The Mine Sequence of the Central Noranda Volcanic Complex: Geology, Alteration Massive Sulphide Deposits and Volcanological Reconstruction

by

Harold L. Gibson, B.Sc., M.Sc.

Thesis submitted to the
Faculty of Graduate Studies and Research
in partial fulfillment
of the requirements for the degree
Doctor of Philosophy

Department of Geology
Carleton University
Ottawa, Ontario, Canada

ABSTRACT

The Mine Sequence, a 3000m thick, primarily tholeiitic, basalt/andesite-rhyolite bimodal succession, was erupted during a period of cauldron subsidence within the upper part of the subaqueous Noranda Shield Volcano. The principal area of subsidence, the Noranda Cauldron, has a crude, oval form (approximately 15 X 20 km) with structural margins defined by the Hunter Creek Fault to the north, Beauchastel-Western Quemont Feeder Dike-Horne Faults to the south and the Flavrian Pluton to the west and Dalembert Shear/Dufault Pluton to the east. The Noranda Cauldron is interpreted to have subsided a minimum of 500m and 1200m along its northern and southern margins respectively to produce an asymmetric, trapdoor-like structure that essentially confined rhyolitic and andesitic formations of the Mine Sequence. Two smaller subsidence structures, the Despina and Delbridge Cauldrons, are nested within and along the southern margin of the Noranda Cauldron. Subsidence, localized along radial and concentric faults, was essentially piece-meal and passive and is interpreted to have occurred in response to partial evacuation of an underlying magma chamber now represented by the Flavrian Pluton.

Rhyolitic flows issued from fissures located primarily along the margins of the cauldron. Lobe-hyaloclastite flows constructed broad, low relief (<20°) plateaus or lava shields that extended along and less than 2km away from their feeding fissure. Blocky rhyolitic flows constructed steep-sided (20-70°), aerially restricted lava domes and ridges that extended less than 1km from their feeding fissure. Massive and pillowed andesitic flows erupted mainly from fissures within the Old Waite Dike Swarm or Paleofissure in the core of the cauldron. Andesitic flows produced broad, low-relief, lava plains that inundated and buried topographic highs produced by rhyolitic volcanism. Pyroclastic eruptions, chiefly phreatomagmatic eruptions that preceded periods of andesitic and rhyolitic volcanism, were minor. Pyroclastic rocks comprise less than 5% of the Mine Sequence.

Mine Sequence rhyolitic and andesitic flows have a complex hydrothermal-metamorphic history. Semiconformable alteration, consisting of diagenesis followed by spilitization, epidote-quartz alteration and locally by silicification, has affected all flows and is interpreted to be the product of alteration within a shallow, subseafloor hydrothermal system within the cauldron. Widespread, pervasive silicification, however, is restricted to the Amulet and Waite upper members which are products of uninterrupted, voluminous (up to 40 km^3), flood-type andesitic eruptions. Silicification is interpreted to result from the interaction of these hot, ponded flows with a silica-saturated, intrastratal hydrothermal fluid, that through rapid heating, was driven through the quartz solubility maximum (<700 bars)

resulting in the replacement of andesitic and rhyolitic glass by quartz, and quartz precipitation. Discordant pipe-like areas of chlorite and sericite cross-cut penecontemporaneous, semiconformable alteration zones and mark fault-controlled conduits that channelled "ore-forming" hydrothermal fluids to the seafloor to form massive sulphide deposits.

Massive sulphide (VMS) deposits are concentrated within and along the margins of the Noranda Cauldron where they occur along synvolcanic radial and concentric faults that also accommodated subsidence and controlled the location of volcanic vents. Although VMS deposits occur throughout the Mine Sequence they preferentially formed during a period of contemporaneous rhyolitic and andesitic volcanism that marks the onset of the second cauldron subsidence cycle. The location of VMS deposits in the Noranda Cauldron and Mine Sequence is thought to reflect this unique period in the evolution of the Noranda Shield Volcano. The Noranda Cauldron was a restricted site of anomalously high heat flow and structural permeability that localized the development of a high temperature hydrothermal system. Metals may have been derived from leaching of aquifer rocks by convecting evolving seawater or from a shallow underlying magma (Flavrian Pluton) that was at its highest position in the crust during cauldron subsidence. Massive sulphide deposits probably formed through a combination of sulphide precipitation and replacement at and below the seafloor in an analogous manner to modern ocean floor sulphide mounds.

TABLE OF CONTENTS

	Page
Acceptance Page	ii
Abstract	iii
Table of Contents	v
List of Figures	xiii
List of Plates	xix
List of Tables	xxiv

1 INTRODUCTION

1.1 LOCATION 1

1.2 RELIEF AND EXPOSURE 1

1.3 PREVIOUS WORK 2

1.4 PURPOSE OF THE STUDY 3

1.5 METHODS 4
1.5.1 Field Methods 4
1.5.2 Laboratory Methods 6

1.6 PRESENTATION 7

1.7 ACKNOWLEDGEMENTS 8

2 REGIONAL GEOLOGY OF THE NORANDA VOLCANIC COMPLEX

2.1 REGIONAL GEOLOGY 13
2.1.1 Blake River Group 15

2.2 GENERAL GEOLOGY OF THE NORANDA VOLCANIC COMPLEX AND NORANDA AREA 17
2.2.1 Noranda Volcanic Complex 17
2.2.2 Noranda Area Geology 19

3 LITHOLOGIC CLASSIFICATION, DEFINITIONS AND STRATIGRAPHIC NOMENCLATURE

3.1 INTRODUCTION 38

3.2 CLASSIFICATION OF FLOWS 38
3.2.1 Field Criteria 38
3.2.2 Petrographic Criteria 40
3.2.3 Chemical Criteria 41

3.3 CLASSIFICATION OF VOLCANIC BRECCIAS 42

3.4 STRATIGRAPHIC NOMENCLATURE AND DEFINITIONS 43

4 THE PETROLOGY, FLOW MORPHOLOGY AND EMPLACEMENT OF SUBAQUEOUS RHYOLITE FLOWS

4.1 INTRODUCTION 46

4.2 LOBE-HYALOCLASTITE FLOWS 47
4.2.1 Flow Facies of Lobe-hyaloclastite Flows 48
4.2.2 Interpretations 57

4.3 BLOCKY RHYOLITIC FLOWS 59
4.3.1 Cranston Member 60
4.3.2 Millenbach-D68 QFP Lava Dome 63

4.4 EMPLACEMENT OF SUBAQUEOUS RHYOLITIC FLOWS 69
4.4.1 Lobe-hyaloclastite Flows 69
4.4.2 Blocky Rhyolite Flows 72

4.5 COMPARISON WITH SUBAERIAL RHYOLITIC FLOWS 74

4.6 COMPARISON WITH SUBGLACIAL RHYOLITIC FLOWS 75

5 THE PETROLOGY, FLOW MORPHOLOGY AND EMPLACEMENT OF SUBAQUEOUS ANDESITIC FLOWS

5.1 INTRODUCTION 107

5.2 ANDESITE FLOW FACIES 108
5.2.1 Vertical Facies Sequence 108
5.2.2 Lateral Facies Sequence 109
5.3 PILLOWED FLOWS 110
5.3.1 Introduction 110
5.3.2 Pillow Facies 111
5.3.3 Structures within Pillows 116
5.3.4 Breccia Facies 119

5.4 MASSIVE FLOWS 123
5.4.1 Massive Facies 124
5.4.2 Lobe Facies 125
5.4.3 Structures 126
5.4.4 Breccia Facies 128

5.5 CONTROLS ON THE FORMATION OF MASSIVE VERSUS PILLOWED FLOWS 131

5.6 FLOW MORPHOLOGY AND EMPLACEMENT OF ANDESITIC FLOWS 132
5.6.1 Pillowed Flows 132
5.6.2 Massive Flows 134

6 TUFF UNITS AND SILICEOUS DEPOSITS

6.1 TUFF UNITS 152
6.1.1 Definition and Description 152
6.1.2 Interpretation 154

6.2 SILICEOUS DEPOSITS 155
6.2.1 Definition and Description 155
6.2.2 Interpretation 156

7 VOLCANIC BRECCIAS

7.1 BEECHAM BRECCIA 160
7.1.1 Description 161
7.1.2 Vent Area 162
7.1.3 Subsurface Distribution 163
7.1.4 Interpretation 163

7.2 RHYOLITIC BRECCIAS 164
7.2.1 Rhyolitic Breccias of the Rusty Ridge Formation 164
7.2.2 Rhyolitic Breccias of the Waite Andesite Formation 166

7.3 BRECCIA DIKES 168
7.3.1 Rhyolitic Breccia Dikes 168
7.3.2 White-Fragment Breccia Dikes 173

8 SYNVOLCANIC INTRUSIONS

8.1 RHYOLITIC INTRUSIONS 186
8.1.1 Lithology 186
8.1.2 Chemical Composition 188
8.1.3 Interpretation 188

8.2 ANDESITIC INTRUSIONS 189
8.2.1 Lithology 189
8.2.2 Chemical Composition 190
8.2.3 Interpretations 191

8.3 COMPOSITE INTRUSIONS 191
8.3.1 Lithology and Field Characteristics 192
8.3.2 Petrography 194
8.3.3 Chemical Composition 198
8.3.4 Interpretation 199

8.4 XENOLITHS 202

8.5 THE DACITE DIKE 202

8.6 DIKE SWARMS ... 203
8.7.1 The McDougall-Despina Dikes ... 203
8.7.2 The Old Waite Dike Swarm ... 204

8.7 ORIENTATION OF SYNVOLCANIC INTRUSIONS ... 206

8.8 MECHANISM OF DIKE EMPLACEMENT ... 206

9 STRATIGRAPHY

9.1 INTRODUCTION ... 225

9.2 MINE SEQUENCE STRATIGRAPHY:FLAVRIAN BLOCK ... 226
9.2.1 Flavrian Formation ... 226
9.2.2 Northwest Formation ... 230
9.2.3 Cranston Member, Northwest Formation ... 234
9.2.4 Rusty Ridge Formation ... 238
9.2.5 Amulet Formation ... 244
9.2.6 Amulet Lower Member ... 245
9.2.7 Amulet Upper Member ... 249
9.2.8 Millenbach Andesite Formation ... 257
9.2.9 Waite Andesite Formation ... 259
9.2.10 Waite Rhyolite Formation ... 264
9.2.11 Millenbach Rhyolite Formation ... 269
9.2.12 Amulet Andesite Formation ... 274

9.3 STRATIGRAPHIC CORRELATION ... 279
9.3.1 Correlation across the Hunter Creek Fault ... 279
9.3.2 Correlation across the Beauchastel/Western QFP Feeder Dike Fault ... 282
9.3.3 Correlation across the Horne Fault ... 284
9.3.4 Correlation with the Mine Sequence at Aldermac ... 286

9.4 ERUPTIVE CENTRES ... 287

10 SYNVOLCANIC FAULTS AND STRUCTURE

10.1 SYNVOLCANIC FAULTS ... 320

10.2 SYNVOLCANIC FAULTS OF THE FLAVRIAN BLOCK ... 321

10.2.1 McDougall-Despina Fault 321
10.2.2 The Des and Dacite Faults 322
10.2.3 The Cranston and Bancroft Faults 323
10.2.4 Trail#1, Quesabe and Watkins Faults 325
10.2.5 Vauze Creek Fault 325
10.2.6 Subsidence within the Flavrian Block 326

10.3 FAULT ORIENTATION 328

10.4 MAJOR STRUCTURAL FEATURES 329

11 THE NORANDA CAULDRON: VOLCANIC RECONSTRUCTION AND SUBSIDENCE HISTORY

11.1 DEFINITION OF THE NORANDA CAULDRONS 335

11.2 SHAPE AND SIZE OF THE NORANDA CAULDRONS 337

11.3 SUBSIDENCE MECHANISM 339

11.4 SUBSIDENCE HISTORY AND CHARACTERISTICS 341

11.4.1 Structural Events 341
11.4.2 Volcanic Events 343
11.4.3 Sedimentary Events 343
11.4.4 Intrusive Events 344

11.5 WATER DEPTH... 345

11.6 CAULDRON CLASSIFICATION 348

12 ALTERATION

12.1 DIAGENETIC ALTERATION 356
12.1.1 Palagonitization of Andesitic and Rhyolitic Vitrophyre and Hyaloclastite 356
12.1.2 Andesitic and Rhyolitic flows 358
12.1.3 Pore space cement and amygdules 369
12.1.4 Chemical changes 361
12.1.5 Summary 361

12.2 SEMI-CONFORMABLE ALTERATION 363
12.2.1 Spilitic alteration 363
12.2.2 Epidote-quartz alteration 365
12.2.3 Silicification 370

12.3 ORIGIN AND EVOLUTION OF SEMI-CONFORMABLE ALTERATION ASSEMBLAGES 380
12.3.1 Diagenetic, Spilitic and Epidote-quartz Alteration 381
12.3.2 Silicification 391
12.3.3 Heat Source 395
12.3.4 Discharge of Hydrothermal Fluids 397

12.4 DISCORDANT ALTERATION 398
12.4.1 Chlorite and Sericite Alteration 398
12.4.2 Origin and Evolution of Chlorite and Sericite Alteration 403

13 CHARACTERISTICS, MODE OF FORMATION AND CONTROLS ON THE LOCATION OF VOLCANOGENIC MASSIVE SULPHIDE DEPOSITS WITHIN THE NORANDA SHIELD VOLCANO AND CAULDRON

13.1 INTRODUCTION 440

13.2 CHARACTERISTICS OF NORANDA-TYPE VMS DEPOSITS 441
13.2.1 Tonnage, Grade and Mineralogy 441
13.2.2 The Massive Sulphide Lens 442
13.2.3 The Stringer Sulphide Zone 444
13.2.4 Metal Zoning 446
13.2.5 Mode of Formation 448

13.3 DISTRIBUTION OF VMS DEPOSITS WITHIN THE NORANDA SHIELD VOLCANO AND CAULDRON 453
13.3.1 Stratigraphic Distribution and Metal Zoning Of VMS Deposits within the Noranda Shield Volcano 453
13.3.2 Cauldron Subsidence and VMS Deposits 456
13.3.3 Controls on the Location of VMS Deposits within the Noranda Cauldron 459
13.3.4 Possible Origins of Hydrothermal Fluids Responsible for Formation of Noranda VMS Deposits 465

14 CONCLUSIONS 478

15 REFERENCES.. 478

APPENDIX A: A PONDED MASSIVE FLOW AND PILLOW VOLCANO AT ANSIL HILL 509
APPENDIX B: SUBAQUEOUS PHREATOMAGMATIC EXPLOSION BRECCIAS AT BUTTERCUP HILL 527
APPENDIX C: RECONSTRUCTION OF THE CORBET BRECCIA PILE AND VOLCANOGENIC MASSIVE SULPHIDE DEPOSIT 559
APPENDIX D: MINE SEQUENCE STRATIGRAPHY OF THE POWELL AND HUNTER BLOCKS, ALDERMAC AREA. CYCLE IV FORMATIONS, AND HORNE MINE STRATIGRAPHY 593
APPENDIX E: VOLCANIC HISTORY OF THE MINE SEQUENCE....... 609
APPENDIX F: CHARACTERISTICS OF ANDESITIC AND RHYOLITIC FLOWS.. 620
APPENDIX G: GEOCHEMISTRY AND CHEMICAL ANALYSES.......... 634

LIST OF FIGURES AND MAPS

Figure 1.1. Location of the Noranda Area, northwestern Quebec............10
Figure 1.2. Major fault blocks, intrusions and reconnaissance traverses............11
Figure 1.3. Synvolcanic faults and Pre-Caldera, Caldera and Post-Caldera sequences............12
Figure 2.1. Stratigraphic map of the Rouyn-Noranda area and part of northeastern Ontario............29
Figure 2.2. Rhyolite Zones and general geology of the Noranda Volcanic Complex............30
Figure 2.3. Fault bounded sectors within the Flavrian Block............31
Figure 2.4. General geology of the Flavrian Block............32
Figure 2.5. Distribution of regional metamorphic isograds............33
Figure 4.1. Feldspar Porphyritic and Quartz Porphyritic rhyolitic flows of the Mine Sequence in the Flavrian Block............78
Figure 4.2. Isopach map of the North and South flows of the Northwest formation............79
Figure 4.3a. Lobe of massive rhyolite in contact with banded rhyolite............80
Figure 4.3b. Quartz amygdule band at contact between massive and banded spherulitic rhyolite (Bedford flow)............80
Figure 4.4. Textures and structures of massive rhyolitic lobes in the lobe-hyaloclastite and massive facies............81
Figure 4.5a. An amygdule band and smooth parallel banding define the margin of a massive rhyolite lobe............82
Figure 4.5b. Autobrecciation of a massive rhyolitic lobe within flowbanded rhyolite............82
Figure 4.6. Columnar jointed massive rhyolite of the South flow of the Northwest formation............83
Figure 4.7. Cross-section through the #3 flow of the Amulet lower member............84
Figure 4.8. Drift wall map showing the lobe-hyaloclastite facies of the Northwest formation............85
Figure 4.9. Gradational contact between rhyolitic lobe and brecciated flow banded rhyolite and hyaloclastite............86

Figures 4.10 A and B. A. Sharp and gradational contacts between a rhyolitic lobe and contorted, brecciated hyaloclastite............ 87
Figure 4.10C. Rhyolitic lobe engulfed within brecciated flow banded rhyolite and hyaloclastite.. 87
Figure 4.11. Geologic map showing the distribution of the massive and breccia facies of the Cranston QFP flow................................ 88
Figure 4.12. Isopach map of the Cranston member................................... 89
Figure 4.13. Isopach map of the Millenbach-D68 lava dome...................... 90
Figure 4.14. Longitudinal section of the Millenbach-D68 lava dome.......... 91
Figure 4.15. Actual profile (upper) and diagrammatic reconstruction of the Millenbach QFP lava dome at the Millenbach Mine......... 92
Figure 4.16. Diagrammatic cross-sections through subaqueous lobe-hyaloclastite and blocky rhyolitic flows.......................... 93
Figure 4.17. Sketch of the southern slope of Blahnukar............................ 94
Figure 5.1. Vertical sequences in basaltic and andesitic flows of the Noranda area.. 135
Figure 5.2. Oblique cross-section through a tube-fed pillowed flow......... 136
Figure 5.3. Cross-sections through a tube-fed pahoehoe flow................. 137
Figure 5.4. Oblique cross-section through a tube-fed pillowed flow......... 138
Figure 5.5. Oblique cross-section through a tube-fed pillowed flow......... 139
Figure 5.6. Structures and amygdule distribution within pillows............ 140
Figure 5.7. Well developed radial joints in tube-fed pillowed flow.......... 141
Figure 5.8. Idealized cross-section through a tube-fed pillowed flow....... 142
Figure 5.9. Vertical facies, structures and amygdule distribution within subaqueous massive andesitic flows........................... 143
Figure 5.10. Idealized cross-section through a massive andesitic flow....... 144
Figure 7.1. Location of volcanic breccias, breccia dikes and synvolcanic faults... 177
Figure 7.2. Isopach map of the Beecham Breccia.................................... 178
Figure 7.3. Beecham Breccia exposed along the 7-02 drift....................... 179
Figure 7.4. Beecham Breccia, 7-02 exploration drift................................ 180
Figure 7.5A. Rhyolitic, andesitic and breccia dikes that occupy the McDougall Fault.. 181
Figure 7.5B. Cartoon illustrating one possible reconstruction of the Beecham Breccia vent area... 182
Figure 7.6. Rhyolitic breccias within the Rusty Ridge formation............. 183
Figure 8.1. Composite dike with a QFP rhyolite interior and fine-grained andesitic margins... 208
Figure 8.2. Irregular, rounded and cuspate andesite xenoliths in hybrid zone.. 208
Figure 8.3. Outcrop sketch of a composite dike...................................... 209
Figure 8.4. Composite dikes adjacent to the McDougall-Despina fault..... 209
Figure 8.5. Diagrammatic sketch of a composite dike............................. 210

Figure 8.6. Chondrite normalized REE plots for the andesitic, rhyolitic and hybrid components of composite dikes.............211
Figure 9.1. Mine Sequence Stratigraphy of the Flavrian Block................291
Figure 9.2. Lithostratigraphic correlation ....in pocket
Figure 9.3. Structural cross-sections...in pocket
Figure 9.4. Structural cross-sections...in pocket
Figure 9.5. Structural cross-sections...in pocket
Figure 9.6. Structural cross-sections...in pocket
Figure 9.7. Surface distribution of the Flavrian formation...................... 292
Figure 9.8. Stratigraphic top contact contour map for the Flavrian formation... 293
Figure 9.9. Isopach map for the Ansil member.......................................294
Figure 9.10. Stratigraphic top contact contour map for the Ansil (A) and Cranston (B) QFP flows.................................295
Figure 9.11. Surface distribution of the Northwest formation and Cranston member...296
Figure 9.12. Stratigraphic top contact contour map for the north and south flows of the Northwest formation........................ 297
Figure 9.13. Surface distribution of the Rusty Ridge formation................ 298
Figure 9.14. Flow stratigraphy of the Rusty Ridge formation.................. 299
Figure 9.15. Stratigraphic top contact contour map for the Rusty Ridge formation... 300
Figure 9.16. Isopach map for the Rusty Ridge formation.........................301
Figure 9.17. Feeder dikes and vent areas for the Rusty Ridge formation.. 302
Figure 9.17A. Cartoon illustrating one possible reconstruction of a reactivated andesitic vent area..303
Figure 9.18. Surface distribution of the #1, 2 and 3 flows of the Amulet lower member..304
Figure 9.19. Surface distribution of the Amulet upper member................ 305
Figure 9.20. Sections detailing the flow stratigraphy and facies of the upper member...306
Figure 9.21. Andesitic feeder dike and vent area for the Amulet upper member, F-Shaft sector..307
Figure 9.22. Stratigraphic top contact contour map for the Amulet upper member..308
Figure 9.23. Reconstructed cross-section through the Amulet upper member... 309
Figure 9.24. Surface distribution of the Waite and Millenbach Andesite formations and location of the Old Waite Dike Swarm..........310
Figure 9.25. Lithostratigraphic correlation of the Waite and Millenbach Andesite formations..311
Figure 9.26. Surface distribution of the #1, 2, 3 and 4 rhyolitic flows of the Waite Rhyolite formation.. 312

Figure 9.27. Flow stratigraphy of the Millenbach Rhyolite formation........ 313
Figure 9.28. Surface distribution of the Amulet Andesite formation.......... 314
Figure 9.29. Geology of the Hunter Block.. 315

Figure 9.30. Geology of the Powell and south part of the Flavrian Blocks..316
Figure 9.31. Generalized geology of the Aldermac area............................ 317
Figure 9.32. Generalized location of the Mine Sequence eruptive centres..318
Figure 10.1. Stratigraphic sections and reconstruction.......... ....in pocket
Figure 10.2. Diagrammatic reconstruction of subsidence and volcanism along the Bancroft Fault... 331
Figure 10.3. Trace of synvolcanic faults of the Northwest formation paleosurface...332
Figure 11.1. Reconstructed north-south cross-section through the Noranda Cauldron post Here Creek Rhyolite volcanism.in pocket
Figure 11.2. Inferred structural margins of the Noranda Cauldron............ 350
Figure 11.3. North-south and east-west cross-sections through the Noranda Cauldron..351
Figure 11.4. Stages in the evolution of the Noranda Cauldron........ in pocket
Figure 11.5. The Tertiary Alnsjo Cauldron, Norway................................. 352
Figure 12.1. Alkali ratio diagram illustrating the spilitic affinity of Mine Sequence rhyoitic flows... 413
Figure 12.2. Alkali ratio diagram illustrating the spilitic affinity of Mine Sequence andesitic flows... 414
Figure 12.3. Alkali ratio diagram illustrating the spilitic affinity of silicified andesitic flows of the Amulet upper member........... 415
Figure 12.4. Alkali ratio diagram illustrating the spilitic affinity of rhyolitic and andesitic sub-volcanic intrusions.......................416
Figure 12.5 Waite Andesite upper member...................................in pocket
Figure 12.6. Distribution of epidote-quartz alteration and silicification within massive and pillowed andesitic flows......................... 417
Figure 12.7. Areas of weak and strong silicification within andesitic flows of the Amulet upper member...................................... 418
Figure 12.8. Wide-beam microprobe traverses across the silicified margins of microlitic sideromelane shards............................ 419
Figure 12.9. Distribution of alteration types and paleo-isotherms............. 420
Figure 12.10.A.Calculated solubilities of quartz in water at temperatures up to 900°.. 421
Figure 12.11.Distribution of sericite and chlorite within an idealized alteration pipe at the Millenbach mine.................................. 422
Figure 12.12.Distribution of chlorite, sericite and epidote-quartz alteration at the Corbet Mine... 422

Figure 12.13. Unfolded tetrahedron after Riverin (1977) showing trends of alteration.......... 423
Figure 12.14. Interpreted evolution of Mg-chlorite and sericite alteration assemblages.......... 424
Figure 12.15. Diagram showing the stability fields of chlorite, kaolinite, sericite and K-feldspar at temperatures from 100 to 250°.......... 425
Figure 13.1. Distribution of Volcanogenic Massive Sulphide and gold deposits.......... 470
Figure 13.2. Cartoon illustrating an interpreted volcanological reconstruction of the rhyolitic Millenbach - D-68 lava dome.......... 471
Figure 13.3. Cartoon illustrating an interpreted volcanological reconstruction of massive sulphide deposits along the Old Waite Dike Swarm.......... 472
Figure 13.4. Cartoon illustrating an interpreted volcanological reconstruction of the Northwest and Rusty Ridge formations.......... 473
Figure A.1. Stratigraphic column for the Ansil Hill flows.......... 520
Figure A.2. Vertical variation in textures and structures within a massive andesitic flow of unit 1.......... 520
Figure A.3. Geological map illustrating the distribution of flow units and fault breccia at Ansil Hill.......... 521
Figure A.4. Idealized cross-sections through Ansil Hill.......... 522
Figure A.5. Representative samples of Ansil Hill flows straddle the tholeiitic - calc-alkaline field boundary.......... 523
Figure A.6. Sketch illustrating the discordant contact between the tube-fed andesitic flow of unit 3 and the massive, ponded andesitic flow of unit 4.......... 524
Figure B.1. General geology of the central part of the Noranda Volcanic complex.......... 550
Figure B.2. Simplified geologic map and cross section of Buttercup Hill.. 551
Figure B.3. Stratigraphic column for Buttercup Hill.......... 552
Figure B.4a. Silicified lobes of andesite.......... 553
Figure B.4b. Plan view of autobrecciated, silicified lobes in flow breccia.. 553
Figure B.5. Sketch of Buttercup Hill looking northeast and along strike of the breccia dikes.......... 552
Figure B.6. Schematic stratigraphic sections of an idealized tuff cone and ring and for Buttercup Hill breccias.......... 554
Figure B.7. Diagrammatic reconstruction portraying the sequence of events leading to the formation of the Buttercup Hill breccia.......... 554
Figure C.1. Simplified stratigraphy of the Corbet Mine.......... 581

Figure C.2. Massive sulphide lenses at the Corbet Mine 581
Figure C.3. Subsurface topography of the Flavrian formation 582
Figure C.4. Geology of Section 600N, looking north 582
Figure C.5. Geology of Section 800N, looking north 583
Figure C.6. Geology of section 4900E, looking west 583
Figure C.7. Schematic north-south cross-section through the Corbet breccia pile 584
Figure C.8. Wall map detailing geology of the #1 draw point 584
Figure C.9. Detailed geology of the 14-3-5 A sublevel 585
Figure C.10. Cartoon illustrating an interpreted paleovolcanolgical reconstruction of the Corbet volcanic edifice and massive sulphide deposits 586
Figure D.1. Surface distribution of the Brownlee Rhyolite formation 600
Figure D.2. Surface distribution of the Joliet Rhyolite formation 601
Figure D.3. Surface distribution of the Quemont Rhyolite formation 602
Figure D.4. Surface distribution of the Powell Andesite formation 603
Figure G.1 Olivine - nepheline - quartz ternary diagram 642
Figure G.2 Classification of Mine Sequence volcanic rocks 643
Figure G.3 Variation of major oxides with respect to SiO_2, andesitic flows 644
Figure G.4 Variation of major oxides with respect to SiO_2, rhyolitic flows 647
Figure G.5 Variation of major oxides with respect to SiO_2, silicified flows, Amulet upper member 650
Figure G.6 A SiO_2-Na_2O+K_2O-Fe_2O_3+MgO ternary diagram 653
Figure G.7 An AFM diagram and Jesen Cation Plot 654
Figure G.8 An AFM diagram and Jesen Cation Plot 655
Figure G.9 An AFM diagram and Jesen Cation Plot 656
Figure G.10 An AFM diagram and Jesen Cation Plot 657
Figure G.11 An AFM diagram and Jesen Cation Plot 658
Figure G.12 An AFM diagram and Jesen Cation Plot 659
Figure G.13 Classification of andesitic flows according to possible tectonic environment 660
Figure G.14 Histogram showing the bimodal character of the Mine Sequence 661

MAP 1 Geological compilation map, 1:10,000 scale .... in pocket
MAP 2 Lithologic maps, 1:2000 scale .... in pocket

LIST OF PLATES

Page

Plate 4.1A. Feldspar porphyritic spherulitic rhyolite of the Amulet lower member (#3 flow)..........100
B. Same as A, flowbanding and quartz amygdules more apparent in plane polarized light
C.and D. Spherulitic and flowbanded border to a rhyolite lobe from the #3 flow of the Amulet lower member
E. Well developed quartz spherulites from the interior of a massive rhyolite lobe (#3 flow, Amulet lower member).
F. Spherulitic corona mantling a quartz filled amygdule within a the chloritized obsidian selvedge of Plate 4.6.
G. Weakly silicified, chloritized obsidian hyaloclastite from the #3 flow of the Amulet lower member.
H. Weakly insitu brecciated, perlitic textured, chloritized obsidian selvedge to a rhyolite lobe of the QFP Cranston flow.

Plate 4.2. Massive, and quartz amygdaloidal rhyolite of the #3 flow, Amulet lower member 101

Plate 4.3. Contorted flow banded spherulitic rhyolite of the Bedford Flow, Amulet upper member.......... 101

Plate 4.4. Large lobe of massive rhyolite partially enveloped by chloritized rhyolite hyaloclastite.......... 102

Plate 4.5. Irregular lobes of rhyolite.......... 102

Plate 4.6. Chloritized obsidian selvedge to rhyolite lobes of the #1 flow of the Amulet lower member..........103

Plate 4.7. Lobe margin - hyaloclastite contact, #3 flow of the Amulet lower member..........103

Plate 4.8. Close-up showing the contact between chloritized obsidian selvedge and hyaloclastite in 4.7.......... 104

Plate 4.9. Carapace breccia to the Cranston Flow.......... 104

Plate 4.10. Crudely bedded flank breccias to the Cranston Flow.......... 105

Plate 4.11. Hammer rests on the obsidian selvedge (black) of a columnar jointed rhyolite lobe, Iceland.......... 105

Plate 4.12. Close-up of 4.12 showing the transition between massive rhyolite of the lobe interior to the banded, spherulitic border zone.......... 106

Plate 4.13. Faintly banded obsidian hyaloclastite mantling lobes in 4.12.......... 106

Plate 5.1A. Pilotaxitic texture where flow aligned plagioclase microlites wrap around amygdules.. 146
B. Fine intersertal texture of andesite from a pillow interior (Rusty ridge formation).
C. Intersertal textured masive andesite with needle-like plagioclase microlites (Rusty Ridge formation).
D. Transitional intersertal-hyalophitic texture.
E. Glomeroporphyritic clots of plagioclase phenocrysts.
F. Concentric joint defined by a thin line of opaque minerals.
G. Laminated quartz crystal tuff.
H. Fragmental matrix to breccias which occupy the Despina Fault.
Plate 5.2. Irregular, densely packed pillows of the Rusty Ridge formation.. 147
Plate 5.3. Bulbous pillows of the Rusty Ridge formations.......................... 147
Plate 5.4. Upper surface of pillowed flow showing the tube-like form of individual pillows... 148
Plate 5.5. Well developed concentric joints... 148
Plate 5.6. Polyhedral fractures within pillows.. 149
Plate 5.7. Parallel striations or corrugations within the pillow crust.......... 149
Plate 5.8. Finger-like lobes of massive andesite.. 150
Plate 5.9. Blocky flow top breccia.. 150
Plate 5.10. In situ brecciation of lobe margins... 151
Plate 6.1. Plane, parallel bedded tuff.. 157
Plate 6.2. Plane parallel bedded, pyritic "C" contact tuff............................ 157
Plate 6.3. Sulphide bearing plane bedded and cross bedded tuffs.............. 158
Plate 6.4. Massive and laminated chert.. 158
Plate 6.5. Massive, recrystallized chert between pillows............................ 159
Plate 6.6. Massive and laminated jasper between pillows.......................... 159
Plate 7.1. Beecham Breccia with lapillistone beds interbedded with thin, parallel laminated deposits of tuff......................... 184
Plate 7.2. Densely packed fragments within a lapillistone bed.................... 184
Plate 7.3. Bomb sag in laminated tuff... 185
Plate 7.4. Rhyolite breccias within the Despina Fault................................. 185
Plate 8.1A. Perlitic cracks in groundmass of a quartz porphyritic rhyolite dike (Old Waite Swarm).. 221
B. Recrystallized spherulitic texture in a massive, homogenous rhyolite dike (Old Waite Swarm).
C. Plagioclase porphyritic, intersertal textured andesite dike.
D. Fine actinolite corona mantling a quartz phenocryst.
E. Myrmekite and "granular" textured quartz rims a quartz phenocryst from the Hybrid zone of a composite dike.
F. Embayed, irregular plagioclase phenocryst.

Plate 8.2A. Ragged plagioclase microlite with myrmekite.......................... 222
B. Gradational contact between an andesitic xenolith and the hybrid zone matrix.
C. Quartz rim mantling a fine grained andesitic xenolith.
D. Quartz-rich rim surrounding an epidotized fragment.
Plate 8.3. Sharp, chilled contact between the andesitic component of a composite dike and silicified andesite flows....................223
Plate 8.4. Massive, quartz-feldspar porphyritic component of a composite dike.. 223
Plate 8.5. Xenolith-rich, hybrid component of a composite dike................ 224
Plate 8.6. Large granitic xenolith.. 224
Plate 10.1. Pyrite-chalcopyrite-pyrrhotite stringer mineralization within the C shaft Fault..333
Plate 10.2. Sharp contact between a flow banded rhyolite dike and adjacent andesite flows...334
Plate 12.1A. Waxy yellow palagonite along the shard margins.................. 429
B. Chloritized obsidian shard.
C. Close-up of the shard in B.
D. Strongly palagonitized basaltic hyaloclastite.
E. Chloritized andesitic hyaloclastite.
F. Cross-nicols photo of E.
G. Arcuate perlitic cracks in chloritized andesitic vitrophyre.
H. Close-up of a perlitic crack in G.
Plate 12.2A. Silicification localized along perlitic cracks........................... 430
B. Pervasively silicified andesitic vitrophyre as in A.
C. Typical least altered, intersertal textured, andesite.
D. Incipient silicification of andesite in C.
E. Complete silicification of andesite in C.
F. Typical pillow margin characterized by microlites and microphenocrysts of plagioclase.
G. Incipient silicification of the pillow margin in F.
H. Epidote-quartz altered andesite.
Plate 12.3A. Oxide-rich crusts and borders to andesitic shards.................. 431
B. The bulbous or coliform structure of mineralogically distinct layers.
C.and D. Silicified and quartz cemented hyaloclastite.
E. Clusters of fibrous, radiating chlorite.
F. Fibrous, radiating clinozoisite.
G. Silicified obsidian hyaloclastite.
H. Silicified rhyolite hyaloclastite as in G.
Plate 12.4A.,B.,C. and D. Silicified, microlitic, sideromelane shard hyaloclastite.. 432

Plate 12.5. Light-green, resistant, irregular epidote-quartz alteration patches....433
Plate 12.6. Epidote-quartz alteration....433
Plate 12.7. Epidote-quartz alteration patches in an andesitic hyaloclastite flow top breccia.... 434
Plate 12.8. Coalescing epidote-quartz alteration patches.... 434
Plate 12.9. Silicified pillow margins, Waite Andesite formation.... 435
Plate 12.10.Siiicified pillows of the Waite Andesite formation.... 435
Plate 12.11.Incipient silicification centred about a mega-amygdule.... 436
Plate 12.12.Silicification preferentially located along an amygdule zone.... 436
Plate 12.13.Irregular, patchy silicification along laminar joints....437
Plate 12.14.Pseudo-flowbanding, a result of silicification....437
Plate 12.15.Silicification of andesitic hyaloclastite and fragments....438
Plate 12.16. Same flow top breccia as in 12.15.... 438
Plate 12.17. Ribbon-like, fluidal structure in an andesitic lobe.... 439
Plate 12.18. Silicification localized along concentric joints within pillows..439
Plate 13.1. Massive crudely banded sulphide at the Millenbach Mine....476
Plate 13.2. Brecciated massive sulphide at the Millenbach Mine....476
Plate 13.3. Massive chalcopyrite stringers mantled by dark chloritc envelopes at the Corbet Mine.... 477
Plate 13.4. Sericite altered Northwest Rhyolite at the Corbet Mine....477
Plate B.1A. Hyalopilitic texture of silicified Amulet andesite....555
B. Conformable, shallow, southeast-dipping contact between the breccia deposit and Millenbach andesite flow.
C. White-fragment breccia dikes merging with conformable breccia.
D.Gradational, brecciated margins of dikes.
Plate B.2A. Hyalopilitic texture of a silicified Amulet andesite fragment.... 556
B. Angular chloritized sideromelane shards.
C. Microlitic, chloritized sideromelane shards.
D. Arcuate fractures, "perlitic cracks," in a chloritized sideromelane shard.
E. Quartz amygdaloidal, opaque-rich rhyolite fragment.
F. Silicified fragment identical to Amulet vitrohyre from breccia dike.
Plate B.3A. In situ brecciated, silicified Amulet andesite.... 557
B. Poorly sorted, angular, variably silicified Amulet andesite fragments that constitute the conformable breccia deposit.
C. Bed characterized by numerous fragments of Millenbach andesite.
D. Crude bedding within conformable breccia deposit.
Plate B.4A. Chloritized sideromelane shards and silicified andesite fragment in matrix of breccia deposit....558
B. Aligned sideromelane shards in a tuff matrix to breccia.
C. "Sagged bedding" in andesitic tuff.

D. Quartz-, chlorite- and opaque-rich laminae define bedding within andesitic tuff.
Plate C.1A. Aphanitic and aphyric weakly quartz amygdaloidal andesite fragment and chloritized shards....587
B. Amygdaloidal andesite fragments.
C. Altered (sericitized) microlitic andesite fragment.
D. Matrix to transported sulphide breccia of the #3 lens.
E. Delicately shaped chloritized shards with ragged margins and tails.
F. Plate-like, angular chloritized shards and minor altered andesite fragments in a finer breccia matrix.
G. Amygdaloidal shards containing numerous fine oxides.
H. Amydaloidal and massive shards.
Plate C.2A. Amygdaloidal andesite fragment....588
B. Strongly amygdaloidal, "scoriaceous" andesite fragments.
C. Broken composite lapilli.
D. Plane bedded tuff showing normal grading and numerous faults.
Plate C.3. Lapilli tuff characterized by numerous altered, angular fragments of andesite in a finer-grained ash-sized matrix....589
Plate C.4. Numerous sericitized andesitic "scoria" fragments....589
Plate C.5. In situ brecciated massive andesite flow....590
Plate C.6. In situ brecciated pillows....591
Plate C.7. Close-up of the breccia in C.7....590
Plate C.8. Amoeboid, highly amygdaloidal, silicified fragments....592
Plate C.9. Transported sulphide, #3 lens....592

LIST OF TABLES

Page

Table 2.1. Volcanic Stratigraphy of the External Zone, Abitibi Greenstone Belt 34
Table 2.2. Lithostratigraphic subdivision of the Noranda Volcanic Complex 35
Table 2.3. Table of Formations for the Noranda Area 36
Table 2.4. Table of Cycle 3 and 4 Formations 37
Table 4.1. Average chemical composition of FP and QFP Rhyolite 95
Table 4.1B. Average composition of the North and South flows of Northwest formation 96
Table 4.2. Estimated volumes of selected FP and QFP Rhyolite flows 97
Table 4.3. Chemical composition of rhyolite lobes, banded rhyolite and breccia, Amulet lower member 98
Table 4.4. Average chemical composition of the Millenbach and Cranston QFP flows 99
Table 5.1. Average chemical composition of the Mine Sequence andesitic flows 145
Table 8.1. Chemical composition of rhyolitic dikes 212
Table 8.2. Average chemical composition of the Mine Sequence rhyolitic and andesitic flows 213
Table 8.3. Major element composition of andesitic dikes 214
Table 8.4. Trace element composition of andesitic dikes 215
Table 8.5. Chemical composition of composite dikes 216
Table 8.6. Trace element composition of composite dikes 218
Table 8.7. Average chemical composition of andesitic, rhyolitic and hybrid components of composite dikes 219
Table 8.8. Chemical composition of the Dacite Dike 220
Table 9.1. Average chemical composition of the Amulet upper member 319
Table 11.1 Evolution of the Noranda Cauldrons 353
Table 12.1. Semiconformable alteration types 426
Table 12.2. Chemical composition of epidote-quartz altered andesite and adjacent least altered andesite 427
Table 12.3. Chemical composition of silicified and adjacent least altered andesite 428
Table 13.1. Grades and tonnages of VMS deposits within the Noranda Cauldron 474
Table A.1. Chemical composition of andesitic flows at Ansil Hill 525
Table A.2. CIPW normative mineralogy of andesitic flows at Ansil Hill 526

Table D.1. Mine Sequence formations in the Hunter Block........................ 604
Table D.2. Mine Sequence strata of the Aldermac area.............................. 605
Table D.3. Post Mine Sequence formations.. 606
Table D.4. Formations south of the Horne Fault and west of Osisko Lake, Powell Block 608
Table F.1A. Andesitic flows of the Flavrian formation, Ansil Sector........... 621
Table F.1B. Andesitic flows of the Flavrian formation, F-Shaft Sector........ 622
Table F.1C. Andesitic flows of the Flavrian formation, Waite Dufault Sector.. 622
Table F.2A. Andesitic flows of the Rusty Ridge formation, Cranston Sector.. 623
Table F.2B. Andesitic flows of the Rusty Ridge formation, Ansil Sector..... 624
Table F.2C. Andesitic flows of the Rusty Ridge formation, Waite Dufault Sector.. 626
Table F.2D. Andesitic flows of the Rusty Ridge formation, F-Shaft Sector. 628
Table F.2E. Andesitic flows of the Rusty Ridge formation, Amulet-Millenbach Sector..629
Table F.3. Andesitic flows of the Millenbach Andesite formation.............. 630
Table F.4. Andesitic flows of the Waite Andesite formation, New Vauze and Ansil Sector.. 631
Table F.5. Flows of the Waite Rhyolite formation.................................... 632
Table F.6. Flows of the Millenbach Rhyolite formation............................. 633
Table G.1. Tables of major and trace element data.................................. 663
Table G.2. Precision of the University of Ottawa XRF Analyses............... 706
Table G.3. Analyses of duplicate fused pellets.. 707
Table G.4. Accuracy and Precision of XRAL XRF Analyses........................ 708
Table G.5. Comparative analyses, Univ. of Ottawa and XRAL.................. 710
Table G.6. Trace element data for Mine Sequence flows.......................... 712
Table G.7. Analyses of duplicate fused pellets.. 715

1. INTRODUCTION

1.1 LOCATION

The Noranda area is located in northwestern Quebec, approximately 600 and 700 km north of Ottawa and Montreal, respectively (Figure 1.1). The centre of the Noranda Volcanic Complex lies 11 km north of the city of Rouyn-Noranda, within Duprat and Dufresnoy townships. Numerous gravel and drill roads provide excellent access to the area.

1.2 RELIEF AND EXPOSURE

Relief ranges from a low of 295m at Dufault Lake to a high of 480m at Beaver Mountain. Topography is rugged by Superior Province standards and is characterized by numerous rolling hills and locally by precipitous cliffs.

The region is well drained with large tracts of low-lying swamp and sand restricted to areas north of Duprat Lake. This results in excellent exposure where the area of outcrop ranges to a high of 80% and commonly exceeds 50%.

1.3 PREVIOUS WORK

The Noranda area is unique in that it not only contains a remarkably well exposed and preserved succession of Archean volcanic rocks but also the "classic" and type examples of Archean, Cu-Zn volcanogenic massive sulphide deposits (VMS). For these reasons the Noranda area is, and will continue to be, one of the most studied regions of the Canadian Shield.

The present understanding of Noranda geology results from the combined work of exploration, university and government geologists. Contributions by exploration geologists have been twofold. The first and perhaps the most direct contribution has been the detailed description of volcanogenic massive sulphide deposits and the physical and chemical controls on their formation and localization (Edwards, Gilmour, Greenwood, Price, Sinclair, Boldy, Spence, Severin, Simmons, Knuckey, Comba, Riverin and Watkins). Many interpretations of the formation of these deposits have stood the test of time and are currently finding further validation through studies of modern seafloor deposits. The second contribution is detailed property mapping that aided stratigraphic subdivision of the Noranda area. Problems and ideas that emerged from this mapping were often the impetus for research by university and government geologists.

University researchers have focused their attention on a spectrum of problems that include regional studies (Dimroth), structure (Goulet, Hubert), metamorphism (Joly), plutonic rocks (Goldie), paleovolcanology and sedimentology (Dimroth, Gelinas, Lajoie, Rocheleau), geochemistry (Baragar, Gelinas, Goodwin) and ore deposits (Hodgson, Riverin, Sakrison, Lickus, Watkinson). Government geologists (Ambrose, Cooke, Wilson) of the Geological Survey of Canada and Quebec Department of Natural Resources provided the first lithologic and stratigraphic maps of the Noranda area. Their accurate and detailed lithologic descriptions and structural/stratigraphic interpretations laid the framework for later studies. A more comprehensive summary of previous work can be found in Comba (1975) and Dimroth and Rocheleau (1979).

1.4 PURPOSE OF THE STUDY

The main objective of this study was to produce a detailed (1:2000) geologic map of the Mine Sequence, within the Flavrian Block (Figure 1.2), that would incorporate data obtained from extensive diamond drilling conducted by Corporation Falconbridge Copper since the 1930's. The map provided the basis for:

1) detailed stratigraphic subdivision of the Mine Sequence within the Flavrian Block and comparisons with the equivalent stratigraphic succession to the north and south.

2) an interpreted reconstruction of the Mine Sequence and a large, 15 x 20 km cauldron, and details regarding the paleovolcanology of each formation with the

Mine Sequence.

3) interpretations regarding the controls on the location of massive sulphide deposits within the Mine Sequence and cauldron, and their mode of formation at and near the seafloor.

4) delineation of semiconformable and conformable alteration types, their mineralogy, chemistry and interpretations concerning their evolutionary relationship to volcanic stratigraphy and history of the Mine Sequence.

5) development of facies models which describe the flow mechanism and emplacement of subaqueous rhyolitic and andesitic flows

1.5 METHODS

1.5.1 FIELD METHODS

Field mapping occupied a period of 16 months during the interval 1979-1984 while in the employ of Corporation Falconbridge Copper. Emphasis was placed on mapping the entire Mine Sequence of the Flavrian Block (Figure 2.6), excluding the Amulet Andesite formation that had been mapped by de Rosen-Spence(1976) and Cousineau and Dimroth (1982). It quickly became apparent, however, that in order to understand and reconstruct the paleovolcanology of the Mine Sequence in the Flavrian Block, the equivalent stratigraphic succession to the north and south had to be examined. Reconnaissance traverses in these areas are shown in Figure 1.2.

Outcrops were mapped at a scale of 1:2000 using enlarged airphotos from the Quebec Department of Natural Resources. Areas were selected for detailed mapping at scales of 1:1000 and 1:10. Distortion inherent in airphoto mapping was minimized by plotting the outcrops on topographic base maps and by "tying in" outcrops to survey triangulation stations and surveyed drill hole collars. Underground mapping was routinely conducted at a scale of 1:240 and selected exposures mapped at a scale of 1:60. Samples collected during mapping were later selected for whole rock chemical analysis or assay.

The author logged some 30,000m of drillcore and supervised the drilling of an additional 70,000m. Data from this drilling and previous and other on-going drill programs totalling more than 500,000m were compiled onto 1:10,000 base maps to produce the first "complete" contour and isopach maps of individual formations and members of the Mine Sequence within the Flavrian Block. These subsurface maps proved invaluable in volcanic and structural reconstruction, in determining the three-dimensional morphology of subaqueous rhyolitic and andesitic flows and in planning drill programs. The interpreted surface geology between the Hunter Creek Fault and Duprat Lake is also based mainly on drill hole data and could not be duplicated if only outcrop data were used. Because of the proprietary nature of the information the original 1:10,000 scale subsurface maps are not included in this study, but, at the discretion of Minnova Inc., may be examined at their Noranda Exploration office. Simplified, reduced copies of these maps are contained in Chapter 9.

Field trips to Cyprus, Hawaii, Iceland, Nevada and the Salton Sea geothermal field provided a much needed background in the flow morphology of subaqueous and subaerial rhyolitic and basaltic flows, ash flow tuffs, volcanic landforms and alteration assemblages in active and fossil hydrothermal systems. Comparison of Noranda geology and alteration assemblages with these modern examples greatly facilitated interpretation of the latter.

1.5,2 LABORATORY METHODS

Laboratory work included:

1) The examination of 350 thin sections with special emphasis on mineralogy and primary textures which served as a basis for lithologic classification and determination of the type and degree of alteration.

2) The selection of 332 samples for chemical analysis. The samples were analyzed for major and trace elements at the University of Ottawa and at X-Ray Assay Laboratories in Toronto using a fused pellet x-ray fluorescence technique. 35 of the above specimens were analyzed at Memorial University for 12 trace elements using a pressed pellet x-ray fluorescence technique. In addition 11 of the samples were analyzed for REE at the CNRS in France.

1.6 PRESENTATION

In spite of initial scepticism about the interpretation of a caldera within the core of the Noranda Volcanic Complex (Figure 1.3;Dimroth et al., 1982) it became apparent during mapping, and later structural and stratigraphic reconstruction described in Chapter 11, that the Mine Sequence of the Flavrian Block was erupted within, and was largely confined to, a subsidence structure herein referred to as the Noranda Cauldron. The first 4 chapters describe the regional geology and setting of the Noranda Volcanic Complex and the lithologies and flow morphologies of units which occupy this structure. Chapters 9 through 11 , provide a detailed description of the Mine Sequence stratigraphy within and outside the cauldron, proposed stratigraphic correlations, reconstruction of the volcanic edifice and cauldron, and outlines the role of synvolcanic faults and intrusions during volcanism and subsidence. The last two major chapters describe a) the distribution, origin and evolution of hydrothermal alteration assemblages in light of processes active in modern hydrothermal systems and b) the localization of massive sulphide deposits within the Noranda Shield Volcano and central cauldron. In each of the chapters an attempt was made to separate descriptions from interpretations. The format for stratigraphic descriptions in Chapter 9 was taken from Lambert (1974).

Map 1 is a 1:10,000 compilation map showing the distribution of major flows, alteration assemblages, mineralization and Mine Sequence formations within the Flavrian Block. The distribution of map units and contacts in Map 1 have been influenced by extensive diamond drill hole data (500,000m). Map 2 is a series of detailed 1:2000 scale lithologic maps that record field observations and notes. Information contained in Map 2 is the basis for all descriptions and interpretations.

1.7 ACKNOWLEDGEMENTS

I am very grateful to my wife, Denise and sons, Jeffrey and Matthew who provided constant encouragement and sacrificed numerous holidays and weekends so that this study could be completed.

Grateful appreciation is extended to Dr. David H. Watkinson who supervised, and was actively involved in this research. Dave's critical reviews, seemingly endless patience and "prodding" made this long-overdue thesis a reality.

This study benefited from numerous discussions and field trips with university and government researchers and explorationists. In particular I would like to thank D.H. Watkins, M.Labrie, A.P. Lichtblau, G. Doiron, G. Riverin and M. Gagnon of Minnova Inc., M.B. Lambert, J.M. Franklin, J.W. Lydon and D.F. Sangster of the Geological Survey of Canada, C.D.A. Comba, C.D. Spence, A. de Rosen-Spence, D.V. Lefbure, J.J.Watkins, H.-U. Schmincke, D. MacNeil, S. Paradis and the late E. Dimroth and L. Gelinas for their insights into Noranda geology, massive sulphide deposits and physical volcanology. C.D.A. Comba and A.D. Hunter introduced the author to Noranda geology and specifically the silicification problem.

The author wishes to thank Corp. Falconbridge Copper for their financial support and "openness" in allowing the author access and permission to use all maps and extensive diamond drill hole information, in particular to M.J. Knuckey and D.H. Watkins for arranging this support and for their keen interest in this research. Noranda Exploration also granted permission for the author to map on their properties. Thanks are also extended to Falconbridge Limited and, in particular, C.D.A. Comba and P.W.A. Severin for providing financial assistance with reproduction costs for this thesis. Funding for field trips to Cyprus and Iceland was provided through NSERC grants to Dave Watkinson and by Corp. Falconbridge Copper.

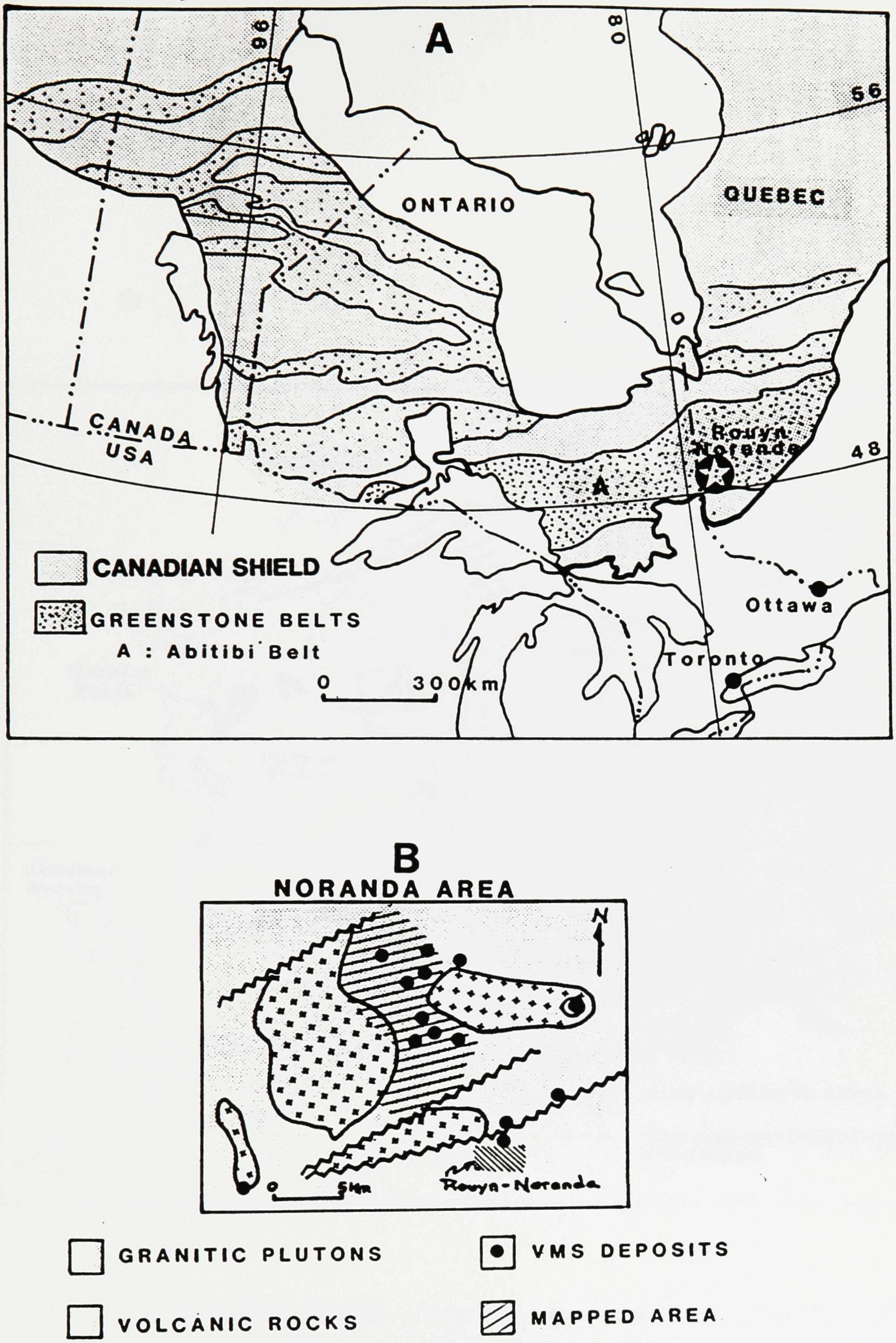

Figure 1.1. Location of the Noranda Area, northwestern Quebec.

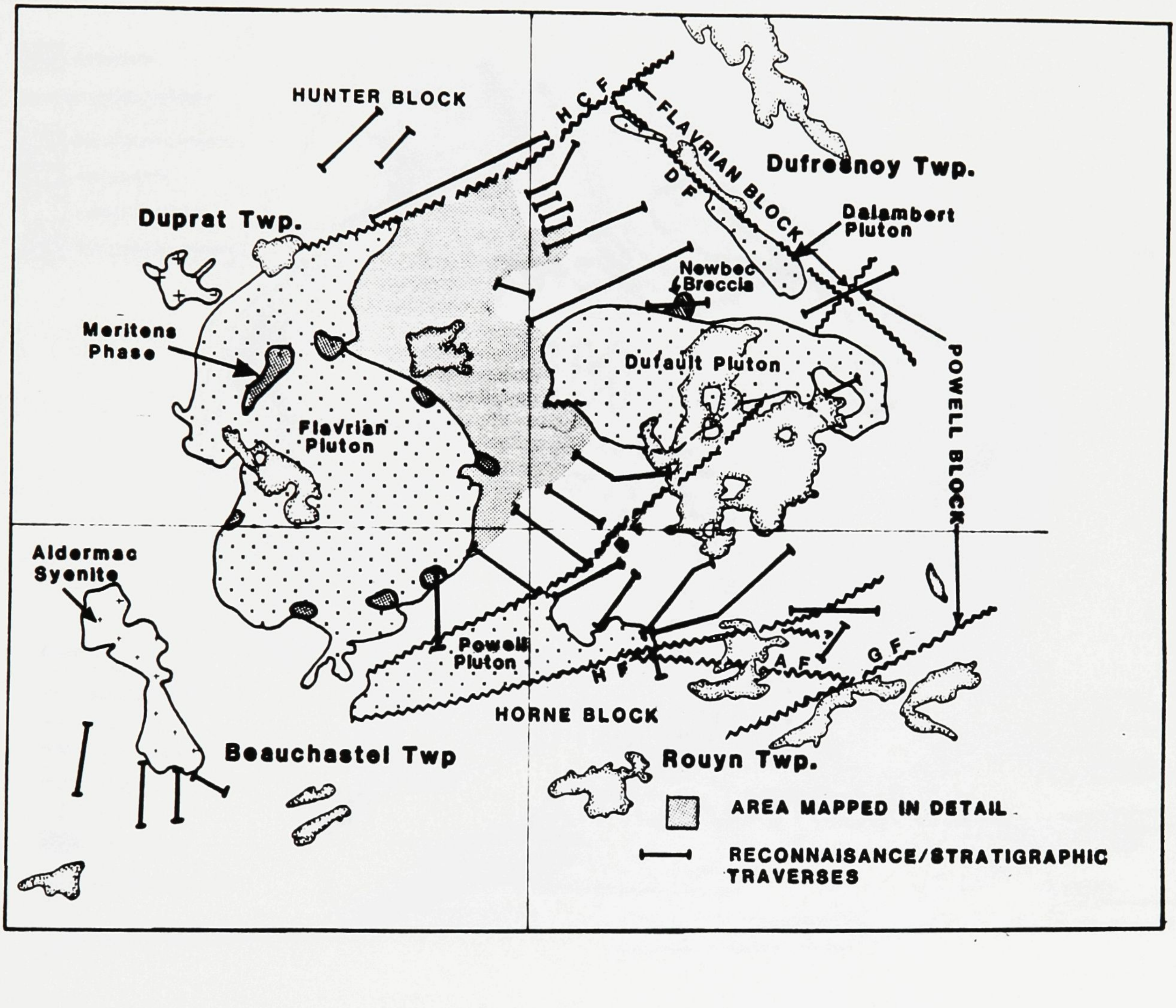

Figure 1.2. Major fault blocks, intrusions and location of mapped areas and reconnaissance traverses (HCF-Hunter Creek Fault, DF-Dalambert Fault/Shear, BF-Beauchastel Fault, HF-Horne Fault, AF-Andesite Fault, GF-Glenwood Fault).

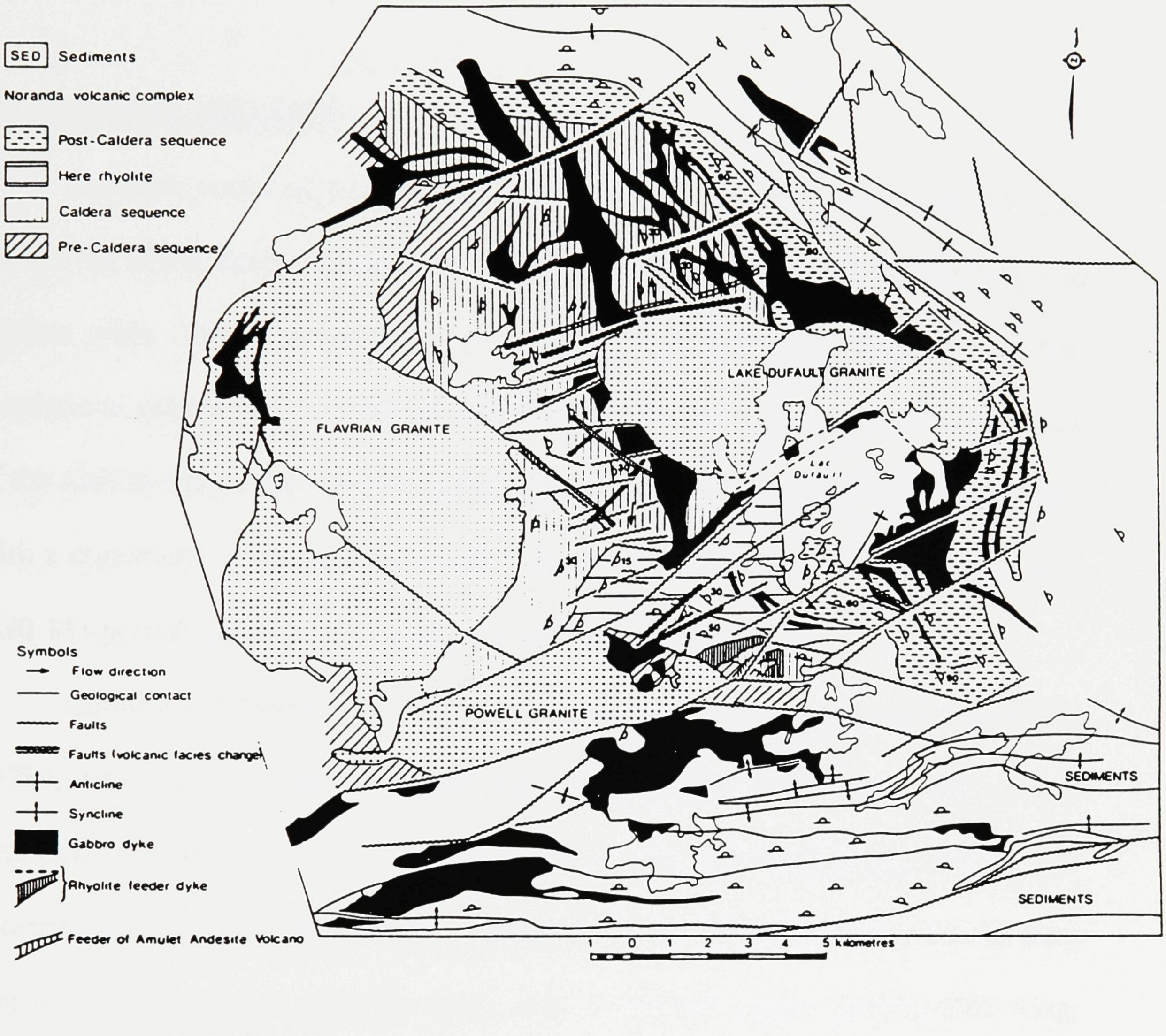

Figure 1.3. Synvolcanic faults and Pre-Caldera, Caldera and Post-Caldera Sequences, after Dimroth <u>et al.</u>, 1982.

2. REGIONAL GEOLOGY OF THE NORANDA VOLCANIC COMPLEX

2.1 REGIONAL GEOLOGY

Volcanic rocks of the Noranda area form the youngest volcanic complex within the Blake River Group of the Abitibi greenstone belt. The 700km long and 200km wide Abitibi greenstone belt has the distinction of being the longest continuous greenstone belt within the Canadian Shield and is the dominant unit of the Abitibi subprovince (Ayres and Thurston, 1985). The Abitibi greenstone belt, with a maximum estimated stratigraphic thickness of 45 km, was deposited within a 30 Ma period (Jensen, 1985; Jensen and Langford, 1985).

Initially subdivided into 9 volcanic and 6 sedimentary groups (Goodwin, 1979), the Abitibi greenstone belt has subsequently been subdivided into a northern "internal zone" and southern "external zone" (Dimroth et al., 1983a) The external zone is subdivided into 3 supergroups in the Timmins-Kirkland Lake area (Jensen, 1985) and on a larger scale, into 4 volcanic cycles (MERQ-OGS Map, 1983; Table 2.1). The cycles, and for that matter the 3 supergroups, are chemostratigraphic units that consist of a basal komatiitic group overlain in turn by tholeiitic, calc-alkaline and alkaline groups.

Dimroth et al., (1983) divided the external zone of Quebec, into 2 cycles (Cycles I and II, Table 1.0 of Dimroth et al., 1983a). Cycle I of Dimroth et al., (1983a) corresponds to Cycle 3 of Table 2.1, and is represented by the Hunter Mine Group, a poorly exposed succession of intercalated basalt and rhyolite. Cycle II of Dimroth et al., (1983a) corresponds to Cycle 2 of Table 2.1, and consists of a 2-7 km thick basal komatiitic succession (Roquemaure-Stoughton Group), a middle 7km thick tholeiitic group (Kinojevis Group) and a 10 km thick upper, complex group of tholeiitic and calc-alkaline volcanics belonging to the Blake River Group (Dimroth et al., 1982). Zircon dates from rhyolites at the top of Cycle 2 and 3 (Table 2.1) indicate that volcanic units of Cycle 2 (19-24km thick) were erupted within an interval of approximately 7 Ma (+/- 4Ma), starting approximately 2710 Ma ago (Jensen, 1985).

Most workers envisage the Abitibi greenstone belt as a succession of overlapping and coalescing volcanos. To explain the origin of this extensive, linear volcanic belt one model invokes an island arc analogy where volcanism was localized above a subducting plate (Dimroth et al., 1982, 1983a and b), whereas in another model volcanism is attributed to crustal rifting above a stationary or moving mantle hot-spot (Goodwin,1977 and 1979; Gelinas et al., 1983). A third model, proposed by Jensen (1985a and b), postulates that the Abitibi greenstone belt formed by a series of megacauldrons (>100 km in diameter) in which primary mantle-derived magmas were progressively transformed into sialic crust by repeated partial melting and fractionation during subsidence.

2.1.1 BLAKE RIVER GROUP

The Blake River Group is the youngest and most extensive volcanic group within the Abitibi greenstone belt and includes all volcanic and sedimentary rocks between the Porcupine-Destor and Cadillac-Larder Lake "Breaks" or Fault Zones. The Blake River Group conformably overlies the Kinojevis Group and is unconformably overlain by sediments of the Temiskaming Group in the Kirkland-Larder Lake area (Table 2.1). The Blake River Group is a succession of ultramafic to felsic volcanic rocks of komatiitic, tholeiitic, calc-alkaline and alkaline affinities. Goodwin (1979) divided the Blake River Group into four informal "subgroups" or volcanic complexes; from west to east and from oldest to youngest they include the Bowman, Garrison, Misema and Noranda subgroups. In the Blake River Group of Quebec, Dimroth et al., (1983a) recognized two central volcanic complexes, the Reneault-Montsbrais and Noranda Complexes (Figure 2.1). These complexes, interpreted as large shield volcanos, are characterized by a concentration of felsic volcanic rocks, rapid facies changes and a marked variation in the thicknesses of individual units (Spence, 1976; Goodwin, 1979; Dimroth, et al., 1983a). Gelinas et al., (1983) also interpreted the Blake River Group, in Quebec, as a large volcanic edifice which they subdivided into nine tholeiitic and calc-alkaline units.

The east-west trending Blake River Group is folded about steeply dipping, east-plunging fold axes that produce east-west trending, doubly plunging anticlinoria and synclinoria (Figure 2.1). In Quebec, Dimroth et al., (1983a) interpreted the Blake River Synclinorium (BRS) and the Baie Fabie synclinal zone (BFS), a northeast trending "synclinal zone" that lies between the Noranda and Montbrais Volcanic Complexes, as first order folds (see Figures 2, 3 and 4 of Dimroth et al., 1983a). Upright and open folds of the BRS and BFS are separated by a central zone that contains three "structural domes", the easternmost dome, the "Noranda dome", is occupied by the Flavrian Pluton (Table 2.3) which forms the core of the Noranda Volcanic Complex. Accordingly, the Mine Sequence, which lies within the "Noranda dome" and is the main focus of this thesis, is characterized by very low strain and shallow east dips. Where the BFS curves around the east margin of the "Noranda dome", and trends southeast, folds within Cycle 5 units (Table 2.3) are isoclinal and overturned with axial planes that dip steeply northeast away from the "Noranda dome". The "tightening" and overturning of folds within the BFS may have resulted from reactivation of the subparallel, steeply north dipping Destor-Porcupine Fault. Dimroth et al., (1983a) interpreted first order folds of the BRS and BFS as early, open, flexure or buckle folds that formed in linear areas of synvolcanic subsidence prior to deformation; later north-south compression resulted in a "tightening up" of the folds. Although the Cadillac-Larder Lake and Destor-Porcupine Faults are now steep, north dipping reverse faults Dimroth et al., (1983a) interpreted these faults to have been vertical during volcanism and sedimentation and to mark the south and north limits of a synvolcanic graben in which the Blake River Group was erupted.

Metamorphic grade within the Blake River group ranges from sub-greenschist to greenschist facies with areas of higher metamorphic grade adjacent to individual plutons (Joly, 1978; 1977). The disposition of metamorphic mineral paragenesis with the Blake River Group, of Quebec, is illustrated in Figure 2.5.

2.2 GENERAL GEOLOGY OF THE NORANDA VOLCANIC COMPLEX AND NORANDA AREA

2.2.1 NORANDA VOLCANIC COMPLEX

The Noranda Volcanic Complex has an approximate diameter of 35 km and represents some 7.5 to 9 km of volcanic strata consisting of tholeiitic and calc-alkaline rhyolitic, andesitic and basaltic flows, and minor pyroclastic rocks. The first lithostratigraphic subdivision of the Noranda Volcanic Complex was proposed by Spence (1967), who grouped informal rhyolitic and andesitic formations into 5 "Rhyolitic Zones" separated by 4 andesitic inter-zone units (Figure 2.2). Spence (1967) interpreted the rhyolitic zones as comprising an eastward-younging homoclinal succession produced by successive periods (1 to 5) of eastward migrating rhyolitic volcanic activity that built the Noranda Volcanic Complex. Rhyolitic zones of Spence (1967) are included in Cycles 1-5 of this study (Table

2.2) where each Cycle consists of an andesitic basal unit (inter zone andesite) and mixed rhyolitic and andesitic upper unit.

Gelinas et al., (1983) who subdivided the Noranda Volcanic Complex into 9 chemostratigraphic units also interpreted these units as representing a homoclinal, albeit folded, eastward younging succession. Dimroth et al., (1983a), however, interpreted the gross structure of the Noranda Volcanic complex to be a syncline and that Cycle 5 units may be older than Cycle 4.

Spence (1967), de Rosen-Spence (1976), and Dimroth et al., (1982,1983a) interpreted the Noranda Volcanic Complex as a large subaqueous shield volcano that, unfolded, had an original diameter of some 40 to 50 km. De Rosen-Spence (1976) likened the Noranda Volcanic Complex or shield volcano to central volcanic complexes in Iceland described by Walker (1963). Dimroth et al., (1982, 1983b) interpreted the Noranda Volcanic Complex as an "island arc" type shield volcano that was built upon a low relief, deep water, lava plain (subaqueous equivalent of flood basalts) composed of the lower Blake River Group and underlying Kinojevis Group. Gelinas et al., (1984), however, interpreted the Noranda Volcanic Complex to have formed in a "continental environment" and the volcanism to be bimodal resulting in construction of an edifice dominated by andesite and rhyolite.

Geochronology

All volcanic and plutonic rocks of the Noranda Volcanic Complex are Archean except for Proterozoic diabase dikes and Cobalt Group sedimentary rocks to the south. Krough and Davis (1971) dated (U-Pb, zircon) samples from the Dufault Pluton (West Body) and Powell Pluton at 2709 Ma and found volcanic rocks from near Mobrun (5^{th} Rhyolite Cycle) to be "a few million years older". Krough also dated washed zircons from the Dufault Pluton which yielded a $^{207}Pb/^{206}Pb$ age of 2701 Ma for this intrusion (Nunes and Jensen, 1980).

U-Pb zircon dating by Mortenson (1986), has established a preliminary age of 2698.7 Ma (minimum age) for Cycle 2 rhyolite, 2697.9 +1.3/-0.7 Ma for Cycle 5 rhyolite and an age of 2701.5 +/-1 Ma for the Flavrian Pluton (trondjemitic phase). If the five Cycles represent a homoclinal succession the data suggest that the 7-9 km thick Noranda Shield Volcano may have formed in as little as 3.5 Ma. The uncertain stratigraphic position of Cycle 5 and the similar age of the latter to Cycle 2 suggests that Cycle 5 formations may be the folded, stratigraphic equivalent of Cycle 2 or, for that matter, Cycle 3 formations.

2.2.2 NORANDA AREA GEOLOGY

The Noranda area refers to the area bounded by the Hunter Creek Fault in the north, the Glenwood Fault to the south, the Flavrian Pluton to the west and the Dufault Pluton to the east (Figure 1.2). The Noranda area is underlain by

Cycles 3 and 4 (Table 2.4) and was interpreted by De Rosen-Spence (1976) to lie within a 15-20 km wide area of synvolcanic subsidence within the upper, central part of the Noranda Volcanic Complex/Shield Volcano. This broad area of synvolcanic subsidence has been referred to as the Noranda Caldera (Watkins, 1980; Dimroth et al., 1982; Gibson et al.,1985; 1986).

Lithostratigraphic (Wilson, 1941; Spence, 1967; de Rosen-Spence, 1976; Dimroth et al., 1982) and chemostratigraphic subdivisions (Gelinas et al., 1983) of the Noranda Volcanic Complex have resulted in the adoption of different stratigraphic units or informal formations by different workers. This has led to some confusion in nomenclature and it appears that stratigraphic subdivision of the Noranda Volcanic Complex is presently in a state of flux. The difficulty in defining and mapping complex chemostratigraphic "formations" containing both calc-alkaline and tholeiitic units, such as those at Noranda, has resulted in a lithostratigraphic subdivision of the Noranda Volcanic Complex in this study. The Table of formations, (Table 2.3, format modified after Lambert, 1988) summarizes the stratigraphy of the Noranda area.

The Noranda area is subdivided by major faults into 4 blocks: from north to south, the Hunter, Flavrian, Powell and Horne Blocks (Figure 1.2). The strike and dip of units within each block differ from those in adjacent blocks. Cycle 3 and 4 formations, found within each block, are listed in Table 2.4.

The Flavrian Block is further subdivided, by subordinate faults and intrusions, into 8 sectors which include, from north to south, the Cranston, Ansil, New Vauze, Norbec, Waite-Dufault, F-Shaft, Amulet-Millenbach, and Despina sectors (Figure 2.3). The strike of units within each sector is uniform but may vary between sectors; dips are generally uniform. Faults which separate both blocks and sectors are interpreted to be synvolcanic structures that accommodated subsidence within the cauldron during extrusion of the Mine Sequence (Chapter 11).

The Volcanic Succession

Cycles 3 and 4 are characterized by long, sinuous alternating rhyolitic and andesitic formations composed principally of subaqueous flows and containing <5% pyroclastic deposits (Figures 2.2 and 2.4 and Table 2.4). The succession is homoclinal and east dipping with the oldest units outcropping in the west, adjacent to the Flavrian Pluton which occurs at the base of the section. In the Flavrian Block strata generally strike north and dip at 10^0 to 45^0 east whereas equivalent strata in the adjacent Hunter and Powell Blocks strike northwest and dip steeply (50 to 90^0) east.

The first formal stratigraphic subdivision of units within the Noranda area was proposed by Wilson (1941), who divided the volcanic succession into 26 alternating rhyolitic and andesitic "belts". Wilson's initial subdivision provided the stratigraphic framework for later studies.

Formations within the Noranda area were grouped into the 3rd and 4th Rhyolite zones and intervening 3-4 andesite by Spence (1967). De Rosen-Spence (1976) subdivided these Rhyolite zones and intervening andesites into 18 rhyolitic and andesitic formations (VI to XXIII; Table 2.4). Formations V and XXIV which underlie and overly the above succession are parts of interzone 2-3 and 4-5 andesites.

Table 2.2, contains the informal formations of the Noranda Volcanic Complex and compares the subdivisions and names used in this study to that of Spence (1967) and de Rosen-Spence (1976). Detailed mapping was restricted to the Flavrian block and encompasses all of the 3rd or Mine rhyolite zone (formations VI-X) and inter zone 2-3 (formation V) and 3-4 (formation XI) andesites. In this study formations numbered V-XI are grouped into one stratigraphic unit referred to as the Mine Sequence. The term "sequence" replaces "zone" which is a biostratigraphic not a lithostratigraphic or time-stratigraphic term; the "Mine" prefix is retained to emphasize the concentration of volcanogenic massive sulphide deposits within this stratigraphic succession.

As will be described, formations which comprise the Mine Sequence are interpreted to define a single geologic event, the development and infilling of a large synvolcanic subsidence structure, the Noranda Cauldron. Andesitic and rhyolitic formations of Cycles 1/2 and 4 are interpreted to be pre-cauldron and post-cauldron successions respectively.

Intrusive Rocks

The main intrusive rocks of the Noranda area (Table 2.3) include, in their interpreted order of intrusion, Here Diorite, Flavrian Pluton, diorite-gabbro intrusions (i.e. Dufresnoy Diorite), Dalembert granodiorite, and Dufault Pluton east body and west body. Late syenite dikes and plugs (Aldermac Syenite), lamprophyre dikes and Proterozoic diabase dikes mark the last intrusive events. The Newbec Breccia is interpreted to have been emplaced after diorite-gabbro dikes but before intrusion of the Dufault Pluton (west body). Numerous synvolcanic andesitic and rhyolitic dikes and sills intrude the volcanic succession.

Flavrian Pluton

The Flavrian Pluton has been referred to as the Flavrian Granite and Flavrian Lake Granite by Dimroth et al, (1982, Figure 1.3) and Spence and de Rosen-Spence (1976, Figure 2.2) respectively. Following the terminology of Goldie (1976) the Flavrian Pluton and its faulted equivalent, the Powell Pluton (Goldie, 1976), are collectively referred to herein as the Flavrian Pluton. The Flavrian Pluton is the most significant, major intrusion within the Noranda Volcanic Complex. The relationship of this plutonic body to surrounding strata and its emplacement have a direct bearing on the volcanic reconstruction described in Chapter 11. Description and interpretations summarized below are from Goldie (1976; 1978; 1979) and from observations of the pluton's east margin encountered during mapping and drilling.

The Flavrian and Powell Plutons are located in the Flavrian and Powell Blocks where they are bounded by the Hunter Creek, Beauchastel, and Horne Faults (Figure 2.4). The Pluton is a multi-phase intrusion composed of numerous sill-like intrusions that are characterized by shallow dips and generally conformable contacts with adjacent strata. The Flavrian Pluton is a passively emplaced, high level intrusion (Goldie, 1976) surrounded by a narrow (<1km), weak, contact metamorphic aureole. Units within this contact aureole are lighter in colour and where previously altered, develop a spotted porphyroblastic texture reminiscent of dalmatianite (Chapter 12). Porphyroblasts are prismatic, range to 3cm in length, and are pseudomorphed by chlorite and actinolite.

Goldie (1976) divided the Flavrian Pluton into 5 main rock types, namely trondjemites, breccias, tonalites, hybrid rocks and quartz-gabbros and diorites. The oldest phase of the pluton is the quartz-gabbroic Meritens Phase. Remnants of this oldest intrusive phase have an annular disposition within the Flavrian Pluton (Figure 1.2) which is interpreted to reflect emplacement along a primary ring fracture (Goldie.1976).

Trondjemitic intrusions constitute the bulk of the pluton and were emplaced in several phases. Early trondjemite was emplaced before complete consolidation of the Meritens Phase and tonalitic and hybrid rocks are interpreted as products of mixing between quartz-gabbro and trondjemite (Goldie,1976). Plugs and dikes of fine grained felsite and mafic dikes within the pluton are interpreted as erosional remnants of subvolcanic feeders that vented ascending magma at surface (Goldie, 1976).

Goldie (1976, 1979) proposed that the chemical similarity of the different intrusive phases to enclosing volcanic strata, their similar age and the sill-like, multiphase form of the pluton indicated that the Flavrian Pluton and enclosing strata are consanguineous. He interpreted the Flavrian Pluton to represent the later intrusive stages of a shallow underlying magma chamber which was emplaced into its own volcanic pile during construction of the Noranda Volcanic Complex. Dimroth et al., (1983b), Gelinas et al., (1984) and Paradis et al., (1988) also interpreted the Flavrian Pluton to be a pre-kinematic, synvolcanic intrusion.

Lake Dufault Pluton

The Lake Dufault Pluton has been referred to as the Lake Dufault Granite and Lake Dufault Granodiorite by Dimroth et al.,(1982, Figure 1.3) and Spence and de Rosen-Spence (1976, Figure 2.2) respectively. This intrusion is referred to herein as the Lake Dufault Pluton or Dufault Pluton. The Lake Dufault Pluton is a composite granodiorite intrusion consisting of east and west bodies. The east body, like the Flavrian Pluton, shows effects of regional deformation and is not surrounded by a pronounced thermal aureole. The west body is a massive, structureless intrusion with a pronounced thermal aureole and contains numerous volcanic xenoliths along its western margin. Metamorphic grades up to amphibolite facies are recognized in volcanic rocks immediately adjacent to the west body (Riverin, 1977). The bodies also differ slightly in their chemical composition, the west body containing more K and Sr than the east body (Webber, 1962).

Diorite-Gabbro Intrusions

Diorite-gabbro intrusions occur (Map unit 6) as large sheet-like dikes and sills that generally strike N15^{0}W and N45^{0}W and dip at >60^{0}E and <45^0 respectively (Figure 2.2). The dikes form a dense network in the area north and west of the Lake Dufault Pluton. The diorite dikes commonly occupy low-angle reverse faults that thrust up strata on their east margins.

Wilson (1941) described the intrusions as ranging in composition from coarse-grained gabbro to quartz-diorite with pegmatitic and granophyric schlieren. The thicker bodies are commonly layered with cm to mm bands of leucocratic gabbro alternating with quartz diorite or gabbro. Magmatic foliations are rare but where observed result from the preferential alignment of plagioclase.

Although altered to an albite-actinolite-chlorite-quartz-epidote assemblage, the primary mineralogy is commonly preserved. Even within the contact aureole of the Dufault Pluton, primary zoned labradorite and augite are recognized. Limited chemical analyses indicate a tholeiitic affinity for these intrusions.

Newbec Breccia

The Newbec Breccia (Figure 1.2) is a coarse intrusive breccia with a maximum length and width of 750 X 550 m respectively (Smith, 1983). The breccia dips 45-70^0 to the west and has sharp and discordant contacts with east-dipping volcanic strata. The breccia is bounded by volcanic rocks on the west, north and east and by the Dufault granodiorite (west body) to the south.

The Newbec breccia is composed of a variety of fragment types that range in size up to 20m and include diorite, gabbro, anorthositic gabbro, quartz-feldspar porphyritic (QFP) rhyolite and aphyric rhyolite. Fragment shapes range from rounded to angular with the majority being subrounded to subangular (Smith, 1983). The breccia matrix is a fine-grained, comminuted QFP rhyolite (1mm - 1cm fragments) or locally fine-grained massive chlorite.

Discordant contacts and ovoid shape indicate a pipe-like form for the Newbec breccia. Variable composition, angularity and size of fragments and brecciated QFP rhyolite matrix that intrudes shattered and veined wall rocks suggest that the Newbec Breccia was emplaced as a volatile-rich, fluidized system (Smith, 1983). The Newbec Breccia may be a product of shallow, subterranean phreatic explosions. The occurrence of diorite-gabbro fragments and absence of granitoid fragments suggest that the breccia was generated and emplaced after intrusion of the diorite-gabbro dikes and prior to or during intrusion of the adjacent Dufault Pluton.

Structure and Metamorphism

Volcanic rocks of the Noranda area have suffered little of the penetrative deformation and metamorphism that typify most Archean terrains. Metamorphic grade is lower greenschist facies and is characterized by the assemblage albite-chlorite-sericite-actinolite-epidote-quartz (Figure 2.5). This mineral paragenesis is typical of most Archean regionally metamorphosed greenschist facies volcanic rocks. However, in the Flavrian Block there is no evidence of penetrative deformation or recrystallization that typify many Archean terrains. Primary volcanic textures are well preserved and are amenable to detailed petrographic analysis.

Folds in the Noranda area are generally east-trending and plunging open structures that parallel the Blake River synclinorium. Folds inferred for the Flavrian Block include the Quebec-Copper anticline, Duprat syncline and Amulet-Dufault anticline (Figure 2.5). These folds have been interpreted as broad and gentle warps in the stratigraphic succession (De Rosen-Spence, 1976). As will be described in Chapter 11, folds within the Flavrian block are now interpreted to be a product of synvolcanic faulting as the location of fold axes lie within areas of subsidence (synclines) or bounding margins (anticlines). The Duprat Syncline (Figure 2.3), in particular, lies within the core of the Noranda cauldron and the apparent fold pattern is interpreted to result from step-like down-faulting of volcanic strata located to the north and south towards the core of the cauldron.

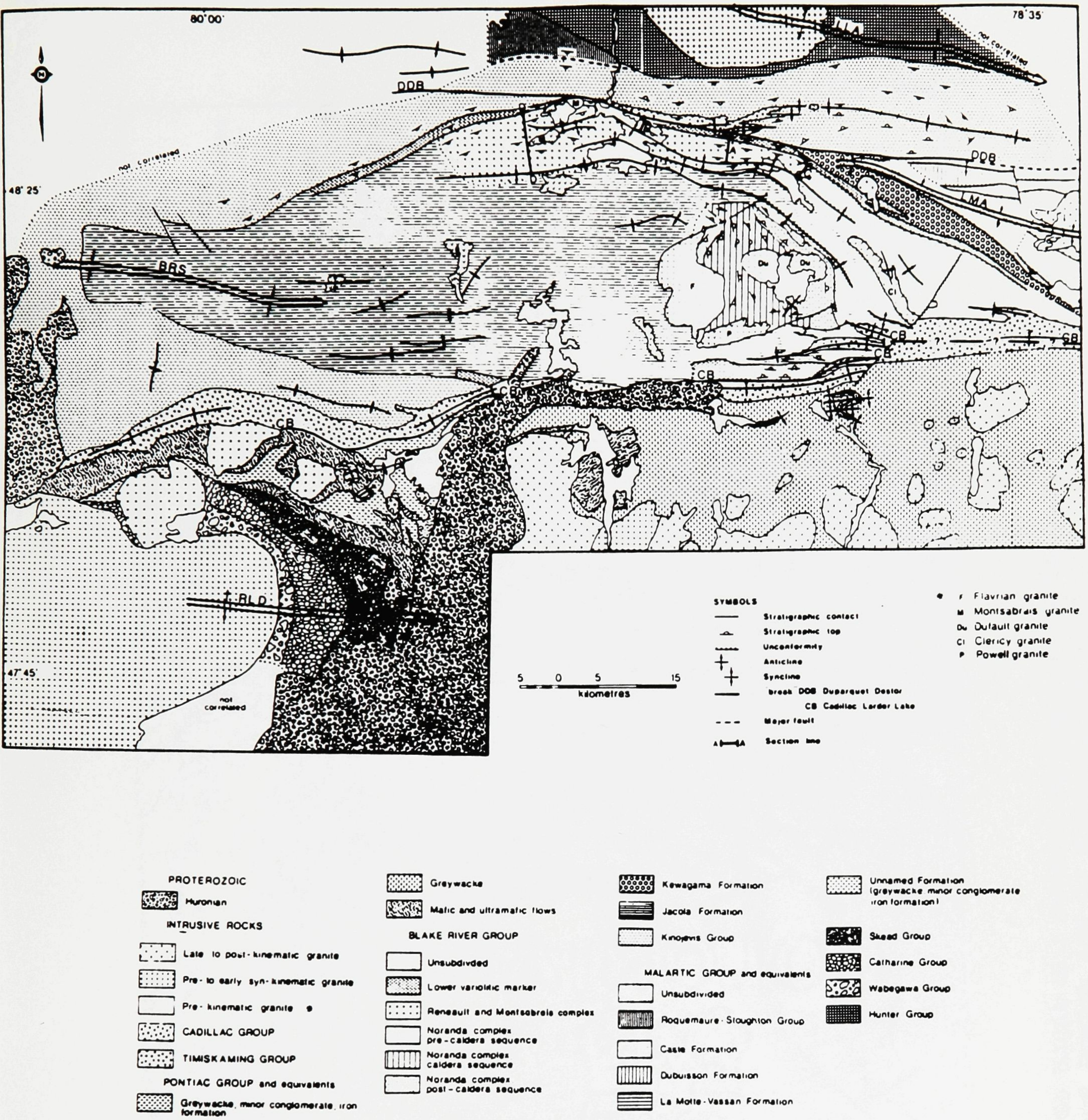

Figure 2.1. Stratigraphic map of the Rouyn-Noranda area and part of northeastern Ontario, after Dimroth et al., (1982).

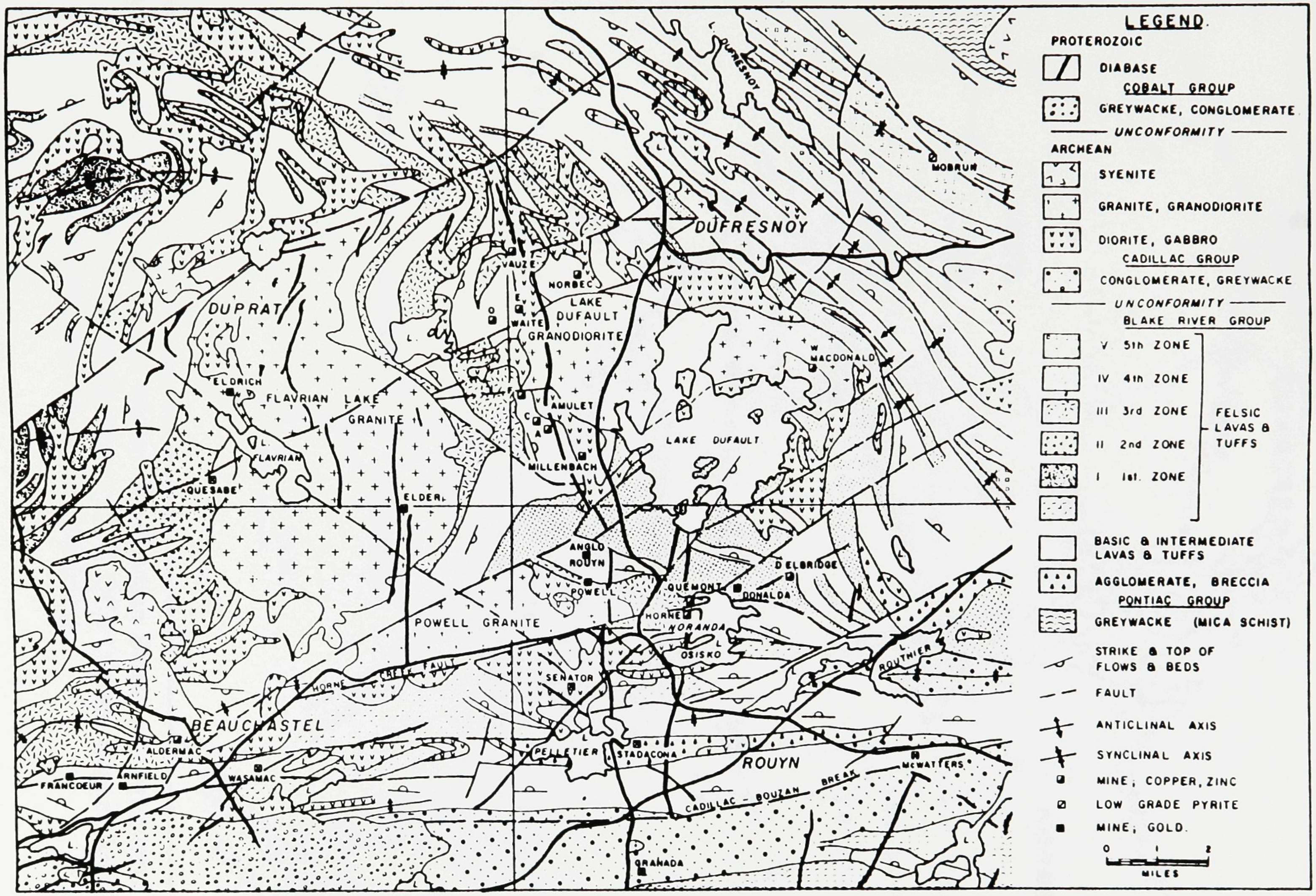

Figure 2.2. Rhyolite Zones and General Geology of the Noranda Volcanic Complex after Spence (1967) and Spence and de Rosen-Spence (1976).

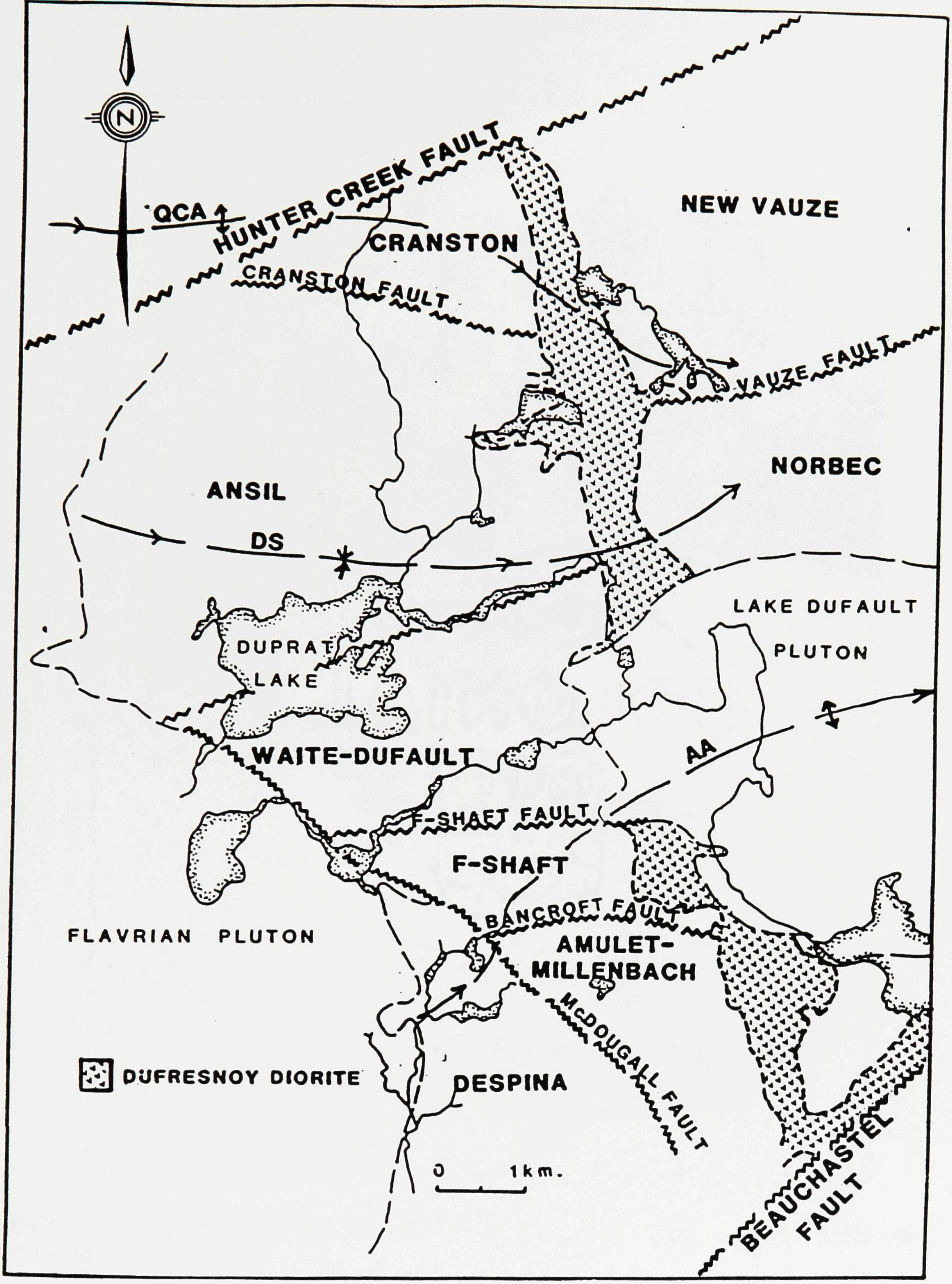

Figure 2.3. Fault bounded sectors within the Flavrian Block and interpreted fold axes after de Rosen-Spence (1976); QCA-Quebec Copper Anticline, DS-Duprat Syncline, AA-Amulet Anticline.

32222

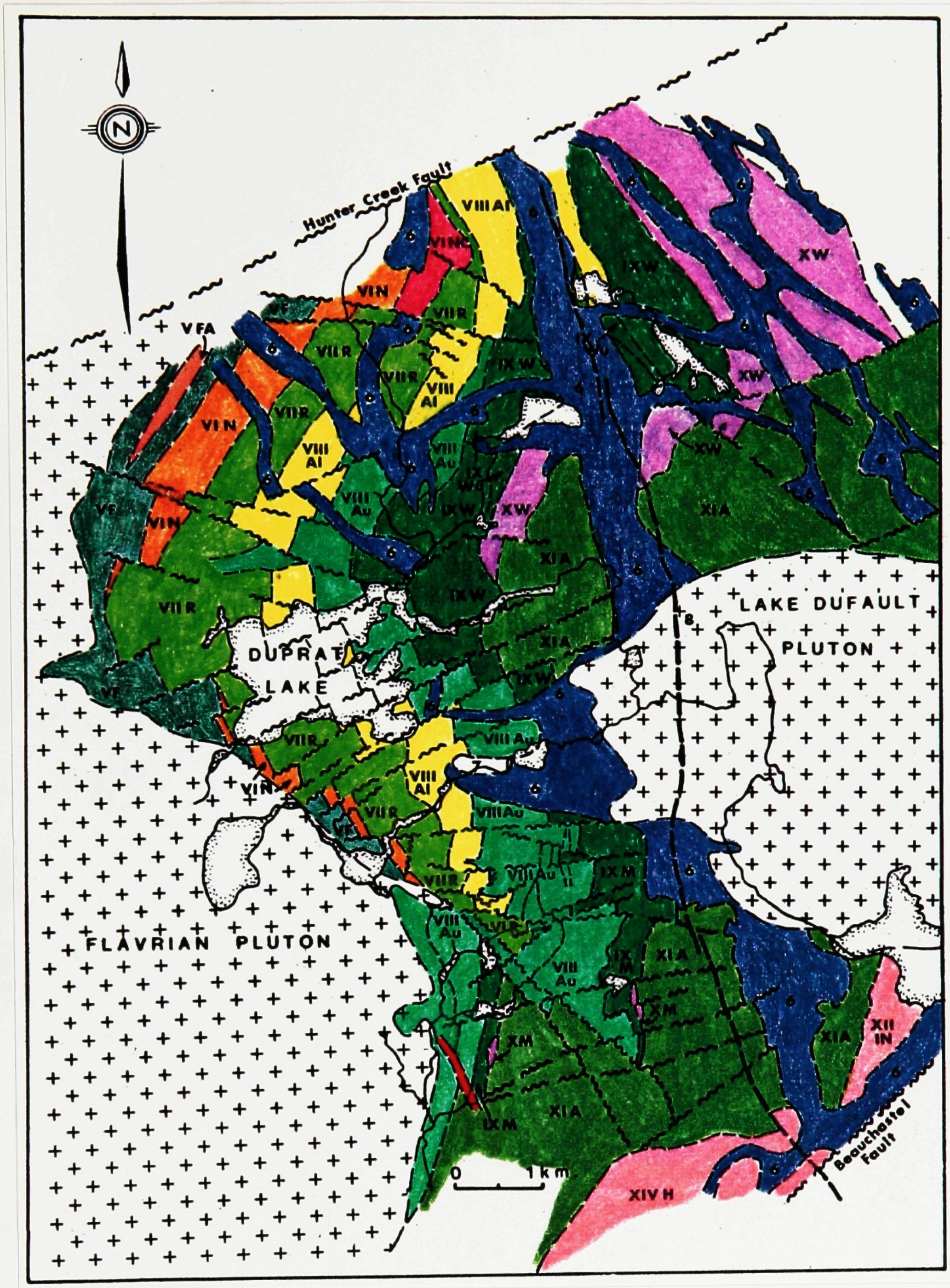

Figure 2.4. General geology of the Flavrian Block. Unit numbers refer to formations of Table 2.3.

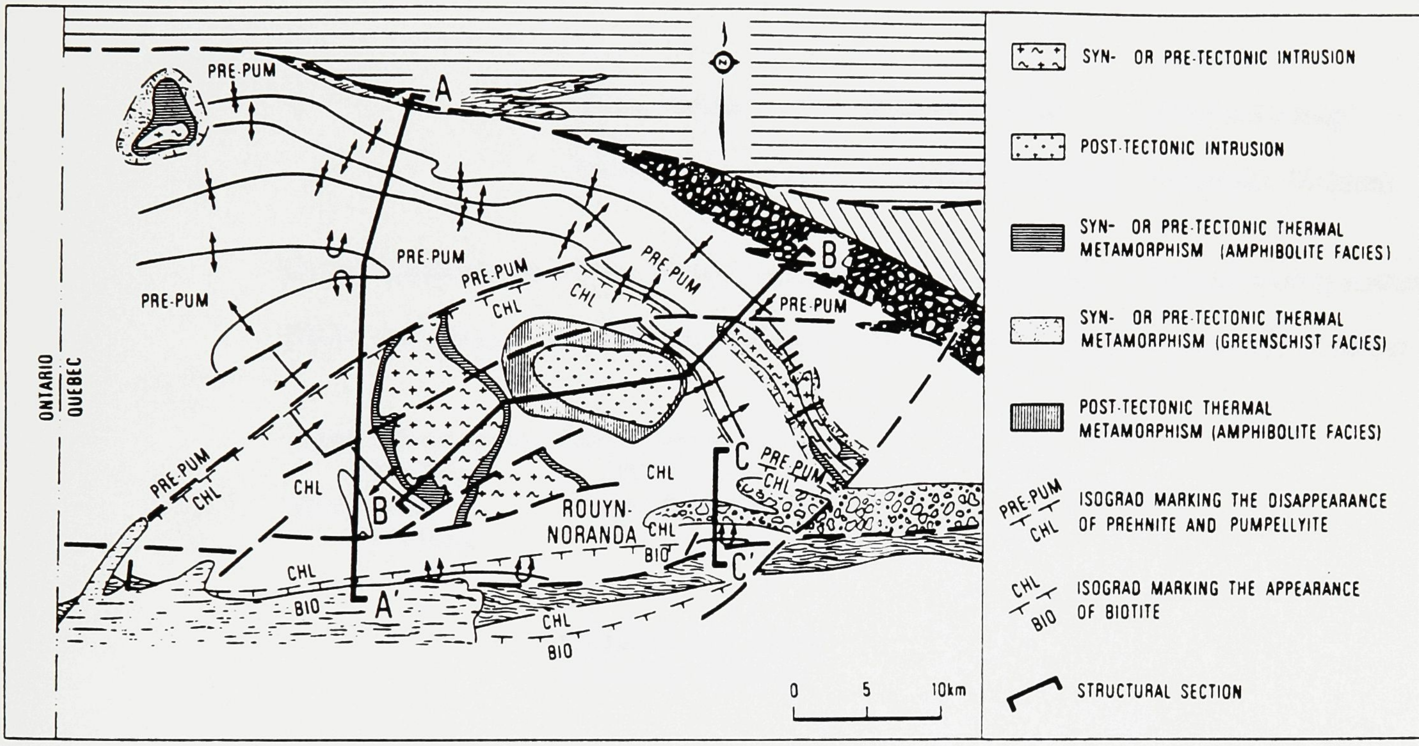

Figure 2.5. Distribution of regional metamorphic isograds and contact metamorphic aureoles, after Dimroth et al., (1982).

TABLE 2.1. VOLCANIC STRATIGRAPHY OF THE EXTERNAL ZONE, ABITIBI GREENSTONE BELT
TIMMINS - KIRKLAND LAKE - NORANDA AREAS *

	TIMMINS NORTH	TIMMINS SOUTH	KIRKLAND LAKE	NORANDA
CYCLE 1			Timiskaming Group (2685 Ma) ^ ^ ^ ^ ^ ^ ^ ^ ^	Timiskaming Group ^ ^ ^ ^ ^ ^ ^ ^ ^
↑		Upper Tisdale Group 2703±2Ma (Varied Division)	Blake River Group 2702±2Ma (Varied Division)	Blake River (Varied Division)
CYCLE 2		Middle Tisdale Group (Tholeiitic Division)	Kinojevis Group (Tholeiitic Division)	Kinojevis Group (Tholeiitic Division)
	Lower Tisdale Group (Mafic Volcanics)	Lower Tisdale Group (Ultramafic Division)	Larder Lake Group (Ultramafic Division)	Stroughton-Roquemaur (Ultramafic Division)
↓ ↑ CYCLE 3 ↓	Upper Deloro Group 2708±2Ma (Kidd Creek Rhyolites)	Upper Deloro Group 2725±2Ma (Varied Division)		
		Middle Deloro Group (Tholeiitic Division)		
		Lower Deloro Group (Ultramafic Division)		

* From MERQ-OGS Map (1983)

TABLE 2.2. LITHOSTRATIGRAPHIC SUBDIVISION OF THE NORANDA VOLCANIC COMPLEX, BLAKE RIVER GROUP

SPENCE (1967) DE ROSEN-SPENCE (1976)	THIS STUDY		SEQUENCE
Rhyolite Zone 5	Cycle 5	}	
Andesite		}	
		} –	Post Cauldron
		}	
Rhyolite Zone 4	Cycle 4	}	
Andesite			
Rhyolite Zone 3	Cycle 3		Cauldron
Andesite	Mine Sequence		
Rhyolite Zone 2	Cycle 2	}	
Andesite		}	
		} –	Pre Cauldron
		}	
Rhyolite Zone 1	Cycle 1	}	

TABLE 2.3. TABLE OF FORMATIONS FOR THE NORANDA AREA

EON (ERA)	CYCLE	FORMATION	MAP SYMBOL	PRINCIPAL LITHOLOGY
PHANEROZOIC				Sand, gravel, alluvium
Unconformity				
PROTEROZOIC				Diabase dikes
Intrusive Contact				
ARCHEAN	INTRUSIONS			Lamprohyre dikes
		Aldermac Syenite		Syenite plugs,dikes
		Dufault Pluton		Composite granodiorite intrusion
		Dalambert Pluton		Granodiorite
		Newbec Breccia		Hetrolithic diatreme breccia
			6	Diorite,gabbro sills and dikes
		Flavrian Pluton		Diorite,trondjemite,tonalite intrusions
		Here Diorite		Diorite,gabbro intrusions
	Intrusive Contact			
	NORANDA VOLCANIC COMPLEX: Cycle 5			Rhyolitic and andesitic flows/breccias
	Cycle 4			Rhyolitic and andesitic flows/breccias
	Cycle 3 — MINE SEQUENCE (HUNTER BLOCK, FLAVRIAN BLOCK, POWELL BLOCK)	HUNTER BLOCK		
		Upper North Duprat Andesite	XI UNDA	Massive and pillowed andesitic flows
		Upper North Duprat Rhyolite	VII-X UNDR	Aphyric, feldspar porphyritic and quartz porphyritic rhyolitic flows
		Lower North Duprat Andesite	VII LNDA	Massive and pillowed andesitic flows
		Lower North Duprat Rhyolite	VI LNDR	Aphyric, feldspar porphyritic and quartz porphyritic rhyolitic flows
		Hunter Andesite	V H	Massive and pillowed andesitic flows
		FLAVRIAN BLOCK		
		Amulet Andesite	XI A	Massive and pillowed andesitic flows, minor tuff
		Waite/Millenbach Rhyolite	X W/M	Feldspar porphyritic and minor quartz porphyritic rhyolitic flows
		Waite/Millenbach Andesite	IX W/M	Massive and pillowed andesitic flows and minor tuff
		Amulet	VIII A	
		Amulet Upper Member	VIII Al	Silicified andesitic flows, minor rhyolite
		Amulet Lower Member	VIII Al	Feldspar and quartz feldspar porphyritic rhyolitic flows and minor breccia (Beecham Breccia) at base of unit
		Rusty Ridge	VII R	Massive and pillowed andesitic flows, minor rhyolitic breccias
		Northwest	VI N	Feldspar phyric rhyolitic flows
		Cranston Member	VI NC	Quartz feldspar porphyritic rhyolitic flow
		Flavrian	V F	Massive and pillowed andesitic flows
		Ansil Member	V FA	Quartz feldspar porphyritic rhyolitic flow
		POWELL BLOCK		
		Powell Andesite	XI P	Massive and pillowed andesitic flows
		Quemont Rhyolite	X Q	Aphyric and quartz-feldspar porphyritic rhyolite
		Joliet Rhyolite	VI J	Feldspar phyric rhyolitic flow
		Brownlee Rhyolite	VI B	Feldspar phyric rhyolitic flow
	Cycle 2			Rhyolitic and andesitic flows/breccias
	Cycle 1			Rhyolitic and andesitic flows/breccias

Roman numeral prefix indicates order of stratigraphic succession
Cycle 5 may be the stratigraphic equivalent of Cycles 2 or 3

Table 2.4. Cycle 3 and 4 Formations of the Hunter, Flavrian and Powell Blocks

	HUNTER BLOCK	FLAVRIAN BLOCK	POWELL BLOCK
CYCLE 4 FORMATIONS			
CYPRUS RHYOLITE		XXIII	XXIII
CYPRUS ANDESITE/DACITE		XXII	XXII
DALEMBERT RHYOLITE		XXI DL	
SOUTH DUFAULT RHYOLITE			XX SD
DALEMBERT ANDESITE upper mem.		XX DL	
MESPI ANDESITE			XX M
MESPI RHYOLITE			XIX M
DELDONA ANDESITE			XVIII DD
DON RHYOLITE			XVII D
DALEMBERT ANDESITE Lower mem.		XVI DL	
SOUTH BAY ANDESITE			XVI SB
DELBRIDGE RHYOLITE			XV DB
FISH-ROE RHYOLITE	XV FR	XV FR	
NORQUE RHYOLITE		XV NQ	
HERE CREEK RHYOLITE		XIV H	XIV H
UPPER NORTH DUPRAT ANDESTE	XIII UND (Upper member)		
NEWBEC ANDESITE		XIII NB	
INSCO RHYOLITE		XII IN	XII IN
CYCLE 3 FORMATIONS			
UPPER NORTH DUPRAT ANDESITE	XI UND (Lower member)		
AMULET ANDESITE		XI A	
POWELL ANDESITE			XI P
UPPER NORTH DUPRAT RHYOLITE	X-XI UND		
WAITE RHYOLITE		X-XI W	
MILLENBACH RHYOLITE		X M	
QUEMONT RHYOLITE			X-XI Q
WAITE ANDESITE		IX W	
MILLENBACH ANDESITE		IX M	
AMULET Upper member		VIII Au	
AMULET Lower member		VIII Al	
LOWER NORTH DUPRAT ANDESITE	VII LND		
RUSTY RIDGE		VII R	
LOWER NORTH DUPRAT RHYOLITE	VI LND		
NORTHWEST RHYOLITE		VI N	
Cranston member		VI NC	
JOLIET RHYOLITE			VI J
BROWNLEE RHYOLITE			VI BR
HUNTER ANDESITE	V H		
FLAVRIAN ANDESITE		V F	
Ansil member		V FA	

3. LITHOLOGIC CLASSIFICATION, DEFINITIONS AND STRATIGRAPHIC NOMENCLATURE

3.1 INTRODUCTION

This chapter outlines the field, petrographic and chemical criteria used to subdivide and classify flows and breccias of the Mine Sequence. All units are metamorphosed and variably altered, but lack a penetrative fabric; for ease in discussion the "meta-"prefix has been omitted from rock names. The effects of hydrothermal alteration on the major element composition of flows is described in Chapter 12.

3.2 CLASSIFICATION OF FLOWS

3.2.1 FIELD CRITERIA

During mapping flows were classified as andesite, dacite and rhyolite. Andesitic flows are recognized by their brown, buff to rusty-brown weathered surface, and dark green to grey-green colour. Andesite is typically aphanitic and fine-grained, aphyric to feldspar porphyritic, and amygdaloidal. Andesitic flows are sheet-like bodies, but thick, aerially restricted, flows are common proximal to their feeding fissure where they are ponded within fault blocks.

Rhyolitic flows are recognized by their light grey to white (pink hue) weathered surface, light grey to grey-green colour, common spherulitic texture that imparts a granular appearance to weathered surfaces, and heterogeneous textures and structures (Chapter 4). Rhyolite is weakly amygdaloidal, typically feldspar or quartz feldspar porphyritic, and is less commonly aphyric. Rhyolitic flows occur as steep-sided stubby lava domes or low relief lava shields and plateaus.

Dacitic flows share characteristics of both andesitic and rhyolitic flows. They are recognized by their brown to white weathered surface, light grey to green colour, ubiquitous mottled colouration (white, siliceous mottled patches), variable hardness, and absence of spherulites and quartz phenocrysts. Dacite is aphanitic to fine-grained, weakly feldspar porphyritic and amygdaloidal. Dacite forms thick, extensive flows with thin, altered vitrophyic (commonly spherulitic), flow-top breccias and lobe facies.

Andesitic, dacitic and rhyolitic successions (formations) are subdivided into individual flows. The term "flow", as used in this study, is equivalent to flow-unit as defined by Walker (1972). In Walker's (1972,1973) definition, a lava flow is the product of a single eruption which may be divisible into one or more flow-units with each flow-unit representing a single pulse or surge of lava that cooled separately (an individual cooling unit). Compound flows are flows that are divisible into two or more flows or flow-units whereas simple flows comprise a single flow or flow-unit. Flows are distinguished by either a change in lithology (composition), texture (aphyric versus porphyritic; size, type and percentage of phenocrysts), grain size (fine <1mm, medium 1-5mm, coarse >5mm) and structure (joint type; percentage, size and distribution of amygdules).

Rhyolitic and andesitic flows are further subdivided into different "facies". Facies, as used by Dimroth (1977) and Dimroth et al., (1978,1979), refers to a part or segment of a flow that differs from other parts of the flow by its appearance and structure. Andesitic and dacitic flows are divisible into a massive, pillow, lobe and breccia facies whereas rhyolitic flows consist of a massive, lobe-hyaloclastite and breccia facies (Chapters 4 and 5).

3.2.2 PETROGRAPHIC CRITERIA

Flows mapped as andesite and rhyolite are characterized by distinctive mineralogy and textures. Andesitic flows are commonly plagioclase porphyritic(<10% albite phenocrysts), rarely pyroxene porphyritic (psuedomorphed by actinolite and chlorite) and have textures ranging from hyalopilitic (felted albite microlites) and pilotaxitic (oriented microlites) to intersertal. The groundmass contains interstitial chlorite, actinolite, epidote and sphene interpreted to replace original glass. Rhyolitic flows are either weakly plagioclase porphyritic (<4% albite phenocrysts) with a spherulitic groundmass or quartz and feldspar porphyritic (5-20%) with a fine-grained felsophyric and/or spherulitic groundmass. Minor chlorite, sericite and trace epidote occur within the groundmass.

Dacitic flows are not as easily classified. Most dacite flows are characterized by textures and mineralogy common to andesitic flows to which they share a similar flow morpholgy. As discussed in Chapter 12, this textural and mineralogical similarity to andesitic flows allows most dacites to be interpreted as silicified andesites.

3.2.3 CHEMICAL CRITERIA

De Rosen-Spence (1976) classified flows in the Noranda area on the basis of their (anhydrous) SiO_2 content as follows:

NAME	% SiO_2
Basalt	< 52
Basaltic Andesite	52 - 55
Andesite	55 - 64
Dacite	64 - 68
Rhyolite	> 68

These chemical subdivisions into andesite, dacite and rhyolite correspond well with andesitic, dacitic and rhyolitic flows distinguished through mapping and petrography and maintain continuity with previous work. Most dacitic flows of the Mine Sequence are interpreted as silicified andesite on the basis of field characteristics, textures and chemical composition (Chapter 12). Dacite has been retained as a descriptive field name to indicate units with an intermediate SiO_2 content. The distinction between basalt, basaltic andesite and andesite is entirely chemical as their colour, hardness, texture and structures are similar. Accordingly andesite, as used herein, refers to rocks of basalt, basaltic andesite and andesite composition.

3.3 CLASSIFICATION OF VOLCANIC BRECCIAS

Volcanic breccias are initially classified on the basis of the size and percentage of contained fragments as proposed by Fisher(1966). Genetic classification follows delineation of units, and careful petrographic and field examination where documentation of fragment types, shape, size, distribution, matrix constituents, degree of sorting and internal structures allows breccias to be further classified on the basis of their interpreted mode of fragmentation and mechanism of emplacement.

In the description of volcanic breccias which follows the terms hydrovolcanic and hydroclastic describe breccias where fragmentation occurred as a result of magma/lava interaction with an external fluid (typically sea water). The result is either an explosive eruption or non-explosive granulation and generation of hyaloclastite (MacDonald,1972; Williams and McBirney,1979; Fisher and Schmincke,1984; Wohletz, 1983; Wohletz and Sheridan, 1983).

Explosive hydrovolcanic breccias can be further classified as phreatic or phreatomagmatic. Phreatic breccias are products of steam eruptions where fragmentation occurred within volcanic units above a magmatic source and juvenile material was not fragmented or incorporated within the associated deposit. Phreatomagmatic breccias are produced by eruptions where juvenile magma is fragmented and incorporated within the resulting deposit. Autoclastic breccias, where fragmentation is a product of mechanical deformation (autobrecciation) during flow, are described along with rhyolitic and andesitic flows in Chapters 4 and 5.

Following the terminology of Dimroth, et al. (1978) hyaloclastite is subdivided into three petrographic types, namely: 1) sideromelane shard hyaloclastite characterized by the presence of chloritized sideromelane globules, granules and or shards (Carlisle, 1963). Where the shards contain phenocrysts or 1-3% microlites they are referred to as vitrophyic shards; 2) microlitic hyaloclastite where the fragments are microlitic andesite with a pilotaxitic or hyalopilitic texture; and 3) pumiceous hyaloclastite where fragments are "lumps" of highly vesiculated sideromelane.

3.4 STRATIGRAPHIC NOMENCLATURE AND DEFINITIONS

The primary criteria for stratigraphic subdivision is lithologic change. This results in a stratigraphy characterized by alternating rhyolitic and andesitic formations. In accordance with the North American Stratigraphic Code lithostratigraphic subdivisions include from largest to smallest, formation, member and flow/bed as defined below. In this work the lithostratigraphic units described are treated as "informal units" and accordingly, the initial letter of the rank or unit term is not capitalized (for example Amulet formation).

Formation

As used herin, a formation is a mappable unit composed predominantly of rhyolitic or andesitic flows. Formation names reflect a geographic locality or proximity to a property or mine. To facilitate stratigraphic correlation a Roman numeral prefixing the formation name indicates the order of stratigraphic succession (de Rosen-Spence, 1976). Thus segments of continuous formations with different names or separate but correlated formations are recognized by the same number.

Member

A member is a recognizable, lithologically distinct mappable unit within a formation that may comprise a bedded pyroclastic succession or a single flow or group of flows. A member is not necessarily as extensive as the formation and may be confined to distinct fault blocks.

Flow/Bed

A flow is the smallest, mappable stratigraphic unit and represents a single flow-unit as defined by Walker (1972). A bed represents a single depositional unit defined by variation in grain size, texture, structure or composition. Individual beds are rarely traceable beyond the limits of a single outcrop.

4. THE PETROLOGY, FLOW MORPHOLOGY AND EMPLACEMENT OF SUBAQUEOUS RHYOLITIC FLOWS

4.1 INTRODUCTION

Mine Sequence rhyolitic flows are divisible into feldspar porphyritic (FP) and quartz-feldspar porphyritic (QFP) flows as illustrated in Figure 4.1. FP rhyolite commonly occurs as lobe-hyaloclastite flows that constructed broad, low relief lava shields or plateaus. QFP rhyolite typically occurs as blocky flows that built steep sided domes and ridges. The main objectives of this chapter are to describe the petrology, flow morphology and emplacement of lobe-hyaloclastite and blocky flows. Features of these subaqueous rhyolitic flows are also compared to subaerial and subglacial rhyolitic flows.

The description and interpretation of lobe-hyaloclastite flows are based on examination of FP rhyolitic flows of the Amulet lower member and Northwest and Waite Rhyolite formations. QFP rhyolitic flows of the Cranston member and Millenbach Rhyolite formation provide examples of blocky flows.

Rhyolitic flows of the Noranda area have been described as quartz latite (Roscoe,1965), calc-alkaline rhyolite (Descarreaux, 1973), Fe-rich dacite (de Rosen-

Spence,1976) and rhyolite (Gelinas et al. 1984). The chemical composition of rhyolitic flows is discussed in Appendix G and average analyses for FP and QFP rhyolitic flows are contained in Table 4.1.

4.2 LOBE-HYALOCLASTITE FLOWS

Lobe-hyaloclastite flows are the most voluminous type of rhyolitic flow within the Mine Sequence. Estimated volumes of selected flows are presented in Table 4.2.

The overall form of lobe-hyaloclastite flows is well illustrated by FP flows of the Northwest formation as depicted on the isopach map in Figure 4.2. The Northwest formation consists of a North flow and a South flow. The North flow forms a northeast-trending, elongate, topographic ridge up to 500m high with gentle slopes of 10-15^0 with a central, northeast-trending, 3.5km long dome (defined by the 300m isopach) that rises from the flow with slopes of 10-20^0. The South flow is a composite body which constructed a 300m high northwest-trending lava dome or ridge. The 200m isopach outlines a N 10^0 W trending ridge which contains four small domes (defined by the 300m isopach) that rise above the flow with slopes of < 20^0. Slopes along the flanks of the south flow range from 10-20^0. Section EE, GG, HH, NN and PP of Figures 9.4 and 9.6, illustrate the morphology and gentle (<20^0) slope of these rhyolitic flows.

The northeast- and northwest-trending, elongate, central domical ridges of the North and South flows, as outlined by the 300m and 200m isopachs, are interpreted to overlie long (3-4km) feeding fissures. Small domes that rise gently above the flow may mark principal vent areas along the underlying fissure.

4.2.1 FLOW FACIES OF LOBE-HYALOCLASTITE FLOWS

Lobe-hyaloclastite flows are characterized by three flow facies which include massive, lobe-hyaloclastite, and breccia facies. The massive facies is composed of massive, banded and weakly brecciated rhyolite. The lobe-hyaloclastite facies consists of irregular lobes of massive rhyolite from 2 to >100m engulfed by intact and weakly brecciated banded rhyolite and hyaloclastite. The breccia facies includes a poorly sorted carapace breccia and crudely layered flank breccia. These flow facies are also common to blocky rhyolitic flows.

Massive Facies

Rhyolite of the massive facies weathers white to light buff-brown, is light grey to green-grey on fresh surface and is massive and homogeneous (Plate 4.2) or banded (Plate 4.3). Subhedral to euhedral albite phenocryts, 1-3mm in size, account for <4% of the flow. Massive rhyolite is characterized by an aphanitic groundmass composed of variably recrystallized spherulites with minor interstitial sericite, chlorite and opaque minerals (Plate 4.1A&B).

Amygdules are typically elongate and commonly occur within bands, up to 40cm wide, which contain 10 to 20% amygdules that range up to 2cm in size (Figure 4.3b). Amygdule bands are best developed in the Bedford flow of the Amulet lower member.

Where banded, rhyolite (Plate 4.3) is composed of parallel, alternating, fine (mm wide) to coarse (cm wide) light coloured spherulitic laminae and darker, more chloritic and recessive weathering laminae. Spectacular, coarsely spherulitic, banded rhyolite of the Bedford flow is illustrated in Plate 4.3. Banding may be either regular, or highly contorted and flow folded. Pockets of brecciated banded rhyolite are common in areas of contorted flow banding.

In banded rhyolite amygdules are stretched and aligned parallel to laminae. Large (up to 12cm) round to ellipsoidal cavities lined with quartz crystals found within amygdule bands are interpreted as lithophysae.

The proportion of massive and banded rhyolite varies within a single flow. Where banded rhyolite occurs in proportions exceeding 30% massive rhyolite occurs as irregular lobes or sheets (2m to >50m) surrounded by banded rhyolite. Where the massive facies contains <10% banded rhyolite, massive lobes (50 to >100m) cannot be traced but are separated by intact banded rhyolite as in Figure 4.3a. Lobes of massive rhyolite, within the massive facies, may represent multiple internal flows or surges of lava separated by margins of banded lava.

The contact between massive and banded rhyolite is either gradational or autobrecciated as illustrated in Figure 4.4. Where contacts are gradational massive rhyolite is finely banded adjacent to banded rhyolite into which it grades; this transition occurs over 5-10cm (Figure 4.5a) and the lobe margin is defined by contorted banding. The second and most common type of gradational contact is defined by an amygdule band (<40cm wide) between massive and banded rhyolite (Figure 4.3b). Amygdule bands are typically coarsely spherulitic (>1mm) and where adjacent to banded rhyolite are often finely banded.

Autobrecciated contacts, (Figure 4.5b) are less common. Angular fragments derived from adjacent lobes of massive rhyolite occur in a matrix of intact to weakly brecciated, contorted, banded rhyolite. Finely banded "matrix" rhyolite is reminiscent of rhyolitic hyaloclastite associated with the lobe/hyaloclastite facies except that the former is intact and lacks shards of chloritized obsidian.

Columnar joints are not common. The best examples were observed in the South flow of the Northwest formation where it overlies the underlying Flavrian formation at the Corbet Mine (Figure 4.6). Laminar jointing typical of many massive andesitic flows is extremely rare in massive rhyolite.

Intraflow breccia dikes, similar to breccia dikes described by Wachendorff (1973) in subaerial rhyolitic flows of Lebombos, southeast Africa, occur at the base of the Bedford flow. The breccia dikes are interpreted as products of small localized steam-blast explosions caused by heated water trapped at the base of the flow (Gibson,1979).

Lobe-Hyaloclastite Facies

The lobe-hyaloclastite facies consists of irregular, ellipsoidal to sheet-like lobes or pods of white to grey weathering massive rhyolite in contact with, and ultimately surrounded by a brown to buff coloured breccia matrix of contorted, banded and brecciated rhyolite and hyaloclastite. The proportion of hyaloclastite breccia within the facies increases toward the top and bottom of rhyolitic flows where it may compose greater than 50% of some exposures. The lobe-hyaloclastite facies has been referred to as heterogeneous rhyolite by de Rosen-Spence (1976) and de Rosen-Spence et al., (1980).

The contact between massive and lobe-hyaloclastite facies is irregular and gradational. As illustrated in Figure 4.7, lobes of massive and banded rhyolite of the massive facies and within the flow interior are gradually engulfed by hyaloclastite breccia to form the lobe-hyaloclastite facies at the flow top and base. This vertical transition also occurs laterally from the feeding fissure toward the flow margin. Plate 4.4, shows rhyolitic lobes mantled and surrounded by hyaloclastite flow breccia at the base of the Amulet lower member in Figure 4.7, whereas in Plate 4.5, a lobe is apparently isolated within hyaloclastite breccia of the flow top.

Lobe Morphology

Lobes have shapes that range from mattress, bun, and irregular amoeboid forms to large sheets. Lobes viewed in outcrop range in size from 1m to >100m; lobes <0.75m are rare. Large lobes are difficult if not impossible to distinguish from massive rhyolite where outcrop exposure is limited. The irregular bulbous shape of lobes is well illustrated by the South flow of the Northwest formation in Figure 4.8.

Textures and Structures of Rhyolitic Lobes

Lobes are composed of massive rhyolite that is identical in colour, texture and mineralogy to rhyolite of the massive facies. Lobes are divisible into three distinct, but gradational zones: an inner core zone, a transitional border zone and an outer margin or selvedge (Figure 4.4).

The core consists of massive, grey to white weathering, homogeneous, aphanitic to fine "granular" textured spherulitic, aphyric to weakly feldspar porphyritic rhyolite. Spherulites (Plate 4.1E) dominate the groundmass with plagioclase phenocrysts (<4%) that range in size to 3mm. Amygdules (<1cm to 3cm) comprise from 1-10% but generally <3% of the lobe core.

The border zone ranges from 5 to 20cm in thickness and is commonly lighter coloured than the inner zone into which it grades. Features of a typical border zone include:

a) a marked increase in the percentage of amygdules (>25%) toward the outer margin that imparts a pumiceous texture to the border zone. Amygdules are typically quartz-filled and are increasingly elongate (up to 3cm long X 3mm wide) toward the lobe margin where they define a wispy banding.

b) a pronounced development of spherulites both in the groundmass and as coronas mantling amygdules. Abundant spherulites within the border zone may account, in part, for its lighter colour.

Flow bands within the border zone typically parallel the lobe margin; however, some flowbands are folded into small recumbent folds whose axial planes parallel the lobe margin. Banding reflects a variation in spherulite size or percentage, or alternating spherulitic and chloritic laminae (Plate 4.1C&D).

The lobe margin marks a transition from massive and banded rhyolite of the lobe to surrounding hyaloclastite flow breccia. Lobe margins range from gradational, where there is often a continuation of textures, structures and flow laminae between the lobe and hyaloclastite breccia, to abrupt where the lobe is isolated from surrounding breccia by a chloritized obsidian selvedge. Figure 4.9, is an example of a gradational margin where contorted, banded, rhyolite of the border zone grades into the surrounding breccia composed of weakly chloritized flow foliated obsidian. Spherulitic laminae within chloritized obsidian continue into adjacent hyaloclastite flow breccia. The lobe margin is placed where flow laminae are contorted and as such defines a regular contact which conforms to the lobe.

Gradational margins are most common where lobes are isolated in a hyaloclastite breccia matrix.

Lobes with an abrupt chloritic obsidian margin or selvedge are most common (Figures 4.10 and Plates 4.6. to 4.8). The chloritic selvedge is fine-grained, weakly flow foliated, porphyritic (if adjacent lobe is porphyritic), weakly amygdaloidal and massive. On close inspection, the selvedge has a fine micro-breccia texture produced by delicate, light coloured, arcuate perlitic cracks that increase toward the outer edge where they grade (over centimetres) into a fine obsidian shard matrix to the hyaloclastite breccia. The chloritic selvedge is an altered obsidian crust similar to chloritized sideromelane crusts mantling pillows (Plate 4.6).

The lobe in Figure 4.10c (Plate 4.7), provides a spectacular example of a well developed obsidian selvedge and spherulitic border zone. The dashed lines in Figure 4.10c, mark transitional contacts which separate the core zone, border zone and chloritized obsidian selvedge. The border zone is divided into an inner part containing elongate quartz amygdules in a massive spherulitic groundmass that grades, over 2-3cm, into an outer part where the groundmass is an intact chloritized obsidian. Amygdules within this outer zone are large (0.5-1.5cm) and mantled by thick spherulitic coronas that double their original diameter (Plates 4.1F and 4.8). The coarsely spherulitic, amygdaloidal border zone abruptly grades, by rapid decrease in amygdules (and spherulites), into a flow-foliated, chloritized obsidian selvedge (Plate 4.8). The chloritized selvedge is in irregular but sharp contact with surrounding breccia composed of fragments of chloritized banded rhyolite, obsidian shard hyaloclastite and devitrified bands of spherulitic rhyolite (Plate 4.8).

Concentric joints are rare in rhyolitic lobes and have been recognized in only two exposures (Northwest formation north of Fourcet Lake and the Amulet lower member north of the Bedford road). Radial joints were not observed, but are reported from rhyolitic lobes of the Delbridge Rhyolite formation (de Rosen-Spence, 1976).

Hyaloclastite Breccia

Hyaloclastite breccia (Plates 4.4 and 4.5) is poorly sorted, chaotic debris, that is devoid of any sedimentary structures. The breccia may compose up to 50% of some lobe-hyaloclastite exposures. The breccia consists of fragments of fine and coarsely banded, weakly chloritized and spherulitic rhyolite in a finer-grained breccia matrix of the same and shards of chloritized rhyolitic obsidian.

The finer matrix contains abundant, angular, chloritized obsidian and vitrophyric shards (Plate 4.1G) and granules. Hyaloclastite shards are interpreted to be derived through disintegration and granulation of obsidian margins; granules and globules may have a similar origin or may, in part, be quenched lava droplets released by mild steam explosions generated where seawater, trapped with fractures, is exposed to fresh lava. In-situ, "ribbon-like spherulitic fragments" are disrupted flow laminae of coarsely spherulitic rhyolite. Irregular light coloured and resistant areas with a vein-network appearance are "in situ" devitrification networks composed entirely of quartz spherulites.

Hyaloclastite breccias locally contain trains of subangular to angular fragments (1cm to >0.3m in size) of massive and banded spherulitic rhyolite. These fragments are identical to rhyolite of the lobe border and core zones and comprise up to 6% of some breccia units.

BRECCIA FACIES

The breccia facies is volumetrically insignificant and aerially restricted. Carapace breccia (Figure 4.8) occurs as localized, discontinuous deposits along the upper surfaces of the flows. Blocky, carapace breccias are matrix to framework supported, unsorted, non-bedded deposits composed of angular fragments of massive and banded rhyolite that range up to 20cm in size in a fine ash-sized rhyolitic hyaloclastite matrix. As illustrated in Figure 4.8, lithic fragments are derived from brecciation of adjacent lobes.

Flank breccia deposits are not common and were only observed at the terminus of the North flow of the Northwest formation, 1.4 km west of Duprat Lake. At this locality the lobe-hyaloclastite facies grades (over 50m) into an intact, poorly sorted, framework to matrix supported breccia containing angular fragments of massive and banded rhyolite ranging to 0.5m in size within a hyaloclastite matrix. The breccia deposit, < 5m thick adjacent to the flow, is overlain by thin (<10cm) deposits of laminated andesitic tuff. The flank breccia extends 150m south of the flow terminus where it thins to <1m thick. Laminated andesitic tuff contains discontinuous lenses of rhyolitic breccia for 30m south of the flank breccias.

4.2.2 INTERPRETATIONS

Lobes are not confined to the lobe-hyaloclastite facies but also occurs within the massive facies of subaqueous flows. The significant differences between lobes of the massive facies versus those of the lobe/ hyaloclastite facies are the absence of obsidian shard hyaloclastite and the larger size of lobes in the former. Lobes within the massive facies were emplaced within the massive interior of flows presumably during endogenous growth where successive pulses of magma emplaced during continued and sustained extrusion are interpreted to have inflated the flow or dome. These internal lobes were not exposed to seawater and consequently did not develop hyaloclastite at their margins.

Massive rhyolite of the lobe-hyaloclastite facies is identical in both texture, structure and composition to rhyolite of the massive facies (Tables 4.2 and 4.3). The different zones which comprise lobes in the lobe-hyaloclastite facies reflect a continuous evolution of textures and structures that formed during extrusion in response to rapid chilling of the lobe by water. The chloritic obsidian margin or selvedge developed in response to rapid quenching of moving lava in contact directly with seawater or within a porous "water soaked" breccia carapace. The border zone marks a transition from quenched obsidian crust to microcrystalline interior. The border zone cooled quickly as indicated by an original glassy groundmass devitrified to spherulites. Parallel and contorted banding at the lobe margin is analogous to banding described in subaerial rhyolitic flows (Loney, 1968; Christianson and Lipman, 1966; MacDonald, 1972) and is interpreted to be a product of shear developed between less viscous (higher temperature, volatile-rich) magma moving within the lobe interior and chilled, more viscous (lower temperature, degassed) lava along the periphery of the lobe.

Amygdules within the border zone were flattened and elongated parallel to the lobe margin during flow. The high percentage (25%) and size of amygdules within the border zone indicate that the lava was volatile-rich. The low percentage of amygdules (<1%) in the chilled crust and within lava of the inner zone (<3%) suggests that volatiles were effectively retained in the lava during extrusion and only exsolved along lobe margins during rapid cooling and flow.

Hyaloclastite breccia mantling lobes is a chloritized obsidian shard hyaloclastite and flow breccia. Lithic fragments within the breccia are identical to the different textural and structural zones of adjacent lobes and are interpreted to be derived through autobrecciation of lobes during flow. The chaotic nature of hyaloclastite breccias, which are devoid of bedding or grading, and the absence of pumiceous fragments, broken phenocryts or Y-shaped shards supports an origin through autobrecciation and not explosive pyroclastic eruptions.

The breccia is interpreted to form through spalling, disintegration and granulation of chilled obsidian crusts and lobe border zones. To account for the volume of breccia, autobrecciation of lobe margins must be a common and on-going process. Spalling and autobrecciation of the selvedge and border zone would have exposed fresh lava to seawater and the development of a new selvedge and border zone would ensue. Successive autobrecciation and regeneration of chilled margins would yield substantial hyaloclastite breccia. Multiple crusts separated by hyaloclastite along the margins of lobes support this interpretation.

Carapace breccias are localized deposits derived through autobrecciation of adjacent rhyolitic lobes. Flank breccias are interpreted as subaqueous debris flow deposits derived through slumping of the flow margins and carapace deposits. The low relief and gentle slopes of lobe-hyaloclastite flows accounts, in part, for the limited development of these breccias.

4.3 BLOCKY RHYOLITIC FLOWS

Blocky rhyolitic flows typically consist of QFP rhyolite and contain up to 15% quartz phenocrysts, 8% albite phenocrysts and <1% amygdules. Blocky rhyolitic flows of the Cranston member and Millenbach Rhyolite formation (Millenbach-D68 QFP lava dome) are described separately followed by a discussion of their principal characteristics. Estimated volumes of selected blocky rhyolite flows are contained in Table 4.2 and the average chemical composition of QFP flows is presented in Table 4.1; the average composition of the Millenbach and Cranston flows are contained in Table 4.4.

4.3.1 CRANSTON MEMBER

The Cranston member of the Northwest formation is a single QFP rhyolitic flow referred to as the Cranston QFP. It is readily divisible into a massive, lobe-hyaloclastite and breccia facies (Figure 4.11). The isopach map of the Cranston member in Figure 4.12, indicates that it is an aerially restricted stubby rhyolitic flow or dome with slopes ranging from 10-40^0. A crude northeast trend to the isopachs suggest that the flow may been fed from fissures striking N 70^0 E.

Massive Facies

The massive facies is composed of white to light pink weathering massive rhyolite containing up to 12% subhedral to anhedral quartz phenocrysts (5mm to 1cm) and up to 10% euhedral to subhedral albite phenocrysts (3 to 8mm) in an aphanitic grey groundmass of fine granular quartz and feldspar, recrystallized quartz spherulites, up to 10% fine albite microlites/crystallites and minor interstitial sericite and chlorite. Banded rhyolite is identical mineralogically and texturally to massive rhyolite except that the former contains alternating 0.5cm to 2cm wide light grey, white and dark grey contorted flow laminae that are more spherulitic than is massive rhyolite. Both massive and banded rhyolite contain <1% quartz-filled amygdules.

The massive facies comprises the majority of surface exposures and increases in thickness from the Cranston Fault northward where it attains a maximum thickness near the centre of the Cranston sector. The 50m isopach effectively outlines the extent of the massive facies in the subsurface and the 200m isopach is coincident with the thickest area of massive and banded rhyolite at surface (Figures 4.11 and 4.12).

Lobe-Hyalocalstite Facies

The lobe-hyaloclastite facies is of very limited extent and is represented in only one outcrop exposure of the Cranston QFP where lobes of massive rhyolite project upward into an overlying carapace breccia. The lobes are irregular in form, have a massive interior and banded margin that is separated from the surrounding breccia by a thin, <4cm wide, chloritized, QFP obsidian selvedge (Plate 4.1H). Angular blocks of massive and banded QFP in the surrounding carapace breccia are identical to the interior and margin of lobes.

Breccia Facies

The breccia facies of the Cranston QFP is divisible into carapace and flank breccias. Carapace breccia consists of poorly-sorted, framework- and, less commonly, matrix-supported deposits containing angular to subangular fragments of massive and banded rhyolite that are identical to underlying massive facies (Plate 4.9). Fragments range in size from several cm to >2m. The matrix consists of fine-grained, weakly foliated to massive, chloritized QFP hyaloclastite and fine (<2cm) lithic QFP fragments.

Carapace breccia mantles the upper surface of the flow (Figure 4.11) and is best developed in the central and northern exposures of the flow where it overlies the massive facies. The contact between carapace breccia and massive facies is gradational with poorly-sorted breccia grading downward into "in situ" brecciated massive and banded rhyolite which in turn grades downward into intact banded and massive rhyolite. Fragments within carapace breccias are interpreted to be derived through autobrecciation of underlying massive facies and lobes.

Flank breccia deposits have an overall wedge shape, being thickest adjacent to the Cranston Fault and thinning with eventual pinch out to the north against massive rhyolite and carapace breccia of the Cranston QFP flow (Figure 4.11). Flank breccia deposits consist of angular, blocky, QFP fragments that are crudely bedded and divisible into distinct depositional units on the basis of fragment/matrix ratios and fragment size. A typical depositional unit consists of a framework supported, blocky breccia base, composed of angular to subangular massive and banded QFP fragments ranging in size to 1m in a fine-grained matrix of lithic QFP fragments (<2cm) and QFP hyaloclastite. The framework supported base grades upward through an increase in matrix and a general decrease in fragment size to a matrix supported top containing <10% QFP fragments. Depositional units range in thickness from 1m to >3m (Plate 4.10). On the isopach map (Figure 4.12), deposits of flank breccia extend for 2km south of the Cranston flow to Ansil Hill. Quartz crystal tuffs are recognized as far south as the Ansil deposit. The breccia forms a blanket-like deposit, mixed with andesitic fragments, that averages 10m in thickness but locally attains thicknesses up to 50m within topographic depressions.

The monolithologic nature of the breccia, the similarity of fragments to massive and banded rhyolite, and thickening of the breccias along the south flank of the flow away from thick, massive rhyolite of the central portion suggests that they are debris flow deposits. The absence (<1%) of amygdules both within the fragments and flow indicate that they are not pyroclastic. The breccias, however, may in part be derived through phreatomagmatic eruptions produced by water trapped within carapace breccias contacting massive lava of the flow interior.

4.3.2 MILLENBACH-D68 QFP LAVA DOME

The Millenbach-D68 lava dome does not outcrop but has been mapped using surface and underground drill holes and underground workings from both the

Corbet and Millenbach Mines. Details of the Millenbach-D68 lava dome are depicted in the isopach map of Figure 4.13, and in a longitudinal section and cross-section of Figures 4.14 and 4.15.

The Millenbach-D68 lava dome is well defined from the McDougall Fault northeast to the former Millenbach mine, a distance of 1.8km. The Millenbach-D68 lava dome was separated into the Upper and Lower QFP flows (Simmons et al., 1973; Comba, 1975; Knuckey et al., 1982). Both the Upper and Lower QFP flows extend the full length (1.8km) of the lava dome and attain a maximum thickness of 240m and 110m respectively. The contact between flows is conformable and defined by a thin, plane-bedded tuff, the Inter QFP Tuff (Comba, 1975), by 13 massive sulphide lenses in the Millenbach and D-68 deposit areas, and by thin andesitic flows in the D68 area.

At Millenbach, the Lower QFP flow lacks internal flow contacts and is a simple flow composed of massive rhyolite enveloped by a carapace breccia. The Upper QFP compound flow, contains separate flows of massive lava encased within carapace breccia and locally separated by deposits of fine tuff (Comba, 1975). In the D-68 area the opposite situation exists where the Lower QFP flow is a compound flow that is internally separable into individual rhyolitic flows by thin andesitic flows (Doiron, 1983). The Upper QFP is a simple flow.

Flow Facies

Like the Cranston QFP flow, rhyolitic flows of the Millenbach-D68 lava dome are divisible into three facies. The massive facies predominates. The 60m isopach (Figure 4.13) defines the margins of a narrow (<0.5km wide) ridge-like dome composed principally of massive and banded rhyolite and overlying carapace breccia over a 1.8km strike length. The ridge attains a height of up to 240m and slopes that range from 30^0 - 70^0.

Both the Upper and Lower QFP flows are characterized by an interior of predominantly massive and banded rhyolite that grades outward into an adjacent, well developed carapace breccia. Doiron (1983) and Ikingura (1984) found that the Upper and Lower QFP flows differed in phenocryst population and size. The Upper flow contains 2-5% subhedral-anhedral quartz phenocrysts <1mm in size and up to 4% subhedral-euhedral albite phenocrysts <2mm in size. The Lower flow is characterized by up to 15% subhedral to anhedral quartz phenocryst <3mm in size and <8% subhedral to euhedral albite phenocrysts <3mm in size. The groundmass of both flows consists of recrystallized quartz spherulites, granular quartz and albite with up to 10% albite microlites (crystallites) with <10% interstitial chlorite, actinolite, sericite, epidote and opaque minerals (Simmons, 1973; Comba, 1975; Ikingura, 1984). The QFP flows contain <1% quartz-filled amygdules.

The lobe-hyaloclastic facies occurs at the transition between massive rhyolite (massive facies) and adjacent carapace breccia (breccia facies). The lobe-hyaloclastite facies is of limited extent and often poorly developed, with massive rhyolite commonly grading directly into adjacent carapace breccia. Where the lobe-hyaloclastite facies is developed, stubby lobes of massive rhyolite occur as finger-like projections from the massive facies into overlying and adjacent carapace breccia. Massive rhyolite of the lobe interior grades into banded rhyolite of the lobe margin which is enveloped by a hyaloclastite selvedge (Comba, 1975). Autobrecciation of lobes is common with direct contribution of lobe fragments to adjacent carapace breccias.

The breccia facies is divisible into both carapace and flank breccias. Carapace breccia mantles the Millenbach-D68 ridge along its length, attains thicknesses of up to 30m, and comprises the bulk of the flow between the 30m and 60m isopachs (Figures 4.13 and 4.15). Carapace breccia is essentially a poorly sorted, framework supported, blocky rubble containing angular fragments derived through autobrecciation of underlying massive and banded rhyolite. Fragments range from <10cm to >5m and rest in fine matrix containing smaller lithic QFP fragments (<2cm), hyaloclastite and fine andesitic tuff. Fine andesitic tuff, with minor chert and sulphides, is locally abundant where it occurs as isolated thin-bedded deposits that have "slumped" between large QFP blocks and serves to mark the contact between carapace breccias of the Lower and Upper QFP flows (Comba, 1975). Carapace breccia locally underlies both the Upper and Lower QFP flows and thus envelopes massive rhyolite of the flow interior (Figure 4.15). Carapace breccia is not graded or bedded; however, fragments along the upper surface of the breccia and margins of the ridge are commonly smaller (<0.5m) and these deposits range from matrix to framework supported. Doiron (1983) and Ikingura (1984) recognized pale coloured, amygdaloidal aphyric fragments (<5%) within the basal breccia of both the Upper and Lower QFP flows in the D-68 area facilitating distinction of the flows where contacts are flow breccias. The fragments are interpreted as xenoliths derived from the chilled margins of underlying QFP feeders dikes and/or underlying Amulet formation that were "flushed" to surface with the first extrusive aliquot. Similar pale, aphyric fragments (up to 10%) were mapped in the basal flow breccia of the Upper QFP flow exposed along the 4-01 exploration drift of the Millenbach mine.

Flank breccia, observed only in drill core and in one surface exposure of a satellite QFP flow (Turcotte flow), contains angular to subangular fragments of QFP rhyolite, accessary fragments of aphyric rhyolite and occasionally andesite in a fine tuff and hyaloclastite matrix. The breccia is poorly sorted with fragments ranging from <2cm to >1m and is both matrix and framework supported. Flank breccia (Figure 4.13), is a uniformly thick (10-15m) blanket-like deposit extending both north and south from the QFP ridge. The flank breccia is more extensive in the Millenbach area and is less well developed and extensive in the D68 area.

Blanket-like flank breccia deposits are interpreted as submarine talus or debris flow deposits derived through collapse and spalling of the steep slopes of the QFP ridge. A possible example of dome collapse and slumping occurs in the area immediately northwest of the Millenbach mine where the smooth upper surface of the Upper QFP flow is broken by a large scour-like depression (Figure 4.15). This depression lies directly up-slope from the most extensive part of the flank breccia deposit which extends for 0.8km northwest of the ridge. Slumping may have been accompanied and/or triggered by phreatomagmatic explosions with debris transported downslope to the northwest.

Discussion

QFP lava of the Millenbach-D-68 ridge issued from northeast trending (N45^{0}E) fissures occupied by QFP feeder dikes. Viscous flows of the Lower QFP flow travelled <0.25km to form a hummocky ridge above and immediately adjacent to its underlying feeding fissure . Hotspring activity was concentrated along the ridge crest, directly above the lower QFP feeding fissure, and at three growing domes along the ridge (Figure 4.14).

Viscous lava of the Upper QFP flow issued from northeast-trending fissures located north of the Lower flow and built up a parallel and adjacent ridge which overlapped and nearly buried the Lower flow. Domes, which rise above the Upper flow with slopes of up to 70^0, are coincident with those of the Lower flow and were constructed directly above the feeding fissure in three main vent areas. Hotspring activity was limited after extrusion of the Upper flow with only five massive sulphide deposits formed above this unit (Figure 4.14). These upper sulphide deposits are also located above the feeding fissure to the Lower QFP flow and are restricted to domes along the ridge crest.

The Upper and Lower QFP flows may represent simultaneous eruptions with different and variable extrusion rates, or the Upper QFP flow was extruded following extrusion of the Lower QFP ridge. Blanket-like deposits of flank breccia extending north and south from the ridge are submarine talus/debris flows, derived through collapse and spalling of the steep ridge slopes and perhaps, through phreatomagmatic explosions.

4.4 EMPLACEMENT OF SUBAQUEOUS RHYOLITIC FLOWS

4.4.1 LOBE-HYALOCLASTITE FLOWS

Lobe-hyaloclastite flows issued from fissures with individual flows travelling < 2km to form low, broad, gentle-sloped (10-20^0) rhyolitic lava shields or plateaus. Small isolated domes dot the upper surface of flows immediately above the underlying fissure.

Lobes within the massive facies represent successive pulses of new magma that were emplaced during endogenous growth of the flow. This new magma inflated the vent area and fed large lobes that carried lava to the flow front.

The similarity of rhyolitic lobes and andesitic tube-fed pillows is striking. Rhyolitic lobes are interpreted as analogs to andesitic tubes and, therefore, lobe-hyaloclastite flows may have advanced in a manner similar to that of andesitic tube-fed flows. Using this analogy rhyolitic lobes, encased within hyaloclastite flow breccia or in direct contact with water, may have followed an irregular path to the flow front where they terminated or branched ("budded") to form smaller lobes. The irregular form of lobes, and finger like protrusions support this interpretation. Lobes at the flow front were continuously buried by advancing lobes. The occurrence of identical textures, structures and amygdule content in rhyolitic lobes located proximal to the fissure to distal lobes located at the flow front suggest that the obsidian selvedge and enveloping hyaloclastite had good insulating properties which may have allowed lava to be delivered to the flow front with little apparent loss of heat or volatiles and attendant increase in viscosity.

Lobe-hyaloclastite flows are compound flows. The massive facies is a multiple flow as it contain lobes that represent individual pulses of lava that essentially cooled as a single unit. The lobe-hyaloclastite facies is a "compound flow" where individual lobes are analogous to single flow-units that cooled separately and independently. Again, using compound andesitic flows (pillow lavas) as an analogy lobe-hyaloclastite flows may be products of sustained, continuous fissure eruptions with low rates of effusion (Walker, 1972; 1973).

A schematic cross-section through an idealized lobe-hyaloclastite flow is illustrated in Figure 4.16a. This diagram illustrates the gentle slope of these rhyolitic flows and an ordered spatial distribution of flow facies where the massive facies is restricted to and characterizes a proximal vent facies and the dominant lobe-hyaloclastite facies characterizes the bulk of the flow. Carapace breccias occur as localized deposits along the upper surface of flows and flank breccias as aerially restricted deposits along the periphery of the flow. Similar facies have been proposed for subglacial rhyolitic flows in Iceland (Furnes et al., 1980) and for rhyolitic flows of the IV cycle, de Rosen-Spence (1976) and de Rosen-Spence et al., (1980). The flow morphology and facies described herein differs from that of de Rosen-Spence, et al. (1980) in that:

a) individual flows have a more limited areal extent than originally proposed (<2km from their feeding fissure). The extensive character of rhyolitic formations which have strike lengths exceeding 10km, is a product of multiple, contemporaneous, overlapping flows erupted along fissures and does not represent the extent of a single flow.

b) hyaloclastite flow breccia associated with rhyolitic lobes is not layered and contains "pockets" of intact and "in situ" brecciated banded rhyolite into which it grades.

c) large scale cross-beds of hyaloclastite and isolated lobes which characterize the distal facies of de Rosen-Spence et al.'s (1980) are absent.

d) well bedded deposits of hyalotuff are not found mantling the upper surface of lobe-hyaloclastite flows.

The flow morphology and facies described by de Rosen-Spence, et al., (1980) are based on rhyolitic flows of the Don Rhyolite formation (Cycle 4) which were erupted in relatively shallow water (100-200m; Lichtblau and Dimroth, 1980) and although the rhyolites were emplaced primarily as flows they have also been interpreted as pyroclastic deposits by Gelinas, et al., (1978) and Gorman (1975). Deposits of cross-bedded hyaloclastite and hyalotuff associated with these flows, and noticeably lacking in the Mine Sequence flows, may be products of localized pyroclastic or hydrovolcanic eruptions.

4.4.2 BLOCKY RHYOLITIC FLOWS

Blocky rhyolitic flows issued as viscous lava which travelled < 0.5km and constructed steep sided (20-70^0) domes immediately adjacent to and above their feeding fissure. A schematic cross-section through an idealized QFP rhyolitic flow illustrating steep slopes and rugged topography which typifies QFP flows is shown in Figure 4.16b.

QFP flows are essentially composed of two facies, an interior of massive and banded rhyolite (massive facies) which grades outward into a carapace breccia that mantles and in part underlies the flow and laterally into flank breccia deposits. The lobe-hyaloclastite facies is poorly developed and commonly absent; where it occurs it marks the transition from intact massive rhyolite of the flow interior to autobrecciated rhyolite comprising the breccia carapace.

Lobes and multiple flows within the massive facies suggest endogenous growth of the flow or dome with concomitant autobrecciation of massive lava at the margins and base to produce thick envelopes of carapace breccia. Carapace breccia was subsequently sloughed off the steep slopes of the flow or dome to be transported downslope as submarine debris flows to form flank deposits.

Although similar in composition, the textures, structures and flow morphology of lobe-hyaloclastite flows suggests that these flows were probably less viscous than blocky rhyolitic flows (Yamagishi and Dimroth, 1985). The lower viscosity attributed to lobe-hyaloclastite flows may be related to a high extrusion temperature and volatile content. Similarly, Hausback (1987) attributed the low viscosity interpreted for extensive subaerial rhyolitic flows to a high volatile content and extrusion temperature. Arguments for a high extrusion temperature and volatile content include:

1) Lobe-hyaloclastite flows were essentially obsidian flows where even the massive facies was comprised of rhyolite containing >85% original glass. The original glassy nature of the flows and low phenocryst content (<4%) as compared to blocky QFP flows suggests that they underwent very little crystallization prior to eruption and may have been extruded above or at liquidus temperatures.

2) The greater amygdule content of lobe-hyaloclastite flows may indicate that these flows had a higher initial volatile content than blocky QFP flows. Amygdule distribution within lobes suggests that the volatiles largely remained in solution during eruption and extrusion of lobe-hyaloclastite flows. Maintenance of volatiles in solution does not necessarily require deep water extrusion. Subglacial rhyolitic flows in Iceland that were extruded passively in < 200m of melt water have identical flow facies, similar amygdule content and distribution and formed similar edifices.

4.5 COMPARISON WITH SUBAERIAL RHYOLITIC FLOWS

Subaqueous lobe-hyaloclastite flows differ from subaerial rhyolitic flows primarily in the abundance of hyaloclastite, isolated lobes and lower relief of the former. Descriptions of the latter however, are based primarily on surface features of recent flows whereas the former are based on observations of sections through individual flows. Subaerial rhyolitic flows/domes described by Loney (1968), Christiansen and Lipman (1966), Wachendorf (1973), MacDonald (1972), Williams and McBirney (1979), Swanson et al., 1987 and Bonnichsen and Kauffman, 1987 are remarkably similar to blocky rhyolitic flows as they are essentially blocky flows composed of a massive and flow banded interior (presumably continuous with vent feeder dike) overlain by a blocky breccia carapace and margin. Fragments are derived through autobrecciation of the massive interior as it advances. The steep slopes of subaqueous blocky flows may reflect the higher angle of repose permitted in a subaqueous environment but more likely reflects preservation through rapid burial by penecontemporaneous andesitic flows.

The internal, terminus to vent, morphology of recent subaerial flows is poorly known, but a few dissected flows suggest some similarities to subaqueous flows. Permian, pyromeride rhyolitic flows described by Rutten (1963) contain lobe-like forms of massive rhyolitic in banded rhyolite (see Figures 2 and 3 of Rutten, 1963) similar to lobes in the massive facies of both subaqueous lobe-hyaloclastite and blocky flows. MacDonald (1972) also described small lobe-like tongues of massive lava that issued from the front of some block flows and Bonnichsen and Kauffman (1987) described lobes mantled by breccia within the terminus of rhyolitic flows in the Snake River Plain.

4.6 COMPARISON WITH SUBGLACIAL RHYOLITIC FLOWS

Although subaqueous lobe-hyaloclastite flows differ in flow morphology from recent subaerial rhyolitic flows they are identical to subglacial dacite and rhyolitic flows observed in Iceland and described by Furnes et al. (1980) and to subaqueous rhyolitic hyaloclastites first described by Pichler (1965). The subglacial, Quaternary dacite flow Blahnukur of the Torfejakull central volcanic complex in south central Iceland is a prime example. Blahnuknur is essentially a lobe-hyaloclastite lava ridge that extends for approximately 3km and is interpreted to overlie its feeding fissure. Massive rhyolite and rhyolitic lobes are interpreted to form the interior of the ridge above the fissure (Furnes et al., 1980). A cross-section oblique to the flow front is shown in Figure 4.17, where Blahnukur overlies an older subaerial rhyolitic flow.

As illustrated in Plates 4.11 through 4.13, the different zones within individual lobes described for subaqueous lobe-hyaloclastite flows at Noranda are identical to those observed in lobes at Blahnukur. Rhyolitic lobes at Blahnukur are characterized by massive, typically columnar jointed microcrystalline interior (Plate 4.11), a chilled vitrophyric, strongly amygdaloidal and flow banded border zone (Plate 4.11 and 4.12) and an in-situ brecciated to intact obsidian selvedge (Plates 4.12 and 4.13). Lobes were observed to range in size from several tens of metres to <5m; lobes <2m in diameter were not observed. Breccia associated with the lobes consists predominantly of fine obsidian hyaloclastite, identical to the lobe crust, and amygdaloidal and massive rhyolite similar to the lobe margin and interior (Plate 4.13). Furnes et al., (1980) refer to this breccia as Type II hyaloclastite and interpret it as a flow breccia derived by disintegration of lobe crusts and margins, with complete autobrecciation of some lobes. They also interpret lobes to be both interconnected and isolated bodies.

At Blahnukur, rhyolitic lobes and associated hyaloclastite breccia (Type II), referred to as "lobe complexes" by Furnes et al., (1980), are separated by massive units of pumiceous hyaloclastite referred to as Type I hyaloclastite (Figure 4.17). Pumiceous hyaloclastite consists predominantly of grey pumice and obsidian fragments which they interpret as a pyroclastic deposit, a product of Surtseyian or Subplinian to Plinian eruptions.

The similarity of Archean lobe-hyaloclastite flows of the Mine Sequence and Quaternary subglacial flows such as Blahnukur is apparent. The only difference between the two, other than age, is the presence of pyroclastic pumiceous hyaloclastite associated with some subglacial flows. Blahnukur is interpreted to have been erupted in a shallow, <200m, glacial lake. The lack of pumiceous hyaloclastite in subaqueous lobe-hyaloclastite flows of the Mine Sequence may reflect their emplacement within deeper water (>200m).

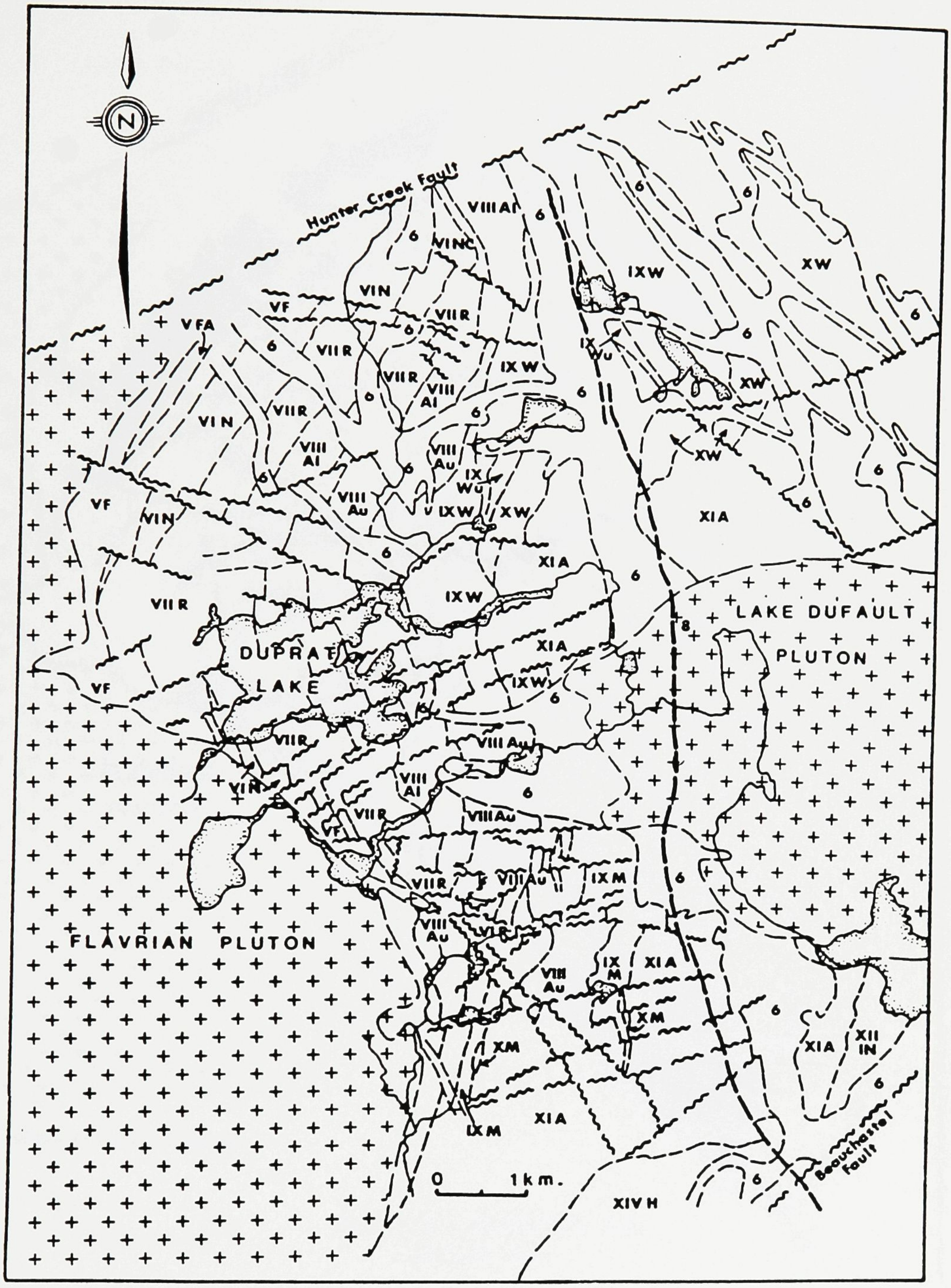

Figure 4.1. Feldspar Porphyritic (yellow) and Quartz Porphyritic (pink) rhyolitic flows of the Mine Sequence in the Flavrian Block.

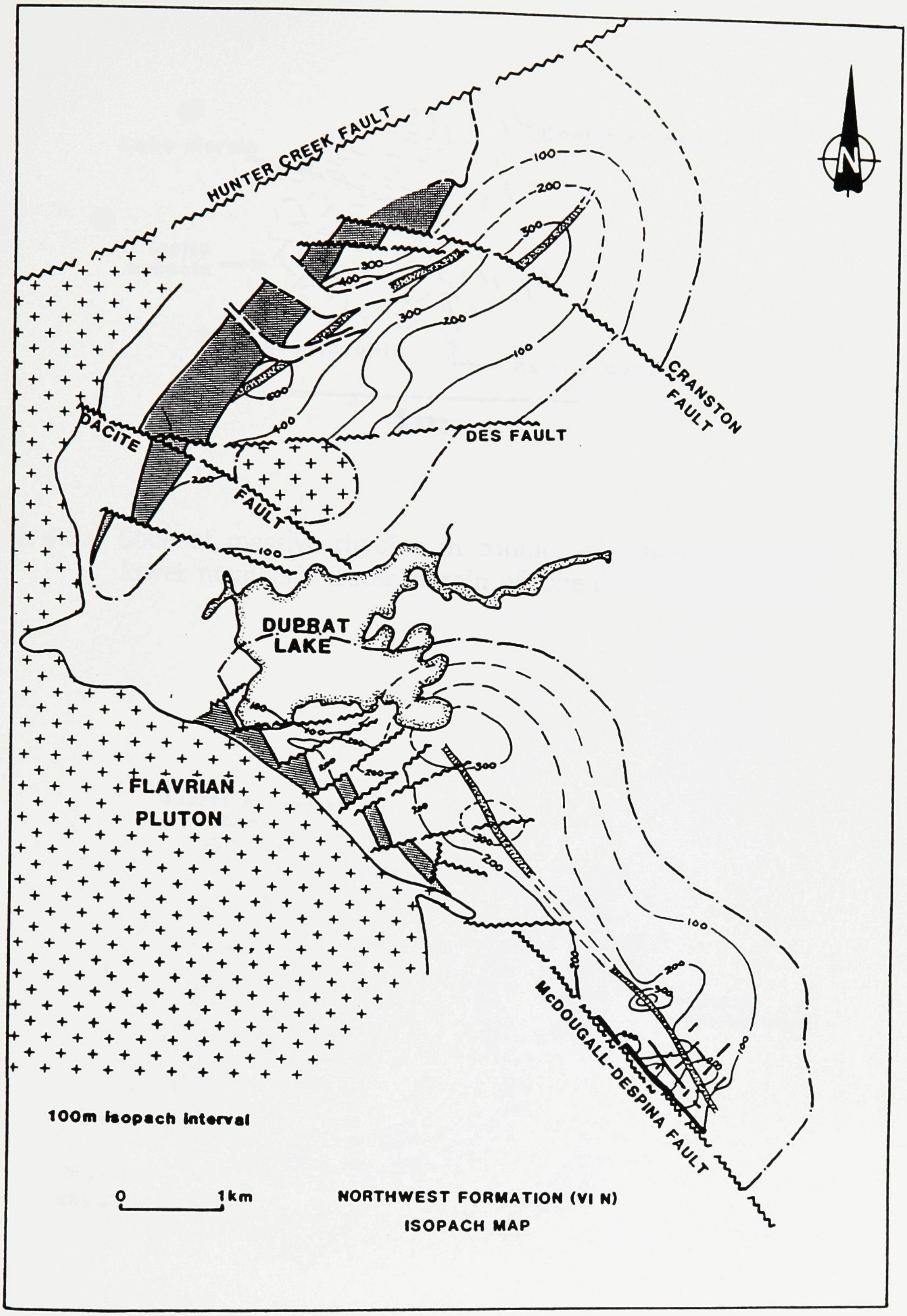

Figure 4.2. Isopach map of the North and South flows of the Northwest formation.

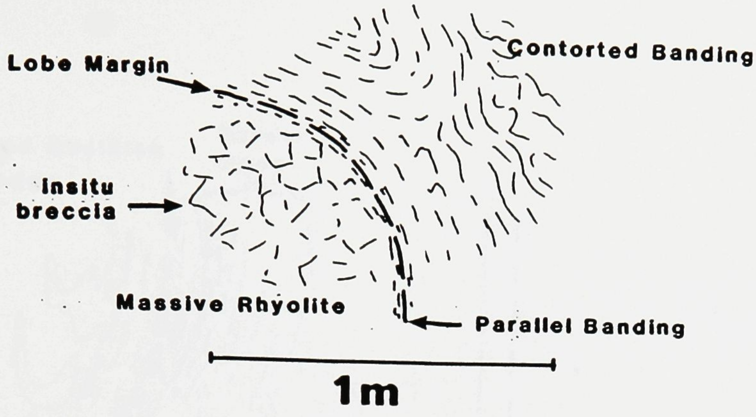

Figure 4.3a. Lobe of massive rhyolite in contact with banded rhyolite (Amulet lower member). Outer margin of lobe defined by banding.

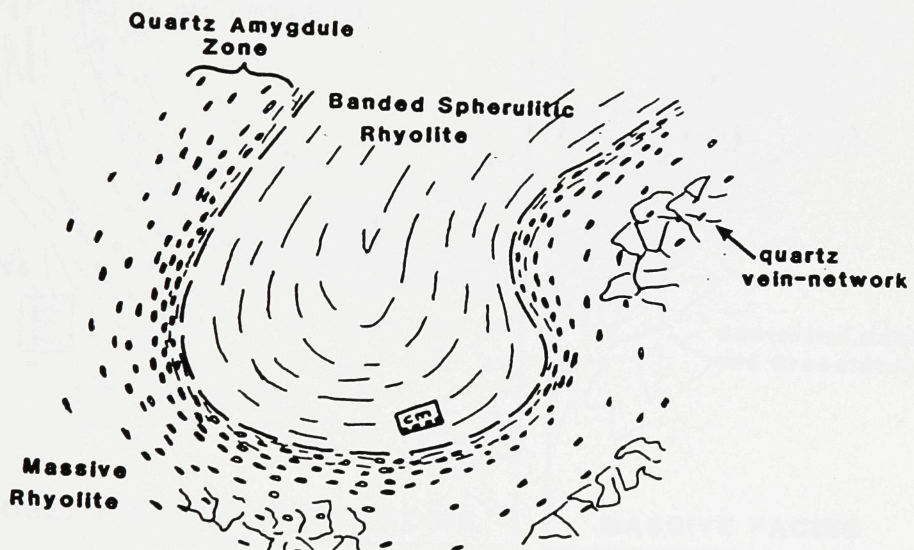

Figure 4.3b. Quartz amygdule band at contact between massive and banded spherulitic rhyolite (Bedford flow).

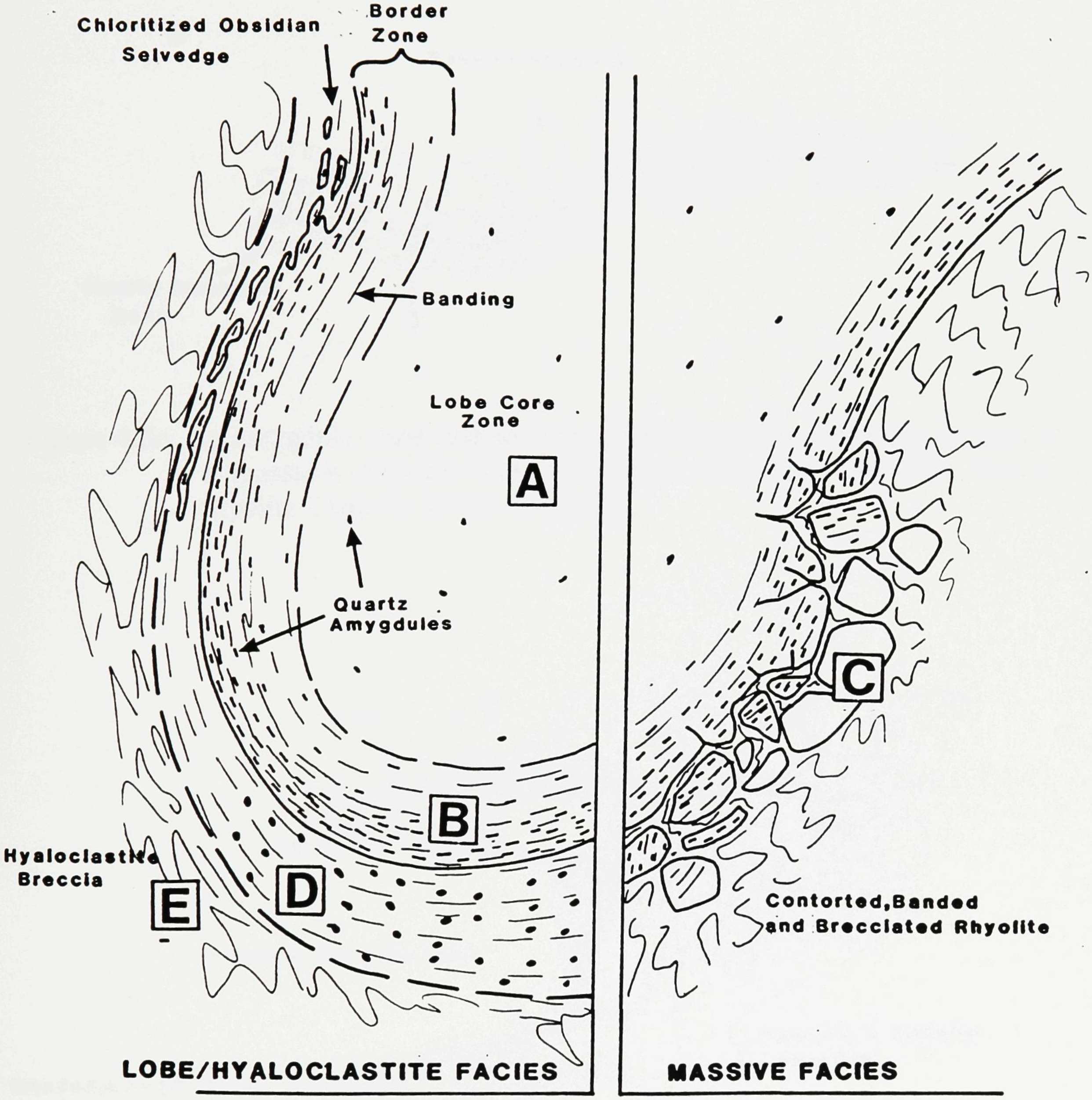

Figure 4.4. Textures and structures of massive rhyolitic lobes in the lobe-hyaloclastite (left) and massive facies (right). Boxes A through E correspond to specimen locations for chemical analyses in Table 4.3.

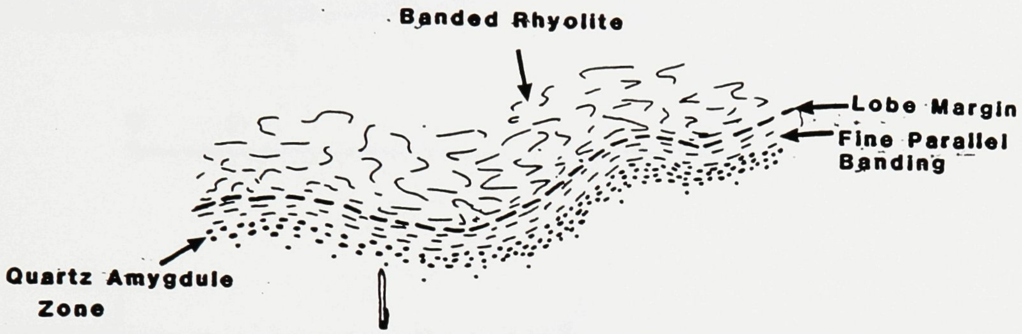

Figure 4.5a. An amygdule band and smooth parallel banding define the margin of a masssive rhyolite lobe in contact with contorted flow banded rhyolite (Amulet lower member).

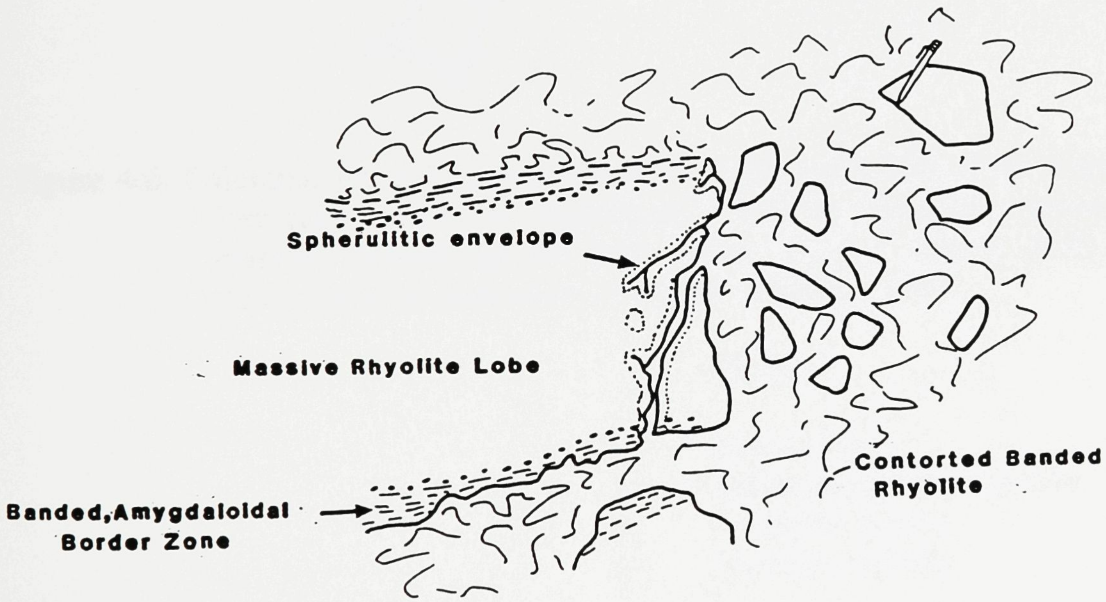

Figure 4.5b. Autobrecciation of a massive rhyolitic lobe within flow banded rhyolite. Fragments of massive rhyolite are rotated and rafted in an intact matrix of contorted flow banded rhyolite (Amulet lower member).

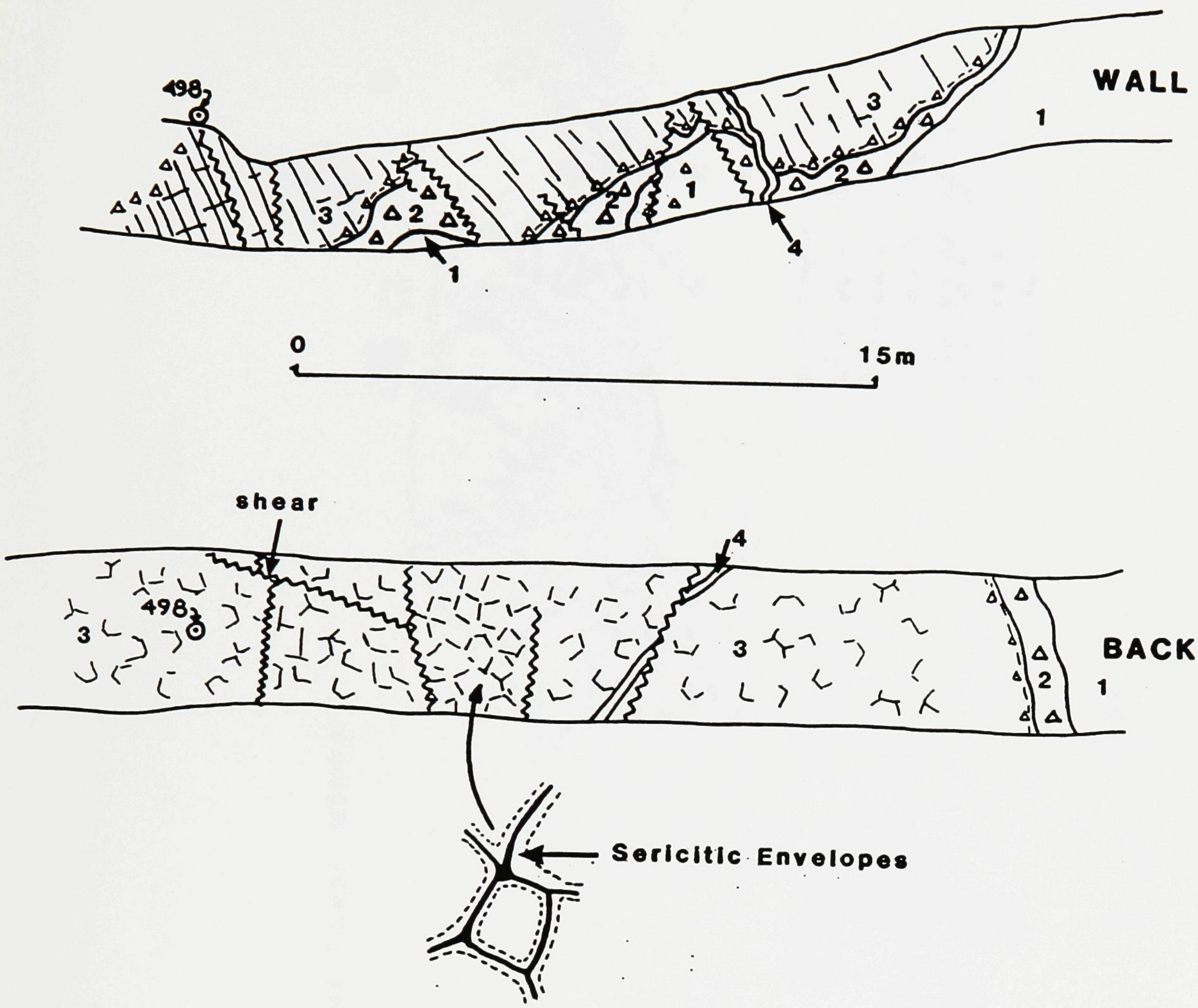

Figure 4.6. Columnar jointed massive rhyolite of the South flow of the Northwest formation where it conformably overlies andesitic breccias and massive sulphide at the Corbet Mine (12-2-1 overcut drift). Note strong sericitic alteration along the columnar joints.

LEGEND

4	Diorite dike
3	Columnar jointed rhyolite
2	Andesitic breccia
1	Massive sulphide

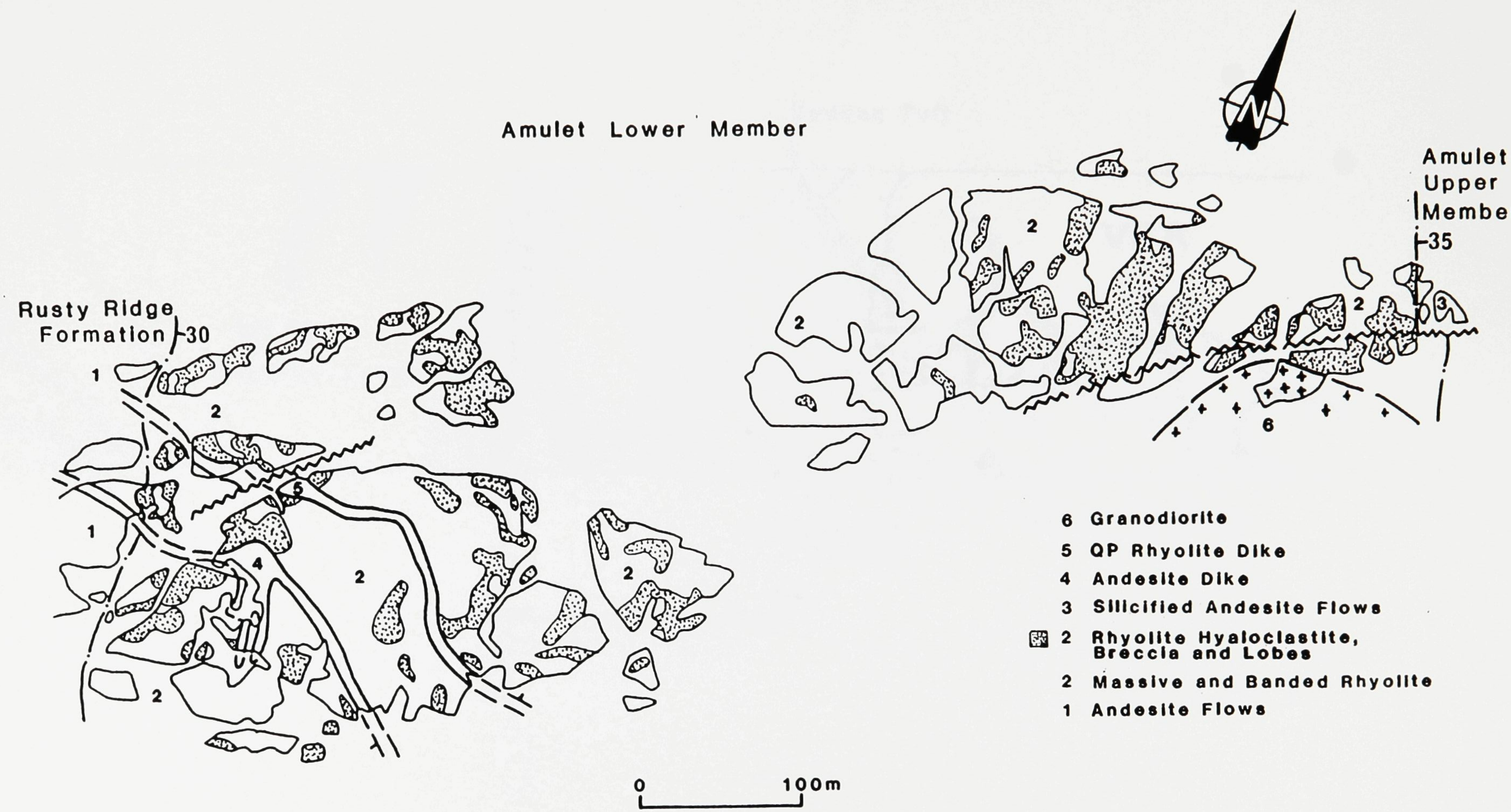

Figure 4.7. Cross-section through the #3 flow of the Amulet lower member near its vent area south of Duprat Lake. Note the vertical transition from predominately massive lava to lobes and hyaloclastite at the flow top.

RHYOLITE LOBE/HYALOCLASTITE FACIES AND CARAPACE BRECCIA

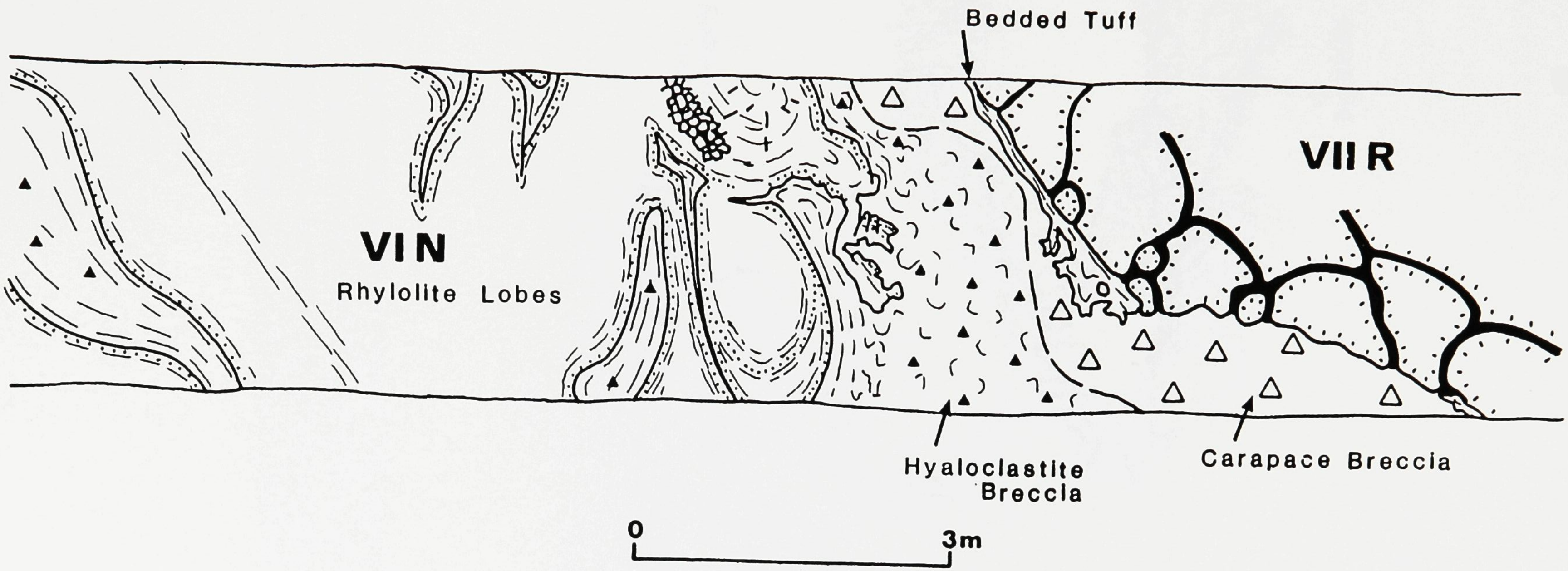

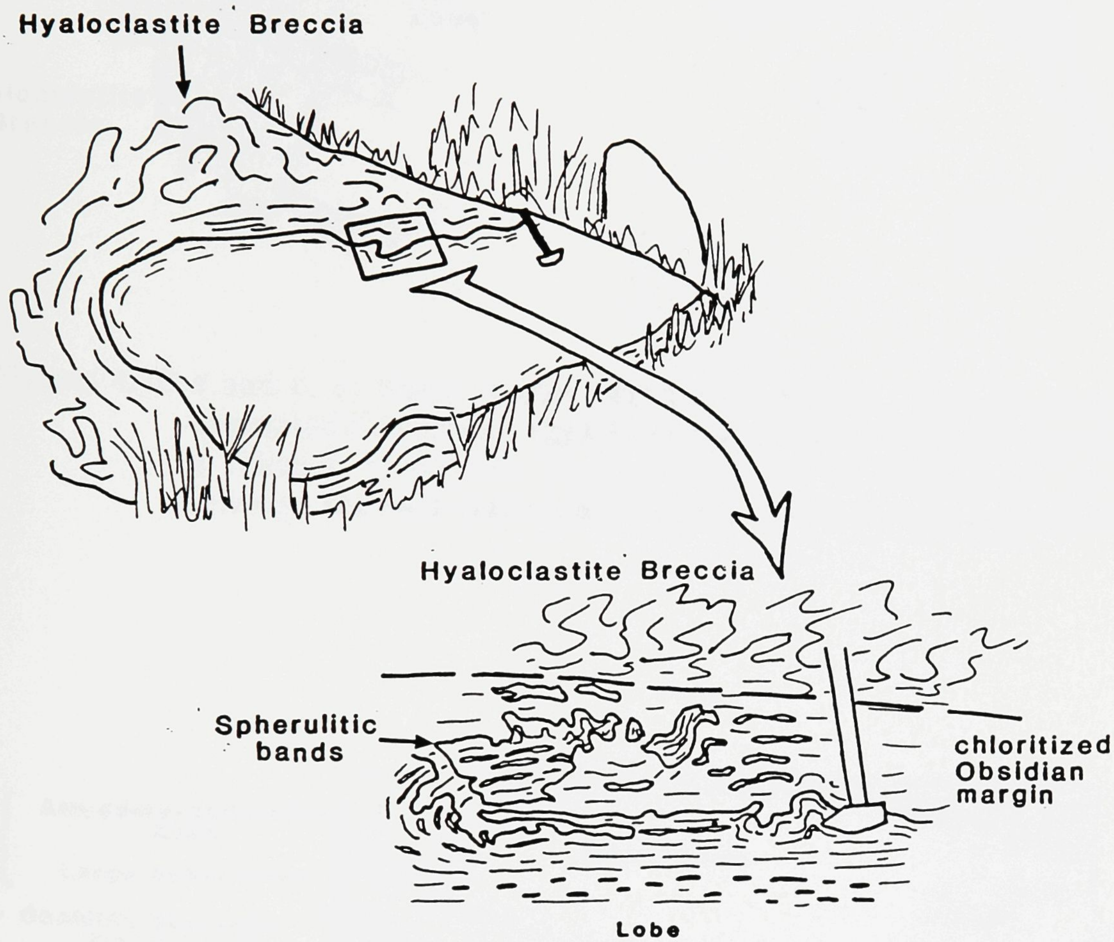

Figure 4.9. Gradational contact between rhyolitic lobe and surrounding, brecciated flow banded rhyolite and hyaloclastite. Note the continuation of spherulitic bands into the chloritized obsidian margin and adjacent hyaloclastite breccia (Amulet lower member).

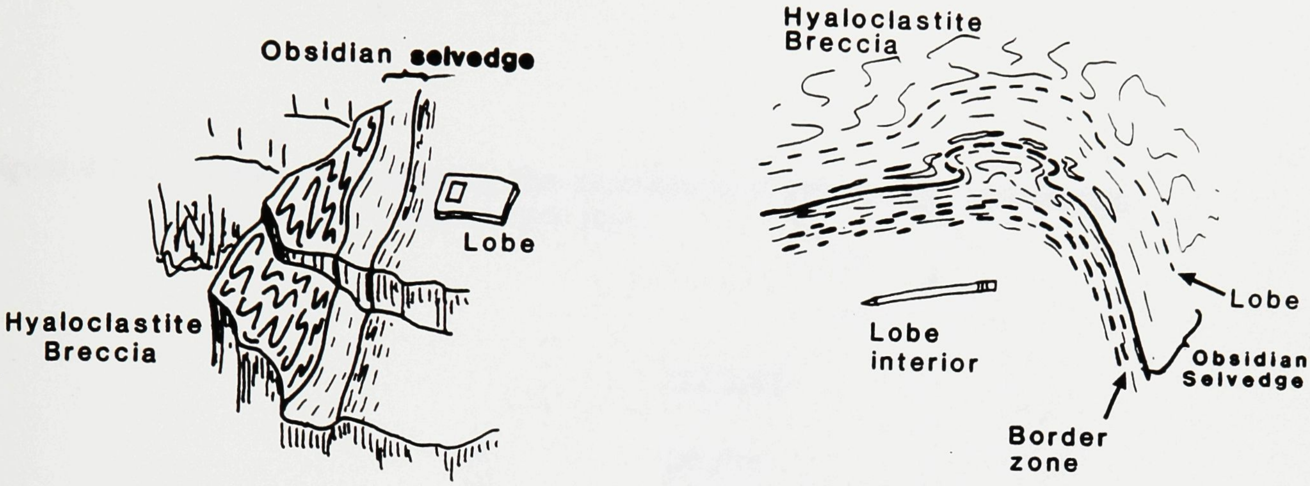

Figures 4.10 a and b. A. Sharp contact between a rhyolitic lobe and contorted, brecciated flowbanded rhyolite and hyaloclastite. Contact defined by a foliated, chloritized obsidian selvedge. B. Chloritized obsidian selvedge shows a gradational but sharp contact with hyaloclastite.

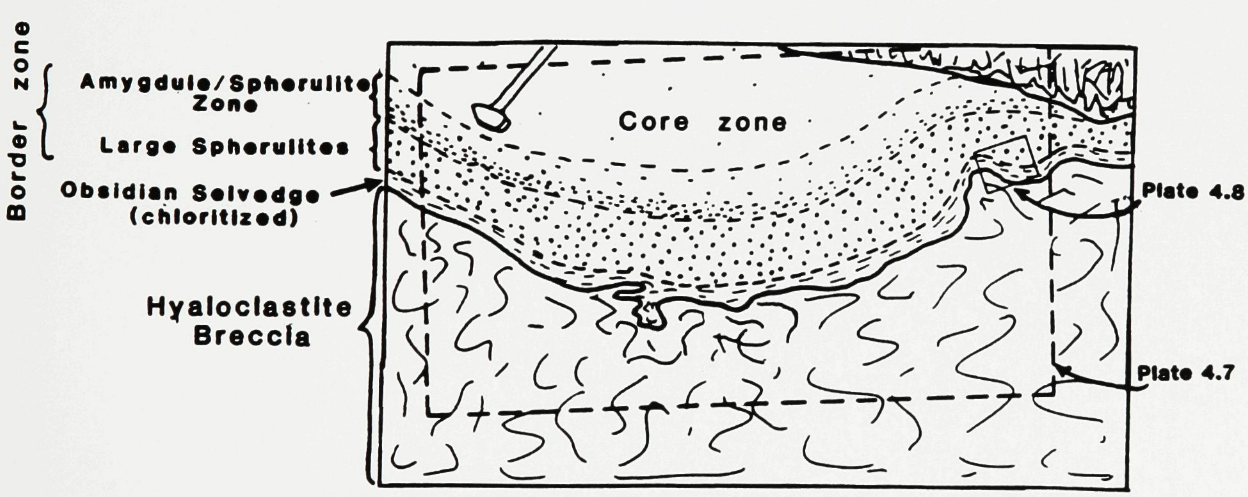

Figure 4.10c. Rhyolitic lobe engulfed within brecciated flowbanded rhyolite and hyaloclastite. Boxes correspond to Plates 4.7 and 4.8.

Figure 4.11. Geologic map showing the distribution of the massive and breccia facies of the Cranston QFP flow.

LEGEND

4	Diorite
3	Rusty Ridge formation
2	Cranston member (QFP Rhyolite)
	Massive and flow banded rhyolite
△	In situ brecciated rhyolite
	Breccia facies
▲	Carapace breccia
▲	Flank Breccia
1	Northwest formation

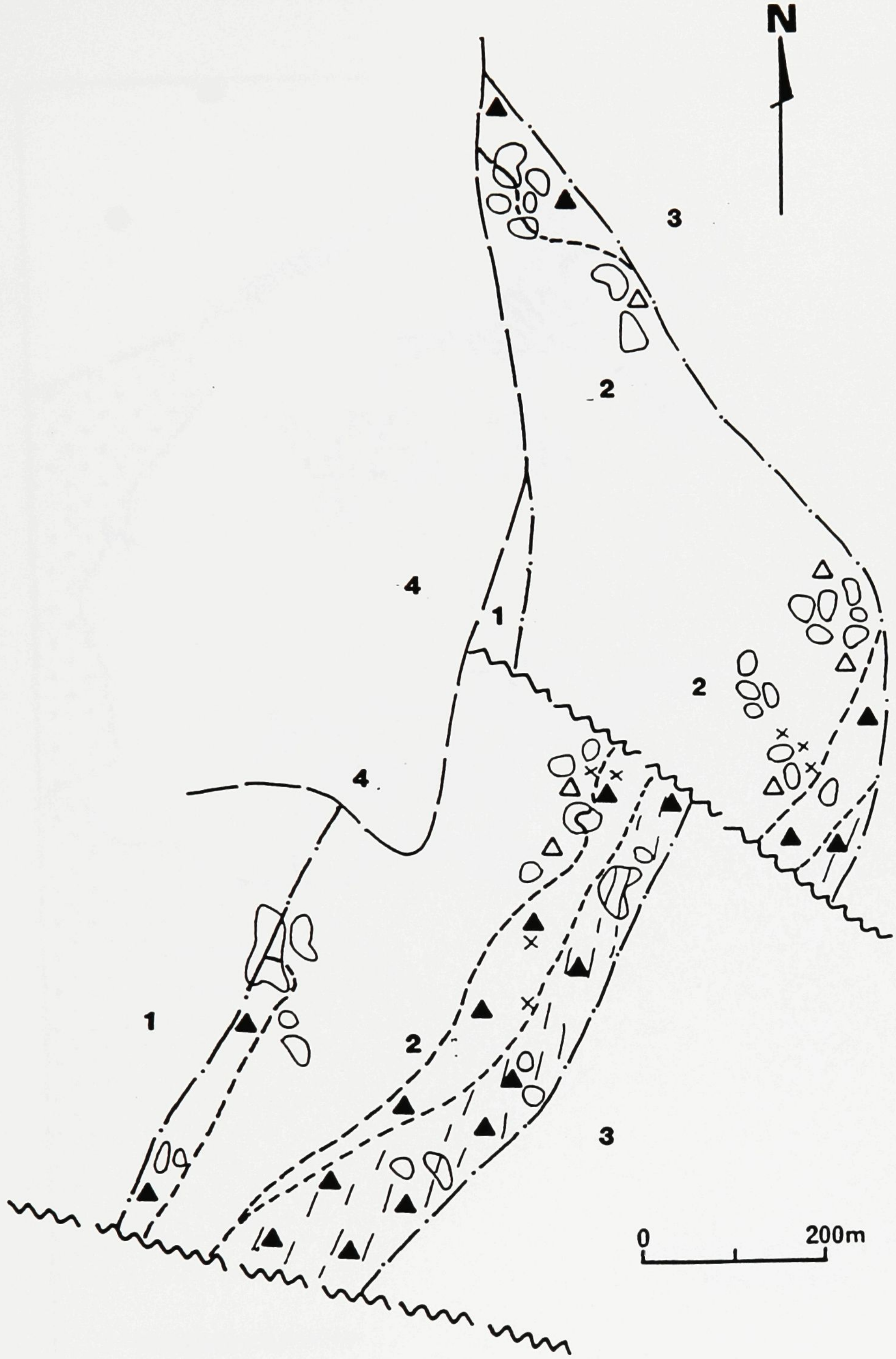
N
3
2
4
1
2
3
4
1
2
3
0
200m

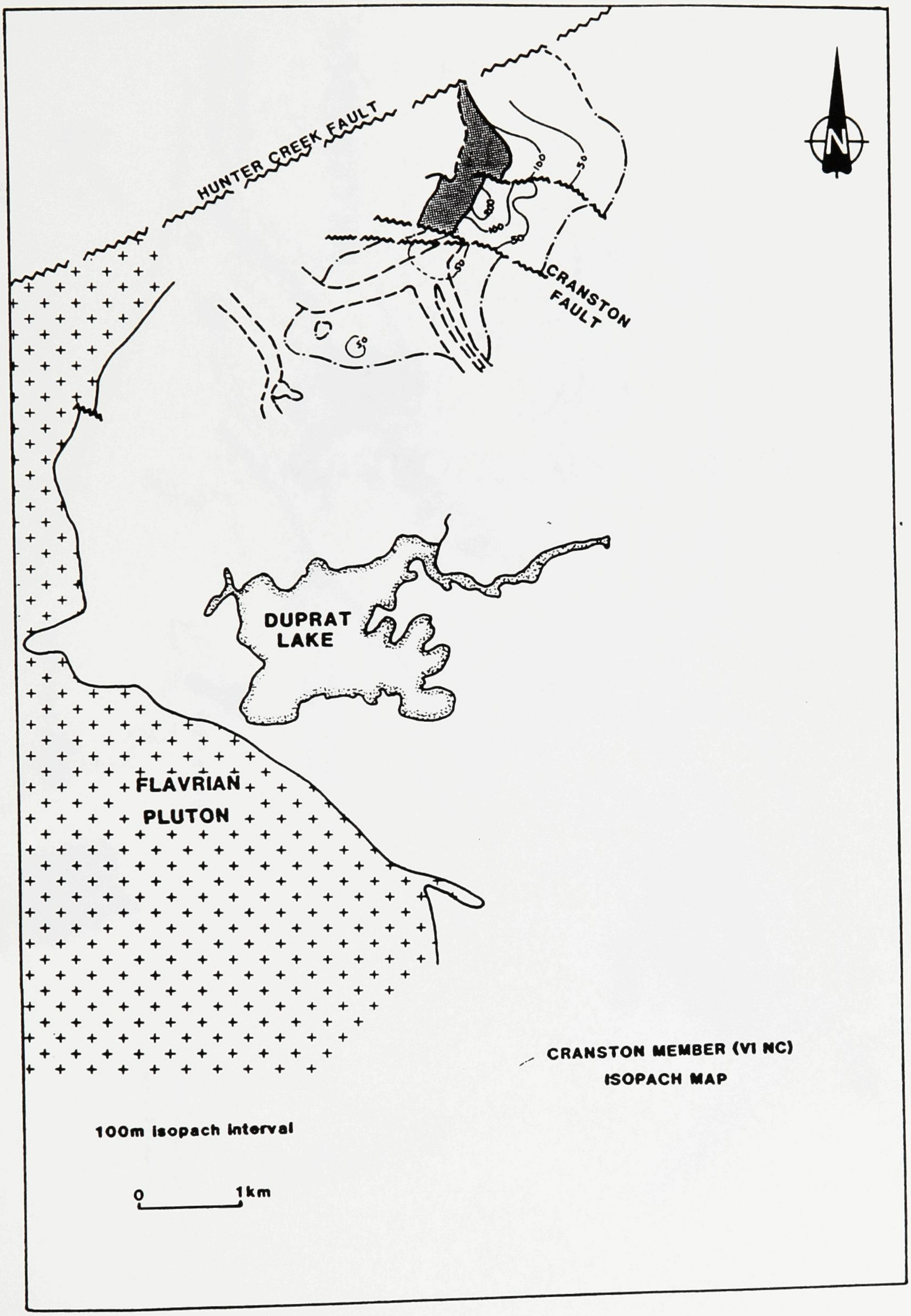

Figure 4.12. Isopach map of the Cranston member.

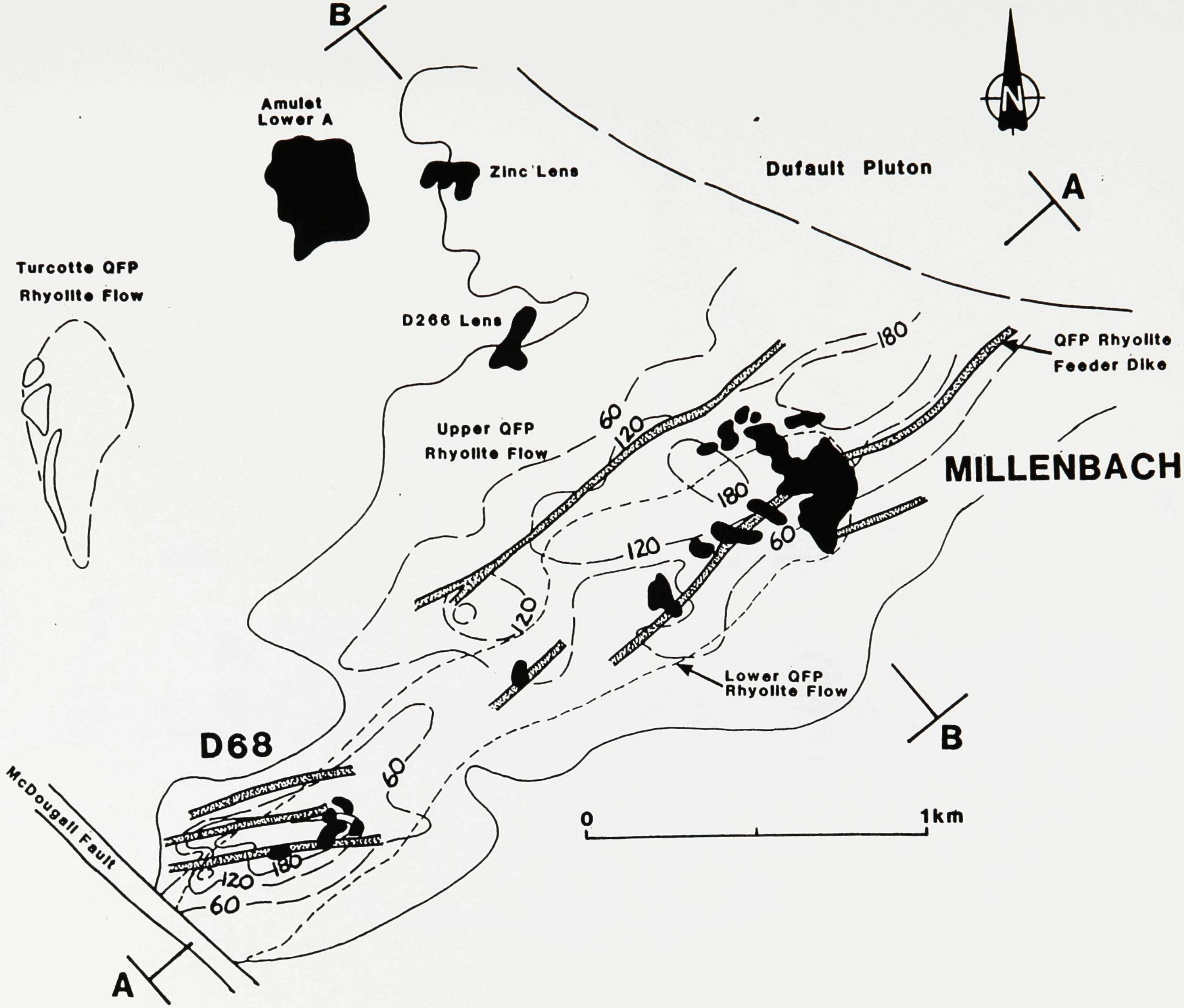

Figure 4.13. Isopach map of the Millenbach-D68 lava dome. Solid forms represent massive sulphide lenses and linear patterned areas are feeder dikes (after Comba and Gibson, 1983).

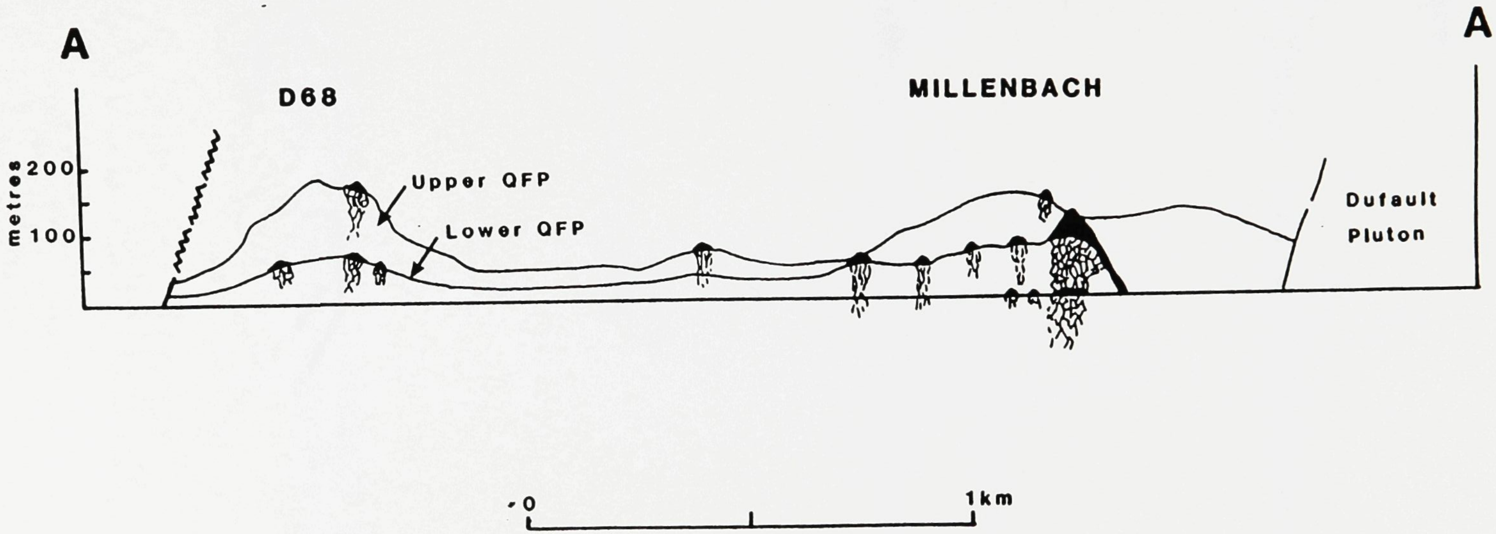

Figure 4.14.Longitudinal section of the Millenbach-D68 lava dome (after Comba and Gibson, 1983)

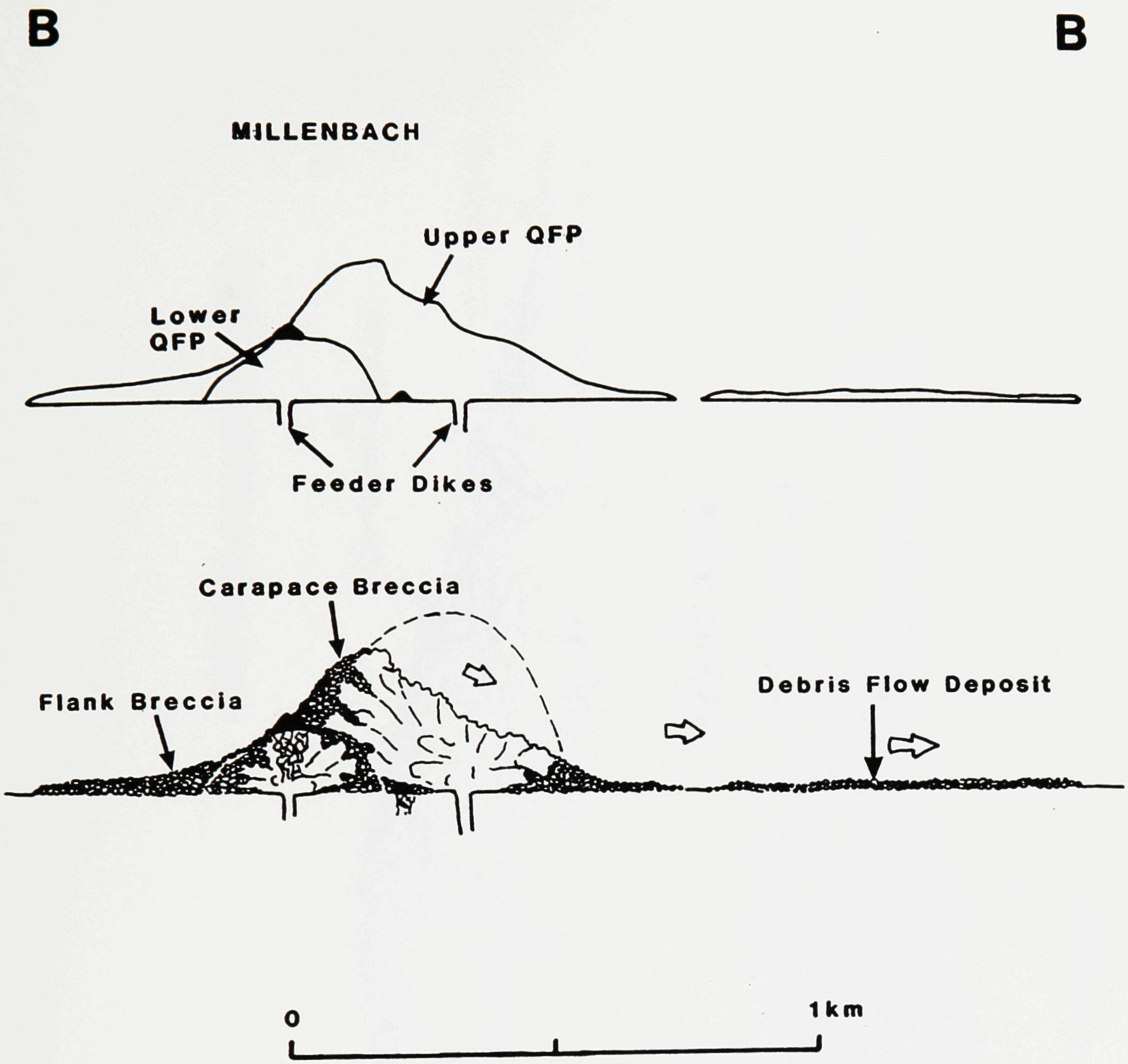

Figure 4.15. Actual profile (upper) and diagrammatic reconstruction of the Millenbach QFP lava dome at the Millenbach Mine after Comba and Gibson (1983).

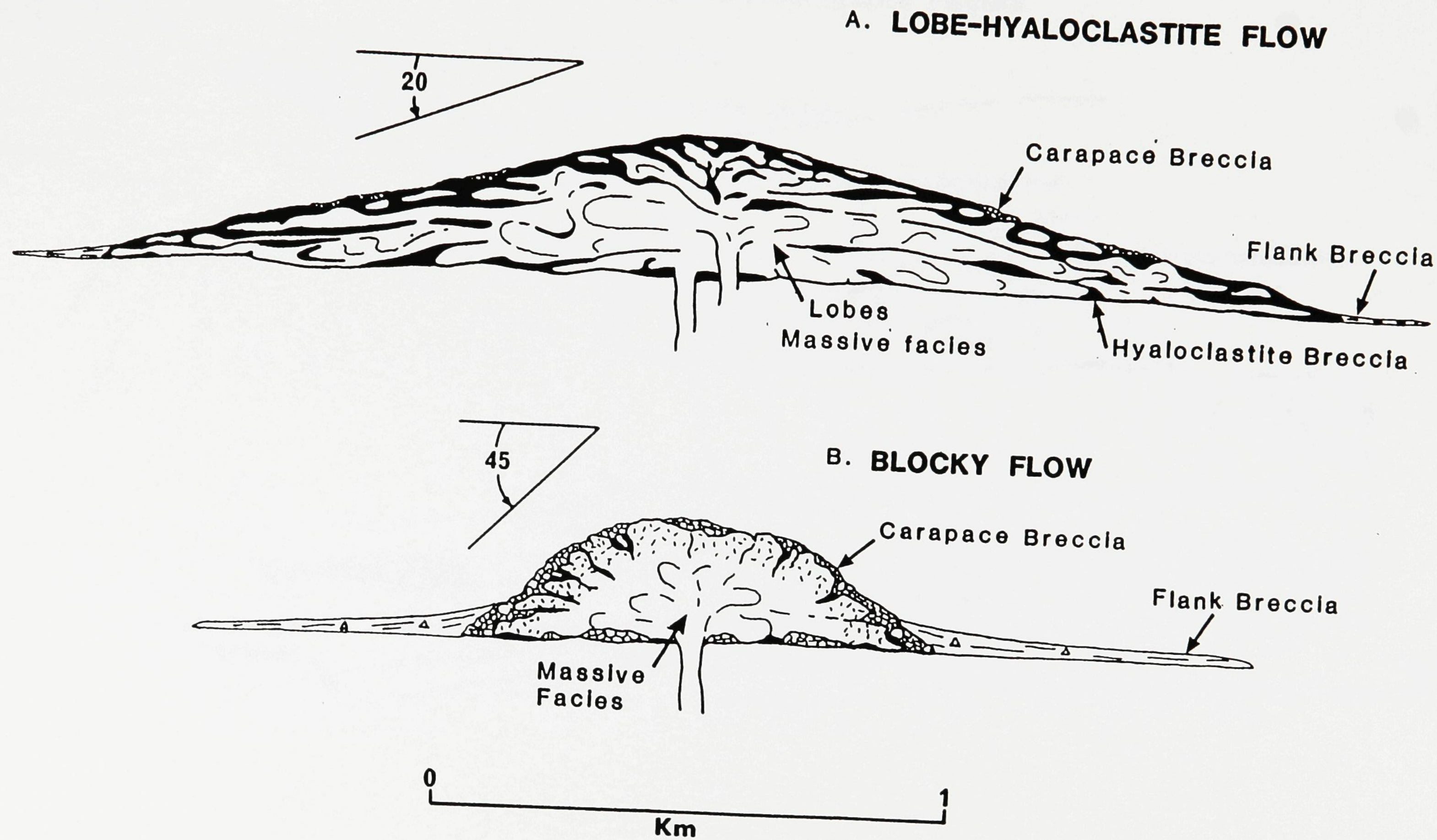

Figure 4.16. Diagrammatic cross-sections through subaqueous Lobe-hyaloclastite (A) and Blocky (B) rhyolitic flows.

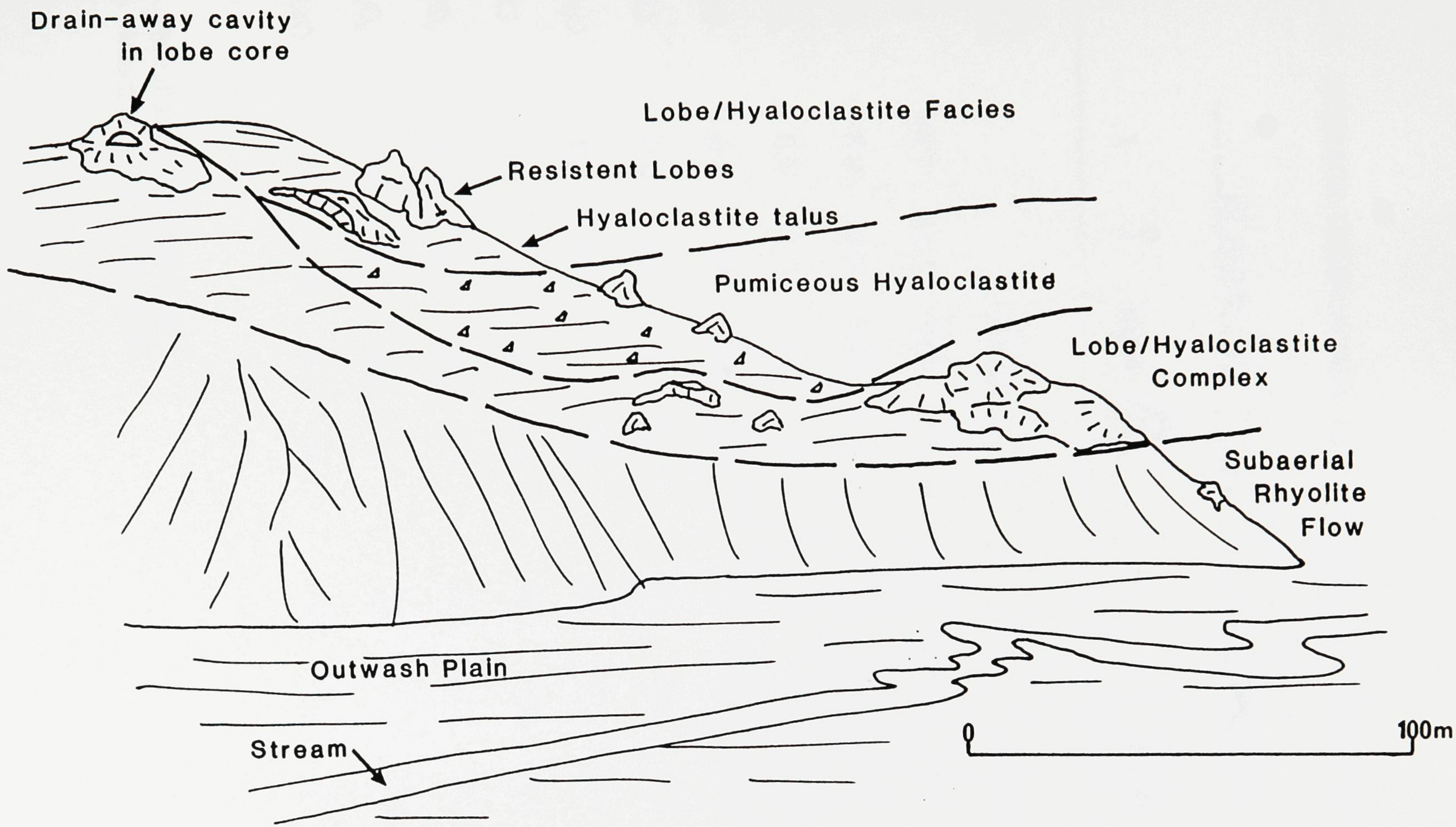

Figure 4.17. Sketch of the southern slope of Blahnukar illustrating lobe/hyaloclastite complexes separated by pumiceous hyaloclastite and underlying, older sub-aerial rhyolitic flow (after Furnes et al., 1980). Note the well developed radial joints within lobes.

TABLE 4.1. AVERAGE COMPOSITION OF FP RHYOLITE AND QFP RHYOLITE

	FP RHYOLITE				QFP RHYOLITE			
	1	2	**Mean**	Std. Dev.	1	2	**Mean**	Std. Dev.
Wt. % Oxides			(80 analyses)				(14 analyses)	
SiO_2	49.7	81.2	**73.0**	4.6	69.7	78.4	**74.4**	2.5
Al_2O_3	8.9	22.5	**11.9**	1.8	9.3	12.1	**11.1**	0.8
Fe_2O_3	0.5	11.5	**4.7**	1.8	1.7	6.5	**4.0**	1.3
MgO	0.1	5.4	**1.9**	1.2	0.3	2.5	**1.3**	0.6
CaO	0.1	6.3	**1.1**	1.2	0.2	1.4	**0.7**	0.4
Na_2O	0.0	5.9	**3.5**	1.6	0.1	4.3	**3.0**	1.1
K_2O	0.0	8.0	**1.5**	1.3	0.8	4.4	**2.1**	1.2
TiO_2	0.2	0.9	**0.3**	0.1	0.2	0.5	**0.3**	0.1
P_2O_5	0.0	0.2	**0.0**	0.0	0.0	0.1	**0.0**	0.0
MnO	0.0	0.3	**0.1**	0.0	0.0	0.2	**0.1**	0.0

1. Minimum value for oxide
2. Maximum value for oxide

TABLE 4.1B. AVERAGE COMPOSITION OF THE NORTH AND SOUTH FLOWS OF THE NORTHWEST FORMATION

	North Flow[1]		South Flow[2]		Combined	
	X	SD	X	SD	X	SD
SiO_2	73.8	1.3	73.5	1.5	73.7	1.4
Al_2O_3	11.9	0.5	12.5	0.3	12.2	0.5
Fe_2O_3	3.6	0.7	4.2	0.6	3.8	0.8
MgO	1.3	0.8	1.5	0.4	1.4	0.7
CaO	1.4	0.6	0.8	0.6	1.2	0.6
Na_2O	4.9	1.2	5.5	0.3	5.1	1.0
K_2O	0.6	1.2	0.1	0.04	0.4	1.0
TiO_2	0.4	0.02	0.4	0.01	0.4	0.02
P_2O_5	0.05	0.01	0.02	0.01	0.04	0.02
MnO	0.04	0.01	0.03	0.004	0.04	0.01
S	-					

[1] Based on 6 analyses
[2] Based on 4 analyses

TABLE 4.2. ESTIMATED VOLUME OF SELECTED FP AND QFP RHYOLITE FLOWS

	Area (Km²)	Volume (Km³)	Maximum Thickness (m)	Flow Units
<u>QFP RHYOLITE FLOWS</u>				
Millenbach-D68 QFP	2.5	0.82	240	2
Cranston QFP	13	0.8	200	1
Ansil	2	0.2	300	1
<u>FP RHYOLITE FLOWS</u>				
Northwest, Formation North Flow	22	2.9	500	1
Northwest, Formation South Flow	15	1.9	300	2

TABLE 4.3. COMPOSITION OF RHYOLITE LOBES, BANDED RHYOLITE AND BRECCIA, AMULET LOWER MEMBER

	A	B	C	D	E
Wt. %					
SiO_2	74.86	75.23	58.85	72.54	72.34
Al_2O_3	11.55	10.62	20.45	12.62	11.75
Fe_2O_3*	3.87	4.40	6.49	4.92	5.22
MgO	1.53	2.11	3.23	1.68	3.15
CaO	0.30	0.30	0.28	0.35	0.24
Na_2O	4.87	2.41	0.21	3.09	0.21
K_2O	0.72	2.44	6.80	2.12	3.12
TiO_2	0.25	0.22	0.46	0.27	0.24
P_2O_5	0.01	0.0	0.05	0.0	0.01
MnO	0.13	0.09	0.10	0.13	0.09
S	0.0	0.03	0.00	0.01	0.0
ppm					
Ba	162	720	1237	478	482
Cr	23	30	23	26	26
Zr	272	246	508	301	268
Sr	29	38	4	29	11
Rb	8	37	124	36	55
Y	59	56	103	66	56
Nb	7	6	17	7	9
Zn	90	57	83	100	83
Ni	0	0	0	0	0
Total	98.16	97.99	96.97	97.85	96.50

A - Lobe core (82-192
B - Lobe border zone (82-182)
C - Chloritized obsidian selvedge (82-183)
D - Banded rhyolite (82-194)
E - Rhyolite breccia (82-201)

as illustrated in Figure 4.4

* Total Fe as Fe_2O_3

TABLE 4.4. AVERAGE CHEMICAL COMPOSITION OF THE MILLENBACH AND CRANSTON QFP FLOWS

	MILLENBACH[1]		CRANSTON[2]	
	X	SD	X	SD
SiO_2	74.2	4.4	74.9	0.4
Al_2O_3	11.7	0.4	11.5	0.2
Fe_2O_3	2.6	0.6	3.0	0.3
CaO	1.1	0.1	0.4	0.9
MgO	1.1	0.4	1.1	0.4
K_2O	2.2	2.2	3.3	0.3
Na_2O	3.5	2.4	3.1	0.7
TiO_2	0.3	0.0	0.2	0.0
P_2O_5	0.03	0.0	0.03	0.0

[1] Based on 9 samples from Riverin (1977).
[2] Based on 2 weakly sericitized samples.

PLATE 4.1

Field of view for all photos is 4mm
Bar in 4.1B is 1mm long

A. Feldspar porphyritic spherulitic rhyolite of the Amulet lower member (#3 flow).

B. Same as A: flowbanding and quartz amygdules more apparent in plane polarized light.

C. and **D.** Spherulitic and flowbanded border to a rhyolite lobe of the #3 flow of the Amulet lower member.

E. Well developed quartz spherulites from the interior of a massive rhyolite lobe (#3 flow, Amulet lower member).

F. Spherulitic corona mantling a quartz filled amygdule within the chloritized obsidian selvedge of Plate 4.6.

G. Weakly silicified, chloritized obsidian hyaloclastite from the #3 flow of the Amulet lower member. Silicification, as fine chalcedony, occurs adjacent to perlitic cracks within shards.

H. Weakly in situ brecciated, perlitic textured, chloritized obsidian selvedge to a rhyolite lobe of the QFP Cranston flow.

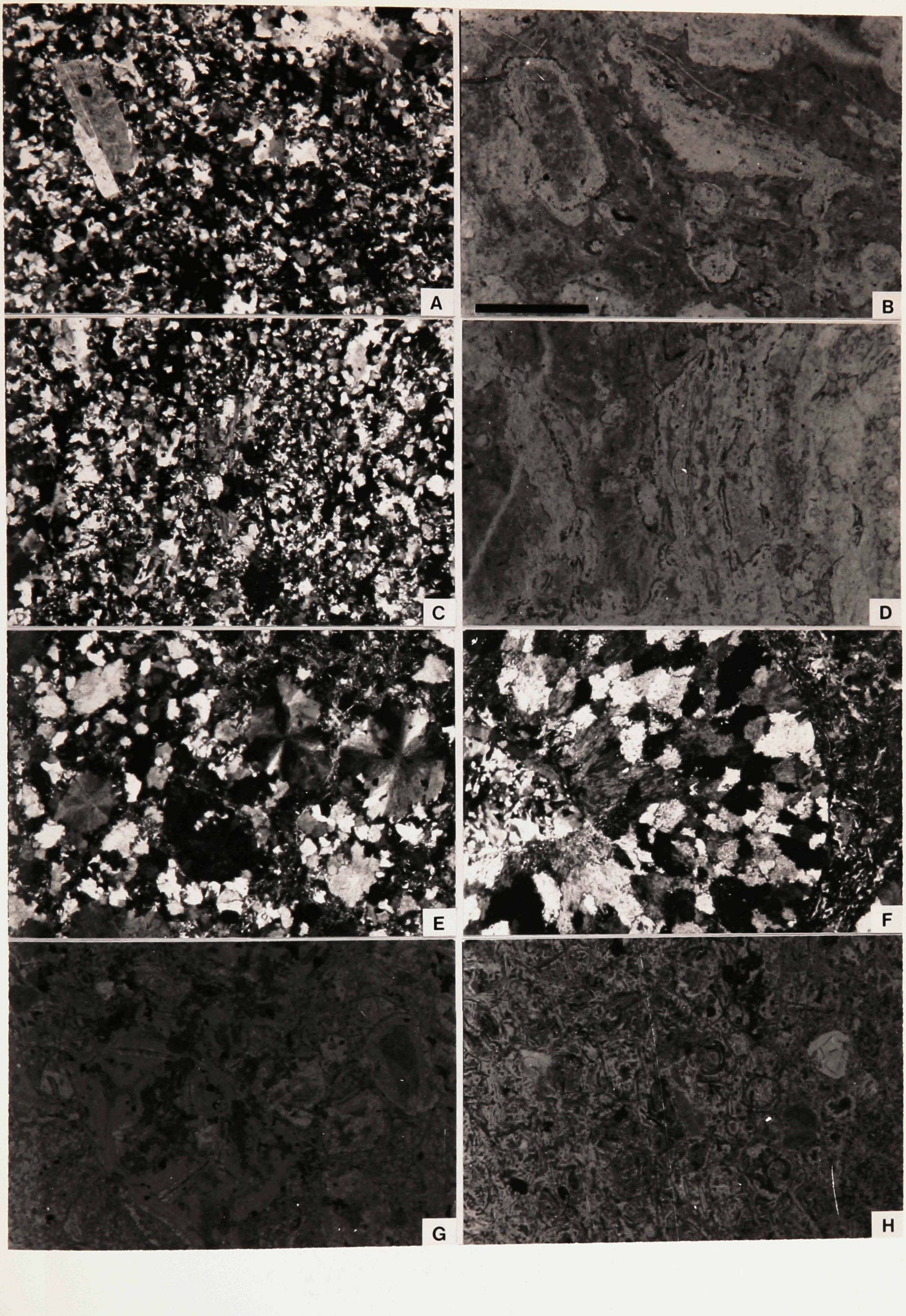
A
B
C
D
E
F
G
H

Plate 4.2. Massive, and quartz amygdaloidal rhyolite of the #3 flow, Amulet lower member.

Plate 4.3. Contorted flowbanded spherulitic rhyolite of the Bedford Flow, Amulet upper member. Banding is defined by contorted laminae of variable spherulite content.

Plate 4.4. Large lobe of massive rhyolite partially enveloped by chloritized rhyolite hyaloclastite, #3 flow of the Amulet lower member.

Plate 4.5. Irregular lobes of rhyolite surrounded by hyaloclastite and flow breccia at the south terminous of the #3 flow of the Amulet lower member.

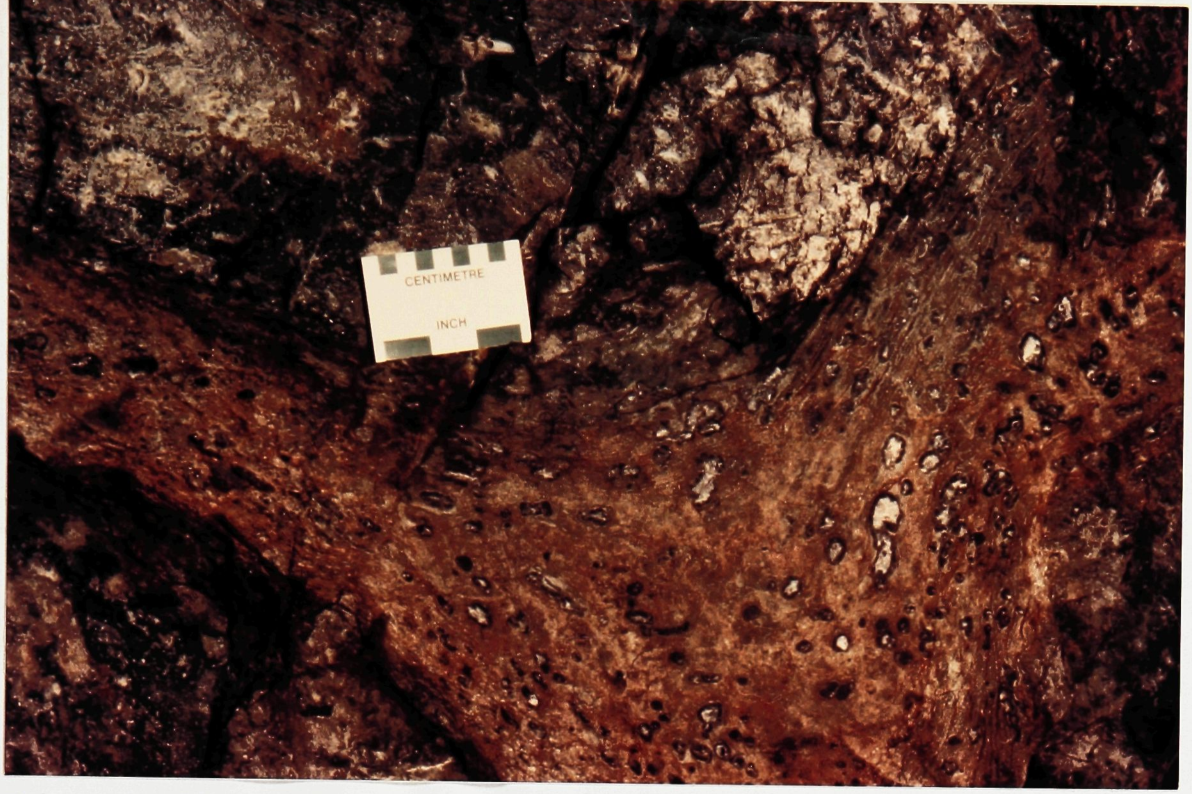

Plate 4.6. Chloritized obsidian selvedge to rhyolite lobes of the #1 flow of the Amulet lower member. The chloritized selvedge has a fine flow foliation and is characterized by spherulitic coronas mantling quartz amygdules (refer to Plate 4.1F).

Plate 4.7. Lobe margin - hyaloclastite contact, #3 flow of the Amulet lower member. Massive rhyolite of the lobe interior (under hammer) grades outward into a spherulitic border and foliated chloritized obsidian selvedge which has an irregular but sharp contact with surrounding hyaloclastite (see Figure 4.10c).

Plate 4.8. Close-up showing the contact between chloritized obsidian selvedge and hyaloclastite in 4.7 (see Figure 4.10c).

Plate 4.9. Carapace breccia to the Cranston Flow.

Plate 4.10. Crudely bedded flank breccias to the Cranston Flow. Hammer rests on the contact between the blocky breccia base to the bed on the right and the finer matrix supported top of the bed on the left.

Plate 4.11. Hammer rests on the obsidian selvedge (black) of a columnar jointed rhyolite lobe, Blaknukar Flow, Iceland.

Plate 4.12. Close-up of 4.11 showing the transition between massive rhyolite of the lobe interior (under hammer) to the banded, spherulitic border zone.

Plate 4.13. Faintly banded obsidian hyaloclastite mantling lobes in 4.11.

5. THE PETROLOGY, FLOW MORPHOLOGY AND EMPLACEMENT OF SUBAQUEOUS ANDESITIC FLOWS

5.1 INTRODUCTION

The following description and discussion of subaqueous andesitic flows is based on flows of the Flavrian, Rusty Ridge, Waite Andesite and Millenbach Andesite formations and the upper member of the Amulet formation. Flows range in composition from basalt to andesite (Tables 5.1 and 8.2). Individual flows were mapped and traced along strike during surface and underground mapping, and sections through flows were examined and described in detail (1:120 and 1:50). Mapping of individual flows facilitated stratigraphic correlation, definition of both the vertical and lateral facies of flows, and delineation of vent areas which allowed reconstruction of the volcanic history. The petrology, flow morphology, and facies of two morphologically distinct flow types, massive and pillowed, are described first followed by a discussion of the organization and emplacement of subaqueous andesitic flows.

5.2 ANDESITE FLOW FACIES

5.2.1 VERTICAL FACIES SEQUENCE

Facies recognized in subaqueous andesitic flows include massive, lobe, pillow and breccia facies. Flows may consist of entirely one facies, i.e., entirely massive and pillowed flows, but flows consisting entirely of a lobe or breccia facies were not observed. Dimroth et al., (1978, 1979) recognized similar facies in andesite and basalt flows of the Noranda area and the vertical sequences in which they observed them to occur are illustrated in Figure 5.1. Dimroth et al., (1978) found that the facies sequence represented by 1a-3a and 1c-3c to be most common, whereas sequences represented by 1b-3b are rare; the latter were interpreted to represent an uncommon transition between massive and pillow facies.

In this study the most common vertical facies sequences are represented by 1a and 2a, and 1c and 2c. The lobe facies, common to most massive flows, was not recognized by Dimroth et al., (1978,1979) or Cousineau and Dimroth (1982) and may have been included within their pillow facies (see Cote and Dimroth, 1976).

The pillow breccia facies of Figure 5.1, is referred to as the breccia facies in this study and is subdivided into flow breccias (massive flows) and pillow breccias (pillowed flows). Only one flow was observed to show an upward transition from massive through pillow to pillow breccia facies, and this transition is considered rare.

Dimroth et al., (1978) interpreted the various vertical facies sequences (Figure 5.1) as variants of a standard " ideal facies sequence" consisting of, in ascending order, a massive , pillow, pillow breccia and hyalotuff facies. Baragar (1984) described just the opposite sequence with a massive facies grading downward into a pillow facies. It should be emphasized that based on Dimroth et al., (1978,1979) work and this study the "ideal vertical facies sequence" is rarely developed.

5.2.2 LATERAL FACIES SEQUENCE

Dimroth et al., (1978, 1979) and Cousineau and Dimroth (1982) interpreted the "idealized standard vertical facies sequence" as lateral equivalents. In their model massive lava undergoes a lateral transition to pillowed lava and eventually to pillow breccia. This transition, was interpreted (Dimroth et al., 1978) to indicate decreasing flow velocity and temperature with concomitant increase in viscosity. Thus, in the above model massive and pillowed flows can be the proximal and distal facies of the same flow (Dimroth et al., 1978; Cousineau and Dimroth, 1982).

The standard vertical facies sequence of massive to pillowed to breccia facies is only ideal and its occurrence is the exception rather than the rule. Thus, if andesitic flows rarely achieve such an ideal vertical facies sequence why should this sequence be well developed laterally in an advancing andesitic flow? Mapping indicates that it is not, and a lateral transition from massive to pillow facies in the same flow is uncommon. Only two examples were observed and in these cases massive lava occurs as sill-like mega-pillows within pillowed flows as illustrated by the pillowed flow (unit 3) in Figure 12.5. As will be discussed later these mega-pillows are interpreted as buried lava streams or channels and do not represent a transition from massive to pillowed flow.

The Rusty Ridge Andesite formation is well exposed and contains thick flows of both massive and pillowed andesite. None of the massive flows of this formation or underlying Flavrian formation grade laterally into an equivalent pillowed facies. The marked lateral continuity and extent of most pillowed flows away from their vent areas (Appendix H, Figure 9.14) and alternation and sharp contacts with massive flows indicate that both pillowed and massive flows are discrete flow types that differ in morphology and are not vertical or lateral facies transitions of a single flow. Thick massive flows may, at their terminus, develop pillow or lobe like forms as described by Ballard et al., (1979) for sheet flows of the Galapagos Rift. The volume and extent of "pillow" lavas produced in this manner is minimal and could not account for pillowed flows with considerable strike length encountered in the field. Thus, the ideal vertical and lateral facies sequences proposed by Dimroth et al., (1977; 1978; 1985) and Cousineau and Dimroth (1982) are not applicable to all andesitic successions in the Noranda area. In the description and discussion which follows massive and pillowed flows are interpreted as morphologically distinct and separate flow types characterized by their own distinct vertical and lateral facies sequence.

5.3 PILLOWED FLOWS

5.3.1 INTRODUCTION

Pillowed flows consist of a pillow facies overlain by a breccia facies. The pillow facies predominates and extends from vent to flow terminus, whereas the breccia facies is not continuous but is more prominent toward the flow terminus. Flow thicknesses range from 2m to 150m and individual flows have been traced for up to 1km. Flows within the Millenbach, Waite and Amulet Andesite formations are more continuous than flows of underlying formations. Cousineau and Dimroth (1982) and de Rosen-Spence (1976) documented flows with lengths up to 14km in the Waite/Millenbach Andesite formations.

5.3.2 PILLOW FACIES

Pillow Shape and Flow Morphology

The pillow facies consists of densely packed "pillows" separated by thin selvedges and hyaloclastite breccia. Interpillow material accounts for <5% of the pillow facies and consists of sideromelane shard hyaloclastite cemented and variably replaced by quartz, epidote, chlorite and massive chert. Discontinuous deposits of massive and plane-bedded chert and tuff are common within and separating pillowed flows where they mantle pillows, fill irregular depressions , and occur as "squeeze ups" between pillows of an overriding flow.

Sill-like pockets of "massive andesite", ranging in size to 10 x 4m, occur within the pillow facies. Massive andesite is identical in both textures and structures to adjacent pillows and occurs near the base, within and near the top of the flow. Contacts conform to the shape of the surrounding pillows from which it is separated by a hyaloclastite selvedge. Pillow-like apophyses or "buds" which project from massive andesite into the surrounding pillows suggest that the former are large "mega-pillows" (Figure 5.8B).

The shape and size of pillows in outcrop are primarily a function of the two dimensional exposure afforded by most outcrops. Pillows shapes have been referred to as mattress, bun, balloon, ball/spherical and irregular/amoeboid (Plates 5.2 and 5.3; Hargraves and Ayres,1979; Dimroth et al., 1978; Cousineau and Dimroth, 1982). Although exposures may consist of predominantly one pillow shape it is not uncommon for all forms to be present in a single cross sectional exposure as illustrated in Figure 5.2. Amoeboid, irregular pillows are rare but are common within the breccia facies. Mattress pillows are large (>1.5m), whereas bun and balloon shaped pillows are commonly smaller (<1.5m). Ball or spherical pillows occupy interpillow areas and are typically <0.2m in diameter. Pillow shapes are identical to pillows observed in Iceland that were extruded into glacial meltwaters as described by Jones (1968) and to cross-sections through pahoehoe toes (MacDonald, 1972).

Superb exposures, topographic relief and shallow dips within the map area commonly allowed the observation of pillows in three dimensions and provided an opportunity to not only walk along flow contacts but upon the upper surface of flows.

Invariably such exposures yield pillows with cross-sectional shapes as described above but in plan the same pillows are long, single and bifurcating tubes that meander, intertwine, and overlap. Individual tubes are traceable for up to 4m before encountering an overlapping tube. Spectacular, classic exposures of pillowed lavas within the Rusty Ridge formation at Ansil Hill (Appendix A) and in the Waite Andesite formation north of Waite Lake (Plate 5.4) are remarkably similar to those from the Mid-Atlantic Ridge rift valley (Ballard and Moore, 1977) and to tube-fed pahoehoe flow surfaces observed at Kilauea and Mauna Ulu in Hawaii.

These field observations are consistent with a pillow facies composed a branching, intertwined mass of interconnected tubes that appear as separate isolated "pillows" or "sacks" in 2-dimensional exposures. Pillowed flows are interpreted as the subaqueous equivalent of subaerial tube-fed pahoehoe flows (Ballard et al., 1979) and are essentially compound flows as each pillow or tube is a separate and small scale flow-unit that cooled independently (Walker, 1972). The similarity between pillows and subaerial tube-fed pahoehoe flows has been noted by numerous workers (Lewis, 1914; Jones, 1968, 1969; Moore et al.,1971, 1973, 1975; Dimroth et al., 1978; Cousineau and Dimroth, 1982; Hargraves and Ayers, 1979 and Baragar, 1984).

The analogy between pillows and tube-fed pahoehoe toes explains the variability in shape and size of pillows observed in cross-section. Figure 5.3, illustrates cross-sections oriented parallel, oblique and normal to an idealized tube-fed flow. Exposures of predominantly mattress and elongate-irregular pillows reflect a sectional view parallel or oblique to the flow (Section B and C), whereas section A, orientated perpendicular to the advancing flow, would yield numerous bun and balloon-shaped pillows. Small, spherical or round pillows occur where a section has "nicked the edge" of a larger tube. Figure 5.3, also illustrates that all pillow shapes may be expected in any 2-dimensional cross-sectional exposure and that isolated pillows would be extremely rare, interpretations consistent with field observations.

Although pillows appear as discrete, separate bodies in cross-section many larger pillows show "necking structure" and reentrant selvedges which indicate they are interconnected. Necking pillows (Figure 5.4) are adjacent pillows connected by a narrow "medial" neck. The medial "neck" marks the connection between pillow and bud (Hargraves and Ayres, 1979). Reentrant selvedges are identical to the selvedge which surrounds pillows but the former occurs within pillows as projections roughly perpendicular to the pillow margin (Figures 5.4 and 5.5). In some pillows reentrant selvedges from both the top and bottom nearly meet and are interpreted as the contacts between tube and bud. The direction of budding observed in cross-sections (Figures 5.4 and 5.5) and branching of tubes observed on flow surfaces (tubes branch down flow) were used to determine crude paleo-flow directions.

Imbrication of pillows, reentrant selvedge and "budding" (Figure 5.5) are consistent with the digital advance of pillows observed by Moore et al., (1975). In Figure 5.5, advancing pillows bud upward to cover and extend beyond the underlying pillow; the budding of new pillows from cracks located along the top of a pre-existing pillow is similar to trap door pillows described by Ballard and Moore (1977) from mid-oceanic ridge pillow basalts.

Internal Subdivisions: Textures and Petrography

Pillows are subdivided into an outer crust or selvedge, a border zone, and an inner core zone (Figure 5.6). The selvedge completely surrounds pillows, is typically <3cm wide and consists of chloritized, devitrified, intact and brecciated sideromelane or vitrophyre. Skeletal albite microlites (0-3%), with swallow-tail and belt-buckle forms, are randomly oriented in an aphanitic massive groundmass of chlorite and minor actinolite, quartz and opaque minerals that are interpreted to replace former sideromelane. Perlitic cracks are common within the selvedge and give way to a hyaloclastite outer rind of brecciated, chloritized sideromelane. Pillow selvedges weather slightly darker brown than the pillow interior.

The border zone ranges from 2cm to 5cm in width, weathers slightly lighter in colour (buff-brown) than the pillow interior, and marks a transition from quenched selvedge to microcrystalline interior. The border zone has a hyalopilitic texture, with 5-20% skeletal albite microlites that range to 0.6mm in size in a groundmass of chlorite and minor actinolite, quartz and opaque minerals which presumably replace original sideromelane. Microlites and to a lesser extent plagioclase phenocrysts are commonly mantled by fibrous spherulitic coronas. Bands of microlites and, commonly, fine amygdules and phenocrysts are often aligned imparting a flow foliation or banding (Plate

5.1A).

The pillow core is characterized by an hyalopilitic or intersertal texture, where elongate plagioclase microlites (30-50%) and phenocrysts define a felted framework with interstitial chlorite, and minor actinolite, quartz, epidote, opaque minerals and sphene (Plate 5.1 A,B&C). Areas of massive, aphanitic chlorite and actinolite, with fine "dusty" opaques constitute up to 20% of the groundmass and are interpreted to replace "pools" of sideromelane (Plate 5.1D).

5.3.3 STRUCTURES WITHIN PILLOWS

Amygdules

Amygdules range in size from <0.5cm to 8cm and constitute between 3-30% of pillows. Amygdules occur throughout the pillow but are preferentially distributed around the periphery and occasionally increase in number toward the interior and top of pillows (Figure 5.6). Radially oriented, tear shaped, pipe amygdules up to 4cm long and 1cm wide are common in some flows (Plate 5.2). Flat bottomed arched topped cavities, up to 30cm x 20cm in size, are interpreted as lava levels (Figure 5.6). These cavities may represent:

a) primary voids produced by partial evacuation of lava "tubes" via draining of lava to feed an advancing flow front, as proposed by Ballard and Moore (1977) for hollow pillows at mid-ocean ridges. b) cavities formed by the concentration of residual gas between the crystallizing rim and molten interior of pillows as proposed by Waters

(1960) and Hargraves and Ayres (1979).

If the cavities formed by the trapping of exsolved volatiles their occurrence may signify relatively shallow water. In either case the flat base of the cavity records the temporary level of lava within the tube and provides a reliable indicator of the horizontal paleosurface.

Joints

Joints are of two main types, concentric and radial. Radial joints (Figures 5.6 and 5.7) are fine cracks or fractures that are oriented roughly perpendicular to the pillow rim. There is no expression of radial joints on the pillow crust. Radial joints are interpreted as radiating columnar joints as they are oriented roughly perpendicular to the cooling surface.

Concentric joints (ribbing or concentric laminations) are parallel and continuous "cracks" that faithfully follow the contours of pillows. The spacing between concentric joints decreases as the number of joints increase towards the pillow margin (Figure 5.6 and Plates 5.3 and 5.5). In three dimensions, concentric joints may be likened to a series of nested cylinders within pillows. The joints consist of fine, elongate, and aligned quartz amygdules, trains of opaque minerals (Plate 5.1F) and flow aligned plagioclase phenocryts and microlites. Although their origin is uncertain concentric joints are early structures as they are dissected by both radial joints and polyhedral fractures (Plate 5.6). Like bands of flow aligned phenocryts in pillows, described by Duffield (1969), concentric joints are likely a product of laminar flow within pillows. They may represent primary planes of weakness that originated in response to shear stresses along and parallel to the pillow margin induced within chilled lava that was increasing in viscosity and decreasing in velocity through a steep temperature gradient along the pillow margin.

A crude polyhedral fracturing occurs in the interior of some pillows. In brecciated and in "situ"-brecciated pillows much of the dislocation and separation of fragments appears to have been governed by polyhedral fractures and radial joints, both of which are superimposed on concentric joints (Plate 5.6).

Pillow Crust Structures

Pillow crusts are normally smooth and featureless except for one exposure of tube-fed pillow flows within the Waite Andesite formation north of Waite Lake. The crusts of these pillows are well exposed and clearly show parallel striations or corrugations along their length (Plate 5.7). The corrugations are 2-4mm high, 2-3mm wide and are spaced at intervals from 0.5-2cm. These corrugations are the first described from Archean flows and may be analogous to corrugations described by Ballard and Moore (1977) in mid-ocean ridge basalts. Ballard and Moore (1977) interpret the corrugations as gouge marks that form perpendicular to the spreading crack during moderately rapid extrusion (pillow budding).

5.3.4 BRECCIA FACIES

The breccia facies, which occurs at the top and terminus of pillowed flows, constitutes less than 15% of individual flows and ranges from <1m to 6m in thickness. Thin discontinuous pockets of breccia occurs between pillows immediately below the flow top.

The breccia contains intact, whole pillows and pillow fragments in a hyaloclastite, pillow fragment matrix. Pillow breccias are poorly sorted, non stratified deposits. Intact pillows and broken pillows do however increase toward the bottom and top of the breccia respectively. The percentage of isolated pillows to broken pillow fragments is variable and either can be the dominant fragment type. Breccias at the base of pillowed flows occassionaly contain isolated, ribbon-like, imbricated pillows.

The upper pillowed surface is irregular and pillow breccia rests directly on and is in sharp contact with pillows. Pillows protrude upward into the breccia and irregular, amoeboid, isolated pillows within the breccia may be detached buds from these protrusions (Figure 5.8 A). Pillows are typically intact but where brecciated they grade upward into a pillow breccia dominated by broken pillow fragments.

Intact Pillows

Intact pillows are isolated amoeboid-shaped bodies that range in size from 8cm to 1m (Figure 5.8 A). Amygdules (<0.5cm typically) are concentrated along the pillow margins where they can constitute up to 30%; concentric joints are common. Pillows are commonly in situ brecciated resulting in an intact but shattered appearance (Plate 5.3); fractures separating individual blocks are filled by quartz (minor epidote) and/or hyaloclastite.

Pillow Fragments

Pillow fragments are derived from the breakup of isolated amoeboid pillows and from brecciation of underlying pillows. It is common to observe intact isolated pillows, "in situ" brecciated isolated pillows and brecciated pillows with rotated, separated and displaced fragments within the same exposure (Figure 5.8 A). Brecciation occurs primarily along fractures, radial joints and to a lesser extent on concentric joints. This results in plate-like fragments possessing one chilled margin and angular, blocky fragments from the interior of pillows. Pillow fragments range in size from <1cm to 25cm with fragments >10cm chiefly plate-like in form.

Matrix

Isolated, intact pillows and pillow fragments constitute from 30 to 45% of most pillow breccias. The matrix is massive and contains fragments ranging in size from 2cm to <1cm within a finer, aphanitic matrix of chlorite, quartz and epidote. The matrix may display a faint "flow foliation" which wraps around and parallels the margins of larger fragments and isolated pillows. Matrix fragments are of two types, chloritized hyaloclastite and lithic fragments.

The hyaloclastite component of the matrix consists of three morphological types as described by Carlisle (1963), namely sideromelane and vitrophyric shards, granules and globules. Shard hyaloclastite predominates.

Globules are ellipsoidal to tear shaped beads of chloritized sideromelane that are commonly dissected and in situ brecciated by fine perlitic cracks. Granules are similar to globules except that they are bounded in part by knife-edged concave or convex margins. Shards have angular, crudely triangular forms with concave-convex boundaries that meet in knife-like points. Perlitic cracks are common but amygdules and phenocrysts rare.

Angular fragments of microlitic andesite similar to the interior of associated pillowed lavas constitute <10% of the matrix to most pillow breccias. Microlitic andesite fragments are derived through brecciation of isolated pillows and underlying pillow lava. Amygdules are common in microlitic fragments and, depending on the vesicularity of isolated pillows and underlying pillowed lava, range from 3-20%.

Hyaloclastite and lithic andesite fragments are cemented by a fine-grained quartz, chlorite and minor epidote and carbonate. The fine "flow foliation" reflects the alignment of hyaloclastite shards.

Interpretation and Summary

Pillow breccias are an integral component of subaqueous tube-fed flows and are gradational into underlying pillows to which they are similar both texturally and mineralogically. Intact irregular pillows within the breccia are detached and isolated buds from underlying tubes which project into the breccia. The irregular shape of pillows within the breccia compared to that of the underlying flow suggests that:

a) they are isolated bodies and therefore, unlike tubes of the underlying flow, are not inflated and supported by lava ponded within or moving through them.

b) isolated pillows are extruded into a chaotic breccia and are not rigidly supported by adjacent pillows. These detached "buds" conform to irregularities in the breccia which would be constantly changing as the breccia shifts during advance of the underlying pillowed flow.

Angular fragments are derived from isolated pillows within the breccia and to a lesser extent from pillows of the underlying flow. Brecciation of isolated pillows takes place along radial joints and polyhedral fractures. Brecciation of pillows and incorporation of fragments within the breccia are likely the result of a shifting, unstable, loose chaotic breccia that is continuously jostled by an underlying advancing flow.

Hyaloclastite fragments are similar to those described by Carlisle (1963) and Honnorez and Kirst (1973). The predominance of platy, angular, nonvesiculated sideromelane shards suggests the hyaloclastite formed through spalling, crumbling and granulation of glassy pillow crusts that were rapidly quenched by seawater. Tear drop and ellipsoidal shaped hyaloclastite globules and granules may be drops of quenched lava released by small scattered steam explosions at an active, advancing flow front.

5.4 MASSIVE FLOWS

Massive flows consist of a massive facies, lobe facies and breccia facies. Flows range from 5m to 200m in thickness and individual flows have been traced for up to 2km.

Cross-sections through idealized, massive flows illustrating their principal flow facies, textures and structures are shown in Figure 5.9. By far the most common type of massive flow consists of a basal massive facies, an upper lobe facies and an overlying breccia facies (Figure 5.9A). Less commonly flows are characterized by a massive facies directly overlain by a breccia facies (Figure 5.9 B.). In all flows the massive facies predominates and flows composed entirely or predominantly of breccia were not recognized.

Massive flows have been interpreted as the subaqueous equivalent of submarine pahoehoe sheet flows (Ballard et al.,1979) and are simple flows as defined by Walker, (1972). Only one compound massive flow was recognized (A-M #5 flow) where two flow-units are distinguished by an internal amygdule zone and poorly developed flow breccia. The flow shows no variation in texture or grain size related to this internal contact; it essentially cooled as a single unit and therefore might better be called a multiple flow (Walker, 1972).

Massive flows represented by a massive, lobe and breccia facies (Figure 5.9A) are similar to "complex massive flows" described by Hargraves and Ayres (1979) whereas flows with only a massive and breccia facies (Figure 5.9B) are similar to their "simple massive flows".

5.4.1 MASSIVE FACIES

The massive facies of thin flows (<50m) consists of aphanitic to fine-grained (0.2 to 0.5mm) andesite. The margins of thin flows have a narrow (1-2cm) aphanitic chilled basal zone but the flow in general lacks a conspicuous variation in grain size. The massive division of thick flows, especially those exceeding 100m in thickness, are characterized by aphanitic margins and interiors that range from fine grained to medium grained (0.3 to 2.0mm).

Intersertal textured andesite characterizes lava of the massive facies (Plates 5.1C and D). Plagioclase phenocrysts constitute from 0-15% of individual flows and are typically stubby, subhedral to euhedral and occur as single crystals or glomeroporphyritic clots (Plate 5.1E). Phenocrysts range in size from <0.5mm to 1.5mm. Subhedral pyroxene phenocrysts (up to 1.5mm in size), pseudomorphed by actinolite, epidote and or chlorite, constitute approximately 2% of some flows. Euhedral to subhedral plagioclase microlites range in size from 0.1 to 1.0mm and constitute from 30-50% of the flow. Microlites form a randomly oriented, felted framework to interstitial massive and fibrous bundles of actinolite, chlorite, clinozoisite, quartz, and minor sphene and opaque minerals which collectively constitute up to 40% of the flow. Homogeneous clots of massive chlorite and/ or actinolite interstitial to microlites are interpreted as "clots" of altered glass and constitute <10% of massive andesite (Plate 5.1D).

The fine to medium grained intersertal textured interior grades into a fine-grained intersertal and less commonly hyalopilitic textured margin. Phenocrysts' size and percentage are the same as in the massive interior. Microlites constitute from 20-40% of the margin and interstitial chloritized "sideromelane" comprises up to 20% of the flow margin.

Rootless, chloritized sideromelane selvedges, <0.5m in length, occur in the upper portion of the massive facies (Figure 5.9A). The selvedges are identical to chilled crusts of overlying lobes and are interpreted as incipient lobes or the base of overlying lobes, with which they are continuous.

5.4.2 LOBE FACIES

The lobe facies consists of irregular finger-like protrusions of massive fine-grained andesite that originate in underlying massive lava and extend upward into the overlying flow-top breccia (Figure 5.9A, Plates 5.8 and 5.9)). The lobe facies is typical of most flows and ranges from 0.5m to >3mm in width with individual lobes attaining lengths of up to 2m. Lobes, like pillows, are mantled by a thin (<3cm) hyaloclastite selvedge that is best developed where lobes are in contact with breccia. Selvedges extend downward into the flow until they abruptly terminate and both lobes and massive lava merge (Figure 5.9A). The lobe interior is texturally and mineralogically identical to underlying fine-grained massive lava, whereas the selvedge and border zones of lobes are identical to those described for pillows.

Interpretation

Lobes are finger-like apophyses of underlying massive andesite that were injected upward into the overlying flow top breccia. Lobes are commonly aligned oblique to the flow contact (Plate 5.9). This angular discordance between lobe elongation and flow contacts was interpreted by Cote and Dimroth (1976) to represent an imbrication produced by shear during flow advance (Plate 5.8). Lobe imbrication, where the acute angle between the lobe and flow contact faces down-flow, was used to determine paleoflow directions.

5.4.3 STRUCTURES

Amygdules

The variation in amgydule content within the massive and lobe facies is illustrated diagrammatically in Figure 5.9. In all flows there is a distinct increase in amygdules toward the flow top.

Amygdules are typically <1cm and commonly <0.5cm in size although amygdules 2-3cm in size are common near the flow top. Some of the large amygdules (>1cm) have flat bottoms and arched tops reminiscent of lava levels and paleo-shelves in pillows. Flat bottomed amygdules range in size from 1-8cm; the amygdule base usually conforms to and coincides with laminar joints in the flow top.

The abrupt zone of amygdule increase near the flow top (Figure 5.9A) typically defines the upper limit of mega amygdules. Mega amygdules refers to amygdules that range in size from 5cm to 28cm, are ovoid in form and account for <1% of the total amygdules present. These large amygdules are filled by quartz and epidote that pseudomorph original fibrous precursor minerals, possibly zeolites, or have botryoidal laminated infillings defined by alternating millimetre wide laminae of quartz, epidote and opaque minerals. Amygdule mineralogy and filling sequences are discussed in Chapter 12.

Within the upper part of the massive and overlying lobe facies amygdules display two basic forms, elongate and spherical. Elongate amygdules are attenuated vesicles that likely formed by volatile exsolution during emplacement of the flow, whereas spherical amygdules are vesicles that may have exsolved from stagnate lava following flow emplacement. The long axis of elongate amygdules was used as a crude indication of flow direction.

Joints

Columnar joints are restricted to the massive facies where columns up to 50cm across were observed. The plunge of columnar joints measured in individual flows are remarkably similar, indicating a relatively flat underlying topography.

Laminar joints are common toward the top and to a lesser degree at the base of massive flows (Figure 5.9). Laminar joints, referred to as ribbing or laminations, are fine, 1-3mm wide, resistant quartz (minor epidote, opaques, chlorite) filled parallel cracks. Trains of quartz amygdules frequently occur along the joints.

As illustrated in Figure 5.9, laminar joints are continuous parallel and planar structures that faithfully follow and conform to flow contacts; the spacing between joints decreases towards the flow contacts. The planar orientation of these joints persists to within several metres of the lobe facies. Thereafter the joints remain parallel but are increasingly contorted and folded as they parallel lobe margins (Figure 5.9A).

Laminar joints are interpreted to be the equivalent of concentric joints found in pillowed lavas; both are primary planes of weakness which conform to cooling surface contacts and are defined by same mineralogy, structures and textures. Pillows provide a cross section through a lava tube, hence conformable laminar joints appear as concentric rings or cylinders, whereas in sections through massive flows laminar joints appear as lines. In three dimensions laminar joints are probably conformable, undulating planes that may have formed in response to shear stresses along and parallel to cooling surfaces during laminar flow where lava was increasing in viscosity and decreasing in velocity through a steep temperature gradient.

5.4.4 BRECCIA FACIES

Breccias overlying massive flows form the uppermost facies of a complete flow unit (Figure 5.9). Flow breccias typically account for <15% of most flows, range in thickness from <1m to 7m and are typically continuous along the length of the flow.

The breccia contains angular, blocky and plate-like fragments with lesser amoeboid "pillow" fragments in a fine matrix composed of andesitic fragments and hyaloclastite

(Plate 5.9). The contact with underlying lobe facies is irregular, with lobes of massive lava projecting upward into the breccia. Contacts between lobes and breccia are sharp with "in situ" brecciation of lobe margins and detachment of plate-like fragments from lobe crusts common (Plate 5.10).

Fragments

The most common fragment type is angular plates similar to those described in pillow breccias. Plate-like fragments range from 4cm to 20cm, typically possess one chilled margin and are identical to lobe and amoeboid fragment margins. Angular blocky fragments are less abundant than the plate variety and are typically <10cm in size. Both angular and plate-like fragments are composed of microlitic andesite with a hyalopilitic to intersertal texture.

Intact, amoeboid "pillows" completely surrounded by an altered sideromelane crust are identical to isolated pillows of pillow breccias (Plate 5.9). They are not a common fragment type and where they do occur, they are located at the base of the breccia. Amoeboid pillows are commonly "in situ" brecciated along fractures normal to their margins, by irregular polyhedral fractures, and along concentric joints. Fragments within "in situ" brecciated amoeboid pillows display various stages of rotation and separation of blocks. Plate-like angular blocks of andesite which predominate in the breccia are in part derived through brecciation of amoeboid pillows.

Matrix

The matrix is a massive, non-sorted, chaotic, medium-to fine-grained breccia with angular fragments ranging from <1cm to 3cm in size. Most fragments are microlitic andesite with hyalopilitic or intersertal textures similar to large angular fragments and the interior of amoeboid fragments within the breccia. Sideromelane and/or vitrophyric hyaloclastite constitutes a minor component. The proportion of hyaloclastite tends to increase toward the base of the breccia near lobe contacts.

Interpretation

Flow breccias are an integral component of subaqueous massive flows and form in an analogous manner to pillow breccias overlying tube-fed flows. Irregular amoeboid "pillows" are interpreted as isolated detached bodies derived from lobes which project into the breccia. Amoeboid pillows are absent in breccias that directly overly the massive lava.

"In situ" brecciation and autobrecciation of amoeboid "pillows" and lobe margins during flow advance would yield lithic fragments to the breccia. Sideromelane shard hyaloclastite, a minor matrix component, is interpreted to be the product of spalling and granulation of glassy crusts that envelopes lobes and amoeboid pillows.

5.5 CONTROLS ON THE FORMATION OF MASSIVE VERSUS PILLOWED FLOWS

Massive and pillowed flows are interpreted as distinct and separate flow types characterized by their own flow morphology and are not facies equivalents of a single flow. The generation of massive versus pillowed flows is not a function of differences in composition, viscosity, or extrusion temperature, as both have similar compositions, mineralogy, textures and amygdule content. The formation of massive or pillowed flows is attributed to the rate and volume of lava effusion (Walker 1972; 1973; Ballard et al.,1979). Massive flows are simple flows and may be the subaqueous analog of subaerial sheet-flood flows which form during brief, but voluminous eruption with high rates of effusion. Pillowed flows are compound flows and may be the subaqueous analog to tube-fed subaerial pahoehoe lava that are products of sustained eruptions with low effusion rates.

According to Walker (1973) the principal factor influencing the length of compositionally similar lava flows is the rate of effusion regardless of slope, topography and volume of lava extruded. Thus massive flows should have a greater areal extent than pillowed flows. This is not always the case in andesitic formations of the Mine Sequence. For example, massive and pillowed flows of the Rusty Ridge formation have similar lengths and, south of Duprat Lake, aerially extensive pillowed flows overly a restricted succession of ponded massive flows (Chapter 9). This seemingly incompatible relationship between flow type and extent may be explained by special circumstances during eruption of the Mine Sequence where mapping has shown flows to be ponded in fault blocks (Chapter 9). It appears that voluminous andesitic eruptions with a high effusion rate were sometimes accompanied by contemporaneous subsidence that restricted the extent of the resulting massive flows.

5.6 FLOW MORPHOLOGY AND EMPLACEMENT OF ANDESITIC FLOWS

5.6.1 PILLOWED FLOWS

Tube-fed pillowed flows are analogous to subaerial tube-fed pahoehoe flows and advance by budding new tubes or pillows. Ballard and Moore (1977) and Moore (1975) interpret that as an individual tube inflates with lava it ruptures along a ring fracture or break in the crust and a protrusion of new lava issues from the break. The protrusion is a new tube that quickly crusts over due to rapid quenching by seawater and as it continues to swell with lava it moves downslope in a caterpillar-tred manner analogous to subaerial lava toes. At some point the new lobe stops and may lie dormant, in which case it is covered by other advancing tubes, or like its predecessor, may bud a new lobe from its end, side or top and continues its course down slope. In this manner the flow front of pillowed flows have a digital advance identical to that described for subaerial tube-fed pahoehoe flows (MacDonald, 1972; Swanson; 1973). The digital advance of the flow front is fed by an intertwined and corded distributary system. Mega pillows may represent buried lava tubes, streams and secondary, smaller distributaries which fed the advancing flow front. These distributaries travel an irregular course to the flow front where they may have issued lava directly or through budding tubes. Lava carried by buried streams or tubes can be expected to reach the flow front at the same or a slightly lower temperature then when it entered the tube (Swanson, 1973). In subaerial eruptions the extent of tube-fed pahoehoe flows depends to a marked degree upon how early lava crusts over and is carried within buried streams (Swanson, 1973). This is even more critical in a submarine setting where interaction with surrounding seawater would quickly cool and impede flows.

In plan, various parts of the flow front were undoubtedly active at different times. The flow front may have advanced, on a large scale, like a prograding pillow delta fed by bifurcating and meandering tubes. Breccias would develop along the margins and upper surface of flows by autobrecciation of pillows, pillow budding and spalling and granulation of sideromelane pillow crusts.

This model for the emplacement of tube-fed submarine pillowed flows (Figure 5.8) is in accord with field observations and differs from Dimroth et al., (1978;1985) model in that:

a) andesite can issue from the vent as pillowed lava. Pillowed flows and small pillow volcanoes (Appendix A) can and do constitute a vent facies.

b) the primary delivery system for lava reaching the flow front is not massive lava that undergoes a facies transition to pillowed lava, but buried, interconnected lava tubes or streams.

c) pillowed flows are a discrete flow type produced by sustained eruptions with low effusion rates.

5.6.2 MASSIVE FLOWS

Assuming massive flows are products of voluminous andesitic eruptions with a high effusion rate, erupted lava would spread laterally (radially) away from its feeding fissure as a rapidly advancing sheet where all parts of the flow front advanced simultaneously (Figure 5.10). Irregularities in the underlying topography may cause some channelization but these would be quickly smoothed out by subsequent flows or surges. Channelization, may however, result in an initial surge of a single flow (cooling unit) to be covered by a later surge of the same lava flow producing a multiple or compound flow (Figure 5.10).

Proximal to the feeding fissure the flow surface may be characterized by either a smooth chilled flow top or thin flow breccia (Figure 5.10 B and C). The lobe and flow breccia facies develops within the upper part of the flow immediately away from its feeding fissure (Figure 5.10 A and B) and increases in proportion to massive lava toward the flow front. Once the lobe and flow breccia facies develop, lava moving within the massive facies would be insulated and could possibly arrive at the flow front with little loss in temperature and volatiles to further advance the flow. During the waning stage of an eruption (lower effusion rate) lobe-like forms and pillows may have developed at the flow front and margins to produce an aerially restricted pillow terminus. The lateral transition from massive and breccia facies to massive, lobe and breccia facies away from the feeding fissure in subaqueous flows may be analogous to the lateral transition from pahoehoe to aa lava in subaerial flows.

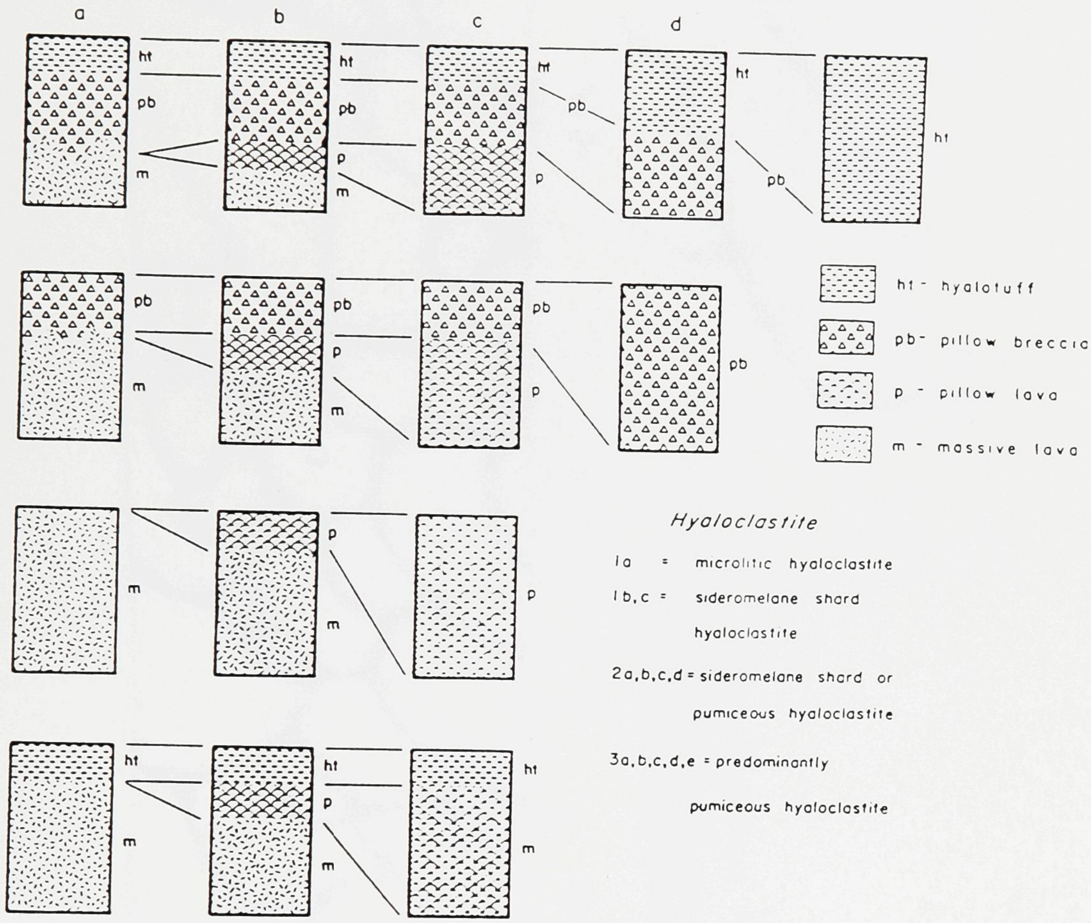

Figure 5.1. Vertical sequences in basaltic and andesitic flows of the Noranda area, after Dimroth et al., 1978.

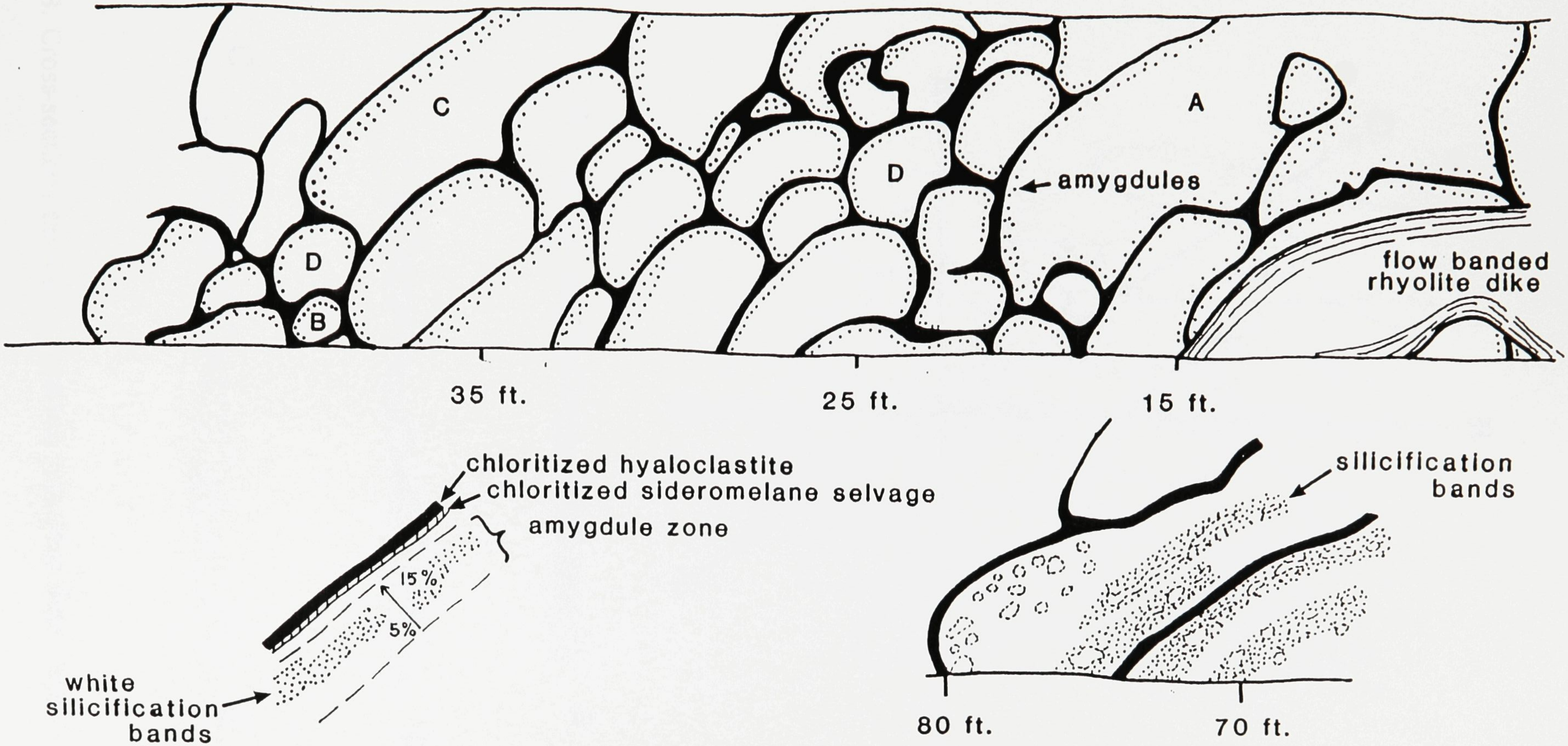

Figure 5.2. Oblique cross-section through a tube-fed pillowed andesitic flow of the Rusty Ridge formation at the Corbet Mine (7-02 drift). Note the diverse pillow shapes; A is a large mega-pillow, B spherical pillows, C mattress pillows and D a bun or balloon-shaped pillow. Amygdules are concentrated along pillow margins and toward the top of pillows.

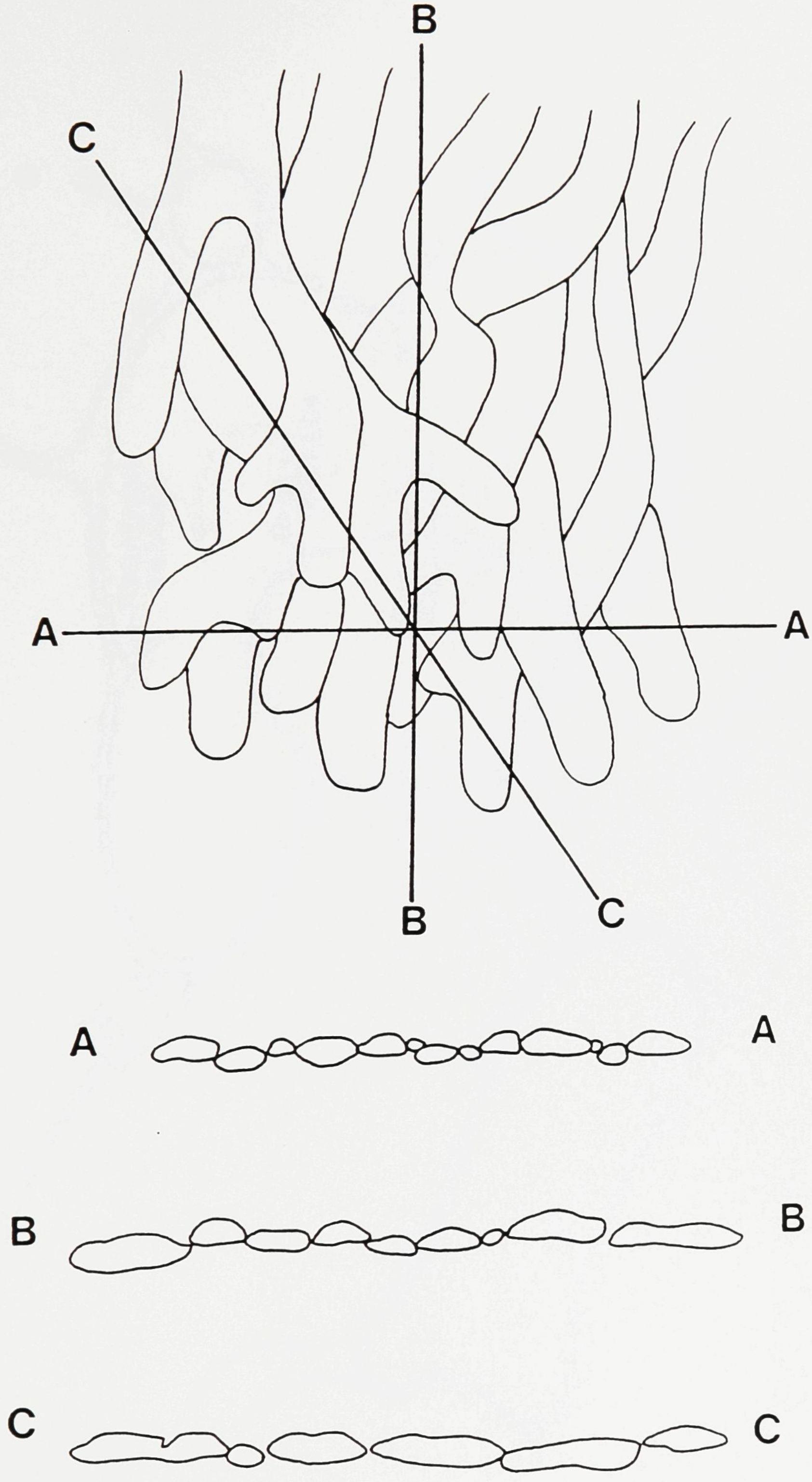

Figure 5.3. Cross-sections through a tube-fed pahoehoe flow, after Jones (1968).

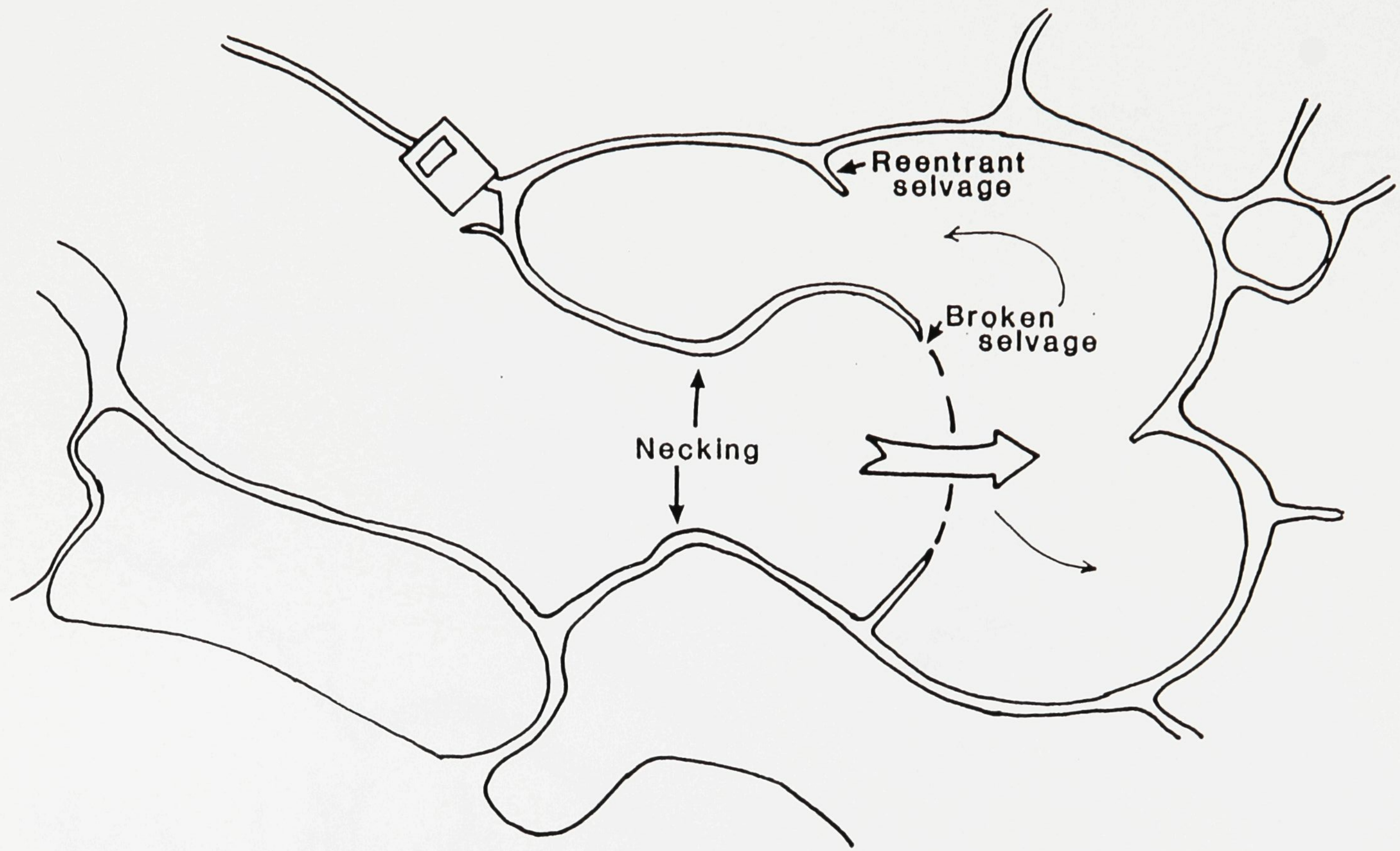

Figure 5.4. Oblique section through a tube-fed pillowed flow of the Millenbach Andesite formation. Broken selvedges and curved re-entrant selvedges suggest a flow direction during budding.

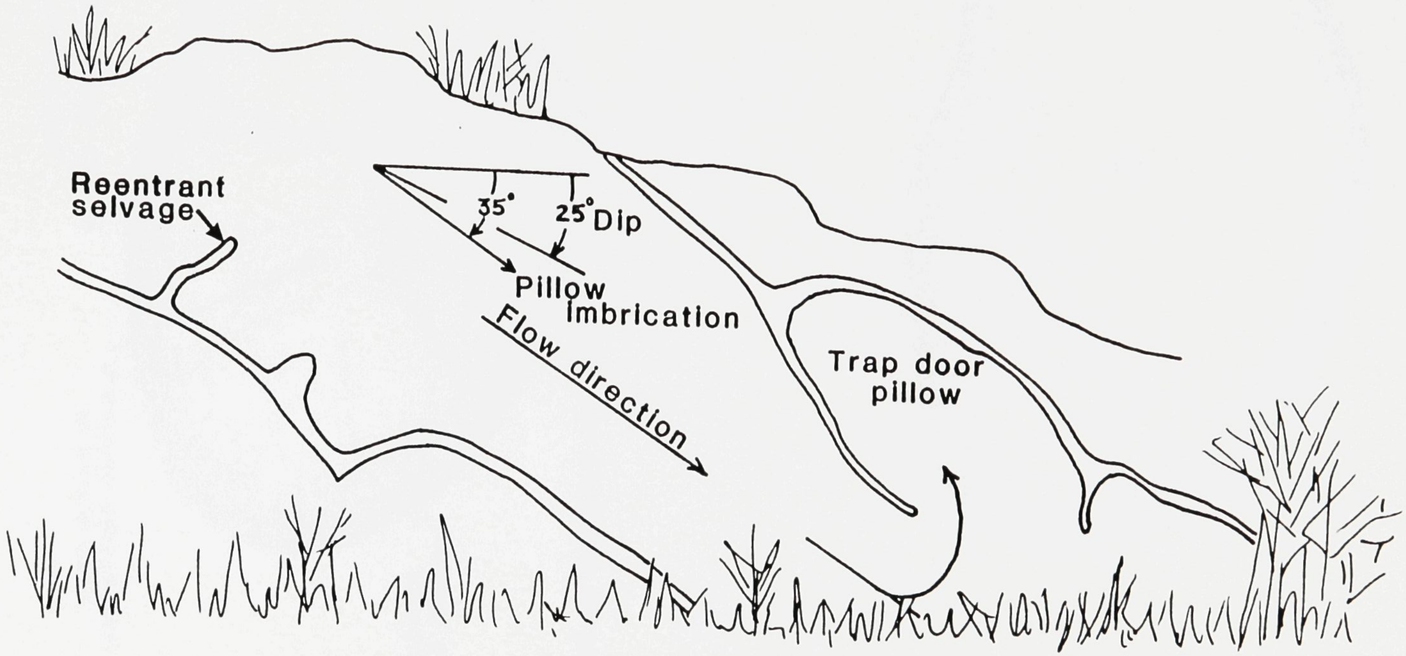

Figure 5.5. Oblique cross-section through a tube-fed pillowed flow of the Millenbach Andesite formation illustrating imbrication of pillows (10° to dip) and upward budding.

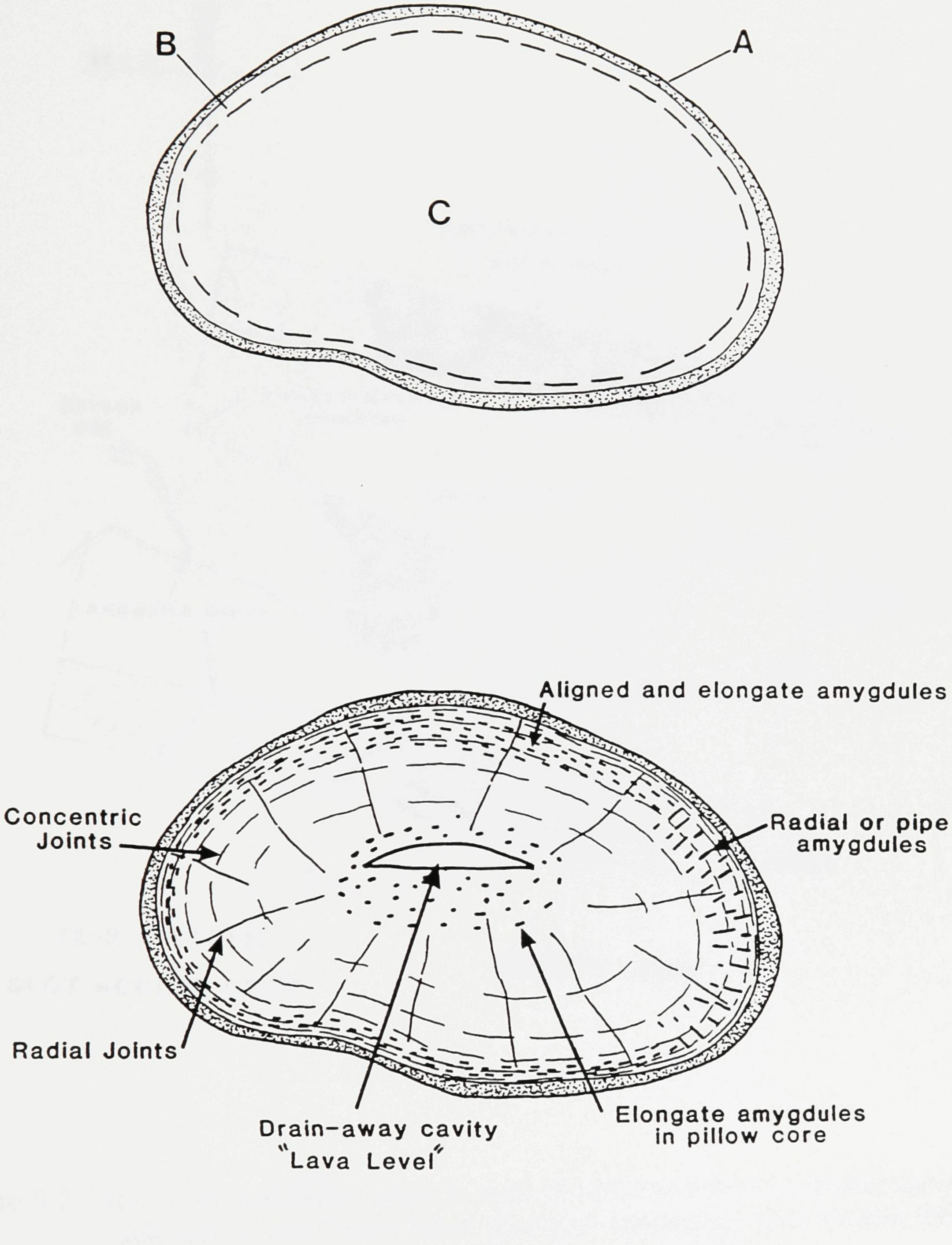

Figure 5.6. Structures and amygdule distribution within pillows.

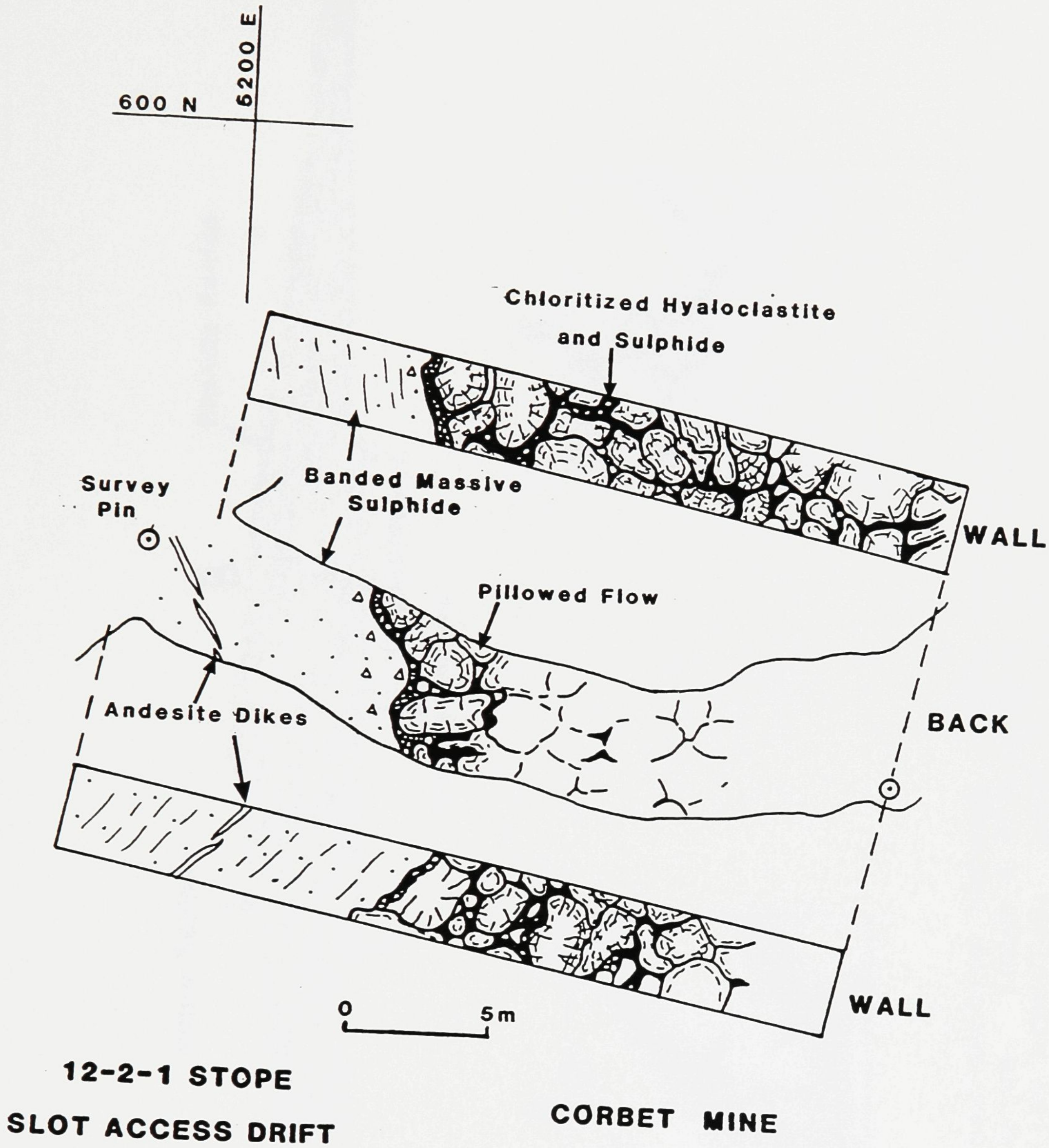

Figure 5.7. Well developed radial joints in tube-fed pillowed flow overlying massive sulphide at the Corbet Mine (Flavrian formation, 12-2 overcut drift). Note the range in size and diverse forms of pillows.

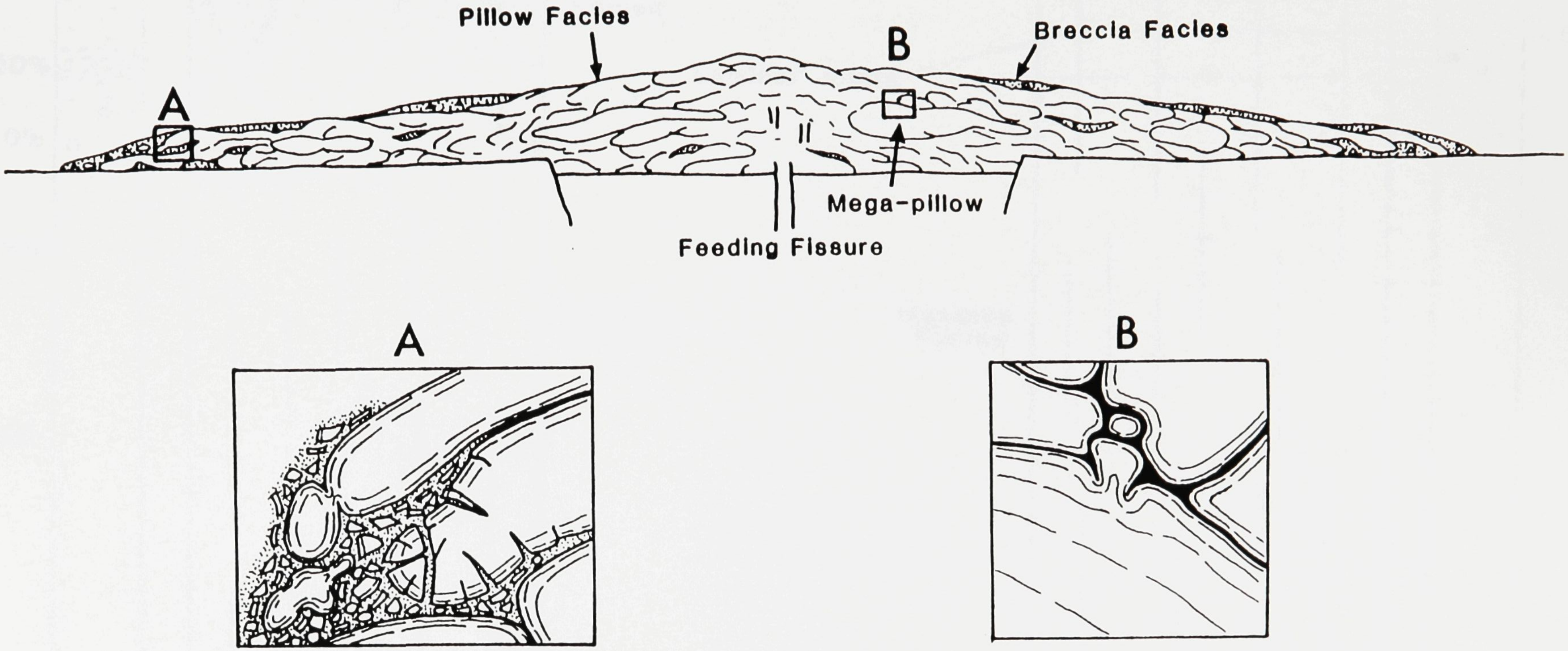

Figure 5.8. Idealized cross-section through a tube-fed pillowed flow showing both vertical and lateral facies. Inset A illustrates auto brecciation of pillows and budding to produce pillow breccias. Inset B illustrates the densely packed pillows which characterize the flow interior. Vertical exaggeration approximately 3X.

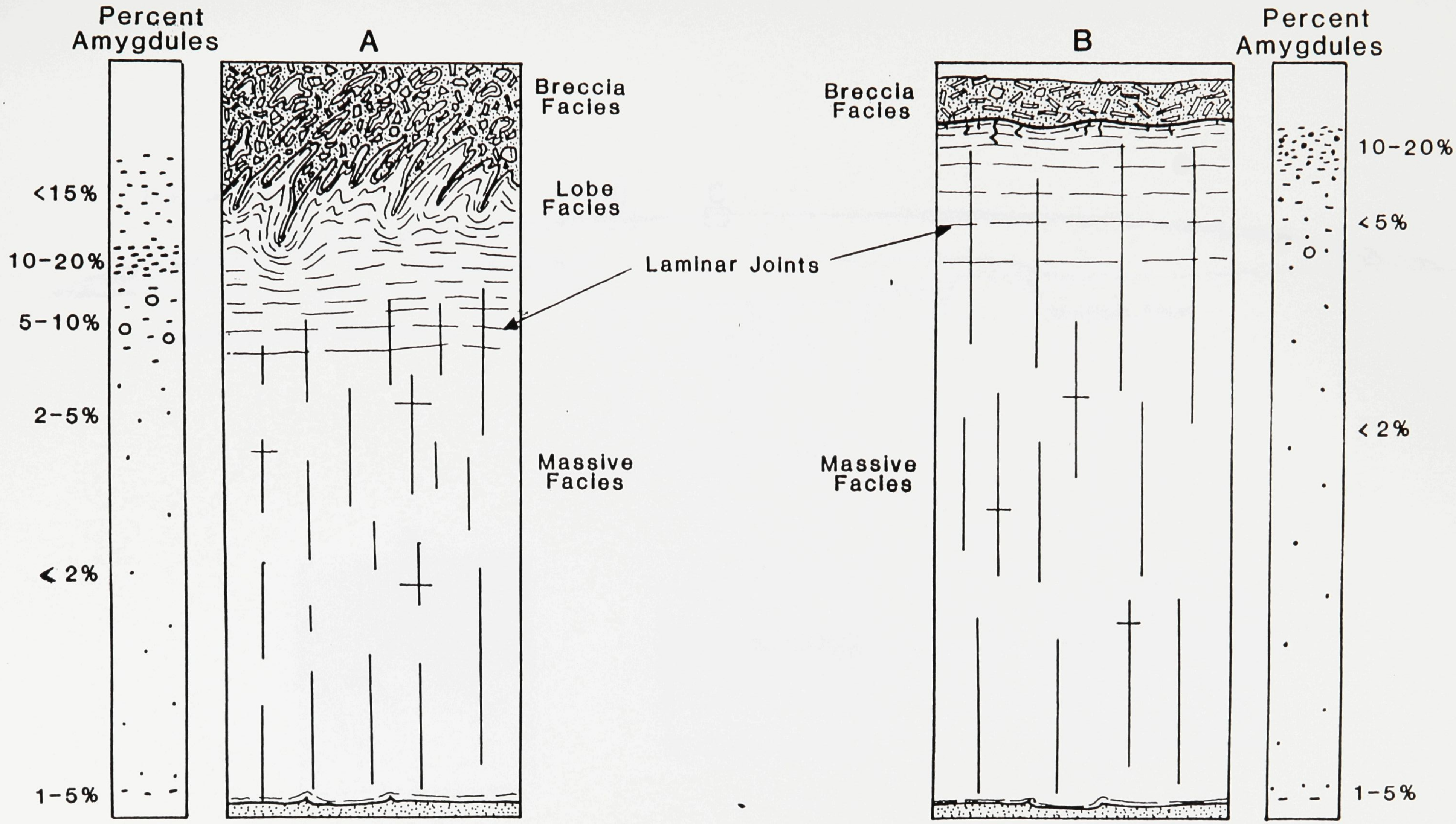

Figure 5.9. Vertical facies, structures and amygdule distribution within subaqueous massive andesitic flows.

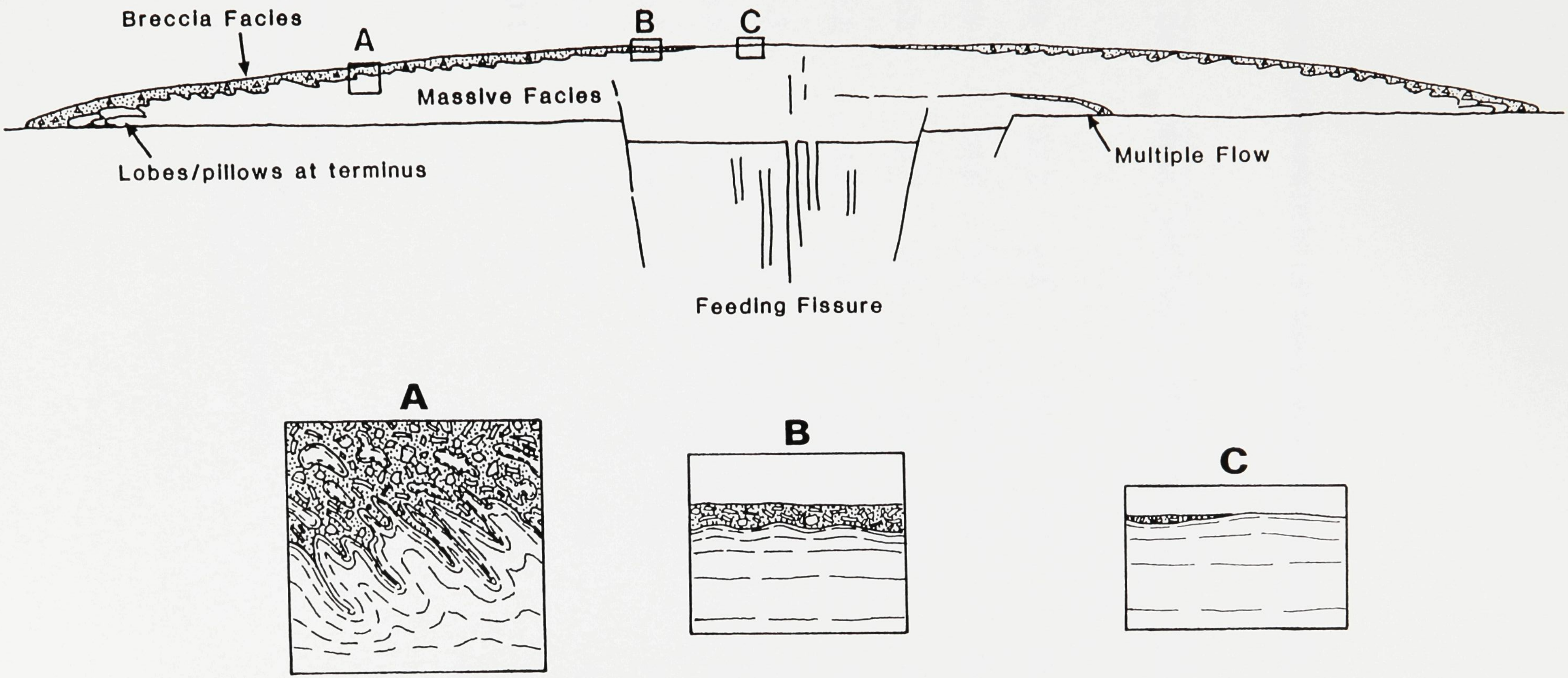

Figure 5.10. Idealized cross-section through a massive andesite flow showing both the vertical and lateral facies. Vertical exaggeration approximately 3X.

TABLE 5.1. AVERAGE COMPOSITION OF MINE SEQUENCE ANDESITIC FLOWS

	1		2		3		4	
	Mean	Std. Dev.	Mean	Std. Dev.	Mean	Std. Dev.	Mean	Std. Dev.
Wt. %								
SiO_2	56.1	3.9	57.7	4.2	63.3	8.4	56.6	2.2
Al_2O_3	15.6	0.8	14.6	1.2	13.8	3.0	16.0	0.8
Fe_2O_3	10.1	2.2	9.7	2.3	6.9	2.4	8.5	1.4
MgO	5.3	1.2	4.5	1.2	2.5	1.7	4.5	1.2
CaO	3.5	1.3	4.5	2.4	5.5	3.9	9.1	2.3
Na_2O	4.7	0.7	4.3	1.2	4.0	1.7	3.2	1.1
K_2O	0.3	0.2	0.5	0.5	0.5	0.4	0.9	0.2
TiO_2	1.3	0.4	1.3	0.2	1.0	0.2	1.2	0.2
P_2O_5	0.2	0.1	0.2	0.1	0.3	0.1	0.0	0.0
MnO	0.3	0.1	0.2	0.1	0.1	0.0	0.2	0.1

1. Flavrian Formation (17 analyses)
2. Rusty Ridge Formation (52 analyses)
3. Waite/Millenbach Andesite Formations (14 analyses)
4. Amulet Andesite Formation (9 analyses)

PLATE 5.1

A. Pilotaxitic texture where flow aligned plagioclase microlites wrap around amygdules filled by quartz, epidote and minor chlorite (pillow border, Flavrian formation). Field of view is 4mm; bar in **B** is 1mm long.

B. Fine intersertal texture of andesite from a pillow interior (Rusty Ridge formation). Note the "belt-buckle" forms of plagioclase microlites and "clots" of massive, homogeneous chlorite that are interpreted to replace former sideromelane. Bar is 1mm long.

C. Intersertal textured massive andesite with needle-like plagioclase microlites (Rusty Ridge formation). Field of view is 4mm.

D. Transitional intersertal-hyalophitic texture where massive, homogeneous chlorite, presumably after former sideromelane, partially surrounds some plagioclase microlites (Rusty Ridge formation). Bar is 1mm long.

E. Glomeroporphyritic clots of plagioclase phenocrysts in an intersertal textured groundmass (Rusty Ridge formation). Note the clots of massive chlorite, after original sideromelane, both within the groundmass and glomeroporphyritic clots. Field of view is 4mm.

F. Concentric joint defined by a thin line of opaque minerals and quartz-filled amygdules that are elongate parallel to the joint (Waite Andesite formation). Field of view is 4mm.

G. Laminated quartz crystal tuff from the Flavrian formation (Corbet Mine). Light coloured angular shards are broken quartz phenocrysts. Bar is 3mm long.

H. Fragmental matrix to breccias which occupy the Despina Fault southwest of the Corbet Mine. Curved, somewhat plate-like faintly flowbanded chloritized rhyolitic shards (P) and wispy, delicate and distinctly flow banded fragments of chloritized obsidian (W) predominate with minor angular fragments of massive rhyolite (M). Andesite fragments (A) although a minor component are ubiquitous as are shards of massive , homogeneous chlorite (S) that are interpreted to replace former obsidian. Bar is 3mm long.

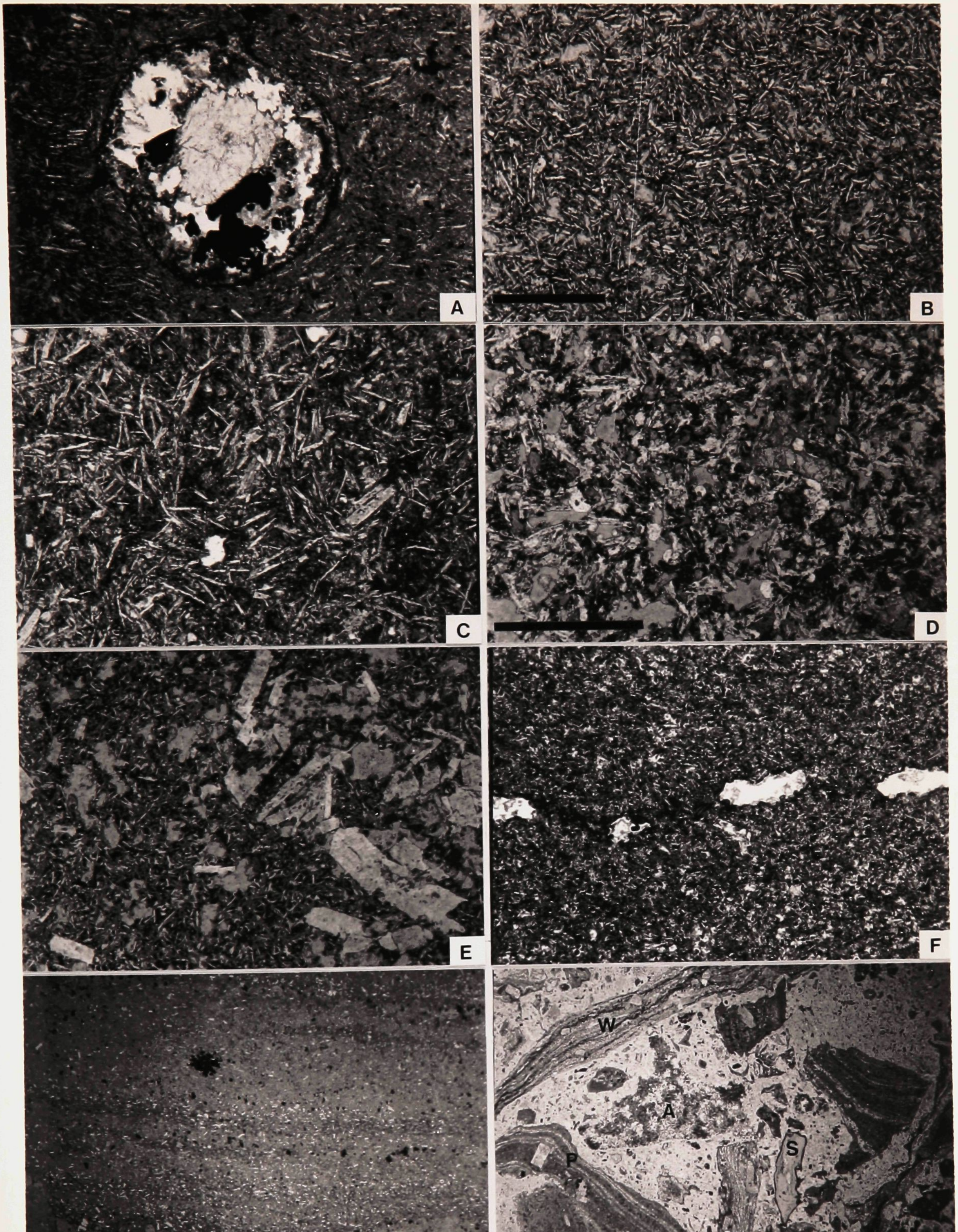

A
B
C
D
E
F
W
A
P
S
G
H

Plate 5.2. Irregular, densely packed pillows of the Rusty Ridge formation. Note the radial, "pipe" amygdules concentrated along the pillow margins and absence of significant hyaloclastite and breccia.

Plate 5.3. Bulbous pillows of the Rusty Ridge formation with well developed concentric joints (refer to Plate 5.5). Note the abundance of pillow breccia and hyaloclastite.

Plate 5.4. Upper surface of pillowed flow showing the tube-like form of individual pillows. Knob in background at right is pillow breccia which overlies the pillowed flow that dips shallowly to the east (left). Waite Andesite formation.

Plate 5.5. Well developed concentric joints which parallel the pillow margin (same flow as in Plate 5.3).

Plate 5.6. Polyhedral fractures within pillows of the Flavrian formation that overlie the #2 massive sulphide lens at the Corbet Mine. The fractures are filled with chalcopyrite, pyrrhotite and pyrite and are mantled by light coloured sericitic envelopes.

Plate 5.7. Parallel striations or corrugations within the pillow crust of pillows in Plate 5.4.

Plate 5.8. Finger-like lobes of massive andesite projecting upward into the overlying flow top breccia. Lobes are elongate and are oriented oblique to the flow contact indicating a right to left flow direction (Cote and Dimroth, 1978).

Plate 5.9. Blocky flow top breccias where plate-like fragments of massive andesite and intact "pillows" sit in a fine breccia and hyaloclastite matrix. Note the irregular contact with underlying lobes.

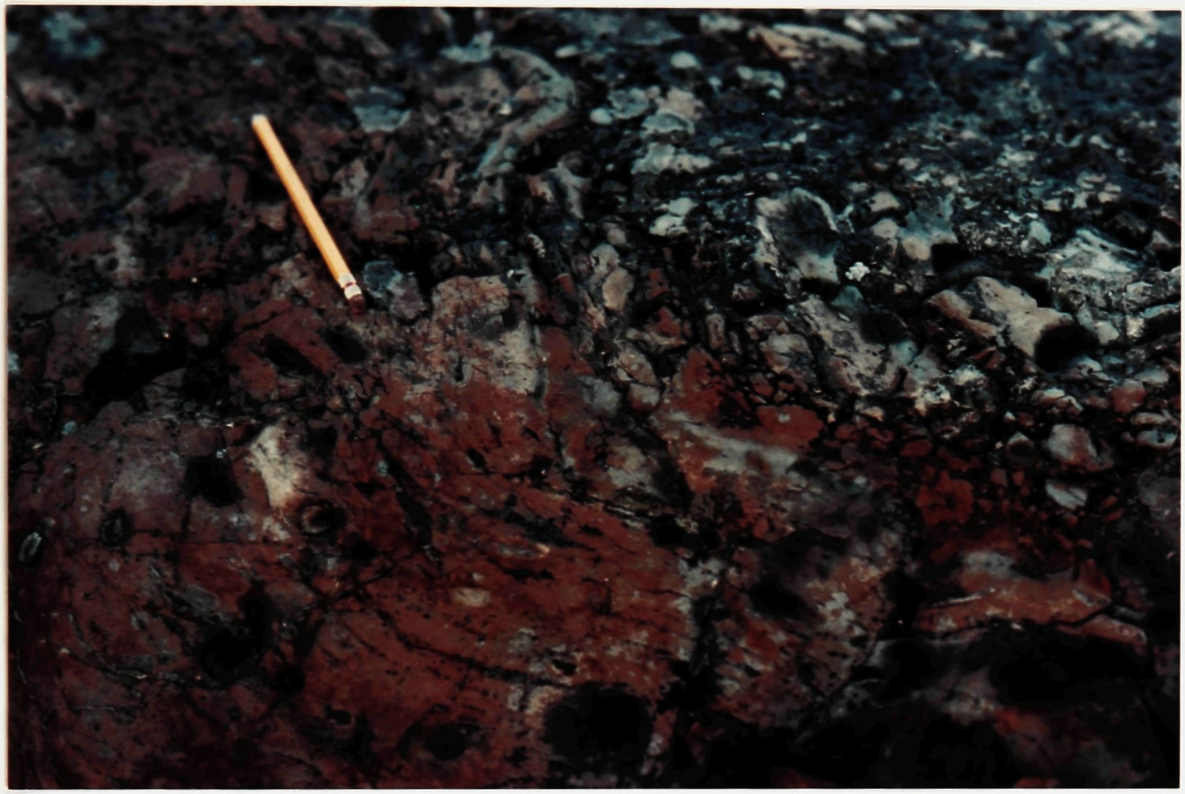

Plate 5.10. In situ brecciation of lobe margins in contact with overlying flow breccia.

6. TUFF UNITS AND SILICEOUS DEPOSITS

6.1 TUFF UNITS

6.1.1 DEFINITION AND DESCRIPTION

Tuff units are distinct, thin, units (< 1cm to 2m) composed of thin-bedded to laminated ash, chert and sulphide that have been referred to as exhalites (Ridler, 1971), tuffaceous exhalites (Comba, 1975) or tuffs (mine terminology). A typical tuff, as shown in Plate 6.1, consists of light coloured laminae containing fine-grained (< 0.01mm) quartz, interpreted as recrystallized chert, with subequal to minor amounts of albite and minor to accessory chlorite and sericite (Plate B.4C). Dark brown to light buff grey laminae consist of fine-grained (<0.01 mm) chlorite, actinolite, quartz and sericite with chloritized sideromelane and hyalopilitic shards, broken albite and occasionally quartz crystals, and small lithic fragments (Plate B.4C). Sulphides, chiefly pyrite with minor pyrrhotite, sphalerite and trace chalcopyrite (rare magnetite), occur as individual laminae or dispersed throughout chert and ash laminae. Crystal-rich tuffs (Plate 5.1G) are not common but have been recognized at both the Corbet and Ansil Mines.

Tuff units principally occur at formation/member contacts within the Mine Sequence and from oldest to youngest they are referred to as the Corbet Tuff (VF/VIN), Lewis Tuff (VIN/VIIR), Beecham Tuff (VIIR/VIIIA), Comba Tuff

(VIIIAL/VIIIAU), "C" Contact Tuff (VIIIA/IX W/M) and Main Contact/Norbec Tuff (XM/XIA; XW/XIA). Tuffs also occur at intraformational flow contacts where they are typically thin (< 0.3m) localized deposits that are rarely traceable for distances exceeding 0.5km. The discontinuous patchy distribution of tuff units at formational or flow contacts and localization within irregularities in the underlying flow may be a primary depositional feature or a function of preservation.

Thin-bedded to laminated, plane-bedded andesitic tuffs and feldspar crystal tuffs constitute a poorly exposed, localized, <10m thick deposit within the uppermost flows of the Amulet Andesite formation 300m south of the former Millenbach deposit. The andesitic tuffs are waterlain tuff and ash deposits that are interpreted to be the time -stratigraphic equivalent of the identical ash-tuff facies of the Powell Tuffs (Lichtblau, 1983) within the Powell Andesite formation of the Powell Block (Figure 9.2).

The "C" Contact Tuff, which is the most regionally extensive and traceable, consists of two facies. In the Amulet-Millenbach, Cranston, Vauze and parts of the Despina sector the unit is a sulphide-facies iron formation consisting of pyrite-rich laminae (> 20% pyrite, minor pyrrhotite and sphalerite) interbedded with black chert and ash beds (Plate 6.2). The sulphide-rich facies is best developed in the vicinity of known massive sulphide deposits in the Amulet-Millenbach sector which occur either at the "C" contact or directly above the "C" Contact in overlying Amulet Andesite and Millenbach Rhyolite formations. Elsewhere in the Flavrian

Block, the "C"-Contact Tuff is composed of chert and ash beds with or without sulphide laminae (< 5% pyrite).

6.1.2 INTERPRETATION

Tuffs are composed of two principal components (Comba, 1975; Kalogeropoulous and Scott, 1989). Plane parallel and mantle bedding indicate that the clastic or tuff component is a fine waterlain ash derived from explosive volcanic activity (subaqueous equivalent of air-fall tuffs). Undulating dune-like forms, cross-bedding and channel structures (Plate 6.3 and Appendix C), although not common, indicate lateral transportation during deposition of some tuffs. This may have been accomplished by reworking of waterlain deposits and transportation by turbidity flows, but other breccias show no evidence of subsequent reworking. Alternatively these structures, which are characteristic of the sandwave facies in base surge deposits (Fisher and Schmincke, 1984) may indicate deposition by subaqueous base surges, generated during phreatomagmatic eruptions (Appendix C). The chert/sulphide component is regarded as a chemical constituent introduced through discharge of submarine hotsprings.

Tuffs therefore, have a dual provenance; it is the latter provenance and association with submarine hotspring activity that has attracted explorationist and researcher for the past 25 years. The "chemical" component of tuffs is a key indicator of hydrothermal activity and discharge that may or may not be associated with deposition of massive sulphide deposits.

6.2 SILICEOUS DEPOSITS

6.2.1 DEFINITION AND DESCRIPTION

Siliceous deposits and the field term "silica-dumping" (Gibson, 1979) describe occurrences of massive to weakly laminated chert (< 0.01mm quartz grains) with or without sulphides (Plates 6.5 and 6.5) in inter-pillow areas and as the matrix to both andesitic and rhyolitic breccias. In the latter example massive chert has a distinctive vein-network appearance where it surrounds fragments of andesite or rhyolite and has been observed to grade upward (Millenbach Andesite, south of Turcotte lake) and laterally (Flavrian formation, Corbet Mine) into chert-rich tuff.

Siliceous deposits typically cover a small area (< 0.04km^2). Significant siliceous deposits occur in the uppermost flows of the Rusty Ridge formation (Amulet-Millenbach sector), in pillow breccias of the Millenbach Andesite formation, south of Turcotte lake, in pillow lavas of the Amulet Andesite formation adjacent to the Upper A deposit and in pillow lavas and breccias of the Flavrian formation at the Corbet Mine. Siliceous deposits resemble localized deposits of massive jasper observed within the Troodos Pillow Lavas immediately adjacent to some massive sulphide deposits (Watkinson et al., ;Plate 6.6).

6.2.2 INTERPRETATIONS

Siliceous deposits are interpreted to reflect high concentrations of chemical sedimentation over a restricted area. Massive chert is identical to the chemical component of tuff units and is interpreted to be a product of submarine hotspring activity. Siliceous deposits may define the discharge site of localized SiO_2-rich hotsprings which may be Archean analogs to low-temperature (< $200^{o}C$) white smokers which deposit various combinations of silica (opal), anhydrite, pyrite, sulphur and barite along active mid-ocean ridges (Hekinian et al., 1980; Styrt et al., 1981.

Like their modern analogs, silica-rich hotsprings in the Noranda area were spatially and temporally associated with VMS deposits. The recognition of siliceous deposits in Archean terrains is of prime importance in exploration as their occurrence can help outline and define paleo-hotspring fields which may contain economic VMS deposits.

Plate 6.1. Plane, parallel bedded tuff overlying a pillowed flow and underlying a massive flow of the Millenbach Andesite formation. The upper siliceous, light coloured bed is squeezed upward to surround fragments within the flow bottom breccia.

Plate 6.2. Plane parallel bedded, pyritic "C" contact tuff exposed on the 13th level of the Millenbach Mine (photo by P.Severin).

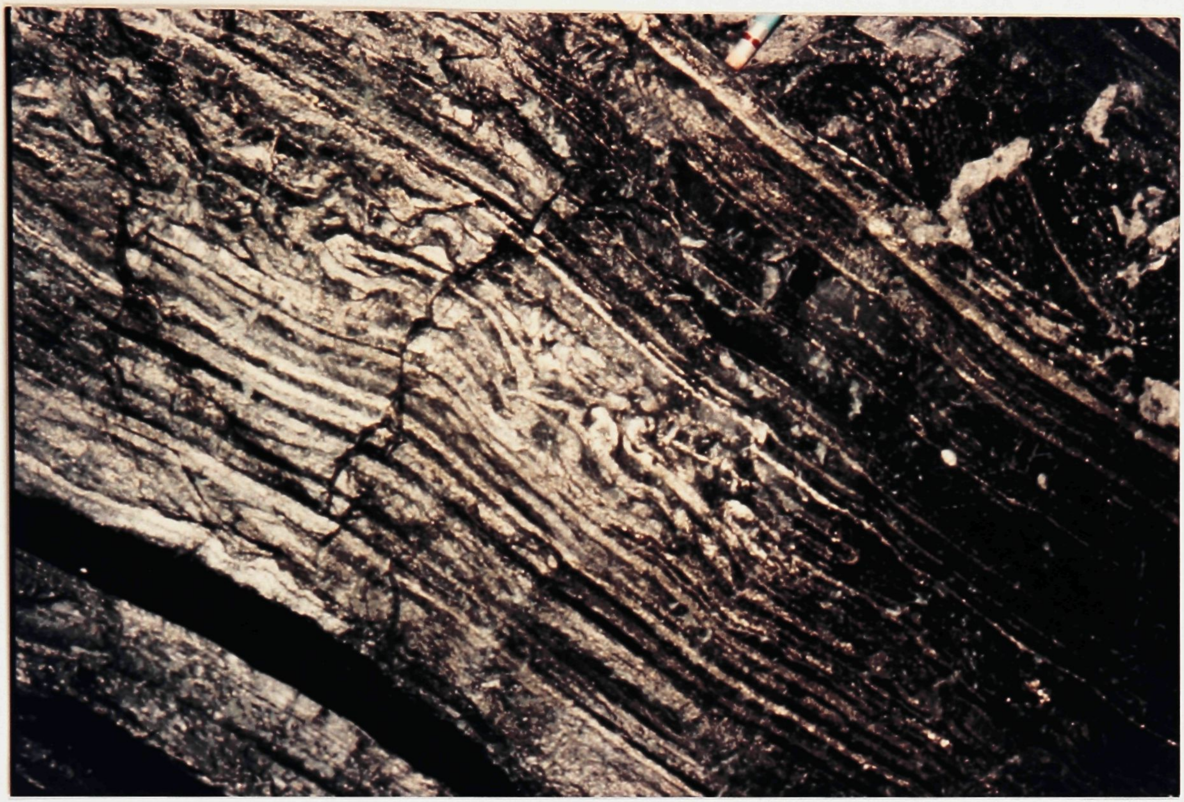

Plate 6.3. Sulphide bearing plane bedded and cross bedded tuffs with convolute bedding and dune-like structures (pencil) intercalated with andesitic flows of the Flavrian formation at the Corbet Mine.

Plate 6.4. Massive and laminated chert containing 1-3% sulphides cementing pillow breccias within the Millenbach Andesite formation.

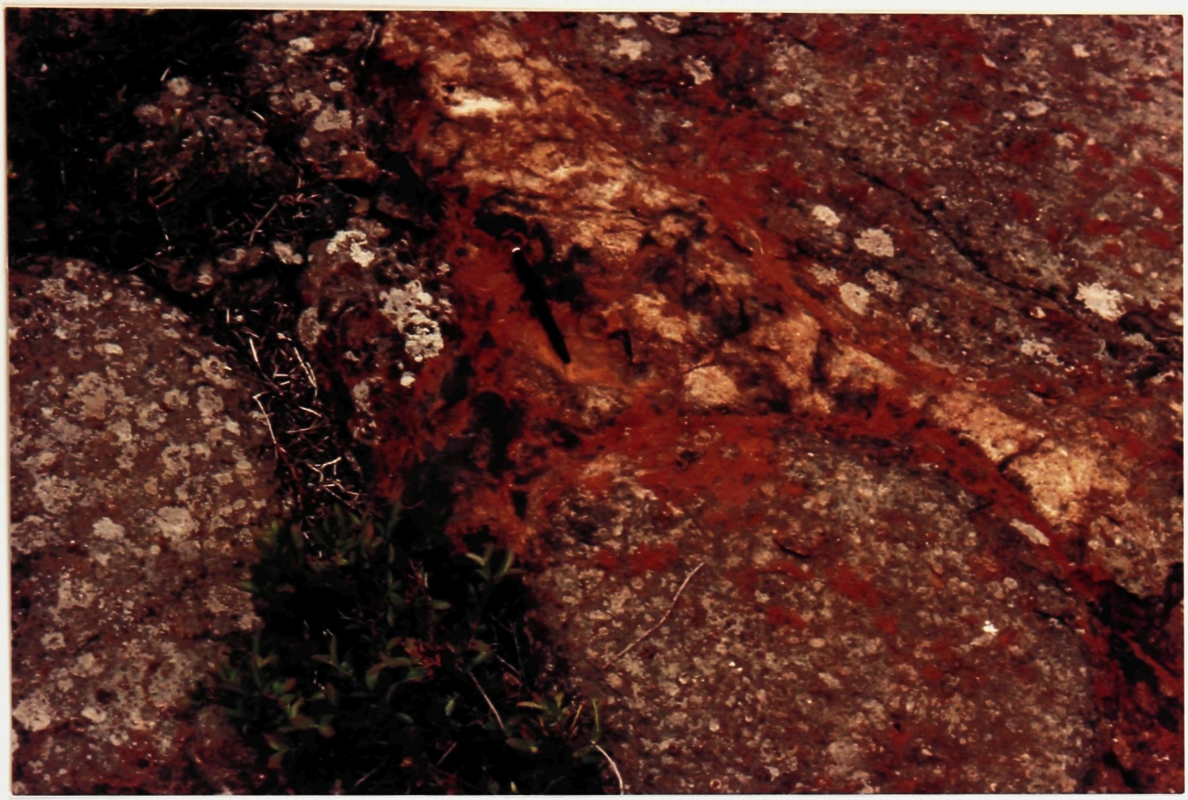

Plate 6.5. Massive, recrystallized chert between pillows at the Amulet Upper A glory hole.

Plate 6.6. Massive and laminated jasper between pillows peripheral to the Peristerka masive sulphide deposit, Cyprus.

7. VOLCANIC BRECCIAS

Pyroclastic breccias comprise less than 5% of the Mine Sequence. The breccias include deposits of monolithologic rhyolitic breccias and hetrolithologic, mixed andesite-rhyolite breccias (minor andesitic tuffs, lapilli tuffs and heterolithic breccias) and breccia dikes. Pyroclastic breccias within the Flavrian Block are described below. Breccias within the adjacent Powell Block have been described by de Rosen-Spence (1976) and Lichtblau and Dimroth (1980).

7.1 BEECHAM BRECCIA

Beecham Breccia is a distinctive marker unit located at the base of the Amulet lower member in the Amulet-Millenbach and F-Shaft sectors (Figure 7.1). West of the McDougall-Despina Fault, in the Despina sector, the breccia has been removed by intrusion of the Flavrian Pluton; the inferred original extent of this unit is illustrated on the isopach map of Figure 7.2.

Beecham Breccia conformably overlies andesitic flows of the Rusty Ridge formation and is conformably overlain by the Bedford and # 3 rhyolitic flows of the Amulet upper and lower members. The description and discussion which follow are based on both surface and underground exposures.

7.1.3 DESCRIPTION

Beecham Breccia consists of poorly sorted thick beds of lapilli tuff and tuff breccia intercalated with thinly bedded, laminated deposits of fine tuff as illustrated in Figures 7.3 and 7.4, and in Plates 7.1 and 7.2. The coarse breccia beds range from 10cm to 4m in thickness, are composed of angular to subangular lithic fragments (<1cm to >20cm), are poorly sorted, non-laminated and framework supported. The matrix, which comprises <20% of the breccia, is a fine, felsic "tuff" that consists of quartz and chlorite. The beds are massive, unstratified deposits but do show crude normal grading with large lithic fragments concentrated at the base of the bed and a marked increase in the proportion of matrix tuff within the upper 10-15cm of the bed.

Fragment types include: 1) amygdaloidal andesitic fragments, some of which are silicified; 2) aphanitic, amygdaloidal white siliceous fragments; and 3) massive and banded, spherulitic rhyolite. Andesitic fragments which have the same rusty brown colour as andesitic flows of the underlying Rusty Ridge formation dominate some breccia beds and in general increase in abundance toward the vent area in Figure 7.2. Strongly amygdaloidal or pumiceous fragments are noticeably absent. The matrix is composed of fine (<0.01mm) quartz with minor chlorite and opaque minerals. Pervasive silicification (both fragments and matrix) obscures primary constituents.

Plane-bedded, laminated, normally graded felsic tuff separates breccia beds and ranges in thickness from 1-10cm. The contact between tuff and underlying breccia is sharp and planar whereas the contact with overlying breccia is irregular and marked by loading structures. The sporadic distribution of tuff along the top of some breccia beds, absence above others, and occurrence as "rip-ups" (Plate 7.1, Figure 7.3) within the breccia suggests that deposits of laminated tuff were commonly eroded by and incorporated within succeeding breccia units.

7.1.1 VENT AREA

The vent for the Beecham Breccia is interpreted to lie within the McDougall Fault 1.7 km north of the Corbet mine and 200m northeast of Buttercup Hill (Figure 7.2). Felsic dikes which occupy the fault north and south of the vent area are massive rhyolite whereas in the proposed "vent area" the fault is occupied by a breccia dike (Figure 7.5). The breccia dike is composed of delicately banded wispy and massive rhyolitic fragments, chloritized rhyolitic hyaloclastite/vitrophyre shards and andesitic fragments. The similarity of fragments within the breccia dike to those within the Beecham breccia, the localized occurrence of the breccia dike within the uppermost flows of the Rusty Ridge formation which underlie Beecham Breccia, and its position within the depositional area of the breccia suggest that the breccia dike is an erosional remnant or neck of a vent from which the Beecham Breccia erupted (Figure 7.5A).

7.1.2 SUBSURFACE DISTRIBUTION

The isopach map in Figure 7.2, illustrates the subsurface distribution of the Beecham Breccia. The breccia occurs for 4km along the length of the McDougall-Despina Fault and extends <1km away from this structure. Beecham Breccia is thickest in distinct pockets immediately adjacent to the fault where it locally attains a maximum thickness of 50m. Comparison of the Beecham Breccia isopach to that of underlying Northwest formation (Figure 4.2), suggests that the breccia, like the intervening Rusty Ridge formation, is controlled by the paleotopography of underlying rhyolitic flows; the breccias are channelized, topographically controlled deposits. The apparent restriction of Beecham Breccia to areas south of the proposed vent may indicate that strata in the F-shaft, Amulet-Millenbach and Despina sectors were tilted to the south-southeast relative to sectors in the north prior to or during eruption and deposition of the breccia.

7.1.4 INTERPRETATION

Beecham Breccia is interpreted to be a subaqueous ash flow deposit. Individual breccia beds and overlying laminated ash units are interpreted to represent a single depositional unit, a product of single subaqueous ash flow (Fiske, 1963; Fiske and Matsuda, 1964; Yamada, 1973).

The coarse breccia base may represent deposits from a high concentration debris flow derived through collapse of an eruption column (Fiske and Matsuda,

1964) and the laminated tuff top, a deposit of intermittent pyroturbidite flows. Bomb sags, where lithic fragments symmetrically indent underlying ash beds (Plate 7.3), indicate subaqueous deposition and the presence of an eruption column that ballistically emplaced some fragments. Because of the total absence of pumiceous or scoriaceous fragments the breccias are interpreted to be products of successive phreatomagmatic eruptions where ascending rhyolitic magma interacted with near surface water preceding the onset of rhyolitic extrusive activity of the Amulet lower member (Chapter 9). The resulting ash flows were channelized by topographic depressions south of their vent.

7.2 RHYOLITIC BRECCIAS

Rhyolitic breccias within the Rusty Ridge and Waite Andesite formations occur as localized, thin, isolated deposits within andesitic flows. The breccias have only been intersected in drill holes and are not known to outcrop.

7.2.1 RHYOLITIC BRECCIAS OF THE RUSTY RIDGE FORMATION

Distribution and Thickness

Rhyolitic breccias of the Rusty Ridge formation in the Ansil sector have been intersected in drill holes south of Ansil Hill (Figures 7.6 and 9.4 Section I-I). The breccias are subdivided into units A, B, and C which occur at different stratigraphic intervals within the Rusty Ridge formation (Figure 7.6) as outlined below:

Unit	Statigraphic Position	Max.Thickness	Areal Extent
A1	<60m from top of VII R	23.4m	0.3 km^2
A2	60-100m from top of VII R	18.9m	0.08 km^2
B	midway within the VII R	25.0m	0.06 km^2
C	50-100m from base of VII R	17.25m	0.05 km^2

Description

Rhyolitic breccias of units A1 and A2 are most extensive and characteristics of this unit typify the others. The breccias are densely packed, framework supported, poorly sorted, chaotic deposits of non-bedded lapilli tuff and tuff breccia. Fragments are angular to subangular, and range from <1cm to 20cm in size. The predominant fragment types are massive aphyric and spherulitic rhyolite with subordinate, typically finer fragments of andesite. Large (10-15cm), subrounded fragments of amygdaloidal andesite identical to underlying flow top breccia occur as isolated blocks (<1%) within the breccia. The matrix is a fine tuff which constitutes <20% of the breccia.

The breccias are massive and unstratified or consist of successive depositional units (>1m) defined by variation in fragment size and proportion of andesitic to rhyolitic fragments. Beds sometimes display crude normal grading. Contacts with overlying and underlying flows are sharp with some incorporation of andesitic fragments. Thin bedded to laminated tuff (<10cm thick) locally occurs at the basal or upper contacts of the breccia.

Interpretation

Although a vent area has not been defined, rhyolitic breccias of units A, B and C are interpreted to be subaqueous hydrovolcanic explosion breccias. The lack of vesiculated fragments and occurrence of predominantly lithic rhyolitic fragments within an andesitic flow succession support an interpretation of explosive interaction of water with an ascending, contemporaneous rhyolitic magma.

7.2.2 RHYOLITIC BRECCIAS OF THE WAITE ANDESITE FORMATION

The Cranston breccia is a localized deposit within the basal flow units of the Waite Andesite formation and is the time-stratigraphic equivalent of breccias at Buttercup Hill (Appendix B). The Cranston breccia was intersected in three drill holes, DT-34 and WL-36-37 which lie north and south of the Cranston Fault (Figure 7.1 and 9.3 Section C-C). The breccias have a maximum thickness of 45m, and an estimated minimum surface area of 0.16 km^2. The Cranston breccia is not appreciably offset by the Cranston Fault (<70m) whereas underlying units show marked offset along this synvolcanic fault (Chapter 9).

Description

The Cranston breccia is an unsorted, non-stratified, framework supported, disorganized tuff breccia that is identical to intrusive breccias within the immediately underlying Cranston breccia dikes (Figure 9.3C). The breccia consists of angular to subangular, amygdaloidal (<3% amygdules) and massive, spherulitic rhyolitic blocks (5cm to >25cm) in a finer matrix composed of angular to subangular andesitic fragments (<1cm-10cm) and fine tuff (<15%). Contacts with underlying and overlying flows are sharp and conformable.

Vent Area

The Cranston White-Fragment (WF) breccia dikes are interpreted as feeder dikes to the immediately overlying Cranston breccia (Figure 9.3C). The predominance of lithic rhyolitic fragments within the breccia dikes and in the overlying Cranston breccia reflects the rock types cross-cut by the breccia dikes which, in this case, are "rooted" in the #1 rhyolitic flow of the Amulet lower member. Andesitic flows of the Amulet upper member are markedly thin in this area and contributed substantially fewer fragments.

Interpretation

The Cranston breccia, like stratigraphically equivalent breccias at Buttercup Hill (Appendix B), is interpreted to be a product of shallow phreatomagmatic eruptions where ascending andesitic magma explosively interacted with water.

7.3 BRECCIA DIKES

Breccia dikes are subdivided into rhyolitic breccias and "white-fragment" breccias. Rhyolitic breccia dikes are interpreted as products of explosive fluid-magma interaction during emplacement of synvolcanic rhyolitic dikes. White-fragment breccia dikes are also interpreted as products of hydrovolcanism, in this case the explosive interaction of ascending andesitic magma with an external fluid.

7.3.1 RHYOLITIC BRECCIA DIKES

Rhyolitic breccia dikes occupy the McDougall-Despina Fault in two areas (Figure 7.1). As described earlier, heterolithic breccia dikes within the McDougall Fault 1.7 km north of the Corbet Mine are interpreted as an erosional remnant of a vent to the Beecham Breccia. The second area lies southeast of the former Corbet mine where rhyolitic breccias and subordinate massive rhyolitic dikes occupy the McDougall and Despina Fault for 1.2 km until they merge with the overlying Here Creek Rhyolite formation (Cycle 4). The latter breccias are described below.

Definition and Description

Rhyolitic breccia dikes are chaotic, unsorted intrusive breccias. Setterfield (1984; 1987) distinguished 3 principal fragment types:

1. curved, angular to somewhat plate-like and faintly banded, chloritized rhyolitic obsidian shards (6cm to <1cm), Plates 4.1H and 7.4.

2. thin, wavy, distinctly banded, elongate wispy fragments of obsidian with length to width ratios of up to 30 to 1, Plates 4.1H and 7.4.

3. blocky, angular fragments of massive rhyolite identical to associated rhyolitic lobes and dikes.

Two additional fragment types are also common. The first are massive andesitic fragments which occur as angular xenoliths up to 1m and rounded microxenoliths <1cm in size (Plates 7.4 and 4.1H). The second, are irregular isolated lobes of spectacularly banded chloritized spherulitic obsidian up to 2m in size, displaying various degrees of boundary disintegration and fragment incorporation into surrounding breccia.

Rhyolitic breccias are intimately associated with massive spherulitic rhyolite identical to that of associated dikes. Massive spherulitic rhyolite in contact with breccia is mantled by an outer distinctly banded, chloritized obsidian margin.

Orientation of the banding changes from parallel laminae adjacent to massive rhyolite (parallel to rhyolite/breccia contact) to irregular contorted banding near the breccia contact. Isolated lobes of banded chloritized obsidian in the breccia are interpreted to be detached protrusions from massive rhyolite. Setterfield (1984; 1987) likened intrusive massive rhyolite and lobes/breccia within the fault to rhyolitic lobes and hyaloclastite typical of subaqueous lobe-hyaloclastite flows. The major differences are the lack of an intact massive obsidian selvage at the banded margin of massive rhyolitic lobes, and occurrence of andesitic xenoliths within the rhyolitic breccia dikes.

The dominant fragment type (Setterfield; 1984, 1987) is angular, curved, shard-like chloritized obsidian which displays smooth concave and convex edges and is replaced by massive chlorite. Individual flow bands are composed of chlorite, quartz and/or epidote. Perlitic cracks, although not common, attest to the original "glassy" nature of the shards. Wavy banded, wispy, fragments, initially interpreted in the field as collapsed pumice (Plate 4.1H), were interpreted by Setterfield (1984, 1987) as chloritized finely banded obsidian and were probably derived through breakup and disintegration of banded obsidian of detached lobes and margins of massive spherulitic rhyolite. Amygdules are not common but some fragments do contain up to 20% amygdules (Setterfield; 1984, 1987). Shard-like obsidian fragments range to <2mm in size where they grade into a fine-grained matrix of granular quartz with minor albite. Phenocrysts of quartz and albite, the latter sometimes broken, are common matrix constituents.

Origin

The absence of pumiceous fragments, rarity of Y-shaped shards and fragment morphology which indicate fragmentation through thermal strain and shattering and not explosive release of juvenile volatiles (Heiken, 1972) led Setterfield (1984, 1987) to conclude that the breccias are a product of hydrovolcanism. Setterfield envisaged passive, non-explosive fragmentation of the massive rhyolite related to interaction of pulses of ascending magma with downward migrating seawater or hydrothermal fluids that were using the faults as discharge channelways. Characteristics of the breccia, however, suggest that fragmentation was not solely passive but that magma/fluid interaction was accompanied by rapid and confined (within a fissure) steam generation that resulted in near surface phreatomagatic explosions at the top of the rising magma column. Evidence for explosive fluid/magma interaction include:

1. fragment morphology is compatible with fragmentation resulting from hydrovolcanism either passive, through thermal strain and granulation and/or through hydrovolcanic explosions.

2. broken phenocrysts are not typical of rhyolite "hyalocastites" but are typical product of explosive fragmentation.

3. restriction of andesitic xenoliths to the breccia led Setterfield, to propose that stoping of fissure walls was accomplished not by rising rhyolitic magma but by unconsolidated breccia. Hydrovolcanic explosions offer a more plausible explanation, with andesitic xenoliths stoped and entrained within a coherent rapidly ascending breccia. Accidental fragments are characteristic of shallow phreatomagmatic explosions and result in typical heterolithologic, unsorted surface deposits (Fisher and Schmincke, 1984).

4. Andesitic xenolith trains up to 5m in length (<0.5m width) aligned parallel to dike margins are more likely to form by forceful stoping and entrainment within a rapidly ascending breccia, rather than by an unconsolidated breccia pushed to surface by underlying magma.

Shallow phreatomagmatic explosions during initial magma ascent may have vented at surface to deposit a thin, localized breccia at the base of the Here Creek Rhyolite formation (Lichtblau, 1983). Massive rhyolite which also occupies the fault and dominates the structure immediately below the Here Creek Rhyolite formation is interpreted by Setterfield (1984, 1987) as feeders to the overlying Here Creek flows. Thus rhyolitic dike emplacement characterized by initial near-surface explosive activity (phreatomagmatic eruption) was followed by passive fissure eruption of rhyolitic lava.

7.3.2 WHITE-FRAGMENT BRECCIA DIKES

Distribution and Orientation

The distribution and surface trace of white-fragment breccia dikes are illustrated in Figure 7.1. Most dikes occur in the Amulet-Millenbach and Despina sectors with a single dike, the Cranston Breccia dike, located in the north part of the Ansil sector 100m south of the Cranston Fault. White-fragment (WF) breccia dikes trend 070^0 and dip steeply at 70^0-80^0 north in the Amulet-Millenbach sector, to north 20-25^0 east and steeply west dipping (70-80^0) in the Despina sector (including Buttercup Hill, Appendix II) and strike 090^0 to 130^0 southeast and have near vertical dips in the Ansil sector. In the Ansil and Amulet-Millenbach sectors white-fragment breccia dikes are oriented perpendicular to flow contacts, whereas in the Despina sector the dikes are oriented approximately parallel to flow contacts. This orientation in the Despina sector suggests that down-faulting of the Despina sector along the McDougall-Despina Fault was accompanied by tilting such that later breccia dikes oriented at a high angle to the McDougall-Despina Fault intersected flow contacts at different angles on either side of the structure. White-fragment breccia dikes also have a distinct stratigraphic control as they all occur within silicified andesite 200m from the top of the Amulet Upper member.

Field Characteristics

Individual WF breccia dikes range in thickness from <10cm to 40m (average 1-2m) and are traceable for up to 180m along strike. The dikes pinch and swell along strike, occur singly or bifurcate.

The breccia wall-rock contacts range from straight to irregular and are either sharp and abrupt or gradational. Where gradational the dike margins are shattered and veined by the dike matrix resulting in an "in situ" where fragments display all stages of detachment from the wall rocks and from each other within the dike (Gibson, 1979).

Fragments within the breccia dikes are dominantly andesite although variably altered and, especially, silicified. In the Cranston WF breccia dike, fragments greater than 10cm are predominantly rhyolite. Andesitic fragments are brown to white weathering (silicified), range to 0.4m in size, are typically quartz and/or quartz-, epidote- and actinolite-amygdaloidal (up to 20% amygdules), finely feldspar-porphyritic (<3%, <2mm phenocrysts) and may be finely banded or display laminar jointing. Fragments are typically angular and blocky but fragments <5cm tend to be subangular. WF breccia dikes are unsorted with respect to fragment shape and size with fragments ranging from 0.5cm to microscopic. The breccias are chaotic and lack any internal structure.

Origin

WF breccia dikes are identical to those at Buttercup Hill described in detail in Appendix B. These discordant breccias are interpreted to be the shallow root zones (erosional remnants) of vents where phreatomagmatic explosion breccias erupted on the sea floor. This relationship is most evident at Buttercup Hill where WF breccia dikes were traced upward into a conformable unsorted breccia that rests on flows of the Millenbach Andesite formation. Identical localized breccia deposits located within the lowermost flows of the Millenbach formation (Appendix B), exposed at surface in the Beaver Meadow area (Figure B.1) and intersected in drill holes (D-416), are interpreted to be hydrovolcanic explosion breccias. As described earlier the Cranston WF breccia dikes are interpreted to feed an overlying, localized rhyolitic breccia that rests conformably on andesitic flows of the Waite Andesite formation.

Unlike rhyolitic breccia dikes of the McDougall-Despina structure where breccias are observed to be directly related to fragmentation of associated massive rhyolite dikes, "high level" dikes were not recognized within structures occupied by WF breccia dikes. Several lines of evidence indicate that WF breccia dikes are products of shallow phreatomagmatic explosions related to emplacement of andesitic dikes during the onset of andesitic surface eruptions:

1. the matrix of white-fragment breccia dikes contain unsilicified shards of chloritized andesitic sideromelane and hyalopilitic andesite that display smooth curved, concave and convex boundaries and shard-like shapes that are typical of fragments derived from hydrovolcanic, not pyroclastic, eruptions. These fragments were not derived from adjacent wall-rocks, but are foreign, and may represent juvenile andesitic magma.

2. the surface deposits of phreatomagmatic eruptions, as at Buttercup Hill, typically occur within the basal andesitic flows of the overlying Millenbach and Waite Andesite formations. Thus phreatomagmatic explosions and emplacement/venting of WF breccia dikes did not occur during a pause in volcanic activity but during the onset of andesitic volcanism that was undoubtedly accompanied by emplacement of high level andesitic feeder dikes and blind intrusions.

The fluid which interacted with rising andesitic magma may have been downward migrating seawater or hydrothermal fluid. It is significant that a period of widespread hydrothermal fluid circulation and discharge followed extrusion of the Amulet upper member (Chapter 12). Ascending andesitic magma would undoubtedly follow existing faults that were also focusing discharge of hydrothermal fluids to the sea floor (Gibson et al., 1983). Widespread shallow hydroclastic explosions that mark this time-stratigraphic interval may be a product of andesite magma-hydrothermal fluid interaction as described in modern and younger hydrothermal systems (Hedenquist and Henley, 1985).

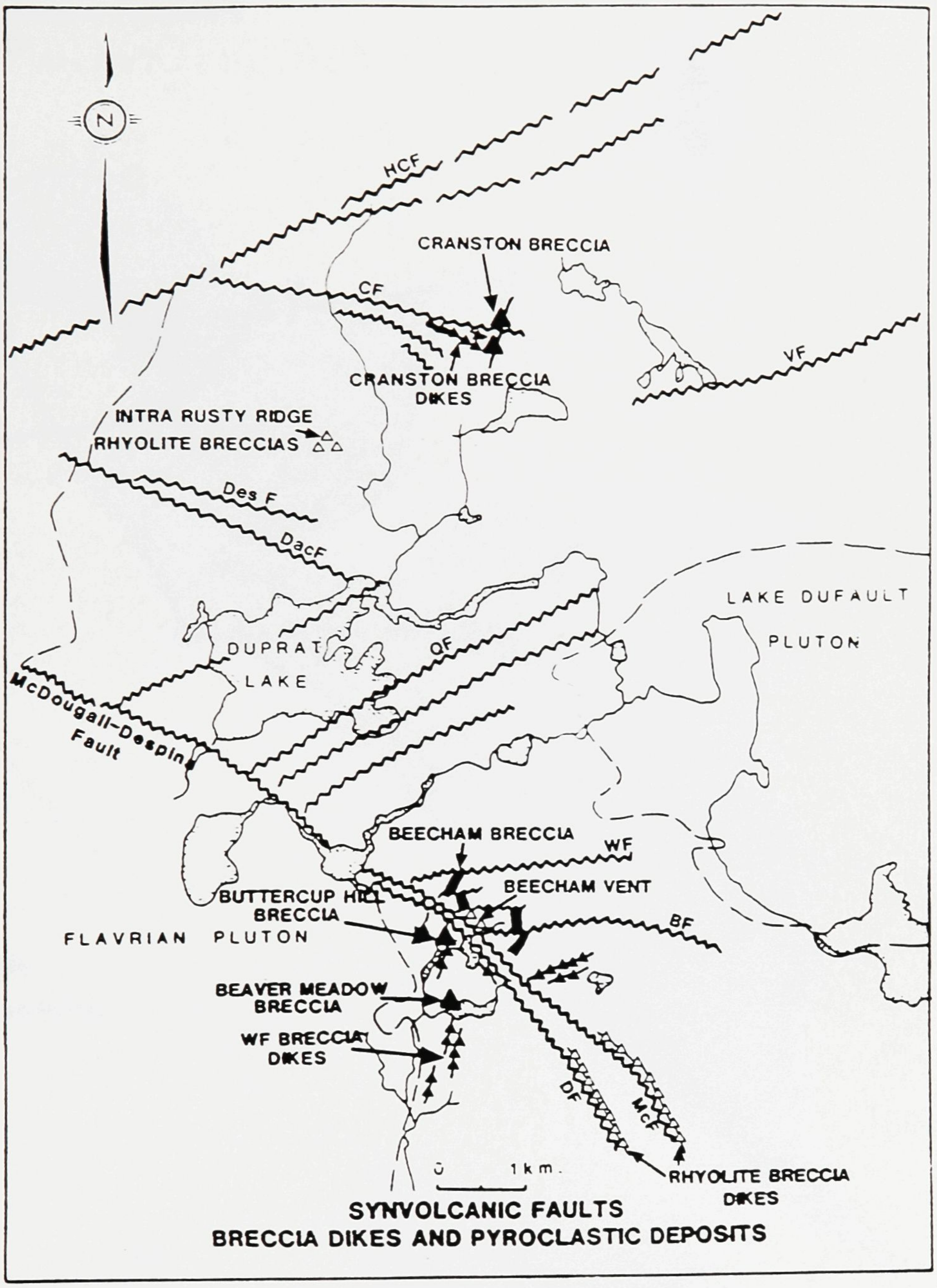

Figure 7.1. Location of volcanic breccias, breccia dikes and synvolcanic faults; HCF-Hunter Creek Fault, CF-Cranston Fault, DacF-Dacite Fault, DesF-Des Fault, QF-Quesabe Fault, WF-Walker fault, BF-Bancroft Fault, McF-McDougall Fault, VF-Vauze Fault and DF-Despina Fault.

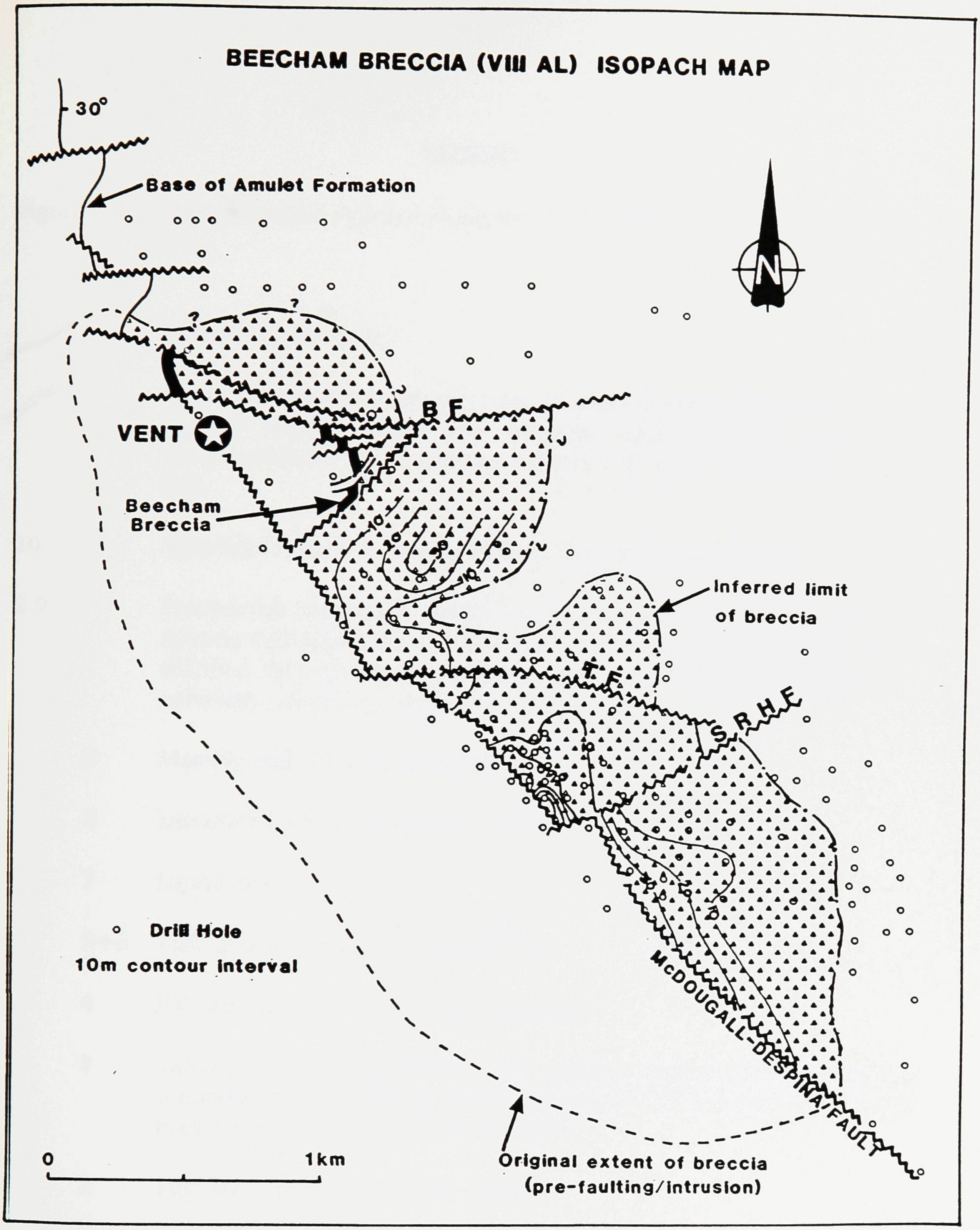

Figure 7.2. Isopach map of the Beecham Breccia (Amulet lower member); BF-Bancroft Fault and SRHF-South Rusty Hill Fault.

LEGEND

Figure 7.3. Beecham Breccia exposed along the 7-02 exploration drift at the Corbet Mine.

Massive pyrite beds.

Thin (1-6cm) discontinuous beds of plane-bedded tuff with smooth, regular basal contacts and irregular upper contacts with well developed flame structures and indented by clasts of overlying breccia bed.

10 Spherulitic rhyolite flow with basal breccia (Amulet lower member).

2-9 Framework supported, poorly sorted breccias containing dark green aphyric and aphanitic, angular andesite fragments -some with white silicified rims and white, amygdaloidal rhyolite fragments in an aphanitic, siliceous matrix (10 - 30%).

- 9 Massive tuff with 15-20% felsic lapilli.
- 8 Laminated tuff with massive pyrite at base.
- 7 Lapilli tuff.
- 5+6 Tuff breccia, crude normal grading.
- 4 Feldspar crystal tuff (15% plagioclase).
- 3 Thin bedded to laminated tuff with massive sulphides. Where tuff has slumped into underlying breccia individual tuff beds are replaced by massive pyrite at contact with breccia.
- 2 Tuff breccia, crude normal grading.

1 Massive andesite flow containing 1-3% pyrite-quartz filled amygdules and irregular, siliceous alteration patches (Rusty Ridge formation).

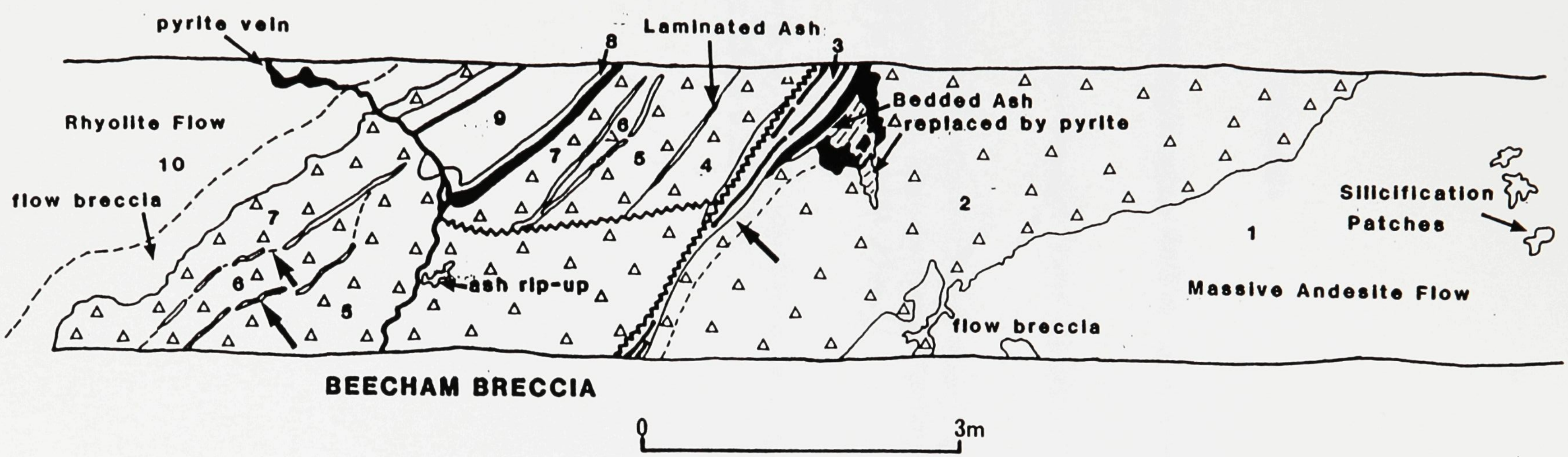
pyrite vein
Laminated Ash
8
3
Bedded Ash
replaced by pyrite
Rhyolite Flow
10
9
7
6
5
4
flow breccia
7
6
5
ash rip-up
2
1
Silicification
Patches
Massive Andesite Flow
flow breccia
BEECHAM BRECCIA
0
3m

LEGEND

Figure 7.4. Beecham Breccia, 7-02 exploration drift at the Corbet Mine.

3	Spherulitic rhyolite flow (Amulet lower member).
2	Poorly sorted, framework supported and crudely graded (normal) tuff breccias and lapilli tuffs. Thin discontinuous deposits of laminated tuff separate coarser depositional units.
1	Massive andesitic flow, weakly silicified along fractures and around amygdules (Rusty Ridge formation).

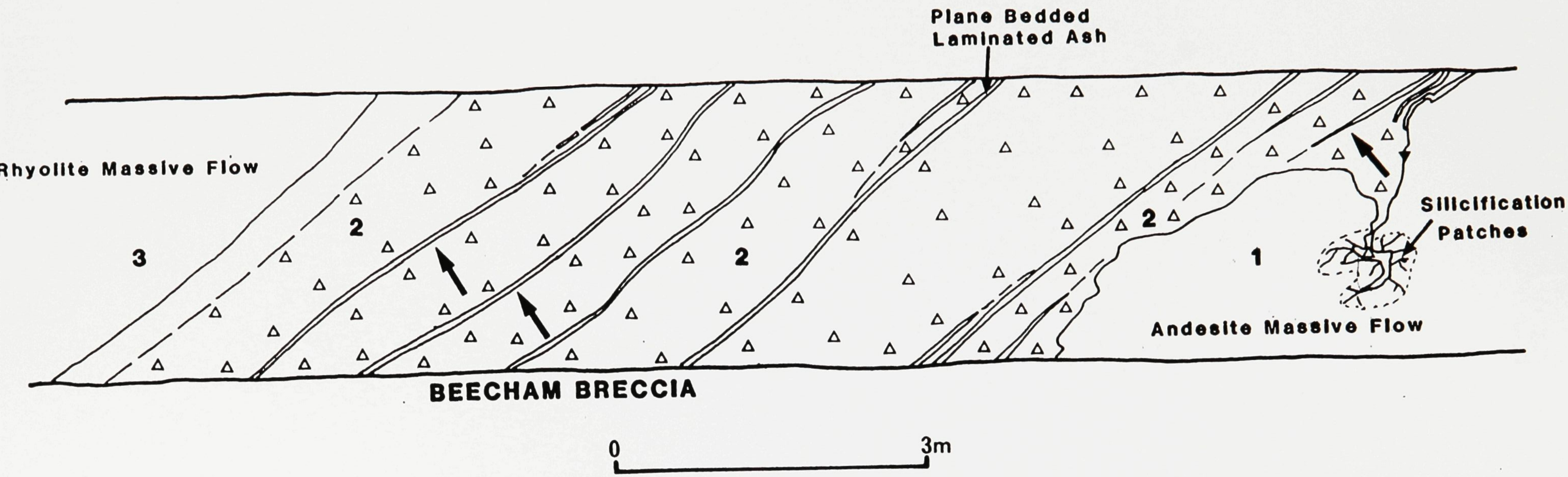
Plane Bedded
Laminated Ash
Rhyolite Massive Flow
3
2
2
2
1
Silicification
Patches
Andesite Massive Flow
BEECHAM BRECCIA
0
3m

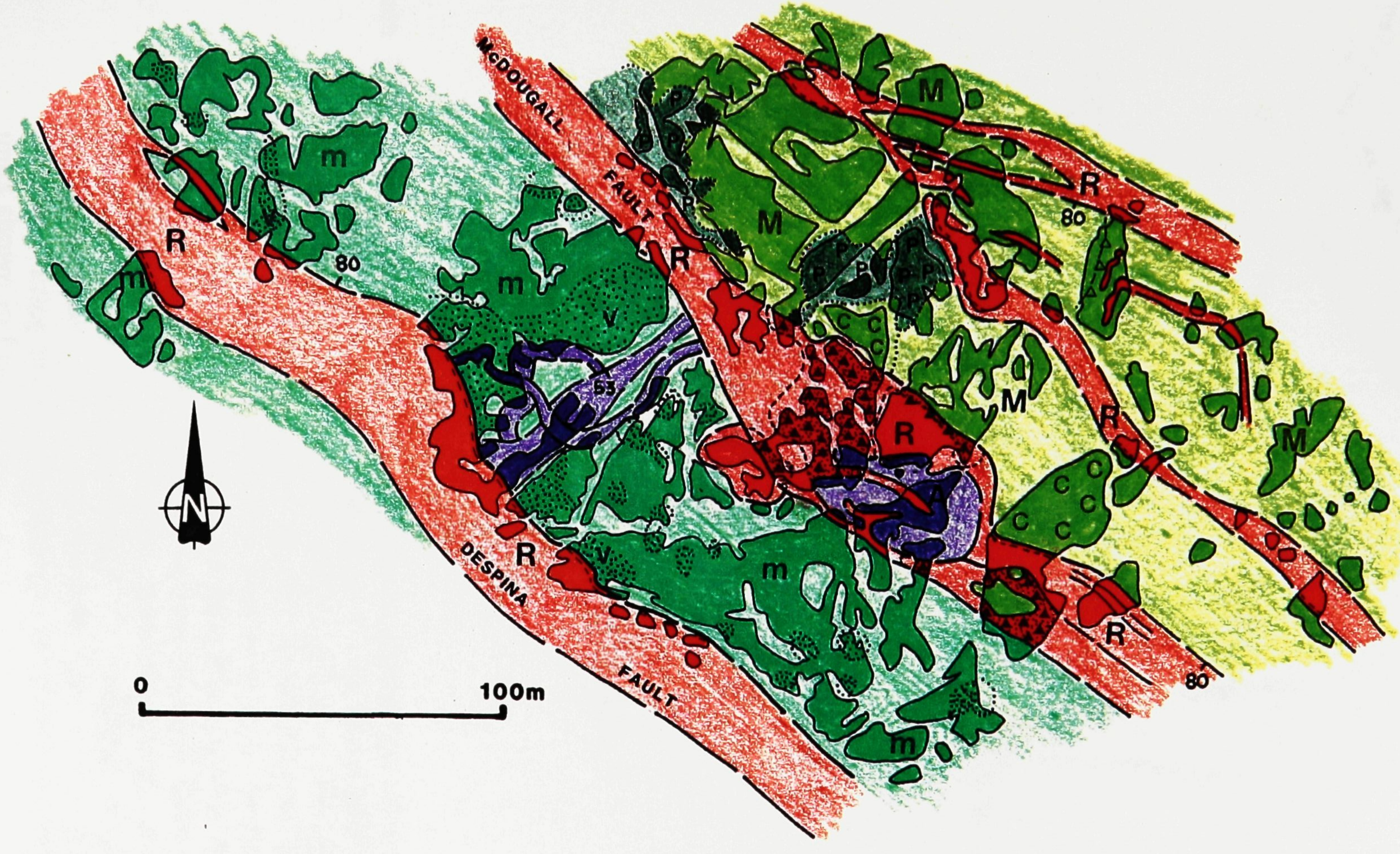
McDOUGALL FAULT
DESPINA FAULT
0
100m
N
R
M
m
80
53

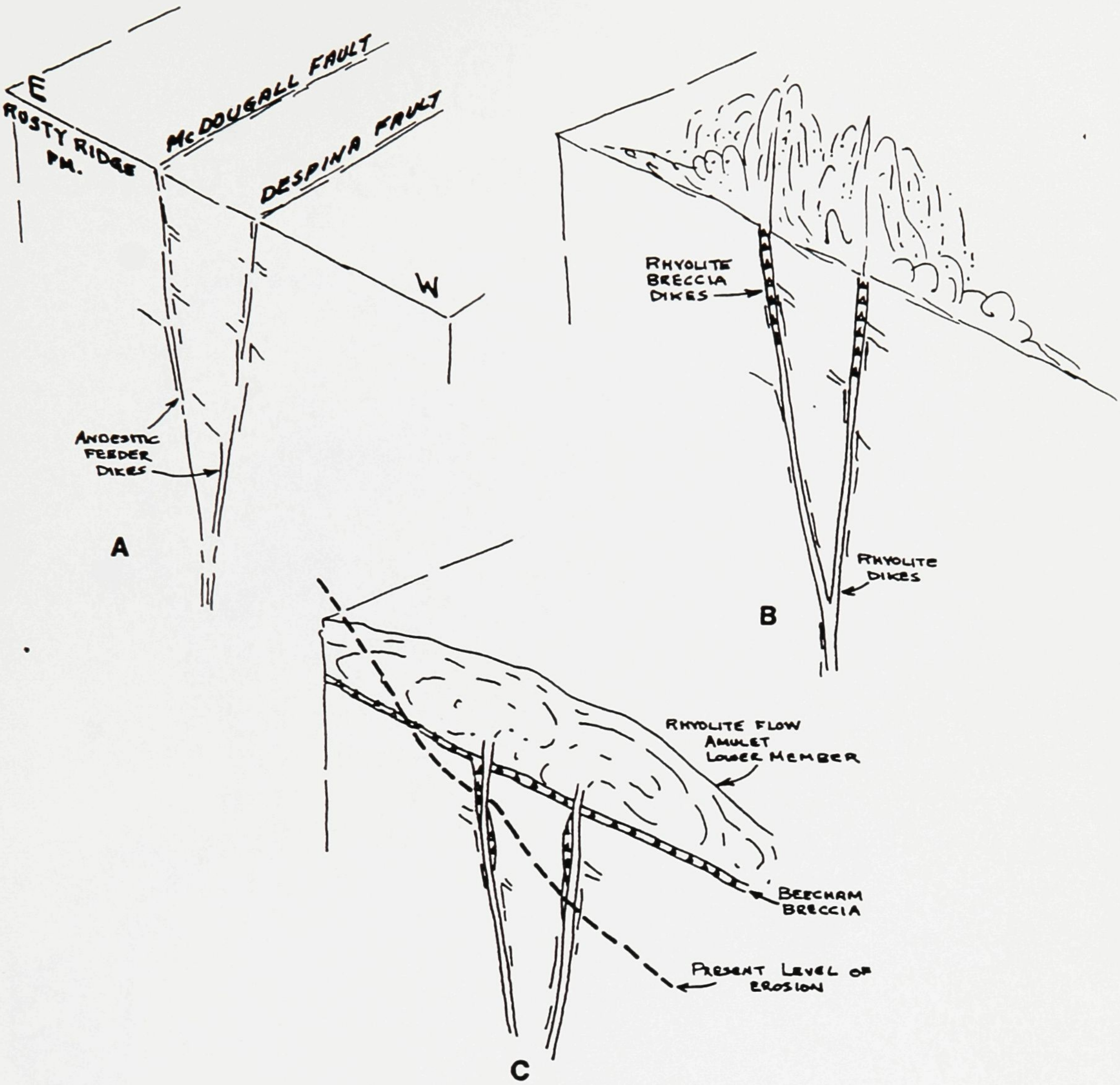

Figure 7.5B. Cartoon illustrating one possible reconstruction of the Beecham Breccia vent area illustrated in Figure 7.5. A. McDougall and Despina Faults occupied by andesitic feeder dikes to the Rusty Ridge formation. B. Emplacement of rhyolite dikes within the faults during the onset of rhyolitic volcanism associated with the Amulet lower member. Explosive interaction of ascending rhyolitic magma with downward migrating seawater or hydrothermal fluids resulted in shallow subsurface and surface phreatomagmatic eruptions and emplacement of Beecham Breccia. C. Pyroclastic eruptions cease during extrusion of the #3 rhyolitic flow of the Amulet lower member. Tilting and erosion results in the present distribution of map units shown in Figure 7.5.

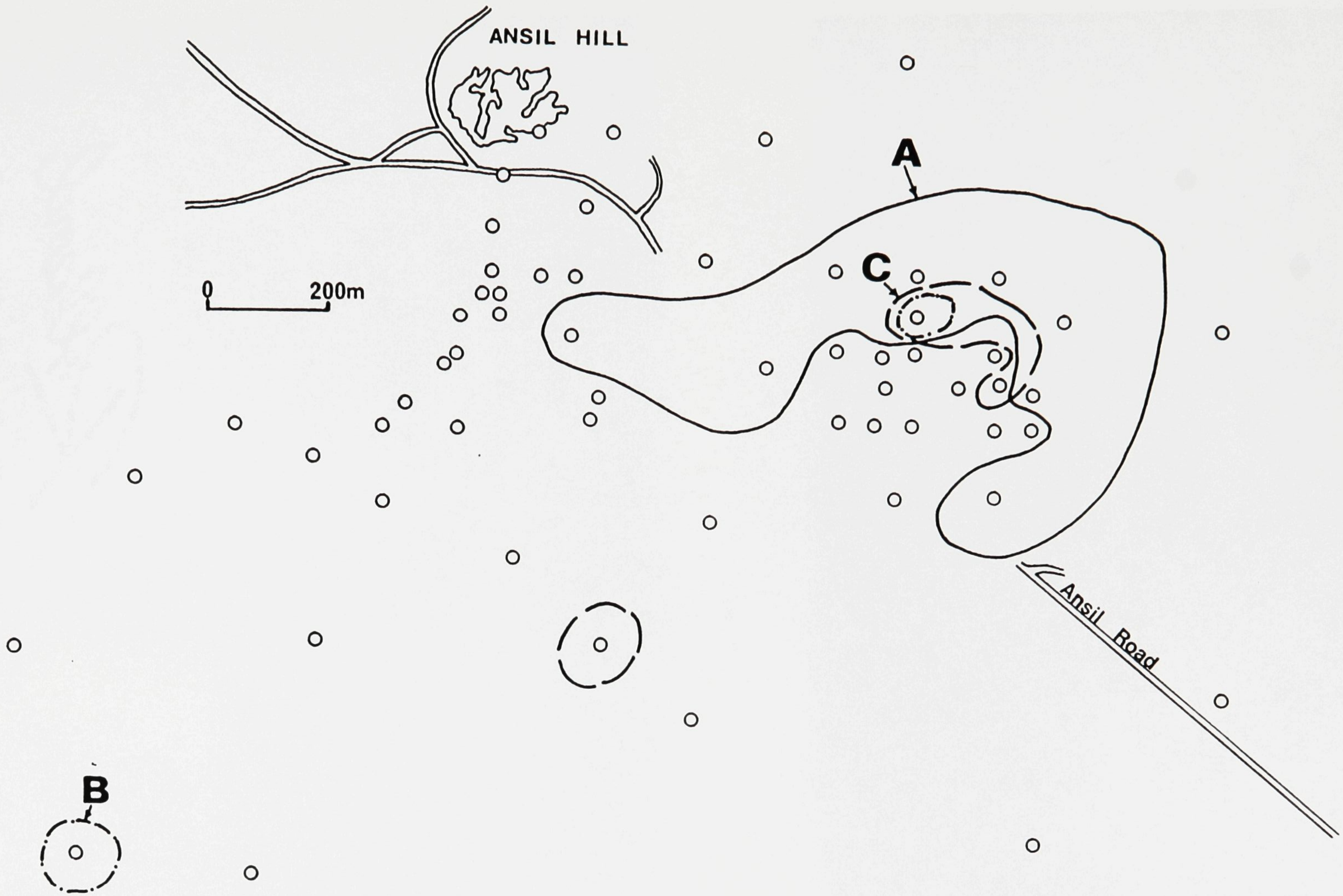

Figure 7.6. Rhyolitic breccias within the Rusty Ridge formation. Circles show collar location of drill holes.

Plate 7.1. Typical Beecham Breccia with lapillistone beds interbedded with thin, parallel laminated beds of tuff. Note the tuff rip-ups within the breccia.

Plate 7.2. Densely packed fragments within lapillistone bed that indent underlying laminated tuff bed (right). Note white siliceous rims on some fragments.

Plate 7.3. Bomb sag in laminated tuff. Symmetrical indentation of the tuff bed indicates subaqueous deposition.

Plate 7.4. Rhyolitic breccias within the Despina Fault southwest of the Corbet Mine. Irregular fragments of flowbanded rhyolite and wispy chloritic obsidian fragments are characteristic. Angular blocks of andesite are common and often occur in "trains" oriented parallel to the dike margin.

8. SYNVOLCANIC INTRUSIONS

Synvolcanic rhyolitic, andesitic, and composite dikes and subordinate sills intrude the Mine Sequence. These intrusions occur singly or in swarms, and are feeders to adjacent and overlying flows and pyroclastic deposits. The mineralogy, texture and chemical composition of synvolcanic intrusions are described first, followed by a summary of their mechanism of emplacement. Breccia dikes are described in Chapter 7.

8.1 RHYOLITIC INTRUSIONS

8.1.1 LITHOLOGY

Rhyolitic dikes weather grey-white to buff and are grey to light blue-grey on fresh surface. Individual dikes pinch and swell along strike and have been traced for 0.8km; dike widths range from <1m to >100m but are typically 2-5m.

The most characteristic feature of rhyolitic dikes is their granular or "sugary" texture on weathered surfaces which reflects a macrospherulitic texture of up to 90% spherulites, 1mm to 1cm in diameter. The dikes have a massive, weakly quartz amygdaloidal (<2%), spherulitic interior (1->100m wide) and finer-grained, spherulitic and/or aphanitic, banded margins (10cm-2m wide). Small recumbent "folds" occur within the banded margins of some dikes where irregular protuberances of the wall rock project inward. Inclusions or xenoliths of adjacent wall rock are not common and have only been observed within the interior of dikes. Dikes composed entirely of banded rhyolite are <1m wide. Rhyolitic dikes are aphyric, feldspar porphyritic or quartz and feldspar porphyritic; porphyritic dikes contain from 1-12% phenocrysts.

The most characteristic feature of rhyolitic dikes is their spherulitic texture. Spherulites (1mm-1cm) account for 65-90% of the groundmass of most dikes and display all stages of recrystallization and replacement by quartz (Plate 8.1B). Perlitic cracks are not common and where developed are overgrown by spherulites (Plate 8.1A). The groundmass mesostasis is a mosaic of quartz, chlorite and sericite (10-30%). Fine (<0.1mm) opaque minerals occur as isolated grains within the groundmass, as an ultra-fine dusting on the outer rim of spherulites and as thin films separating radially oriented quartz within spherulites. Banding is characterized by laminae with different amounts and/or sizes of spherulites alternating with thin (<.2mm) chlorite-sericite laminae. Subhedral to euhedral plagioclase phenocrysts (<1.5mm) are commonly replaced by quartz or sericite and subhedral to anhedral quartz phenocrysts (up to 1cm) often have irregular embayments. Texturally and mineralogically the rhyolitic dikes are identical to associated flows.

8.1.2 CHEMICAL COMPOSITION

The major element analyses of five rhyolitic dikes are contained in Table 8.1. Sample I-82-28 is chloritized (note the low Na_2O and high Fe_2O_3 content) and sample MDC-28 is sericitized (high K_2O and low Na_2O content). The average composition of rhyolitic dikes is similar to the average composition of Mine Sequence rhyolitic flows (Tables 8.2).

8.1.3 INTERPRETATION

Banding developed at the margins of a massive rhyolitic dike, by analogy with that in rhyolitic flows, is interpreted to be a product of viscous laminar flow. The restriction of banding to the margin of large dikes or throughout narrow dikes (<1m) is interpreted to reflect higher viscosity, primarily a function of rapid cooling and attendant velocity decrease (drag) along and parallel to the dike margin during emplacement. The dike interior is presumably insulated by the chilled margin and consequently is less viscous. Shear developed parallel to the dike margin between a more rapidly moving, less viscous, interior and viscous chilled margin may have resulted in heterogeneous volatile exsolution along shear planes that were drawn-out during viscous flow to form parallel flow laminae. Recumbent folds in the outer chilled margin are interpreted as drag folds which develop where laminar flow was disrupted by irregularities in the wall-rock contact.

Like consanguineous and chemically similar flows, rhyolitic dikes underwent negligible crystallization prior to their emplacement. Spherulitic textures which typify these dikes and perlitic cracks indicate that the original magma was quenched to an obsidian or vitrophyre.

8.2 ANDESITIC INTRUSIONS

8.2.1 LITHOLOGY

Andesitic dikes weather rusty brown, brown to green-brown and are grey-green to green on fresh surface. Dikes vary in thickness along their strike and individual dikes have been traced for 0.5km and locally attain widths up to 50m; thick massive columnar jointed sills in the Amulet A and C area attain thicknesses up to 200m. Columnar jointing has not been recognized in dikes.

Dikes range from aphanitic to medium-grained (<5mm) and are sometimes difficult to distinguish from massive andesitic flows. Feldspar phenocrysts constitute 1-5% of most dikes and amygdules (1-10%), up to 2cm in diameter, filled by quartz, chlorite, epidote and actinolite are common. Dike/wall rock contacts are sharp, with dike margins typically chilled and laminar jointed over a 5-15cm interval. Amygdules commonly increase in abundance toward either the dike margin or interior.

Fine-grained and aphanitic andesitic dikes have an intersertal textures with <1.0mm plagioclase microlites (45-55%) forming a mesh-like texture with interstitial (40-45%) actinolite, epidote, chlorite, sphene and opaque minerals

(Plate 8.1C); biotite (up to 10%) is common within the contact metamorphic aureole of the Dufault Pluton. Plagioclase phenocrysts (<2mm) are subhedral to euhedral and constitute < 5% of most dikes. Elliptical to spherical amygdules are filled with quartz, chlorite, opaque minerals and epidote (minor actinolite and calcite). Medium-grained dikes are similar mineralogically but have a subophitic to ophitic texture with occasional equant actinolite pseudomorphs, after pyroxene (up to 1mm), surrounding randomly oriented lath-like, subhedral-euhedral plagioclase microlites.

8.2.2 CHEMICAL COMPOSITION

Five samples from andesitic dikes were analyzed for 11 major elements. These analyses along with a single analysis of an andesitic feeder dike to the Amulet Upper member and a calculated "average composition" for andesitic dikes are presented in Table 8.3. Three of the andesitic dike samples and the Amulet feeder dike were also analyzed for 18 trace elements (XRF, pressed pellet analysis; Table 8.4) The andesitic dikes are remarkably consistent in both major and trace element composition and the average composition is similar to that of Mine Sequence andesitic flows (Table 8.2).

The Amulet upper member feeder dike is comparable to least altered upper member andesitic flows (Chapter 12) and is also similar to the andesitic component of a composite dike within the Amulet Upper member (Table 8.6)

8.2.3 INTERPRETATIONS

The fine-grained and aphanitic texture of andesitic dikes and sills, occurrence of amygdules and thin chilled margins are features consistent with high-level synvolcanic intrusions. Their chemical, mineralogical and textural similarity to andesitic flows of the Mine Sequence into which they are locally continuous support this interpretation.

8.3 COMPOSITE INTRUSIONS

Composite intrusions consist of distinct rhyolitic and andesitic components. This intimate association of two compositional end-members is interpreted to result from the contemporaneous association of both rhyolitic and andesitic magmas within a single conduit. The complex temporal and spatial association of contemporaneous mafic and felsic rocks has been described by Blake et al., 1965; MacDonald and Katsura, 1965; Walker and Skelhorn, 1966; Philpotts 1971; 1980; Weibe 1973; Vogel and Walker, 1975; Anderson, 1976; Gelinas et al., 1976; Sparks and Sigurdson, 1977; Sigurdsson and Sparks, 1981; Volgel and Wilband, 1978; Echilberger, 1975; 1978; Echelberger and Gooley, 1977; and Taylor et al., 1980. These descriptions and reviews leave no doubt that magmas of such contrasting compositions coexisted within the same locale.

8.3.1 LITHOLOGY AND FIELD CHARACTERISTICS

Composite dikes have only been recognized in eruptive centres characterized by major zones of synvolcanic faulting and dike emplacement such as the Old Waite and McDougall-Despina dike swarms. Individual dikes range from <2m to 12m in width and are rarely traceable for >300m before being cut-off by other composite or associated homogeneous rhyolitic and andesitic dikes (Map 2).

Figures 8.1 to 8.5, illustrate the main features which typify composite dikes. Composite dikes are divisible into 3 main components: an outer margin of andesite, an intermediate hybrid zone and a core of rhyolite. The hybrid zone which typifies most composite dikes is not always present (Figure 8.4).

The andesitic component ranges from 20cm to 2m in width and is symmetrically disposed on both margins of the dike (Figure 8.1). Andesite weathers brown to rusty brown, is fine-grained to aphanitic, weakly feldspar porphyritic (1-2%, <3m crystals), massive to weakly flow laminated and commonly amygdaloidal (up to 10% amygdules <1.5m in size); virtually identical to andesite of associated homogeneous dikes and flows. Amygdules are not typical of chilled and aphanitic margins but occur within 10-15cm of the dike/wall-rock contact and often increase in abundance toward the dike interior. The contact between the andesite and wall-rock is sharp and marked by a thin, <1cm wide, dark grey to black, aphanitic selvedge (Plate 8.3). Inward the grain size ranges from aphanitic to fine-grained. Epidote-quartz alteration patches (Figure 8.5 and Plate 8.3) commonly occur within the dike if adjacent andesitic flows are similarly altered. The contact between the andesitic component and hybrid zone is typically sharp and abrupt without evidence of chilling (Figures 8.1 and 8.2) and occasionally, is gradational over a 5-10cm interval.

The rhyolitic component ranges from <1m to 5m in width and is located within the dike core (Figures 8.1 to 8.5), but not always at its centre. Off-centred "rhyolite intrusions" are more common in shallowly (<30^0) dipping dikes. The rhyolitic component is similar to associated homogeneous rhyolitic dikes and flows and is subdivided into quartz-feldspar porphyritic (QFP) and feldspar porphyritic (FP) varieties; both weather light grey to white although QFP varieties often have a pink hue (Plate 8.4). Feldspar phenocrysts constitute 1-3% (<2mm) of feldspar porphyritic rhyolite whereas QFP rhyolite contains up to 15% (<5mm) quartz phenocrysts and 10% feldspar phenocrysts. Amygdules are not common but when present are typically found in FP rhyolite. Irregular xenoliths of feldspar porphyritic andesite constitute <5% of the rhyolitic component of composite dikes. Contacts between rhyolite and intervening hybrid zones are irregular and gradational and defined by a rapid decrease in the percentage of andesitic xenoliths in the latter (Plate 8.4, Figure 8.2). Where the hybrid zone is absent contacts are sharp but not chilled.

An irregular "mixed" or "hybrid zone", up to 1m wide, typically separates the andesitic and rhyolitic components of composite dikes. This is essentially a xenolith-rich zone containing up to 35% platy, irregular, cuspate and amoeboid shaped xenoliths that range from <1cm to 25cm in size (Plates 8.4 and 8.5, Figures 8.1, 8.2 and 8.5). The xenoliths are composed of aphanitic, and feldspar porphyritic aphanitic and fine-grained andesite that are identical to the adjacent andesite. The groundmass is light grey, more siliceous and displays sharp but irregular contacts with xenoliths. Unlike that of adjacent andesite, the hybrid zone groundmass is distinctly feldspar porphyritic and contains approximately the same percentage of phenocrysts as does the rhyolite. In most examples the phenocryst assemblage within the hybrid zone groundmass changes from feldspar to quartz plus feldspar toward the QFP rhyolitic component. Contacts between the hybrid zone and rhyolite are gradational whereas contacts with adjacent andesite are typically sharp but not chilled.

8.3.2 PETROGRAPHY

The mineralogy and textures of the andesitic component are identical to those of associated homogeneous andesitic dikes of similar width. Where andesite at the composite dike margin is <1m wide the groundmass is typically hyalopilitic with up to 35% skeletal (swallow-tail and belt-buckle morphology) plagioclase microlites within a homogeneous matte of fibrous and acicular actinolite (40-50%), quartz (10%), epidote (1%) and opaques (6%) that replace original glass. Thick andesitic margins, >2m have groundmass textures ranging from hyalopilitic to intersertal at the outer margin to fine-grained and subophitic toward the rhyolitic component. Fine-grained subophitic andesite consists of up to 50% randomly oriented albite microlites (<1mm) partly engulfed by equant actinolite pseudomorphs after pyroxene (30-40%) and interstitial fibrous actinolite (<15%), chlorite (<15%), quartz (<10%), epidote (<2%), sphene (trace) and opaque minerals (1-5%). Ubiquitous euhedral to subhedral plagioclase phenocrysts (0.8-2.5mm) constitute <3% of the andesite.

The hybrid zone is best described as heterogeneous. Andesitic xenoliths ranging from <1mm to >25cm characterize this unit. Andesitic xenoliths are classified as two main types. The first, and most common, consists of massive andesite with hyalophitic to fine-grained intersertal texture (Plates 8.5 and 8.2C); the mineralogy texture, and grain size of the andesitic xenoliths are identical to adjacent andesite along the dike margins. The second type ranges from 5mm to <1mm and occurs as irregular clot-like to globular forms consisting of fine-grained massive and/or acicular epidote with minor actinolite quartz and opaque minerals (Plate 8.2B and D). Massive epidote xenoliths lack any evidence of original texture and are interpreted as altered and replaced andesitic glass (Plate 8.2D).

Xenoliths typically display sharp contacts with the groundmass but some grade imperceptibly into the groundmass (Plate 8.2D and B). This is particularly a problem in that fine microxenoliths (<1mm) are often difficult to distinguish from clotted actinolite and albite of the groundmass. Although not common, thin

0.1 to 0.4mm "reaction" rims or rinds of fine-grained epidote, actinolite, quartz and opaque minerals mantle xenoliths (Plate 8.2C).

The hybrid zone groundmass consists of randomly oriented (30-40%) subhedral plagioclase microlites (<0.8mm) with ragged, seriate boundaries with interstitial prismatic and fibrous actinolite (20%), granular blocky quartz commonly with myrmekitic texture (15%), quartz spherulites (10%), granular epidote (<10%) and fine opaque minerals (<5%). Contacts between plagioclase and quartz are commonly myrmekitic (Plate 8.2A). The percentage of plagioclase microlites, actinolite and quartz varies considerably within the hybrid zone but the groundmass appears more "siliceous" than analyses indicate. The "andesitic composition" for the hybrid zone, indicated by whole rock analyses in Tables 8.5 and 8.7, reflects numerous andesitic xenoliths.

Phenocrysts of anhedral to subhedral plagioclase (1-4%, <2.6mm) are common and as a rule the hybrid zone is distinctly feldspar porphyritic compared to adjacent andesite. Anhedral, embayed quartz phenocrysts (1-6%) occur throughout the groundmass but like plagioclase phenocrysts tend to occur in clusters. Stubby, prismatic megacrysts of actinolite, presumably after pyroxene phenocrysts are rare and are only present where adjacent andesite contains similar megacrysts.

Evidence of disequilibrium within the hybrid zone includes:

a) actinolite coronas or reaction rims (after original pyroxene?) mantling quartz phenocrysts (Figure 8.1D).

b) myrmekitic coronas and concentric myrmekite and quartz rims on quartz phenocrysts (Figure 8.1E).

c) embayed, <u>anhedral</u> plagioclase phenocrysts or xenocrysts with seriate boundaries, often mantled by coronas of myrmekite and quartz (Plate 8.1F).

d) "ragged" plagioclase microlites with myrmekite developed in contact with quartz (Figure 8.2A).

e) thin (0.1-0.4mm) "reaction rims" of fine (<0.1mm) actinolite, epidote, quartz (myrmekite) and opaque minerals mantling xenoliths (Plate 8.2C).

The rhyolitic component, although similar in field characteristics and composition to associated homogeneous rhyolitic dikes differs substantially in both texture and mineralogy. The rhyolitic groundmass is similar to the felsic groundmass of the hybrid zone into which it grades. The rhyolite consists of up to 25% fine ragged plagioclase microlites (<0.5mm) and/or skeletal quenched plagioclase microlites (<10%) in a groundmass of fine granular quartz, mrymekite with <5-20% spherulites, <10% fine prismatic and acicular actinolite (minor chlorite), <10% epidote and <6% opaque minerals. Andesitic xenoliths range from 10cm to <1mm microxenoliths. Phenocrysts of anhedral embayed quartz (4-12%) and subhedral to anhedral albite (1-4%) are reminiscent of those within the hybrid zone and are commonly rimmed by coronas of fine granular quartz and myrmekite.

8.3.3 CHEMICAL COMPOSITION

The fourteen samples from five composite dikes (Tables 8.5 and 8.6) were chosen to reflect the greatest range in megascopic and petrographic variations across individual dikes. QFP rhyolite is characterized by higher SiO_2 and lower Al_2O_3, Fe_2O_3, CaO, P_2O_5 and TiO_2 contents relative to FP rhyolite. This distinction is the same as in associated rhyolitic flows and the calculated average compositions are similar.

The chemical composition of andesitic components are remarkably consistent in both major and trace elements, with the exception of I-82-114 which is more SiO_2-rich and is chemically similar to least altered andesite of the Amulet upper member. Samples I-82-18,-17,-16 are from a cross-section through an andesitic component or margin to a composite dike (Figure 8.5). These samples illustrate a consistent trend of high SiO_2 and Na_2O toward the hybrid zone with concomitant low Fe_2O_3, MgO, K_2O and TiO_2. This "trend" could be primary but may be secondary, a product of mixing between the outer andesitic dike and inner rhyolitic dike represented macroscopically by the hybrid zone. The average composition of the andesitic components is similar to average compositions of associated homogeneous dikes and flows of the Mine Sequence. The hybrid zone has a major and trace element composition intermediate between adjacent massive rhyolite and andesite, consistent with mixing between the two end-member magmas.

Chondrite normalized REE data (Figure 8.6) show:

1. marked enrichment of all REE of rhyolitic component relative to the andesitic component.

2. parallel REE patterns of andesitic and rhyolitic components with that of the hybrid zone intermediate and parallel to the two compositional end-members.

3. the rhyolitic, andesitic and hybrid components have flat REE patterns (low La:Lu ratios) with weak negative Eu anomalies, typical of primitive tholeiites.

8.3.4 INTERPRETATIONS

1. The symmetric distribution of andesite on both margins of the composite dike and restriction of chilled margins to wall-rock contacts indicate that they originally comprised a single dike now separated by rhyolite.

2. Rhyolite was emplaced separately within the andesite while the latter was still fluid. The globular, amoeboid, rounded and cuspate forms of andesitic xenoliths indicate their fluid nature during incorporation in the margin of ascending rhyolite. There are no angular xenoliths that might reflect brittle behaviour during emplacement of the rhyolite.

The textural and mineralogical similarities of homogenous andesite along the dike margins to incorporated xenoliths and the restriction of xenoliths to hybrid zones located at internal contacts indicate that xenoliths were derived from adjacent andesite and are not mafic segregations, or cumulates carried by the rhyolite.

3. The hybrid zone is a zone of mixing of contemporaneous andesitic and rhyolitic magmas within a single dike. Mixing occurred at the interface of existing andesitic and a somewhat later rhyolitic magma. During emplacement of the rhyolite the still fluid andesite is interpreted to have broken into irregular globules which were incorporated into the margins of the ascending rhyolitic magma. Unlike large subvolcanic bodies where "convective stirring" (Eichelberger and Gooley, 1977; Anderson, 1976) would result in globules strewn throughout the magma body, rapid cooling of the magma within a narrow high level dike combined with vertical movement during ascent is interpreted to have concentrated the xenoliths along the margin of the rhyolite. Direct mixing of andesitic and rhyolitic magmas was probably minor as the globules crystallized quickly within the rapidly cooled and emplaced dikes. Limited interaction and disequilibrium during the mixing of two magmas is suggested by thin rinds mantling some xenoliths, embayed phenocrysts of both quartz and plagioclase mantled by coronas of granular quartz and myrmekite and gradation of microxenoliths into the hybrid zone and rhyolitic groundmass. Similarly, abundant epidote within the rhyolitic groundmass is atypical of associated homogeneous rhyolitic dikes and flows and may indicate resorption of an originally Ca-rich phase (plagioclase) into the rhyolitic magma during mixing.

The absence of a macroscopic hybrid zone separating rhyolite and andesite in some composite dikes suggests that the hybrid zone did not develop along the entire length of the rhyolitic dike.

4. Two general models have been proposed to explain the origin of coexisting, chemically distinct magmas. One is silicate liquid immiscibility and another is magma mixing. Liquid immiscibility versus magma mixing models may be evaluated using REE data. Watson (1976) and Ryerson and Hess (1978) provide trace element partition data for immiscible silicate liquids which indicate that REE are enriched in the basic magma by a factor of 5-10. However, during fractional crystallization or fractional melting of a single parent (Yoder, 1973) REE are enriched in felsic magma (Vogel and Wilband, 1978; Taylor et al., 1980). The consistent enrichment of REE within rhyolite relative to associated andesite indicates that the two coexisting magmas are not a product of silicate liquid immiscibility but are two distinct magmas.

It is significant to note that within the interpreted subvolcanic magma chamber now represented by the Flavrian Pluton, Goldie (1976) has described evidence for large-scale magma mixing between an early quartz dioritic magma (Meritens phase) and subsequently emplaced trondjhemite to produce hybrid tonalitic rocks. Thus shallow, near-surface magma mixing within composite dikes may have coincided with large scale magma mixing during emplacement of the underlying magma chamber.

5. Cross-cutting composite dikes and associated homogeneous rhyolitic and andesitic dikes indicate ascent and limited near-surface magma mixing of contemporaneous andesitic and rhyolitic magmas feeding surface eruptions.

8.4 XENOLITHS

Although not common, medium- to coarse-grained "granite" xenoliths occur within both andesitic and composite dikes. Rounded xenoliths (<25cm) occur within an andesitic dike and rhyolitic dike of the Old Waite dike swarm and a large (2m X 1m) leucocratic fine-grained aplitic xenolith occurs within a narrow (<1m wide) quartz-feldspar porphyritic rhyolitic dike south of Duprat Lake. The occurrence of such a large xenolith in the narrow dike illustrated in Plate 8.6, implies emplacement within an originally wider fissure during a period of extension.

In all cases the xenoliths have sharp contacts with enclosing dike, are subrounded and occur within the central part of the enclosing dike. Similar "granitic" xenoliths were noted in the Millenbach-D68 lava dome at the Millenbach mine (C.D.A. Comba, personal communication, 1985).

8.5 THE DACITE DIKE

The Dacite Dike is an intrusive body of intermediate composition (Table 8.8) that lies adjacent and subparallel to the Dacite Fault (Figure 9.19, Map 1).

The dike has limited surface exposures but has been intersected in numerous drill holes (Table 8.8) where it is interpreted to cross cut the Flavrian, Northwest and Rusty Ridge formations and Amulet lower member. The similarity in chemical composition (Gibson and O'Dowd, 1981) and textures (massive, fine-grained intersertial texture) between the Dacite Dike and least altered flows of the Amulet upper member and its interpreted morphology (Figure 9.4 Section G-G) suggest it is a feeder to the upper member andesitic flows. Recently, conformable sill-like intrusions or thick massive flows of chemically and texturally identical dacite have been recognized in the drill core from the Amulet upper member in the Ansil sector (G. Riverin, personal communication 1989).

8.6 DIKE SWARMS

Individual rhyolitic and andesitic dikes occur throughout the Mine Sequence; however, two "dike swarms", the McDougall-Despina and Old Waite swarms define major paleo-fissures or vent areas for andesitic and rhyolitic flows.

8.6.1 THE McDOUGALL-DESPINA DIKES

The N40^{0}W trending McDougall and Despina Fault are occupied by rhyolitic and to a lesser extent andesitic dikes along their 4.8 km strike length. Up to 11 discrete rhyolitic dikes have been observed to occupy the fault (Setterfield, 1984); rhyolite breccia dikes occupy the faults south of the Corbet deposit. Numerous ancillary rhyolitic, composite and to a lesser extent andesitic dikes parallel and increase in abundance toward the faults. As described in Chapter 9 rhyolitic and andesitic intrusions that occupy the faults are feeder dikes to flows of the Flavrian, Northwest, Rusty Ridge, Amulet and Amulet Andesite formations.

8.6.2 THE OLD WAITE DIKE SWARM

The Old Waite dike swarm lies near the centre of the Flavrian block and is best exposed along the south shore and northeast of Duprat Lake. The dike swarm strikes east-northeast (070^0), normal to strata, has a minimum strike length of 3.0km and ranges in width from 1.4km in the west to 0.9km in the east (Map 1). The dike swarm comprises a plexus of predominantly andesitic and subordinate composite and rhyolitic dikes that have variable strike, and dip 80^0-20^0 to the north or south. Individual dikes range in width from <1m to 50m and may be traced for up to 300m; more typically, dikes range from 1-5m in width and are traceable for a few tens of metres before being cut off by other dikes.

The complex, multiply intrusive nature of the dike swarm is evident on Maps 1 and 2; the best exposures of the dike swarm lie between Duprat Lake and the former Old Waite mine. The myriad of cross-cutting andesitic, rhyolitic and composite dikes vary in grain size, amygdule content and structure but are similar in both chemical composition and mineralogy. The core of the dike swarm contains up to 85% dikes whereas the margin contains 25-45% dikes. Within the dike swarm intervening flows occur as discontinuous screens between dikes.

The Old Waite Dike Swarm intrudes strata of the Rusty Ridge, Amulet and Waite Andesite formations and abruptly terminates in the lowermost flows of the Amulet Andesite formation. Lack of outcrop west of Duprat Lake does not allow definition of the north-south limits of the dike swarm but drill holes in this area intersect numerous dikes and attest to its occurrence within the Flavrian formation.

Dikes within the Old Waite Dike Swarm were the principal feeders to andesitic flows of the Flavrian, Rusty Ridge, Waite Andesite and Amulet Andesite formations (Chapter 9). Rhyolitic dikes were feeders to the Number 3 flow of the Amulet lower member, and the Waite Rhyolite dome at the East Waite Mine (Chapter 9). The west to east section through the Old Waite Dike Swarm affords an excellent cross-section through a reactivated, synvolcanic fissure system which fed both rhyolitic and andesitic flows. The dike swarm increases not only in width but also in the number of cross-cutting dikes from east to west as would be expected with continued reactivation and dike emplacement along this structure. Assuming an average dike density of 50% and an average width of 1.0km for the dike swarm, strata have been dilated a minimum of 0.5km over a 1km width, in a north-south direction. Although individual faults are recognized, offset along dikes is also common (Maps 1 and 2) indicating that north-south dilation during dike emplacement was accompanied or followed by repeated down-faulting of volcanic strata within the dike swarm relative to equivalent stratigraphic units to the north and south. There is also a general trend for strata north of the Old Waite Dike Swarm to be down-faulted relative to those on the south side.

8.7 ORIENTATION OF SYNVOLCANIC INTRUSIONS

Synvolcanic dikes and breccia dikes trend northeast or northwest, typically at a high angle to strata, dip steeply north or south, and commonly are parallel to associated synvolcanic faults. Within dike swarms, individual dikes have trends that generally parallel the swarm, but often have variable dips. Rhyolitic dikes occupying the McDougall-Despina Fault and ancillary parallel dikes have a crudely arcuate surface trace.

8.8 MECHANISM OF DIKE EMPLACEMENT

1. Synvolcanic intrusions were emplaced during periods of extension consistent with successive tumescence of the volcanic edifice preceding surface eruptions.

2. Magmatic stoping was a minor aspect of passive dike emplacement during intrusion of rhyolitic, andesitic, and composite dikes whose xenoliths appear to be derived from an underlying basement. Stoping of wall-rock was common during emplacement of breccia dikes.

3. Emplacement of multiple dikes within a single fissure and occurrence of major dike swarms (eruptive centres, Chapter 9) that fed successive eruptions

indicate that dikes are localized by fundamental and long-lived zones of weakness: i.e., major synvolcanic faults. Faults continuously reactivated during tumescence preceding eruption, controlled magma ascent, localized surface eruptions, focused ascent and discharge of hydrothermal fluids (formation of VMS deposits) , and accommodated subsidence.

4. The dike-like form of synvolcanic intrusions as opposed to isolated plugs or stocks is consistent with fissure eruptions versus eruptions from a central vent.

5. Synvolcanic intrusions are oriented northeast and northwest parallel to synvolcanic faults. Some rhyolite dikes have a crude arcuate surface trace.

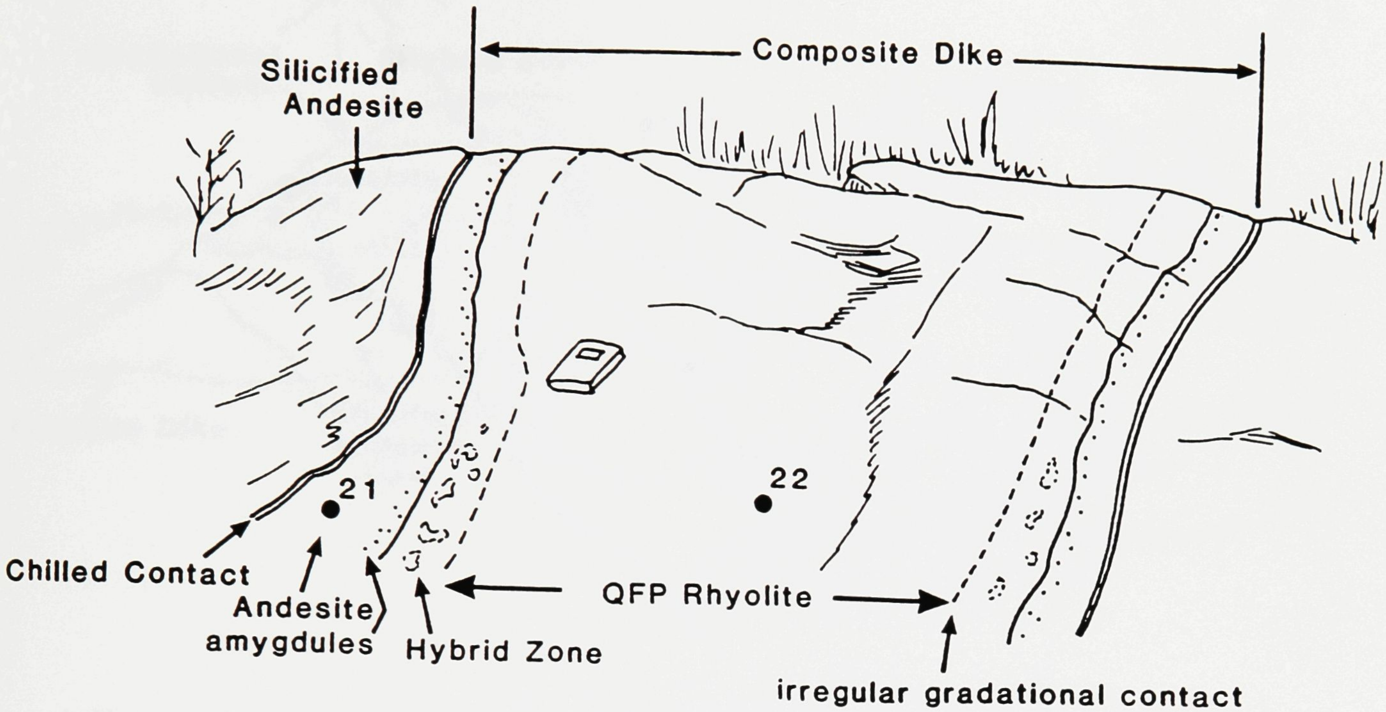

Figure 8.1. Composite dike with a QFP rhyolitic interior and fine-grained andesite at margins. Contacts between rhyolite and andesite are sharp, but not chilled (Old Waite Dike Swarm). Numbers refer to analyses in Table 8.5.

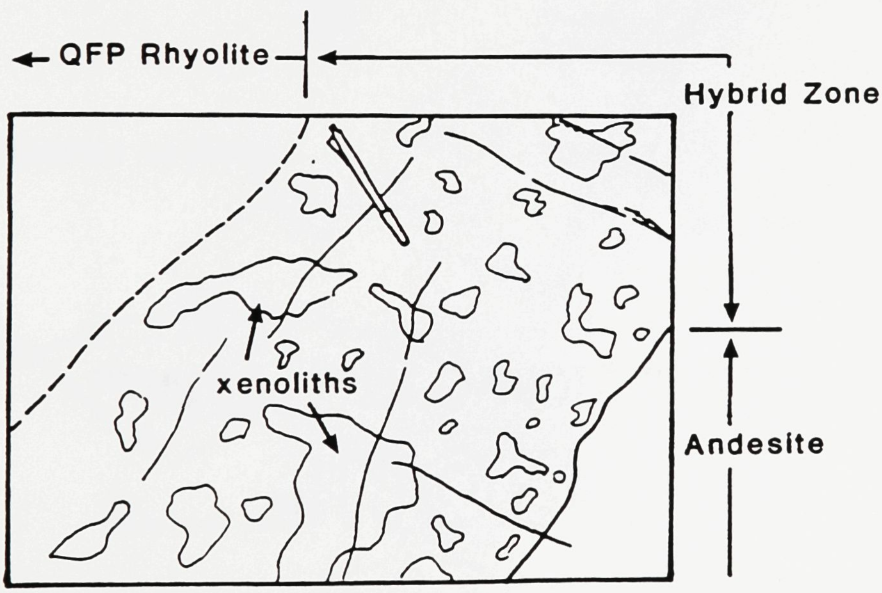

Figure 8.2. Irregular, rounded and cuspate andesitic xenoliths in hybrid zone. (Old Waite Dike Swarm).

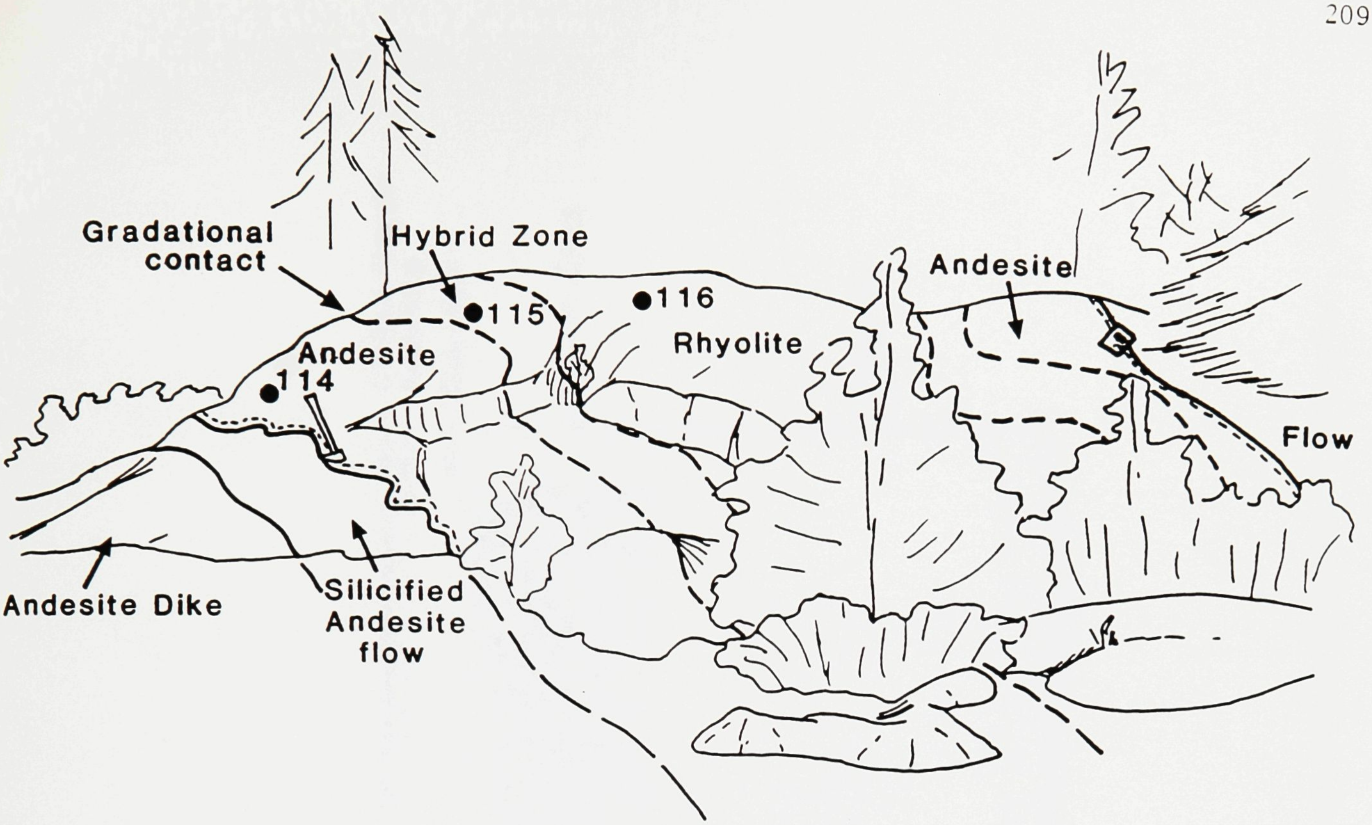

Figure 8.3. Outcrop sketch of a composite dike in silicified flows of the Amulet upper member (Old Waite Dike Swarm). Numbers refer to analyses in Table 8.5.

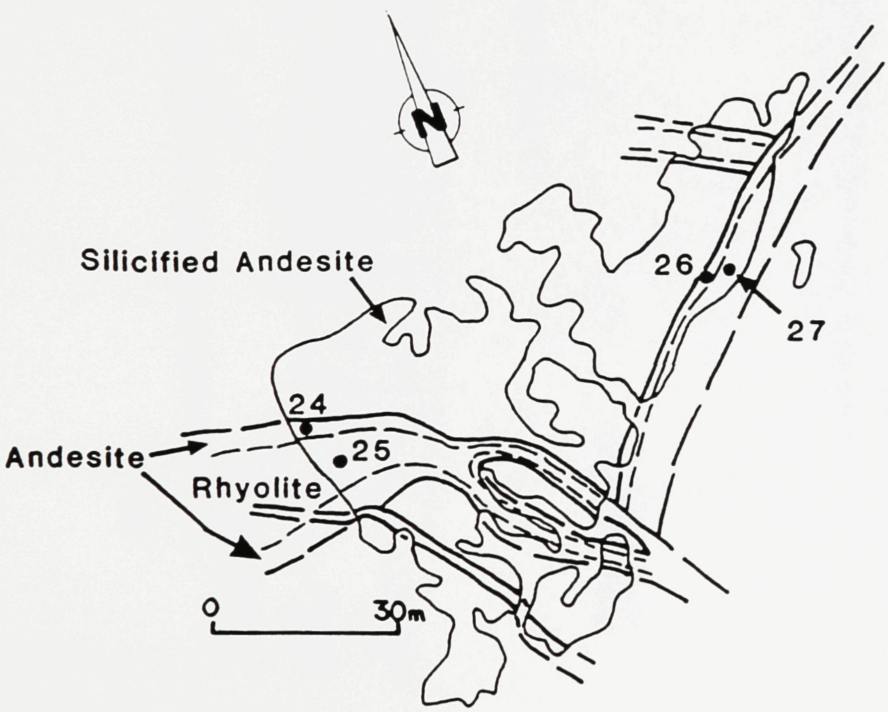

Figure 8.4. Composite dikes adjacent to the McDougall-Despina fault. Numbers refer to analyses in Table 8.5.

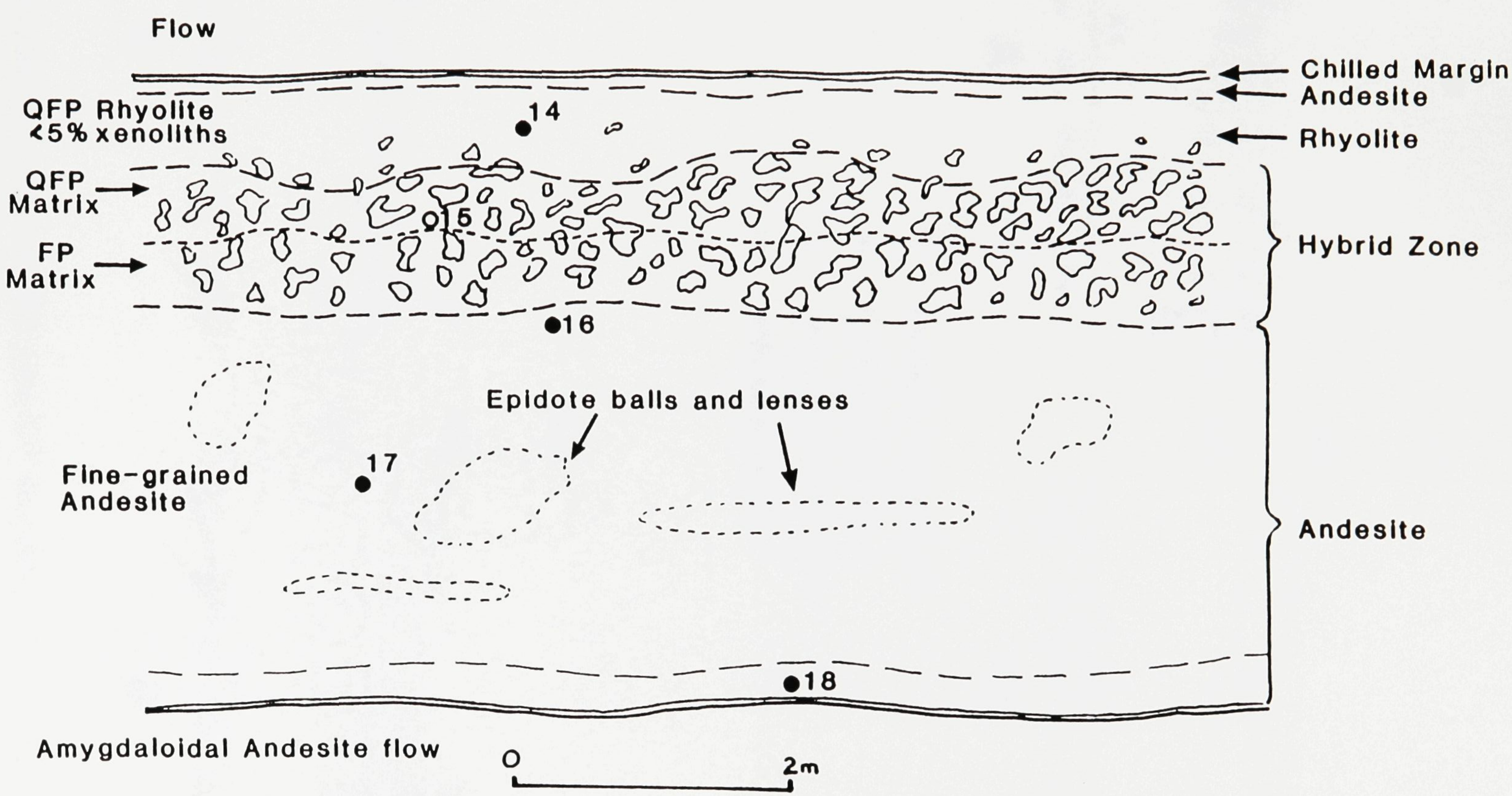

Figure 8.5.Diagrammatic sketch of a composite dike from the Old Waite Dike Swarm. Numbers refer to analyses in Table 8.5.

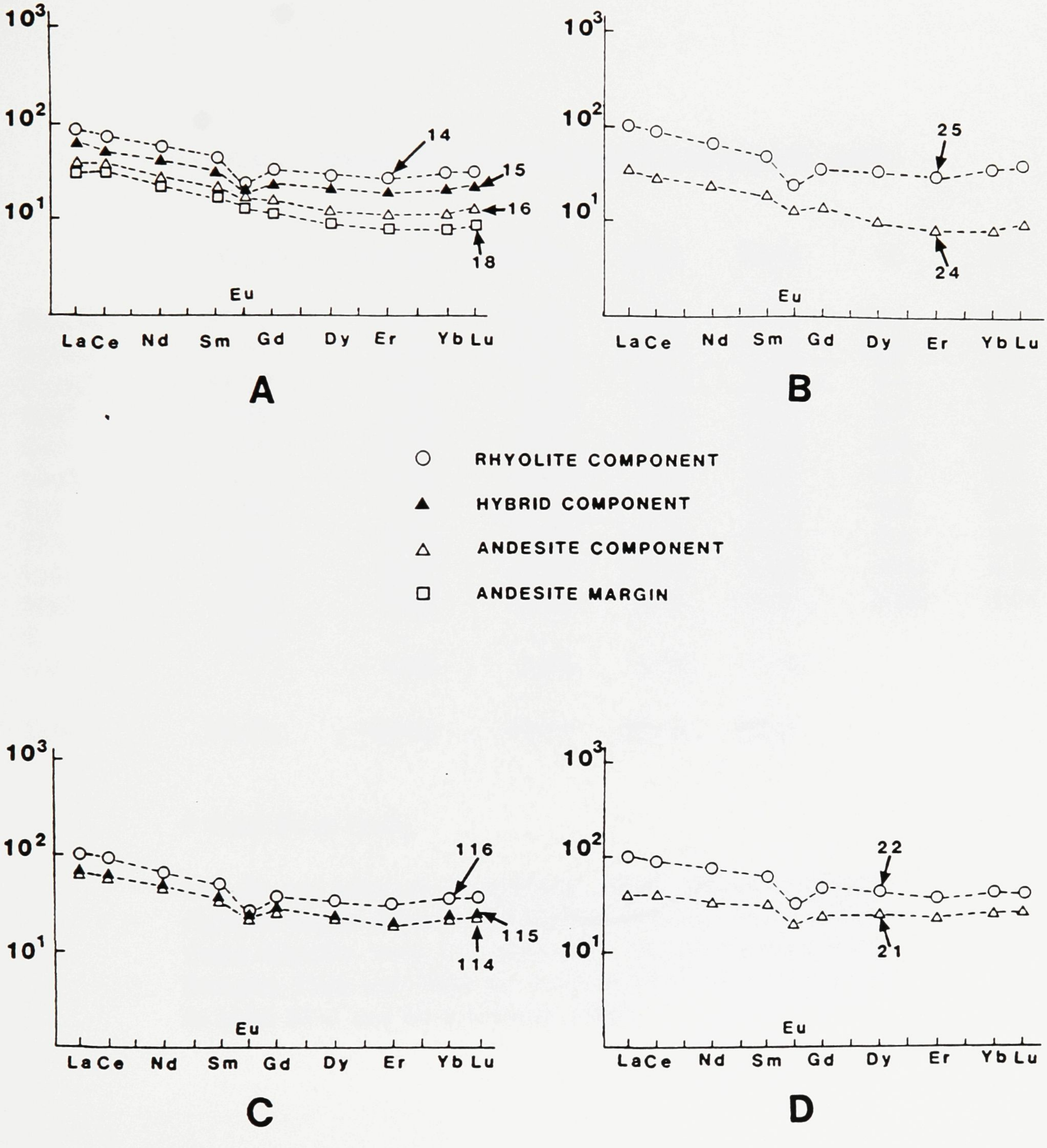

Figure 8.6. Chondrite normalized REE plots for the andesitic, rhyolitic and hybrid component of composite dikes.

TABLE 8.1. CHEMICAL COMPOSITION OF RHYOLITIC DIKES

	I-82-28	MDC-14	MDC-28	3566	9802	X	SD
SiO_2 %	67.77	72.50	72.30	72.60	74.20	73.1	0.9
Al_2O_3	11.65	12.50	12.20	11.30	11.40	11.7	0.6
Fe_2O_3*	11.25	4.53	7.05	4.47	3.70	4.2	0.4
MgO	2.58	2.54	2.69	1.99	0.55	1.7	1
CaO	0.30	0.27	0.11	1.21	1.88	0.6	0.8
Na_2O	0.0	3.76	0.09	4.98	4.37	4.3	0.6
K_2O	1.52	1.48	2.14	0.07	1.10	0.8	0.7
TiO_2	0.75	0.40	0.38	0.32	0.28	0.3	0.06
P_2O_5	0.22	0.07	0.07	0.04	0.02	0.04	0.02
MnO	0.17	0.03	0.05	0.06	0.11	0.06	0.04
S	0.00	-	-	-	-		
LOI	-	1.85	2.85	1.08	1.70		
Total	96.21	99.93	99.93	98.12	99.31		

* Total Fe as Fe_2O_3

I-82-28 and MDC-28 (Setterfield, 1984), weakly chloritized rhyolitic feeder dikes to the Bedford Rhyolite flow and Here Creek Rhyolite, were not included in the calculated averages. Samples 3566 and 9802 are from rhyolitic dikes intersected in holes 81-3 and 80-3 (Clarke, 1983).

TABLE 8.2. AVERAGE COMPOSITION OF MINE SEQUENCE RHYOLITIC AND ANDESITIC FLOWS

	ANDESITIC FLOWS				RHYOLITIC FLOWS			
	1	2	**Mean**	Std. Dev.	1	2	**Mean**	Std. Dev.
Wt. % Oxides			(92 analyses)				(94 analyses)	
SiO_2	50.4	77.1	**58.2**	5.4	49.7	81.2	**73.1**	4.3
Al_2O_3	7.5	18.7	**14.8**	1.7	8.9	22.5	**11.8**	1.7
Fe_2O_3	2.7	19.3	**9.2**	2.5	0.5	11.5	**4.7**	1.9
MgO	0.6	8.5	**4.3**	1.5	0.1	5.4	**1.9**	1.2
CaO	0.3	17.7	**4.9**	2.9	0.1	6.3	**1.0**	1.1
Na_2O	0.0	6.4	**4.2**	1.3	0.0	5.9	**3.4**	1.7
K_2O	0.0	1.8	**0.5**	0.4	0.0	8.0	**1.5**	1.3
TiO_2	0.7	1.9	**1.2**	0.3	0.2	0.9	**0.3**	0.1
P_2O_5	0.1	0.4	**0.2**	0.1	0.0	0.2	**0.0**	0.0
MnO	0.1	0.4	**0.2**	0.1	0.0	0.3	**0.1**	0.1

1. Minimum value for oxide
2. Maximum value for oxide

TABLE 8.3. MAJOR ELEMENT COMPOSITION OF ANDESITIC DIKES

	I-82-4	I-82-5	I-82-12	I-82-19	I-82-20	82-79	X	S
SiO_2 %	58.27	55.08	58.17	53.70	55.20	64.76	56.0	2
Al_2O_3	15.43	15.29	15.30	17.15	15.89	13.50	15.8	0.8
Fe_2O_3*	7.31	9.49	8.45	11.37	10.40	7.82	9.4	1.6
MgO	5.33	4.67	4.79	4.95	6.59	3.11	5.2	0.8
CaO	7.59	8.98	5.51	3.84	3.32	1.53	5.8	2.3
Na_2O	3.28	2.73	4.51	5.33	3.98	3.94	3.9	1
K_2O	0.41	0.79	0.46	1.53	2.57	0.97	1.1	0.9
TiO_2	1.11	1.17	1.18	1.42	1.02	0.93	1.18	0.1
P_2O_5	0.04	0.00	0.15	0.25	0.11	0.24	0.11	0.09
MnO	0.17	0.17	0.14	0.22	0.19	0.13	0.18	0.03
S	0.05	0.01	0.00	0.00	0.01	0.01	-	-
Total	98.99	98.38	98.66	99.76	99.28	99.28		

* Total Fe as Fe_2O_3

Sample 82-79 is a feeder dike to andesite flows of the Amulet Upper member and was not included in the calculated average composition.

TABLE 8.4. TRACE ELEMENT COMPOSITION[1] OF ANDESITIC DIKES

	I-82-5	I-82-12	I-82-20	82-79
Pb ppm	0	1	8	6
Th	2	0	1	4
U	1	0	0	3
Rb	17	7	54	15
Sr	164	166	114	51
Y	30	35	22	56
Zr	112	138	101	208
Nb	8	8	6	10
Zn	79	54	101	79
Cu	54	0	20	0
Ni	42	37	20	0
La	15	7	5	10
Ba	148	170	743	318
Ti (%)	1.11	1.30	1.14	1.07
V	297	245	300	56
Ce	24	31	26	33
Cr	23	12	36	0
Ga	15	19	11	14

[1]Pressed Pellet XRF analyses, Memorial University, Nfld.

TABLE 8.5. CHEMICAL COMPOSITION OF COMPOSITE DIKES

	(R) I-82-14	(H) I-82-15	(A) I-82-16	(A) I-82-17	(A) I-82-18	(A) I-82-21	(R) I-82-22
SiO_2	72.01	61.04	59.69	54.03	51.67	48.73	72.69
Al_2O_3	11.84	14.59	15.37	18.02	17.40	17.84	12.93
Fe_2O_3*	4.01	7.67	7.69	9.11	9.78	13.18	3.40
MgO	1.25	3.76	4.95	5.50	6.84	7.84	0.69
CaO	3.51	5.64	4.30	6.73	6.13	3.23	2.82
Na_2O	4.40	4.19	5.84	2.87	3.21	3.97	5.24
K_2O	0.38	0.88	1.50	1.63	2.80	1.46	0.32
TiO_2	0.29	0.61	0.65	0.82	0.86	0.96	0.25
P_2O_5	0.0	0.01	0.05	0.06	0.03	0.11	0.0
MnO	0.07	0.14	0.14	0.15	0.15	0.24	0.05
S	0.00	0.00	0.00	0.00	0.00	0.02	0.02
Total	97.76	98.53	100.18	98.92	98.87	97.58	98.41
La	21.87	16.13	9.97	-	7.86	8.35	26.05
Ce	48.40	33.94	24.72	-	21.37	19.40	58.37
Nd	29.18	20.28	13.03	-	10.87	11.18	32.02
Sm	7.06	4.86	3.36	-	2.62	2.84	7.84
Eu	1.31	1.06	0.95	-	0.77	0.77	1.47
Gd	7.13	4.86	3.21	-	2.37	3.03	7.74
Dy	7.84	5.24	3.03	-	2.34	2.48	8.79
Er	4.63	3.06	1.80	-	1.33	1.35	5.18
Yb	5.40	3.48	1.90	-	1.33	1.32	6.28
Lu	0.85	0.57	0.34	-	0.23	0.25	1.07
Y	54.47	35.89	20.12	-	14.68	15.49	63.06

A, H, R - denote Andesite, Hybrid or Rhyolite components
Samples I-82-14/-15/-16/-17/-18; and I-82-21/-22 are from two composite dikes

* Total Fe as Fe_2O_3

TABLE 8.5. CHEMICAL COMPOSITION OF COMPOSITE DIKES

	(A) I-82-24	(R) I-82-25	(A) I-82-26	(R) I-82-27	(A) I-82-114	(H) I-82-115	(R) I-82-1
SiO_2	51.16	66.01	53.45	70.43	64.43	65.62	74.56
Al_2O_3	12.97	13.60	15.47	11.90	14.69	14.04	12.00
Fe_2O_3*	15.31	7.70	13.32	4.81	7.89	6.84	3.51
MgO	4.49	1.07	6.21	1.83	2.49	2.12	0.70
CaO	7.98	3.91	3.32	1.77	2.25	2.63	1.59
Na_2O	1.93	3.75	3.83	3.88	6.16	5.54	5.34
K_2O	1.65	1.35	0.74	1.14	0.18	0.20	0.24
TiO_2	1.53	0.80	1.66	0.38	0.95	0.81	0.31
P_2O_5	0.04	0.12	0.17	0.03	0.23	0.17	0.02
MnO	0.28	0.10	0.16	0.06	0.08	0.08	0.04
S	0.00	0.01	0.01	0.00	0.01	0.01	0.00
Total	97.34	98.42	98.34	96.23	99.36	98.06	98.31
La	9.79	25.29	-	-	16.58	17.01	26.07
Ce	25.60	60.51	-	-	39.60	40.75	61.05
Nd	15.90	37.36	-	-	22.45	21.74	32.08
Sm	4.76	9.93	-	-	5.58	5.74	8.11
Eu	1.17	1.88	-	-	1.37	1.25	1.41
Gd	4.97	10.19	-	-	5.75	5.49	7.80
Dy	6.11	11.17	-	-	5.73	5.86	8.83
Er	3.60	6.51	-	-	3.31	3.49	5.25
Yb	4.09	7.51	-	-	3.80	4.12	6.32
Lu	0.68	1.14	-	-	0.63	0.67	0.97
Y	42.38	76.58	-	-	39.67	41.52	60.08

A, H, R - denote Andesite, Hybrid or Rhyolite components
Samples I-82-24/-25, I-82-26/-27; and 82-114/-115/-116 are from three individual composite dikes

* Total Fe as Fe_2O_3

TABLE 8.6. TRACE ELEMENT COMPOSITION OF COMPOSITE DIKES

	(A) I-82-16	(A) I-82-21	(R) I-82-22	(A) I-82-24	(A) I-82-114	(H) I-82-115	(R) I-82-1
Pb	5	2	1	3	2	10	1
Th	6	0	4	2	0	0	7
U	1	0	0	0	0	0	3
Rb	24	32	7	28	4	4	5
Sr	126	144	143	114	51	71	56
Y	33	14	72	50	44	48	66
Zr	148	71	297	126	192	201	251
Nb	8	5	17	10	9	10	15
Zn	87	181	30	165	32	30	7
Cu	2	0	6	0	0	0	5
Ni	52	101	2	26	0	0	0
La	5	8	8	9	12	10	17
Ba	521	447	109	372	72	71	89
Ti	0.74	1.09	0.26	1.43	1.08	0.92	0.34
V	164	263	29	444	132	112	17
Ce	19	21	29	23	28	36	27
Cr	81	161	0	0	0	0	0
Ga	12	13	17	17	15	13	12

TABLE 8.7. AVERAGE CHEMICAL COMPOSITION OF THE ANDESITIC, RHYOLITIC AND HYBRID COMPONENTS OF COMPOSITE DIKES

	Andesite[1]	Andesite	Rhyolite[2]	Rhyolite	Hybrid	Hybrid
No. of Samples	6		4		2	
	X	SD	X	SD	X	SD
SiO_2 %	53.2	3.7	72.4	1.7	63.3	3.3
Al_2O_3	16.2	1.9	12.1	0.5	14.3	0.4
Fe_2O_3*	11.4	2.9	3.9	0.6	7.3	0.6
MgO	5.9	1.2	1.1	0.5	2.9	1.2
CaO	5.3	1.9	2.4	0.9	3.1	0.6
Na_2O	3.6	1.3	4.7	0.7	4.8	0.9
K_2O	1.6	0.6	0.5	0.4	0.5	0.5
TiO_2	1.08	0.4	0.3	0.05	0.7	0.1
P_2O_5	0.07	0.05	0.01	0.01	0.09	0.1
MnO	0.19	0.06	0.05	0.01	0.11	0.4

[1] Average excludes sample 82-114 which has a high SiO_2 content and is interpreted to be a feeder dike to the Amulet upper member.

[2] Average excludes sample I-82-25 which is compositionally similar to the Hybrid component.

* Total Fe as Fe_2O_3

TABLE 8.8. CHEMICAL COMPOSITION OF THE DACITE DIKE

Hole No.	AN-53		AN-53		AN-56		AN-59	AN-66		AN-46*		AN-47	
Interval (m)	826-944		0-100		545-585		470-486	0-313		0-290		0-165	
No. Samples	4		5		2		1	9		8		6	
	X	SD	X	SD	X	SD		X	SD	X	SD	X	SD
Cu ppm	69	14	40	5	41	2	52	43	19	187	13.7	48	8
Zn ppm	132	36	87	5	49	9	26	83	19	433	20	108	59
Fe %	5.61	0.45	5.67	0.17	4.9	0.98	4.63	5.2	0.42	6.62	0.53	5.56	0.23
Mg %	1.41	0.11	1.3	0.21	1.2	0.58	0.78	1.44	0.35	1.28	0.15	1.3	0.35
CaO %	2.4	0.52	2.0	0.64	3.39	0.43	3.81	1.95	0.6	-	-	-	-
Na_2O%	4.26	0.43	5.1	0.31	4.93	0.87	4.69	5.29	0.26	3.74	0.72	5.31	0.36
K_2O %	0.35	0.08	0.7	0.17	0.18	0.01	0.27	0.33	0.13	-	-	-	-
SiO_2 %	61.7	0.31	62.5	0.60	62.96	0.49	64.3	60.1	3.02	63.08	0.86	63.35	1.8
TiO_2 %	0.86	0.14	0.93	0.25	0.90	0.06	0.95	0.93	0.05	0.96	0.05	0.96	0.13

* Hole AN-46 is anomalous, with a higher average Cu, Zn, Fe and lower Na_2O content than dacite intersected in other holes.

PLATE 8.1

Field of view for all photos is 4mm.
Bar in Plate 8.1A is 1mm long

A. Perlitic cracks in the groundmass of a quartz porphyritic, rhyolitic dike (Old Waite Swarm).

B. Recrystallized spherulitic texture in a massive, homogenous rhyolite dike (Old Waite Swarm).

C. Plagioclase porphyritic, intersertal textured andesitic dike from the Old Waite Swarm. Clots of massive, homogeneous chlorite are interpreted to replace original sideromelane.

D. Fine actinolite corona mantling a quartz phenocryst in the hybrid zone of a composite dike.

E. Myrmekite and "granular" textured quartz rims on quartz phenocryst from the hybrid zone of a composite dike.

F. Embayed, irregular plagioclase phenocryst from the hybrid zone of a composite dike.

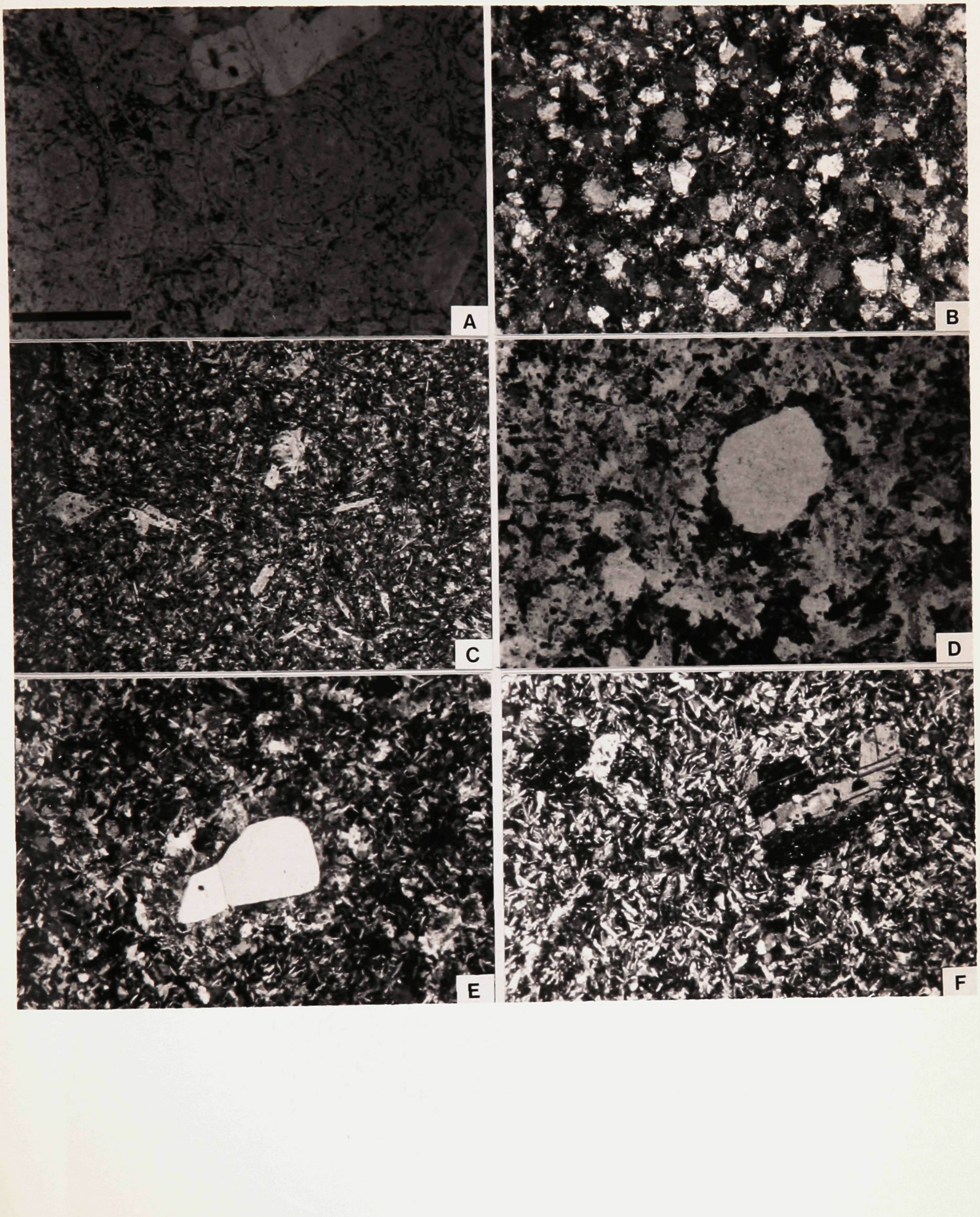
A
B
C
D
E
F

PLATE 8.2

A. Ragged plagioclase microlite with myrmekite in the groundmass. Bar is 1mm long.

B. Gradational contact between an andesitic xenolith (actinolite and quartz) and the hybrid zone matrix. Bar is 1mm long.

C. Quartz rim mantling a fine grained andesitic xenolith within the hybrid zone. The xenolith contains fine microlites. Field of view is 4mm.

D. Quartz-rich rim surrounding an epidotized andesitic xenolith. Field of view is 4mm.

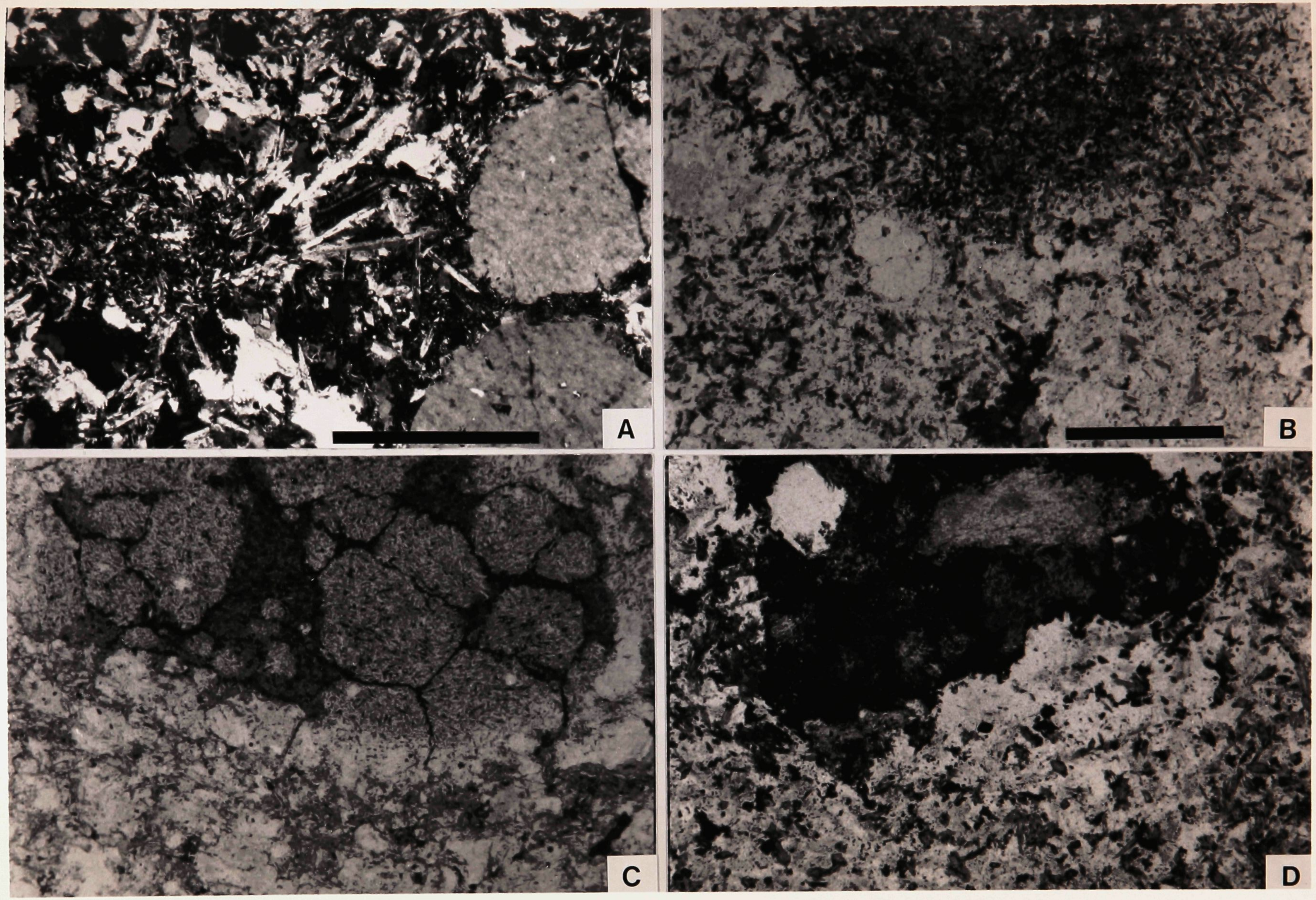
A
B
C
D

Plate 8.3. Sharp, chilled contact (under pencil) between the andesitic component of a composite dike and silicified andesitic flows of the Amulet upper member. Epidote-quartz alteration patches within the dike are elongate parallel to the dike contact.

Plate 8.4. Massive, quartz-feldspar porphyritic component of a composite dike. Hybrid component occupies lower part of photo below pencil.

Plate 8.5. Xenolith-rich, hybrid component of a composite dike. Irregular, amoeboid and cuspate andesite xenoliths occur within a massive feldspar and quartz-feldspar porphyritic, "rhyolitic" matrix.

Plate 8.6. Large granitic xenolith within a narrow QFP rhyolitic dike containing numerous irregular andesitic xenoliths. White paint defines the dike margins.

9. MINE SEQUENCE STRATIGRAPHY

9.1 INTRODUCTION

This Chapter is divided into three parts. The first part describes, in detail, the Mine Sequence of the Flavrian Block (Figure 9.1, Tables 2.3 and 2.4). The second part outlines a proposed lithostratigraphic correlations between the Hunter, Flavrian and Powell Blocks and the third part defines the principal Eruptive Centres for the Mine Sequence. For purposes of lithostratigraphic correlation, the Mine Sequence of the Powell and Hunter blocks and Aldermac area along with Cycle IV formations and Horne Mine stratigraphy are summarized in Appendix D. Proposed lithostratigraphic correlations are illustrated in Figure 9.2.

In the stratigraphic description which follows, each formation is described separately. The subsurface characteristics of formations VF to VIIR within the Flavrian block include isopach and top-contact contour maps based on >500,000m of drill core and structural cross-sections located on Map 1 and illustrated in Figures 9.3 to 9.6. Interpretations, which include vent areas and paleotopography, follow the description of each formation. Lithologic descriptions of rhyolitic and andesitic flows and breccias are contained in Chapters 4 through 7. Unless otherwise stated thicknesses referred to are true thicknesses.

9.2 MINE SEQUENCE STRATIGRAPHY: FLAVRIAN BLOCK

9.2.1 FLAVRIAN FORMATION (VF)

Definition, Distribution and Thickness

The Flavrian formation (VF) is stratigraphically and structurally the lowest formation within the Mine sequence and consists of andesitic flows and a single quartz-feldspar porphyritic (QFP) rhyolitic flow, the Ansil member (V FA). The formation is poorly exposed and occurs at surface in the Ansil, Waite Dufault and F-Shaft sectors and is intersected in drill holes within the Amulet-Millenbach sector for a total north-south length of 10km (Figure 9.7).

In both the Waite Dufault and F-Shaft sectors the formation is dissected by numerous dikes and minimum thickness estimates are difficult to determine. The type section for the Flavrian formation is located in the Ansil sector where the formation consists of 5 andesitic flows and a single QFP rhyolitic flow for a total thickness (minimum) of 500m (Figure 9.7).

The Ansil member (VFA) is not exposed at surface and was delineated through relogging of surface drill holes (Gibson and O'Dowd, 1981). The Ansil member is thickest (200m) in the north part of the Ansil sector (Figure 9.9) and thins to the south where it pinches out (Figure 9.10A). The Ansil member was not intersected in drill holes within the Waite Dufault and F-Shaft sectors. Quartz crystal tuffs interbedded with andesitic flows at the Corbet mine may be the time stratigraphic equivalent of the Ansil QFP flow.

Contact Relations

The base of the Flavrian formation is not exposed as the Flavrian Pluton intrudes the formation along its strike. Within 500m of the Flavrian Pluton andesitic flows of the Flavrian formation display effects of weak contact metamorphism manifested by a light "grey" colouration, recrystallization and locally, where altered, by the development of prismatic mafic porphyryoblasts pseudomorphed by chlorite/actinolite that are shown as spotted alteration in Map 2.

The Flavrian formation is conformably overlain by rhyolitic flows of the Northwest formation. However, in the southwest part of the Ansil sector and southeast part of the Amulet-Millenbach sector, where mapping and drill holes indicate a pinch out of the Northwest formation, the Rusty Ridge formation conformably overlies the Flavrian formation.

The Flavrian/Rusty Ridge contact is marked by a pyritic, thinly bedded to laminated tuff (<0.3m thick) referred to as the Lewis Tuff (Comba, 1975). Drill hole data and limited surface exposures indicate that the Lewis Tuff occurs as localized deposits. In the Amulet-Millenbach sector the Corbet VMS deposit occurs within the upper 200m of the Flavrian formation.

Flow units within the formation are conformable and in any one sector have the same attitude. Aerially restricted, thin deposits of laminated tuff are recognized in drill holes but are not correlative. The Flavrian Pluton intrudes the base of the Ansil member (Section EE and FF, Figure 9.4) and the rhyolitic member is conformably overlain by andesitic flows of the Flavrian formation except to the northeast where the Northwest formation conformably overlies the Ansil member.

Lithology

Five andesitic flows comprise the Flavrian formation of the Ansil sector whereas only two flows define the formation in the Waite Dufault and F-Shaft sectors (Table F.1). At the Corbet mine, in the Amulet-Millenbach sector, the formation is a 400m thick succession of massive and pillowed flows and pyroclastic breccias (Appendix C).

The Ansil member consists of a single QFP flow, the Ansil QFP, that is mineralogically and chemically similar to QFP flows of the Millenbach Rhyolite formation (Gibson and O'Dowd, 1981). The flow consists of massive and subordinate flow brecciated rhyolite containing 10% quartz and 5% albite phenocrysts in a felsophyric to spherulitic groundmass.

Subsurface Characteristics

Flavrian Formation

Uniform, regularly spaced, parallel and straight contour lines which follow the surface trace of the formation (Figure 9.8) suggest a flat, planar, upper surface for much of the Flavrian formation. This regular contour pattern is disrupted adjacent to the McDougall-Despina Fault, in the Corbet mine area, where a detailed contour map (Watkins, 1980; Appendix C) indicates a paleotopographic high in the andesitic formation extending from just south of the Corbet orebody northward for 1.2 km along and parallel to the McDougall-Despina Fault.

Ansil Member

The isopach map of Figure 9.9, and section F-F of Figure 9.4, show the Ansil member to be an aerially restricted dome or stubby flow with slopes of 20^0 - 30^0.

Interpretation

Vent Areas

Limited surface exposures and removal of unknown volumes of the formation by the Flavrian Pluton has hampered definition of vent areas. The best defined vent area for andesitic flows of the Flavrian Formation is the McDougall-Despina Fault in the Corbet mine area (Appendix C). Andesitic dikes within the Old Waite dike swarm west of Duprat lake are probable feeders to adjacent Flavrian andesitic flows (Chapter 8). The classical dome form of the Ansil member suggests that it is a restricted, short stubby flow or lava dome that is likely situated above its vent.

Paleotopography

The contour map for the Flavrian formation indicates a smooth, flat paleotopography, except in the immediate area of the Corbet mine. Topographic irregularities imposed by the comparatively steep-sided rhyolitic Ansil member are eliminated by almost total burial by penecontemporaneous andesitic flows.

9.2.2 NORTHWEST FORMATION (VIN)

Definition, Distribution and Thickness

The Northwest formation (VI N) consists of two main rhyolitic flows and a single QFP rhyolitic flow, the Cranston member (VI NC), which is described separately. Surface exposures of the Northwest formation extend from the Cranston Sector in the north to the F-Shaft sector in the south, a distance of 7km (Figure 9.11). Numerous drill hole intersections define the formation in the Amulet-Millenbach sector.

The Northwest formation is composed of a North and South flow. The North flow is a simple flow that, in the Ansil sector, attains a maximum thickness of 500m west of Ansil Hill and thins both to the northeast, and south where it pinches out west of Duprat Lake as illustrated in sections E-E and G-G of Figure 9.4, and Map 1.

The South flow is a composite flow. In the Amulet-Millenbach and Waite-Dufault sectors a thin tuff (DDH D-278) and andesitic flow separates flow units.

The South flow ranges from 15m to a maximum thickness of 300m above the Corbet deposit (Section P-P of Figure 9.5).

Contact Relations

The Northwest formation conformably overlies and is conformably overlain by the Flavrian and Rusty Ridge formations respectively. These contacts are each exposed in two localities at surface (Map 1) but are well exposed in underground workings at the Corbet mine (Figure 4.8).

Lithology

The North and South flows consist of FP rhyolite as described in Chapter 4. The quartz porphyritic flow at the base of the South flow in the Waite Dufault sector is of limited areal extent and is identical to overlying FP rhyolite except that it contains 3-5%, fine (1-3mm) quartz phenocrysts (Gibson and Doiron, 1982).

Subsurface Characteristics

Contour and isopach maps for the North and South flows are illustrated in Figures 9.12 and 4.2. The North flow is a northeast-trending elongate topographic dome with slopes ranging from 10^0 - 20^0 and a central 3.5km ridge (defined by the 300m isopach) that trends N55^{0}E (Figure 4.2). Contour lines are regular, parallel and conform to the shape of the isopached flow indicating a relatively smooth surface except in the vicinity of the 500m isopach where contours are contorted, possibly reflecting surface irregularities at the top of the flow in this area (Figure 9.12).

The South flow is an elongate, northwest-trending flow (Figure 4.2). The 200m isopach defines a 4.0km, N40^{0}W trending topographic ridge that contains 4 smaller "domes" defined by 300m isopachs. This topographic ridge is adjacent and subparallel to the McDougall-Despina Fault. In the Corbet mine area a N45^{0}E trend is also apparent as indicated by the alignment of two small "domes" and by the distinct northeast trend to the 200 and 250m isopachs. This northeast trend is similar to that of the North flow, to the stratigraphically higher Millenbach Rhyolite formation which occurs 1km to the east-southeast and to the strike of underlying rhyolitic feeder dikes (Appendix C). Slopes along the flanks of the South flow range from 10^0 - 15^0.

Interpretation

Vent Areas

Although the surface trace of the North flow is a section oblique to the actual flow direction a thickening of the flow is readily apparent in the Ansil Hill area (cross-sections EE, GG and HH of Figure 9.4). Thickening of the North flow at surface and in section with a concomitant decrease in thickness of the overlying Rusty Ridge formation indicates that the North flow was a topographically positive feature that attained a maximum height of 500m immediately south of Ansil Hill.

The isopach map indicates that the Ansil Hill dome lies at the south end of a 3.5 km long topographic ridge which trends N55^{0}E. This ridge is interpreted to overlie the feeding fissure to the North flow. Rhyolitic lava that issued from this fissure flowed less than 2km.

Similarly, the South flow may have issued from a 4km long, northwest-trending fissure. Four domes, with thicknesses in excess of 300m, occur along and above this feeding fissure (Figure 4.2).

Rhyolitic feeder dikes to the North flow have not been recognized at surface because of the low outcrop density. This is not the case for the South flow where underground workings at the Corbet mine provide ample exposures of the South flow and underlying Flavrian formation. Flow banded, aphyric to feldspar porphyritic, spherulitic dikes, identical to the overlying South flow occur within the Flavrian formation with two distinct trends: northwest, parallel and subparallel to the McDougall-Despina Fault, and northeast (Appendix C). These dikes are interpreted as feeders to the South flow and their trends match those inferred from the isopach map.

Paleotopography

The North and South flows formed two large rhyolitic ridges or plateaus rising 500m and 300m above the relatively flat Flavrian formation with slopes of

10^0 - 20^0.

9.2.3 CRANSTON MEMBER, NORTHWEST FORMATION (VI NC)

Definition, Distribution and Thickness

The Cranston member of the Northwest formation is a single QPF rhyolitic flow referred to as the Cranston QFP. Outcrops of this unit are found only in the Cranston sector (Figure 9.11) but drilling indicates that it extends east, across the Dufresnoy Diorite, in the New Vauze sector and south of the Cranston Fault to Ansil Hill (Section A-A, B-B of Figure 9.3). The Cranston member has not been recognized in the adjacent Hunter Block; its northward extension was perhaps blocked by the Hunter Creek Fault.

Contact Relations

Diorite intrudes the Cranston member and obscures the contact with underlying Northwest formation in the north part of the Cranston sector (Figure 4.11). To the south, massive and weakly flow-brecciated rhyolite of the Cranston QFP directly and conformably overlies a feldspar porphyritic flow of the Northwest formation. Thin-bedded to laminated tuff occurs as lenses along this contact (Map 1).

To the southeast, andesitic flows separate the Cranston member from underlying Northwest formation (section AA, Figure 9.3). These andesitic flows are thickest in the immediate area of the Cranston Fault (section BB, Figure 9.3).

South of the Cranston Fault, in the Ansil sector, the Cranston member is a breccia (Chapter 4) which conformably overlies the North flow at Ansil Hill area but, adjacent to the Cranston Fault, is separated from underlying North flow by andesitic flows (section B-B, Figure 9.3).

A thin tuff occurs locally at the upper contact of the Cranston member. Rusty Ridge formation conformably overlies the Cranston member in both the Cranston, Ansil and New Vauze sectors.

Lithology

The Cranston QFP consists of quartz and albite porphyritic rhyolite containing a maximum of 20% phenocrysts. A detailed lithologic description is contained in Chapter 4.

Subsurface Characteristics

Isopach and stratigraphic top-contact contour maps for the Cranston QFP are illustrated in Figures 4.12 and 9.10B. The Cranston QFP is a small, aerially restricted rhyolitic lava dome or stubby flow that attains a maximum thickness of 250m and slopes of 10^0 - 30^0. The area of maximum flow thickness corresponds with an area of predominantly massive lava at surface. A crude northeast trend to the isopachs suggest that the lava-dome may have been fed from fissures trending N70^{0}E and S60^{0}E.

South of the Cranston Fault the Cranston member is a QFP rhyolitic breccia that forms a blanket-like deposit covering the north part of the Ansil sector (section B-B, Figure 9.3). It is typically <10m thick but locally up to 50m thick within isolated depressions. Quartz crystal tuffs which overlie the North flow of the Northwest formation at the Ansil mine may be the stratigraphic equivalent to the Cranston QFP flow.

Interpretation

Vent areas

Surface exposures and the isopach map indicate that the QFP flow is thickest in an area dominated by massive rhyolite within the centre of the Cranston sector. This dome of massive rhyolite is interpreted to overlie the main vent which may be controlled by northeast and southeast trending structures.

Andesitic flows which separate the Cranston member from the underlying North flow are interpreted to have been erupted contemporaneously from vents along the Cranston Fault. These andesitic flows may be precursors to, or contemporaneous with flows of the Rusty Ridge formation. The latter interpretation is preferred but either interpretation indicates contemporaneous rhyolitic and andesitic volcanism and perhaps temporal overlap between eruption of the Northwest and Rusty Ridge formations.

Paleotopography

Extrusion of the Cranston QFP flow, with slopes of 10^0 - 30^0, on the north flank of the North flow produced a "rugged" topographically high dome or barrier along the Hunter Creek Fault in the north part of the Flavrian Block. This barrier accounts, in part, for the rapid decrease in thickness of the overlying Rusty Ridge formation. The apparent restriction of the Cranston member to the Flavrian Block suggests that the Cranston flow may have built up against an ancestral fault scarp now represented by the Hunter Creek Fault.

9.2.4 RUSTY RIDGE FORMATION (VII)

Definition, Distribution and Thickness

The Rusty Ridge formation (VII) is a complex succession of basaltic to andesitic flows, minor dacitic flows and thin localized units of rhyolitic breccia. The formation extends south from the Hunter Creek Fault in the Ansil Sector to the McDougall Fault in the F-Shaft Sector (Figure 9.13). The Rusty Ridge formation is variable in thickness (Table E.2) but attains a maximum thickness of 1000m in the Duprat lake area. The formation thins to the northeast where it is 300m thick at Ansil Hill; north of Ansil Hill the formation thickens to 500m. In the Cranston sector the formation is thickest near the Cranston Fault (350m) and thins northwards to 60m at the Hunter Creek Fault. South of Duprat Lake the Rusty Ridge formation thins to <300m adjacent to the McDougall Fault.

Thin (<25m thick), localized, inter-andesite flow, rhyolitic breccia units were encountered at three stratigraphic intervals within the Rusty Ridge formation of the Ansil sector (Figure 7.6). In the Cranston sector, and north part of the Ansil sector, the uppermost flows of the Rusty Ridge formation contain a "dacitic" unit composed of silicified massive flows that are similar to flows of the upper member of the Amulet formation (Table E.2).

Contact Relations

The Rusty Ridge formation rests conformably on underlying Northwest formation and, where the latter is absent, on the Flavrian formation. Bedded tuff occurs sporadically at this contact; the best exposure is located 300m east of Fourcet Lake where laminated tuff (<1.5m thick), fills irregular depressions of the underlying rhyolitic flow breccia. The Rusty Ridge formation is conformably overlain by the Amulet formation; Beecham Breccia and tuff occur at this contact.

A northeast striking discordant breccia occurs at the Rusty Ridge/Amulet formation contact adjacent to the McDougall Fault, in the Amulet-Millenbach sector (Maps 1 and 2). There, north-south striking andesitic flows of the Rusty Ridge formation terminate against the breccia which separates the andesitic flows from the northeast striking Bedford rhyolitic flow of the Amulet formation (VIII Au). The breccia ranges in thickness from <0.5m to 10m and comprises angular to rounded fragments (<0.3m) of strongly chloritized rhyolite and andesite in a fine-grained, chloritized breccia matrix with discontinuous quartz veins. The breccia is interpreted as a synvolcanic fault breccia as the Bedford rhyolitic flow is chilled against it.

In the F-shaft sector, the lowermost flows of the Rusty Ridge formation are in fault contact with a quartz-porphyritic dioritic intrusion (Meritens phase) of the Flavrian Pluton which occupies the McDougall-Despina Fault.

Lithology

Details of the mineralogy, textures, structures and flow morphology of andesitic flows are described in Chapter 5. Andesitic flows which comprise the Rusty Ridge formation are described in Table F.2.

Figure 9.14, constructed from data contained in Appendix F, illustrates details of the flow stratigraphy and correlation of individual flows within the Waite Dufault sector (Figure 9.13). From Figure 9.14 it is apparent that :

a) the formation decreases in thickness from 550m to 345m south of Duprat Lake. This decrease is not related to an increase in thickness of the underlying Northwest formation.

b) individual flows such as #1, 3, 5, 7, 8, 9 and 10 end abruptly at faults whereas underlying and overlying flows continue uninterrupted across these faults.

c) the marked thickening and increase in number of flows which comprise flow #11, between the Quesabe and Watkins Faults, suggest primary ponding within a fault block.

d) massive and pillowed flows have a similar lateral extent.

Subsurface Characteristics

The parallel, straight and regular spacing of contours (Figure 9.15) suggests a relatively flat topography for the Rusty Ridge formation. Closer spacing of contours indicates that dips are somewhat steeper north of Ansil Hill and south and east of Duprat Lake or that the formation thins in these directions. Variation in thicknesses of the formation at surface support the latter interpretation.

An isopach map of the Rusty Ridge formation is shown in Figure 9.16. The data are limited and only general variations in thicknesses are indicated;

a) in the Cranston Sector the formation thins from approximately 400m at the Cranston Fault to <100m near the Hunter Creek Fault. This in part reflects underlying topography as the Cranston member is thickest and forms a topographic barrier or dome where the Rusty Ridge formation is thinnest.

b) in the Ansil Sector the Rusty Ridge formation increases in thickness north, east and south of Ansil Hill along the flanks of a topographic ridge in the underlying Northwest formation. The Rusty Ridge formation increases in thickness from 300m at Ansil Hill to >500m, at the Ansil Mine located only 0.5km to the east-southeast. (Section G-G and H-H of Figure 9.4).

c) the Rusty Ridge formation exposed on the south shore of Duprat Lake has a maximum thickness of 550m and thins to the southeast where it is <100m thick 1km south of the Corbet Mine. Thinning of the formation to the southeast corresponds in part with an increase in thickness of underling Northwest formation in the Amulet-Millenbach sector.

Interpretations

Vent Areas

The main vent area for andesitic flows the Rusty Ridge formation lies within the northeast striking Old Waite Dike Swarm in the Duprat Lake area (Chapter 8). Evidence that supports this interpretation includes:

a) fine-grained to aphanitic andesitic dikes along the south shore of Duprat Lake Maps 1 and 2 are identical to adjacent Rusty Ridge flows. In one example, illustrated in Figures 9.17 and 9.17A, an amygdaloidal andesitic dike is traceable into an overlying massive flow. This feeder dike is identical and parallel to numerous andesitic dikes which comprise the Old Waite Dike Swarm (<2m to >10m wide) and are collectively interpreted as feeders to andesitic flows of the Rusty Ridge and overlying younger andesitic formations.

b) paleo-flow directions measured from budding pillows (cross-sections) and branching tubes (plan) indicate a general north to south flow direction for andesitic flows of the Rusty Ridge formation in the Waite Dufault sector.

c) the marked thinning of the Rusty Ridge formation away from the dike swarm.

Other "vent areas" were recognized and these include;

a) an east-west trending (40m wide) columnar jointed andesitic dike similar to those of the Old Waite Dike Swarm north of Fourcet Lake, in the Waite Dufault sector, is interpreted to be a feeder dike. This dike and a narrower one located 300m to the north may have fed andesitic flows of the Rusty Ridge formation in the south part of the Waite Dufault and adjacent F-Shaft sectors.

b) at Ansil Hill, a narrow (<2m wide) northwest striking andesitic feeder dike cross-cuts a massive andesitic flow and flow-top breccia and grades into an overlying pillowed flow (Appendix A).

c) the Rusty Ridge formation adjacent to the Cranston Fault is >300m thick and thins both to the north and south away from this structure. Paleo-flow directions obtained in the upper most flows of the Rusty Ridge formation at Ansil Hill suggest a north-south flow direction from a possible vent area in vicinity of the Cranston Fault.

d) paleo-flow directions for the uppermost andesitic flows in the Amulet-Millenbach sector indicate a south to north flow direction, away from the McDougall-Despina Fault. Large blocks of massive andesite within rhyolitic breccia dikes which occupy the Fault north of the Bedford road may be remnants of feeder dikes to Rusty Ridge flows.

Rhyolitic breccias within the Rusty Ridge formation are localized deposits. Vent areas for these deposits have not been recognized.

Paleotopography

The paleotopography following extrusion of the Rusty Ridge formation is interpreted to have been relatively flat with irregular topographic ridges and domes of the underlying Northwest formation inundated by Rusty Ridge andesitic flows. Evidence in support of this interpretation includes;

a) the smooth, regular contours

b) absence of a shoaling sequence or increase in amygdule contact of flows at the top of the 1 km thick formation

c) occurrence of a regionally extensive, plane-bedded tuff and localized breccia (Beecham Breccia) along this upper contact.

d) low primary slopes inherent to edifices built by andesitic flows; even rhyolitic flows of the Northwest formation and Amulet Lower member have slopes $<20^0$.

9.2.5 AMULET FORMATION (VIII A)

Definition, Distribution and Thickness

The Amulet formation (VIII A) is composed of flows ranging in composition from andesite to rhyolite and a localized breccia unit, the Beecham Breccia. The

Amulet formation is one of the best exposed formations within the Flavrian Block and extends from the Cranston sector south to the Despina sector. The formation attains a maximum thickness of 1.2 km in the Waite Dufault and F-Shaft sectors.

The Amulet formation is divided into an upper member of predominantly silicified andesite and a lower member composed of rhyolitic flows (Gibson, 1979). The members are distinctive units even where the upper member is strongly silicified. Only where they are strongly chloritized or sericitized were chemical analyses required to establish their contact.

Reference (Type) sections for the Amulet formation are located in Figures 9.18 and 9.19, and illustrated in Figure 9.20. The Amulet lower and upper members are described separately.

9.2.6 AMULET LOWER MEMBER (VIII AL)

Definition, Distribution and Thickness

The lower member extends from the Hunter Creek Fault south to the Bancroft Fault (Figure 9.18) and attains a maximum thickness of 300m and 450m in the Ansil sector and Waite Dufault sector respectively. The lower member is composed of three rhyolitic flows and a localized breccia unit, the Beecham Breccia (Figure 9.18).

Contact Relations

The lower member rests conformably upon the underlying Rusty Ridge formation. The contact is well exposed with andesitic flows of the Rusty Ridge formation in direct contact with rhyolitic flows of the lower Amulet member or with Beecham Breccia. Beecham breccia is a well bedded lapilli tuff to tuff breccia and ash deposit (Chapter 7) that defines the base of the lower member in the Amulet-Millenbach and F-Shaft sectors and totally comprises the lower member in the former. The Bedford rhyolitic flow of the upper member conformably overlies Beecham Breccia (lower member) in the Amulet-Millenbach sector.

The contact between the members is irregular but conformable. Between the Bancroft and the Cranston Faults, where the contact is not obscured by alteration, massive silicified andesitic flows of the upper member rest conformably on rhyolitic hyaloclastites and lobes of the lower member. A thin bedded, pyritic tuff, the Comba Tuff, occurs at this contact north of Duprat Lake between the Des and Dacite Faults and 10m above this contact in andesitic flows of the upper member 100m north of the Bedford road within the F-Shaft sector.

In the Cranston sector, the rhyolitic lower member is conformably overlain by the Waite Andesite formation (IX). A pyritic tuff, the C Contact tuff, is exposed in trenches at this contact.

Lithology

The #1 and #3 flows of the lower member are FP rhyolites. The #2 flow is an aerially restricted QFP flow containing from 3-10%, <5mm quartz and 3% plagioclase phenocrysts in a fine-grained spherulitic groundmass. Unlike QFP rhyolitic flows described in Chapter 5, the #2 flow has a well developed lobe/hyaloclastite facies and based on limited exposures has a flow morphology similar to FP flows. Beecham Breccia is interpreted as a subaqueous ash flow deposit (Chapter 7).

Interpretations

Vent Areas

The vent area for Beecham Breccia lies within the McDougall-Despina fault north of the Bedford road (Chapter 7). Vents for the three rhyolitic flows are defined on the basis of facies mapping (Chapter 4), and thickness variations (Figure 9.18).

The #1 flow extends from the Hunter Creek Fault in the north to the just south of the Dacite Fault where it pinches out. In the Cranston sector the flow thickens toward the north and a second vent for this flow is inferred to lie close to the Hunter Creek Fault which may also confine the #1 flow to the Flavrian Block. In the Ansil sector a second vent is inferred to lie south of or within the Cranston Fault as the #1 flow is thick in this area and thins to the south. An increase in thickness of the #1 flow, south of Ansil Hill, may be a product of faulting or indicate a third vent in the vicinity of the Dacite and Des Faults.

The #2 flow is the most aerially restricted. The flow is thickest along the north shore of Duprat Lake and thins northward where it overrides the #1 flow. The #2 flow is interpreted to overlie its vent located on the north shore or within Duprat Lake. Quartz-feldspar porphyritic dikes and the rhyolitic component of composite dikes within the Old Waite Dike Swarm may be feeders to this flow.

The #3 flow is thickest immediately south of Duprat Lake. The southward thinning of the #3 flow and concomitant decrease in the proportion of massive lava to lobe/breccia facies suggest that the principal vent area lies immediately south of or within Duprat Lake. Spherulitic rhyolitic dikes within the Old Waite Dike Swarm and south of Duprat lake may be feeders to this flow.

Paleotopography

Variations in thickness of the Beecham breccia reflect the underlying paleotopography (Chapter 7). Assuming a relatively horizontal paleotopography following Rusty Ridge volcanism, the distribution of Beecham breccia relative to its vent suggests that the F-shaft, Amulet-Millenbach and Despina sectors may have been tilted to the south-southeast relative to sectors in the north prior to or during deposition of the breccia.

Following extrusion of rhyolitic flows the paleotopography was dominated by rhyolitic plateaus and domes with slopes of 10^0 - 20^0. These gently sloping rhyolitic edifices were built upon the relatively flat, horizontal surface of the Rusty Ridge formation.

Synvolcanic faulting and subsidence accompanied volcanism as shown by the north and south confinement of the #1 and 3 flows and tilting of stratigraphy prior to deposition of Beecham Breccia (Chapter 7).

9.2.7 AMULET UPPER MEMBER (VIII Au)

Definition, Distribution and Thickness

The Amulet upper member consists of flows that range in composition from andesite to rhyolite and have been variably altered (silicified and chlorite/sericite altered). The Amulet upper member extends from the Despina sector north to the Ansil sector where it ends abruptly at the Cranston Fault (Figure 9.19). The upper member attains a maximum thickness of 0.9km in the F-Shaft sector.

In the F-Shaft sector two rhyolitic flows occur within the upper member. The lower rhyolitic flow, the Bedford flow, extends south into the Amulet-Millenbach and Despina sectors and conformably overlies Beecham Breccia of the lower member in the former. The F-Shaft flow occurs near the top of the Amulet upper member immediately west of the F-Shaft deposit. A third, small and poorly exposed FP rhyolitic flow occurs near the top of the upper member north of

Duprat Lake.

Lithology

Flows comprising the upper member are interpreted to be altered, silicified andesite (Table 9.1, Chapter 12). The emphasis of this description is their flow morphology, stratigraphy and mode of emplacement.

The upper member consists of thick massive flows (50-400m thick) characterized by:

a) a massive facies of brown weathering (white siliceous patches), green, plagioclase porphyritic andesite that is hyalophitic to intersertal textured, medium to fine-grained and contains <5% amygdules in the flow interior that grades into an aphanitic, laminar jointed and amygdaloidal (8-20%) flow top. Narrow (<1m), amygdule-rich bands (10-20% amygdules) and breccia separate individual flows or surges within thick, composite flows.

b) a lobe facies of brown to white weathering (silicified) aphanitic, massive or laminar jointed porphyritic amygdaloidal (<20% amygdules along lobe margins) andesite (Appendix B). The lobe facies is best developed near the flow terminus (Figure 9.23).

c) a purple-green, hyaloclastite and or vitrophyre breccia facies consisting of massive and banded, spherulitic, "in situ" brecciated, chloritized and silicified amygdaloidal (<30% quartz amygdules) andesitic sideromelane. The breccia facies occurs as isolated pockets on massive andesite or mantling poorly developed lobes proximal to the vent and is associated with a well developed lobe facies near the flow terminus. At the flow terminus, the breccia contains isolated lobes and lobe fragments and the matrix contains a significant component of silicified microlitic shard hyaloclastite derived through lobe autobrecciation.

Sections detailing the flow stratigraphy and facies of the upper member are illustrated in Figure 9.20; the sections correspond to reference sections of Figure 9.19 . Massive flows are extensive and correlative between fault blocks. Three flows comprise the upper member north of the F-Shaft Fault. The lower flow increases in thickness near a vent (Dacite unit) north of Duprat Lake, but pinches out along the flanks of the #1 rhyolitic flow of the lower member. The upper two flows extend to the Cranston Fault, but the massive facies of the upper flow thins and ends within breccia. The upper flow extends south into the Despina sector but the underlying two flows merge into a thick (400m), massive columnar jointed compound flow proximal to its main vent, in the F-Shaft sector. This thick flow extends across the F-Shaft sector, but in the Amulet-Millenbach sector is represented by three flows, two of which are compound. In the Despina sector the upper flow was traced south where it eventually terminates against the Flavrian Pluton; the underlying flows pinch out along the flanks of the Bedford flow. The decrease in thickness of the upper member south of the McDougall-Despina Fault indicates a pinch out against the underlying Bedford flow and possibly ponding of flows north of the McDougall-Despina Fault.

Another important aspect illustrated in Figure 9.20, is a lateral increase in thickness and continuity of both the lobe and breccia facies toward the flow terminus (and upper member); and to a lesser degree, vertically, between flows at the base and top of the member. Thick, massive compound flows of the upper member undergo a lateral facies change to simple flows with a concomitant increase in the lobe and breccia facies away from their vent. Pillowed flows occur as localized units within the upper member; four flows have been recognized as described below:

1) a strongly silicified, 12m thick flow occurs within a compound flow immediately adjacent and south of the F-Shaft Fault.

2) a 70m thick pillowed flow and 50m thick massive flow occurs at the base of the upper member immediately adjacent to and north of the Bancroft Fault. The flows extend 300m to the north where they pinch out along the flanks of the #3 flow of the lower member. The flows are not silicified and are conformably overlain by the Bedford flow.

3) a single outcrop of pillowed andesite conformably overlies the Bedford flow at the Bedford deposit south of and adjacent to the McDougall-Despina Fault. The flow is not silicified.

4) a silicified pillowed flow occurs within massive flows near the top of the upper member in the Despina sector, 1.4 km south of the McDougall-Despina

Fault.

The Bedford and F-Shaft flows consist of aphyric to FP spherulitic rhyolite, identical to that of the lower member. The F-Shaft flow occupies a stratigraphic position between the upper two massive andesitic flows of the F-Shaft sector. The Bedford flow occurs at the base of upper member in the Amulet-Millenbach sector but overlies pillowed and massive flows, immediate to the Bancroft Fault, in the F-Shaft sector.

Contact Relations

South of the Cranston Fault and north of the Bancroft Fault the upper member conformably overlies the lower member. South of the Bancroft Fault the Bedford flow conformably overlies Beecham Breccia of the lower member.

The rhyolitic flow within the upper member of the Despina sector is correlated with the Bedford flow in the Amulet-Millenbach sector, the former is intruded by the Flavrian Pluton (Figure 9.19). The base of the upper member is not exposed, nor has it been intersected in drill holes within the Despina sector. The Bedford deposit, a volcanogenic stringer sulphide deposit, occurs at the top of the Bedford rhyolitic flow in the Despina sector (Atkinson and Watkinson, 1979).

In the Ansil sector the upper member is conformably overlain by the Waite Andesite formation (IX W), whereas in sectors to the south Millenbach Andesite (IXM)) conformably overlies the Amulet upper member. The regionally extensive

C Contact Tuff occurs at this upper contact. Six small volcanogenic massive sulphide deposits are located along the upper contact of the Amulet member; they include from north to south, the F-Shaft, D-62 lens, Moose Head, Amulet C, Amulet #11 shaft and Lac Dufault No. 1 deposits.

Tuffs do not occur between thick, silicified massive flows of the upper member.

Interpretations

A reconstructed north-south section through the upper member, assuming a horizontal upper paleosurface (Figure 9.23), illustrates the flow morphology and facies of individual flows and the upper member as a whole. Thick, massive, compound and simple flows of the upper member are interpreted as products of a brief, voluminous eruption (approximately 40 km^3) with a high effusion rate. Voluminous outpourings of lava spread quickly away from vents as proximal, compound flows and distal, simple flows that flooded underlying rhyolite topography only to have become ponded to the north (Cranston Fault) and possibly to the south (Beauchastel Fault). The absence of any kind of interflow sediment or tuff, common to associated andesitic and many rhyolitic formations, is unique to the 900m thick upper member, and is consistent with rapid extrusion and emplacement of this unit.

The F-Shaft flow represents contemporaneous eruption of a small rhyolitic lava dome during a waning andesitic eruption; the vent for the F-Shaft flow lies directly above the principal feeding fissure to underlying andesitic flows. The Bedford flow although included within the upper member, lies at its base. This flow may simply be a continuation of lower member rhyolitic volcanism separated by a period of localized subsidence and andesitic extrusion (along the Bancroft Fault) prior to flood-type eruptions of andesitic flows.

Andesitic Vent Areas

Thick, massive, andesitic flows issued from three main vents; two are located in the F-shaft sector and one is located in the Ansil sector as illustrated in Figure 9.19.

The F-Shaft sector vent is an east-west striking andesitic feeder dike that parallels and lies adjacent to the Walker Fault (Figure 9.21). The andesitic feeder dike is <2m wide where it transects the rhyolitic lower member and widens to 50m over a distance of 100m at the top of the lower member. Andesite within the dike is amygdaloidal and columnar jointed where it merges imperceptively with a massive, columnar jointed andesitic flow of the upper member.

A second east-west trending amygdaloidal, andesitic feeder dike cross-cuts the Bedford flow of the upper member, adjacent to the Bancroft Fault (Maps 1 and 2). Although not observed to grade upward into flows, andesite within the dike is identical to overlying least altered andesitic flows of the upper member.

The Dacite Dike is an intrusive body, of intermediate composition, that may be a feeder to andesitic flows in the Ansil sector (Chapter 8, Figure 9.4 Section G-G). Localized, thin, pillowed flows within the upper member are interpreted to have erupted from nearby vents located adjacent to the F-Shaft, Bancroft, and McDougall Faults.

Rhyolitic Vents

The Bedford flow issued from two vents, both of which are located in the Amulet-Millenbach sector. The most northerly vent is a massive spherulitic rhyolitic dike that intrudes the upper flows of the underlying Rusty Ridge formation, and Beecham Breccia, and grades into banded spherulitic lava of the Bedford flow (Maps 1 and 2). The dike has an amygdaloidal interior, numerous fine andesitic fragments (<2cm) and blocks and distinct chilled and banded margins.

A second vent is interpreted to lie in the McDougall Fault which is now occupied by later rhyolitic dikes. Massive rhyolite of the Bedford flow, adjacent to the McDougall Fault, is intrusive into and chilled against a fault breccia that separates it from the adjacent Rusty Ridge formation. Further to the northeast massive rhyolite grades into flow-banded and massive rhyolite which conformably overlies Beecham Breccia. The truncation of Rusty Ridge andesitic flows against this fault and its control on the location of a Bedford flow feeder dike indicate that it is a synvolcanic structure. The pinch-out of massive andesitic flows of the upper member along the flank of the Bedford flow, in the Despina sector, may be related to doming of the rhyolitic flow above another possible vent.

The F-Shaft flow is confined to the F-Shaft sector and is an aerially restricted flow or dome that is interpreted to overlie a vent area that is not exposed at the present erosion surface.

Paleotopography

Following extrusion of the Amulet upper member the paleotopography is interpreted to have been relatively flat and horizontal. Irregular topographic ridges and plateaus of rhyolite that comprise the lower member were completely buried by andesitic flows, except in the Cranston sector. A relatively flat, horizontal paleosurface for the upper member is indicated by:

a) smooth, regular and evenly spaced contours (Figure 9.22).

b) the occurrence of a regionally extensive, plane-bedded tuff at this contact.

9.2.8 MILLENBACH ANDESITE FORMATION (IXM)

Definition, Distribution and Thickness

The Millenbach Andesite formation (IX M) consists of basaltic to andesitic flows and intercalated tuffs. Millenbach Andesite was first recognized as a separate stratigraphic unit at the Millenbach Mine where it was referred to as "Millenbach Dacite" (Simmons et al., 1973). Millenbach Andesite in the Amulet C and Turcotte Lake areas has been previously referred to as the "Upper McDougall Dacite" and "Black Rhyolite" respectively (Knuckey et al., 1982). The most recent stratigraphic mapping (de Rosen-Spence, 1976) included surface exposures of the Millenbach Andesite with the Amulet Andesite formation (XIA). In the Amulet-Millenbach sector flows A1 - A5 of the Amulet Andesite formation (de Rosen-Spence, 1976) are here interpreted as constituting the Millenbach Andesite formation.

Surface exposures of Millenbach Andesite are restricted to the F-Shaft, Amulet-Millenbach and Despina sectors where the formation has a strike length of 4.5km. The Millenbach formation is correlated with the Waite Andesite formation (Figure 9.24). The Millenbach Andesite formation attains a maximum thickness of 350m in the F-Shaft area, where the Dufresnoy Diorite intrudes the upper part of the unit. At the Millenbach mine, Millenbach Andesite has a maximum thickness of 60m but it thins to the southwest where it pinches out before reaching the D-68 deposit area.

Contact Relations

Millenbach Andesite (IX) conformably overlies the Amulet formation (VIII) and is conformably overlain by the Amulet Andesite formation (XI) and locally by the Millenbach Rhyolite formation (XM). The Main Contact Tuff lies conformably along the upper contact. Four massive sulphide lenses (#19, #6, #3 and D-266) at Millenbach and two massive sulphide lenses at the Amulet deposit (Lower A and Bluff) occur at the upper contact of the Millenbach Andesite formations.

The upper part of the Millenbach Andesite in the F-Shaft sector and probably the entire formation in the Waite Dufault sector has been intruded by the Dufresnoy Diorite.

Flow contacts within the Millenbach Andesite formation are sharp and conformable. Thin discontinuous units of laminated, pyritic tuff are commonly intercalated with the andesitic flows. Well exposed examples of interflow tuffaceous unit occur between flows A4 and A5 in the F-Shaft sector (Buck, 1981) and along the south-east and north shore of Turcotte lake in the Amulet-Millenbach sector.

Lithology

Andesitic flows which comprise the Millenbach Andesite formation in the Amulet-Millenbach sector are described in Table F.3.

9.2.9 WAITE ANDESITE FORMATION (IX W)

Definition, Distribution and Thickness

The Waite Andesite formation (IX W) consists of flows ranging in composition from basalt to rhyolite with minor interbedded tuff. The Waite Andesite formation extends from the Hunter Creek Fault south to the Old Waite Mine in the Ansil sector, a distance of 6km (Figure 9.24). Waite Andesite attains a maximum thickness of 1200m in the Ansil Sector.

Waite Andesite is interpreted to be the time/stratigraphic equivalent of Millenbach Andesite to the south (Figure 9.24). West and southwest of the Old Waite Mine weakly feldspar porphyritic, silicified pillowed lavas with radial amygdules and concentric jointing have been previously grouped with the Amulet Andesite formation (XIA) (de Rosen-Spence, 1976; Cousineau and Dimroth, 1983) but are here interpreted to be the uppermost flows of the Waite Andesite formation. This correlation is based on the similarity in flow morphology, phenocrysts, structure and silicified character to Waite Andesite flows in the north. This interpretation places the Waite Andesite formation in the Waite-Dufault sector, east of Duprat Lake where it is separated from stratigraphically equivalent Millenbach Andesite by the Dufresnoy Diorite (Figure 9.24, and Map 1).

South of Waite Lake and north of the New Insco road three massive flows (#1, 3, and 4) and a pillowed flow (#2) characterized by intense, pervasive silicification and quartz mega-amygdules comprise the uppermost units of the

Waite Andesite formation and are grouped into a separate unit, the Waite Andesite upper member (Figures 9.24 and 12.5). Silicified flows of the upper member attain a maximum thickness of 100m and were previously interpreted as dacitic flows and grouped with overlying Waite Rhyolite formation (#2 flow of de Rosen-Spence, 1976).

The Waite Andesite upper member is recognized east of the Dufresnoy diorite in the New Vauze sector where it was previously interpreted as the Amulet formation (de Rosen-Spence, 1976). In this sector the upper member attains a maximum thickness of 240m and extends 2.2km northwest of the Vauze Fault (Figures 9.24 and 9.25, Maps 1 and 2). The Waite Andesite upper member is conformably overlain by a pillowed flow, thin rhyolitic flow, silicified andesitic flows and a thin massive andesitic flow (Maps 1 and 2). This succession attains a maximum thickness of 300m adjacent to the Vauze Creek Fault and thins northward to the Hunter Creek Fault.

Contact Relations

The Waite Andesite formation conformably overlies the Amulet formation. Waite Andesite is conformably overlain by Waite Rhyolite in the Ansil sector and by both Waite Rhyolite (subsurface at the E. Waite Mine, Figure 9.3D) and Amulet Andesite in the Waite Dufault sector. Although not exposed at surface, thinly bedded tuff units are intersected in drill holes along the upper contact. The lowermost massive sulphide lens at the Old Waite Mine is interpreted to lie on the upper contact of the Waite Andesite formation (Section D-D of Figure 9.3). The contact between the upper member and underlying Waite Andesite is sharp and conformable; a thin (5-10cm) cherty tuffaceous sediment occurs locally along this contact.

In the New Vauze sector the Waite Andesite formation is conformably overlain by the Waite Rhyolite formation and conformably overlies the #1 rhyolitic flow of the Amulet lower member. The C Contact Tuff occurs at this lower contact. North of Vauze Lake the upper member and overlying and underlying pillowed flows pinch out along the flank of the Amulet lower member #1 flow whereas the overlying rhyolitic flow and silicified flows conformably overlie the Amulet lower member (Figures 9.24 and 9.25, Maps 1 and 2).

Lithology

Andesitic and rhyolitic flows that comprise the Waite Andesite formation are described in Table F.4.

Interpretations

Vent Areas

The main vent area for the Waite/Millenbach Andesite formations is interpreted to lie east and northeast of Duprat Lake within the 070-trending Old

Waite Dike Swarm (Chapter 8). The Waite Andesite formation attains its maximum thickness in this area, and north of Duprat Lake, while the stratigraphically equivalent Millenbach Andesite formation thins to the south away from the proposed vent. Aphanitic to fine-grained, amygdaloidal andesitic dikes which comprise the dike swarm are feeders to texturally and mineralogically identical Waite andesitic flows.

In the north part of the Ansil sector, paleo-flow directions obtained from pillowed lavas indicate a north to south flow direction. This suggests an additional vent may occur in the north part of the Ansil/Cranston sectors.

In the New Vauze sector the upper member is overlain by a succession of andesitic flows which are thickest adjacent to the Vauze Creek Fault and thin to the north. These andesitic flows are included within the Waite Andesite formation and may have erupted from vents within the New Vauze sector with their southward extension blocked by subsidence along the Vauze Creek Fault (Figure 9.25).

Paleotopography

By analogy with underlying andesitic units the paleotopography following extrusion of the Waite/Millenbach Andesite formations is assumed to be relatively flat and nearly horizontal. The pinch out of the Waite upper member and overlying pillowed flow against the Amulet lower member indicates considerable topographic relief that was eventually subdued and covered by a rhyolitic flow and silicified andesitic flow in the New Vauze sector. The remarkable continuity of individual flows within the Waite and Millenbach Andesite formations (up to 5km; de Rosen-Spence, 1976 and Cousineau and Dimroth, 1982) also suggests a relatively flat paleosurface.

9.2.10 WAITE RHYOLITE FORMATION (X W)

Definition, Distribution and Thickness

The Waite Rhyolite formation (X W) consists of rhyolitic and minor andesitic flows. Waite Rhyolite extends from the Hunter Creek Fault south to Duprat Lake (Figure 9.26), a distance of 5.5km. In the Ansil sector the Waite Rhyolite formation is a single rhyolitic flow that has a maximum thickness of 270m south of Waite Lake and pinches out immediately north of the Old Waite Mine. The same flow at the Vauze Mine has a minimum thickness of 450m. Waite Rhyolite in the Norbec sector is interpreted to be the faulted offset (across the Dufresnoy Diorite and Vauze Creek Fault) of the formation in the Ansil sector (Figure 9.2). In the Vauze sector the Waite Rhyolite formation attains a maximum thickness of 600m adjacent to the Vauze Creek Fault and thins northwest toward the Hunter Creek Fault. Waite Rhyolite of the Vauze sector was previously divided into 3 thin andesitic flow units and 6 rhyolitic units (de Rosen-Spence, 1976). The lowermost two flows, a lower rhyolite and overlying silicified andesitic flow are now included with the underlying Waite Andesite formation.

In the New Vauze sector, the Waite Rhyolite formation consists of 4 rhyolitic flows and 2 andesitic flows as outlined in Table E.5, and illustrated in Figure 9.26. The lowermost rhyolitic flow (#1 flow) is correlated with the Waite Rhyolite flow in the Ansil sector although the latter may in part be younger (Smith, 1984; de Rosen-Spence, 1976). Outcrops of Waite Rhyolite in the Norbec sector are limited but are texturally, mineralogically, and chemically similar (Smith, 1984) to the #1 Waite rhyolitic flow in the Ansil and Vauze sectors . In the Norbec sector, the Waite Rhyolite formation has been intersected in more than 200 drill holes and is traced for 3.5km east of the Norbec mine.

Contact Relations

The Waite Rhyolite formation conformably overlies Waite Andesite; drill holes intersect bedded tuff at this contact. In the Ansil and Norbec sectors Waite Rhyolite is conformably overlain by the Amulet Andesite formation. An extensive, thin bedded to laminated tuff, the Norbec Tuff, occurs at the upper contact of the #1 flow. The Norbec Tuff is exposed at surface and is intersected in numerous drill holes within the Ansil and Norbec sectors. The Norbec Tuff is the time/stratigraphic equivalent of the Main Contact Tuff in the Amulet-Millenbach sector (Figure 9.2). Four volcanogenic massive sulphide deposits, located along the upper contact of the #1 flow of the Waite Rhyolite formation, are from west to east, the E. Waite, Vauze, D-Zone and Norbec deposits.

In the Vauze sector the Waite Rhyolite formation is conformably overlain by the Newbec Andesite formation (XIII NB); bedded graphitic tuff was intersected in drill holes at this contact (de Rosen-Spence, 1976). Internal contacts between rhyolitic and andesitic flows are conformable and sharp. Thin-bedded tuff at contacts between the #1/#2 and #3/#4 flows in the Vauze Sector may be correlative with the Norbec Tuff.

Lithology

Rhyolitic and andesitic flows which comprise the Waite Rhyolite formation are briefly described in Table F.5.

Interpretations

Vent Areas

In the Ansil sector two distinct rhyolitic domes define specific vent areas for the #1 flow: the first, located at the Vauze mine and the second at the East Waite mine. At the Vauze mine a steep sided (>30^0) rhyolitic dome, the Vauze dome, is located along and was later offset by the Vauze Creek Fault. The Vauze dome attained a minimum thickness of 450m, with the upper part of the dome removed by faulting and diorite intrusion (Spence, 1976). A single rhyolitic flow issued from this vent and extended 1.7km to the south. Detailed facies mapping by

Smith (1984), indicates that the #1 flow has a north to south paleo-flow direction, directly away from the Vauze dome.

The north flank of the Vauze dome is offset along the Vauze Creek Fault and comprises the #1 flow of the Waite Rhyolite formation in the Vauze sector. This flow is 500m thick adjacent to the Vauze Fault and extends for 3.6km to the north where it thins to 130m. The southeast flank of the Vauze dome is represented by surface outcrops of Waite Rhyolite in the Norbec sector.

At the East Waite mine, a steep-sided (40^0) rhyolitic dome, the E. Waite dome, defines a second major vent for the #1 flow (Figure 9.3D). Rhyolite that issued from the E. Waite vent is contemporaneous with rhyolite of the Vauze vent and collectively they constructed a low, broad rhyolitic plateau that extends a minimum of 2.0km east of the Norbec mine. The E. Waite dome is located on the southwest margin of the #1 flow; rhyolite which issued from the vent is not symmetrically disposed about the vent as it extends only to the north, south and east and is conspicuously absent at the Old Waite mine located 0.7km to the west (Section DD, Figure 9.3). The asymmetry of the E. Waite lava dome with respect to its vent is atypical and suggests that the flow erupted on a paleosurface that was tilted to the east prior to or during volcanism. Rhyolitic and composite dikes of the Old Waite Dike Swarm are interpreted as feeders to the dome and flows (Chapter 8).

Three rhyolitic flows which overlie the #1 flow in the New Vauze sector, were erupted from vents located on the north flank of the Vauze dome. The northward increase in thickness of the QFP flow suggests that its vent may lie in the north part of the Vauze sector or adjacent to the Hunter Creek Fault. A QFP rhyolitic dike located stratigraphically below the QFP flow was interpreted by C.D. Spence (personal communication, 1985) to be a possible feeder to this flow. The uppermost two flows of the Waite Rhyolite formation attain maximum thickness in the central part of the Vauze sector and thin both to the north and south; the upper flow pinches out before reaching the Hunter Creek Fault. By analogy with other rhyolitic flows, the vent areas for these two flows are interpreted to occur where the flows are thickest, as illustrated in Figure 9.26. A flow-banded rhyolitic dike lies stratigraphically below the vent areas and may be a feeder to one or both of these flows (Maps 1 and 2).

Andesitic flows within the Waite Rhyolite formation are thin discontinuous units. Vent areas for these flows have not been recognized but their occurrence in a growing rhyolitic dome complex suggests contemporaneous rhyolitic and andesitic volcanism.

Paleotopography

Flows of the Waite Rhyolite formation formed a low broad plateau with slopes from 10^0 - 20^0. Rhyolitic domes constructed above principal vent areas rise above the rhyolitic plateaus with slopes between 30^0 and 45^0. The marked absence of rhyolitic flows extending west of the E. Waite dome suggests that the paleosurface was tilted east prior to or during eruption of the Waite Rhyolite formation.

9.2.11 MILLENBACH RHYOLITE FORMATION (XM)

Definition, Distribution and Thickness

The Millenbach Rhyolite formation consists of the Millenbach-D68 lava dome and Turcotte flow in the Amulet-Millenbach sector and the K-Rhyolite flow in the Despina Sector (Figure 9.26). Minor, intercalated bedded tuff deposits and andesitic flows occur within the Millenbach-D68 lava dome. The Millenbach Rhyolite formation is interpreted to be the time/stratigraphic equivalent of the Waite Rhyolite formation in the Ansil, New Vauze and Norbec sectors to the North (Figure 9.2).

The Millenbach-D68 lava dome constitutes the bulk of the formation and although it does not outcrop it has been delineated and mapped using surface and underground drill holes and underground workings from the Corbet and Millenbach mines. At the Millenbach mine alone, 3,629 drill holes and 13km of drift have provided information and access to the lava dome. Exploration drilling and development in the D-68 area, from the Corbet shaft, have provided additional information. The lava dome is described in detail in Chapter 4.

The lava dome extends from the McDougall Fault northeast to the former Millenbach Mine, a distance of 1.8km (Figure 9.26). The Dufault Pluton defines the eastern limit of the lava-dome and the McDougall Fault is generally assumed, as in this study, to define the western limit. Recent drilling programs have, however, intersected the lava dome west of the McDougall-Despina Fault in the Despina sector but information is limited and proprietary at this time.

The lava dome is divisible into two main flows, the Upper QFP and Lower QFP (Simmons et al., 1973; Comba, 1975; Knuckey et al., 1982). Both flows extend the full length (1.8km) of the lava dome and attain a maximum thickness of 240m and 110m respectively. Stratigraphic sections through the Millenbach-D-68 lava dome in the Millenbach mine and D-68 deposit areas are illustrated in Figure 9.27.

The Turcotte QFP rhyolitic flow occurs at the same stratigraphic position as the Millenbach-D-68 lava dome to which it is interpreted to be a contemporaneous, satellite body. The Turcotte flow is 50m thick at surface and is directly underlain by a thick andesitic sill; the flow extends for 400m in a north-south direction (Figure 9.26).

The K-Rhyolite outcrops in the Despina sector approximately 1.1km west of the Corbet Mine (Figure 9.26). The K-Rhyolite flow has a maximum thickness of 40m at surface where it is exposed over a strike length of 100m. The flow extends for 0.7km in a northeast direction where it is intersected in a surface drill hole and from underground holes located on the 10th level of the Corbet Mine.

Contact Relations

Stratigraphic sections in Figure 9.27, illustrate internal contacts within the Millenbach-D-68 lava dome and contacts with underlying formations. In the Millenbach mine area the lava dome conformably overlies the Millenbach Andesite formation (1XM) from which it is locally separated by the Main Contact Tuff (Comba, 1975). In the D-68 deposit area the lava-dome rests conformably on the Amulet formation (VIIIA); the C Contact Tuff (Comba; 1975; Knuckey et al., 1982) typically separates the two units. The absence of the Millenbach Andesite formation in the D-68 area corresponds with the marked north-south thinning and pinch out of the unit observed at surface (Figure 9.24).

The lava-dome is conformably overlain by andesitic flows of the Amulet Andesite formation. The contact is locally defined by a thin, massive to plane bedded tuff, the Top-Contact Tuff (Comba, 1975). Where the Top-Contact Tuff is absent the rubbly brecciated top of the lava-dome lies in sharp contact with overlying andesitic flows.

In the Millenbach mine area the contact between the flows is conformable and locally defined by a thin, plane-bedded tuff, the Inter QFP Tuff (Comba, 1975), and by 10 and 3 massive sulphide lenses in the Millenbach and D-68 areas, respectively. In the D-68 deposit area meticulous logging of surface drill holes by

Doiron (1983) and Ikingura (1984) allowed distinction of the Upper and Lower QFP flows on the basis of differences in the size and population of quartz and feldspar phenocrysts.

The Lower QFP flow in the Millenbach area lacks internal flow contacts and is a simple flow. The Upper QFP flow is a compound flow, containing distinct pods/flows of massive lava encased within breccia and locally separated by lenses of tuffaceous sediment (Comba, 1975). In the D-68 area the opposite exists where the Lower QFP flow is a compound flow that is internally separable into individual flows by thin andesitic flows (Doiron, 1983). The upper QFP flow appears to be a simple flow.

The Turcotte QFP and K-Rhyolite flows are simple flows that conformably overlie and are conformably overlain by the Millenbach Andesite (IX) and Amulet Andesite (XIA) formations respectively. An andesitic sill underlies the massive phase of the Turcotte flow, north of the Corbet haulage road.

Lithology

Rhyolitic and andesitic flows which comprise the Millenbach Rhyolite formation are described in Table F.6.

Subsurface Characteristics of the Millenbach-D68 Lava Dome

The morphology of the Millenbach-D68 lava dome is discussed in detail in Chapter 4, and well displayed in structural cross-sections PP and QQ of Figure 9.6, and in an isopach map and cross-sections of Figures 4.13 to 4.15.

Interpretations

Vent Areas

QFP lava of the Millenbach-D-68 ridge was extruded along N45^{0}E trending fissures. Viscous flows of the lower QFP flow formed a hummocky ridge above its feeding fissure and in 3 principal vent areas constructed domes that rise above the ridge with slopes of up to 70^0.

The Upper QFP flow issued from feeder dikes located north of the Lower flow and built up a parallel and adjacent ridge which overlapped and nearly buried the Lower flow. Hotspring activity localized above the Lower QFP feeder dike in the three principal vent areas formed 13 and 5 massive sulphide lenses above the Lower and Upper QFP flows respectively.

Inter-Lower QFP andesitic flows in the D-68 area thicken to the northwest (Doiron, 1983; Ikingura, 1984) which suggests that the west end of the lava dome acted as a barrier to contemporaneous andesitic flows erupted from vents located to the north or northwest. These andesitic flows were both ponded by, and intermittently covered the Lower QFP flow; the absence of flank-talus breccias in this locale may reflect rapid burial by contemporaneous andesitic flows. Extrusion of the Upper QFP flow nearly buried the Lower flow in the D-68 area and a positive volcanic edifice was constructed as shown by the aerially restricted breccia deposits to the north and south of the ridge.

Inter-QFP andesitic flows may be the time-stratigraphic equivalent of the Amulet Andesite (XIA) or Millenbach Andesite (IX M) formations. If correlative with the latter, rhyolitic volcanism commenced at the west end of the ridge (D-68 area) and progressed eastward.

The Turcotte flow, a satellite body to the main Millenbach-D68 ridge issued from a vent located near the present surface exposures. The K-rhyolite flow with a limited north-south dimension (<200m) and marked east-west extent (0.7km) may have issued from a northeast-trending fissure below the flow.

Paleotopography

The 240m high Millenbach-D-68 ridge formed a localized area of rugged topography with slopes ranging up to 70^0 along the ridge crest to 10^0 - 20^0 along the ridge flanks. The symmetry of QFP flows about their feeding fissure indicates a relatively horizontal paleo-surface. The Turcotte and K-rhyolite flows formed small domes on the relatively flat underlying topography of the Millenbach and Amulet Andesite formations.

9.2.12 AMULET ANDESITE FORMATION (XI A)

Definition, Distribution and Thickness

The Amulet Andesite formation is the uppermost formation of the Mine Sequence in the Flavrian Block. The formation consists of basaltic to andesitic flows, minor breccias and intercalated tuffs. A thin (<100m) rhyolitic flow, the Norbec Rhyolite, occurs near the top of the formation in the Norbec Sector. Amulet Andesite extends from the Vauze Creek Fault south to the Beauchastel Fault, (Figure 9.28) a distance of 10.5 km. The Dufault Pluton and Dufresnoy Diorite effectively separate the Amulet Andesite in the Norbec/Ansil sectors from that in the F-Shaft/Amulet-Millenbach sectors. The Amulet Andesite formation attains a maximum thickness of 500m in the Norbec sector, 1000m in the Amulet-Millenbach sector, and 1000m in the Despina sector.

Contact Relations

The Amulet Andesite formation conformably overlies the Amulet, Millenbach, Waite Andesite, Millenbach Rhyolite and Waite Rhyolite formations, from which it is locally separated by thin deposits of bedded tuff. Massive sulphide lenses of the Old Waite and Amulet Upper A deposits occur with andesitic flows within several hundred metres of the base of the formation.

Amulet Andesite is conformably overlain by the Newbec Andesite formation in the Norbec sector and by Insco Rhyolite in the east half of the Amulet-

Millenbach sector. The discordant Newbec Breccia obliterates the upper contact of the Amulet Andesite formation in the south part of the Norbec sector. In the south part of the Despina and Amulet-Millenbach sectors north-south striking and east dipping flows of Amulet Andesite are unconformably overlain by east-west striking, shallow south dipping rhyolitic flows of the Here Creek Rhyolite formation.

Intraformational flow contacts are conformable and sharp and are locally marked by thin (<1m) units of bedded tuff. Localized deposits of plane bedded, andesitic hyaloclastite occur at the top of the formation in the Norbec and Amulet-Millenbach sectors (Cousineau and Dimroth, 1982).

Lithology

The Amulet Andesite formation has been subdivided into 18, 31 and 19 individual flows in the Norbec/Ansil, Amulet-Millenbach and Despina sectors (de Rosen-Spence, 1976; Cousineau and Dimroth, 1982). Flows from the lower half of the formation are extensive and variable in both structure and mineralogy which facilitates correlation between sectors (de Rosen-Spence, 1976). The Norbec Rhyolite is an aerially restricted, thin, <50m thick, spherulitic FP flow.

Interpretations

Vent Areas

Andesitic flows of the Amulet Andesite Formation extruded from at least 3 main fissures (Figure 9.28) as described below:

a) Old Waite-Norbec Fissure

Cousineau and Dimroth (1982) interpreted andesitic flows of the Amulet Andesite formation to have been erupted from a 3.0km long, northeast striking (070^0) fissure that extends from the Old Waite Mine east to the Norbec Mine. They defined the fissure on the basis of a change from predominantly massive "proximal flows" along the fissure to predominantly "distal" pillowed flows away from the fissure and by paleo-flow directions which indicated that flows moved north and south away from the fissure. As described in Chapter 8, andesitic dikes of the Old Waite Dike Swarm define their fissure west of the East Waite Mine.

b) Amulet-Millenbach Fissure

Reconnaissance mapping of the Amulet Andesite formation in the Amulet-Millenbach sector suggests that a second vent may extend from southeast and southwest of the C orebodies to the Millenbach and Corbet Mine, approximately 2 and 1 kms respectively. The trend of these proposed fissures parallels the McDougall-Despina Fault/ Millenbach QFP feeder dikes and it is characterized by a predominance of thick massive flows, and numerous thick andesitic sills and dikes similar to those described as feeder dikes in the Old Waite Dike Swarm.

c) McDougall-Despina Fissure

A plug-like body of fine-grained amygdaloidal massive and columnar jointed andesite occurs within the Despina Fault 1.0km south of the Corbet Mine. This andesitic plug is crudely discordant to adjacent flows with which it has gradational contacts (west contact). Although intruded by later rhyolitic dikes this andesitic body is interpreted to be a feeder dike to Amulet Andesite flows in the Amulet-Millenbach and Despina sectors (Setterfield, 1984). A similar but narrower andesitic dike which occupies the McDougall Fault 0.6km south of the Corbet mine may be a remnant of an andesitic feeder dike.

Paleotopography

Detailed maps of the Amulet Andesite formation by Greenwood (1957), de Rosen-Spence (1976) and Dimroth and Cousineau (1982) indicate that, unlike underlying formations, andesitic flows of the Amulet Andesite formation are laterally extensive. The marked lateral extent of these flows indicates:

a) underlying topography was relatively flat and horizontal during extrusion and that

b) faulting and subsidence adjacent to andesitic vent areas did not accompany volcanism; if subsidence occurred it was localized along major boundary faults with large fault blocks subsiding relative to each other and not by piece meal faulting within the Flavrian block.

Andesitic flows of the Amulet Andesite formation and time-stratigraphic equivalent Powell Andesite formations (de Rosen-Spence, 1976; Lichtblau and Dimroth, 1980) are interpreted to have filled in and were confined to a volcanic-tectonic depression. The andesitic flows were blocked by the Waite Rhyolite dome complex and Vauze Creek Fault to the north, and Western Quemont Feeder Dike Faults and Quemont Rhyolite formation, of the Powell Block, to the south. In the Norbec sector a shoaling sequence within the Amulet Andesite formation was described by Cousineau and Dimroth (1982) who recognized a marked increase in the amygdule content of the uppermost flows (up to 35% amygdules compared with <15% amygdules in the lower flows). This upward increase in amygdules and occurrence of stratified hyaloclastite breccias in the uppermost flows suggests decreasing water depth during extrusion.

9.3 STRATIGRAPHIC CORRELATION

Correlation of Mine Sequence formations between the Hunter, Flavrian and Powell Blocks, and Aldermac are described below. These Blocks are separated by the Hunter Creek, Beauchastel/Western Quemont Feeder Dike and Horne Creek Faults. Stratigraphic correlation across these major faults and within the Flavrian Block is illustrated in Figure 9.2 and Tables 2.3 and 2.4.

9.3.1 CORRELATION ACROSS THE HUNTER CREEK FAULT

Lithostratigraphic correlation of Mine Sequence formations across the Hunter Creek Fault is based on the work of Spence and Karis (1963, as quoted in de Rosen-Spence, 1976), Simmons (1972) and Mattinen, (1974) and is illustrated in Figures 9.29 and 9.30. The correlation is tentative, the lack of outcrop, detailed mapping and drilling in the Hunter Block hampering both definition of formations and correlations with the Flavrian Block. It should also be noted that the Hunter Creek Fault is not a single fault but rather a fault zone that consists of numerous parallel structures (Map 1).

The Fish-Roe Rhyolite (XV) and Newbec (XIII NB)/Upper North Duprat Andesite, upper member (XIII UND) formations which are traceable from the Hunter Block to the New Vauze and Norbec sectors of the Flavrian Block provide the basis for correlation. Strata which underlie these formations comprise the Mine Sequence in the Flavrian and Hunter Blocks. Accordingly, the following correlations are inferred:

a) the lower member of the Upper North Duprat Andesite, (XI UND) is correlated with the Amulet Andesite formation (XI A) in the Norbec sector of the Flavrian Block; the absence of this unit in the intervening Vauze sector may reflect restriction by the Waite Rhyolite lava dome and Vauze Creek Fault.

b) the Upper North Duprat Rhyolite formation (X UND) is correlated with the Waite Rhyolite formation (X W). The correlation is based on the stratigraphic position of these formations below the Newbec/Upper North Duprat Andesite formations and the textural and chemical similarities between the two flows of the X UND with flows 1 and 5 of X W (de Rosen-Spence, 1976).

c) the Lower North Duprat Andesite formation (VII LND) is correlated with the Rusty Ridge formation (VII R) as both are tholeiitic as compared to the younger Waite Andesite formation (IX W) which is calc-alkaline (de Rosen-Spence, 1976). This allows correlation of the underlying Lower North Duprat Rhyolite formation (VI LND) with the Northwest formation (VI N) of the Flavrian Block.

d) the Hunter Andesite formation (V H) is correlated with the Flavrian formation (V F) in the Flavrian Block.

Rhyolitic and andesitic formations of the Mine Sequence in the Hunter Block are interpreted to have issued from a centre north of the Hunter Creek Fault whereas the Mine Sequence of the Flavrian Block was largely confined to and erupted from vents within the Flavrian Block.

The Waite Andesite formation (IX W), Amulet lower member(VIII Al) and possibly the Cranston member(VI NC) of the Flavrian Block are not represented in the Mine Sequence of the Hunter Block. The latter two members are thickest and have vent areas immediately south of the Hunter Creek Fault and their restriction is not apparently a function of underlying topographic relief. This confinement of formations is interpreted to represent synvolcanic subsidence of the Flavrian Block relative to the Hunter Block; the combined thickness of the Waite

Andesite and Amulet lower member adjacent to the Hunter Creek Fault indicates a minimum subsidence of approximately 450m. The difference in thickness of the Mine Sequence (from base of VI N) in the Flavrian Block (2.2 km, as measured from sections C, E, F, and S-3B) versus that in the Hunter Block (1.2km, as measured from section S-1A), suggests 1km of subsidence.

9.3.2 CORRELATION ACROSS THE BEAUCHASTEL/WESTERN QFP FEEDER DIKE FAULTS

Correlation of the Mine Sequence of the Flavrian Block south, across the Beauchastel Fault, is based on the work of de Rosen-Spence (1976), Lichtblau and Dimroth (1980), and Lichtblau (1983) and through reconnaissance traverses and field trips with the latter two workers.

The Here Creek Rhyolite formation (XIV H) which occurs in both the Powell and Flavrian Blocks provides the basis for stratigraphic correlation across the Beauchastel and Western QFP Feeder Dike Faults (Figure 9.30). Andesitic flows of the Amulet Andesite formation which underlie the Here Creek Rhyolite formation in the Flavrian Block are interpreted as the stratigraphic equivalent of the Powell Andesite formation which underlies the Here Creek Rhyolite formation in the Powell Block.

The Powell Andesite formation (XI P) defines the top of the Mine Sequence in the Powell Block. West of the Western Quemont Feeder Dike (section S-8, Figures 9.2 and 9.30) the Powell Rhyolite occurs within a 300m thick succession of bedded andesitic tuffs and rhyolitic breccia within the upper third of the Powell Andesite formation. The Brownlee Rhyolite formation occurs as a thin wedge between the overlying Powell Andesite formation and Powell Pluton. De Rosen-Spence (1976) correlated the Brownlee Rhyolite formation with the Amulet formation (VIII A) whereas Lichtblau and Dimroth (1980) correlated the Brownlee Rhyolite with the Northwest formation (VI N); the latter authors also correlated the Powell Rhyolite with the Millenbach formation (X M).

The stratigraphic correlation proposed differs somewhat from the above. The andesitic Powell Tuffs are correlated with identical, localized andesitic tuffs which occur in the upper third of the Amulet Andesite formation in the Amulet-Millenbach sector, 100m south of the Millenbach Mine portal (Figure 9.2). The Brownlee Rhyolite formation is correlated with texturally and chemically similar rhyolitic flows of the Northwest formation (VI N) and may be the faulted equivalent of identical rhyolitic flows comprising the Joliet Rhyolite formation on the east side of the Western Quemont QFP Feeder Dike.

The Western Quemont QFP Feeder Dike marks a zone of distinct stratigraphic change. The feeder dike separates the 900m thick Powell Andesite formation and underlying Brownlee Rhyolite formation to the west from the lowermost flows of the Quemont Rhyolite formation and underlying Joliet Rhyolite formation. Andesitic flows of the Powell Andesite formation conformably overlie a portion of member 4 of the Quemont Rhyolite formation east of the Western Quemont Feeder Dike. The Western Quemont Feeder Dike and identical dikes to the east are interpreted as feeders to the upper members (4-7) of the Quemont Rhyolite formations not covered by the Powell Andesite formation. The Quemont Rhyolite formation is correlated with the upper flows of the Waite Rhyolite formation (X) as both formation are in part covered but ultimately restrict the north and south extent of the Amulet/Powell Andesite formations. The QFP Powell Rhyolite may be a contemporaneous satellite body of the lower QFP flows of the Quemont Rhyolite formation.

Assuming these correlations, strata of the Powell Block are down-faulted in a series of steps toward the Flavrian Block and on a larger scale the Mine Sequence of the Flavrian Block probably subsided relative to the Mine Sequence in the Powell Block. In the Powell Block, the Mine Sequence (VI J-X Q measured in section S-10) is 0.8km thick whereas the equivalent stratigraphic succession in the Flavrian Block (VIN-XW/M measured from sections G, H, and J) is 2.0km thick; this suggests that the Flavrian Block subsided approximately 1.2km, relative to the Flavrian Block, following extrusion of the Northwest formation (VI N).

9.3.3 CORRELATION ACROSS THE HORNE FAULT

Any correlation across the Horne Fault must be regarded as tentative due to lack of both distinctive marker units and recent detailed mapping along and south of the fault. A description of strata south of and adjacent to the Horne Fault and VMS deposit is contained in Table D.4.

De Rosen-Spence (1976) interpreted the Horne Rhyolite as the lithostratigraphic equivalent of the Joliet and Quemont Rhyolite formations (VI to X) of the adjacent Powell Block. The Horne Rhyolite, however, differs from these formations in that it contains well bedded breccias and laminated ash deposits of possible ash flow or epiclastic origin (S.Walker, Noranda Mines Ltd., personal communication, 1984), lacks quartz phenocryts and crystals, and is underlain and overlain by andesite not rhyolite. An alternative interpretation is described below.

The Horne Fault separates two distinctly different "packages" along its strike (Figure 9.30). To the north, a predominantly rhyolitic and andesitic flow package of Mine Sequence and Cycle 4 formations strikes N20^{0}W and abuts against the fault at a high angle. To the south, a predominantly basalt-andesite package, west of Osisko Lake, strikes N65^{0}W and intersects the fault at an oblique angle. The Horne fault has a consistent 080^0 strike but near Delbridge it has been interpreted to swing to the southeast at 110-120^0 (de Rosen-Spence, 1976), to separate the Delbridge formation from the basalt-andesite package to which it appears conformably overlie. There is no evidence in the field or in drilling (J.Bonneau; Corp. Falconbridge Copper, personal communication, 1985) to suggest such a southeast bend and continuation of the fault. The logical and interpreted east continuation of the fault is an 080^0 striking splay that offsets the Delbridge formation (verified by drilling; J.Bonneau, personal communication, 1985). Thus, the Delbridge formation, on the south side of the postulated Horne Fault (<100m offset) may conformably overlie the older basalt-andesite package (Figure 9.30), whereas north of the fault underlying 4 Cycle formations and the Mine Sequence (approximately 4 km of stratigraphy) terminate against the fault and adjacent older basalt-andesite package.

In this interpretation the Horne Fault defines the south margin of the subsidence structure against which flows of the Mine Sequence and Cycle 4 are ponded. Eruption of the Delbridge rhyolitic flows, from feeders along and parallel to the fault, over-ran the margin onto an older basalt-andesite succession. The location of the Horne deposit 2.5 km to the west and presumably lower in the stratigraphy suggests that it may be older than the Mine Sequence and younger strata to the north. Dimroth et al., (1982) also interpreted the Horne Mine strata to be older than the Mine Sequence.

Alternatively, the Horne Deposit and immediate rhyolitic rocks, could represent a fault slice of the Mine Sequence separated from the older andesite-basalt package to the west and south by a northeast fault in Osisko Lake and the east-west Andesite Fault respectively. This interpretation is consistent with numerous other faults slices south of the Horne Fault and would suggest that stratigraphy south of the Horne fault is not a conformable succession.

9.3.4 CORRELATION WITH THE MINE SEQUENCE AT ALDERMAC

Lithostratigraphic correlation of the Mine Sequence in the Flavrian Block with that at Aldermac is based on the Amulet Andesite formation. This formation extends south from the Despina sector and continues around the south end of the Flavrian Pluton to Aldermac where it overlies the Aldermac Rhyolite (Hunter and Gibson, 1986; Figure 9.31). The Aldermac Rhyolite and overlying Macanda rhyolitic dome are correlated with the Waite, Millenbach and Quemont Rhyolite formations of the Flavrian and Powell Blocks (Figure 9.31). Andesitic flows which underlie the Aldermac Rhyolite are correlated with the Waite and Millenbach Andesite formations.

Based on these correlations the thickness of the Mine Sequence at Aldermac is equivalent to that in the Flavrian block which suggests minimal subsidence of strata in the Flavrian Block relative to strata at Aldermac.

9.4 ERUPTIVE CENTRES

Six eruptive centres are defined and their location is illustrated in Figure 9.32. Eruptive centres are rhyolitic and andesitic vent areas that have been continuously reactivated during extrusion of the Mine Sequence. Eruptive centres are defined by the occurrence of: 1) dike swarms that "fed" adjacent and overlying flows; 2) thick accumulations of successive rhyolitic or andesitic formations; 3) numerous individual feeder dikes or necks that fed successive flows.

Eruptive Centre I

Eruptive centre I is defined by the Old Waite Dike Swarm. Dikes within it were the principal feeders to andesitic flows of the Flavrian, Rusty Ridge, Waite Andesite and Amulet Andesite formations. Rhyolitic and the rhyolitic component of composite dikes were feeders to the Number 3 flow of the Amulet lower member, and the Waite Rhyolite dome at the East Waite mine.

Eruptive Centre II

Eruptive centre II is defined by the McDougall-Despina Fault and dike complex. The McDougall-Despina Fault are northwest trending synvolcanic faults that have a crudely arcuate surface trace, and a combined vertical offset of 0.75km (Chapter 10). Intrusions within the faults, plus numerous adjacent and ancillary parallel dikes were feeders to flows of the Flavrian, Northwest, Rusty Ridge, Amulet, Amulet Andesite and Here Creek Rhyolite formations. A parallel structure marking a proposed fissure between the Amulet and Millenbach Mines and the roughly perpendicular northeast-trending Millenbach QFP feeder dikes are included in this eruptive centre.

Eruptive Centres III and IV

Eruptive centres III and IV are defined on the basis of thick, localized accumulations of the Ansil QFP and Northwest formation (North flow), including the Cranston QFP and Cranston breccia dike in centre III (950m), and the Waite Rhyolite formation (flows 1-4, 600m) in centre IV. Feeder dikes were not recognized. Eruptive centres III and IV are located along the faulted, north margin of the Flavrian Block. Proposed vents for Rusty Ridge andesitic flows along the Cranston Fault and at Ansil Hill are included in centres III and IV.

Eruptive Centre V

The Quemont and Delbridge feeder dikes define eruptive centre V which is also characterized by a thick (2500m) succession of proximal rhyolitic flows and pyroclastic breccia without intervening andesite. Three QFP rhyolitic dikes in the Quemont-Joliet mines area, north of the Horne Fault, are feeders to the Quemont flows 4 through 7 (de Rosen-Spence, 1976; Lichtblau and Dimroth, 1980 and Dimroth et al., 1983). From west to east the northeast-striking, steeply dipping dikes are 350, 90 and 400m in width; the middle dike merges with massive banded lava of the number 4 flow. Feeder dikes to the underlying Joliet Rhyolite formation, presumably destroyed by later dike emplacement, are interpreted to have vented in this area. Further to the east rhyolitic flows of the Delbridge Rhyolite formation (post Mine Sequence) were fed from two dikes in the Delbridge mine area (Boldy,1968).

The Quemont feeder dikes were emplaced along synvolcanic faults (de Rosen-Spence, 1976; Lichtblau and Dimroth, 1980 and Dimroth et al., 1983) and the whole of eruptive centre V lies along the Horne Fault and south margin of the Powell Block.

Eruptive Centre VI

Eruptive centre VI is defined on the basis of two rhyolitic vent areas. The Aldermac Rhyolite and Macanda dome define a proximal vent facies that is intruded by a pumiceous tuff dike. Eruptive centre VI is located west of the Flavrian Pluton.

SUMMARY

Eruptive centres III, IV, V and VI, characterized by rhyolitic eruptions, constructed broad lava shields and domes along major synvolcanic faults. Eruptive centre I, the principal andesitic centre, occurs within the down-faulted core of the Flavrian Block. Flows from successive andesitic eruptions spread away from this centre to cover rhyolitic flows and domes to the north and south.

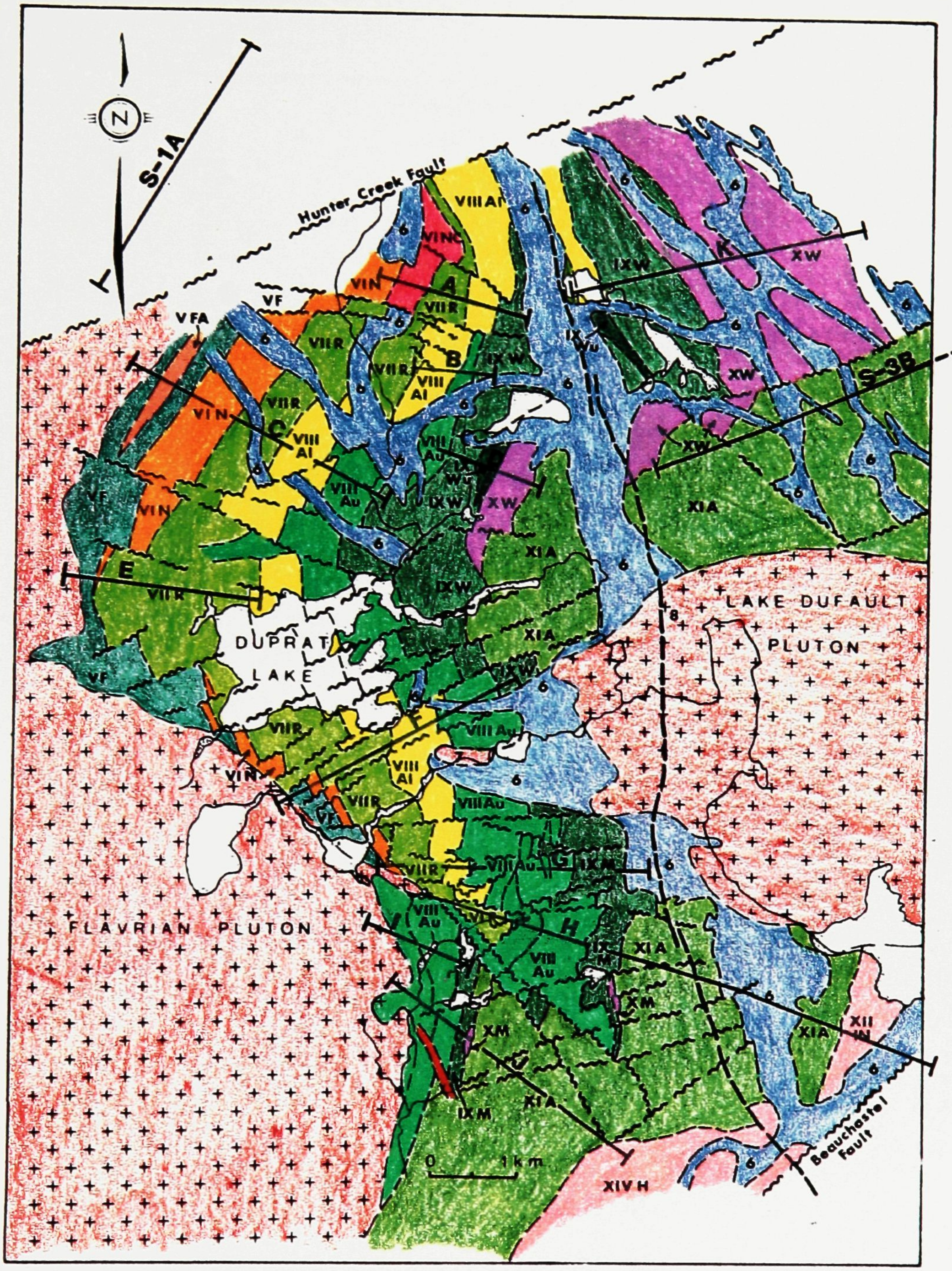

Figure 9.1. Mine Sequence Stratigraphy of the Flavrain Block. Lines mark the location of stratigraphic sections in Figure 9.2.

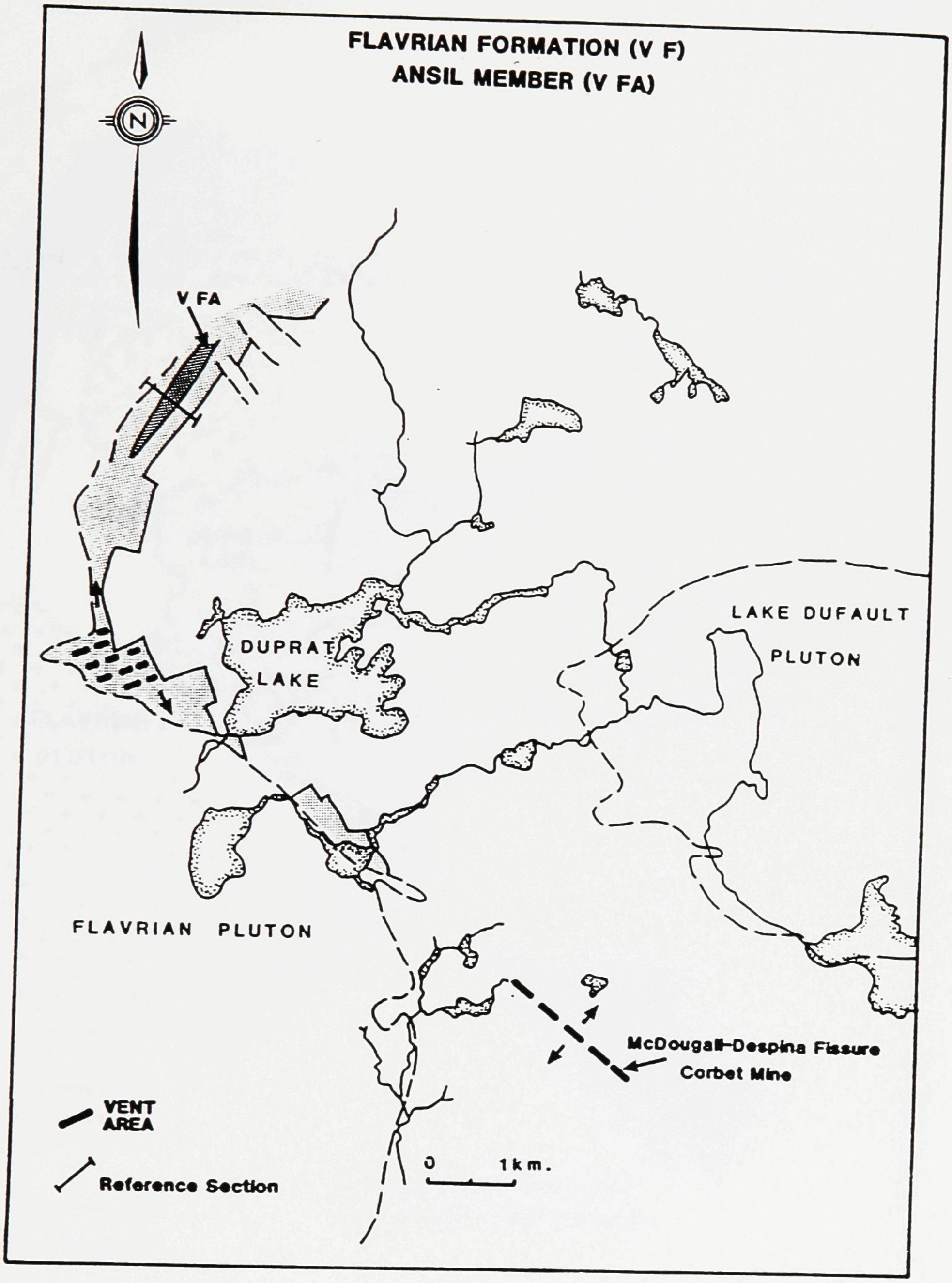

Figure 9.7. Surface distribution of the Flavrian formation; arrows indicate inferred flow direction.

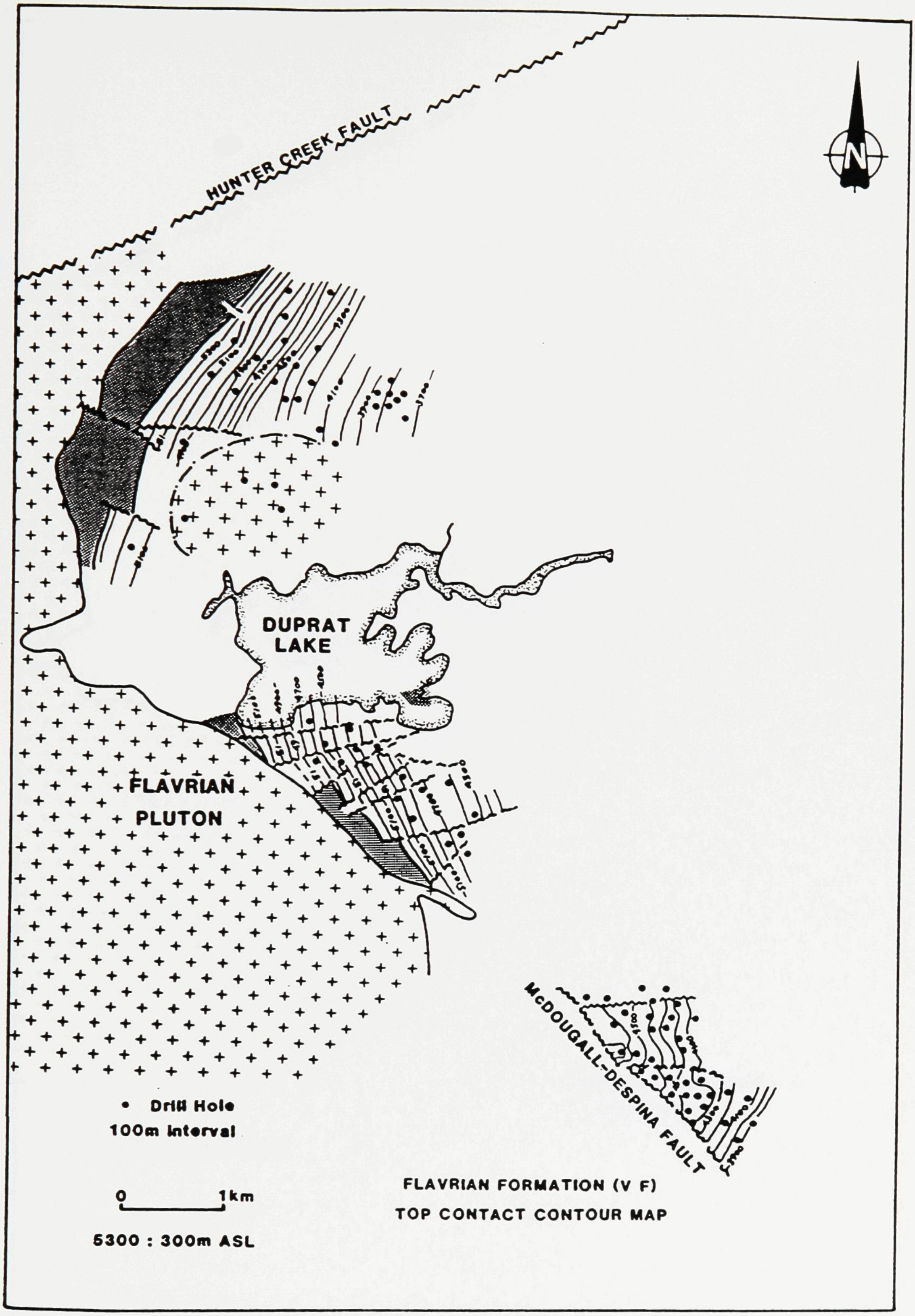

Figure 9.8. Stratigraphic top contact contour map for the Flavrian formation.

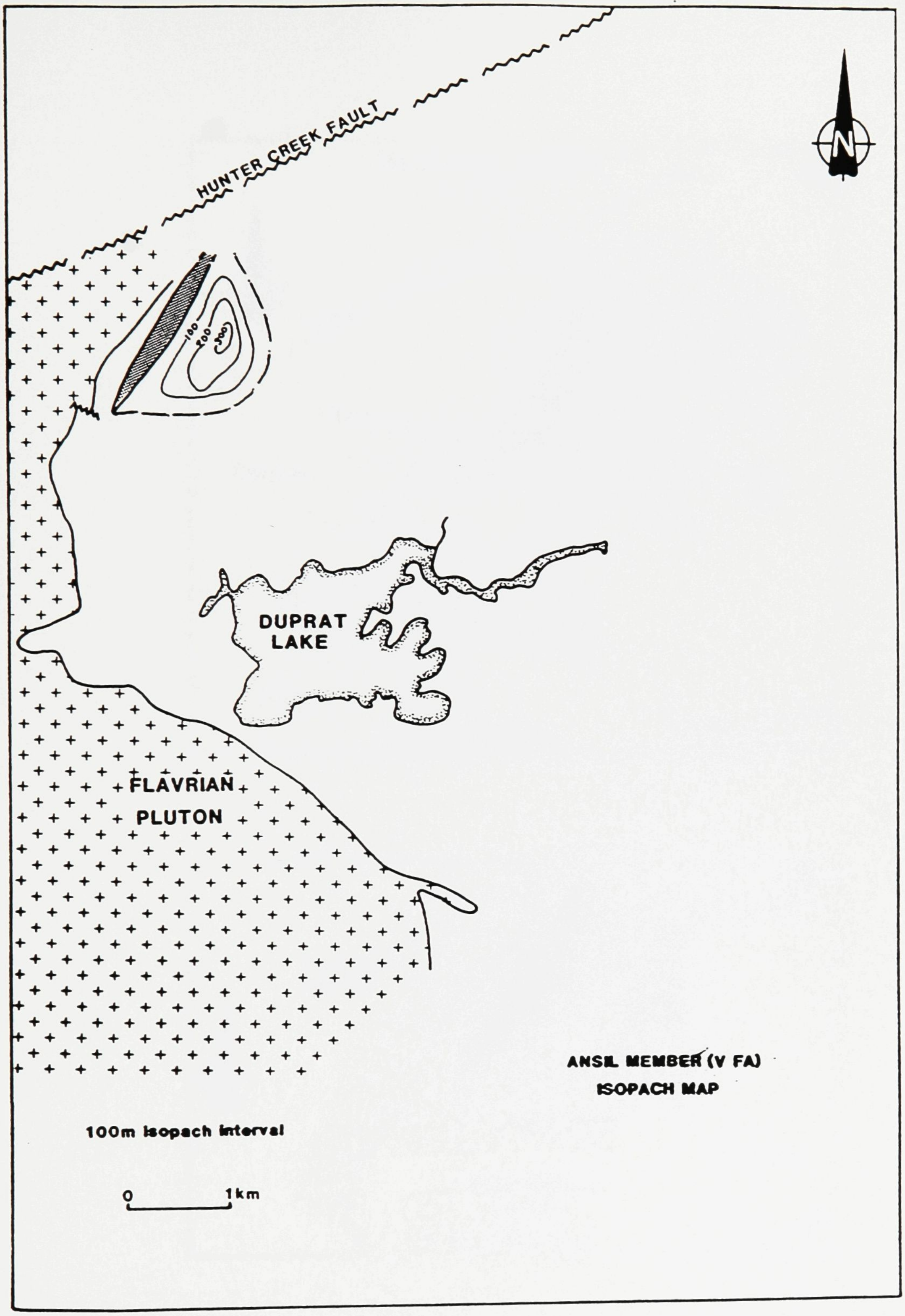

Figure 9.9. Isopach map for the Ansil member (QFP flow).

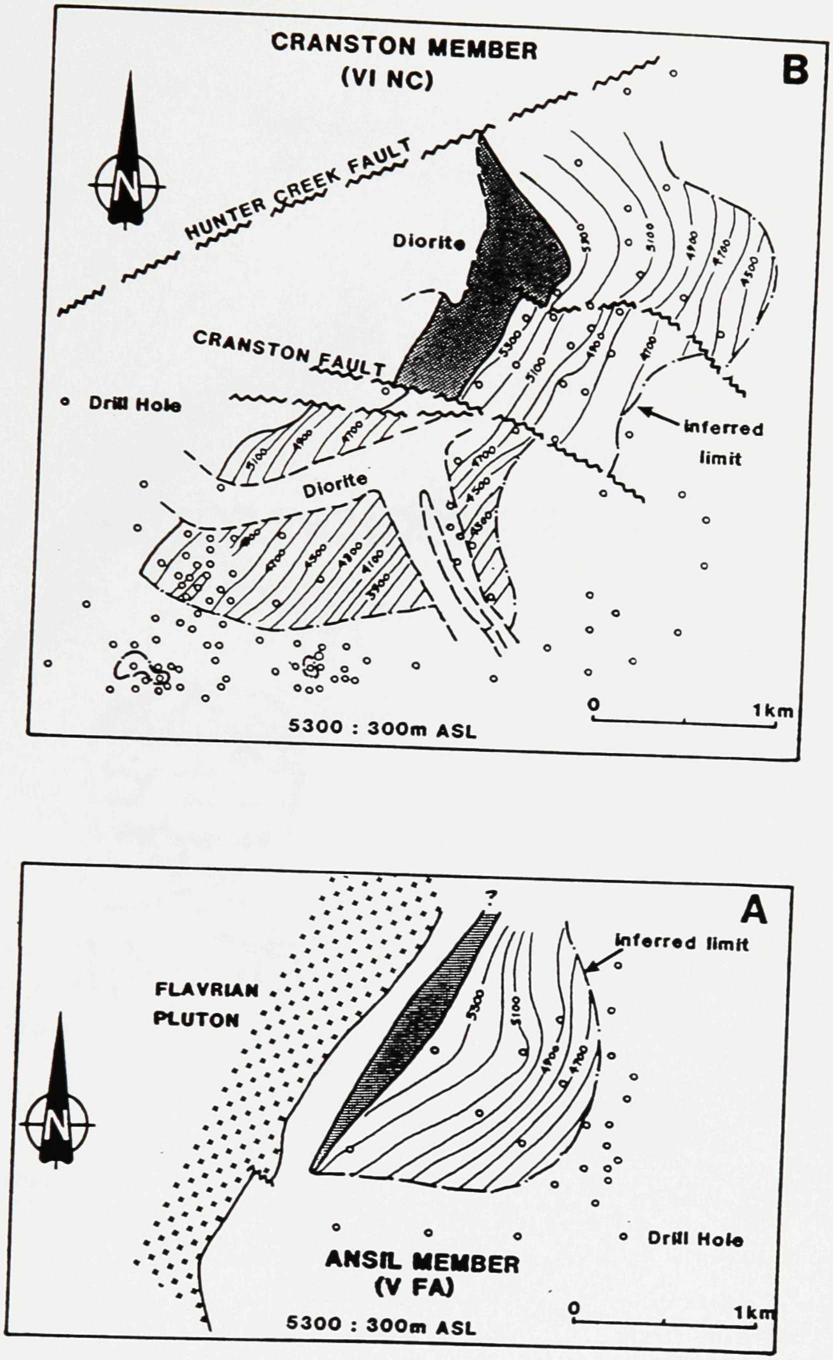

Figure 9.10. Stratigraphic top contact contour map for the Ansil (A) and Cranston (B) QFP flows.

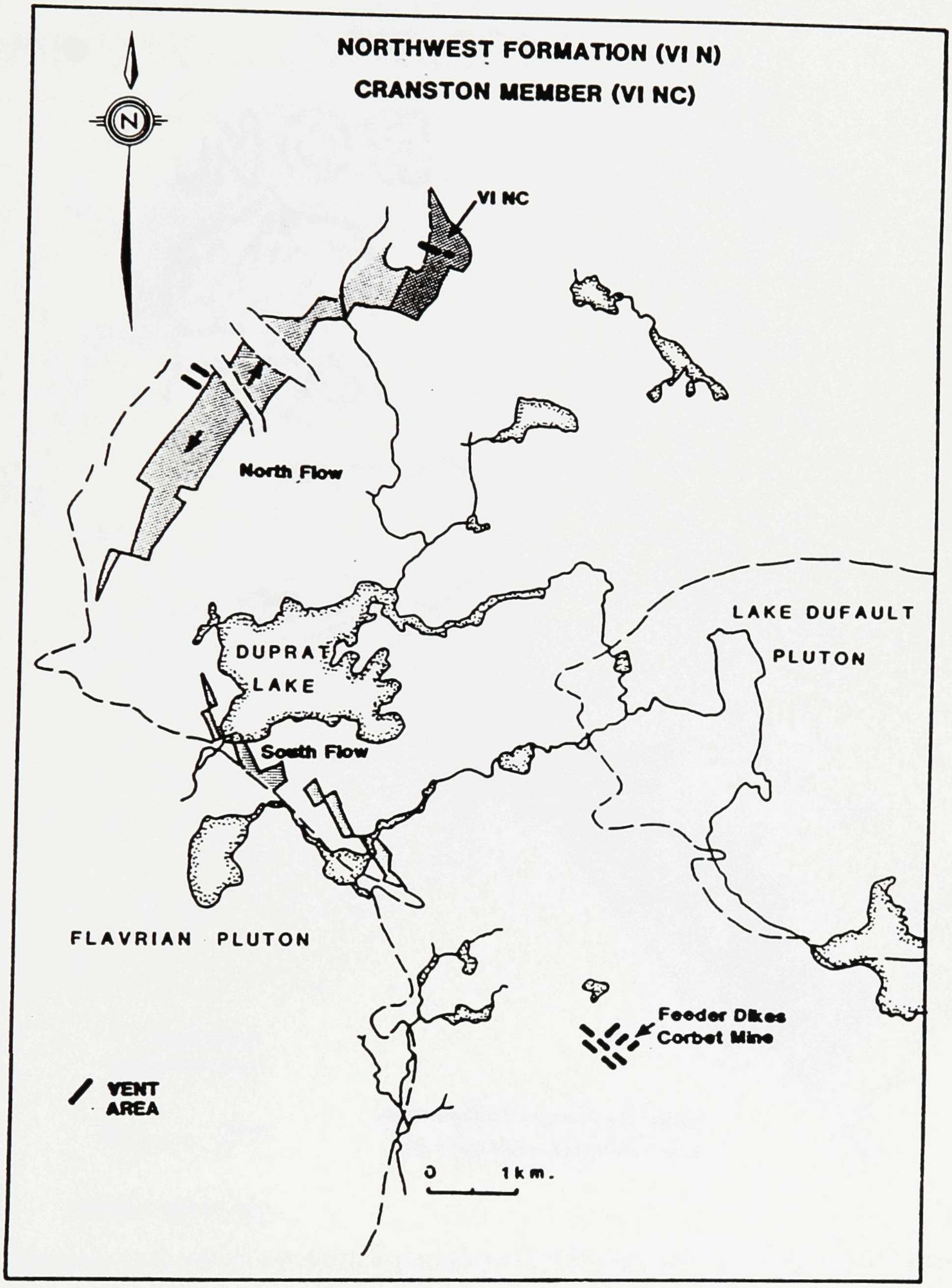

Figure 9.11. Surface distribution of the Northwest formation and Cranston member; arrows indicate inferred flow directions.

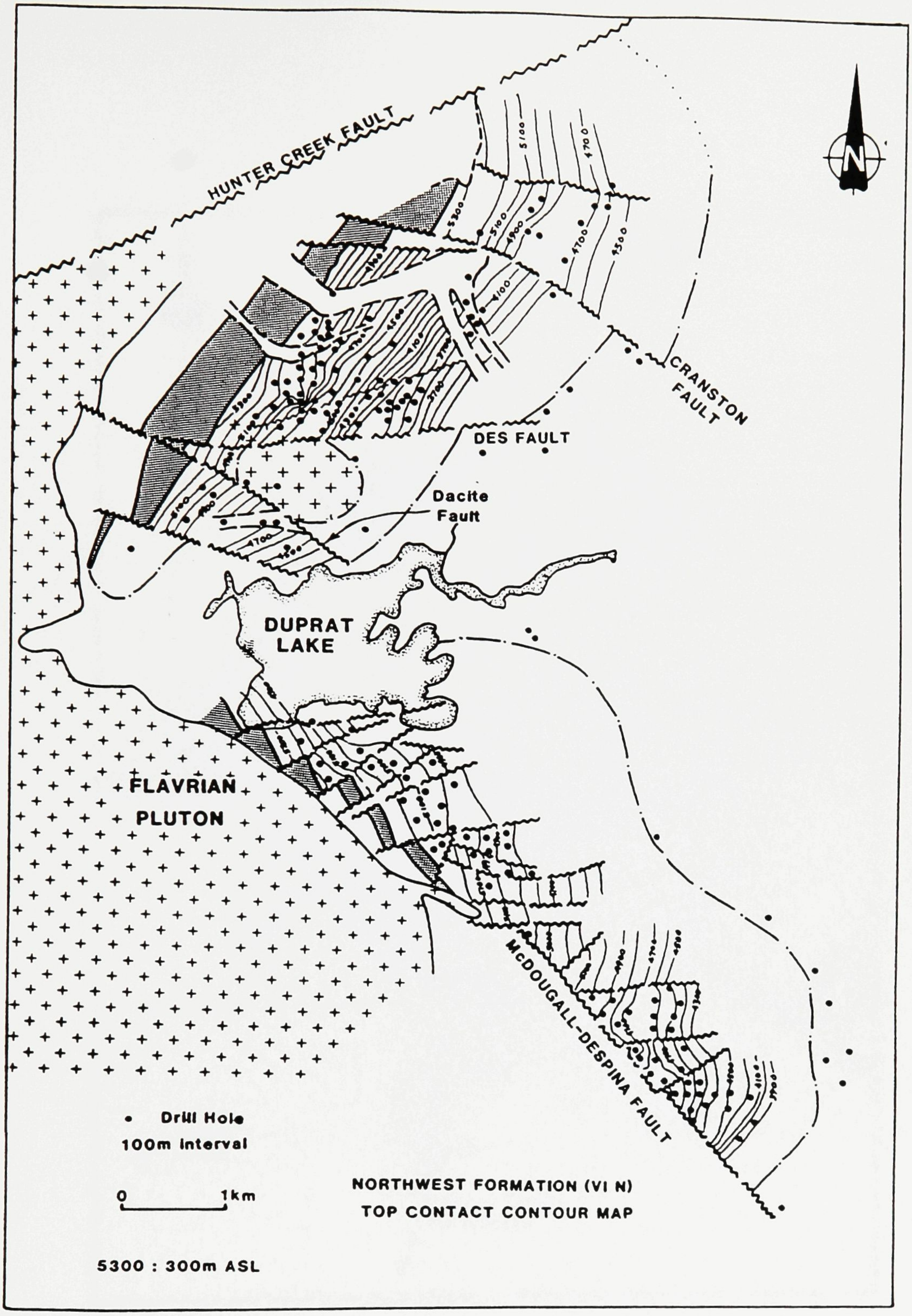

Figure 9.12. Stratigraphic top contact contour map for the north and south flows of the Northwest formation.

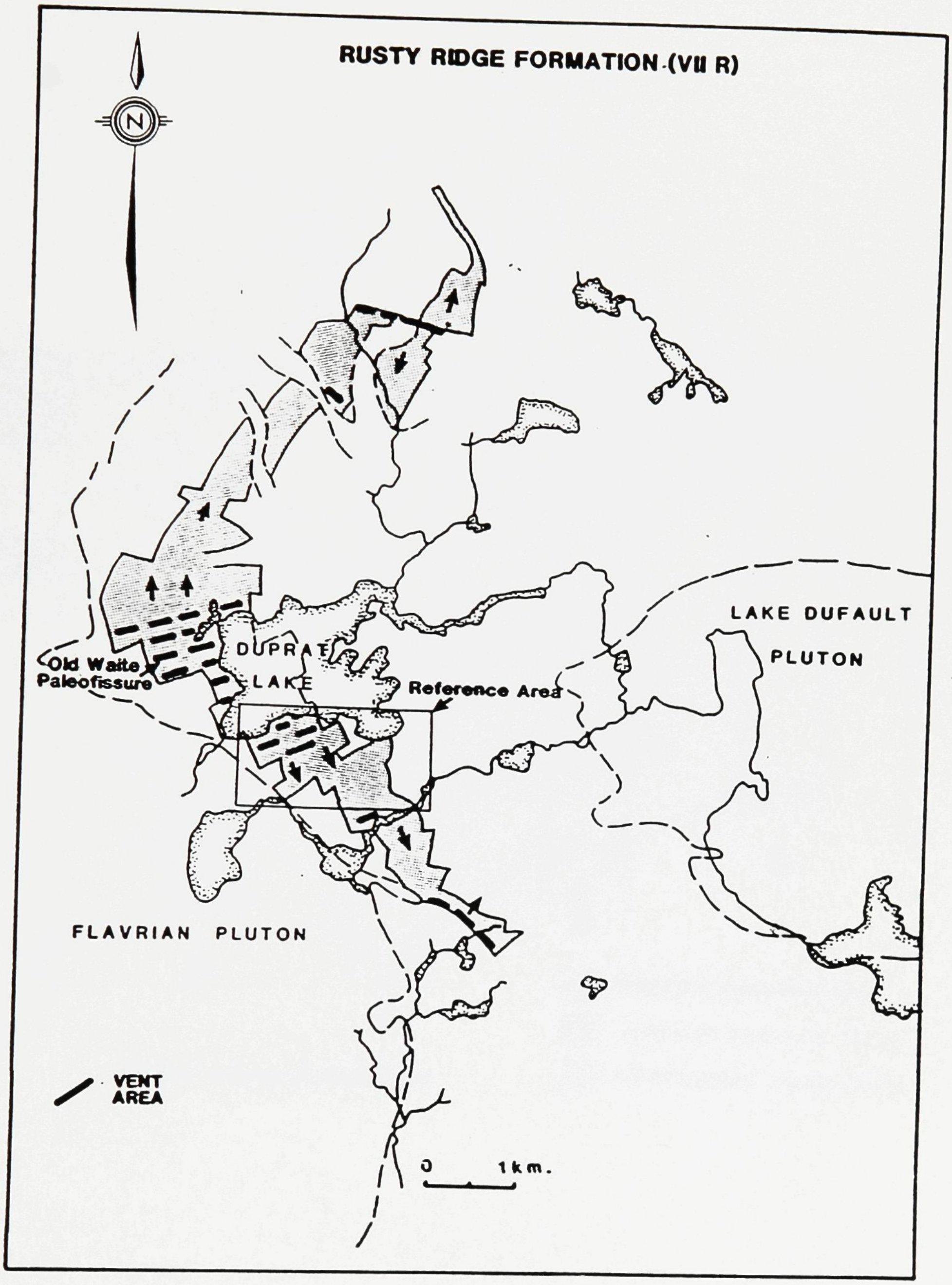

Figure 9.13. Surface distribution of the Rusty Ridge formation; arrows indicate inferred flow direction. Flow stratigraphy in Reference area described in Figure 9.14.

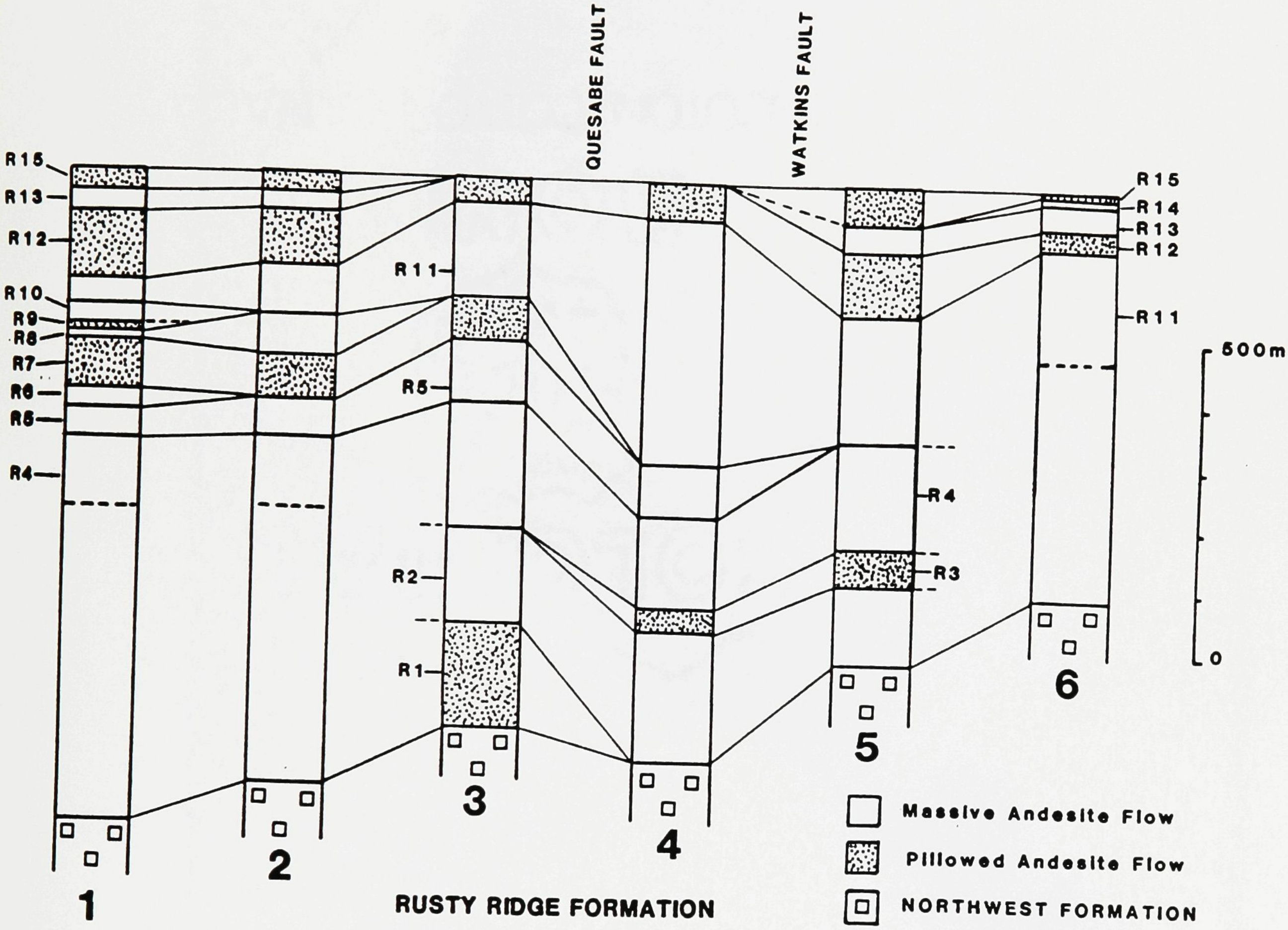

Figure 9.14. Flow stratigraphy of the Rusty Ridge formation south of Duprat Lake (Reference area of Figure 9.13).

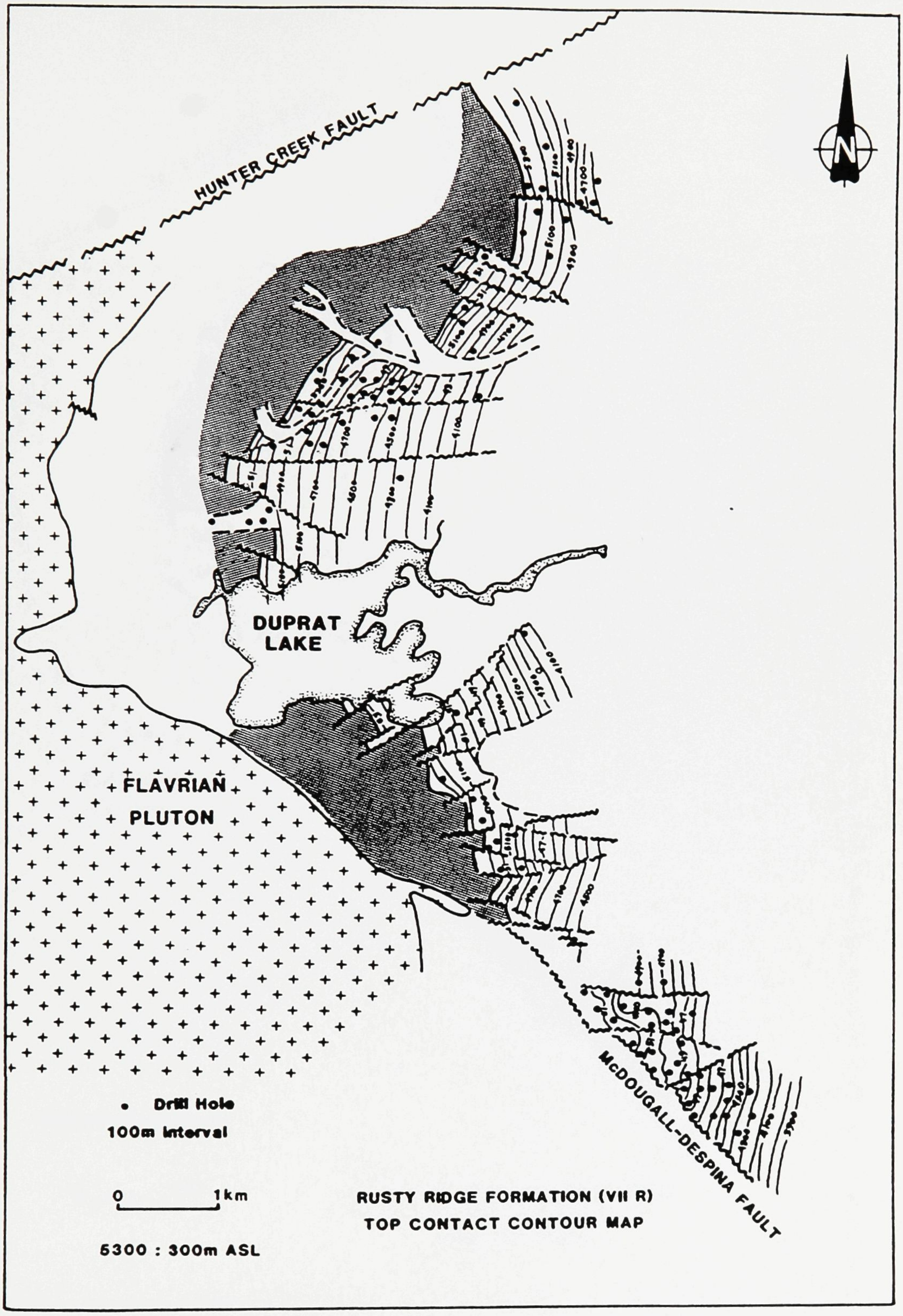

Figure 9.15. Stratigraphic top contact contour map for the Rusty Ridge formation.

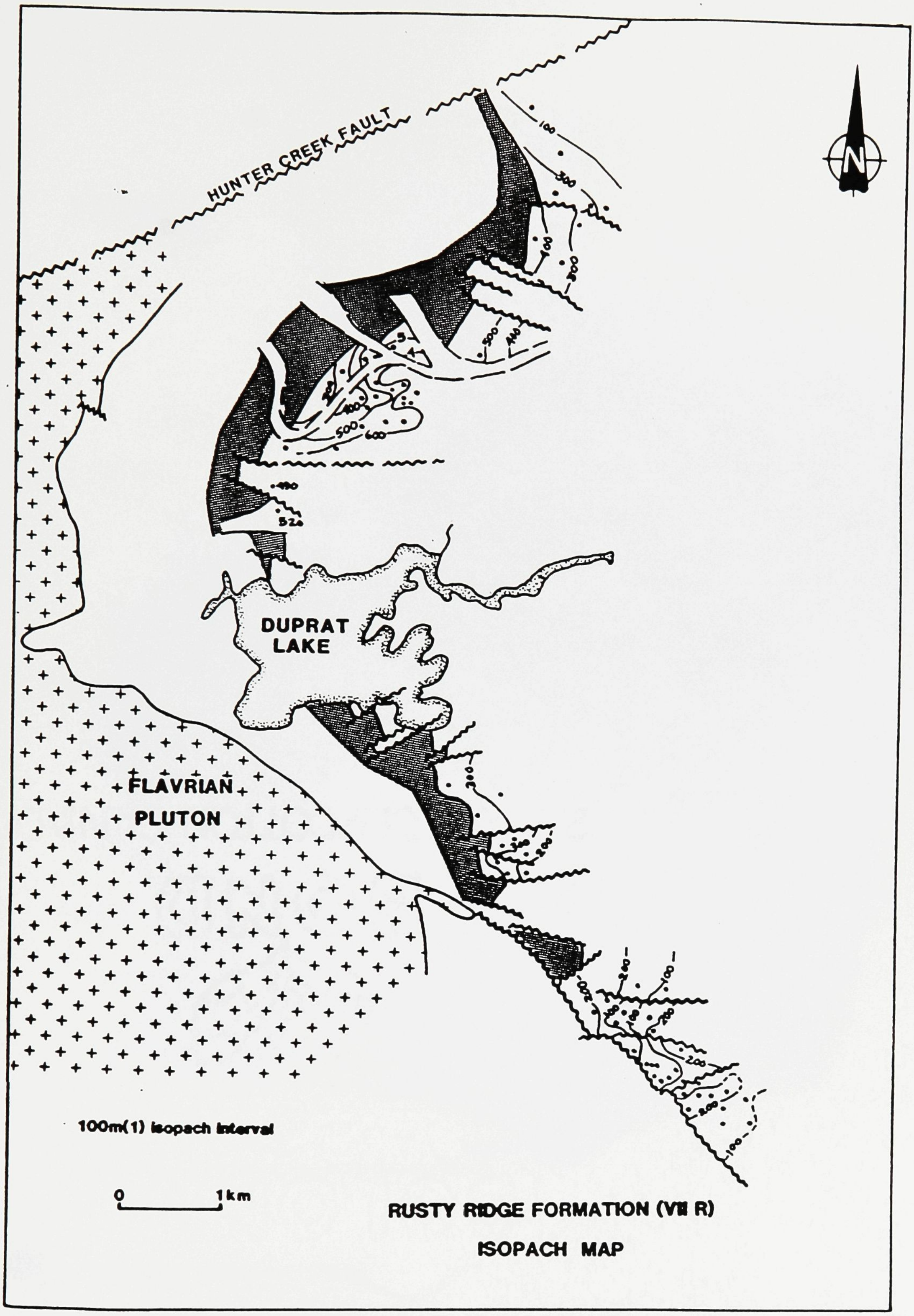

Figure 9.16. Isopach map for the Rusty Ridge formation.

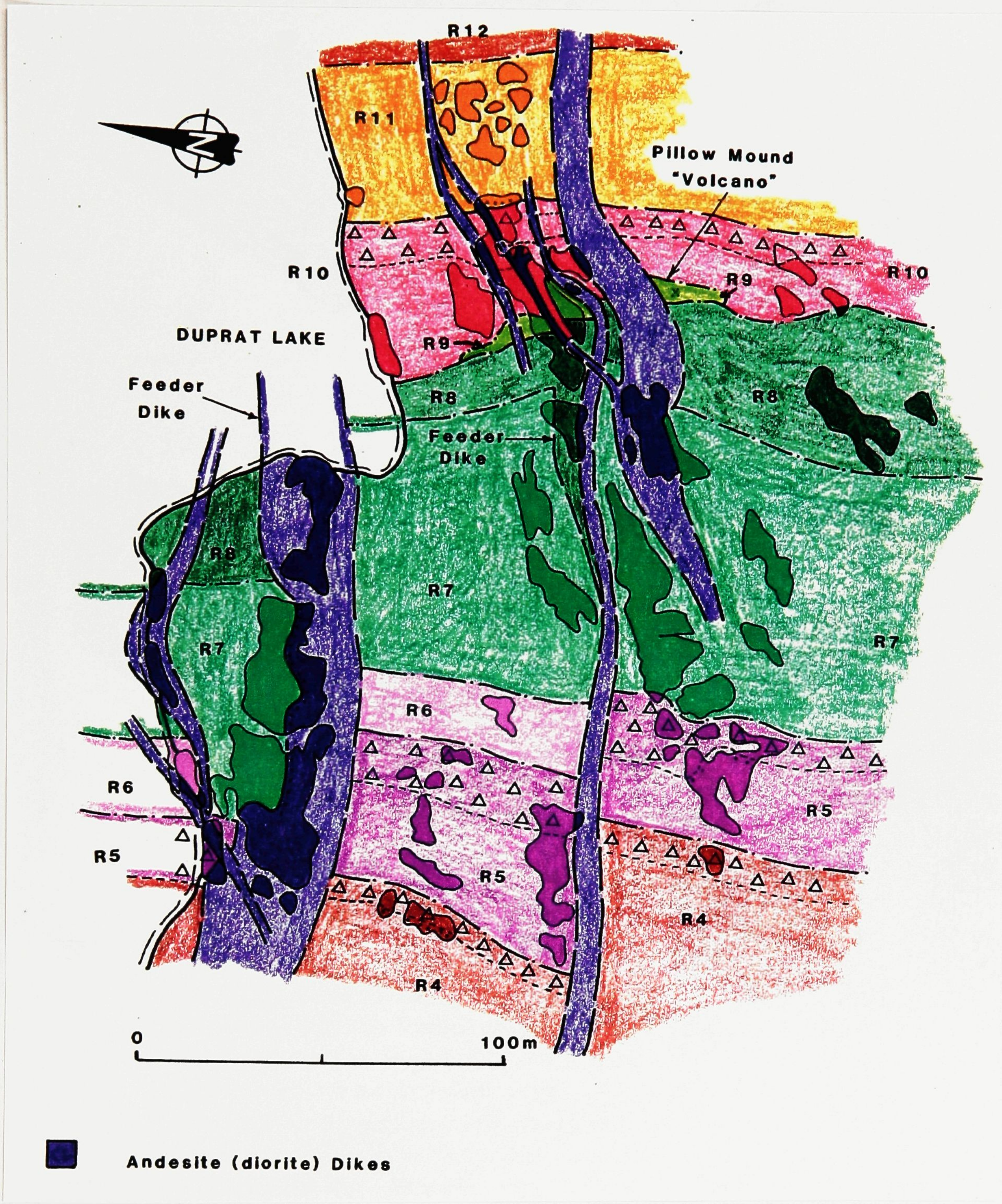

Figure 9.17. Feeder dikes and vent areas for the Rusty Ridge formation south of Duprat lake.

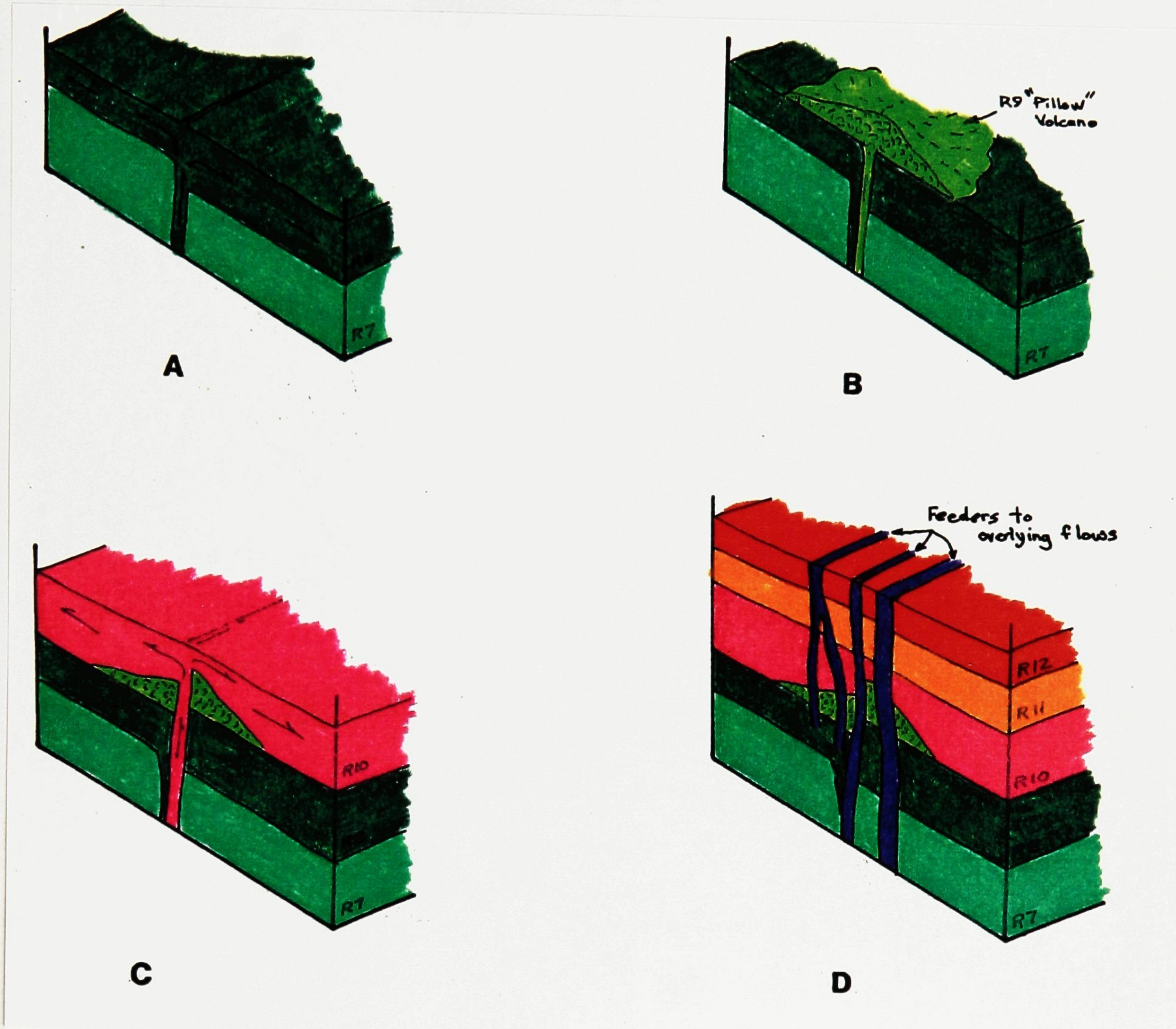

Figure 9.17.A. Cartoon illustrating one possible reconstruction of the reactivated andesitic vent area in Figure 9.17. A. Extrusion of a massive andesitic flow (R8) from a narrow, 080°-trending fissure. B. Extrusion of pillow lava (R9) to form a small, localized pillow mound or volcano directly above the feeding fissure. C. Reactivation of the fissure with emplacement of an andesitic feeder dike and extrusion of a massive flow (R10) which completely buried the underlying pillow volcano. Volcanism accompanied by minor subsidence along the fault/fissure. D. Extrusion of massive and pillowed andesitic flows which completely bury the fissure. Feeder dikes to overlying flows localized along to the former vent area suggesting continued reactivation of this structure.

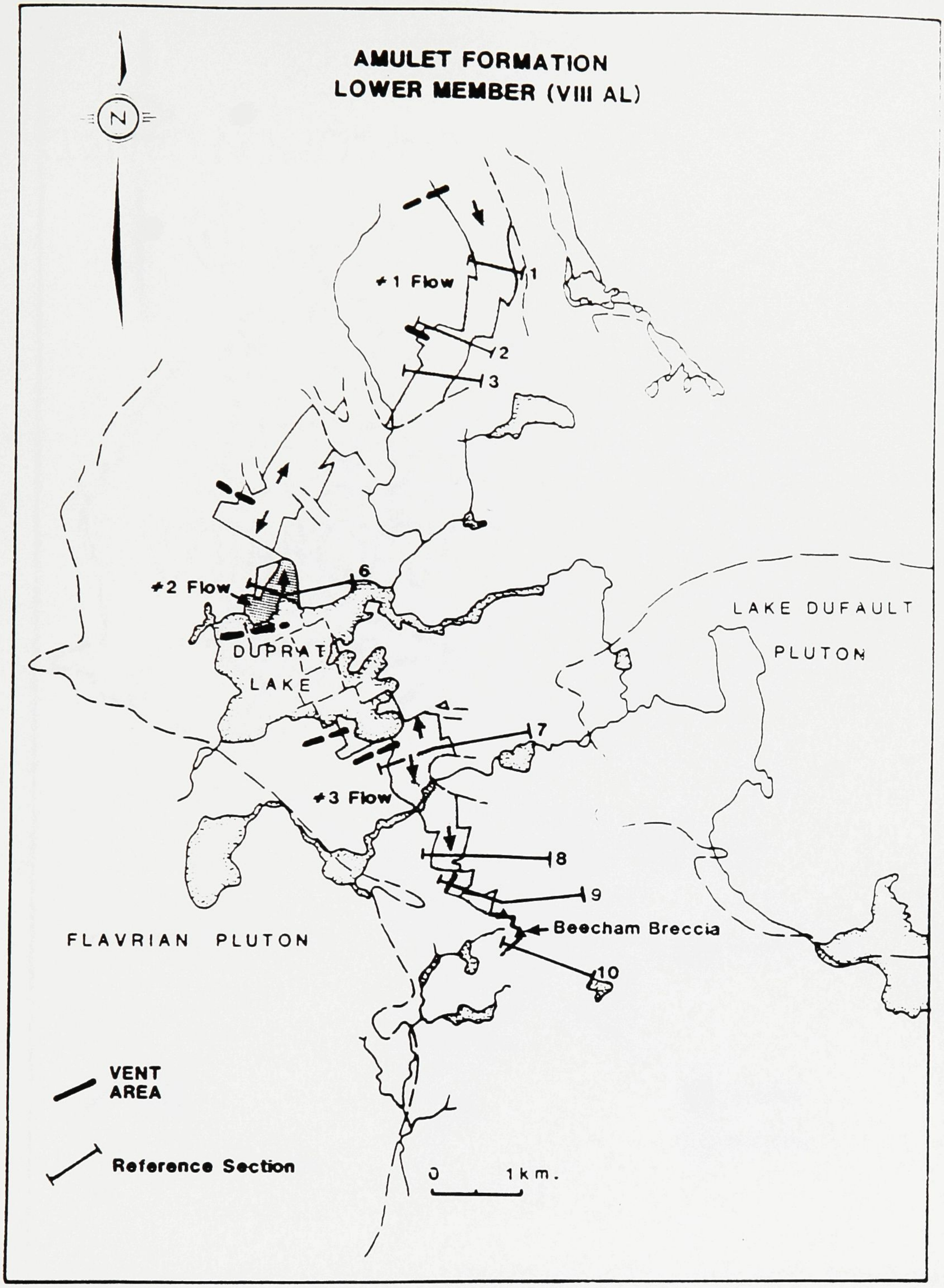

Figure 9.18. Surface distribution of the #1, 2 and 3 flows of the Amulet lower member; arrows indicate inferred flow directions. Numbered sections refer to stratigraphic sections of Figure 9.20.

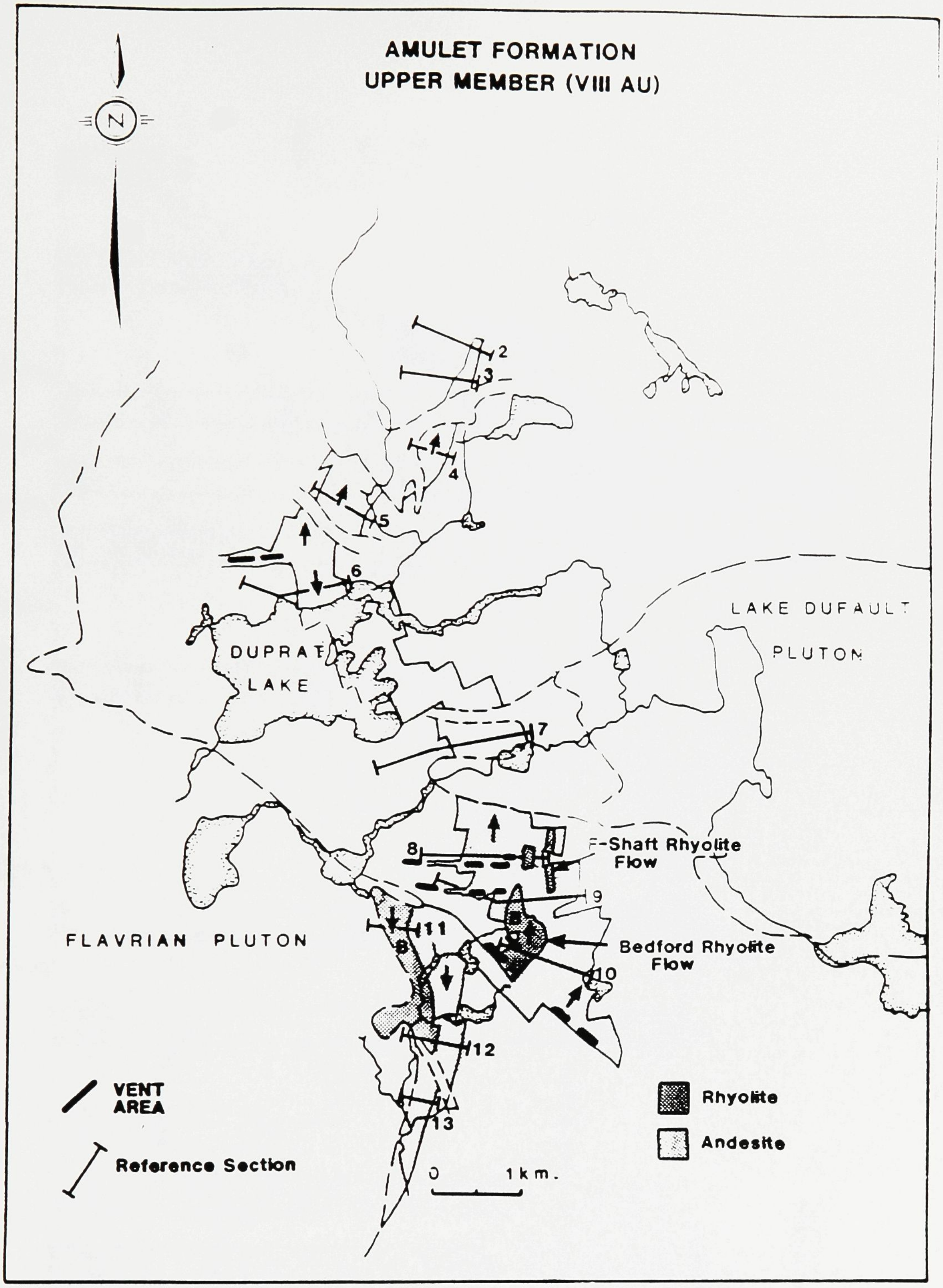

Figure 9.19. Surface distribution of the Amulet upper member; arrows indicate inferred flow directions. Numbered sections refer to stratigraphic sections in Figure 9.20.

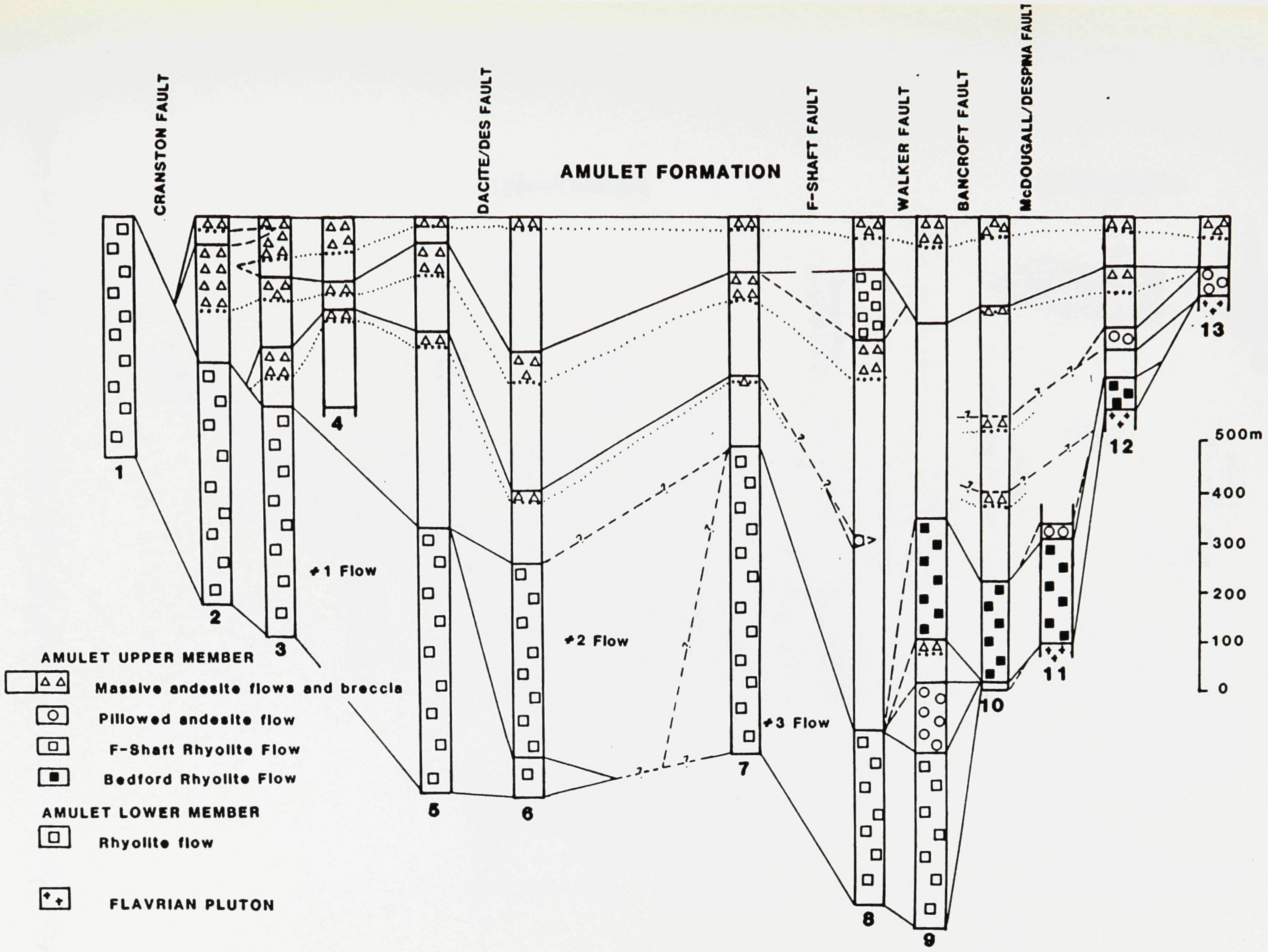

Figure 9.20.Sections detailing the flow stratigraphy and facies of the Amulet upper member.

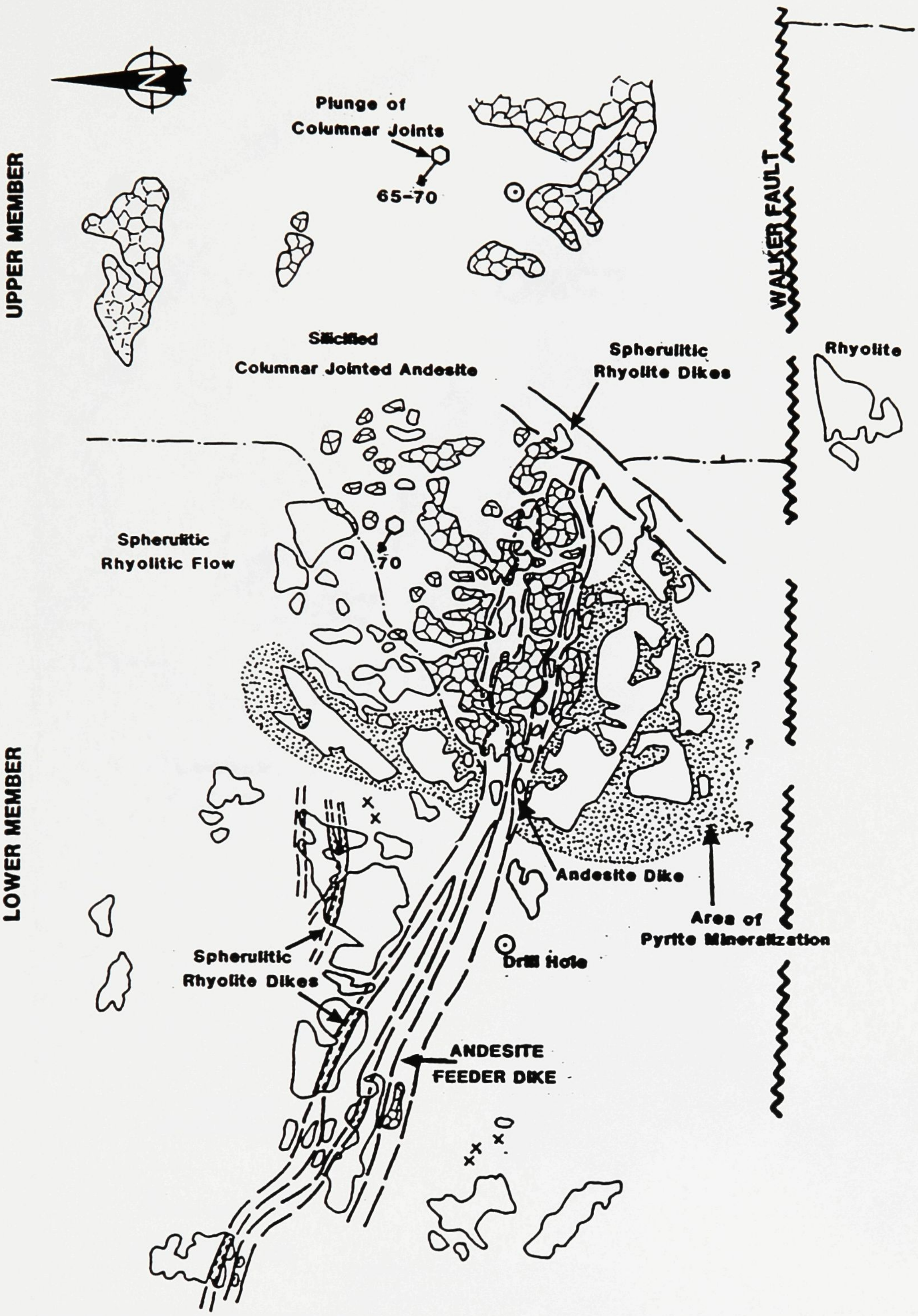

Figure 9.21. Andesitic feeder dike and vent area for the Amulet upper member, F-Shaft sector.

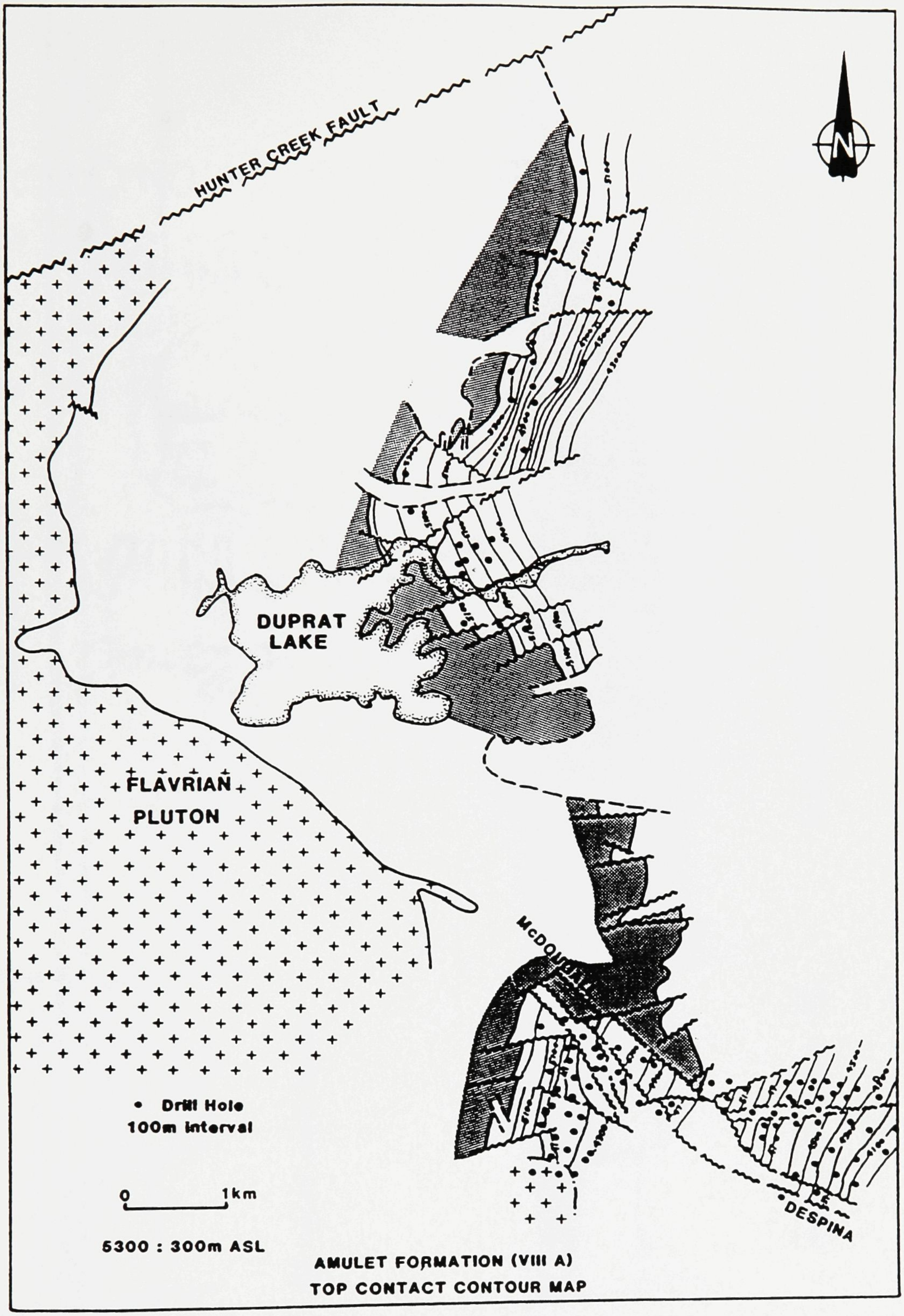

Figure 9.22. Stratigraphic top contact contour map for the Amulet upper member.

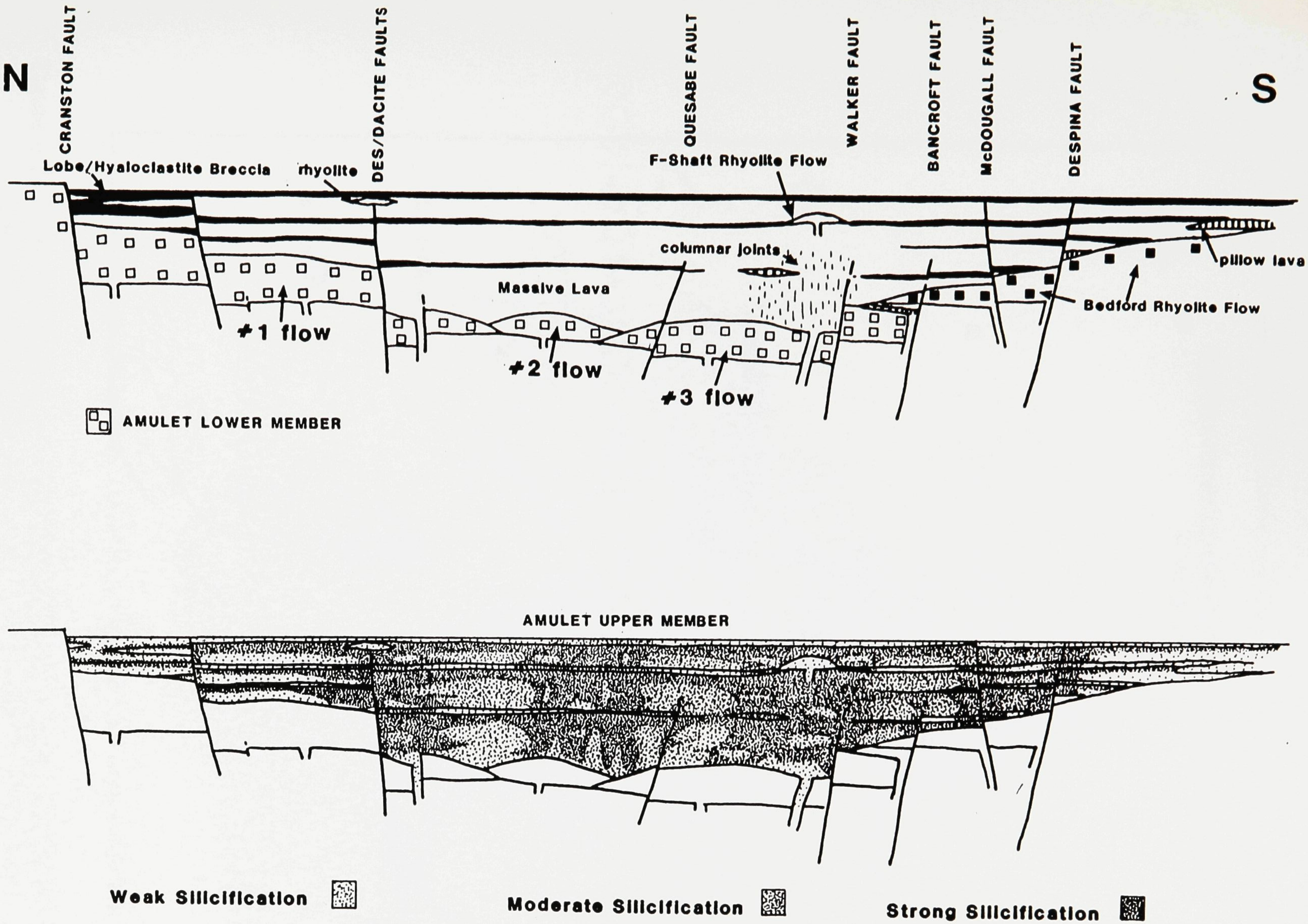

Figure 9.23. A - Reconstructed cross-section through the Amulet upper member prior to Millenbach-Waite Andesite volcanism.
B - Areas of weak to strong silicification within the upper member.

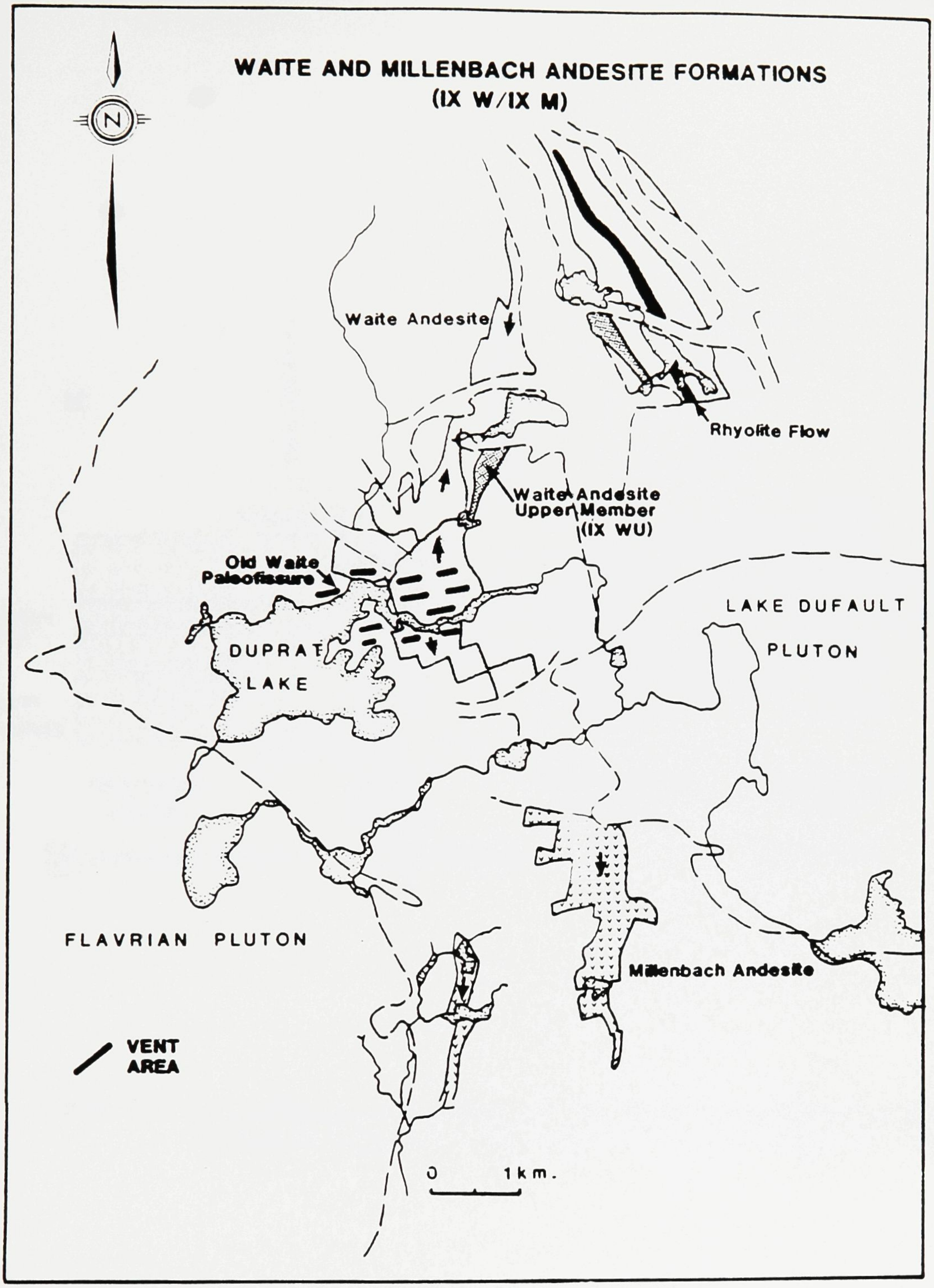

Figure 9.24. Surface distribution of the Waite and Millenbach Andesite formations and location of the Old Waite Dike Swarm or Paleofissure; arrows indicate inferred flow directions.

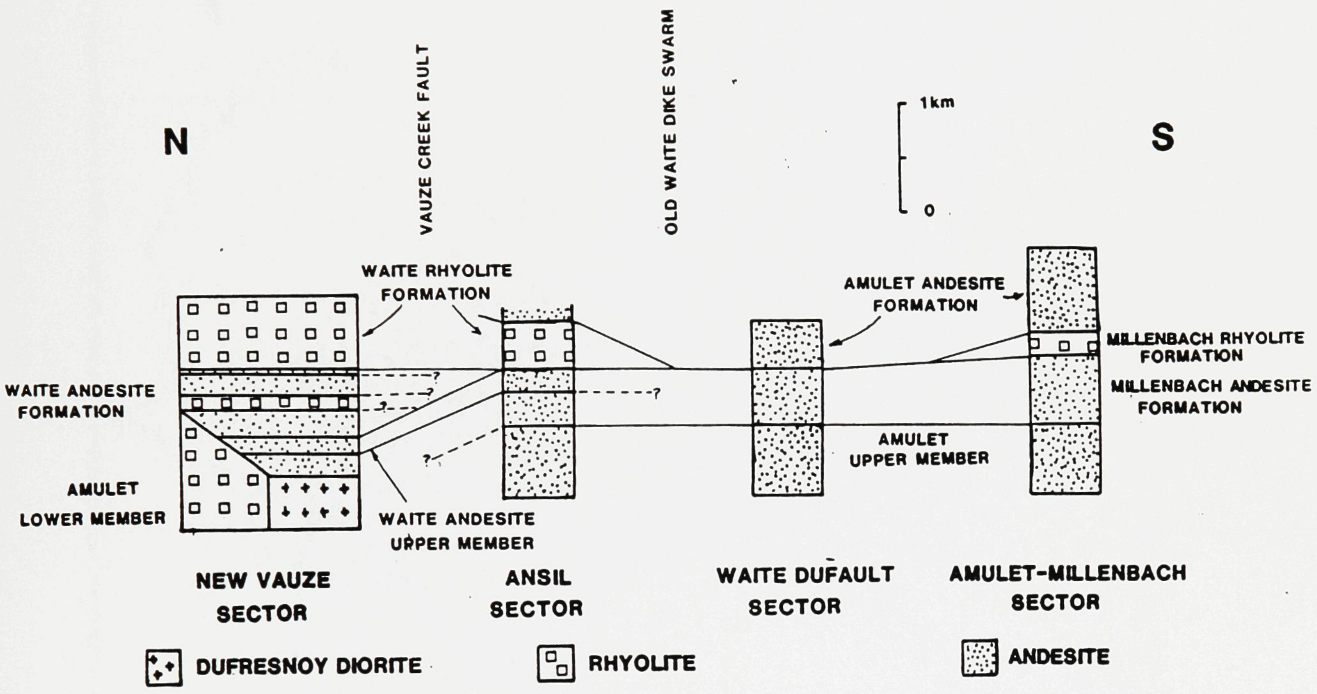

Figure 9.25. Lithostratigraphic correlation of the Waite and Millenbach Andesite formations between the New Vauze and Amulet-Millenbach sectors.

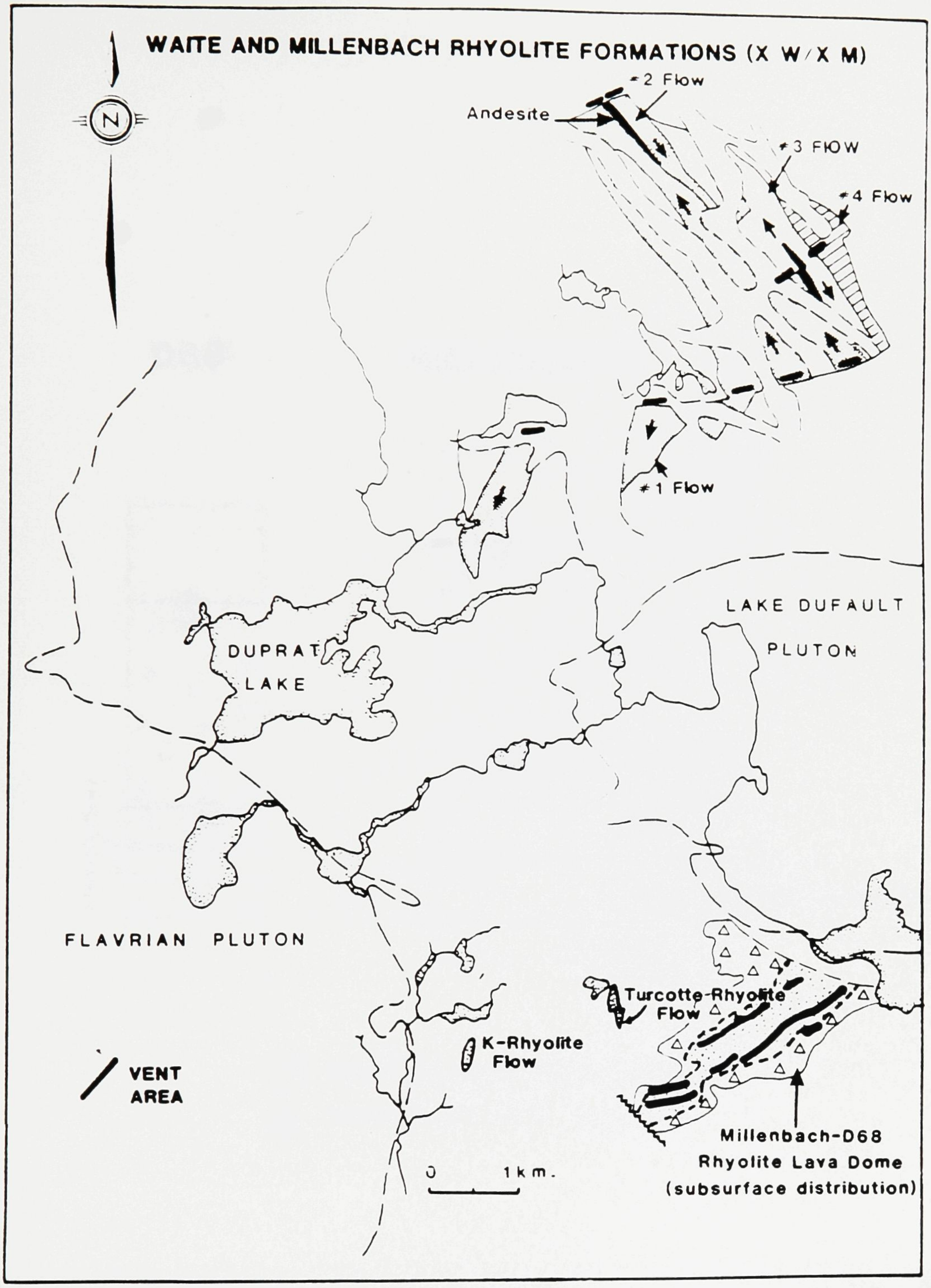

Figure 9.26. Surface distribution of the #1, 2, 3 and 4 rhyolitic flows of the Waite Rhyolite formation and subsurface distribution of the Millenbach-D68 lava dome; arrrows indicate inferred flow directions.

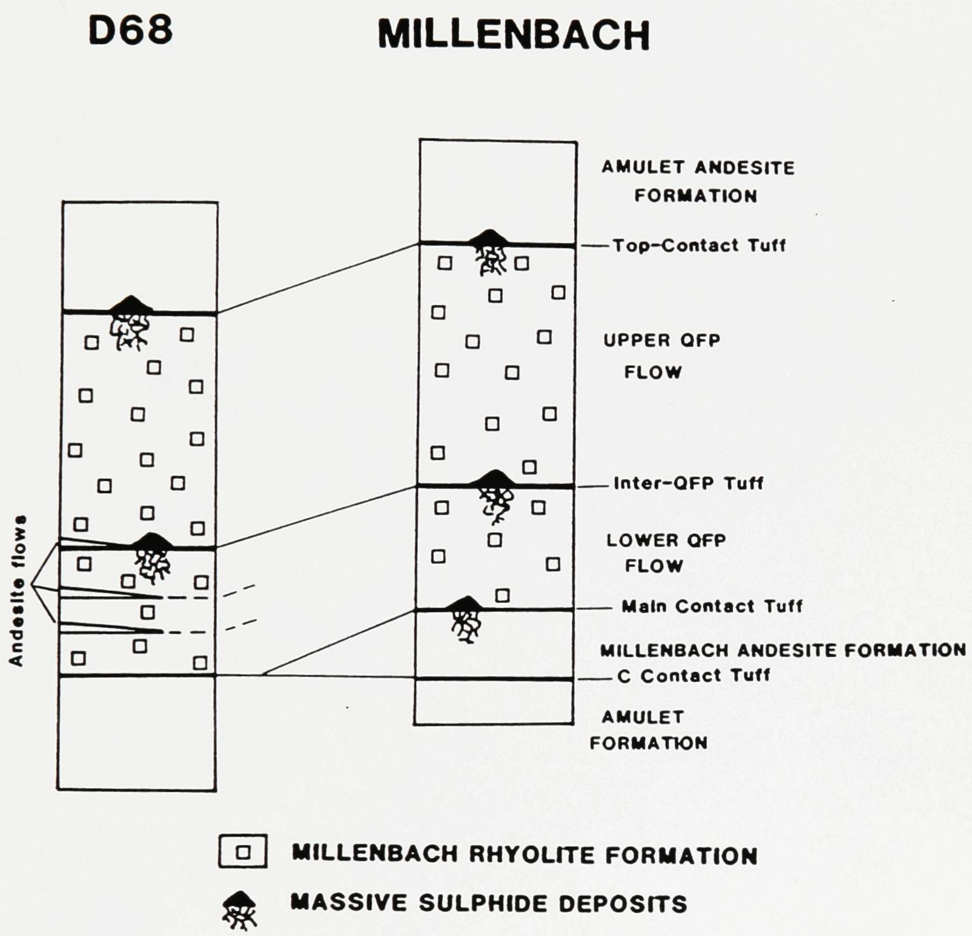

Figure 9.27. Flow stratigraphy of the Millenbach Rhyolite formation at Millenbach and in the D68 area.

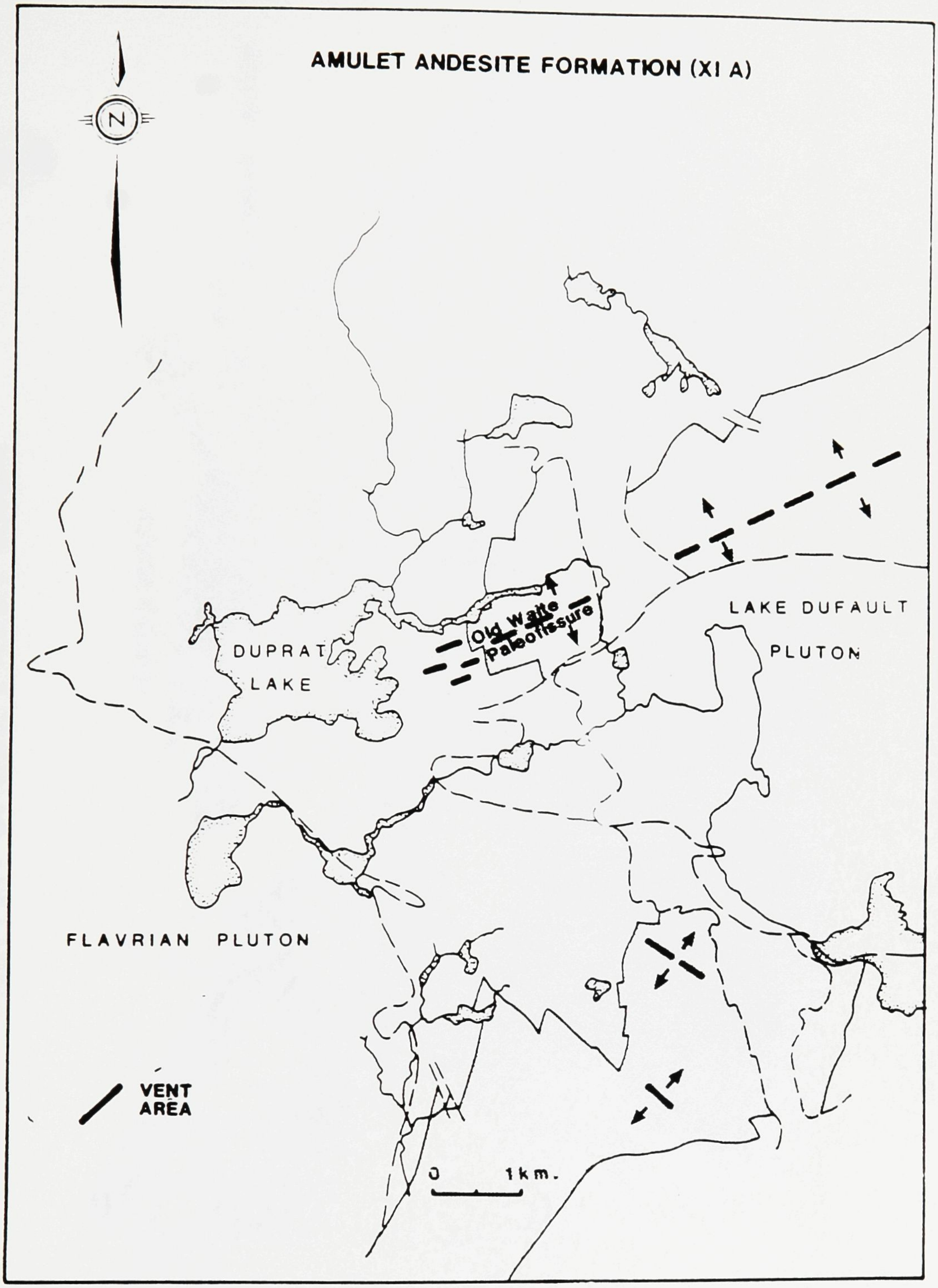

Figure 9.28. Surface distribution of the Amulet Andesite formation and location of the Old Waite Paleofissure; arrows indicate inferred flow directions.

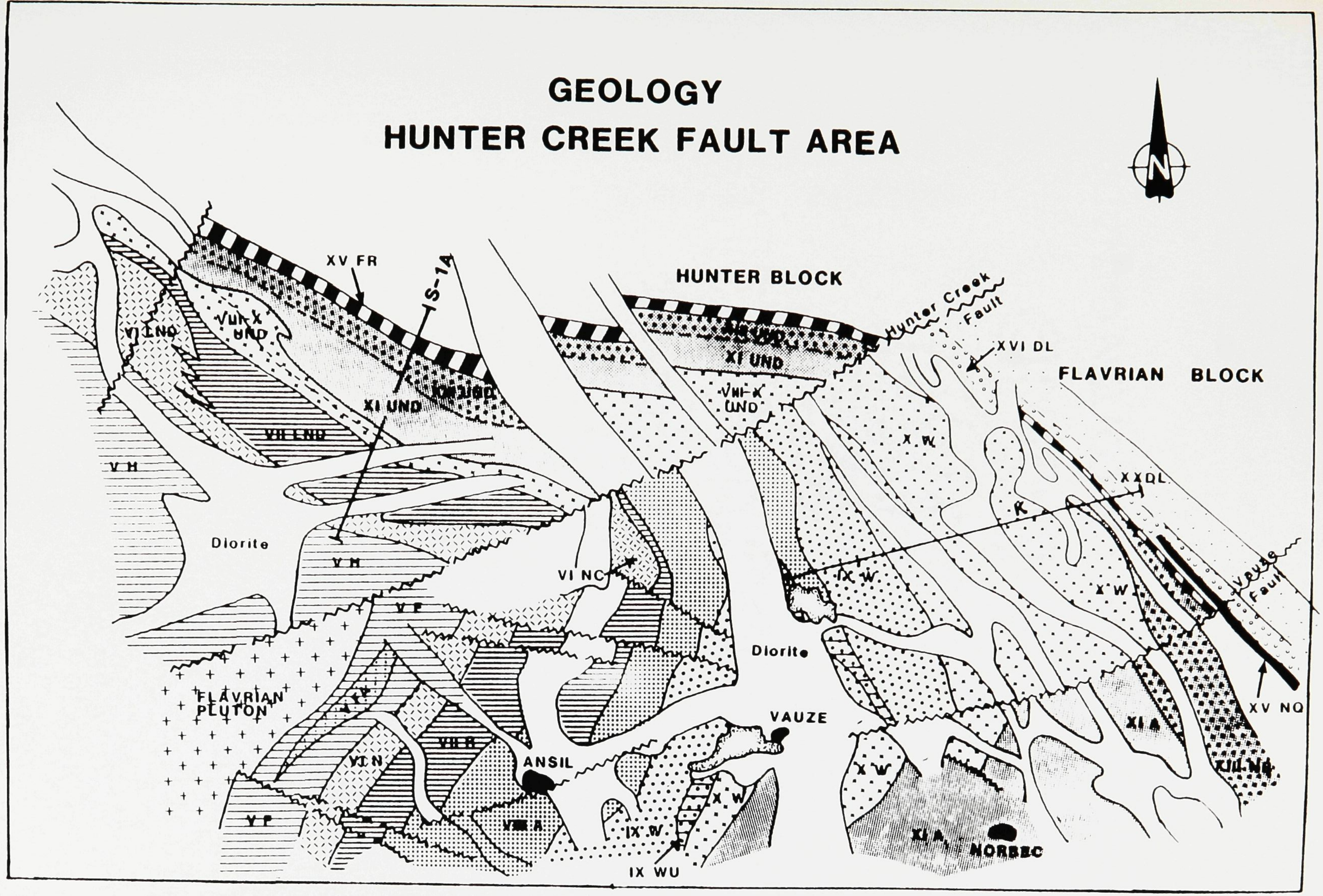

Figure 9.29. Geology of the Hunter Block and north part of the Flavrian Block (modified after de Rosen-Spence, 1976). Sections S-1A and k refer to stratigraphic sections in Figure 9.2.

Figure 9.30. Geology of the Powell and south part of the Flavrian Blocks and Horne Mine area, Sections S-8 to -10 refer to stratigraphic sections of Figure 9.2 (modified after de Rosen-Spence, 1976)

17	Wilco Andesite formation
16	Osisko Andesite formation
15b	Horne Rhyolite, upper member
15a	Horne Rhyolite, lower member
14	Cyprus Rhyolite and Andesite formations
13	South Dufault Rhyolite formation
12	Mesipi Andesite formation
11	Mesipi Rhyolite formation
10	Deldona Rhyolite formation
9	Don Rhyolite formation
8	South Bay Andesite formation
7	Delbridge Rhyolite formation
6	Don Rhyolite formation
5	Insco Rhyolite formation
4	Powell Andesite formation
3	Quemont Rhyolite formation
2	Joliet Rhyolite formation
1	Brownlee Rhyolite formation

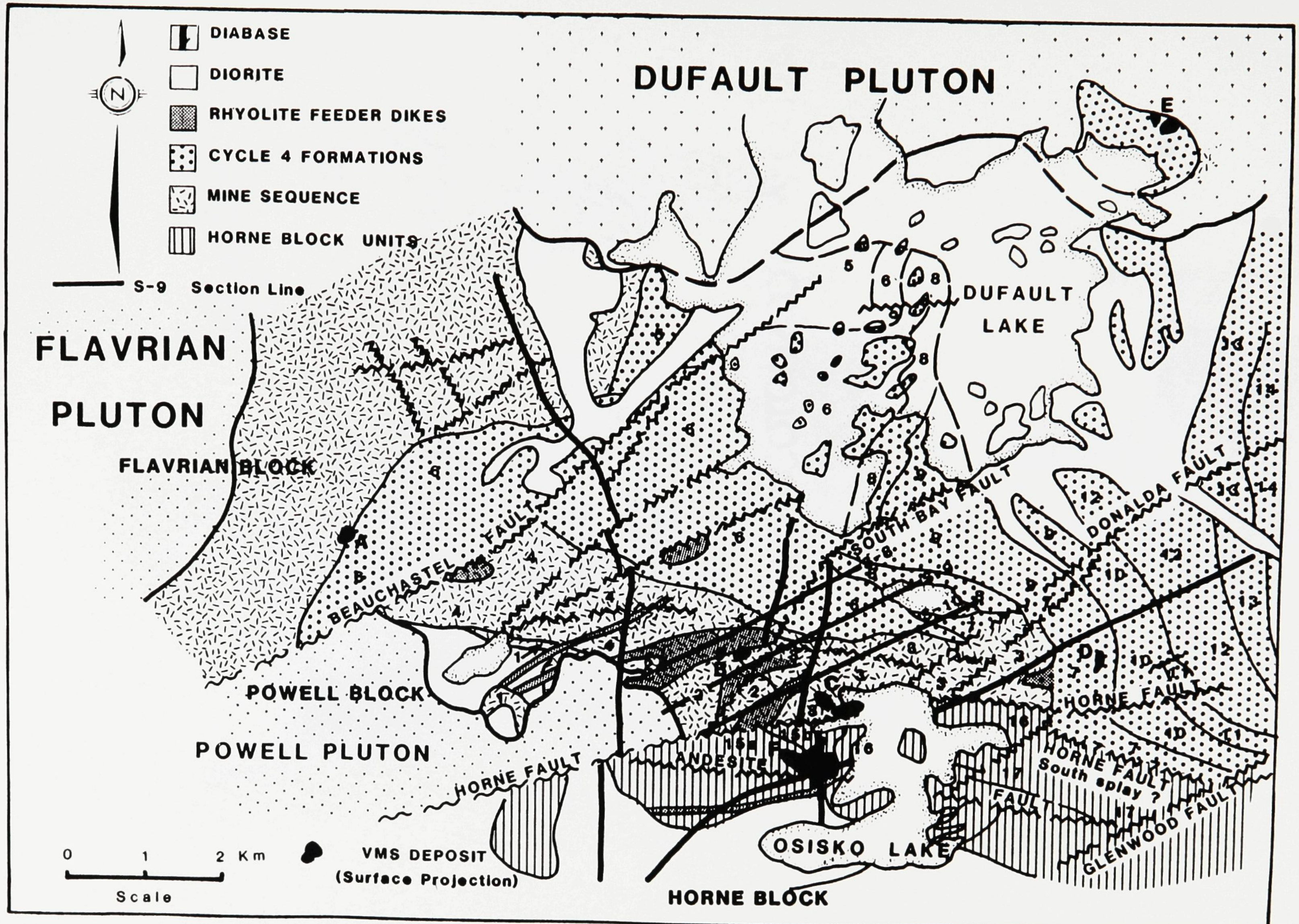
DIABASE
DIORITE
RHYOLITE FEEDER DIKES
CYCLE 4 FORMATIONS
MINE SEQUENCE
HORNE BLOCK UNITS
S-9 Section Line
N
DUFAULT PLUTON
DUFAULT LAKE
FLAVRIAN PLUTON
FLAVRIAN BLOCK
BEAUCHASTEL FAULT
SOUTH BAY FAULT
DONALDA FAULT
POWELL BLOCK
POWELL PLUTON
HORNE FAULT
HORNE FAULT
HORNE FAULT South splay ?
GLENWOOD FAULT
ANDESITE
OSISKO LAKE
HORNE BLOCK
VMS DEPOSIT (Surface Projection)
0 1 2 Km
Scale

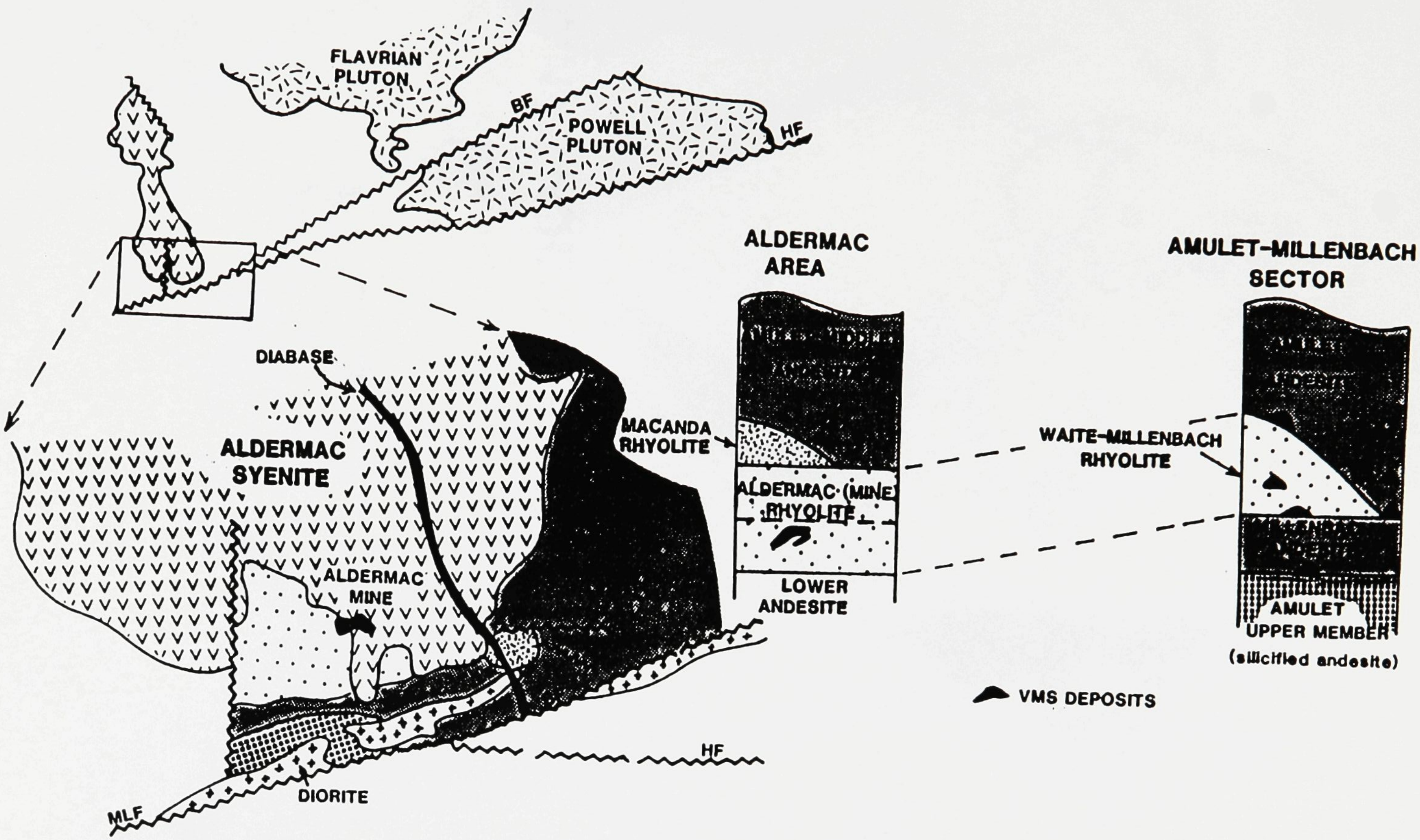

Figure 9.31. Generalized geology of the Aldermac Area and proposed lithostratigraphic correlations with the Mine Sequence of the Amulet-Millenbach Sector (from Hunter and Gibson, 1986).

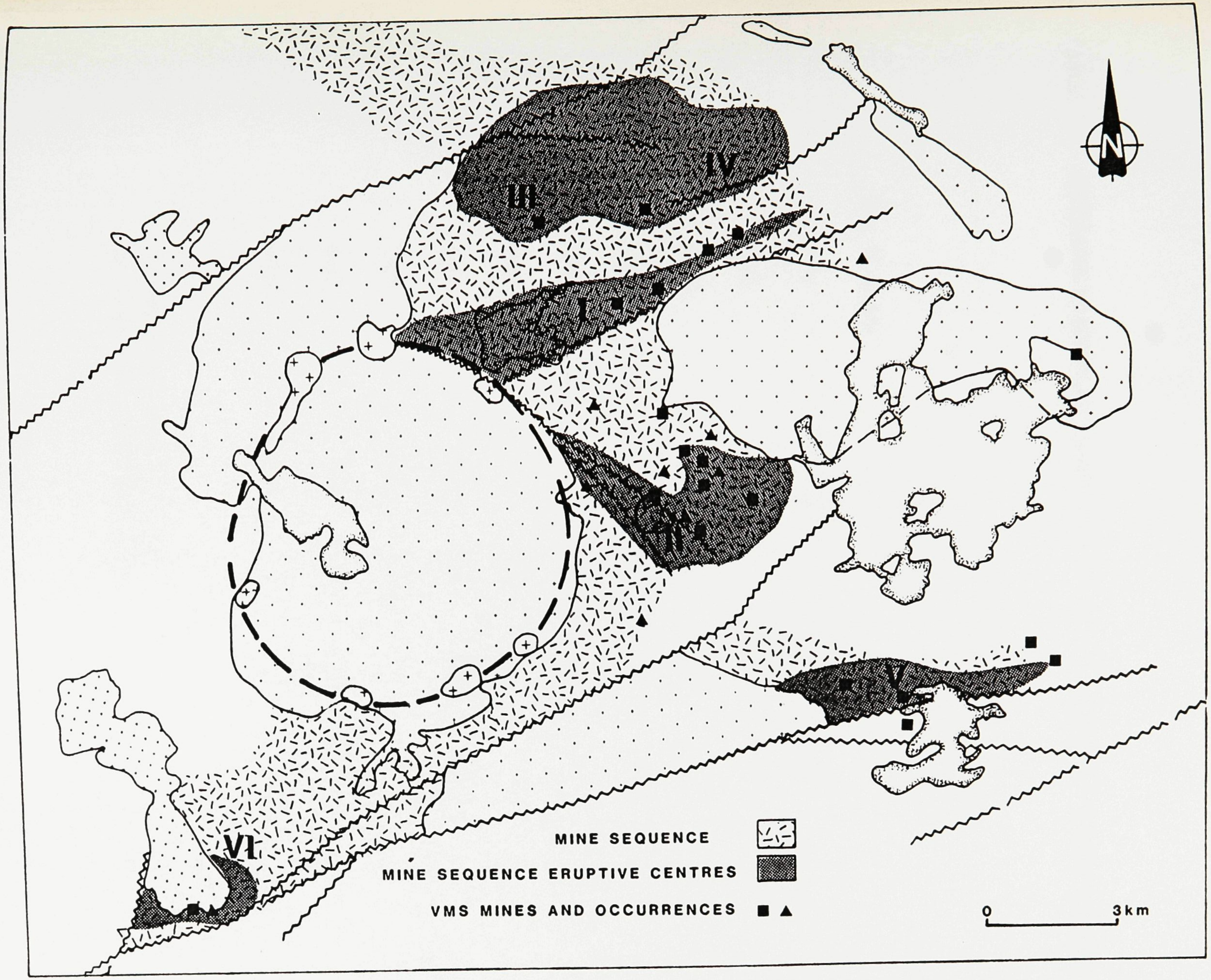

Figure 9.32. Generalized location of the Mine Sequence eruptive centres, former and current Massive Sulphide Mines and Occurrences.

TABLE 9.1. AVERAGE CHEMICAL COMPOSITION OF THE AMULET UPPER MEMBER

	(119 analyses)			
	1	2	**Mean**	Std. Dev.
Wt. % Oxide				
SiO_2	52.7	79.6	**64.6**	4.8
Al_2O_3	11.4	17.0	**14.0**	1.1
Fe_2O_3	0.1	16.6	**7.7**	2.2
MgO	0.2	6.6	**3.2**	1.4
CaO	0.2	7.6	**2.6**	1.5
Na_2O	0.0	6.4	**4.5**	1.4
K_2O	0.0	3.2	**0.6**	0.7
TiO_2	0.5	1.9	**1.0**	0.3
P_2O_5	0.0	0.6	**0.3**	0.1
MnO	0.0	0.6	**0.1**	0.1

1. Minimum value for oxide
2. Maximum value for oxide

10. SYNVOLCANIC FAULTS AND STRUCTURE

10.1 SYNVOLCANIC FAULTS

A synvolcanic fault is one which was or is active during extrusion of the volcanic sequence in which it occurs. Synvolcanic faults are significant in that they:

a) effect the topography of volcanic terrains and therefore influence the disposition, extent and thickness of extrusive units.

b) control the location of volcanic vents.

c) accommodate subsidence.

d) provide channelways for ascending hydrothermal solutions and thus govern the location of submarine hotsprings and massive sulphide deposits.

Synvolcanic faults may be reactivated with continued volcanism or through unrelated, later tectonic events. Before a meaningful reconstruction of the volcanic history can be addressed, synvolcanic faults must be identified. Synvolcanic faults were recognized during mapping and reconstruction using drill hole data. A fault was interpreted to be synvolcanic if it a) controlled the distribution of individual flows, members or formations, b) was occupied by rhyolitic or andesitic feeder dikes (Plate 10.2) or c) contained mineralization (Plate 10.1) and was mantled by chlorite and sericite alteration envelopes that are identical mineralogically and chemically to the chlorite and sericite alteration associated with VMS deposits (Chapter 13). Significant synvolcanic faults within the Flavrian Block are described first, followed by a description of the major structural feature of the Noranda area. Evidence for synvolcanic nature of major faults such as the Hunter Creek, Beauchastel, Western Quemont Feeder Dike and Horne Faults which separate the Hunter, Flavrian and Powell Blocks have been described (Chapter 9).

10.2 SYNVOLCANIC FAULTS OF THE FLAVRIAN BLOCK

10.2.1 McDOUGALL-DESPINA FAULT

The most prominent and important fault within the Flavrian Block is the McDougall-Despina Fault (Figure 7.1). This fault consists of two N40^{0}W trending faults, the McDougall and Despina. These faults, although offset by numerous northeast trending faults, have a crude, gently arcuate surface trace (Figure 7.1) over their 4.8 km strike length (Setterfield 1984, 1987). The faults cut strata at a high angle and converge to the northwest (lower in the stratigraphic succession) and diverge to the southeast (Figure 7.1).

The easternmost fault, the McDougall dips 75-80^0 west whereas the Despina Fault dips at 70^0-80^0 to the east. At the Corbet Mine the two faults converge at depth (Figure 9.6) and dip steeply east as a single structure. The fault has a combined minimum vertical displacement (south side down) of 750m as indicated by measured offset of the Millenbach-D68 lava dome (J.Bonneau, personal communication; 1985). The displacement represents synvolcanic movement as the fault does not appreciably offset or cross-cut the Here Creek formation and dikes which occupy this structure were feeders to this formation as well as the Flavrian, Northwest, Amulet, and Amulet Andesite formations.

The McDougall-Despina Fault, like ring fractures within the Flavrian Pluton (Goldie, 1976), controlled the emplacement of the earliest intrusive phase (Meritens phase) of the Flavrian Pluton prior to or at the onset of Mine Sequence volcanism (Figure 9.6 Section P-P, Appendix C). The uniform, but different level of emplacement of the Flavrian Pluton north and south of the McDougall and Despina Fault suggests that this fault also controlled the emplacement of later phases of the pluton within the Mine Sequence.

10.2.2 THE DES AND DACITE FAULTS

The Des and Dacite Faults in the Ansil sector are similar to the McDougall-Despina Fault as they converge to the northwest (Maps 1 and 2, Figure 9.12). Strata between the faults are down faulted and the faults define a synvolcanic graben or basin. The main evidence for the faults, besides offset of formational contacts established through surface mapping and drilling, is the absence of the Northwest formation in 4 drill holes located between the faults; Northwest formation was intersected in drill holes north and south of the Des and Dacite Faults (Figure 9.12).

A north-south structural cross-section G-G (Figure 9.4), through the fault block shows these features. There is a marked increase in the thickness of the Rusty Ridge formation in its vent area west and northwest of Duprat Lake and thinning to the north and south. This is reflected in section G-G (Figure 9.4) where the Rusty Ridge formation between the Des and Dacite Faults is a minimum of 600m in thickness, while north of the Des Fault the formation is only 370m thick.

The decrease in thickness of the Rusty Ridge formation is not totally in response to topography of the underlying North flow of the Northwest formation. The Rusty Ridge formation is 1.0km thick west of Duprat Lake while the combined thickness of Northwest and Rusty Ridge formations, at surface, at Ansil Hill is only 0.7km. This difference in thickness plus a marked increase in thickness of the Rusty Ridge formation south of the Des Fault (section G-G) is interpreted to reflect ponding of andesitic flows, similar to that proposed for the Rusty Ridge formation south of Duprat Lake (Chapter 9). Synvolcanic subsidence south of the Des Fault down faulted the Northwest formation which was subsequently removed by intrusion of the Flavrian Pluton (Figures 9.12).

10.2.3 THE CRANSTON AND BANCROFT FAULTS

The Cranston and Bancroft Faults have a demonstratable synvolcanic offset (Maps 1 and 2, Figure 7.1). The Cranston Fault and its south splay do not appreciably offset conformable rhyolitic breccias within the lowermost flows of the Waite Andesite formation (Figure 9.3, Section C-C). Underlying Amulet, Rusty Ridge and Northwest formations are, however, offset. Approximately 700m right lateral or 400m vertical ,south side down, displacement is indicated prior to eruption of the Waite Andesite formation. The Cranston

Fault also confines the north extent of Amulet upper member and the Cranston breccia dikes are localized along its south splay.

Two southeast striking faults offset the Rusty Ridge formation (VII R) and Amulet lower member (VIII A1) contact 300m south of the Cranston Fault and do not continue through the lower member or offset its contact with the upper member (Maps 1 and 2). The two faults are interpreted as synvolcanic and to have been active prior to or during extrusion of the Amulet lower member.

The Bancroft Fault is one of the best examples of a synvolcanic fault (Figures 7.1 and 10.2). The #3 flow of the Amulet lower member, is ponded on the north side and terminates against this fault. Beecham breccia, which underlies the #3 flow occurs on both sides of the Bancroft Fault and is offset 550m (apparent left lateral displacement, north side down). South of the fault Beecham Breccia underlies the Bedford rhyolitic flow within the upper member of the Amulet formation. The Bedford flow extends northward, uninterrupted, across the Bancroft Fault (80m apparent offset); north of the fault the Bedford flow is underlain by silicified flows of the upper member. These field relationships indicate the following sequence of events portrayed in Figure 10.2:

a) the Bancroft Fault was operative (or reactivated) following deposition of Beecham breccia (VIII Al) and before extrusion of the Bedford flow (VIII Au).

b) following deposition of Beecham breccia, subsidence of the F-shaft sector relative to the Amulet-Millenbach sector occurred along the Bancroft Fault (approximately 400m vertical movement). The #3 flow was ponded against this fault scarp. Infilling of the subsided block by flows of the Amulet upper member followed and the Bedford flow (extruded from vents in the Amulet-Millenbach sector) crossed the paleo-fault scarp without significant offset.

10.2.4 TRAIL#1, QUESABE AND WATKINS FAULTS

The Quesabe Fault and parallel structures (Watkins and Trail Faults) south of Duprat Lake control the extent and distribution of Rusty Ridge andesitic flows and are interpreted as synvolcanic structures (Figure 7.1). Thick, massive andesitic flows with limited areal extent (low aspect ratio) are ponded within fault blocks now defined by these faults (Figure 9.14). This is further supported by the disappearance of individual flows within adjacent fault blocks whereas underlying and overlying flows are continuous between the fault blocks. The Quesabe and Watkins Faults contain QFP rhyolitic dikes and the former, plus the Trail#1 Fault, merge into a plexus of synvolcanic dikes of the Old Waite Dike Swarm.

10.2.5 VAUZE CREEK FAULT

The location of a large rhyolitic dome (500m thick) within the #1 flow of the Waite Rhyolite formation, and Vauze VMS deposit along this fault, along with ponding of the upper units of the Waite Andesite north of this fault (Figure 9.26) or a parallel structure suggest that the Vauze Creek Fault (Figure 7.1) marks an ancestral synvolcanic structure. Later reactivation (pre diorite intrusion) offsets the Waite and Amulet Andesite formations.

10.2.6 SUBSIDENCE WITHIN THE FLAVRIAN BLOCK

Two main areas of subsidence are recognized within the Flavrian Block. The first is the Despina Sector where strata south of the McDougall and Despina Fault and north of the Beauchastel-Western Quemont Feeder Dike Faults subsided relative to sectors north of the McDougall Fault.

The second is a broad area of subsidence between the McDougall and Hunter Creek Faults. The step-like down- faulting of the Mine Sequence inward from these north-south fault margins is evident Map 1. This faulting is interpreted to be synvolcanic and accommodated along faults described above, and numerous parallel structures.

Synvolcanic subsidence along these faults is best illustrated in Figure 10.1, a north-south cross-section through the Mine Sequence between the Hunter Creek Fault and the Bancroft Fault. Figure 10.1, differs from other stratigraphic sections in that it was constructed assuming that the top contacts of selected formations were horizontal after extrusion. Sections 1 and 2 assume the top of the Rusty Ridge formation to have been horizontal. Section 3 assumes that the top of the Amulet upper member was horizontal after extrusion.

It is apparent in section 1, that to maintain a horizontal or nearly horizontal surface for the Rusty Ridge formation, underlying formations must have undergone considerable down-faulting prior to or during extrusion of the Rusty Ridge formation. Faults that are interpreted to have been active at this time interval include the Cranston, Des, Dacite, Trail, Quesabe and other unnamed faults.

Inspection of section 2, which assumes a horizontal Rusty Ridge paleosurface, suggests that extrusion of rhyolitic flows of the Amulet lower member may not have been accompanied by significant piece-meal subsidence. Minor movement is interpreted along the Cranston and Des/Dacite Faults. This is not the case, however, for extrusion of the Amulet upper member where maintence of a horizontal Rusty Ridge paleosurface requires a steep-sided constructional edifice within the upper member. There is absolutely no evidence for such an edifice in the Amulet upper member and the assumption of a flat underlying topography during upper member extrusion is not tenable.

In section 3, the top of the Amulet formation is assumed to have been horizontal and therefore underlying Amulet lower member and Rusty Ridge formation were down-faulted. Faults interpreted to be active pre or during extrusion of the Amulet upper member include the Cranston, Des, Dacite, Trail and Quesabe.

Figure 10.1, suggests that extrusion of andesitic formations may have been accompanied by piece-meal down faulting, with subsidence occurring along numerous synvolcanic faults. Extrusion of rhyolitic formations, such as the Amulet lower member, appears to have been localized along major bounding faults, such as the Hunter Creek and Bancroft Faults, with the block subsiding as an intact wedge.

10.3 FAULT ORIENTATION

The synvolcanic faults described and other parallel faults are northeast and northwest striking, steeply dipping structures. These two orientations result in an orthogonal fault pattern that has been described as controlling the location of VMS in the Noranda camp (Scott, 1980). On the scale of the Flavrian Block, the faults have a distinct radial pattern evident in Map 1 and Figure 7.1. This radial orientation is best illustrated in Figure 10.3, where the fault traces are shown on the Northwest formation paleosurface (contours removed for clarity). Faults south of Duprat Lake trend northeast-southwest, whereas faults north of Duprat Lake trend northwest-southeast and maintain a perpendicular orientation to the contact of the Flavrian Pluton.

These radially oriented faults controlled the piece-meal down faulting of the Mine Sequence within the Flavrian Block. Radial faults and associated concentric or ring faults have been interpreted to be generated by tumescence of the subsidence area prior to eruption (Anderson, 1936; Smith and Bailey, 1968; Chistiansen etal, 1965; MacDonald; 1972 and Williams and McBirney, 1979). Model studies suggest that radial and concentric fractures form directly above a rising magma body where magma pressure (due to ascent) exceeds lithostatic pressure (Koide and Bhattacharji, 1975). Radially oriented synvolcanic faults within the Flavrian Block are interpreted to have formed above a shallow magma body, now represented by the Flavrian Pluton.

Smith and Bailey (1968) defined ring faults as "fractures or faults that bound or are sympathetic to the displaced mass within the cauldron ..... usually circular arranged but not always". Accordingly, the Hunter Creek, Cranston and perhaps the Vauze Creek Faults in the north and Western Quemont Feeder Dike, Horne and possibly Beauchastel Faults to the south which bound and accommodated subsidence of the central Flavrian Block may be interpreted as ring faults.

Vertical feeder dikes to the Quemont Rhyolite formation which occupy the Western Quemont Feeder Dike Fault and adjacent subparallel dikes may be remnants of ring dikes. The steep northeast dipping McDougall-Despina Fault is also interpreted as a ring dike/fault as it clearly accommodated subsidence of the Despina Block, is occupied by feeder dikes, and has controlled the emplacement of the earliest phases of the Flavrian Pluton, interpreted by Goldie (1976) to have been intruded along ring fractures.

10.4 MAJOR STRUCTURAL FEATURES

The major structural feature of the map area is a large area of synvolcanic subsidence (Flavrian Block) between the Hunter Creek Fault in the north and the Western Quemont Feeder Dike and Horne Faults to the south. This subsidence area was first recognized by de Rosen-Spence (1976) and was referred to as the Noranda Caldera by Dimroth et al., (1982) and Gibson et al., (1984, 1986). The large subsidence structure contains a separate and smaller area of subsidence within the Despina sector. The definition and interpreted origin of this structure and subsidence mechanism are described in Chapter 11.

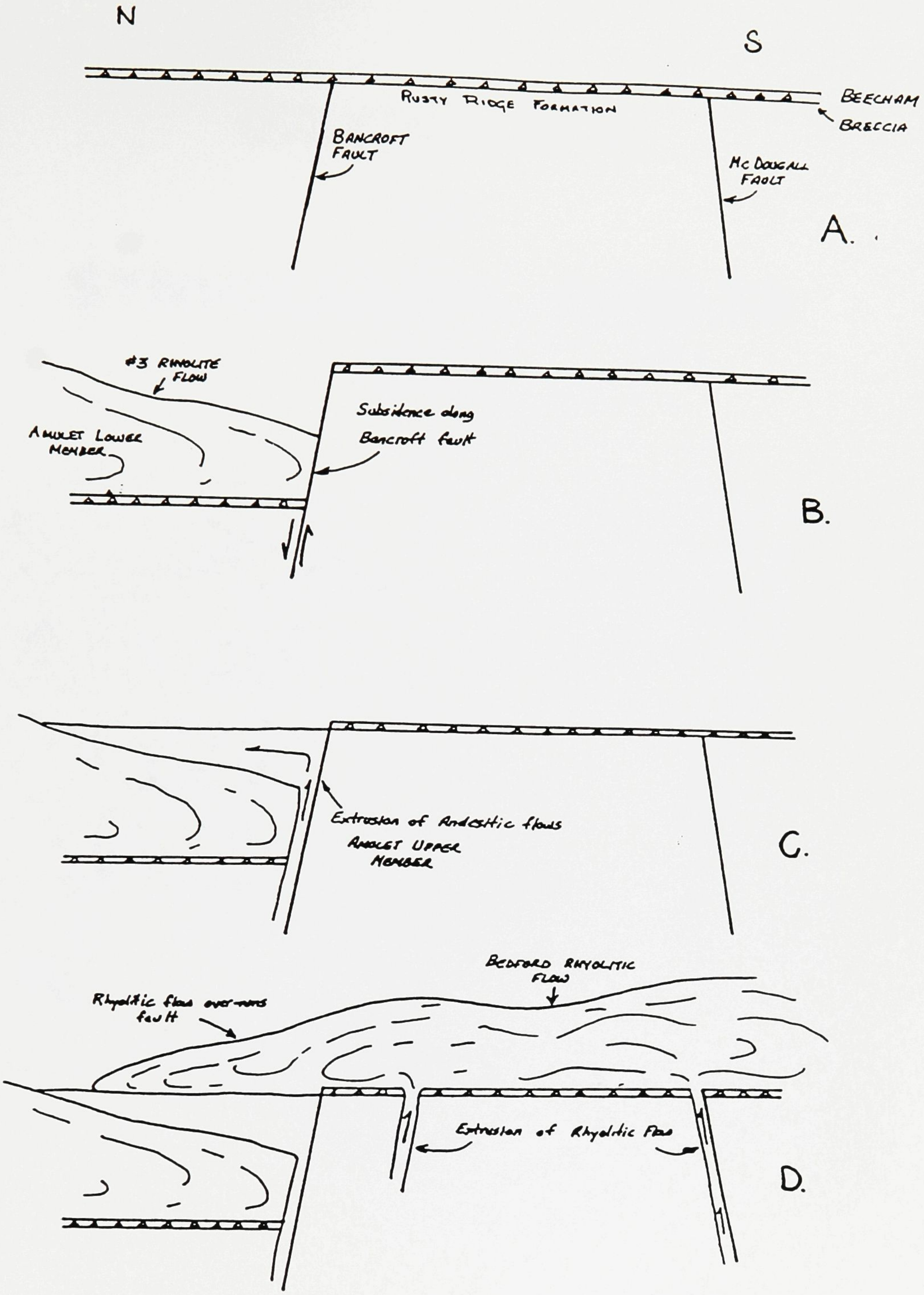

Figure 10.2. Diagrammatic reconstruction of subsidence and volcanism along the Bancroft Fault. A. Volcanic stratigraphy and faulting post emplacement of the Beecham Breccia. B. Subsidence along the Bancroft Fault, probably contemporaneous with rhyolitic volcanism, restricted the southward advance of the #3 flow of the Amulet lower member. C. Eruption of andesitic flows of the Amulet upper member from fissures along and parallel to the Bancroft Fault. D. Eruption of the Bedford Rhyolite flow from vents within the McDougall and Despina faults and immediately south of the Bancroft Fault. The rhyolite flow extends northward, across the Bancroft Fault, and is not offset or restricted by this structure.

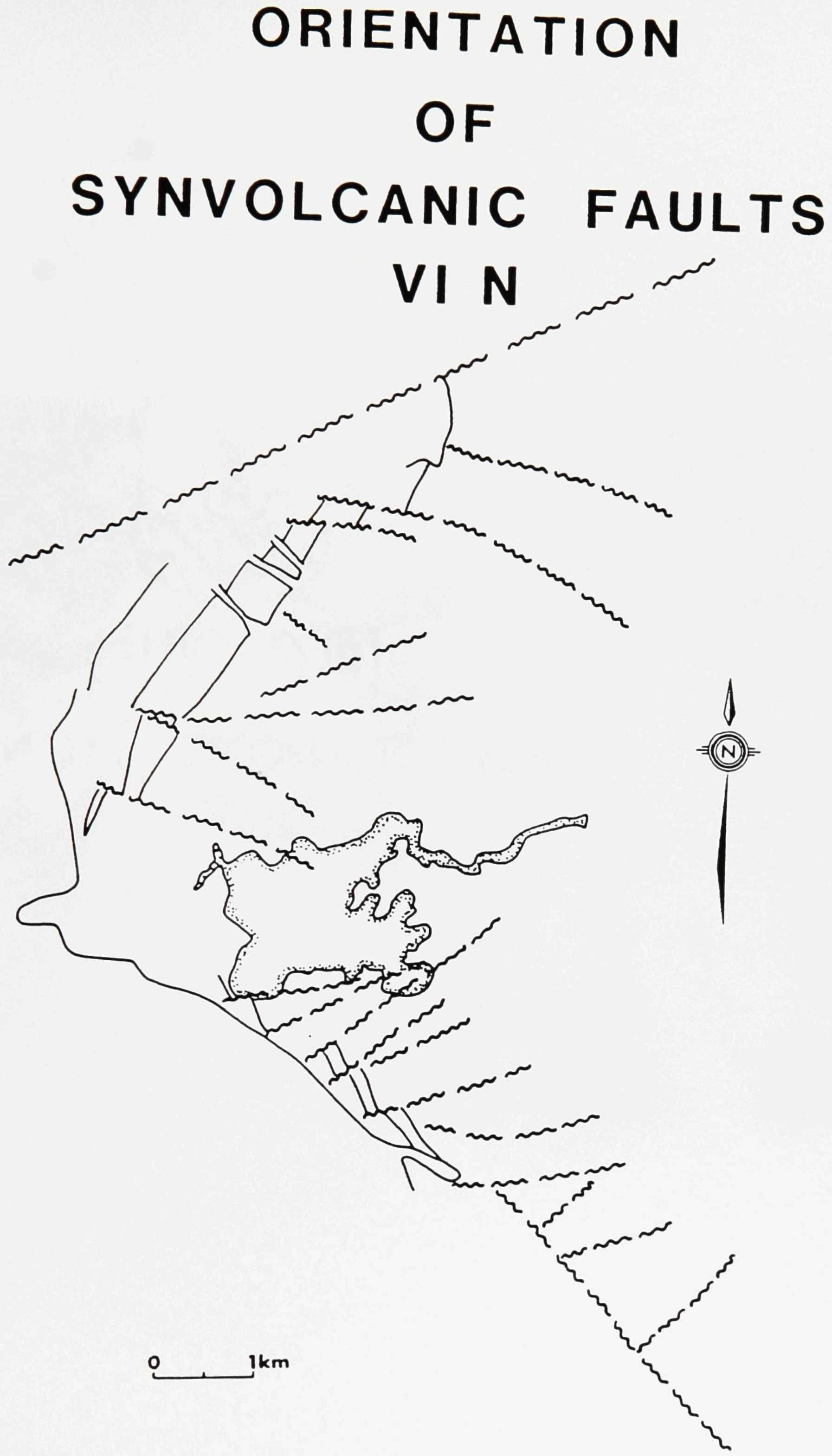

Figure 10.3. Trace of synvolcanic faults on the Northwest formation paleosurface.

Plate 10.1 Pyrite-chalcopyrite-pyrrhotite stringers within the C shaft Fault. The buff-brown colour of adjacent silicified andesite (Amulet upper member) reflects its pervasive chloritization.

Plate 10.2. Sharp contact between a flowbanded rhyolitic dike that occupies the Despina Fault and adjacent andesitic flows.

11.THE NORANDA CAULDRON: VOLCANIC RECONSTRUCTION AND SUBSIDENCE HISTORY

11.1 DEFINITION OF THE NORANDA CAULDRONS

The large area of synvolcanic subsidence between the Hunter Creek and Cranston Faults in the north and Western Quemont Feeder Dike and Horne Creek Faults to the south is interpreted as a cauldron subsidence structure, referred to here as the Noranda Cauldron. Lichtblau and Dimroth (1980), Dimroth et al.,(1982) and Gibson et al., (1984, 1986) referred to this subsidence structure as a caldera. The term cauldron is preferred over caldera as the latter, although a subsidence-produced structure, refers to a "circular" topographic depression. "Cauldron" as defined by Smith and Bailey (1968) "includes all volcanic subsidence structures regardless of shape, size, depth of erosion or connection with surface volcanism", a definition which is applicable to the east-tilted and dissected Noranda structure.

Based on measured fault offset and stratigraphic reconstruction the Noranda Cauldron is interpreted to have subsided a minimum of 0.5 to 1km along the northern margin and 1.2km along the southern margin, producing an asymmetric collapse structure. A reconstructed north to south cross-section through the Noranda Cauldron, following extrusion of the Here Creek Rhyolite formation, is illustrated in Figure 11.1, which displays all vent areas and faults on a single section.

The second, smaller but distinct, area of subsidence in Figure 11.1, is named the Despina Cauldron. The McDougall-Despina ring dike defines the north and part of the east margin of this cauldron. The south margin is not well defined and could lie in an area now represented by the Beauchastel Fault or along the south margin of the larger Noranda Cauldron. The high level of intrusion by the synvolcanic Flavrian Pluton into the Despina Cauldron limits volcanic-subsidence interpretations of this structure to events that post date extrusion of the Amulet formation. A minimum subsidence of 750m occurred during the interval represented by extrusion of the Millenbach and Here Creek Rhyolite formations.

A third, and tentative, smaller area of subsidence, referred to as the Delbridge Cauldron, is inferred for the Delbridge mine area. Approximately 300m of subsidence along the south margin of the Delbridge Cauldron (Deldona Fault) is interpreted to have followed extrusion of the Southbay Andesite formation and effectively ponded the Don Rhyolite formation to areas north of the Donalda Fault. The north margin of the Delbridge Cauldron is obscured by the Dufault Pluton.

Collectively, the Noranda, Despina and Delbridge Cauldrons are referred to as the Noranda Cauldrons. Subsidence of this large structure probably began during eruption of the Flavrian formation (emplacement of the Meritens Phase) and likely ceased along the north margin following extrusion of the Waite Rhyolite formation (Figures 9.2 and 11.1). Major subsidence along the Western Quemont Feeder Dike Fault at the south margin of the Noranda Cauldrons is interpreted to have ended after extrusion of the Amulet/Powell Andesite formations. Minor subsidence of the Despina Cauldron occurred during extrusion of the Here Creek Rhyolite formation. Subsidence along the Horne Creek Fault undoubtedly continued with Cycle 4 volcanism and included limited subsidence along the Donalda Fault (Delbridge Cauldron), on the south margin of the Noranda Cauldron.

11.2 SHAPE AND SIZE OF THE NORANDA CAULDRONS

The Noranda area provides an oblique cross-section through the cauldrons which permits a unique view into the mechanisms and timing of subsidence but severely limits factual data pertaining to their original size and shape. The north and south structural margins are reasonably well defined and indicate a north to south width of 15 km for the Noranda Cauldron and an approximate 5 km width for the Despina Cauldron (Figures 11.2 and 11.3).

The west structural margin of the cauldron is interpreted to have been removed by erosion and is now represented by ring fractures within the Flavrian Pluton (Figures 11.2 and 11.3). The west margin may be a fault or a "hinge zone" where strata further to the east are downfaulted producing a "trap door" subsidence. The Noranda and Despina Cauldrons possibly share the same west margin.

The east structural margin of the cauldron is interpreted to be buried by younger, post-subsidence formations of Cycle 4. If Cycle 5 formations are older then Cycle 4 (Chapter 2) than the eastern limit of the Mine Sequence must underly Cycle 4 and may, therefore, be represented by a wide, poorly defined zone (Figures 11.2 and 11.3) delineated by: a) the northwest-trending, steeply dipping, Dalembert shear zone which contains the Dalembert Pluton. This may be a reactivated fault localized along the cauldron margin, b) the west body of the Dufault Pluton, that was perhaps emplaced along a primary zone of weakness. The Gallen VMS deposit occurs in a "roof pendant" within this pluton and may have originally formed along the east margin, c) massive rhyolitic dikes which occur, adjacent and parallel to the Dalembert shear, along the Dufault Pluton's west contact, and occur as segments around and south of the pluton.

With interpreted structural margins as defined above (Figure 11.2) the Noranda Cauldron has a crudely oval form with approximate north-south and east-west widths of 15 and 20 km. The Despina and Delbridge Cauldrons, nested within the Noranda Cauldron, have estimated diameters of 5km and 2km respectively. The topographic margin of the cauldron cannot be ascertained but would, undoubtedly, lie outside of the proposed structural margins.

11.3 SUBSIDENCE MECHANISM

Radial and ring faults, which accommodated both subsidence and concomitant volcanism, are interpreted to have formed during tumescence of the Noranda Shield Volcano during emplacement of the subvolcanic pluton at a shallow level within the crust (Koide and Bhattacharji, 1975; Anderson, 1936). Subsidence of the cauldrons and internal fault blocks was passive, a result of magma withdrawal, to feed concomitant eruptions within and possible flank eruptions north of the Noranda Cauldron.

The synvolcanic Flavrian Pluton is interpreted as the late magmatic equivalent of a shallow magma chamber which intruded its own volcanic pile (Goldie, 1979; 1976). The sill-like form of individual intrusions within the pluton and a bulge or dome on its upper surface is consistent with a high level intrusion which was accommodated within the crust by downward displacement of underlying strata and doming and brittle fracture of overlying rocks (Goldie, 1976). The pluton directly underlies and marks the west margin of the Noranda Cauldron. The north and south extent of the pluton are limited by the Hunter Creek and Horne Faults which also define the north-south structural margins of the cauldron. Radially oriented faults within the cauldron are perpendicular to the erosional upper surfaces of the Flavrian Pluton and along with concentric ring faults, such as the McDougall and Despina and possibly the Western Quemont Feeder Dike Faults, allowed subsidence of the overlying volcanic pile.

The inferred asymmetric shape and trap door-like subsidence of the Noranda Cauldron, with most displacement localized on the south margin, may reflect original irregularities in the top of the magma chamber with emplacement of cupolas or apophyses of the magma chamber at higher stratigraphic levels in these areas and more intense faulting and brecciation along this margin. The present position of the Flavrian Pluton (Figure 11.1) at a higher stratigraphic level below the Despina Cauldron and south margin of the Noranda Cauldron supports this interpretation.

The progression from an initially large cauldron to the progressively smaller Despina and Delbridge Cauldrons with time, is common to cauldron subsidence structures and is interpreted to indicate continued rise (and emplacement) of the magma chamber during extrusion and subsidence cycles (Steven and Lipman 1976; Lambert, 1974; Hodgson and Lydon, 1977). The location of the Delbridge Cauldron east of the Noranda and Despina Cauldrons may be a product of erosion of the east-tilted structure or an eastward shift in magma emplacement, subsidence and volcanism during the 4th cycle.

11.4 SUBSIDENCE HISTORY AND CHARACTERISTICS

Evolution of the Noranda Cauldrons is divided into eight stages characterized by specific structural, volcanic, sedimentary and intrusive events (modified from Smith and Bailey, 1968) as illustrated in Figure 11.4, summarized in Table 11.1, and described in detail in Appendix E. Figure 11.4 illustrates the variable paleotopography of the cauldron and growth through coalescence of rhyolitic and andesitic eruptive centres that are, in their own right, individual volcanoes. The eight stages are subdivided into two cauldron cycles characterized by an initial period of tumescence (Stages I and IV) followed by contemporaneous cauldron eruptions and collapse. The two cauldron cycles are separated by a cauldron-wide hiatus in volcanic activity (stage III).

Stage VII and VIII may represent a 3rd cauldron cycle during extrusion of the Cycle IV formations. The amount of subsidence during this cauldron cycle is uncertain (possibly 2km) and was localized along the Horne Creek Fault at the south margin of the Noranda Cauldron.

General characteristics of the structural, volcanic, sedimentary and intrusive events which characterize the two main cauldron cycles are summarized below.

11.4.1 STRUCTURAL EVENTS

1. Subsidence of the Noranda Cauldron occurred by step-like downfaulting of the cauldron floor from the margins in toward the centre of the cauldron at Duprat lake. Piece-meal collapse is typical where subsidence is slow, as might be

expected where magma withdrawal from an underlying chamber is a result of lava effusion rather than voluminous pyroclastic eruption. Rapid magma withdrawal, during voluminous pyroclastic eruption, results in subsidence where the cauldron floor subsides as an intact wedge (Steven and Lipman, 1976; Smith and Bailey, 1968).

2. The centre of the Noranda Cauldron coincides with the Old Waite Dike Swarm, the principal eruptive centre for andesitic formations. As there is no evidence for the Old Waite Dike Swarm in pre- and post- cauldron formations it is interpreted as an apical or central graben produced during initial distension of volcanic strata during regional tumescence that preceded volcanism and subsidence. Its location may be controlled by an older rift on which the cauldron was later located; such rift and dike swarm zones are associated with other cauldrons such as in Hawaii (MacDonald, 1972), central Iceland (Bodvorsson and Walker, 1964), and in eroded Tertiary calderas such as Mull and Ardnamurchan (Ritchey, 1961). Once formed, this graben was the focus of andesitic eruptions and cauldron collapse.

3. The floor of the Despina Cauldron appears to have subsided as a single, intact block; there is no evidence of step-like downfaulting of the cauldron floor.

4. Two main periods of subsidence are recognized. The first period commenced with tumescence, generation of ring and radial faults and apical graben, followed by subsidence during extrusion of formations V to VIII. The

second period commenced with tumescence, and reactivation of faults, followed by subsidence during extrusion of formations IX to XI. Subsidence of the Despina Cauldron occurred during the second period of subsidence.

11.4.2 VOLCANIC EVENTS

1. Volcanism and subsidence were contemporaneous, and a topographically positive edifice was not constructed.

2. Topographic relief produced during eruption of rhyolitic flows was subdued and buried by andesitic flows.

3. Both andesitic and rhyolitic flows issued from fissures.

4. Effusive rhyolitic and andesitic fissure eruptions dominated "Hawaiian Type" volcanic activity. Pyroclastic eruptions were few, aerially restricted, and their products constitute <5% of the Mine Sequence.

5. Andesitic vent areas are typically located within the cauldron, whereas rhyolitic vents are located adjacent to major bounding faults at the cauldron margins and to a lesser extent within the cauldron.

11.4.3 SEDIMENTARY EVENTS

1. The two periods of volcanism and subsidence within the Mine Sequence are separated by a brief hiatus in volcanic activity. During this interval the C Contact tuff was deposited and covered the cauldron floor. Similar tuff units occur stratigraphically above and below the C contact but they are of limited areal extent and represent "brief" and localized breaks in volcanic activity within the

cauldron.

2. The Mine Sequence is totally devoid of epiclastic sediments indicating subaqueous extrusion below storm wave base, and distance from an elevated subaerial landmass.

3. Epiclastic debris derived by erosion or avalanches from fault scarps, typical of many subaerial calderas (Stevens and Lipman 1976, Lambert, 1974) are distinctly lacking. This may reflect the small volumes of such deposits and/or the passive and contemporaneous volcanic/subsidence history of the Noranda Cauldron.

4. Submarine hot spring activity occurred throughout the Mine Sequence but was most extensive during deposition of the C Contact tuff and during the initial stages of the second period of volcanism and subsidence.

11.4.4 INTRUSIVE EVENTS

1. Regional tumescence and generation or reactivation of ring and radial faults that preceded each volcanic/subsidence cycle are interpreted to result from the emplacement of high level intrusions of the Flavrian Pluton within its volcanic edifice.

2. Goldie (1976) interpreted the final emplacement of the Flavrian Pluton to have occurred during eruption of the Amulet Andesite (XI) or Here Creek Rhyolite (XIV) formations. Final crystallization of the pluton may have occurred during Cycle 4 and 5 volcanism. Emplacement of the Dufault Pluton (east body) and Dalembert Pluton may have coincided with final emplacement of the Flavrian

Pluton.

3. Contemporaneous ascent and eruption of andesitic and rhyolitic lavas (bimodal volcanism), implies two different sources of magma and/or a strongly zoned magma chamber.

4. The volumetric increase of porphyritic rhyolite relative to aphyric rhyolite as extrusion of the Mine Sequence continued, and the preponderance of porphyritic rhyolite in post-cauldron formations of Cycle 4 is consistent with successive tapping of a zoned magma chamber (Hildreth, 1981).

11.5 WATER DEPTH

The water depth during extrusion of the Mine Sequence can only be qualitatively estimated. De Rosen-Spence (1976) estimated a maximum water depth of 2000m, whereas Watkins (1980) estimated water depths of 160m and 100m during extrusion of the Flavrian and Millenbach Rhyolite formations.

Phreatomagmatic and Strombolian eruptions and highly vesiculated andesitic flows (+20% amygdules) during the waning stages of Flavrian volcanic activity suggest an initial water depth of <300m. This depth is in agreement with observations of Moore and Fiske (1969), Moore (1965), Moore and Schilling (1973), Jones (1970) and Allen (1980) who suggest that pyroclastic eruptions in tholeiitic basalt are limited by a maximum water depth of 100-200m.

Water depth during extrusion of the Mine Sequence and subsidence of the Noranda Cauldron, may have ranged from <100m to 1000m. The total absence of epiclastic debris indicates a minimum water depth greater than storm wave base. The insignificant volume of rhyolitic pyroclastic rocks versus flows within the Mine Sequence has traditionally been interpreted to indicate deep water, >1000m, eruptions. This, however, is not necessarily the case as subglacial rhyolitic flows in Iceland were extruded passively without significant or any pyroclastic activity in < 200m of melt water (Furnes et al., 1980). Andesitic pillow lavas have similar amygdule content and size to subglacial basalt flows in Iceland which erupted in water depths of <400m (Jones, 1970). Ash flow tuffs hosting VMS deposits at Aldermac, on the west margin of the cauldron, are correlated with rhyolitic flows of the Waite/Millenbach and Quemont rhyolites within the cauldron. The ash flows suggest relatively shallow eruptions (<200m) along the cauldron margin whereas contemporaneous rhyolitic flows, within the cauldron, may have been emplaced in deeper water (<400m).

The shoaling sequence recognized in the uppermost flows of the Amulet and Powell Andesite formations indicate that the formation was emplaced in increasingly shallow water (Cousineau and Dimroth, 1982), during final infilling of the cauldron. A water depth of <100m for tuffs in the Powell Andesite and Quemont Rhyolite formations was proposed by Lichtblau and Dimroth (1980).

Assuming an initial water depth of 300m and a final water depth of <100m, extrusion of the 3.0 km thick Mine Sequence implies that approximately 2.8 km of subsidence occurred. The amount of subsidence calculated in this manner is greater than the 1.2 km proposed based on stratigraphic reconstruction and measured fault offsets, but does not include subsidence along the Horne Creek Fault which may have been substantial. The additional 2.2 km of subsidence not accounted for in the reconstruction may be a product of this subsidence and/or widespread subsidence of the volcanic edifice. Cycle 4 formations (3 km thick) were also erupted subaqueously which required continued subsidence along the cauldron south margin that is not recognized in the reconstruction.

Widespread general subsidence of the Noranda shield volcano may be analogous to that occurring in active Hawaiian volcanoes where downwarping of the crust occurs in response to isostatic re-equilibration under the load of the overlying edifice and magma chamber (Moore, 1970). For Hawaii, the annual volume of subsidence exceeds, by 5 times, the average annual volume of basalt erupted (Moore, 1970).

11.6 CAULDRON CLASSIFICATION

Williams and McBirney (1979) classified calderas into seven principal types. The Noranda Cauldrons do not fit neatly into any one type, but share features common to several types. The Noranda Cauldron is similar to Hawaiian and Galapagos types as cauldron development and subsidence is interpreted to have occurred during the late-stage growth of a large shield volcano. Collapse accompanied lava eruptions along ring fractures at the cauldron margins (Galapagos) and through fissure eruptions within and possibly outside the caldera (Hawaiian). They differ in that Hawaiian and Galapagos calderas are associated with eruptions of basalt whereas Noranda Cauldron subsidence is characterized by contemporaneous bimodal volcanism. Piece-meal collapse of the Noranda Cauldron is typical of Hawaiian and also Krakatoan calderas.

The disposition of the Mine Sequence about an intrusive body, the Flavrian Pluton, is remarkably similar to dissected cauldron subsidence structures in Scotland and Norway (Smith and Bailey, 1968). The Alnsjo Cauldron in the Oslo region of Norway is remarkably similar to the Noranda Cauldron; Figure 11.5, allows a comparison of the two cauldrons. The shape of the intrusions in both are similar as is the disposition of volcanic units. Smith and Bailey (1968) interpreted cauldron subsidence structures in Scotland and Norway to be the subvolcanic analog of resurgent cauldrons. The Noranda Cauldron, although having similar evolutionary stages, differs from resurgent cauldrons: a) resurgent cauldrons are associated with rapid, catastrophic, and voluminous ash flow eruptions, not quiet, effusive fissure eruptions. Both, however, are characterized by bimodal volcanism, b) the Noranda Cauldron lacks a resurgent structural dome, but this may be only a recognition problem at Noranda, c) resurgent cauldrons are not known to form during the late-stage growth of shield volcanoes, d) the cauldron floor subsides as an intact wedge in resurgent cauldrons not by piece-meal collapse which typifies the subaqueous Noranda Cauldron.

Although the Noranda Cauldron shares characteristics of various subaerial cauldron types, its location within a shield-like volcanic edifice is most reminiscent of Hawaiian shield volcanos, and particularly, to Tertiary and Quaternary Central Volcanic Complexes in Iceland (Walker, 1963). Features shared by both the Noranda Volcanic Complex and Icelandic Central Volcanic Complexes include: a) development of a broad, primarily basaltic shield-like edifice (Blake River Group) with a central core (Noranda Area) characterized by a bimodal succession of basalt/andesite and rhyolite, b) caldera development and subsidence within this central core area, c) restriction of high-temperature hydrothermal systems to the core area and particularly to a central caldera or cauldron (Walker, 1963).

Although the Noranda Volcanic complex is thought to be most reminiscent of Icelandic Central Volcanic Complexes this is not meant to imply that the Noranda Volcanic Complex is interpreted to have formed in a mid-oceanic ridge environment. Many structural, stratigraphic and geochronological problems must be addressed before the paleo-tectonic environment of the Noranda Volcanic Complex can be interpreted.

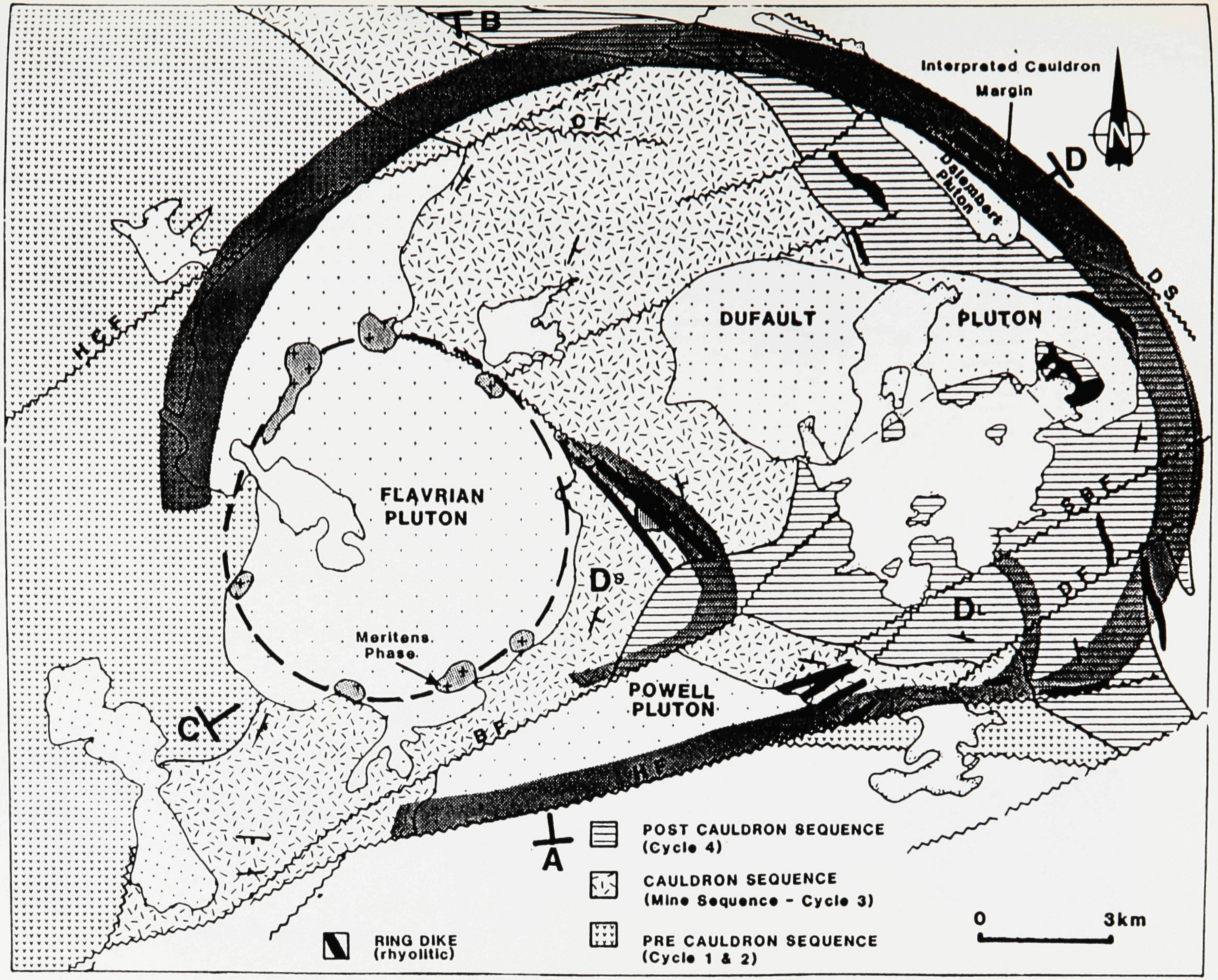

Figure 11.2. Inferred structural margins of the Noranda Cauldron and smaller Despina (Ds) and Delbridge (Db) cauldrons (HCF-hunter Creek Fault, CF-Cranston Fault, BF-Beauchastel Fault, HF- Horne Fault, SBF-South Bay Fault, DF-Deldona Fault and DS-Dalembert Shear)

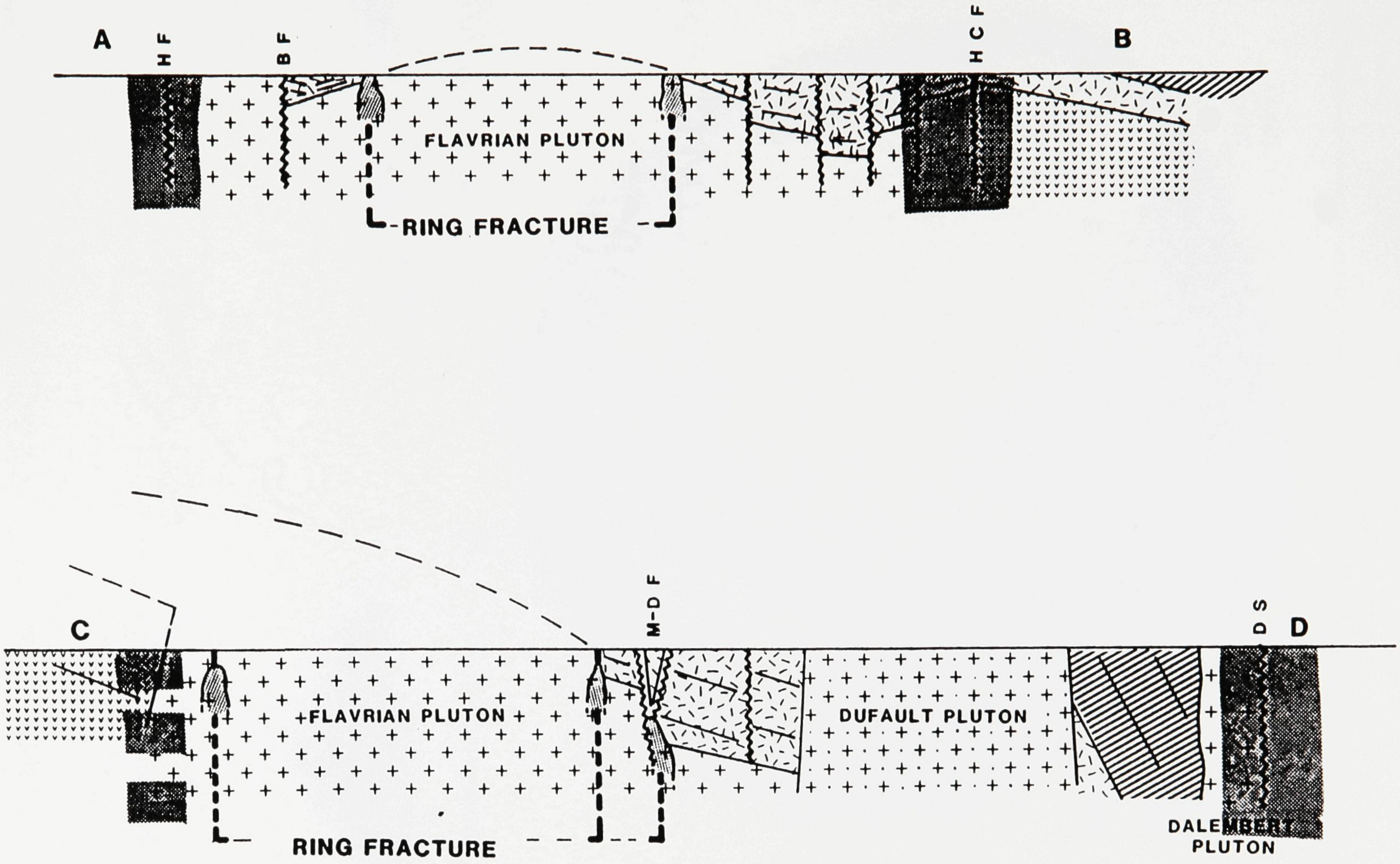

Figure 11.3. North-south and east-west cross-sections through the Noranda Cauldron (fault abbreviations as in Figure 11.2; M-DF-McDougall-Despina Fault).

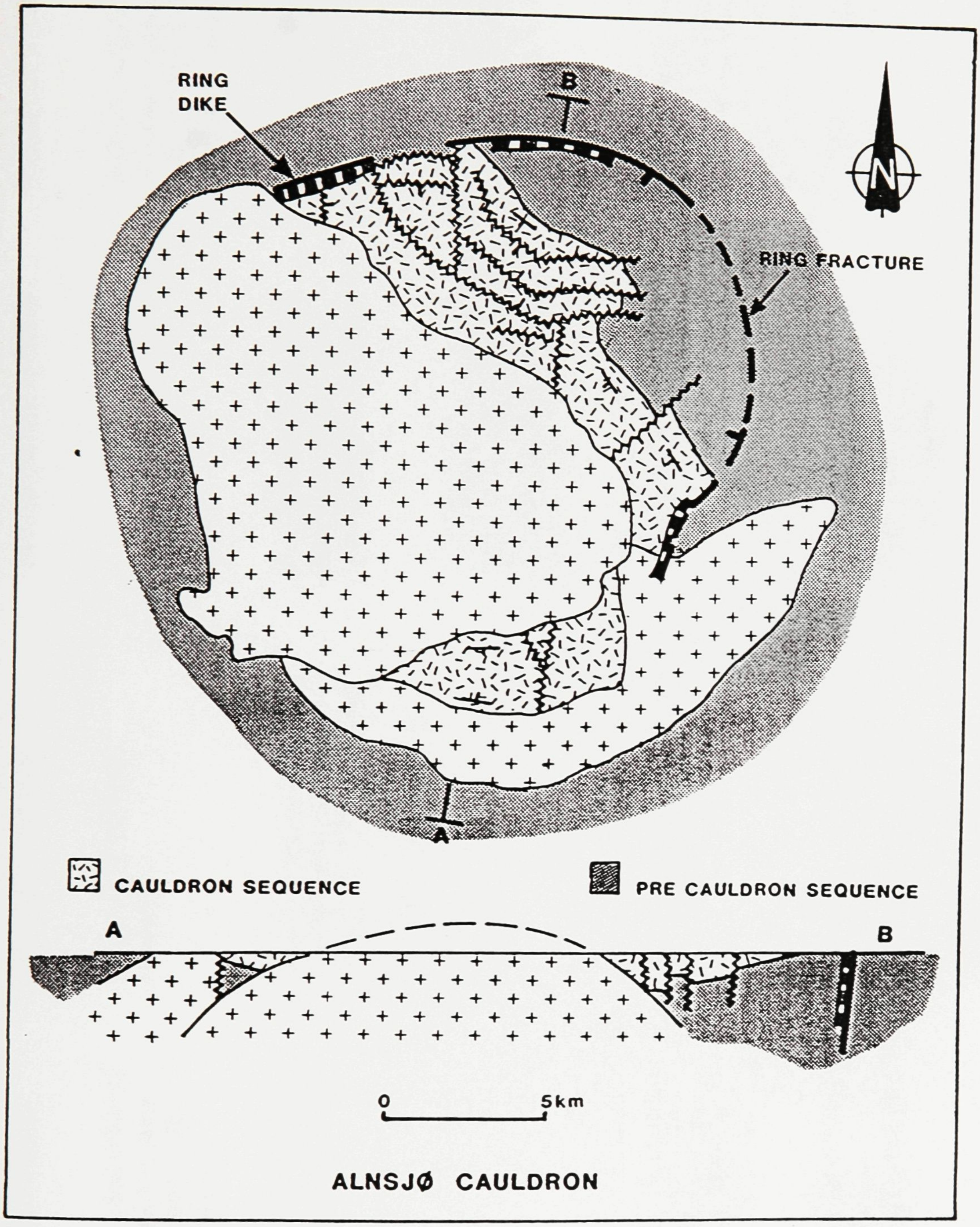

Figure 11.5. The Tertiary Alnsjo Caulldron, Norway (from Smith and Baily. 1968).

TABLE 11.1. EVOLUTION OF THE NORANDA CAULDRONS

STAGE:	STRUCTURAL EVENTS:	VOLCANIC EVENTS:	SEDIMENTARY EVENTS:	PLUTONIC EVENTS:
Cycle 1				
1	Tumescence, generation of ring and radial fractures and apical graben - Old Waite Dike Swarm	Eruption of Flavrian formation		Shallow emplacement of earliest phases of Flavrian pluton along ring faults - Meritens phase
2	Cauldron subsidence along radial/ring faults (Noranda Cauldron)	Contemporaneous rhyolitic and andesitic volcanism, eruption of formations VF to VIII A (Overlap with Stage 1)	Tuff deposited, localized hotspring activity and generation of VMS deposits	Magma withdrawal from shallow chamber
3	Quiet	Quiet	Tuff deposited on cauldron floor, widespread hotspring activity and generation of Zn-rich VMS deposits	Static period following magma withdrawal and before magma resurgence
Cycle 2				
4	Tumescence, reactivation of ring and radial faults (Overlap with Stage 3)	Eruption of Waite/Millenbach andesitic formations	Overlap with Stage 3	Magma resurgence, with continued rise of magma in crust as high level intrusions along ring faults
5	Cauldron subsidence along ring/radial faults (Noranda/Despina cauldrons)	Contemporaneous rhyolitic and andesitic volcanism, eruption of formations IX-XI and infilling of cauldron (Overlap with Stage 4)	Minor tuff deposits, localized hotspring activity and generation of VMS deposits	Withdrawal of magma from shallow chamber
6	Quiet	Quiet	Minor tuff deposited, brief hiatus following infilling of cauldron	Static period

TABLE 11.1. EVOLUTION OF THE NORANDA CAULDRONS (Con't)

STAGE:	STRUCTURAL EVENTS:	VOLCANIC EVENTS:	SEDIMENTARY EVENTS:	PLUTONIC EVENTS:
Cycle 3				
7	Tumescence, reactivation of ring and radial faults	Eruption of Newbec andesitic and Insco/Here Creek rhyolitic formations of Cycle 4	Minor tuff deposited	Magma resurgence with final emplacement of high level intrusions
8	Minor, localized subsidence along south margin of cauldron (Delbridge cauldron)	Contemporaneous rhyolitic and andesitic volcanism, final eruption of Cycle 4 volcanic units (Overlap with Stage 7)	Minor tuff deposited, localized hotspring activity and generation of VMS deposits	Magma withdrawal balanced by replenishment as final intrusions of Flavrian pluton emplaced

12. ALTERATION

Alteration types within the Mine Sequence are divisible into two types, semiconformable and discordant. Semiconformable alteration includes diagenesis, spilitization, epidote-quartz alteration and silicification. Discordant alteration includes chloritization and sericitization associated with VMS deposits and stringer sulphides within faults. Previous studies (de Rosen-Spence, 1969; Hall, 1980; Atkinson and Watkinson, 1980; Riverin and Hodgson, 1980; Watkins, 1980 and Gibson et al., 1983) have concentrated on describing the chemistry, mineralogy and origin of individual alteration types but have not addressed their spatial, temporal and evolutionary relationship within the Mine Sequence. The emphasis of this study was to map alteration types (Maps 1 and 2), in order to define their spatial distribution, temporal relationships and possible relationship to attendant VMS deposits and discuss their evolution within the framework of processes active in modern hydrothermal systems. The distribution, field characteristics, mineralogy and chemistry of both semiconformable and discordant alteration types are described, but first petrographic evidence of an initial diagenetic alteration is examined.

12.1 DIAGENETIC ALTERATION

Intuitively and by analogy with studies of recent subaqueous volcanic rocks, rhyolitic and andesitic flows of the Mine Sequence must have undergone an initial stage of low temperature (<200^{0}C) alteration or diagenesis (Fisher and Schmincke, 1984). Textures and structures outlined by fine-grained oxides and pseudomorphed by secondary chalcedony, chlorite, epidote and minor carbonate suggest the former presence of palagonite, clay minerals, zeolites and Fe-Ti oxides attributed to this early alteration. Minerals, textures and chemical changes that characterize sea floor weathering are described by Staudigel and Hart (1982), Bohlke (1980), Dimroth and Lichtblau (1979), Baragar et al., (1977), Andrews (1977), Scarfe and Scott (1977), Scott and Hajash (1976), Hekinian and Hoffet (1975), Hay and Ijima (1968), Moore (1966) and Nayudu (1964). These studies provide a framework that facilitated interpretation of relict textures within andesitic and rhyolitic hyaloclastites and microcrystalline flows.

12.1.1 PALAGONITIZATION OF ANDESITIC AND RHYOLITIC VITROPHYRE AND HYALOCLASTITE

Andesitic and rhyolitic vitrophyre and hyaloclastite have relict textures of former palagonite, authigenic clay minerals and zeolites. Palagonitization is a process of hydration and devitrification (Hay and Ijima, 1968) where glass is transformed to a yellow-brown resinous substance, palagonite. Palagonite initially forms on any free surface such as the margin of shards, internal cracks and vesicle walls and progresses inward; it may completely replace entire shards or leave "islands" of glass (Plate 12.1A). Peacock (1926) identified two textural varieties of palagonite; gel-palagonite is massive or banded and is adjacent to unaltered sideromelane, whereas fibro-palagonite has a fibrous, radiating texture and forms adjacent to gel-palagonite.

Oxidation which accompanies palagonitization leaves fine opaque minerals (Fe-Ti oxides) as thin bands separating palagonite from glass and within palagonite as diffuse fine opaques, oxide spherules or granules and oxide-rich liesegang rings or crusts on free surfaces (Plate 12.3A). Relict textures of former palagonite are described below.

Andesitic vitrophyre is typically composed of massive homogeneous chlorite, but, perlitic cracks filled by fine opaque minerals and quartz (Plate 12.1G), attest to its original glassy nature. A thin band of fibrous, optically oriented chlorite aligned normal to the cracks is interpreted to have replaced former fibro-palagonite. Relict palagonite rims of chloritized sideromelane shards in Plate 12.3A , are defined by successive concentric oxide-rich bands of different colour intensity and black oxide-rich crusts.

The chloritized obsidian shard in Plate 12.1B and C, displays the relict texture of former palagonite. Concentric banding at the margin as defined by thin, parallel oxide-rich bands is derived from former fibro-palagonite whereas botryoidal oxide-rich liesegang rings may have formed by rhythmic precipitation of oxides in former gel-palagonite. Banding of massive chlorite adjacent and parallel to perlitic cracks within chloritized andesitic vitrophyre of Plate 12.1H may pseudomorph concentric banding of former palagonite. Fibrous chloritic "granules" in chloritized andesitic shards of Plates 12.1E amd F may replace former zeolites; for comparison similar appearing "fibrous granules" in strongly palagonitized shards are shown in Plate 12.1D.

12.1.2 ANDESITIC AND RHYOLITIC FLOWS

Massive rhyolitic and andesitic flows are relatively impermeable in comparison to vitrophyric and hyaloclastite flow breccia and consequently do not display effects of diagenetic alteration to the same degree or intensity .
Relict palagonitization textures occur in perlitic textured flow and pillow margins but have not been recognized in hyalopilitic and intersertal textured andesitic flows. Patches of massive chlorite (Plate 5.1D and E), within the flow groundmass are interpreted, by analogy with associated hyaloclastite, to be chloritized sideromelane mesostasis. Fine granular and fibrous epidote, sphene, quartz and opaques within chloritized sideromelane may have replaced former zeolites or authigenic clay minerals.

Devitrification textures are abundant in rhyolitic flows. The occurrence of fine oxides along perlitic cracks, oxide crusts, and fibrous chalcedony, presumably replacing former clay minerals and perlite, are interpreted as former diagenetic alteration.

12.1.3 PORE SPACE CEMENT AND AMYGDULES

Minerals which cement hyaloclastite breccias and infill amygdules include chalcedony, chlorite, epidote and opaques. The fibrous and parallel orientation of these minerals suggest that they pseudomorph original fibrous or platy precursors such as clay minerals, zeolites and amorphous silica. Form and optically oriented fibrous chalcedony, which is interpreted to replace the palagonite margins of chloritized sideromelane shards in Plate 12.3 C and D, is identical to chalcedony within the matrix. Matrix chalcedony is interpreted to pseudomorph original amorphous silica and is not riddled with fine oxides as is chalcedony that replaced the margins of adjacent chloritized sideromelane shards. Commonly a fine oxide crust separates the silicified, chalcedonic rim from matrix chalcedony, although the two appear continuous. Matrix chalcedony crystals are fewer, but larger away from shard boundaries. Irregular clots of massive or fibrous chlorite and fibrous epidote, presumably after clay or zeolitic precursors, is the final cement.

The hyaloclastite matrix cement (Plates 12.4A to D) may indicate successive precipitation of opaline silica, clays and zeolites now represented by successive encrustations of chalcedony, chlorite and clusters of fibroradial epidote. The filling sequence of amygdules within shards, is identical to the cement sequence within the breccia matrix. The amygdules have an inner margin of chalcedony, that is often continuous with chalcedony replacing the andesitic groundmass, followed by chlorite and epidote.

Within flows, amygdules often display a distinct mineralogical zonation that is interpreted as successive growths or encrustations. Oxide crusts, precipitated on free surfaces during infilling of amygdules, separate successive encrustations between and within monomineralic zones. The amygdule in Plate 12.3B, illustrates successive encrustations of chalcedony, presumably after opaline silica, and opaque minerals. Up to 8 encrustations of opaline silica, clay minerals and oxides now represented by chalcedony, chlorite, epidote and opaques have been recognized in a single amygdule. Similarly, the radiating clusters of fibrous chlorite and epidote in Plates 12.3E and F, are interpreted to replace former zeolites that initially infilled the amygdule.

In summary, chalcedony and fibrous and radiating clusters of chlorite and epidote which occur in monomineralic zones within the matrix cement of breccias and amygdules are interpreted to pseudomorph former opaline silica, authigenic clay minerals and zeolites produced during diagenetic alteration. The fibrous, oriented texture of monomineralic zones and their botryoidal or laminar structures indicates that the primary minerals grew by centripetal growth from the pore wall inward. The continuity between matrix chalcedony and that interpreted to replace palagonite along fragment margins suggests that silicification was accompanied by silica cementation.

12.1.4 CHEMICAL CHANGES

Replacement of original alteration minerals by later hydrothermal assemblages does not allow direct assessment of chemical changes that occurred during diagenetic alteration. Alteration studies of sea floor basalts and recent volcanic rocks can, however, provide an insight into possible chemical changes that occur during sea floor weathering.

Hay and Iijima (1978), Scott and Hjash (1976), Baragar et al., (1977), Scarfe and Smith (1977), Andrews (1977) and Furnes (1978) indicate that palagonitization of basaltic glass is accompanied by significant chemical changes. Assuming constant volume metasomatism, palagonitization is characterized by a net gain in H_2O, Fe and possibly K, Ti and Si and a net loss in Si, Al, Mg, Ca and Na (Table 12.1). Components lost during palagonitization may not have been removed from the system but accommodated within authigenic clay minerals, zeolites, calcite and opal precipitated in open pore-space of breccias and within vesicles (Hay and Iijima, 1968).

Chemical changes that accompany diagenetic alteration of more crystalline rhyolitic and andesitic flows (loss of Ca,S, Mg, Na, and Fe) are not as great, perhaps due to their lower initial permeability and smaller volume of unstable glass (Scott and Hajash, 1976; Baragar et al., 1977 and Andrews, 1977).

12.1.5 SUMMARY

Andesitic and rhyolitic hyaloclastites and to a lesser extent flows and dikes underwent an initial stage of low temperature (<200^{0}C) diagenetic alteration characterized by the development of palagonite, clays and zeolites. The physical and chemical effects of this early diagenetic alteration include a) a reduction in porosity due to precipitation of authigenic minerals and compaction, b) a net gain in H_2O and Fe in glassy rocks and loss of Si, Al, Mg, Ca and Na, and c) oxidation with development of oxide-rich crusts on free surfaces.

Diagenetic alteration described for the Mine Sequence may be analogous to "zeolite facies" alteration which typifies the upper part of high-temperature hydrothermal systems in Iceland (Tomasson and Kristmannsdottir, 1972; Kristmannsdottir, 1975). The inferred primary filling sequence of quartz-clay minerals-zeolites, within amygdules and breccia cements, may have formed in response to increasing temperature, during progressive burial, as proposed for

Tertiary basaltic lavas in Iceland (Walker, 1960A and 1960B).

12.2 SEMICOMFORMABLE ALTERATION

12.2.1 SPILITIC ALTERATION

Distribution and Field Characteristics

Spilitic alteration is characteristic of all formations within the Mine Sequence. The alteration does not result in characteristic textures or morphology but is a pervasive, widespread alteration that appears to uniformly affect all rock types.

Mineralogy and Textures

Spilitic alteration is characterized by the assemblage chlorite-albite-epidote-quartz in andesite and sericite (chlorite)-albite-epidote-quartz in rhyolite. Albite occurs as pseudomorphs after euhedral plagioclase microlites and phenocrysts. Chlorite, sericite and quartz occur within the groundmass of flows where they, along with interstitial, granular epidote, replace an original sideromelane or obsidian mesostasis. As described previously, the spilitic assemblage pseudomorphs original palagonite, clays and zeolites within the groundmass of flows, amygdules and pore-space cements.

Chemistry of Spilitized Flows

Least altered andesite and rhyolite of the Mine Sequence commonly have low Ca and high Na contents relative to typical compositions for unaltered equivalents (Le Maitre, 1976). The spilitic affinity of rhyolitic, andesitic and silicified flows and subvolcanic intrusions is also indicated in an alkali ratio diagram (Figures 12.1 to 4) that distinguishes spilites and keratophyres from "normal" igneous rocks. The occurrence of normative corundum (CIPW) within these spilitized subalkaline volcanics indicates a pseudo-peraluminous composition due to Ca depletion (Gelinas et al., 1977).

Discussion

The spilitic mineral assemblages ubiquitous to Mine Sequence rhyolitic and andesitic flows are also typical of low grade regional metamorphism (Winkler, 1974) and to "greenschist facies" hydrothermal metamorphism in high-temperature hydrothermal systems in Iceland (Kristmannsdottir, 1975; Viereck et al., 1982; Mehegan et al., 1982)

The remarkable textural preservation of the flows and lack of a recognizable metamorphic fabric are not typical of most Archean, regionally metamorphosed volcanic rocks. This, coupled with their occurrence as pseudomorphs after diagenetic alteration phases and the typical spilitic chemistry (Valence, 1974) suggests that the chlorite-sericite-albite-epidote-quartz assemblage may be a product of hydrothermal metamorphism, but does not preclude an origin through regional metamorphism of an earlier alteration assemblage.

Similar, spilitic alteration assemblage described from ophiolites (Spooner and Fyfe, 1973; Spooner, 1977; Heaton and Sheppard, 1977; Lydon and Jamieson, 1984), the Stekenjokk volcanics of the central Sweedish Caledonides (Rickard and Zweifel, 1975; Stephens, 1982; Zachrisson, 1982; Vivallo and Wilden, 1968) and from Mattagami, Quebec (MacGeehan, 1978) are also attributed to an early hydrothermal metamorphism.

12.2.2 EPIDOTE-QUARTZ ALTERATION

Distribution and Field Characteristics

Epidote-quartz alteration occurs in all andesitic formations of the Mine Sequence, including silicified andesitic flows of the Amulet and Waite upper members, but is noticeably absent in rhyolitic flows and or pyroclastic rocks. Characteristics of epidote-quartz alteration, as typified by altered andesitic flows of the Waite upper member (Figures 12.5 and 12.6), differ and are unique from quartz and epidote produced during regional, isochemical, greenschist facies metamorphism in that:

a) epidote-quartz alteration occurs as grey to grey-green, distinct, resistant, round to irregular amoeboid spots or patches (Plates 12.5 to 12.8) from <1cm to

2m in size. The alteration patches display both sharp and diffuse contact with adjacent andesite. Epidote-quartz alteration patches are morphologically identical to hydrothermal epidote patches observed in drill core from the Salton Sea geothermal field. In the Salton Sea geothermal system hydrothermal epidote forms where temperatures exceed 300°C (Keith et al., 1968, McKibben et al., 1987)

b) like silicification (Gibson et al., 1983), the distribution of epidote-quartz alteration is controlled by the original permeability of the flow as indicated by an increase in alteration toward flow contacts (Figures 12.5 and 12.6), and development around amygdules (Plate 12.6). In pillows, the alteration occurs both within the core and margin (Figure 12.6) and also within interpillow hyaloclastite. Unlike silicification, epidote-quartz alteration patches commonly occur in massive, non amygdaliodal andesite and cross fragment boundaries within andesitic breccias (Plates 12.5 and 12.7).

Although epidote-quartz alteration occurs throughout andesitic formations there is a marked increase in the density of alteration spots adjacent to VMS deposits, synvolcanic intrusions and faults. For example, andesitic flows adjacent to the Corbet (Watkins, 1980) and Upper A VMS deposits are more pervasively epidote-quartz altered than the same flows away from the deposits (Figure 12.12). Similarly, at Ansil, where the mineralized and chloritized alteration pipe extends 300m above the deposit, andesite adjacent to the pipe is strongly epidote-quartz altered; however, the North rhyolitic flow of the Northwest formation, is not.

Andesitic flows within and adjacent to the Old Waite Dike Swarm and the Watkins, Quesabe and McDougall Faults are also characterized by more pervasive epidote-quartz alteration (Maps 1 and 2).

Thus, like silicification, epidote-quartz alteration is a semi-conformable stratabound alteration that is, however, somewhat better developed within areas inferred to have had anomalously high permeability and heat flow. Unlike silicification it does not occur as large (50 x 50m) areas of pervasive epidote-quartz alteration, nor is it confined to specific members within andesitic formations and is rarely developed in rhyolitic flows.

Mineralogy and Textures

Unlike silicification, in which albite microlites, phenocrysts and original textures are preserved, epidote-quartz alteration is destructive and primary features are largely obliterated. Epidote-quartz alteration is characterized by the assemblage epidote and quartz in ratios of 0.5 :1 to 2:1 with minor accessory opaque minerals, calcite, actinolite and chlorite.

The alteration patches are characterized by a granular texture with fine (<0.1mm) prismatic epidote and irregular, granular quartz (Plate 12.2H). The alteration is commonly pervasive and feldspar phenocrysts and microlites are not recognizable but, where the alteration is less intense, epidote pseudomorphs after feldspar phenocrysts are common. Amygdules are filled by massive granular and fibrous prismatic epidote and, less commonly, by chalcedony, epidote and chlorite as sequential encrustations (Plate 12.2H). Laminar and concentric joints are recognizable as quartz-filled parallel fractures in some epidote-quartz patches.

Epidote-quartz patches have diffuse contacts with adjacent andesite where the amount of epidote and quartz gradually decrease and microlitic texture gradually becomes recognizable. This transition occurs over intervals of 2mm to 10cm.

In silicified andesite, epidote-quartz alteration is more restricted and typically occurs as envelopes or halos mantling amygdules and fractures but only rarely occurs as isolated patches unrelated to these features as is common in non-silicified andesite. The alteration is texturally and mineralogically identical to that in non-silicified andesite and adjacent fractures or amygdules are filled by massive and fibrous epidote. The quartz-rich outer margin observed on the outer fringe of some epidote-quartz alteration patches mantling amygdules in silicified flows is not a product of epidote-quartz alteration (Gibson, 1979) but is interpreted as an artifact of a previous, more widespread silicification centred about the amygdule.

Chemistry of Quartz-Epidote Altered Andesite

Representative analyses of epidote-quartz altered andesite and adjacent andesite are listed in Table 12.2. Samples 83-210 and -211 are from the Waite Andesite Upper member and Sample 82-87 and -88 from the Rusty Ridge formation. Ca increases, whereas Si, Al and Fe are relatively constant and Mg, Na, K, Ti, P and Mn decrease in quartz-epidote altered andesite relative to adjacent andesite (Table 12.1). These variations are the same as the chemical gains and losses, assuming constant volume metasomatism, calculated by Gibson (1979) for weakly epidote-quartz altered andesite of the Amulet upper member and by Marzouki et al., (1977) for epidote-quartz altered diorite at Al Hadah, Saudi Arabia.

Smith (1968), in describing identical epidote-quartz alteration of Ordovician basalts and andesites in New South Wales, Australia, noted a similar variation as did Harrigan and MacLean (1975), who described epidote-quartz alteration of gabbro dikes at Matagami, Quebec, assuming constant Al_2O_3. The apparent depletion in Ba, Cr, and Zr, addition of Sr and relatively constant Y in epidote-quartz altered andesite relative to adjacent andesite was also noted by Marzouki et al., (1979).

The chemical changes that accompany quartz-epidote alteration correspond well with mineralogical changes. The ubiquitous increase in Ca and relatively constant Al and Si correspond with the development of epidote and quartz. The depletion in Na, K, Ti correspond with the destruction of plagioclase and decrease in Mg, and Fe correspond with replacement of primary clay minerals or chlorite by epidote and quartz. Strongly altered samples are often characterized by normative wollastonite which, according to Gelinas et al.,(1977), is indicative of

Ca addition.

Discussion

Epidote-quartz alteration is interpreted to be a product of fluid-rock interaction within a sub-seafloor hydrothermal system. The restriction of alteration to permeable areas within flows, transfer of elements to and from the alteration sites and conversion of an originally anhydrous to a hydrous mineralogy supports the presence of a fluid phase during alteration.

Harrigan and MacLean, (1975) and Marzouki et al.,(1979) interpreted mineralogically and chemically identical alteration of gabbro and diorite dikes to be a product of hydrothermal alteration during interaction of a fluid with cooling intrusions. Epidote-quartz altered andesitic and basaltic flows at Matagami (MacGeehan,1978), and ophiolites of east Liguria, Italy (Spooner and Fyfe, 1973) and Cyprus (Heaton and Sheppard, 1977; Spooner,1977; Lydon and Jamieson, 1984) are interpreted as hydrothermally altered flows, a product of fluid/rock interaction within a sub-seafloor hydrothermal system.

12.2.3 SILICIFICATION

Distribution

Silicification, unlike other types of semi-conformable alteration, is not widespread. Pervasive, intense silicification is restricted to andesitic flows of the upper members of the Amulet and Waite Andesite formations. Silicification characterizes these members and is so well developed that they were originally mapped as rhyolites (Wilson,1941; de Rosen-Spence, 1976).

Silicification of andesitic flows in the Amulet Andesite, Millenbach Andesite, and Rusty Ridge formations although locally as intense and pervasive is not widespread. The alteration is restricted to a few individual flows (Map2) where it occurs as localized patches and bands at pillow margins or along the top of thick massive flows. The one exception is silicification of flows and volcaniclastic breccias of the Flavrian formation at the Corbet Mine. At Corbet complete silicification of scoriaceous fragments (Plate C.4) and margins of lithic fragments (Plate C.3) within volcaniclastic breccias that underlie and overlie the massive sulphide deposit are common (Appendix C). Massive and pillowed flows are also locally silicified.

Silicification of rhyolitic flows, although not described in detail in this study, does occur. Recognition of silicification within rhyolite is hampered by a) the white colour inherent to the flows which does not contrast with silicification patches and b) difficulty in distinguishing devitrification areas in rhyolite, especially where spherulites are recrystallized to blebby granular quartz. The occurrence of silicification patches and halos mantling amygdules and high SiO_2 content attest to silicification of rhyolitic flows.

Previous work (Gibson, 1979) concentrated on defining the mineralogical and chemical changes that accompany silicification within a single section through the Amulet upper member. Consequently this earlier study did not address large scale structural or stratigraphic controls on silicification or the occurrence of silicification within other formations, such as the Waite Andesite upper member.

Perhaps the best exposed and accessible unit of silicified andesite is the Amulet upper member. This unit was mapped and sampled in detail in order to describe vertical and lateral variations within a single, silicified stratigraphic unit. The dotted pattern in Maps 1 and 2 and Figure 9.23 and 12.7 illustrate, qualitatively, the pervasiveness of silicification. Although there is an increase in silicification toward the top of individual flows and the member in general, the most pronounced variation is lateral. Silicification is most widespread and pervasive within the proximal facies of andesitic flows adjacent to their vents and where the member attains its maximum thickness. The distal facies of flows, which consist predominantly of breccia and were, perhaps, the most permeable, are not as pervasively silicified.

From the above description it is apparent that silicification is a semi-conformable alteration; however, pillowed flows of the Waite Andesite formation west of the Old Waite Mine (Map 2) are an exception. West of the Old Waite Mine silicified pillows clearly define a 400m wide and 600m long discordant "alteration corridor" within and along the south margin of the Old Waite Dike Swarm; pillows of the same flow outside of this corridor are not silicified. A second narrow, discordant zone of silicified pillows lies along the northern margin of a large dioritic intrusion immediately south of the dike swarm (Map 2).

Within this alteration corridor pervasively silicified pillows occur as screens between dikes. Silicified pillows (Plate 12.10) grade outward into "unaltered pillows" through a transition zone at the margin of the dike swarm where silicification is restricted to pillow margins (Plate 12.9). Silicification is so pervasive that pillows of the Waite Andesite formation are difficult to distinguish from silicified lobes and pillows of underlying Amulet upper member.

Field Characteristics

Detailed field descriptions of silicified massive andesitic flows of the Amulet upper member, are provided by Gibson, 1979 and Gibson et al., 1983. Characteristics of silicified massive and pillowed andesitic flows and hyaloclastite breccias of the Waite upper member, south of Waite Lake (Figures 12.5 and 12.6), typify features common to all silicified flows and are described below.

The Waite upper member (Figure 12.5) consists of three massive andesitic flows and a pillowed flow. The flows are characterized by well developed laminar and concentric joints and by 1% round to elongate mega-amygdules infilled by massive and finely laminated quartz and epidote interpreted to replace an original opaline infilling.

The flow morphology and amygdule distribution of these flows are identical to that described in Chapter 5, and to flows of the Amulet upper member.

Idealized cross-sections through a typical massive flow and pillowed flow in Figure 12.6, illustrate the distribution and morphology of both silicification and quartz-epidote alteration.

In massive flows the degree of silicification increases toward the flow top. Irregular, white-weathering patches, as large as 3 m , occur along the flow top and locally develop around mega-amygdules (Plate 12.11). These large patches have diffuse but abrupt margins and commonly coalesce to form large areas of pervasive silicification. Smooth, regular and contorted siliceous ribbon-like forms reflect silicification along amygdule trains (Plate 12.2) and both planar and contorted laminar joints. Individual lobes are pervasively silicified or altered along their laminar jointed, amygdaloidal margins; lobe selvedges are not commonly silicified. Amoeboid, detached lobes within the flow top breccia are silicified along their margin and/or along internal amygdule zones and laminar joints (Plates 12.13 and 12.14); small lobes (<0.3m) are pervasively silicified. Selective silicification of amygdule bands or laminar joints in irregular lobes results in the ribbon-like forms of Plate 12.17. The flow breccia matrix, composed of microlitic and minor sideromelane shard hyaloclastite, is locally and variably silicified and cemented by quartz (Plates 12.5 and 12.6). Silicification is best developed and most pervasive within the lowermost flow top breccia.

Pillows are silicified both along their margin and interior (Figure 12.6). Diffuse silicification patches dot the interior of pillows and silicified concentric joints at pillow margins impart a vein-network pattern (Plate 12.18). Thin, 1-2cm wide chloritized sideromelane selvedges are not commonly silicified but interpillow hyaloclastite (Figure 12.6) may be silicified and or quartz-epidote altered. Pillow breccia mantling the upper surface of the pillowed flow is pervasively silicified.

Mineralogy and Textures

Silicified andesite is characterized by the mineral assemblage quartz and albite. Unlike epidote-quartz and chlorite/sericite alteration, silicification did not destroy primary textures in even the most intensely altered rocks. Silicified andesite of the Amulet upper member (Plates B.1A and B.2A) illustrate the hyalopilitic texture of a silicified andesite flow and fragment that are composed of albite microlites and phenocrysts in a groundmass of chlorite with minor actinolite, quartz, epidote and opaque minerals; the occurrence of blebby quartz in these examples is attributed to silicification. In silicified andesitic flows albite microlites and phenocyrsts are preserved, but the groundmass consists almost entirely of blebby and fine granular quartz with minor, interstitial chlorite and epidote.

The mineralogical and textural changes from least altered to silicified flows also occur on the scale of a single thin section (Plates 12.2C to E). Unaltered andesite from a pillow margin (Rusty Ridge Formation) has a hyalopilitic texture with albite microlites in a groundmass of homogeneous chlorite and minor epidote and opaque minerals (Plate 12.2C). The first manifestation of silicification is the occurrence of irregular quartz blebs (<0.3mm) in the groundmass. Individual quartz blebs consist of a core of microgranular quartz surrounded by a rim of finer, granular quartz which grades into the chloritic groundmass. With increasing intensity of silicification quartz blebs are more abundant and coalesce leaving only remnants of the former glassy groundmass now represented by chlorite (Plate 12.2D). With complete silicification the groundmass is almost totally replaced by quartz which completely surrounds intact albite microlites (Plate 12.2E).

The development of blebby quartz within the flow groundmass was not a random process, but was probably controlled by primary structures and textures. Blebby quartz preferentially developed and is most intense adjacent to amygdules, along concentric or laminar joints and perlitic cracks from which it progressed outward to replace the groundmass. In vitrophyric andesite blebby quartz preferentially developed around albite microphenocryts and their spherulitic coronas (Plates 12.2F and G) which presumably mark microfractures within an originally homogeneous and structurally isotropic groundmass.

The mineralogical and textural changes that accompany silicification of sideromelane shard and microlitic hyaloclastite are similar to those described for flows. Silicification of chloritized andesitic vitrophyre (Plates 12.1G) occurs preferentially along perlitic cracks where optically oriented, length-slow chalcedony is interpreted to replace former fibro-palagonite (Plates 12.1H and 12.2A).

Similarly in rhyolitic flows, silicification of intact obsidian hyaloclastite occurs along perlitic cracks (Plate 12.3G) where chalcedony replaces shard margins leaving a core of massive chlorite after obsidian. Where obsidian shard hyaloclastite is silicified, botyroidal liesegang rings of former palagonite are preserved in shards replaced by chalcedony (Plate 12.3H).

In chloritized sideromelane hyaloclastite, shard margins are commonly silicified and replaced by fibrous chalcedony apparently pseudomorphing original fibro-plagonite (Plates 12.3C and D). Fibrous chalcedony replacing the shard margin is identical to adjacent chalcedony matrix cement (after original amorphous silica) except that the latter is riddled with fine oxides as in adjacent chloritized sideromelane. A fine oxide crust separates the silicified rim from matrix cement although the latter appears continuous.

Chemical Composition of Silicified Andesite

Direct comparison of the composition of silicified andesite and least altered andesite from the Amulet upper member, and pairs of silicified and least altered andesite from the Rusty Ridge formation, Amulet upper member and Waite Andesite formation (Table 12.3) indicate that silicified andesite is enriched in Si and depleted in Fe, Mg, Mn, Ca, Al and Ti relative to their least altered equivalent.

This apparent variation is also similar to that obtained from wide beam microprobe traverses across the silicified margins of two microlitic sideromelane shards from the Waite Andesite upper member (Figure 12.8). Thus, the apparent increase in Si and decrease in Al, Fe, Mg, Ca and Ti from the chloritic shard interior across its silicified margin mimics the variation obtained from whole rocks.

This apparent trend was first described by Gibson (1979) and Gibson et al., (1983), who also calculated the gains and losses attendant with silicification using a computational method that relates compositional variation to volume changes (Gresens, 1967; Babcock, 1973). Assuming constant volume metasomatism, silicified andesites are depleted in Al, Fe, Mg, Mn, Ti and Ca and enriched in Si relative to least altered andesite. The somewhat variable behaviour of Ca in weakly silicified samples (Gibson, 1979) reflects epidote-quartz alteration of these samples. The Na and K contents of andesites do not show any consistent variation related to their Si contents (Appendix G). This erratic behaviour is apparent in both whole rock and microprobe analyses.

The assumption of constant volume during silicification was based on the preservation of primary volcanic textures (Gibson, 1979; Gibson, et al. 1983). Recent work by Lesher et al., (1986) indicates that volume changes as large as 30% may have accompanied silicification. These calculations assumed immobility of the REE and HFS elements as indicated by relatively constant interelement ratios in silicified and least altered andesite. A 30% volume change corresponds to a 9.1% linear change (Lesher et al., 1986) which would be difficult to resolve in the fine-grained mesostasis of these flows and is therefore not inconsistent with their excellent textural preservation. A 30% volume change does, however, allow for an assumption of constant SiO_2 and Al_2O_3 during silicification.

Constant Al_2O_3 was assumed by Harrigan and Maclean (1976) and MacGeehan (1978) in their calculations of the chemical gains and losses that accompanied epidote-quartz alteration and silicification at Matagami. Constant SiO_2 or Al_2O_3, during silicification, requires a volume change of 2-12% and 3-35% respectively (Gibson, 1979). The assumption of constant SiO_2 or Al_2O_3 only affects the magnitude of the chemical changes described above; silicification of andesite results in the depletion of Fe, Mg, Mn, Ca and Ti (Gibson,1979).

The chemical changes that accompany silicification result from the replacement of groundmass glass, now chlorite, by quartz, thereby releasing Fe, Mg, Mn and Ti. Preservation of albite microlites and phenocrysts accounts for the relatively constant Al_2O_3, Na_2O, K_2O and depleted CaO content of silicified andesite.

Discussion

The restriction of intense, pervasive silicification to flow tops and faults, and the localization of silicification in areas surrounding individual amygdules and amygdule zones, to fine microfractures or joints, perlitic cracks and shard margins indicates that silicification is a product of fluid-rock interaction that was controlled by the primary permeability of the flows. Silicification occurred in an open system where the fluid responsible was able to transport chemical components to and away from alteration sites. Silicification was attributed by Gibson (1979), Gibson et al.,(1983), MacGeehan (1978) and Skirrow (1987) to hot water-rock interaction in a shallow sub-seafloor hydrothermal system.

De Rosen-Spence (1976) and de Rosen-Spence et al.,(1980) interpreted silicified flows to be a product of seawater interaction with cooling flows on the seafloor. The main evidence against seafloor silicification is:

a) fine granular and fibrous chalcedony produced during silicification is interpreted to replace former palagonite, clay minerals and zeolites attributed to prior seafloor weathering and diagenesis.

b) synvolcanic dikes within the Old Waite Dike Swarm are locally silicified.

c) silicification, if a normal product or consequence of seafloor water/rock interaction should be a common alteration within subaqueous volcanic terrains. This is definitely not the case; silicified flows have only been recognized locally and silicification appears to be a geologically uncommon alteration process (MacGeehan, 1977; Gibson, 1979; Strong et al., 1979; Dostal and Strong, 1983; Skirrow, 1987). There are no known examples of silicified flows on the present-day seafloor.

12.3 ORIGIN AND EVOLUTION OF SEMI-CONFORMABLE ALTERATION ASSEMBLAGES

In the foregoing discussion semi-conformable alteration assemblages within the Mine Sequence are interpreted as relics of a fossil hydrothermal system and not as products of an isochemical, regional low grade metamorphism. Semiconformable alteration assemblages are compared to and interpreted in light of the mineralogy and processes active in modern hydrothermal systems and to results obtained from fluid/rock interaction experiments. The former offers a "real world" comparison but suffers from uncertainties in the exact physical and chemical processes responsible for mineral transformations, whereas experimental results are plagued by problems of metastable phases, actual fluid/rock ratios, uncertain pH, duration times, and use of rock powders that limit their direct applicability to natural systems.

12.3.1 DIAGENETIC, SPILITIC AND EPIDOTE-QUARTZ ALTERATION

The Flavrian Block is interpreted to represent a section through a large hydrothermal system within the Noranda Cauldron. The size and shape of the hydrothermal system responsible for semi-conformable alteration is huge as it includes all formations of the Mine Sequence. The exceptions are rhyolitic flows which, although spilitized and showing relict textures of former diagenetic alteration, are not epidote-quartz altered.

The conformable character of the alteration and its location within permeable areas of flows suggests that within the hydrothermal system fluid flow was essentially parallel to stratigraphy. Numerous faults within and along the cauldron margin undoubtedly permitted cross-stratal fluid migration and focused discharge at the seafloor during hiatuses in volcanic activity.

The temperature of the fluid responsible for semi-conformable alteration assemblages and the original spatial distribution of these assemblages at Noranda may be estimated by comparison with assemblages found in younger and active hydrothermal systems. As the Mine Sequence consists of basaltic, andesitic and rhyolitic formations, comparison with high-temperature hydrothermal systems in Iceland, particularly the Krafla geothermal field, is appropriate (Tomasson and Kristmannsdottir, 1972). The similarity in semiconformable alteration assemblages at Noranda to those described from the Troodos pillow lavas in Cyprus also invokes a comparison with the latter (Spooner, 1977; Lydon and Jamieson, 1984).

At Krafla the hydrothermal solution is evolved meteoric water and the hydrothermal system is localized within a large cauldron located 2-3km above an underlying magma chamber (H.Trygvason, personal communication,1983). In the Troodos pillow lava succession evolved seawater is interpreted to have penetrated the volcanic succession to depth of 2-3km and may have interacted with the upper part of the underlying igneous complex (Spooner, 1977 ;Heaton and Sheppard, 1977).

The upper part of the Krafla hydrothermal system is characterized by a diagenetic "zeolite facies" alteration assemblage that persists at depth until temperatures exceed 230-250°C (Kristmannsdottir,1975, 1985); the conversion of calcic plagioclase to albite occurs at temperatures lower than 200°C (Arnorsson et al., 1982a and 1982b; Mehegan et al., 1982). A "greenschist facies" assemblage of chlorite (sericite)-epidote-albite-quartz occurs in the 250-300°C temperature range, and at temperatures above 300°C an epidote-quartz (actinolite) assemblage appears (Kristmannsdottir, 1975; Mehegan et al., 1982). Hydrothermal epidote in the Salton Sea geothermal system, which is morphologically similar to epidote-quartz alteration patches in Noranda, formed where temperatures exceeded 300°C (Keith et al., 1968). At Krafla the maximum geothermal gradient is approximately 300°C/km (Kristmannsdottir, 1975; H.Tygvason, personal communication, 1983).

Identical alteration assemblages within the Troodos pillow lava succession have a similar vertical distribution and are interpreted to have formed within a similar temperature range and geothermal gradient (Spooner, 1977; Heaton and Sheppard, 1977). Epidote-quartz alteration within the Troodos Pillow lavas is identical to that at Noranda and is interpreted to have formed at temperatures >300°C, within the deeper part of the hydrothermal system.

Figure 12.9A illustrates an interpreted simple, single-pass hydrothermal system within the Mine Sequence after extrusion of the Rusty Ridge formation.

Assumptions made to construct this model include:

1) The temperature range for the alteration assemblages and geothermal gradient are similar to those at Krafla and those interpreted for the Troodos pillow lavas.

2) The different semiconformable alteration types namely diagenetic (palagonite, clay minerals, zeolites recognized through relict textures), spilitic (chlorite,epidote,albite) and epidote-quartz alteration are predominantly temperature dependant and had an original disposition similar to assemblages at Krafla (Kristmansdottir, 1975) and in the Troodos pillow lavas (Spooner, 1977; Heaton and Sheppard, 1977 and Lydon and Jamieson, 1984). Other factors such as composition of the immediate host rock and changing composition of an evolving fluid will also influence the mineralogy of the alteration assemblage as elaborated below.

3) Synvolcanic intrusions, vent areas and synvolcanic faults channelling ascending hydrothermal fluid constitute local thermal anomalies within the hydrothermal system. These thermal anomalies disrupt and distort subhorizontal isotherms and disposition of mineral paragenesis or alteration types within the hydrothermal system.

4) The fluid responsible for alteration is evolved seawater.

In Figure 12.9A, cold seawater is interpreted to have entered the system over a wide area and migrated downward and to a lesser extent laterally. Influxing cold seawater hydrated glass to palagonite. During palagonitization the glass acquired H_2O and Fe and lost Al, Mg, Ca, Na and Si to solution which, along with Na and Mg from seawater, are fixed within authigenic clay minerals, zeolites and opaline silica precipitated in pore-spaces and vesicles (Hay and Iijima,1968; Viereck et al.,1982 and Mehegan et al., 1982). Palagonite and zeolites form over temperatures ranging from 0 - 100°C but the rate of palagonitization increases rapidly at temperatures above 50°C. Zeolites continue to form as a stable alteration phase until temperatures exceed 230-250°C; however, above 100°C clay minerals tend to form instead of palagonite as shown by seawater/basalt interaction experiments where layered silicates or clay minerals are the common alteration phase in the temperature range 150 - 350°C (Bischoff and Dickson, 1975; Seyfried and Bischoff, 1977 and 1979; Mottl et al., 1979).

At higher temperatures (200°C), Na fixation is accomplished by replacement of Ca-plagioclase by albite and balanced by the release of Ca to solution. Albitization which starts in the "zeolite facies" persists into the "greenschist facies" where albite along with chlorite and minor epidote and quartz constitute a spilitic assemblage characteristic of "greenschist facies" mafic volcanic rocks. The change to spilitic alteration is largely a mineralogical transformation as the main chemical changes to the flows continues to be hydration, a loss in Ca (Si) and net gain in Na and Mg (Table 12.1).

The common alteration products of basalt/seawater interaction experiments in the temperature range inferred for zeolite-greenschist facies alteration assemblages (150 - 300°C) are clay minerals or chlorite. In these experiments Mg-hydrolysis predominates and $Mg(OH)_2$ is precipitated and incorporated into the smectite/chlorite alteration assemblage whereas Ca is removed and incorporated into seawater. Addition of Na to the rock occurred in experiments with water/rock ratios of 5 - 10; however, Mottl (1983) using data from altered seafloor basalts calculated Na addition to occur at water/rock ratios of < 35, a more realistic ratio for alteration within the upper parts of the hydrothermal system which, presumably, would be characterized by higher water/rock ratios. During experiments with water/rock ratios of <50 the solution initially acquired Fe, Zn, Mn and Si and a lower pH but with depletion of Mg from "seawater", the pH of the solution increased and its heavy metal concentration decreased.

In summary, the experimental results mimic the chemical changes but not the complex mineralogical changes that are inferred to have accompanied diagenetic and spilitic alteration. The experiments also suggest that solution chemistry evolved from original seawater to a Si- saturated solution containing less Na and Mg and more Ca and perhaps Mn and Al. The low K content of the flows may preclude a substantial increase in K in the solution.

In modern hydrothermal systems, chemical and mineralogic changes are accompanied by a significant reduction in permeability due to precipitation of authigenic minerals in pore-spaces and vesicles. Reduction in permeability results in decrease in fluid flow and therefore water/rock ratio (W/R) with time and at depth. A decrease in permeability and therefore W/R ratio with depth is well illustrated within the Troodos pillow lava succession where Heaton and Sheppard (1977) calculated a minimum W/R of >1 for the upper part of the fossil hydrothermal system characterized by zeolite and greenschist facies assemblages and W/R of <0.1 for the underlying sheeted dike complex and areas of epidote-quartz alteration. The decrease in permeability at depth, although not obvious in the simple single-pass model of Figure 12.9A, results from the lowermost flow with a spilitic assemblage having been once at surface and undergone early self-sealing with diagenetic alteration during burial. This decrease in permeability with progressive alteration during burial may account, at Noranda, for the widespread and pervasive character of diagenetic and spilitic alteration assemblages and the more restricted, patchy character of epidote-quartz alteration.

The change from a spilitic "greenschist" assemblage to epidote-quartz assemblage is interpreted to occur at temperatures of 300-350°C (Figure 12.9A). On comparing the chemical gains and losses that accompany diagenetic and spilitic alteration of andesite (Na-Ca exchange) they are the complement of that associated with epidote-quartz alteration. These opposite but balanced gains and losses are compatible with related processes controlled by the Na/Ca ratio of the fluid. Marzouki et al.,(1979) proposed that the Na/Ca ratio of the fluid, in this case evolved seawater, may result in either the formation of albite or epidote as represented by the reaction:

$$3NaAlSi_3O_8 + 2Ca^{2+} + OH^- \rightleftharpoons Ca_2Al_3Si_3O_{12}(OH) + 3Na^+ + 6SiO_2$$

During diagenetic and spilitic alteration the composition of the fluid is continuously modified through loss of Na (and Mg) and addition of Ca (and Si). At some point the decreasing Na/Ca ratio may favour epidote over albite and the alteration is interpreted to evolve from one of spilitization to epidote-quartz alteration where Ca (Si)is added to andesite and the alkalis, Mg and Fe are removed. As epidote-quartz alteration occurs in the deeper parts of the hydrothermal system the water/rock ratio is inferred to be low and fluid flow essentially lateral. The localized and rare development of epidote-quartz alteration in spilitized rhyolitic formations may reflect the low CaO content of the flows which translates to less Ca added to the fluid and absence of an quartz-epidote assemblage within these rocks. This control of host rock lithology on alteration assemblages is consistent with low water/rock ratios (Mehegan et al., 1982).

Experiments where an evolved seawater solution (Mg-depleted, Ca-Na-K-Cl fluid) reacted with basalt at temperatures ranging from 350 - 500^{0}C and low water/rock ratios (<3) resulted in mineralogical and chemical changes similar to those proposed for epidote-quartz alteration (Rosenbauer and Bischoff, 1984; Seyfried and Janecky, 1985). Clinozoisite-tremolite-actinolite were the observed alteration products (Seyfried and Janecky, 1985, Seyfried et al., 1988) and Ca-hydrolysis rather than Mg-hydrolysis dominated reactions and formation of Ca-silicates. As in epidote-quartz alteration the fluid acquired Si, Fe, Mn, Zn and Cu.

Na fixation in experimental runs differs from Na leaching indicated for epidote-quartz alteration and may reflect a higher Na content in the reacted seawater solution compared to the inferred Na-depleted character of the solution responsible for epidote-quartz alteration. The behaviour of Mg in the experiments was not addressed but in epidote-quartz alteration Mg is leached from andesite. In diagenetic and spilitic alteration, Mg added to andesite during Mg-hydrolysis is coupled and balanced by dissolution of Ca. Perhaps during epidote-quartz alteration Ca, added during Ca-hydrolysis, was balanced by dissolution of Mg.

The single-pass model illustrated in Figure 12.9A, is characterized by separate areas of diagenetic, spilitic and epidote-quartz alteration that change with depth. Although this pattern may be typical of modern hydrothermal systems such as at Krafla and fossil systems such as in the Troodos pillow lavas, it is definitely not the case in the Mine Sequence where a single outcrop or handspecimen may contain domains of spilitized, epidote-quartz altered and, for that matter, silicified andesite. Although the distribution of alteration types within the Mine Sequence at first appears at odds with modern systems their juxtaposition may be explained by progressive superposition of alteration types during burial and continued volcanism. In the explanation below it will be argued that the distribution of alteration assemblages at Krafla and Troodos represent only a "snap shot" during the evolution of a hydrothermal system within an active volcanic environment.

With continued eruptions and infilling of the Noranda cauldron flows at the top of the succession were continuously buried and as a result underwent progressive hydrothermal alteration. This is illustrated in Figure 12.9B, where andesitic flows of the Rusty Ridge formation and their alteration assemblages produced by an earlier hydrothermal system are buried by rhyolitic flows of the Amulet lower member. Continued hydrothermal alteration during and following extrusion of the younger rhyolitic flows resulted in the superposition of quartz-epidote alteration on previously spilitized andesite such that the two alteration types are juxtaposed. Similarly, phases produced by diagenetic alteration are now replaced by a spilitic assemblage only to become epidote-quartz altered with continued volcanism and burial.

Alternatively, Smith (1968) interpreted juxtaposed areas of spilitic and quartz-epidote altered andesite to processes occurring simultaneously within the area of a single outcrop. Elements added to andesite during epidote-quartz alteration are obtained from adjacent areas undergoing spilitization and vice versa. Thus the two alteration process are coupled and represent only "local" element mobility with rearrangement of elements into juxtaposed domains. In support of this interpretation Smith's (1968) calculated bulk composition for the altered flows, based on the proportion and composition of spilitized and epidote-quartz altered domains within a single 5m x 6m outcrop approximated a basaltic or basaltic andesite composition inferred for the flows.

Field evidence such as 1) the common occurrence of epidote-quartz alteration patches centred on amygdules within larger areas of spilitized and or silicified andesite and never the reverse and 2) the common amygdule and pore-space infilling sequence of chalcedony-chlorite-epidote, the latter two minerals commonly pseudomorphs of former zeolites, however, support superposition of these chemically related but spatially separated alteration types.

In summary, a word of caution is warranted. Epidote-quartz altered andesite is interpreted to have undergone a complex evolution including previous diagenetic and spilitic alteration. It should be apparent that the composition of epidote-quartz altered andesite is not simply a product of this last alteration but is a culmination of early alteration types. Thus, in any study attempting to calculate the "actual gains and losses" attendant with a single alteration type, within a complex system, the element fluxes are only an approximation and, in part, reflect chemical changes inherited from early alteration.

12.3.2 SILICIFICATION

Unlike other semi-conformable alteration types the mineral assemblage or chemical characteristics of silicified andesite have not been duplicated in experimental fluid/rock interaction studies. This fact and the lack of known analogs within modern hydrothermal systems severely limits interpretation regarding the origin of this distinctive alteration type.

The size and shape of the hydrothermal system responsible for silicification is shown by the area underlain by silicified rock in Maps 1 and 2 and Figures 9.23 and 12.7. It is apparent that pervasive, widespread silicification is not common, but is restricted to the upper members of the Amulet and Waite formations within the Mine Sequence. Formations which underlie and overlie these members are not silicified indicating that processes or conditions responsible for pervasive silicification were operative for only two "brief" periods during extrusion of the Mine Sequence and infilling of the Noranda Cauldron. Widespread silicification is not recognized in pre- and post-cauldron formations.

The special eruptive history of these two members is interpreted to account, in part, for the conditions responsible for their pervasive silicification. Typically, Mine Sequence andesitic formations represent accumulations of flows built up through successive eruptions separated by periods, albeit brief, of quiescence. The Amulet and Waite upper members are unique as they formed during single, brief, voluminous eruptions in which, because of concomitant subsidence, flows were ponded within large, fault bounded depressions.

Figure 12.7, depicts the hydrothermal system after extrusion of the Amulet Upper member and qualitatively outlines areas of pervasive silicification within this unit. Silica saturated solutions (responsible for diagenetic and spilitic alteration) circulating within the underlying hydrothermal system with a high Na/Ca ratio are interpreted to be the fluids responsible for silicification. Downward migrating fresh seawater, if analogous to modern seawater, although possessing a high Na/Ca ratio does not contain significant silica (Thompson, 1984) as required by the alteration process.

Silica saturated solutions derived from areas lateral to and below the upper member are likely to have been in the 150-300°C temperature range and in equilibrium with quartz (Figure 10.B;Fournier and Rowe, 1966). Within this temperature range silica is present entirely as $Si(OH)_4$ (Fournier, 1985). The solubility of silica generally increases with temperature and salinity but is also pressure dependant (Kennedy, 1950; Fournier, 1985). Assuming that the solution had the same salinity as modern seawater (3.2 wt.%; Bischoff and Rosenbaurer 198) the solubility of quartz is only slightly increased and would closely approximate that of pure water (Kennedy, 1950; Fournier, 1985; Figure 10). Quartz has a solubility maximum that is pressure dependant and extends from 340°C at the vapour pressure of solution to 550°C at 900 bars (Figure 12.10A). From Figure 12.10A ,it is interpreted that silica saturated solutions in equilibrium with quartz and in the 150-300°C temperature range upon interaction with the hot, ponded flows of the Amulet (or Waite) upper member may have been rapidly heated above the silica solubility maximum for that given pressure resulting in quartz precipitation.

Thus, rapid heating of a silica saturated solution to temperatures above its solubility maximum can account for silica addition; however, silicification is also characterized by dissolution of Fe, Mg, Mn, Ca, Ti, and Zn primarily from volcanic glass. In diagenetic and spilitic alteration Mg-hydrolysis is the dominant H^+ producing reaction that lowers solution pH and allows effective leaching of heavy metals and other elements from andesite (Seyfried and Bischoff, 1981). During silicification Mg is not added but removed from andesite indicating that Mg-hydrolysis had no role in silicification. It is proposed that with rapid silica oversaturation, Si fixation within volcanic glass and precipitation within pore-spaces, coupled with Na fixation during albitization of plagioclase (favoured by the high Na/Ca ratio of the solution) may have been balanced by the removal of Mg, Mn, Ca, Ti, Fe, Zn and possibly minor Al from glass.

This model for silicification was first proposed by MacGeehan (1978) to explain silicification at Mattagami and by Gibson (1979) for silicification within the Amulet upper member. This mechanism is strongly temperature dependant and is consistent with field observations of the Amulet and Waite upper members which indicate the following:

a) pervasive silicification occurs along permeable flow contacts where both temperature and fluid flow were highest, allowing maximum interaction between the fluid and hot andesitic flows. Because of the high temperature required, silicification was restricted to "hot", permeable volumes within flows such as massive amygdaloidal lava inward from lobe/flow/pillow margins whereas adjacent selvedges and surrounding hyaloclastite are less commonly altered.

b) on a regional scale, silicification is most pervasive where heat was retained the longest such as in its principal vent areas where the unit also attains maximum thicknesses. Thinner, but more permeable, distal parts of the upper member are characterized by less pervasive silicification.

The proposed model also accounts for a), the restriction of silicification to specific stratigraphic units within a hydrothermal system, whereas underlying and overlying formations are not silicified and b), the localized occurrence of thin silicified flow tops and lobe margins in thick massive flows within other andesitic and rhyolitic formations.

The apparent discordant nature of silicification within the andesitic flows of the Waite Andesite formation east of the Old Waite deposit is also consistent with the model. Silicification there was confined to the vent area of pillowed flows within the Old Waite dike Swarm which represents an area of anomalously high heat flow and permeability. Silicified areas within flows of other formations are also located adjacent to the Old Waite Dike Swarm and McDougall-Despina Fault.

12.3.3 HEAT SOURCE

The heat required to initiate and sustain a large scale hydrothermal system within the Mine Sequence of the Noranda Cauldron, that may have affected some 900 km^3 of rock, was derived from both a high geothermal gradient and high-level intrusions. Based on a comparison with Krafla and temperatures inferred for alteration of pillow lavas in Cyprus, a geothermal gradient of 300°C/km has been assumed during extrusion of the Mine Sequence. Like Krafla, the postulated hydrothermal system at Noranda occurs in a basalt-andesite -rhyolite succession localized within a large cauldron, 2-3 km above an underlying magma chamber now represented by the Flavrian Pluton. The Flavrian Pluton was emplaced during extrusion of the Mine Sequence and forms the base of the succession. The Meritens phase of the pluton was locally emplaced within 0.5km of surface (Appendix C) which suggests that the estimated 300°C/km geothermal gradient may be a minimum.

Maintenance of a 300-350°C hydrothermal system, even within the upper part of the 3km thick Mine Sequence, is in accord with computer modelling studies of hydrothermal systems. Cathles (1983) and Elders et al.,(1984) indicate that temperatures of 350°C can occur up to 3km from a magma body if the intrusion has a cross-sectional area of >15km^2; the Flavrian Pluton has a minimal cross-sectional area of 65 km^2.

High-level intrusions, such as feeder dikes that occupy the McDougall-Despina Fault and constitute the Old Waite Dike Swarm, might act as local heat sources. These local heat sources, although not contributing significantly to the overall heat flow (Cathles, 1978), are thermal anomalies that distort the geothermal gradient and result in areas of higher heat flow. In this regard the Amulet and Waite upper members essentially acted as a high level heat source that distorted the "normal" temperature regime within the hydrothermal system which resulted in the silicification of these units.

12.3.4 DISCHARGE OF HYDROTHERMAL FLUIDS

Fluids responsible for semi-conformable alteration must eventually be discharged at the seafloor. Active faults undoubtedly are the principal conduits that allow ascent of hydrothermal fluids and focus their discharge. The chert-rich component of bedded tuffs (Chapter 6) which occur throughout the Mine Sequence may represent accumulations of discharged, silica saturated solutions.

Localized siliceous deposits (Chapter 6) are interpreted to have formed near discharge sites with silica precipitated both at and below the seawater/rock interface due to cooling of an ascending, hot, silica-saturated solution. This "silica dumping" (Gibson, 1979) is particularly common toward the tops of formations and, in part, is a self-sealing process that would not only inhibit outflow but also inflow of water into the system (Facca and Tonai, 1967). Self-sealing, due to silica dumping accompanying discharge and silicification, was widespread within the uppermost flows of the Amulet and Waite upper members. The combined effects of these processes may have resulted in the formation of a relatively impermeable cap rock at the top of these formations. The decrease in the pervasiveness of alteration from widespread, near-uniform, spilitization to more restricted, patchy epidote-quartz alteration is interpreted to be a function of decreasing permeability (W/R ratio) deep within the hydrothermal system due to self-sealing.

12.4 DISCORDANT ALTERATION

12.4.1 CHLORITE AND SERICITE ALTERATION

Chlorite and sericite alteration typify alteration pipes, the discordant, crudely cylindrical volumes of altered rock, that underlie and less commonly overlie proximal VMS deposits. As a result of their close association with VMS deposits and usefulness as an exploration tool, chlorite and sericite alteration have received considerable attention by researchers and explorationists alike. Areas of chlorite and sericite alteration also mantle some synvolcanic faults such as the McDougall and Despina (Maps 1 and 2). Many of these faults contain veins of chalcopyrite and quartz.

Significant studies of alteration pipes in the Noranda Camp include Price (1948, Horne Mine), Lickus (1965, Vauze Mine), Sakrison (1966, Norbec Mine), Riverin (1977) and Riverin and Hodgson (1980, Millenbach Mine), Atkinson and Watkinson (1980, Bedford deposit), Watkins (1980, Corbet Mine), Hall (1982, amulet Mine) and Ikingura et al., (1989, D68 deposit) . These studies provide a wealth of data pertaining to the size, shape, mineralogy, textures, and chemistry of alteration pipes that is only summarized herein. The emphasis of this study is directed at developing a model that explains the spatial, temporal and chemical relationships of chlorite and sericite within alteration pipes, to surrounding, larger, semicomformable alteration zones.

Spatial Distribution

Chlorite and sericite occur in crudely cylindrical zones within alteration pipes immediately below and less commonly above VMS deposits. A typical alteration pipe, as described by Riverin and Hodgson (1982) and Knuckey et al., (1982) for the Millenbach deposit, but representative of others, contains an inner chloritic zone surrounded and "capped" by an outer sericitic zone (Figure 12.11). The sericite and chlorite zones are gradational. Chlorite and sericite alteration mantling faults has a similar zoning with an inner chlorite zone and narrow outer fringe of sericite.

Based on observations at both Millenbach and Corbet the sericite alteration zone is best developed at the top and "leading edge" of the pipe. As illustrated in Figure 12.11, massive sulphide lenses at Millenbach, Corbet and Ansil occur at different positions within an alteration pipe. At Millenbach, where the alteration pipe is largely restricted to the footwall, massive sulphide is underlain by sericite whereas at Ansil, where the alteration pipe extends for at least 300m into the hangingwall, the sulphide lens is underlain (and overlain) by the chlorite zone. The significance of the variable position of a massive sulphide lens and alteration type vertically within the pipe will become apparent in later discussion.

The cross-sectional shape and size of an alteration pipe is governed by the permeability of the footwall and hangingwall lithologies. With relatively impermeable footwall rocks such as flows at Millenbach the pipe has a crudely circular shape and is no larger in diameter than the overlying massive sulphide lens. With permeable footwall rocks composed of breccia, as at Corbet, the alteration pipe is irregular in form and considerably larger in diameter (2x) than the massive sulphide lens (Gibson, 1982).

Alteration pipes extend for significant distances below VMS deposits. Deep underground and surface drill programs conducted by Corp. Falconbridge Copper successfully traced the alteration pipes to both the Millenbach main lens and Lower A deposits greater than 1000m into the Flavrian formation. The length of these alteration pipes suggests that the fluids responsible, in part, for chlorite and sericite alteration originated from a deep source. It is significant that in these deep holes only chlorite alteration was recognized within the alteration pipe at depth. This may reflect preferential position of drill holes within the core zone of pipes or a predominantly chlorite alteration assemblage at depth.

Mineralogy, Textures and Chemistry of Chlorite/Sericite Altered Rocks

Mineralogy and Textures

Sericite alteration is characterized by the assemblage sericite and quartz with minor epidote and chlorite. Plagioclase phenocrysts are pseudomorphed by quartz and sericite, within a groundmass of granular quartz, sericite, minor epidote and chlorite. Pyroxene phenocrysts, like those in adjacent non-sericitized flows, are pseudomorphed by chlorite. The sericite zone grades outward into "fresh" rocks through a decrease in sericite and preservation of plagioclase.

Chlorite alteration consists of the assemblage chlorite and minor quartz. Primary textures and structures are largely destroyed; pseudomorphs after plagioclase and even quartz phenocrysts may not be recognizable in intensely altered samples. The chlorite zone is readily subdivided into an inner core zone or spine containing anomalous blue birefringent, Fe-rich chlorite and an outer zone or envelope of anomalous brown birefringent, Mg-rich chlorite (Riverin, 1977; Atkinson and Watkinson, 1979; Watkins, 1980, and Riverin and Hodgson, 1980). The chlorite-sericite transition is characterized by the assemblage chlorite, sericite and quartz. Petrographic evidence indicates that chlorite replaces former sericite within this zone (Riverin, 1977; Ikingura, 1984).

Sulphide minerals may also show a marked zonation with respect to the chlorite and sericite zones, with pyrite and sphalerite dominant in the sericite zone, and pyrrhotite and chalcopyrite in the chlorite zone. Chlorite and sericite altered faults have an identical Cu-Zn zoning.

The mineral assemblages described for the chlorite and sericite zones typify all VMS deposits of the Noranda camp except those within the contact metamorphic aureole of the Dufault Pluton where they have been recrystallized to a hornblende-hornfels assemblage (Sakrison, 1966; de Rosen-Spence,1969). Contact metamorphism caused the development of a porphyroblastic or spotted texture within the altered rocks that was named "spotted dog" or "dalmatianite" by early workers (Cooke,1930; Wilson,1941). Metamorphic minerals that characterize the former chlorite zone include cordierite and anthophyillite or gedrite, whereas biotite dominates in the former sericite zone (Riverin and Hodgson,1980; Hall,1982). Contact metamorphism resulted in significant mineralogical and textural changes within the alteration pipe but was essentially isochemical (Riverin, 1977; Riverin and Hodgson, 1980).

Chemistry of Chlorite and Sericite Altered Rocks

The chemical changes that accompany chlorite and sericite alteration at Millenbach, as described by Riverin, (1977), Riverin and Hodgson, (1980) and Knuckey et al., (1982), have been verified through studies of other deposits with different host rocks (Atkinson and Watkinson,1979; Watkins,1980 and Hall,1982).

Using Gresens (1967) equations and assuming constant volume metasomatism, Riverin (1977) found that relative to "unaltered equivalents", Ca and Na are depleted and K is enriched within the sericite zone corresponding to plagioclase breakdown and an increase in sericite. Ca, Na and K are strongly depleted and Mg and Fe enriched within the chlorite zone; the core of the chlorite zone is Fe-rich. Si and Al are least mobile although the latter is slightly enriched in the sericite zone and slightly depleted in the chlorite zone. These chemical changes are graphically displayed in the unfolded tetrahedron (MgO+FeO)-(CaO+Na_2O)-(Al_2O_3-K_2O) (Figure 12.13).

Chlorite and sericite zones mantling faults show the same chemical trends as those in alteration pipes (Figure 12.13, Gibson et al., 1983). The similar chemistry and silicate/sulphide zoning of fault-related chlorite and sericite alteration to that of alteration pipes and the presence of sulphide stringers suggests that fault controlled alteration may represent a lower part of a discharge conduit that channelled ascending solutions to the seafloor (Gibson et al., 1983).

12.4.2 ORIGIN AND EVOLUTION OF CHLORITE AND SERICITE ALTERATION

Chlorite and sericite alteration are products of intense, pervasive metasomatism where a rapidly ascending fluid interacted with its wallrock. The composition and source of the fluid responsible for alteration and the physicochemical conditions that prevailed during both alteration and formation of Cu-Zn massive sulphides, at Noranda and elsewhere, has been the focus of much controversy and debate (see discussion by Lydon, in Franklin et al., 1981). The conceptual "model" outlined below is an attempt to integrate the evolution of chlorite and sericite alteration with contemporaneous hydrothermal processes responsible for regional, semiconformable alteration of the footwall to VMS deposits at Noranda.

Although the chemistry of ascending solution responsible for chlorite/sericite alteration may reflect a composition buffered and in equilibrium with alteration assemblages of a deep hydrothermal reservoir (Riverin and Hodgson, 1980; Franklin et al., 1981), assemblages within the pipe may not. The uniform bulk composition within the core of alteration pipes regardless of the original lithology they transect, and a +2 per mil shift in the ^{18}O of chlorite and sericite, at the D68 deposit(Ikingura et al., 1989), indicates a high fluid/rock ratio and therefore a high rate of fluid flow (Seyfried and Bischoff, 1979). Because of the high fluid flow and fluid/rock ratio, changes in mineralogy across and upward within an alteration pipe are not interpreted to result from wallrock/ fluid interaction, but changes in fluid chemistry induced by temperature changes as a result of mixing with seawater and/or boiling.

The interpreted model (Figure 14A) depicts the evolution of an ascending high temperature "primary fluid" and its alteration assemblages during mixing with 1) a high temperature intrastratal, solution in the medial part of regional hydrothermal system and 2) downward migrating ambient seawater and cooler hydrothermal fluids.

Field evidence indicates that the primary ore fluid was derived from a deep aquifer or magmatic source (Chapter 13) and not from a hydrothermal system in the immediate footwall to the deposits. The primary fluid was probably a reduced (H_2S-bearing), mildly acidic, chloride solution, with the metals (Fe, Cu, Zn, and

Pb) carried predominantly as Cl^- complexes (Franklin et al.,1981). Based on the compositions of fluids discharging from "Black Smokers" and high temperature fluid/rock interaction and metal solubility experiments, the fluid was likely Mg-poor, silica-saturated and > 300°C in temperature (Seyfried and Bischoff, 1981; Styrt et al.,1981; Crerar and Barnes, 1976).

The pronounced spatial association of VMS deposits and areas of chlorite/sericite alteration with synvolcanic faults, and their marked alignment along these structures, indicate that faults were the main conduits for ascending hydrothermal fluids and concentrated their discharge on the seafloor. Driven by a large hydraulic head, the difference in density of the fluid deep within the source area and the seafloor (Franklin, 1986), and perhaps through tectonic movement, "seismic pumping" of Sibson et al., (1975), the primary fluid was rapidly channelled to the seafloor (3-5m/sec.). The fluid probably ascended adiabatically and arrived at the near seafloor environment without suffering a significant temperature drop due to cooling (Mottl, 1983). During ascent, however, the primary fluid must have come in contact with both high and low temperature hydrothermal fluids also using this structure, and downward migrating, ambient seawater. The possible effects of this interaction or mixing will be examined.

During ascent the fluid would encounter high temperature solutions (>300°C), involved in epidote-quartz alteration and silicification within <1-2km of the seafloor (Figure 14A). Because of rapid ascent, interaction may have been restricted to mixing at the margins and top of the rising fluid column. With mixing, the fluid may have cooled, acquired additional Fe and Zn from the intrastratal fluid, but more significantly acquired Mg. Interaction between the mixed, now Mg-bearing fluid and wall rocks is interpreted to have resulted in formation of Mg-rich chlorite during Mg-hydrolysis that was balanced by the removal of Na and Ca to produce a classic Na and Ca depleted chlorite alteration zone (Riverin and Hodgson,1980. A possible temperature decreases during mixing may have resulted in the precipitation of Fe- and Cu- and to lesser extent Zn-sulphides and quart; this may explain the anomalous copper and zinc values commonly encountered deep within alteration pipes.

While the inferred mixing occurred at the periphery, the composition and temperature of the fluid within the core of the rising fluid column is interpreted to have remained unchanged. Interaction between wall rocks and fluid within the "core" may, therefore, have been dominated by Fe-hydrolysis and the formation of Fe-chlorite balanced by removal of both Na and Ca. Thus, at this point in time, a discordant alteration pipe could have formed which was characterized by a core of Fe-chlorite and margin/top of Mg-chlorite, typical of Noranda VMS deposits.

As the ascending fluid approached the seafloor it undoubtedly interacted with cooler intrastratal fluids responsible for diagenetic and spilitic alteration and downward migrating seawater in the temperature range of 25-250^{0}C (Figure 14A). Mixing of these fluids and the ascending fluid may have been substantial in the upper 500m of the system where fluid flow was greatest. Discharge of mixed fluids at the seafloor may have resulted in a localized and accentuated draw down of ambient seawater near to the vent promoting increased mixing (Franklin,1986) through the generation of a shallow, seawater dominated secondary convection cell (Figure 14A).

Apparently the main effect of mixing cooler hydrothermal fluids, primarily cold seawater, with a higher temperature, reduced and mildly acidic ascending fluid is a rapid drop in the temperature, increase in pH and fO_2 (Large, 1977; Franklin et al., 1981). As illustrated in Figure 12.15, a rapid drop in temperature would drive a fluid initially in equilibrium with chlorite (in this case Mg-chlorite such as at point A), before mixing and cooling, into the sericite field. Subsequent fluid/rock interactions would result in the formation of sericite and development of a sericitic fringe and cap to the alteration pipe.

The temperature drop would also result in silica oversaturation and precipitation of quartz and undoubtedly sulphides. As shown by Large (1977), the zoning from a predominantly chalcopyrite-pyrrhotite-chlorite zone to a sphalerite-pyrite-sericite fringe, both across and vertically within the alteration pipe, may be a function of decreasing temperature and increasing fO_2, a result of seawater mixing. Knuckey et al.,(1982) also attributed the Cu-Zn zoning at Millenbach to be a function of decreasing temperature.

The rapid precipitation of silica and sulphides within fractures, pore spaces and amygdules and attendant development of alteration minerals would reduce permeability and mark the onset of a self-sealing process (Facca and Tonai, 1967). Self-sealing would best develop in the upper part of the discharge site where mixing was dominant.

As the system is not static, continued ascent of hydrothermal fluid and mixing with seawater could substantially reduce the permeability and slowly but progressively restrict the migration of seawater and cooler hydrothermal fluid into the discharge area. Consequently, there would be less mixing, gradually higher temperatures in the discharge area would result, and a progressive, upward migration of the chlorite zone (and Fe-chlorite over Mg-chlorite) at the expense of sericite would occur as indicated from petrographic evidence (Riverin and Hodgson, 1980; Ikingura, 1984).

Within a long-lived and sustained system the upward advancing chlorite zone could approach or reach the seafloor as at Millenbach and Corbet (Figure 14A and B). In some instances where the hydrothermal vents are buried, but not sealed by contemporaneous flows, such as at Ansil and the Amulet deposits, the hydrothermal system and prograding alteration assemblages could continue upward into the hanging wall (Figure 14C). Thus, the occurrence of sericite or chlorite below, or for that matter above, a massive sulphide lens may be totally a function of the longevity of the discharge site and not a function of initial water depth as proposed by Watkins, (1980) and Franklin (1986).

In summary, the end result would a pipe-like alteration zone with a core of Fe-rich chlorite, a periphery of Mg-rich chlorite and an outer fringe and cap of sericite. Riverin and Hodgson (1980) envisaged chlorite and sericite alteration to form simultaneously due to progressive reaction and evolution of a single, homogeneous solution with the rocks as the fluid moved outward and upward within the discharge area. The model outlined herein also involves the simultaneous formation of chlorite and sericite but in response to steep vertical and horizontal thermal gradients, due to mixing with seawater or boiling, within the discharge area.

A multi-fluid model for chlorite and sericite alteration is also indicated by recent oxygen isotope data (Ikingura et al., 1989). They found that sericite and chlorite alteration in the D-68 deposit (Millenbach) maybe associated with two, isotopically different fluids that are unlikely to represent the same fluid at different temperatures. The data also suggest the fluids to be evolved seawater, with the fluid producing sericite less evolved (through secondary mixing with seawater?) than that producing chlorite which may have a magmatic component, interpretations which are consistent with the proposed model.

The Mg-Depletion Problem

The Mg-chlorite fringe to alteration pipes, although overemphasized, is ubiquitous to Noranda VMS deposits and has been particularly difficult to explain with an ore fluid presumably depleted in Mg as indicated in fluid/rock interaction experiments (Seyfried and Bischoff, 1981; Mottl, 1983) and from measurements of the fluid composition of "Black Smokers". In order to overcome this Mg-depletion problem Franklin (1986), proposed that Mg added to the ore fluid was from seawater that migrated or was drawn down around the discharge vent. This model may be adequate to explain Mg enrichment (chlorite/talc) immediately below the seafloor, as initially proposed by Roberts and Reardon (1978) for the Mattagami Lake VMS deposit. However, it seems rather unlikely that seawater could be drawn more than 1000m vertically and immediately below a VMS deposit or retain its Mg content over this distance as would be required at Noranda.

The Mg-addition process outlined above is appealing as it provides a "sink" for Mg leached during quartz-epidote alteration and or silicification; this would then be added to the ascending fluid as it rises and interacts with wall rocks. The model also suggests that in volcanic environments not characterized by Mg-generating epidote-quartz alteration or silicification, the alteration pipes will lack a Mg-rich mineral assemblage but still contain an Fe-rich assemblage such as Fe-chlorite or perhaps Fe-carbonate as described at Mattabi (Franklin et al., 1975).

Depth of Seawater and Boiling

The depth of water at which the hydrothermal fluids discharged onto the seafloor will also affect the physical and chemical process that occur at the discharge site. The most critical aspect of water depth is whether or not the solutions boiled. Boiling, at or below the seawater/rock interface, would both lower the temperature and decrease the volume of the fluid, evolve CO_2/H_2S and result in the precipitation of sulphides and probably silica (Drummond and Ohmoto, 1985). Boiling, like mixing with ambient seawater, would result in development of a strong, vertical thermal gradient in the conduit (Riverin and Hodgson,1980) that could account for the vertical change from chlorite to sericite alteration assemblages below Noranda massive sulphide deposits.

There is no unequivocal evidence that boiling did or did not take place during alteration and sulphide deposition at Noranda. Tables of water depth vs boiling, calculated from temperature-pressure-salinity curves for NaCl solutions by Ridge (1973) and used to evaluate seafloor sulphide deposition, can be used to crudely ascertain if boiling took place.

Water depth during extrusion of the Mine Sequence probably ranged from 300m to 500m, but for simplicity in use of Ridge's data, a water depth of 460m is assumed. Ridge (1973) used a 5 wt.% NaCl solution to approximate the ore fluid salinity, as fluid inclusions from Kuroko deposits have salinities in this range. Based on the temperature of fluids exiting from "Black Smokers" the temperature of the fluid responsible for the formation of Noranda VMS deposits was probably in the 300-350°C temperature range. Assuming a 300°C temperature, the exiting fluid would be boiling if the water depth was less than 725m. Thus, it may be reasonable to assume that the fluids responsible for the formation of VMS deposits at Noranda were boiling and that sulphide deposition, Cu-Zn zonation and possibly the shift from chlorite to sericite alteration are products of the physical and chemical changes that accompanied boiling and/or mixing with ambient seawater (Drummond and Ohmoto, 1985).

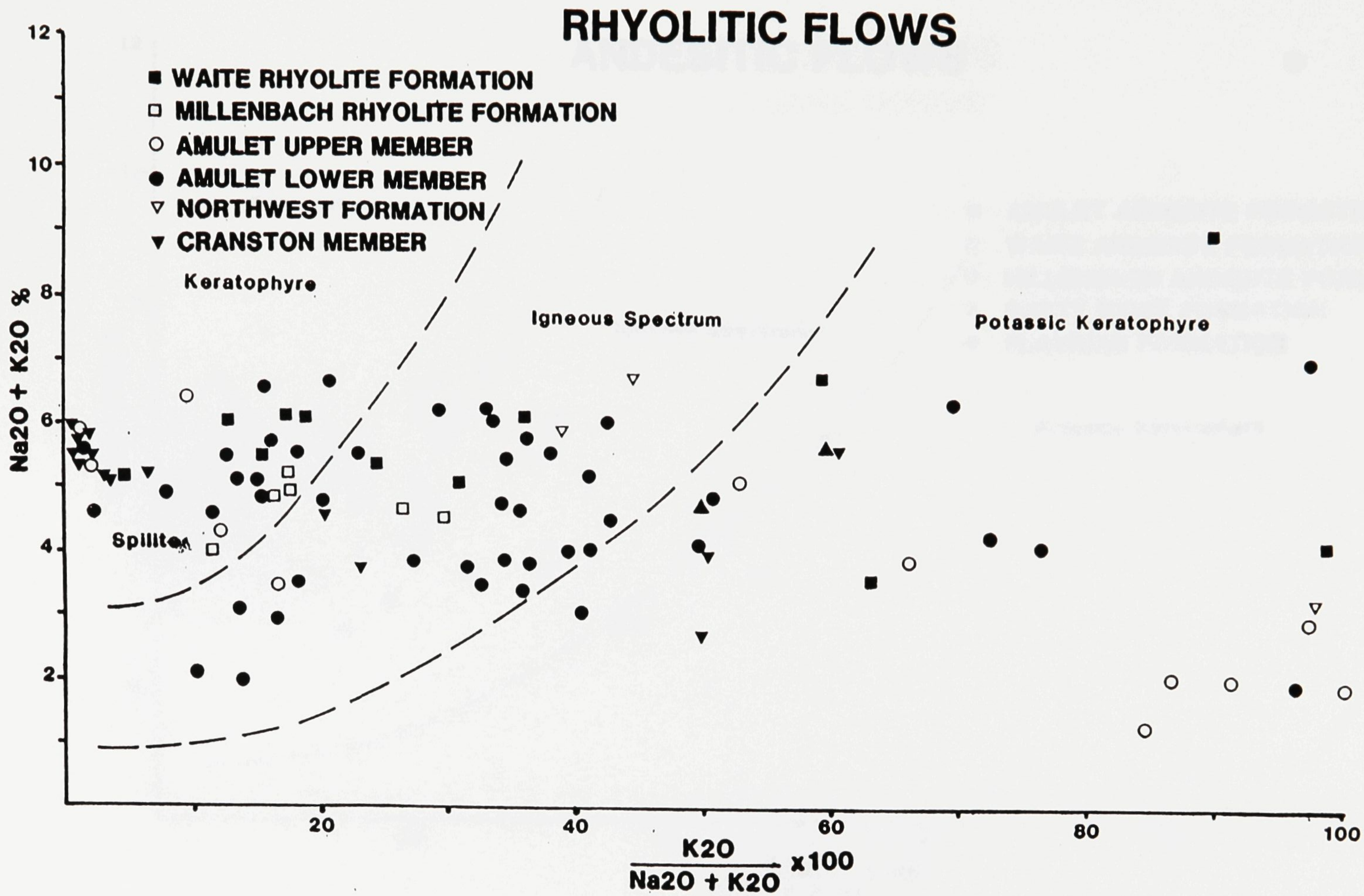

Figure 12.1. Alkali ratio diagram (Hughes, 1976) illustrating the spilitic affinity of Mine Sequence rhyolitic flows.

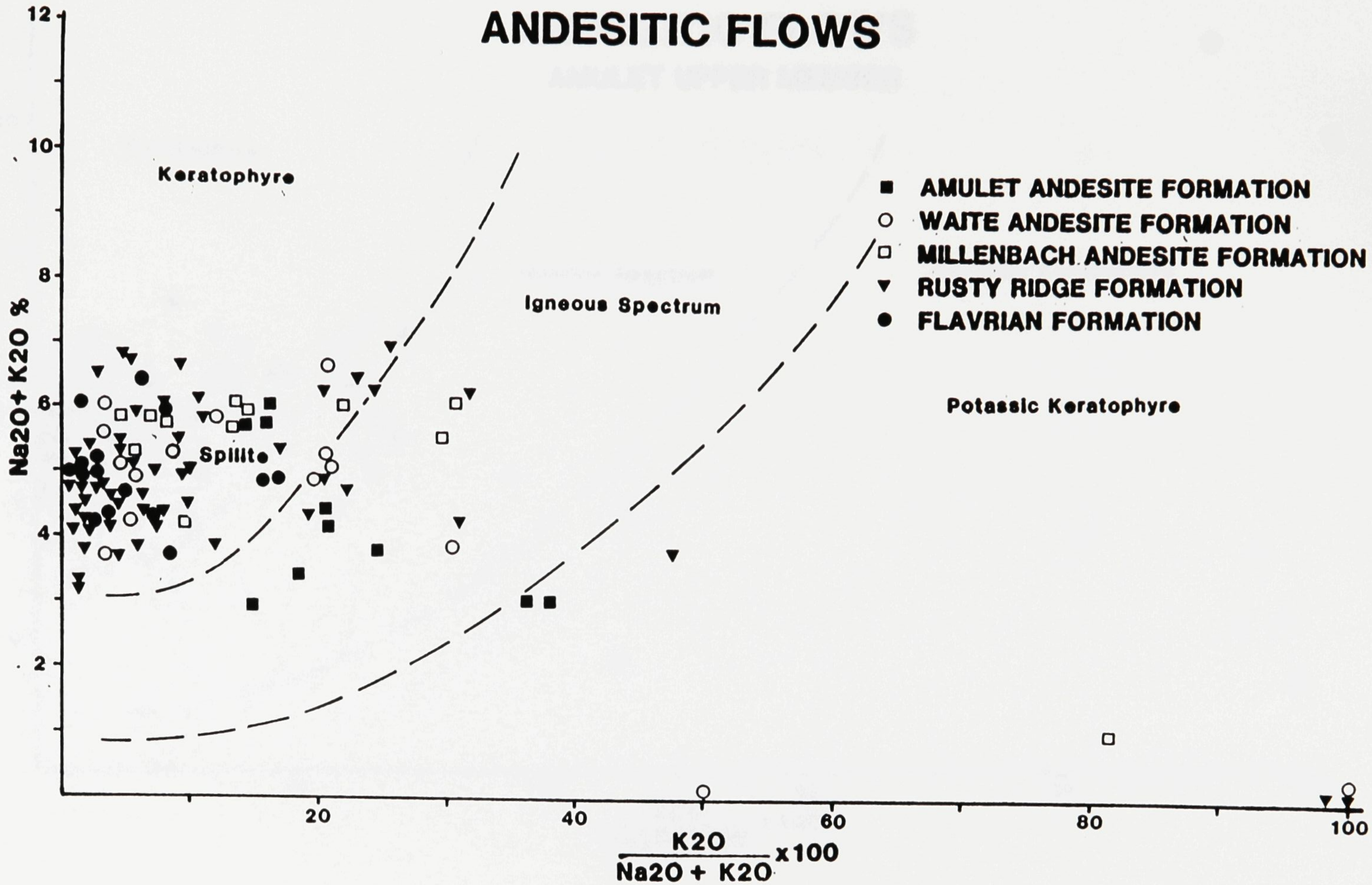

Figure 12.2. Alkali ratio diagram (Hughes, 1976) illustrating the spilitic affinity of Mine Sequence andesitic flows.

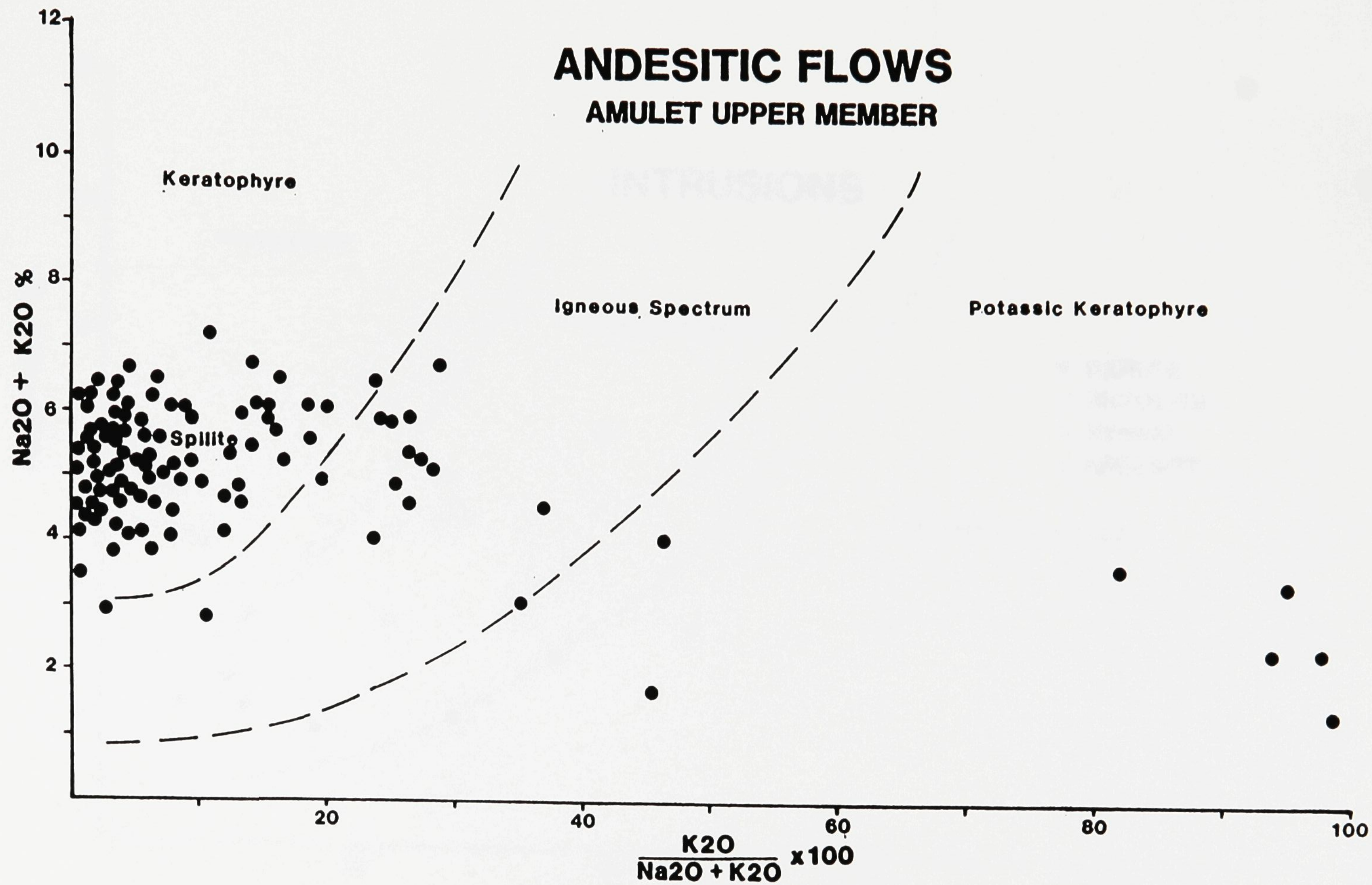

Figure 12.3. Alkali ratio diagram (Hughes, 1976) illustrating the spilitic affinity of silicified andesite flows of the Amulet upper member.

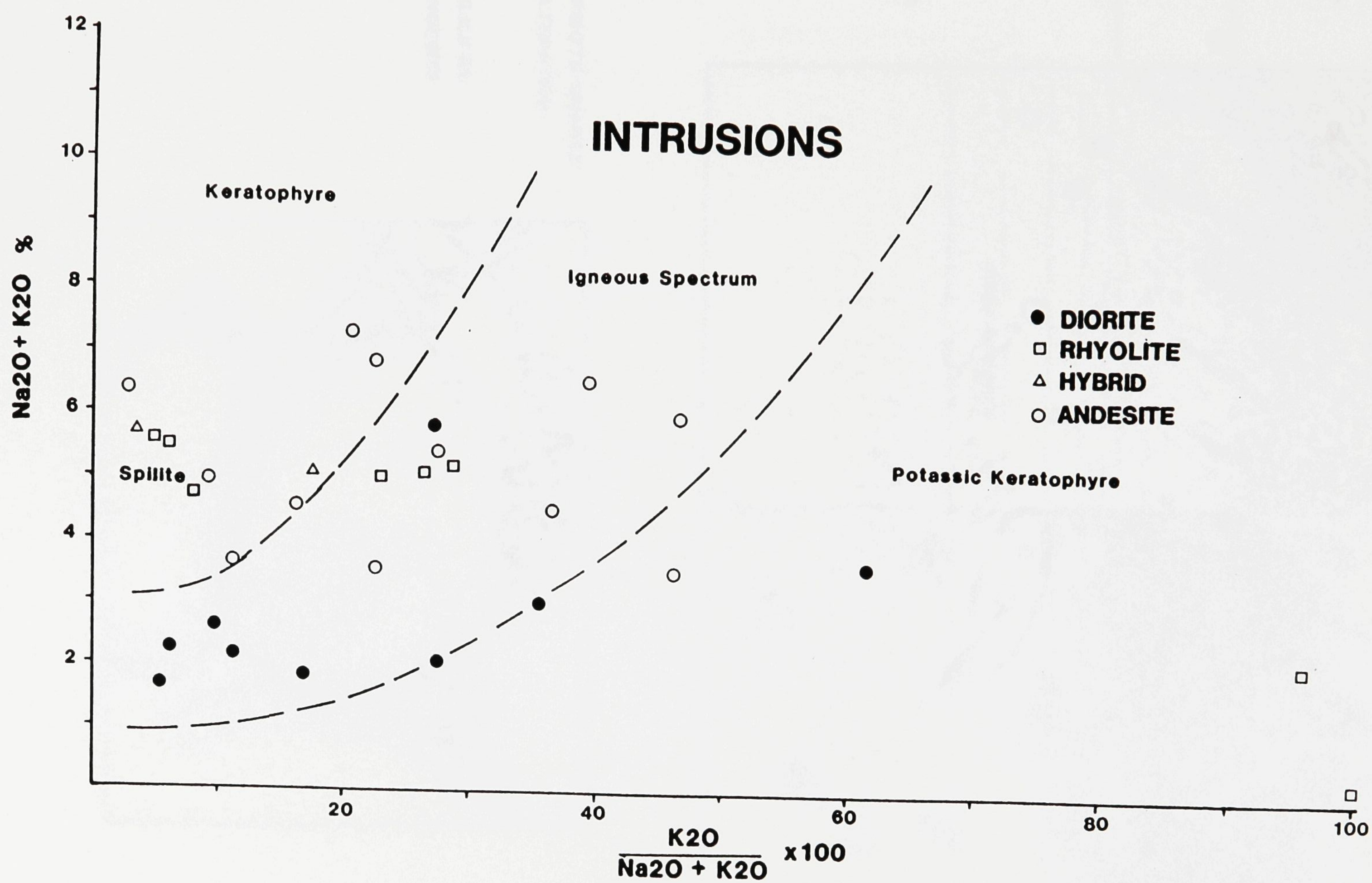

Figure 12.4. Alkali ratio diagram (Hughes, 1976) illustrating the spilitic affinity of rhyolitic and andesitic sub-volcanic intrusions. Note, that except for 1 sample, data for the later diorite intusions fall in the igneous spectrum field.

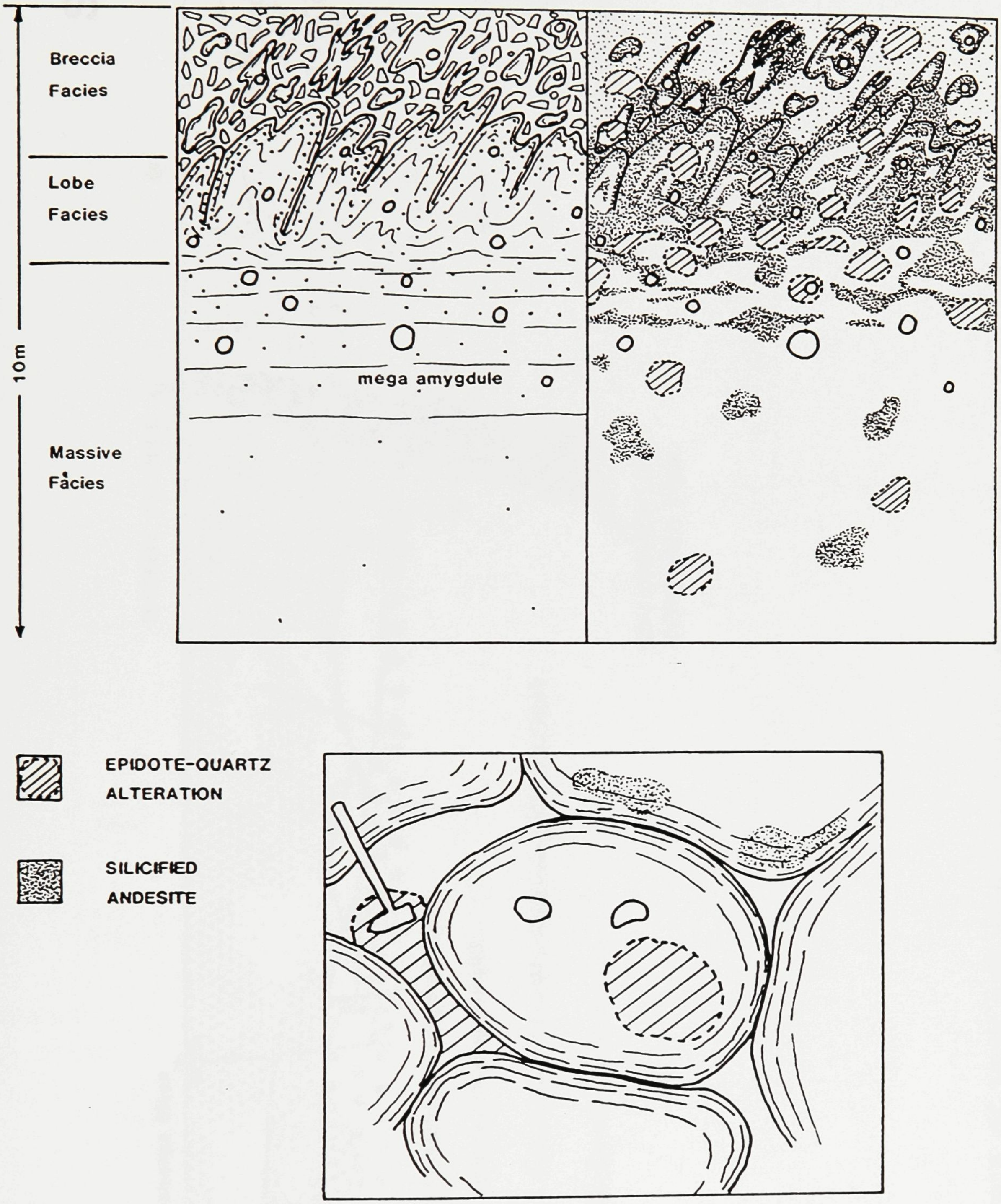

Figure 12.6. Distribution of epidote-quartz alteration and silicification within massive and pillowed andesitic flows of the Waite upper member.

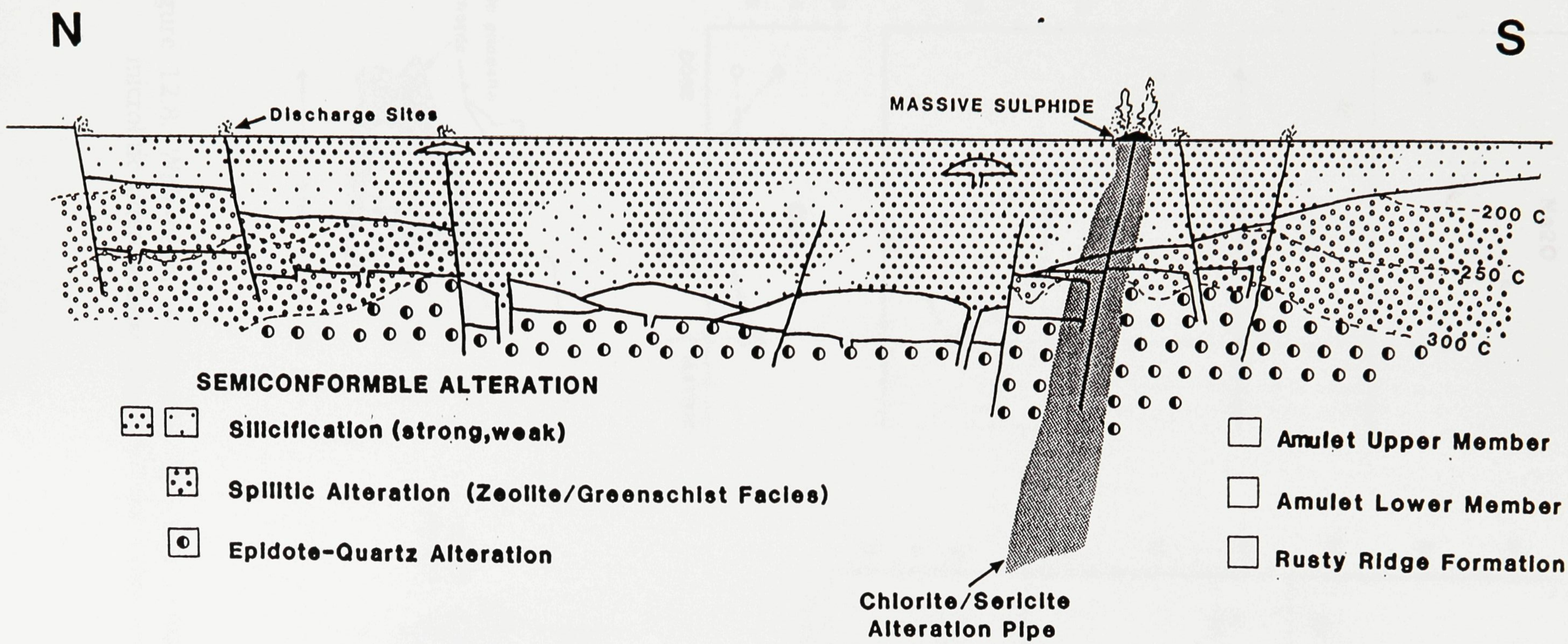

Figure 12.7. Areas of weak and strong silicification within andesitic flows of the Amulet upper member.

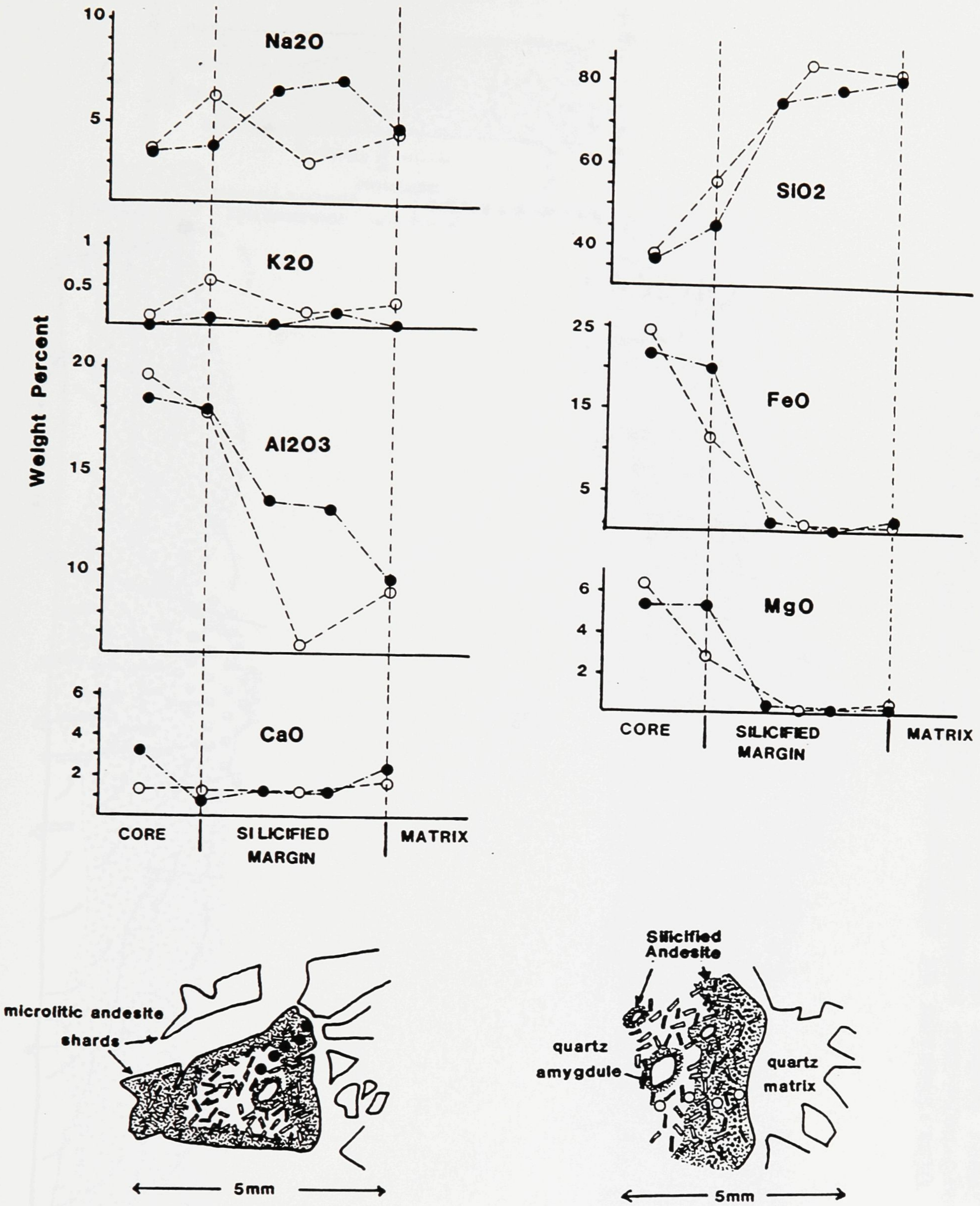

Figure 12.8. Wide-beam microprobe traverses across the silicified margins of microlitic sideromelane shards (Waite upper member).

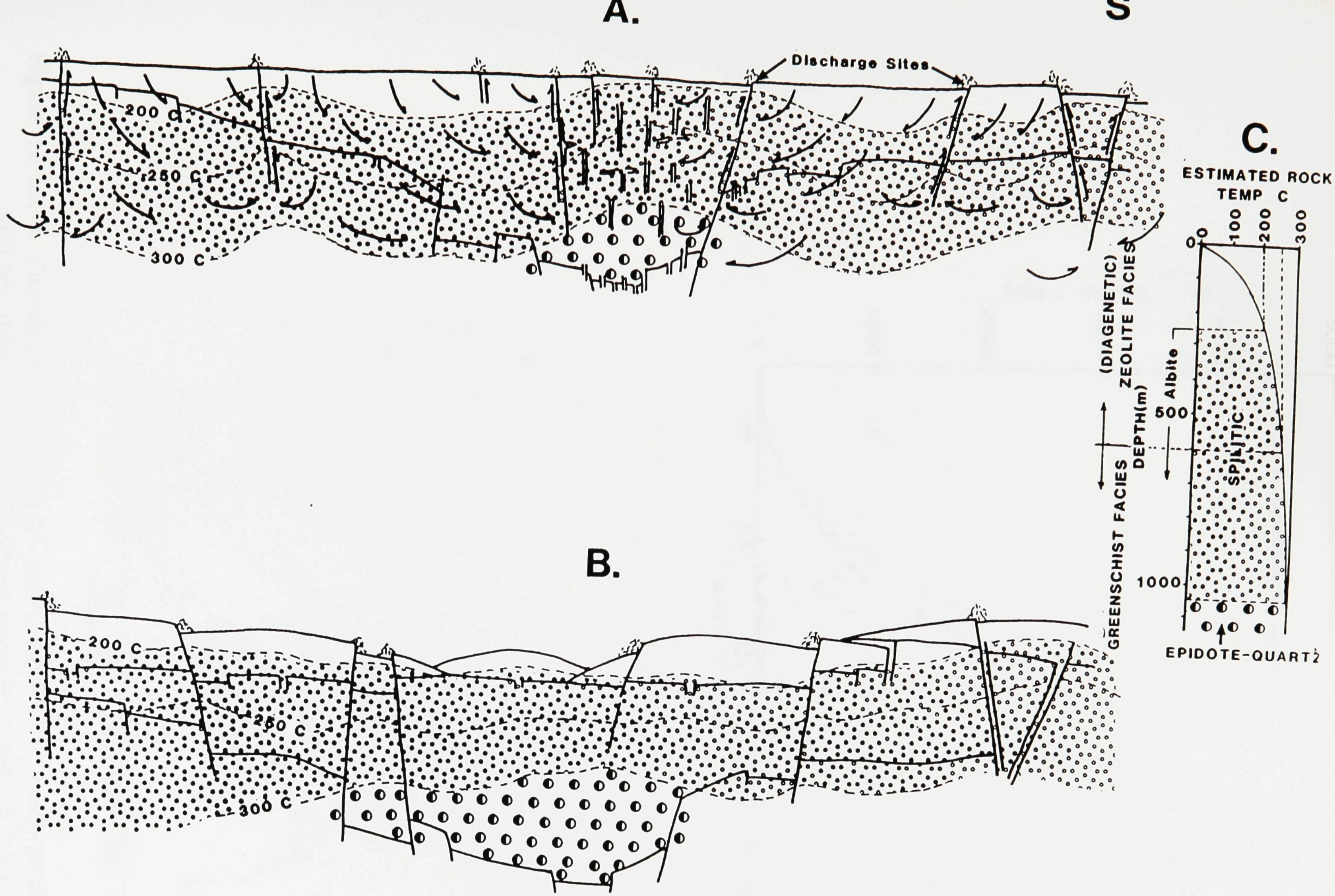

Figure 12.9. Distribution of alteration types and paleo-isotherms within a sub-seafloor hydrothermal system post extrusion of the Rusty Ridge formation (A) and Amulet lower member (B). Temperature data from Spooner (1975), Heaton and Sheppard (1975) and Mehegan <u>et al.,</u> (1982).

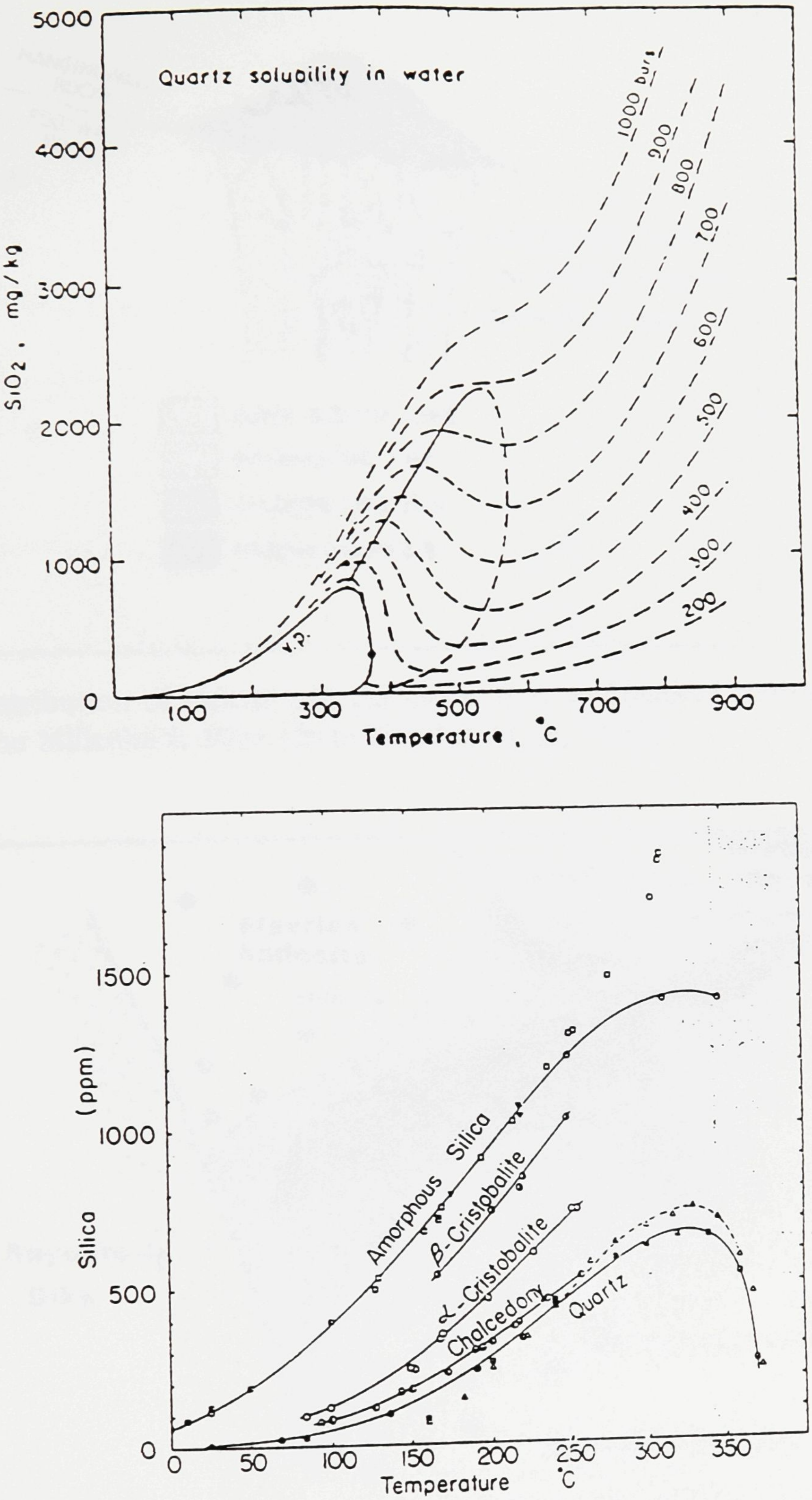

Figure 12.10. A. Calculated solubilities of quartz in water at temperatures up to 900 and indicated pressures (from Fournier, 1985). B.The solubilities of quartz,chalcedony, cristobolite and amorphous silica at the vapour pressure of the solutuon (from Fournier and Rowe, 1966).

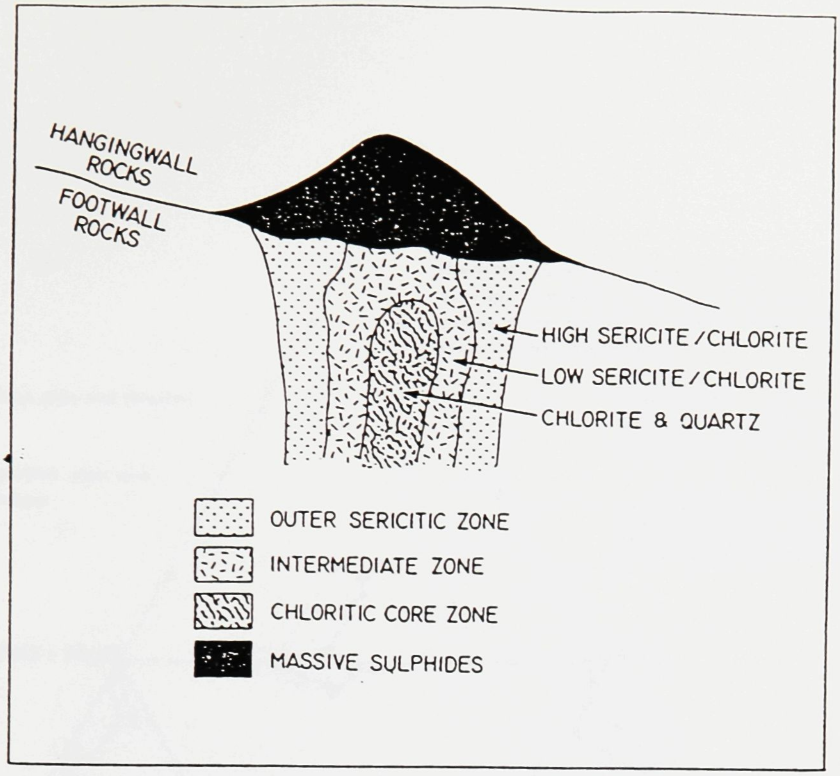

Figure 12.11. Distribution of sericite and chlorite within an idealized alteration pipe at the Millenbach Mine (from Knuckey et al., 1982).

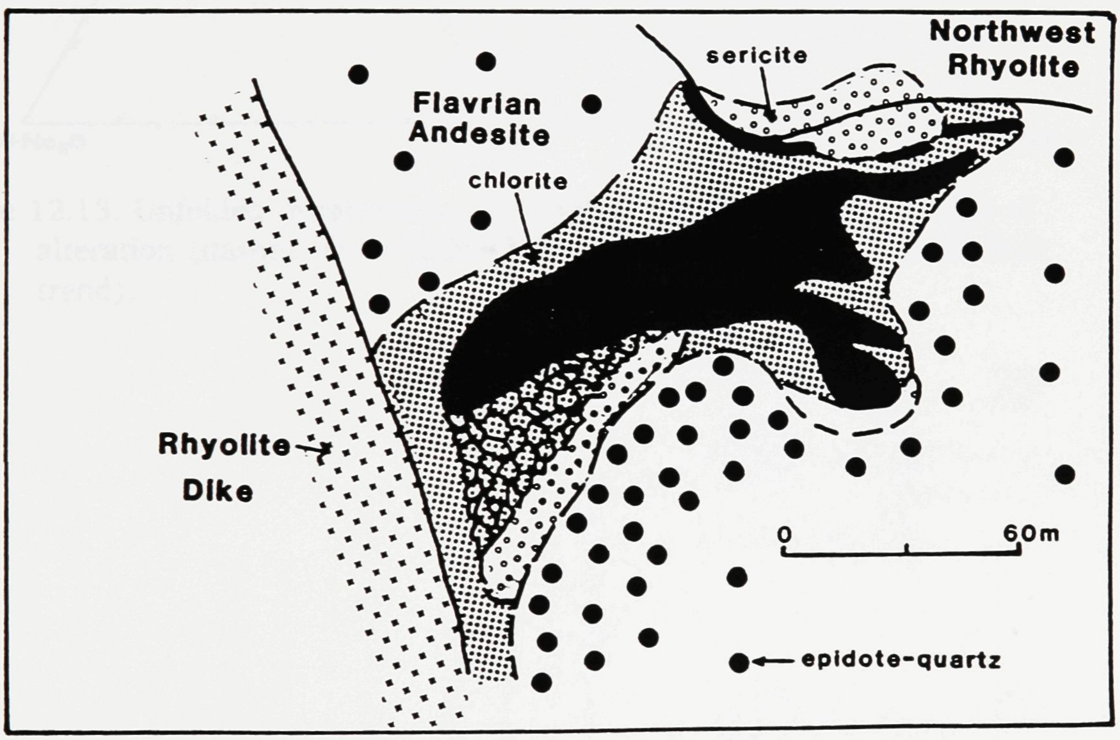

Figure 12.12. Distribution of chlorite, sericite and epidote-quartz alteration at the Corbet Mine, section 800N (after Watkins, 1980). Compare with Figure C.5.

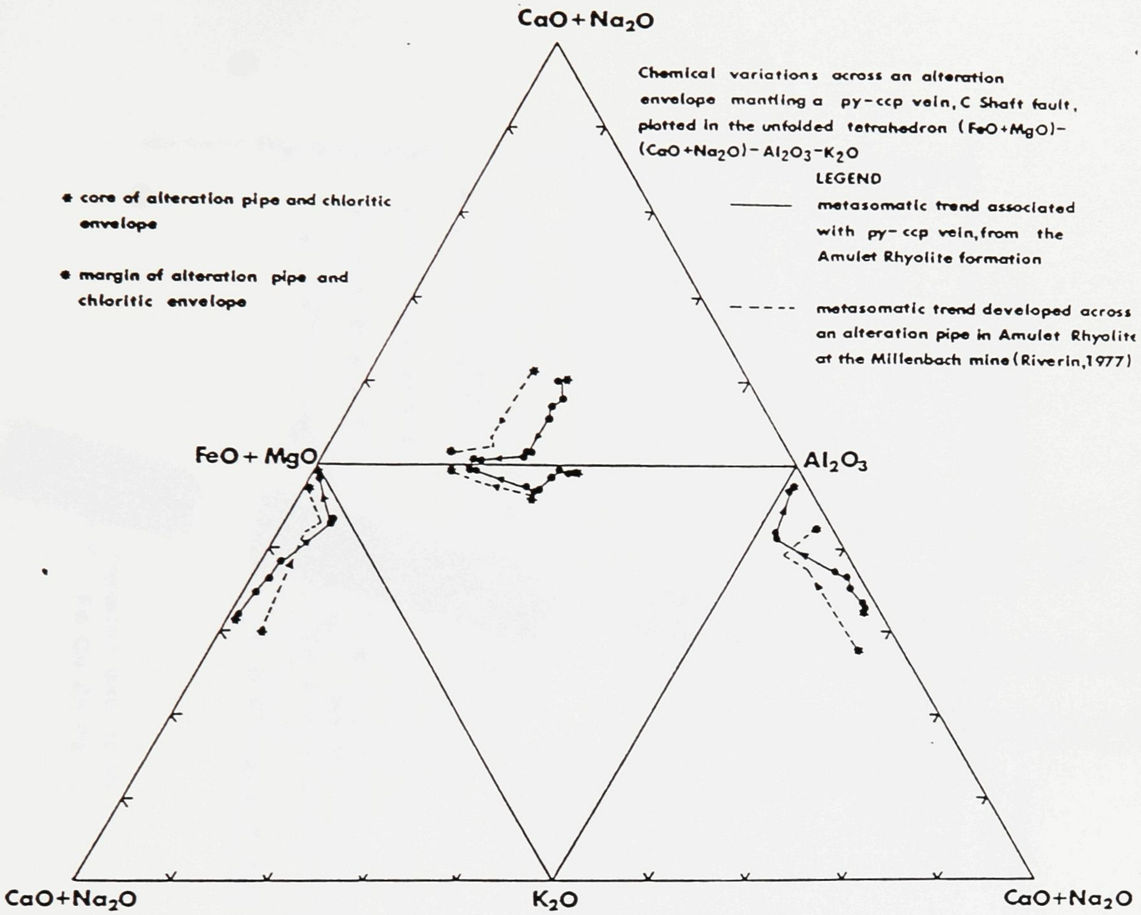

Figure 12.13. Unfolded tetrahedron after Riverin (1977), showing trends of alteration (dashed line = Millenbach trend, solid line = C shaft fault trend);

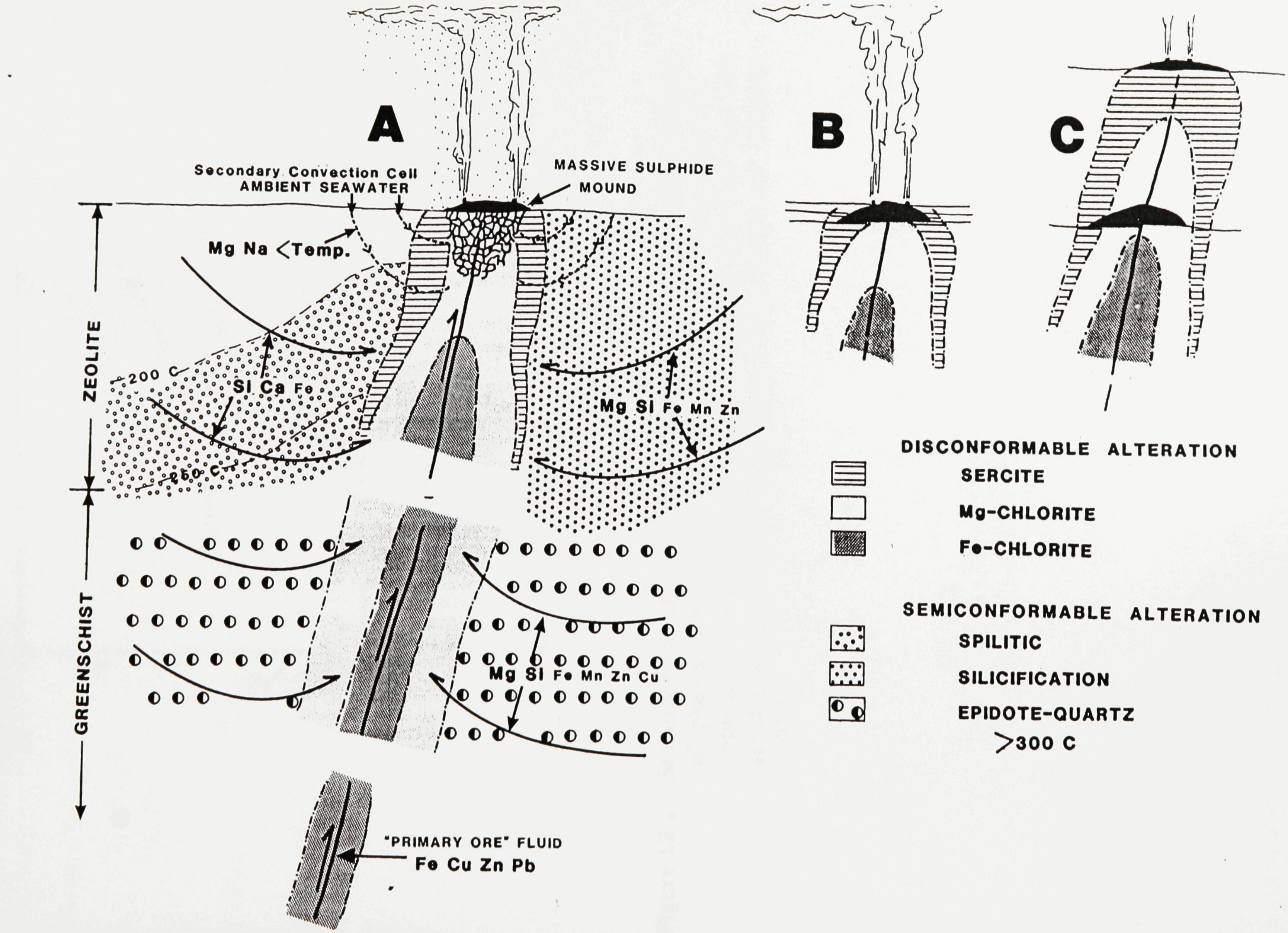

Figure 12.14. A - Interpreted evolution of Mg-chlorite and sericite alteration assemblages during mixing of an ascending "primary ore fluid" with high temperature intrastratal fluid and downward migrating seawater.
B, C - Progressive upward migration of the alteration assemblages in a long-lived discharge site.

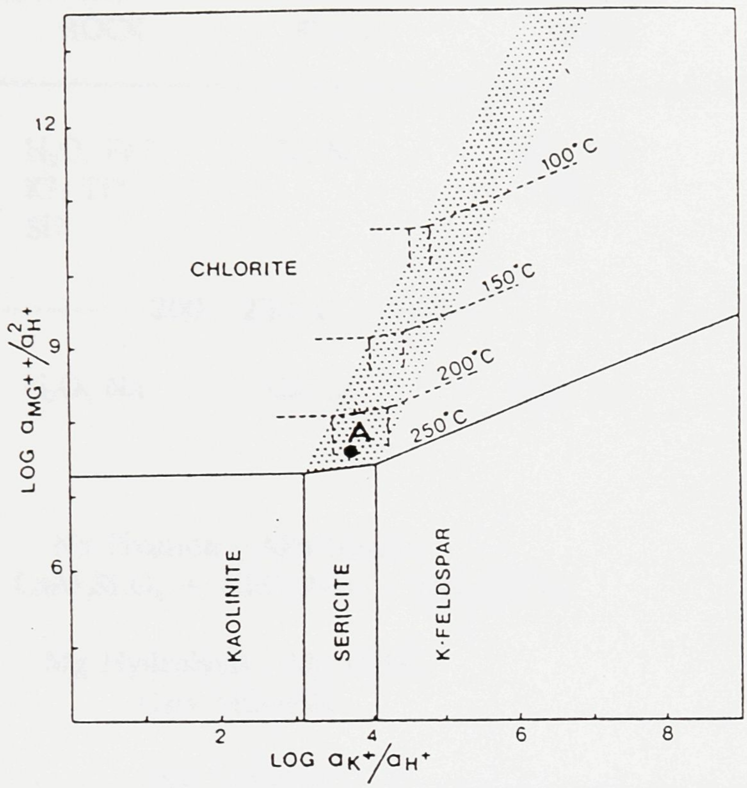

Figure 12.15. Stability fields of chlorite, sericite, kaolinite and potassium feldspar; all phases in equilibrium with quartz. Shaded area outlines the approximate limits of composition of solution which will react with sericite-bearing rocks to form chlorite. After Riverin and Hodgson, (1980).

TABLE 12.1. SEMICONFORMABLE ALTERATION TYPES

ALTERATION TYPE	CHEMICAL CHANGES[1] FLUID	ROCK	EXPERIMENTAL RESULTS[2] FLUID	ROCK	MINERALOGY
Diagenetic	Si, Al, Mg Ca, Na, Fe?	H_2O, Fe? K?, Ti? Si?	Ca, Si	H_2O, Na Mg	Palagonite Zeolites Clays Oxides
200 - 250°C					
Spilitic	Ca, Mg?	H_2O, Na	Ca, Si	H_2O, Na	Chlorite Sericite Epidote Albite

Na Fixation - Albitization

$$2Na + CaAl_2Si_2O_8 + 4SiO_2 \rightleftharpoons Ca + 2NaAlSi_3O_8$$

Mg Hydrolysis - Mg $(OH)_2$
Clay Minerals

ALTERATION TYPE	CHEMICAL CHANGES[1] FLUID	ROCK	EXPERIMENTAL RESULTS[2] FLUID	ROCK	MINERALOGY
300 - 330°C					
Epidote-Quartz	Mg, Na, K Ti, Cu, Zn	Ca	Si, Fe, Mn Cu, Zn	Ca, Na?	Epidote Quartz

(Ca Hydrolysis)

$$3NaAlSi_3O_8 + 2Ca + OH \rightleftharpoons Ca_2Al_3Si_3O_{12}(OH) + 3Na + 6SiO_2$$

ALTERATION TYPE	CHEMICAL CHANGES[1] FLUID	ROCK	EXPERIMENTAL RESULTS[2] FLUID	ROCK	MINERALOGY
Silicification	Fe, Mg, Ca Ti, Mn, Zn Al?	Si			Quartz Albite

Additions
[1] Assumed and calculated
[2] Measured in experiments

References: Bishop and Dickson, 1975
Gibson, 1979 and Gibson et al, 1983
Lesher et al, 1986
Mottl and Holland, 1979
Mottl, 1983
Rosenbauer and Bischoff, 1984
Seyfried and Bischoff, 1977 and 1979
Seyfried and Janecky, 1985
Seyfried et al, 1988

TABLE 12.2. CHEMICAL COMPOSITION OF EPIDOTE-QUARTZ ALTERED ANDESITE AND ADJACENT LEAST ALTERED ANDESITE

	Least Altered	Epidote Quartz Altered	Least Altered	Epidote Quartz Altered
	83-210[2]	83-211[2]	82-88[1]	82-87[1]
SiO_2 %	57.7	54.0	57.4	58.0
Al_2O_3	16.2	17.2	15.6	14.6
Fe_2O_3*	10.1	6.9	8.8	8.4
MgO	2.4	0.6	2.9	0.0
CaO	2.9	17.7	5.4	15.1
Na_2O	5.2	0.1	4.5	0.2
K_2O	0.7	0.1	0.1	0.0
TiO_2	1.1	0.8	1.5	1.1
P_2O_5	0.4	0.3	0.2	0.0
MnO	0.2	0.15	0.2	0.1
LOI	2.0	2.4	-	-
Ba ppm			30	0
Cr	20	<10	45	34
Zr	220	130	131	99
Sr	110	220	129	393
Rb	20	<10	0	0
Y			37	27
Nb			2	4
Zn			91	1
Ni			1	0

* Total Fe as Fe_2O_3

XRF Fused Pellet Analyses, Ottawa University[1] and X-Ray Assay Laboratories[2]

TABLE 12.3. CHEMICAL COMPOSITION OF SILICIFIED AND ADJACENT LEAST ALTERED ANDESITE

	Least Altered	Silicified	Least Altered	Silicified
%	BH-1	BH-2	83-210	83-212
SiO_2	62.9	73.7	57.70	77.10
Al_2O_3	14.1	12.2	16.20	9.65
Fe_2O_3*	10.1	3.19	10.10	2.70
MgO	2.61	0.91	2.42	0.59
CaO	2.10	3.18	2.86	3.57
Na_2O	3.95	4.61	5.15	3.57
K_2O	0.19	0.16	0.71	0.13
TiO_2	0.96	0.52	1.10	0.88
P_2O_5	0.29	0.13	0.37	0.29
MnO	0.20	0.07	0.18	0.05
LOI			2.00	0.85
ppm				
Ba	140	80		
Cr	5	3	20	10
Zr	233	267	220	180
Sr	90	143	110	100
Rb	2	2	20	10
Y	43	40		
Nb				
Zn	160	60		
Ni				

* Total Fe as Fe_2O_3, LOI = loss on ignition

BH-1 and BH-2, Amulet upper member at Buttercup Hill.

83-210 and 83-212, Waite upper member.

PLATE 12.1

A. Waxy yellow palagonite along shard margins display the laminar and botryoidal form that is typical of gel palagonite. Subglacial basaltic hyaloclastite from Laugarvatin, Iceland.

B. Chloritized obsidian shard from the matrix of rhyolitic breccias that occupy the Despina fault.

C. Close-up of the shard in **B.** showing the laminar and botryoidal forms of former gel palagonite now replaced by massive, homogeneous chlorite. Fine oxides define the laminar and botryoidal forms within chlorite.

D. Strongly palagonitized basaltic hyaloclastite with circular to ovoid fibrous textured granules. The granules may represent zeolites within shards or possibly filling amygdules. Note the concentric palagonite rims surrounding the granules.

E. Chloritized andesitic hyaloclastite from the Rusty Ridge formation showing similar fibrous, chloritic granules as in **D.** Former glassy groundmass is replaced by chlorite.

F. Crossed-nicols photo of **E.** shows silicification of the andesitic hyaloclastite. Quartz is interpreted to replace former glass or palagonite leaving the chloritic granules intact.

G. Arcuate perlitic cracks in chloritized, plagioclase porphyritic, andesitic vitrophyre from the Amulet upper member.

H. Close-up of a perlitic crack in **G.** where chalcedony has a laminar, banded and fibrous habit interpreted to have replaced former palagonite

Field of view in A, B and G is 4mm.
Field of view in D, E, F, is 3mm.
Field of view in C and H is 0.9mm.

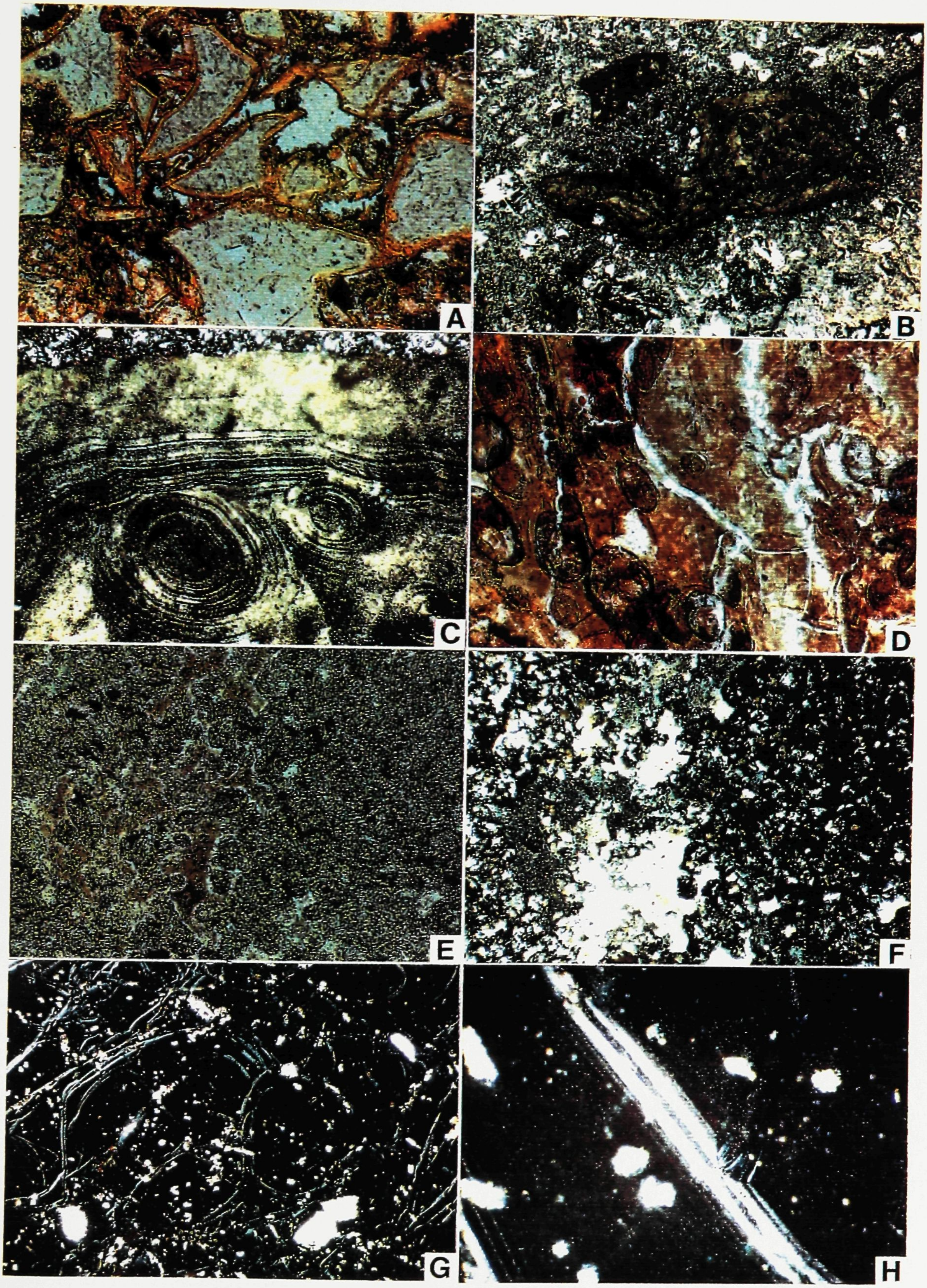
A
B
C
D
E
F
G
H

PLATE 12.2

A. Silicification localized along perlitic cracks in vitrophyre of Plates 12.1 G and H. Optically and form oriented chalcedony replaces vitrophyre (now chlorite) adjacent to perlitic cracks; fine oxides define the crack.

B. Pervasively silicified andesitic vitrophyre as in **A.** Perlitic cracks acted as the loci for alteration that resulted in the replacement of former glass, now chlorite, by chalcedony.

C. Typical least altered, intersertal textured, andesitic massive flow. Rusty Ridge formation, south of Duprat lake.

D. Incipient silicification of andesite in **C**. Silicification is characterized by the occurrence of quartz blebs in the groundmass where fine, chalcedony is interpreted to replace former glass leaving the microlites intact. Individual quartz blebs coalesce to produce larger silicified areas.

E. Complete silicification of andesite in **C**. Quartz blebs are still apparent within a pervasively silicified, microlitic groundmass. Original glass, now chlorite, occurs as isolated islands within the silicified groundmass.

F. Typical pillow margin characterized by microlites and microphenocrysts of plagioclase in a groundmass of massive, homogeneous chlorite that presumably replaced former glass. Note the dendritic albite crystallites nucleated on the quenched microlite.

G. Incipient silicification of the pillow margin in **F**, where the former glassy groundmass, now chlorite, is replaced by chalcedony leaving albite microlites and phenocrysts intact.

H. Epidote-quartz altered andesite from the Waite upper member. The intersertal texture is obliterated as are the primary minerals leaving a granular assemblage of epidote and quartz. The amygdule is also filled by epidote.

Field of view in A, F and G is 0.9mm.
Field of view in B, C, D, E and H is 4mm.

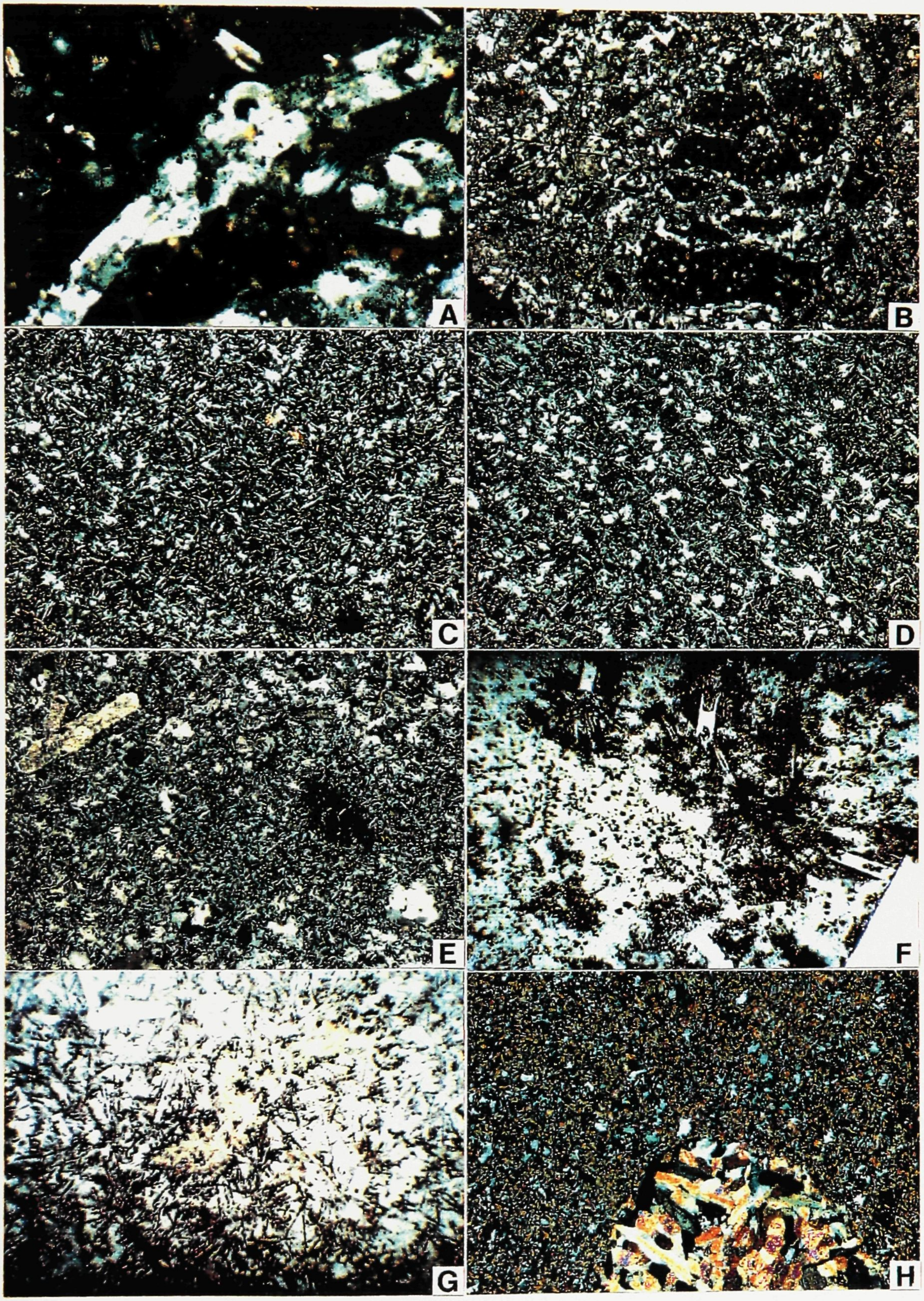
A
B
C
D
E
F
G
H

PLATE 12.3
Field of view for all photos is 4mm

A. Oxide-rich crusts and borders to andesitic shards. Hyaloclastite flow top breccia, Amulet upper member. Bar is 1mm long.

B. The bulbous or coliform structure of mineralogically distinct layers is consistent with successive encrustations during amygdule infilling (Waite upper member).

C.and D. Silicified and quartz cemented hyaloclastite flow top breccia of the Rusty Ridge formation. Form and optically oriented chalcedony replaces shard margins and is similar to chalcedony that cements the fragments except that the former contains numerous fine opaque minerals. A fine oxide crust, which mantles most shards, separates the silicified shard rim from matrix chalcedony.

E. Clusters of fibrous, radiating chlorite which infill this amydule are interpreted to replace former zeolites or an intermediate precursor mineral such as pumpellyite (Northwest formation).

F. Fibrous, radiating clinozoisite which infills this amygdule is interpreted to pseudomorph former zeolites or an intermediate precursor mineral (Northwest formation).

G. Silicified obsidian hyaloclastite from the #3 flow of the Amulet lower member. Fine chalcedony replaces former glass, now chlorite, along perlitic cracks. The fibrous, form oriented nature of the chalcedony, which contains numerous fine oxides suggests, is consistent with replacement of former palagonite.

H. Silicified rhyolite hyaloclastite as in **G.** Ring-like. botryoidal forms outlined by fine opaque minerals are interpreted as relict forms of former gel-palagonite or saponite now replaced by chalcedony (refer to Plate **12.1C**).

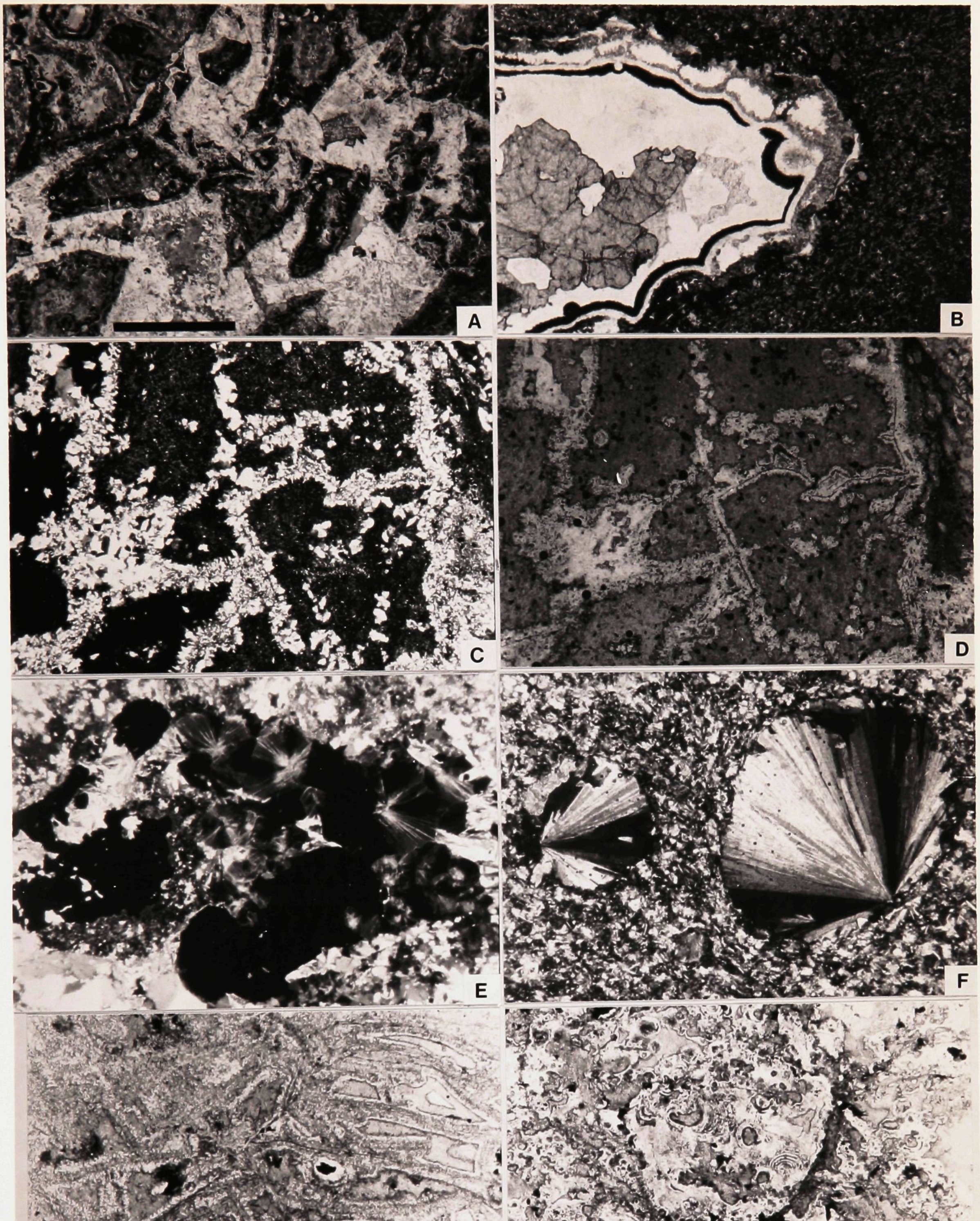
A
B
C
D
E
F
G
H

PLATE 12.4

A.,B.,C. and D. Silicified, microlitic, sideromelane shard hyaloclastite of the Waite upper member. Shards were silicified and replaced by chalcedony externally, along their margins, and internally, adjacent to contained amydules, leaving cores of chloritized microlitic sideromelane. Numerous fine opaque minerals within the chalcedony, its fibrous, form oriented character and the occurrence of oxide crusts on shards suggests that the chalcedony may have replaced former palagonite. A thin crust of chalcedony commonly mantles both shard and amygdule margins which suggests that silicification was accompanied by silica deposition within pore spaces that, in some instances as in **D.**, completely cemented the breccia. The typical mineralogical zonation in both the matrix and amygdules from chalcedony to chlorite to epidote is interpreted to replace a primary filling sequence of chalcedony, clay minerals and zeolites respectively.

Field of view in A.B.and C. is 4mm.
Bar in C. is 1mm long

Field of view in D. is 3mm
Bar is 1mm long.

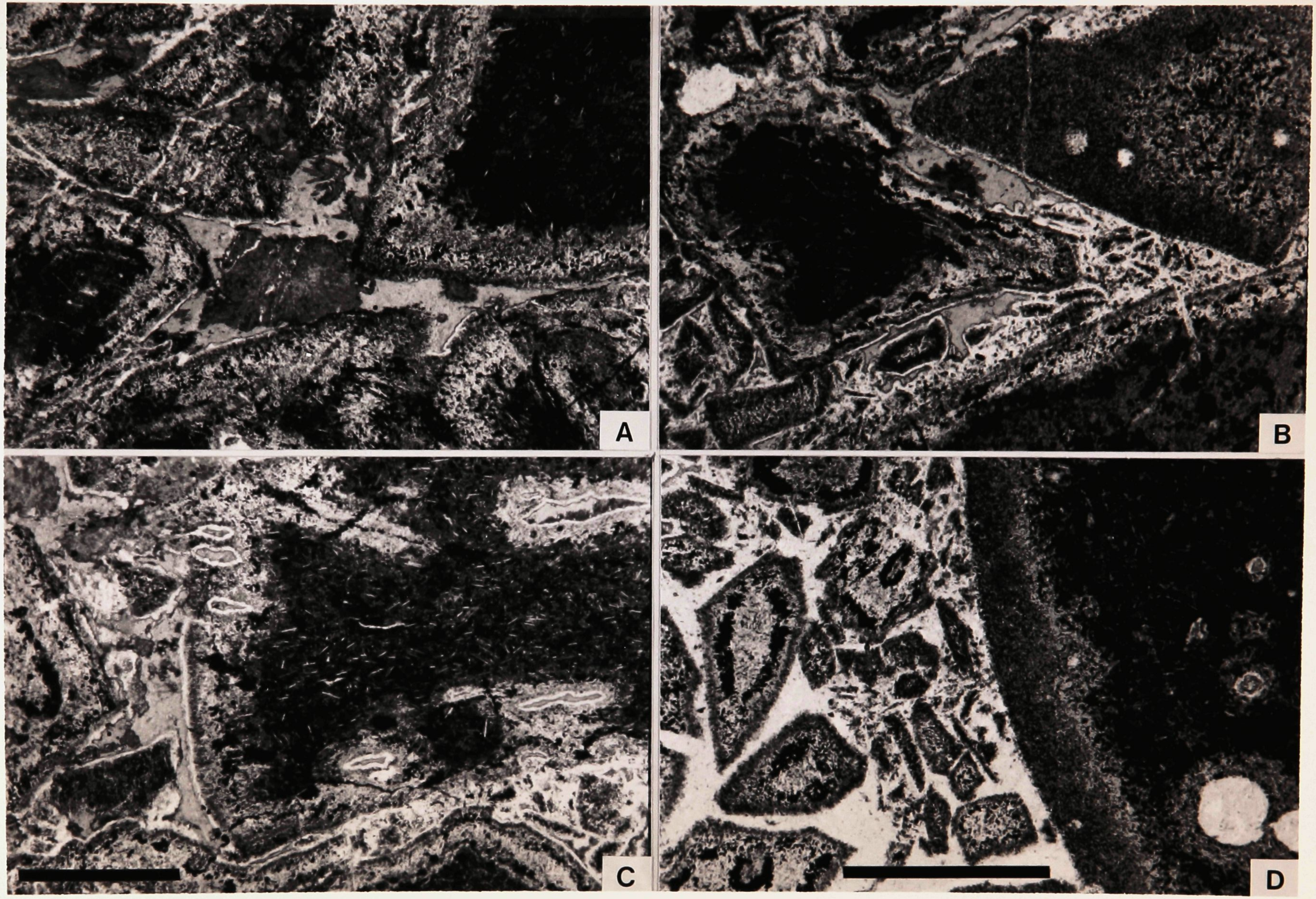
A
B
C
D

Plate 12.5. Light-green, resistant, irregular epidote-quartz alteration patches in andesitic massive flow, Rusty Ridge formation.

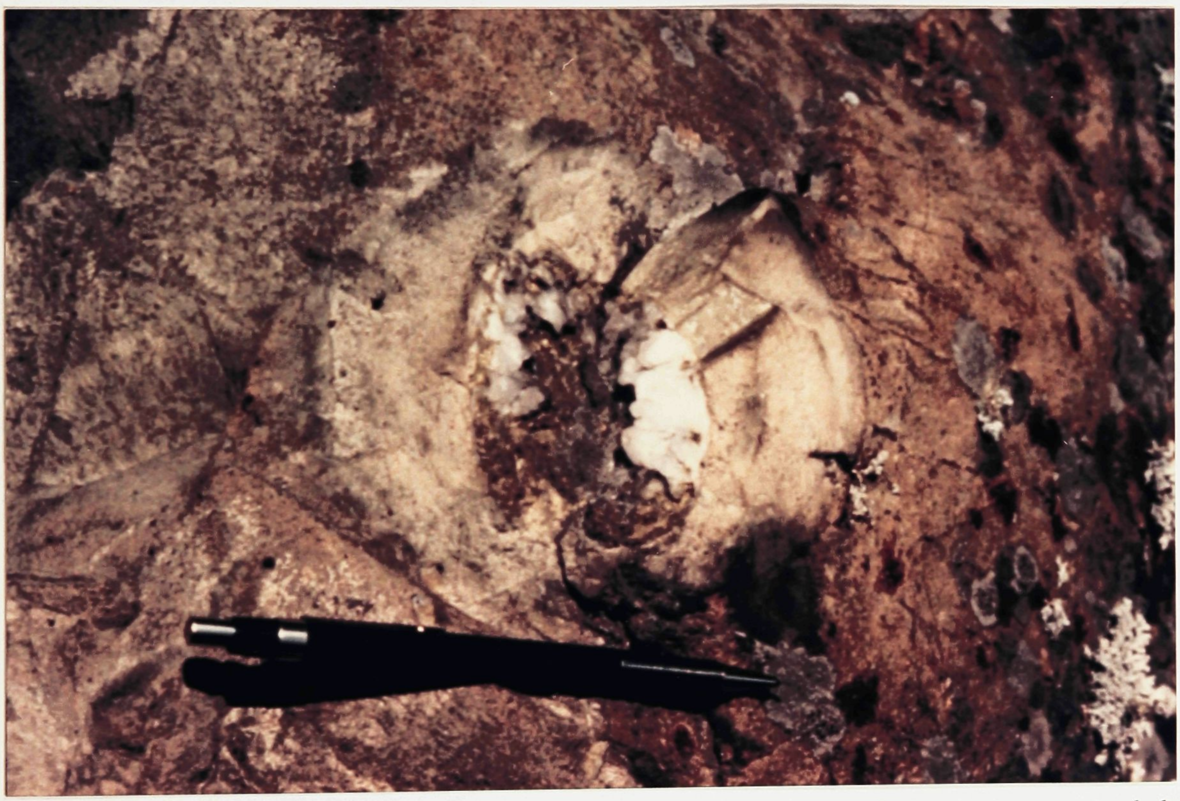

Plate 12.6. Epidote-quartz alteration patch centred on a large mega-amygdule infilled by quartz and epidote (Rusty Ridge formation).

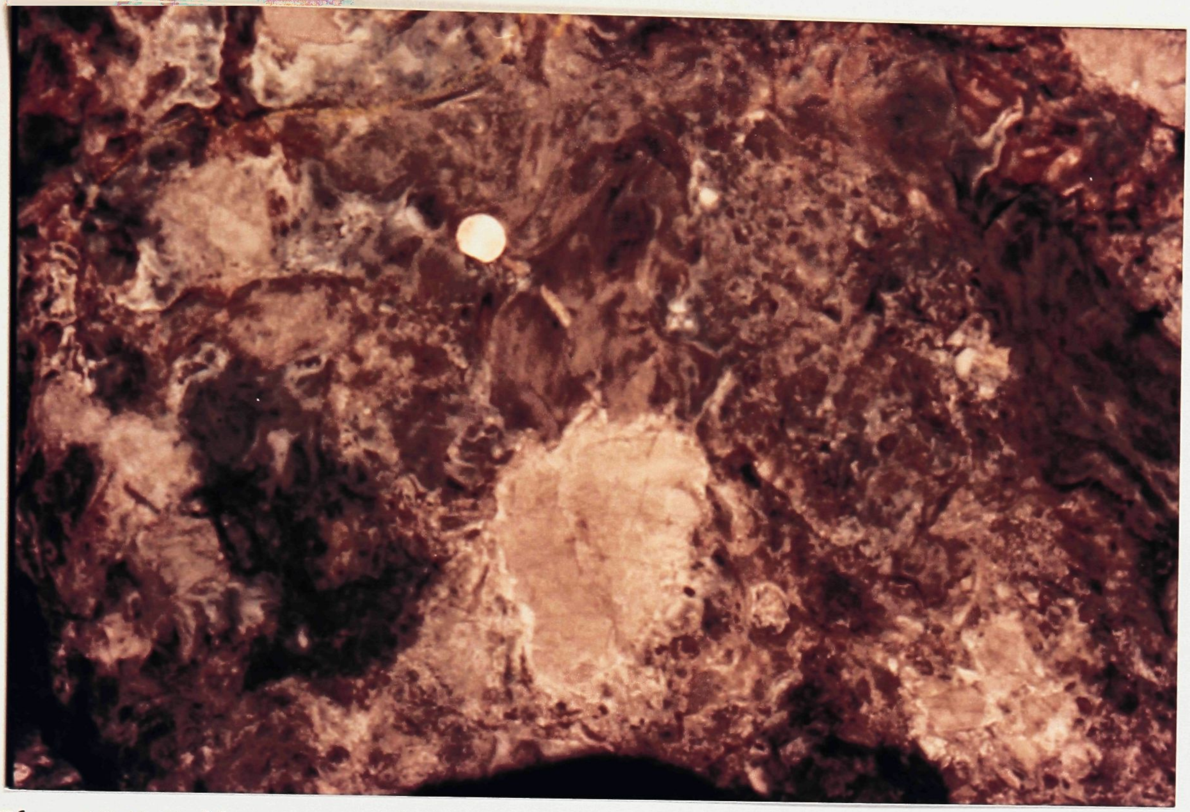

Plate 12.7. Epidote-quartz alteration patches in an andesitic, hyaloclastite flow top breccia. The alteration patches occur both with fragments and matrix and often cross fragment boundaries (Waite upper member).

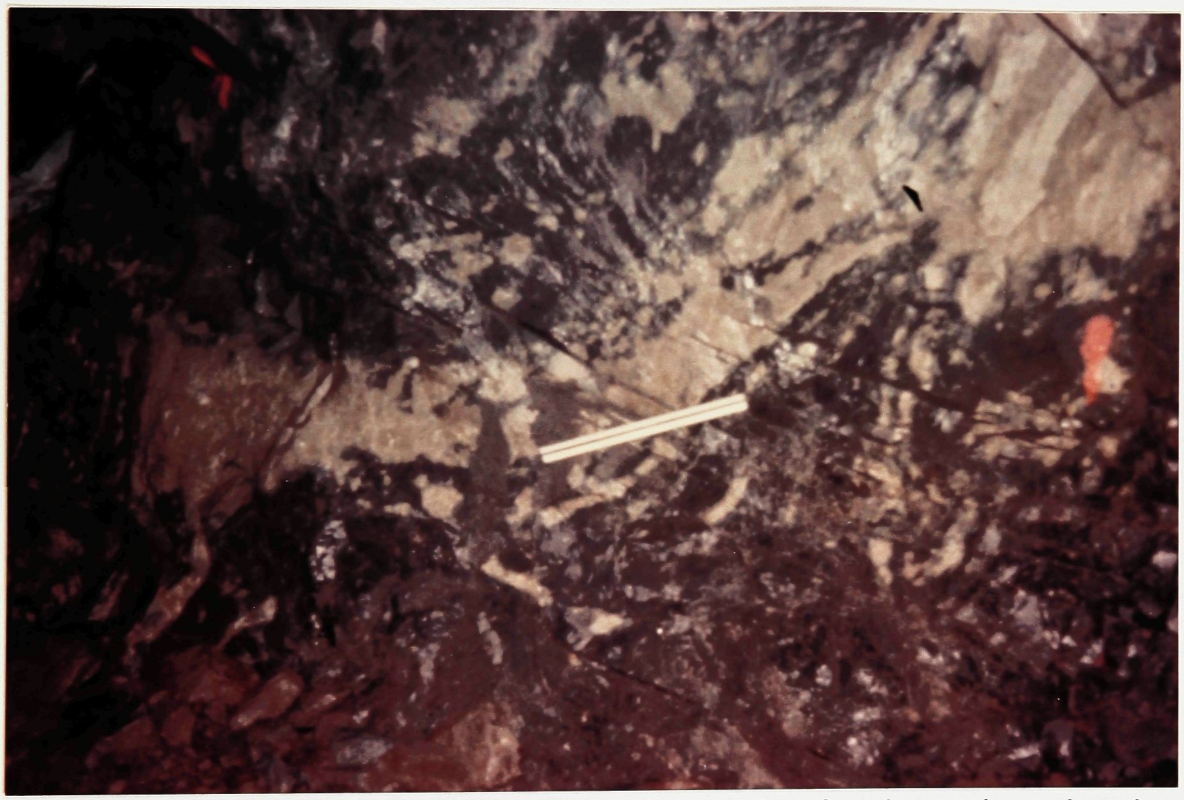

Plate 12.8. Coalescing epidote-quartz alteration patches forming an irregular pipe-like body within the upper member of the Amulet formation at the Millenbach Mine.

Plate 12.9. Silicified pillow margins, Waite Andesite formation.

Plate 12.10. Completely silicified pillows of the Waite Andesite formation. Note the chloritized pillow selvedges are not silicified.

Plate 12.11. Incipient silicification centred about a mega-amygdule (Waite upper member). The granular, diffuse character of the silicified area reflects the development of blebby quartz within the groundmass (refer to Plate 12.2 D and E). The amydule is infilled by laminar chalcedony and epidote.

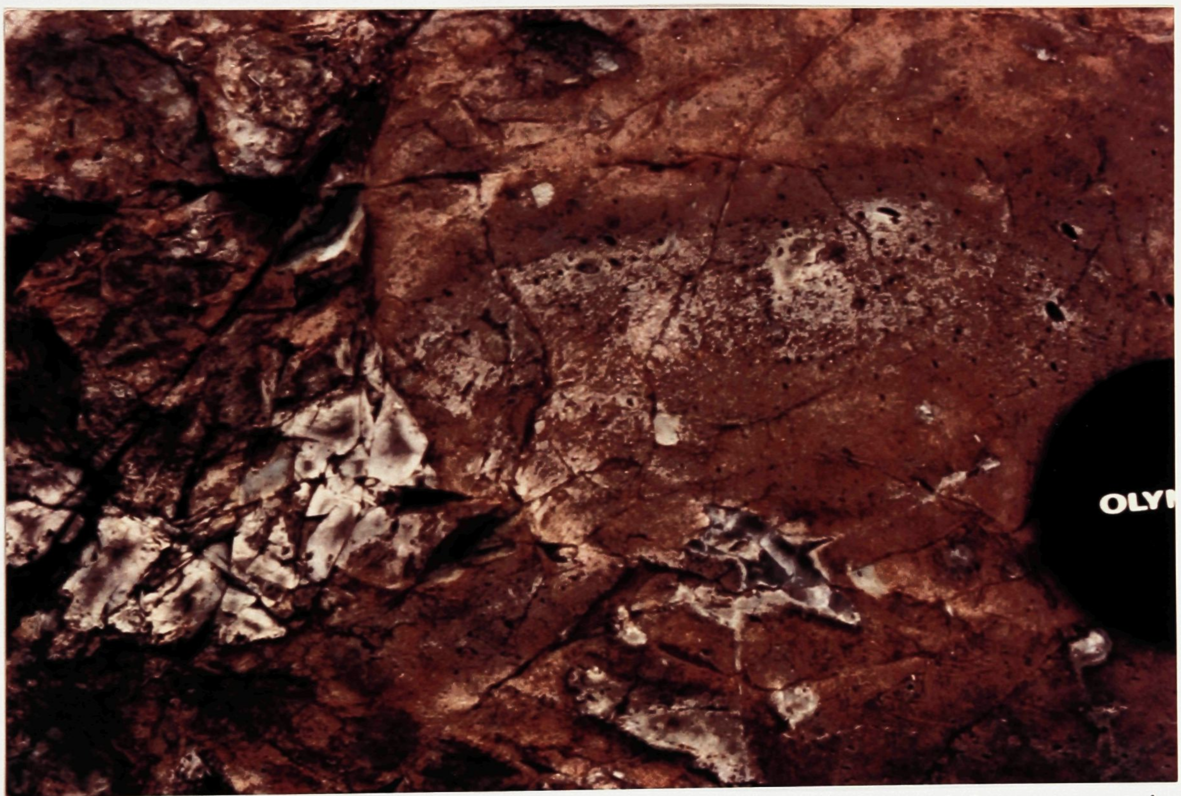

Plate 12.12. Silicification preferentially located along an amygdule zone, Waite upper member.

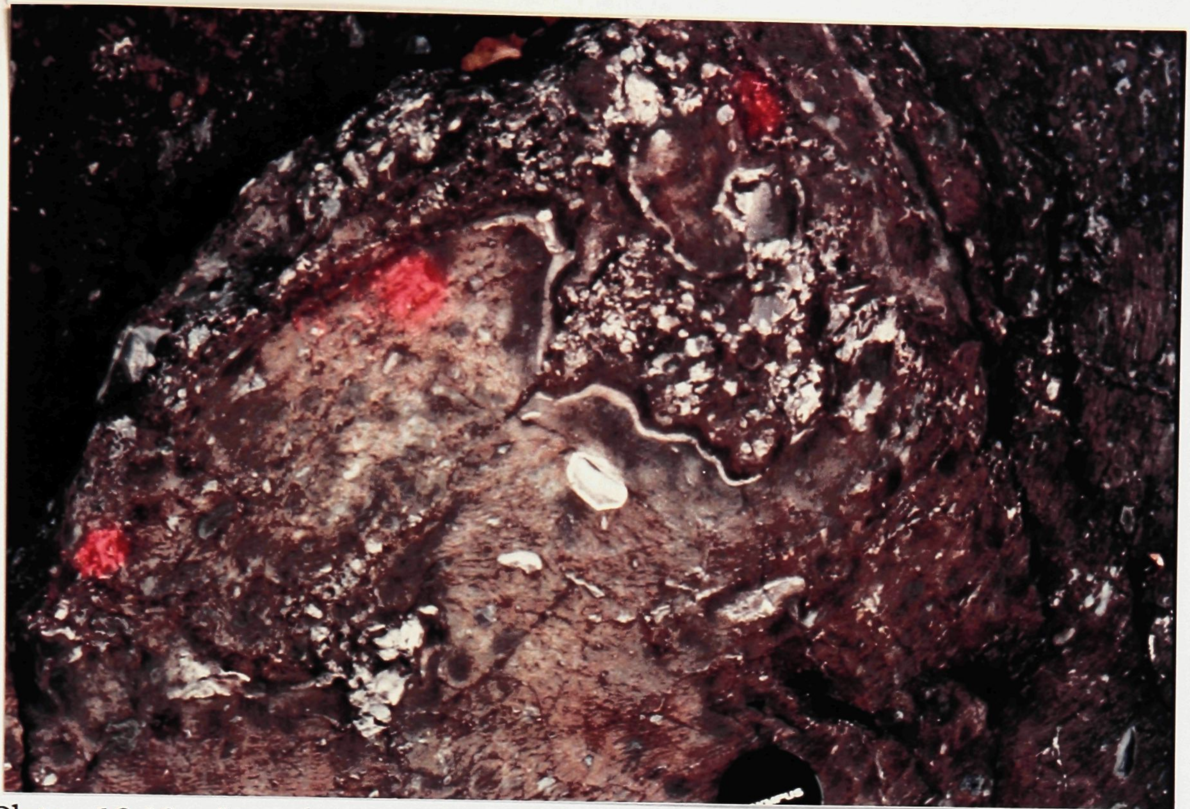

Plate 12.13. Irregular, patchy silicification along a laminar jointed and amygdaloidal flow top in contact with overlying flow breccia.

Plate 12.14. Pseudo-flowbanding, a result of silicification along an amygdule zone and laminar joints.

Plate 12.15. Silicification of andesitic hyaloclastite and fragments within a flow top breccia (Waite upper member). Note the preferential silicification of shard margins and quartz within the breccia matrix. Plate 12.4 A,B,C and D from this locality.

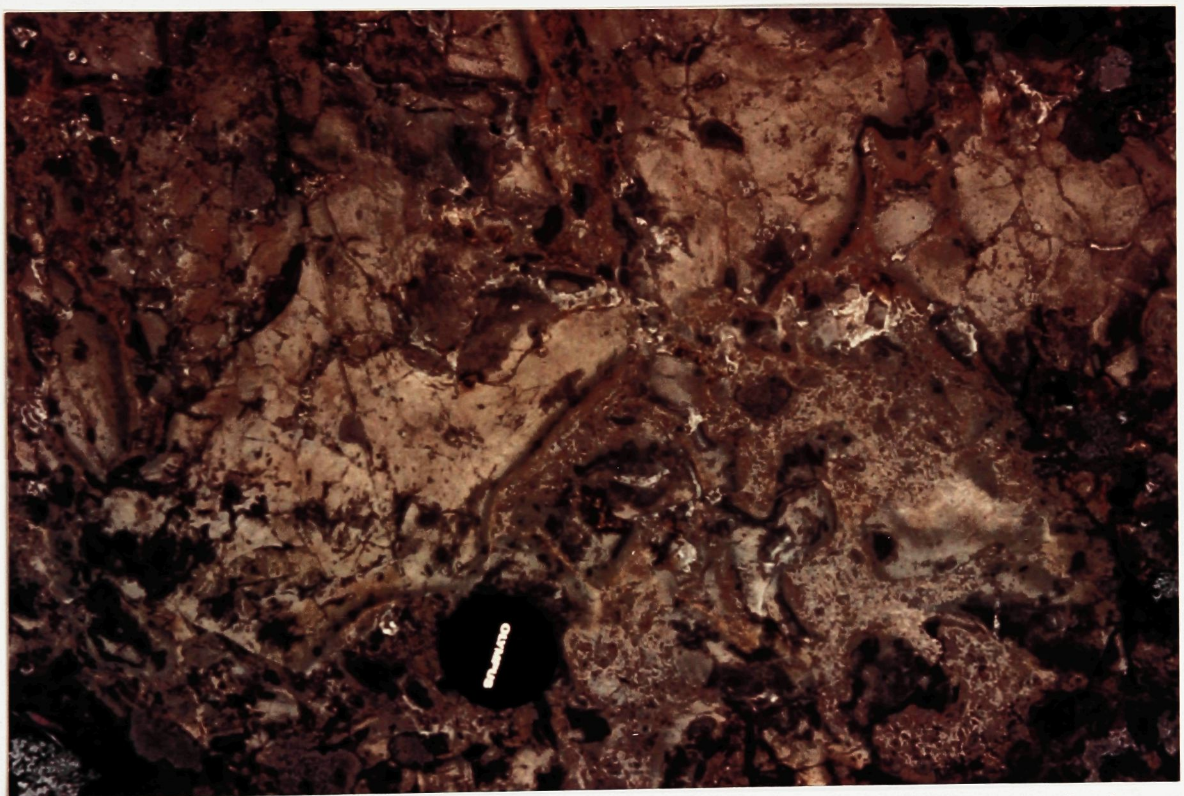

Plate 12.16. Same flow top breccia as in **12.15** except that the breccia is not silicified.

Plate 12.17. Ribbon-like, fluidal structure in andesitic lobe results from the preferential silicification of laminar joints and amygdule bands.

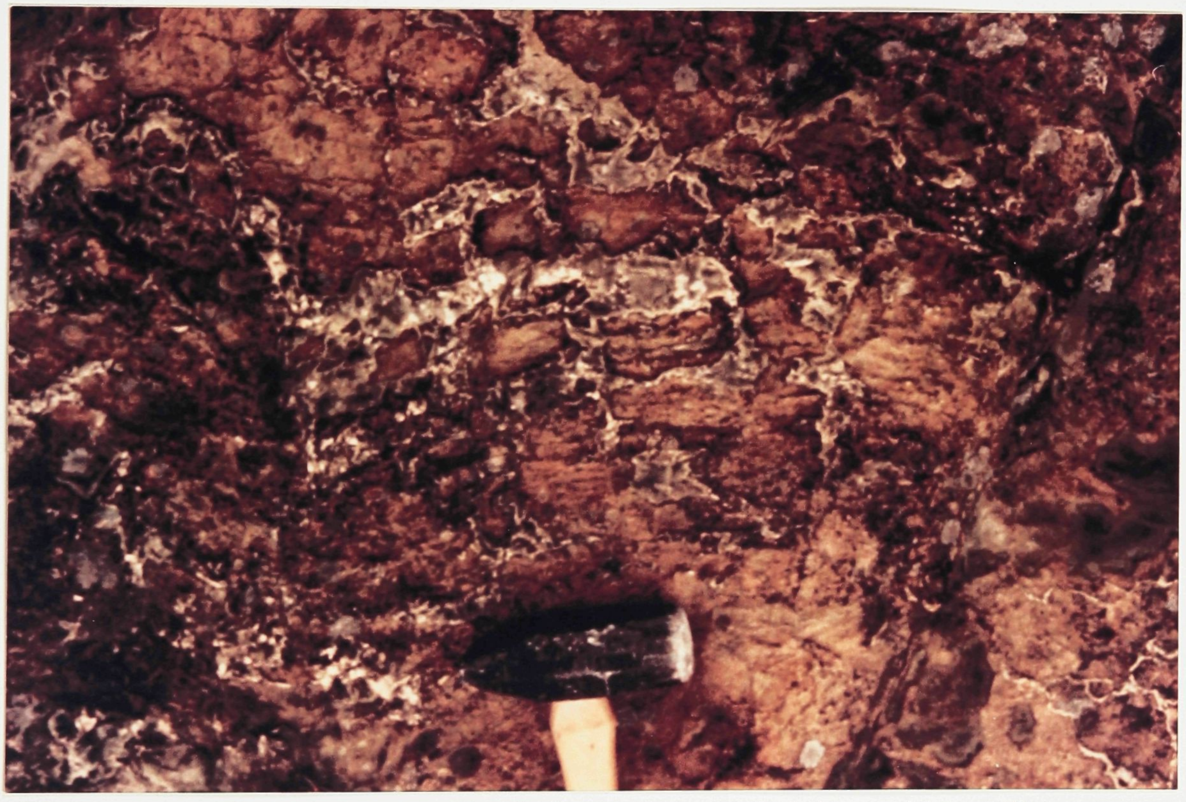

Plate 12.18. Silicification localized along concentric joints within pillows.

13. CHARACTERISTICS, MODE OF FORMATION AND CONTROLS ON THE LOCATION OF VOLCANOGENIC MASSIVE SULPHIDE DEPOSITS WITHIN THE NORANDA SHIELD VOLCANO AND CAULDRON

13.1 INTRODUCTION

The Noranda area is one of Canada's premier base metal and gold camps. To date 22 massive sulphide deposits and 16 gold deposits have been discovered. Discoveries in 1985, 1986 and 1987 by Noranda (Ribago deposit), Nuinsco (Aldermac area) and Audrey Resources (Mobrun area) indicate the continued potential of this camp.

Volcanogenic massive sulphide deposits (VMS) of the Noranda camp are referred to as Noranda-Type and characteristics of these deposits are thought to typify Archean, Cu-Zn massive sulphide deposits. The main objectives of this chapter are to:

a) Describe the characteristic features of Noranda-Type VMS deposits, and propose a model for their formation that is consistent with these features and in accord with processes actively forming sea floor sulphide mounds.

b) Describe stratigraphic, structural and lithologic controls on the location of VMS within the Noranda Shield Volcano and specifically of deposits within the Noranda Cauldron. Recognition and definition of these controls are fundamental to continued, successful exploration both within and outside the Noranda camp.

c) Comment on the origin of hydrothermal fluids responsible for these deposits.

13.2 CHARACTERISTICS OF NORANDA-TYPE VMS DEPOSITS

Noranda-Type VMS deposits are proximal deposits that consist of a concordant lens of massive sulphide (>50% sulphides) overlying a discordant stockwork zone of sulphide stringer mineralization within a pipe-like envelope of altered rock.

13.2.1 TONNAGE, GRADE AND MINERALOGY

The tonnage and grade of VMS deposits in the Mine Sequence and in stratigraphically younger and older formations are summarized in Table 13.1. Deposits consist of either a single massive sulphide lens and stringer zone such as at Ansil, E. Waite and Norbec or of multiple lenses. The best example of the latter is the Millenbach deposit, which consisted of 15 individual massive sulphide lenses that ranged in size from 4,000 tons to 1.8M tons (Knuckey et al., 1982).

The deposits are polymetallic and minerals ubiquitous to all deposits include pyrrhotite, pyrite, chalcopyrite, sphalerite, galena and magnetite. Common accessory minerals include native gold and silver, tetrahedrite, mackinawite, chalcocite, barite, electrum, telluride, tennantite and cassiterite (Knuckey et al., 1982, Watkins, 1980; and Clarke, 1983). Typical gangue minerals include chlorite, quartz, biotite, actinolite and calcite.

13.2.2 THE MASSIVE SULPHIDE LENS

Morphology, Textures, Structures and Mineral/Metal Zoning

A typical massive sulphide lens has an irregular shape in plan but is more regular in cross section with shapes that range from steep sided cones with slopes of up to 45^0 to flat lensoid bodies with slopes of $<5^0$ (Figure 12.11). Examples of the former include Millenbach, the Amulet deposits, Quemont and Norbec; examples of the latter include Delbridge, Mobrun, Gallen and Aldermac with E. Waite, Old Waite and Ansil examples of deposits with shapes intermediate between the two (Figures 9.3 D-D and 9.6 P-P/Q-Q). The irregular outline of the Corbet main lens, in both plan and section, reflect its location within a crater (Appendix C). Contacts of massive sulphide with underlying and overlying rocks are sharp.

The textures, structures and mineral zoning within an individual massive sulphide lens have been described by Simmons (1973), Spence (1975) and

Knuckey et al., (1982). A typical lens consists of an inner discordant cone or spine that sits directly above the stringer zone and narrows toward the top of the lens. The spine consists of massive, fine to coarse-grained pyrrhotite with irregular patches and elongate vertical bands of chalcopyrite with minor pyrite and sphalerite. Surrounding the spine is either massive and or crudely banded sulphide (Plate 13.1) or a framework supported sulphide breccia or "in situ brecciated" massive sulphide; matrix separating fragments is typically massive pyrrhotite, chalcopyrite and pyrite (Plate 13.2). Fragments range to 3m in size, are angular to subrounded and consist of fine to coarse grained massive sphalerite, weakly banded pyrite-sphalerite with minor pyrrhotite and chalcopyrite and massive chalcopyrite. Banding in fragments is discontinuous and lensoidal. The flanks of the sulphide lens consist of coarse grained crudely bedded and well bedded sulphide that thins toward the top and centre of the sulphide lens. The bedded flanks consists of thin bedded to laminated pyrite and alternating pyrite-sphalerite beds which range from 1mm to >15cm in width. Thin beds composed of pyrite framboids (up to 1.5cm in diameter) with interbeds of tuff may occur locally within laminated sulphides.

The proportion of brecciated and massive sulphide in many deposits is unknown. In some deposits, such as the Vauze, sulphide breccias (Main lens) deposited along the flanks of a rhyolitic dome constituted 75% of the massive sulphide lens (Spence, 1975). At Corbet, slumped and transported sulphide breccia also form a significant part of the ore (Appendix C).

From the above description it is apparent that the massive sulphide lens is strongly zoned with respect to base-metal mineralogy. The pyrrhotite and chalcopyrite spine grades laterally to a pyrite and sphalerite-rich flank and ultimately to a pyritic fringe. Massive magnetite occurs as discrete zones at the base of the pyrrhotite-chalcopyrite rich core at both Ansil and Corbet (Watkins, 1980).

13.2.3 THE STRINGER SULPHIDE ZONE

Morphology, Textures, Structures and Mineral Zoning

The stringer zone consists of sulphide veins which form a cross-cutting, discordant, anastomosing network within hydrothermally altered footwall rocks and occasionally in overlying hanging wall rocks. The zones have a crude circular or oval form in plan that is typically of smaller diameter than the overlying massive sulphide lens. In section they are pipe-like to conical and crudely perpendicular to the basal contact of the massive sulphide lens (Figure 9.6 P-P/Q-Q).

Contacts between sulphide stringers and overlying massive sulphide are gradational where sulphide veins ranging from <1cm to 2.0m in width increase in number and size laterally toward the core of the zone and upward toward the massive sulphide lens. Contacts with surrounding host rocks are gradational where sulphide veins grade within 1 to 3m into non-mineralized host rocks often containing disseminated sulphides.

The shape of a stringer zone is governed, in part, by the permeability of the footwall rocks. At Millenbach, where stringer sulphides are located within an rhyolitic lava dome they have a regular, narrow pipe- or cone-like form of smaller diameter than the overlying massive sulphide lens. However, in andesitic and silicified andesitic flows stratigraphically below the rhyolitic dome the stringer zone widens by a factor of 2 or 3x where sulphides replace pillow margins or occur as the matrix to pillow and flow breccias. At Corbet, stringer sulphides constitute the matrix of volcaniclastic breccias that underlie sulphide lenses forming a semi-conformable sulphide zone (Appendix C).

Stringer sulphides above deposits "connect" VMS lenses located at different stratigraphic intervals or are "blind" and end abruptly in overlying units. The Amulet 11 shaft, Lower A and Upper A deposits are connected by one stringer zone over a stratigraphic interval of 400m and provide an excellent example of "stacked" deposits (Figure 9.6, Q-Q). Ore-grade stringers at the Ansil deposit continue above the massive sulphide lens for 300m, and are an example of a "blind" stringer zone (Figure 9.4 E-E). Further exploration may yet find stratigraphically higher deposits associated with this blind zone.

Stringer zones, like overlying massive sulphide, consist of a central core of chalcopyrite-pyrrhotite stringers (Plate 13.3) which grades into a fringe of sphalerite-pyrite stringers (Plate 13.4). The pyrrhotite- and chalcopyrite-rich core grades into the overlying pyrrhotite-chalcopyrite core of the massive sulphide lens. At Corbet, metre-wide stringers of vertically banded chalcopyrite in pyrrhotite occur immediately below similar vertically "banded" sulphide within the core of the overlying massive sulphide lens.

The stringer sulphide core generally constitutes "economic" stringer mineralization, with grades decreasing with depth. Economic stringers persist up to 150m below massive sulphide and, at Norbec, for as much as 500m below the main sulphide lens (Figure 9.3 D-D). Stringer mineralization can contribute significantly to the tonnage of each deposit; at Millenbach, 52% of the ore mined was from stringer zones.

13.2.4 METAL ZONING

Metal Zoning in a Single Lens

Individual massive sulphide lenses are characterized by a concentric metal zonation where a copper-rich spine grades outward into a zinc-rich fringe. This base metal zonation was first documented by Boldy (1968) and has been described further and in other Noranda deposits by Comba (1975), Knuckey, (1975), Spence and de Rosen-Spence (1975), Knuckey et al., (1982) and Knuckey and Watkins (1982),.

Zinc-rich massive sulphide is also enriched in lead relative to the core zone. Precious metals tend to vary systematically within a deposit but not between deposits; at Millenbach higher gold and silver values occur in the copper-rich areas whereas at Corbet they are typical of zinc-rich areas (Knuckey et al., 1982; Watkins, 1980).

Metal Zoning Between Lenses

In multi-lensed deposits, such as Millenbach and Amulet, the overall Cu/Cu+Zn content of individual massive sulphide lenses defines a crude "concentric" pattern of increasing copper content toward the main discharge areas marked by the Amulet lower A and Millenbach Main lens (Knuckey et al., 1982). Knuckey et al., (1982) interpreted this large scale metal zoning between massive sulphide lenses to reflect a systematic increase in the precipitation of chalcopyrite, relative to sphalerite, within conduits that fed peripheral lenses a result of a systematic decrease in temperature coupled with longer solution paths and greater mixing with sea water.

The lower copper content of the Amulet Upper A deposit compared to the underlying Lower A deposit has been interpreted to reflect a vertical metal zoning resulting from an increase in the zinc content of the hydrothermal fluid with time (Spence and de Rosen-Spence, 1975). The higher copper content of successively lower massive sulphide lenses located within the same alteration pipe (discharge conduit) is now interpreted as a product of dissolution and replacement of preexisting sulphide in "older" deposits by continued ascent of hydrothermal fluids through the same conduit to form stratigraphically higher, younger deposits (Knuckey et al., 1982). Evidence which supports the latter interpretation includes:

1. Where the alteration pipe and stringer zone to the No. 16 lens at Millenbach cross-cuts the Zn-rich (<1% Zn), pyritic, C Contact Tuff, pyrite is replaced by chalcopyrite and pyrrhotite and the Cu/Cu+Zn ratio changes from 15 outside the pipe to >30 in the pipe.

2. Massive sulphide lenses at Millenbach occur at 3 stratigraphic intervals, the stratigraphically highest lenses having a Cu/Cu+Zn ratio greater than underlying lenses.

3. There is no systematic stratigraphic variation in the overall Cu/Cu+Zn ratio of deposits within the Mine Sequence.

13.2.5 MODE OF FORMATION

Most massive sulphide lenses formed as hard, encrusting sinters as initially proposed by Boldy (1968). Geologic evidence, such as the steep-sided cone shape of deposits (slopes >45^0), their location on steep slopes and within volcanically and seismically active volcanic vent areas, angularity of fragments in transported sulphide breccias and angular sulphide fragments within overlying flows and tuffs support this interpretation.

Mid-ocean ridge massive sulphide mounds, which form through a combination of chimney collapse, plume fall out and replacement and deposition from within, may be the best modern analog to Archean VMS deposits (Speiss et al., 1980, Styrt et al., 1981, Hayman and Kastner, 1981, Ouideu et al., 1981, Hayman 1982, Goldfarb et al., 1983, Paradis et al., 1988, Hekinian and Foquet 1985 and Hekinian et al., 1983,1980). An internal replacement model has also been proposed for Miocene Kuroko deposits (Barton, 1978 and Eldridge et al., 1983) and was initially proposed for VMS deposits in Noranda (Price, 1948; Wilson, 1941; Dresser and Denis, 1960). The early replacement model for VMS deposits in Noranda envisaged sequential mineral (metal) replacement as occurring after lithification within structural/stratigraphic traps whereas now researchers envisage the "stewing" and replacement process to have occurred on and below the sea floor.

Using the sulphide mound model as an analogy, the growth of Noranda massive sulphide deposits is inferred to result from the following:

1. An initial, vertical Cu-Zn zonation within the discharge conduit is interpreted to have formed by cooling of ascending hydrothermal fluids through mixing with intrastratal fluid and ambient seawater and/or boiling. Based on their relative solubilities Zn and Fe sulphides would precipitate in the upper part of the conduit whereas less soluble Cu and Fe sulphides would be deposited at depth. By analogy with modern smokers (Styrt et al., 1981) the discharged fluids would be in the 250 - 350°C range and would have precipitated a Zn and Fe sulphide sinter at the discharge site due to rapid cooling and decompression and/or through

boiling(Large, 1977; Chapter 12). This initial sulphide sinter may have grown below or replaced an initial, lower temperature, SiO_2 sinter which impeded discharging fluids, trapped sulphide particles and acted as mat or growing surface for the later sulphides much the way early anhydrite/barite deposits are interpreted to have provided a sub-stratum for ocean-ridge VMS deposits (Campbell et al., 1985; Lydon, 1988). Hydrothermal explosion breccias (Muffler et al., 1971; Hedenquist and Henley, 1985) deposited around the discharge site may also have acted as a substratum for sulphide deposition; violent hydrothermal explosions would also provide a mechanism for producing a funnel shaped area of brecciation, below the massive sulphide, "healed" by sulphide stringer mineralization (Lydon, 1988). Sulphide particles, entrained within plumes that jetted from chimneys growing on the upper surface of the mound, would be largely dispersed, but may, in part, have settled out to form bedded sulphide muds above and along the flanks of the growing sulphide mound.

2. The mound is interpreted to have grown primarily from the collapse of inactive chimneys and brecciation of pre-existing sulphide by hydrothermal explosions. Breccias produced through chimney collapse or hydrothermal explosions would both increase the volume of the lens and provide a substratum for sulphide deposition, primarily between fragments, that may have resulted in the formation of "healed" sulphide breccias and "in situ" breccias typical of these ancient deposits. Hydrothermal explosions may not only have fractured and brecciated sulphide "in

situ" but also have dislodged sulphide fragments and deposited them peripheral to the vent as may have been the case at the Vauze Mine (Spence, 1975).

3. During mound growth sulphide and silica deposited within and in the immediate footwall to the lens may have lowered the permeability of the vent such that both fluid outflow (discharge) and inflow of ambient seawater was restricted. Accordingly, mixing between the ascending hydrothermal fluid and seawater would have decreased and the hydrothermal fluid would have both a higher temperature and metal content, especially Cu. Thus self-sealing of the vent may have resulted in a progressive upward increase in temperature and corresponding mineral stabilities and dissolution and replacement of zinc sulphides by copper sulphides within the core of the stringer zone and in the overlying massive sulphide lens.

4. Restricted fluid outflow would have "trapped" high-temperature fluids within the sulphide lens and, as is postulated in modern seafloor sulphide mounds, a steep thermal gradient from the mound core (+300^{0}C) to the mound surface (<100^{0}C) would be established. This thermal gradient would have initiated and sustained convection of trapped interstitial fluid and may have resulted in corresponding mineral stability gradients such that previously formed Zn sulphides, unstable in the hot core zone would be replaced by Cu sulphides (Eldridge etal, 1983). Zn-rich fluids moving away from the mound core would deposit Zn sulphides resulting in the formation of a concentrically zoned massive sulphide lens as at Noranda.

The "mound model" is consistent with the textures and structures, paragenetic sequence, and metal/mineral distribution of Noranda VMS deposits and offers an efficient mechanism to form economic deposits (Franklin, 1986). In contrast, metals precipitated during discharge from Black Smoker chimneys are effectively entrained in the rising plume and are dispersed rather than concentrated at the site of discharge (Mottl, 1983; Hayman and Kastner, 1981; Lydon, 1984).

Black Smokers, however, may be modern analogs for discharge responsible for the formation of metal-rich tuff units associated with some deposits. The Norbec Tuff occurring over a 2.5km^2 area, is not zoned but contains Zn and Cu in the same average proportion as the Norbec orebody (Knuckey et al., 1982). The anomalous Cu and Zn content of the Norbec Tuff may be a product of initial and or contemporaneous Black Smoker-type discharge during formation of the Norbec deposit. The pyritic "C" Contact Tuff in the Amulet-Millenbach sector and numerous other metal-rich tuffs of the Noranda Camp may have had a similar origin.

13.3 DISTRIBUTION OF VMS DEPOSITS WITHIN THE NORANDA SHIELD VOLCANO AND CAULDRON

13.3.1 STRATIGRAPHIC DISTRIBUTION AND METAL ZONING OF VMS WITHIN THE NORANDA SHIELD VOLCANO

The distribution of VMS deposits in the Noranda Shield Volcano is illustrated in Figure 13.1, and the stratigraphic position of these deposits summarized in Table 13.1. The Magusi River and New Insco deposits are not included in Table 13.1. These deposits are located 15 km north of the Hunter Creek Fault and although interpreted to occur within the Mine Sequence by some workers (Spence and de Rosen-Spence, 1975; Boldy, 1977), are of uncertain stratigraphic position. Similarly, the stratigraphic position of the Horne deposit (Chapter 9) is uncertain.

By far the most significant cluster of economic VMS deposits occurs within the cauldron-filling Mine Sequence (Cycle 3) where 17 VMS deposits and three new discoveries occur within 3000m of volcanic strata. As will be described later these deposits occur within and along the margins of the Noranda Cauldron (Figure 13.1).

Pre-cauldron Formations

Pre-cauldron Cycles 1 and 2 do not contain an economic VMS deposit. Cycle 1 does, however, contain the 4-Corners, Inmont and Ivanex deposits. The

Inmont and 4-Corners deposits are chalcopyrite-pyrrhotite stringer zones and are interpreted as the erosional remnants of former VMS deposits (Lefebure, personal communication 1984). The Ivanex prospect is a well bedded zinc-rich, pyritic, transported massive sulphide lens without an underlying stringer zone.

Post Cauldron Formations

Post-cauldron Cycle 4 contains the Delbridge, Deldona and Gallen (West MacDonald) deposits and 1 prospect. Although not located within the cauldron filling Mine Sequence the Delbridge and Deldona deposits are located along the inferred south margin of the cauldron (Horne Fault) and the Gallen deposit occurs along the inferred east margin of the structure.

The zinc-rich, pyritic Deldona and Delbridge deposits (Delbridge No.#1 and 2 deposits of Boldy, 1968) are located within a rhyolitic vent complex of the Delbridge Rhyolite formation. The Delbridge deposit is underlain by a Cu-rich stringer zone and chlorite alteration pipe. The Zn-rich, pyritic Gallen deposit occurs within a pendant of the South Dufault Rhyolite formation (Spence, 1975) within the east body of the Dufault Pluton. The Gallen deposit exhibits numerous soft-sediment features, lacks a distinct stringer/alteration zone and is interpreted by McEwen and Watkinson (1981) as a transported and slumped massive sulphide deposit.

Post-cauldron Cycle 5 hosts the Zn-rich, pyritic Mobrun deposits. It consists of 4 massive sulphide lenses but a distinct zone of discordant stringer mineralization has not been recognized. A second massive sulphide lens (approximately 18M tons) has recently been discovered either along strike of the existing deposit or at a different stratigraphic interval.

Metal Zoning of VMS Deposits within the Noranda Volcano

The Cu/Cu+Zn ratio for VMS deposits within the Noranda Shield Volcano are contained in Table 13.1. These values are calculated from average grades which include both massive and stringer ore types and multiple lenses. The data indicate that:

1. The Mine Sequence is characterized by deposits that are distinctly copper rich. There is no systematic (vertical) variation in the Cu/Cu+Zn ratio of deposits located at different stratigraphic intervals within the Mine sequence. Deposits located at the C Contact are, however, distinctly zinc-rich.

2. Deposits located in post-cauldron Cycles are typically zinc rich and pyritic. Except for Delbridge, these VMS deposits do not have a well developed stringer zone.

3. Massive sulphide deposits within pre-cauldron Cycles, such as the Ivanex deposit are zinc-rich. Stringer zones at Inmont and 4-Corners are Cu-rich. The Cu-rich character of these zones does not indicate that they are remnants of Cu-rich

deposits. For example, the zinc-rich Delbridge deposit is also underlain by a chalcopyrite-rich stringer zone (Boldy, 1968). If an analogy can be made with Norbec deposit and its associated metal-rich tuffs which have a similar Cu/Cu+Zn ratio, then the mineralized 4-Corners tuffs (Cu/Cu+Zn ratio of 22 for 15 holes averaging .38% Cu/.93% Zn; personal communication, D. Lefebure, 1983) peripheral to the 4-Corners stringer zone suggest that the eroded massive sulphide lens was probably zinc rich.

13.3.2 CAULDRON SUBSIDENCE AND VMS DEPOSITS

The pronounced spatial and temporal relationship between VMS deposits to a large cauldron subsidence structure in Noranda has also been recognized in other VMS camps. A genetic relationship between cauldrons and VMS deposits has been proposed for Kuroko-type deposits by Hodgson and Lydon (1977), Kouda and Korde (1978), and Ohmoto and Takahashi (1983), and for deposits in the Bathurst-Newcastle district by Harley (1979). Sangster (1980) interpreted the clustering of Archean VMS deposits within mining districts and their occurrence within felsic centres to reflect an association with submarine calderas.

Cauldron subsidence and volcanism represent a unique stage in the evolution of the Noranda Shield volcano not duplicated in pre- or post-cauldron formations. Cauldron formation is interpreted as a "focusing event" that restricted contemporaneous and "intense" structural, volcanic, plutonic and hydrothermal events to a small area during a brief period in the evolution of the Noranda shield volcano. During cauldron subsidence both volcanism and subsidence was accommodated along ring and radial faults that formed directly above a rising, shallow (1-3km) magma chamber now represented by the Flavrian Pluton. As a result the Noranda cauldron represented a restricted area of anomalously high heat flow and structural permeability as compared to the larger shield volcano. The high heat is interpreted to have resulted in the development of a high-temperature hydrothermal system directly above the magma chamber and within the Noranda cauldron. Numerous faults, continuously reactivated during subsidence and volcanism, provided access for recharge fluid (seawater) and acted as conduits for cross-stratal fluid flow for fluids from both deep and shallow aquifers and ultimately focused their discharge to form deposits both within and along the cauldron margins. Hydrothermal discharge peripheral to the cauldron would likely have been insignificant and of lower temperature compared to that within the cauldron.

VMS deposits formed during the onset of two cauldron subsidence cycles (Chapter 11, Figure 11.4). This particular interval in cauldron development is one which combines maximum heat flow (following regional tumescence and intrusion) with greatest structural permeability (and reactivation) during volcanism and subsidence, and is therefore particularly favourable, but not exclusively so, for generating and sustaining a high-temperature hydrothermal system.

The copper content of deposits varies with stratigraphic position within the Noranda Shield volcano. Deposits in pre- or post-cauldron formations are zinc-rich (Cu/Cu+Zn ratios <30: Table 13.1), whereas deposits of the Mine Sequence are copper-rich (Cu/Cu+Zn ratios >40: Table 13.1). The small, zinc-rich massive sulphide deposits located at the C Contact is the only exception. The copper- or zinc-rich character of deposits is interpreted to be a function of the amount of copper contained within discharging hydrothermal fluids which is, in part, dependant upon temperature (Crerar and Barnes, 1976; Styrt etal, 1981). The higher copper content of VMS deposits within the Noranda cauldron supports discharge from a higher-temperature hydrothermal system that prevailed during a period of higher heat flow which accompanied cauldron development. Zn-rich VMS deposits of pre- and post-cauldron formations are interpreted as products of a "lower" temperature hydrothermal system. "Lower" is a relative term, as these deposits are products of hydrothermal systems above 250°. Zn-rich massive sulphide lenses at the C contact formed during a hiatus in volcanic, plutonic and structural activity that separated two cauldron subsidence cycles (Chapter 11) and are interpreted as products of a "lower" temperature system that was operative during a static period characterized by decreased heat flow immediately following magma withdrawal and collapse.

13.3.3 CONTROLS ON THE LOCATION OF VMS DEPOSITS WITHIN THE NORANDA CAULDRON

Stratigraphic Control

Volcanic reconstruction indicates that economic deposits within the Noranda cauldron formed during active volcanism and subsidence at the onset of two cauldron cycles that were preceded and initiated by magma resurgence. The Corbet and Ansil deposits formed during a period of volcanism and subsidence that marked the onset of cauldron development during the first or earliest recognized cauldron cycle. Similarly, the Millenbach-D68, Amulet, Old Waite, East Waite, and Norbec deposits formed during a period of active volcanism and subsidence during onset of the second cauldron subsidence cycle. Small, Zn-rich deposits at the "C" contact (C, Dufault, Moosehead and F-Shaft deposits) formed during a hiatus in volcanism and subsidence between the two cauldron cycles. Similarly, the small Newbec deposit formed during a hiatus in volcanic activity which followed in-filling of the Noranda Cauldron.

The Quemont deposit, located along the south margin of the Cauldron, formed during an interval that spanned mineralization of both cauldron cycles. The large size of the Quemont deposit, which almost equals the combined tonnage of deposits within the cauldron, may reflect continued, uninterrupted hydrothermal discharge that, unlike the intra cauldron deposits, was not interrupted or forced to shift by contemporaneous volcanic activity.

Structural Control

Perhaps the most important and fundamental control on the location of VMS within the Noranda Cauldron is their location along synvolcanic faults and less well defined paleostructures or lineaments, as has been proposed for Kuroko deposits in Japan (Scott, 1980) and for Cyprus deposits (Adamides, 1980). In Noranda, the northeast and northwest alignment of VMS deposits has been interpreted to reflect an underlying structural control (Sangster, 1972; Knuckey 1975, Knuckey et al., 1982; Scott, 1980).

Synvolcanic faults, generated and reactivated during regional tumescence that preceded volcanism and subsidence provided cross-stratal permeability for ascending hydrothermal fluids and focused their discharge within the Noranda cauldron. Once established, these faults were continually reactivated and controlled the location of subsequent VMS deposits at different stratigraphic intervals. Synvolcanic faults also acted as conduits for ascending and commonly contemporaneous magma accounting for the common occurrence of deposits within rhyolitic and andesitic vent areas.

The Corbet deposit occurs within an andesitic vent area that is localized where the South Rusty Hill Fault intersects the McDougall-Despina Ring Fault (Appendix C). A paleovolcanologic reconstruction of the andesitic vent area and Corbet deposit is illustrated in Figure C.10. The McDougall-Despina Ring Fault and ancillary, parallel faults define the northern margin of the Despina Cauldron, a smaller subsidence structure within the Noranda cauldron. Massive sulphide deposits (Corbet, D-68), volcanogenic stringer zones (Bedford, Rusty Hill) and areas of anomalous mineralization and alteration (Watkins, 1980; Setterfield, 1984), located at different stratigraphic intervals along this fault indicate that ascending hydrothermal fluids were continuously focused along the ring-fault during subsidence and volcanism.

The South Rusty Hill Fault, normal to the McDougall-Despina Fault, is interpreted as a radial fault to the Despina cauldron. This fault, traced stratigraphically upward some 1000m localizes QFP feeder dikes and VMS deposits at Millenbach. Noranda's Ribago deposit is also located within the Despina cauldron (Figure 13.1).

VMS deposits at Millenbach and D-68 occur at the base of, within, and on top of a growing rhyolitic ridge. The deposits occur along the length of the 2.0km northeast trending rhyolitic ridge where they directly overly the northeast trending feeder dike to the lower rhyolitic flow (Figure 13.2). The feeder dike defines the trace of a northeast striking radial fault (South Rusty Hill Fault) oriented perpendicular to the margin of the Despina cauldron. VMS deposits at D-68 are situated at the southwest end of the rhyolitic ridge and immediately adjacent to the margin of the Despina cauldron (Figure 13.2).

The alignment of the Amulet C, Bluff, Lower and Upper A, Lac Dufault zinc and D-266 deposits and Millenbach main lens define a northwest-trending lineament, the Amulet-Millenbach lineament, which parallels the McDougall-Despina Fault located 1.5km to the south. The coincidence of the Amulet-Millenbach lineament with a feeding fissure for the Amulet Andesite formation suggests that the former may mark the position of a deep-seated structure. Deposits along this lineament occur over a 300m stratigraphic interval (Figure 13.2) indicating reactivation and continued ascent of hydrothermal fluids along this structure during volcanism and subsidence. The Amulet F deposit and D-62 lens lie on a northwest trending line, the F-shaft lineament, which parallels the Amulet-Millenbach lineament and McDougall-Despina Fault. The F-shaft lineament it is interpreted to be similar to the Amulet-Millenbach lineament and collectively they are interpreted as parallel ring fractures developed along and parallel to the margin of the Despina cauldron.

The pronounced east-northeast alignment of the Old Waite, East Waite, D-Zone, Norbec and Newbec deposits parallels and is coincident with the east-northeast trend of the Old Waite dike swarm and Amulet Andesite feeding fissure, a graben-like andesitic fissure and subsidence zone within the centre of the Noranda cauldron. Synvolcanic faults and andesitic fissures, now represented by andesitic dikes, controlled the location of both volcanic vents and VMS deposits.

The diagrammatic reconstruction in Figure 13.3, illustrates the pronounced structural control on the location of these deposits as well as the diverse geological environments in which spatially associated and contemporaneous deposits formed. The Old Waite deposit formed at the base of the Amulet Andesite formation within the core of the dike swarm and was dissected by numerous feeder dikes to overlying flows. On a mine scale the geologic environment of the Old Waite deposit is similar to that of Cyprus VMS deposits within the lower Pillow Lavas. In marked contrast the East Waite deposit, located only 0.5km to the east, formed on top of a rhyolitic lava dome (Waite Rhyolite). The Norbec and D-zone deposits formed along the flank of a large Waite Rhyolite flow and immediately adjacent to the Amulet Andesite feeding fissure. The Newbec deposit formed within the Amulet feeding fissure and at the top of the Amulet Formation. The Vauze deposit formed along the south flank the Waite Rhyolite flow (Spence, 1975) immediately north of the Old Waite dike swarm.

The Ansil deposit is located on the south flank of the North Rhyolite flow of the Northwest formation and north of the Old Waite dike swarm. The deposit, as illustrated in Figure 13.4, is in part underlain by flows of the Rusty Ridge formation and is interpreted to have formed along the margin of an actively subsiding fault-bounded basin contemporaneous with andesitic eruptions of the Rusty Ridge formation (Figure 13.4).

The Quemont deposit lies within a rhyolitic vent area of the Joliet and Quemont Rhyolite formations along the intensely faulted south margin of the Noranda cauldron (Figure 11.4). The deposit formed within a down-faulted block sandwiched between the Horne and Quemont Feeder Dike Faults along the cauldron margin. The occurrence of the stratigraphically higher (4^{th} cycle) Delbridge and Deldona deposits north of, but adjacent to, the Horne Creek Fault suggests that these deposits also formed in a fault block , referred to as the Despina Cauldron, along the cauldron margin. The Horne deposit also lies immediately adjacent to, but south of, the Horne Creek Fault. Although the stratigraphic position of the Horne deposit is uncertain its location along the cauldron margin suggests it may be related to this structure.

The Aldermac deposit and Nuinsco's recent discovery occur along the west margin of the Noranda cauldron and 1500m north of the MacKay Lake Fault, the western continuation of the Horne Creek and Beauchastel Faults. The intense block faulting in this area (Hunter, 1979) suggests that the deposits formed along the west margin of the Noranda cauldron. The Gallen (West MacDonald) deposit is interpreted to have formed along the east margin of the Noranda Cauldron (4^{th} cycle). Emplacement of the Dufault Pluton (East Body), in part controlled by the faulted east margin of the cauldron, preserved the deposit within a roof pendant <1km from the inferred cauldron margin.

In summary, VMS deposits have been discovered within and along the inferred west, south and east margins of the Noranda cauldron, but to date, deposits have not been discovered along the north margin. Areas of alteration and sulphide mineralization do occur along the north margin and the absence of deposits may merely reflect minimal exploration, especially diamond drilling. There are, however, fundamental differences in the structural and volcanic history of the north and south margins that may have favoured the localization of deposits on the south margin. As illustrated in the reconstructed cross-section (Figure 11.1) the south margin was more structurally active and characterized by greater subsidence, as evidenced by the higher level of emplacement of the Flavrian Pluton, and less volcanism than the north margin.

13.3.4 POSSIBLE ORIGINS OF HYDROTHERMAL FLUIDS RESPONSIBLE FOR FORMATION OF NORANDA VMS DEPOSITS

The essential constituents of the hydrothermal fluid responsible for the formation of Noranda-type VMS deposits include Fe, Cu, Zn, Pb, S, Au and Ag. Alteration assemblages associated with stringer mineralization suggest the fluid also contained Mg and Si (Chapter 12). The metals may have been transported as chloride complexes in an acidic, reduced fluid or as bisulphide complexes in an alkaline, sulphur-rich fluid (Franklin et al., 1981). The source of the metals and the origin of the "primary" ore fluid are still the subject of much controversy

(Franklin et al., 1981). A seawater source for the metals, proposed by Kajiwara (1973), is usually dismissed because of the low concentrations of metals in modern seawater (Franklin et al., 1981).

Currently, the most popular hydrodynamic model for the formation of VMS deposits is the convection cell model where the metals are considered to be "leached" from underlying, footwall rocks through interaction with evolved, convecting seawater. Seawater convection is interpreted to be driven by the heat of a high level magma source and cooling flows and intrusions. The fluid is interpreted to leach metals from rocks during its passage through the system and is discharged at the seafloor to form VMS deposits. The convection model is appealing because of the: a) existence of hydrothermal convection cells in modern oceanic crust and b) the occurrence of fossil hydrothermal systems in pillow lavas of the Troodos Ophiolte, that host "Cyprus-type" VMS deposits (Spooner, 1977: Heaton and Sheppard, 1977). At Noranda, the leaching model is supported by the occurrence of semiconformable, hydrothermal alteration zones within the footwall rocks to the VMS deposits. Of particular significance are areas of epidote-quartz alteration which, based on experimental work and constant volume calculations, can yield significant amounts of Cu and Zn to the fluid (Rosenbauer and Bischoff, 1984; Seyfried and Janecky, 1985; Harrigan and MacLean, 1976; Gibson, 1979; Skirrow, 1987). Thus, epidote-quartz alteration, within the deeper part of the Mine Sequence hydrothermal system, may be a possible source of metals for the VMS deposits. Lower temperature hydrothermal alteration (spilitic and diagenetic) although capable of adding Fe, minor Zn and other elements (Si, Mg) to the fluid are not interpreted as a significant metal source but may have modified the composition of the ascending fluid, through mixing, during ascent (Chapter 12).

The convection cell, leaching model assumes that the formation of VMS deposits is an integral part of subseafloor hydrothermal systems. The occurrence of VMS deposits and their erosional remnants throughout the Noranda Shield volcano supports this interpretation and indicates that ore-forming hydrothermal systems operated during construction of this edifice. The convection model, however, does not explain a) the preferential location of most and in some cases all deposits to one stratigraphic interval, such as the Mine Sequence, at Noranda, and b) the numerous apparently barren volcanic successions within greenstone belts that show evidence of similar hydrothermal alteration but contain no known deposits. If VMS deposits formed solely by hydrothermal convection than most greenstone belts should contain VMS deposits; unfortunately, for explorationists, this is not the case.

One possible explanation for the selective occurrence of VMS deposits is that the metals and the deposits themselves represent a direct contribution from an underlying magma chamber: i.e., a magmatic component to the convecting hydrothermal fluid. A magmatic component to the fluid is appealing as it would allow the periodic expulsion of fluid within a short time span thus explaining the clustering of deposits at one stratigraphic interval, the occurrence of "sporadic", apparently isolated deposits within a volcanic edifice, and the absence of deposits within some submarine volcanic successions. Thus, the sporadic location of VMS deposits within a volcanic edifice such as the Noranda Shield Volcano may represent periodic tapping of magmatic fluids by deep faults during construction of the edifice. The clustering of deposits within the Noranda cauldron and Mine Sequence, a cauldron-fill succession, is interpreted to reflect a combination of volcanic, plutonic and structural events during cauldron subsidence that are unique to this particular stage in the evolution of the Noranda Shield Volcano. During cauldron subsidence deep seated faults that are continuously reactivated during subsidence and volcanism could, perhaps, more easily penetrate a magma chamber that is emplaced at its highest level within the crust (1 - 3km below surface). A high level magma chamber might also be penetrated by convecting intrastratal fluid; this interaction would facilitate leaching of metal from a cooling and crystallizing magma. Once tapped, ascending magmatic fluids would undoubtedly mix with contemporaneous intrastratal fluids to be discharged primarily within and adjacent to the cauldron.

A magmatic component, additional to the convecting seawater source of the "ore fluid", cannot be discounted especially if one considers that:

a) evidence in favour of a convection model is for the most part circumstantial. Areas of hydrothermally altered rock within the footwall to deposits in Noranda, Cyprus (Spooner, 1977; Heaton and Sheppard, 1977; Lydon and Jamieson, 1984) and in Japan (Urabe et al.,1983; Green et al., 1983) indicate the presence of fossil hydrothermal systems, but provide no direct, unequivocal evidence that metals released to solution during alteration were responsible for contemporaneous VMS deposits. Furthermore, isotopic studies generally do not distinguish between a direct magmatic source or a magmatic signature obtained through fluid interaction with volcanic rocks (Franklin et al., 1981).

b) experimental work (Holland, 1972; Barnes, 1979) suggests that metals and chlorides can be efficiently partitioned into a coexisting early aqueous phase during magmatic differentiation.

c) alteration pipes extend for more than a kilometre below the massive sulphide deposits; for example, the Millenbach and Amulet Lower A "pipes" were traced into the Flavrian Formation. The length of these pipes suggests that the "ore fluid" was not derived from a shallow convection cell but rather a deep "stratal aquifer", as proposed by Lydon (1988), or possibly the underlying Flavrian Pluton.

d) hydrothermal alteration and uneconomic porphyry copper-style mineralization common to synvolcanic intrusions associated with VMS bearing successions, such as in the Flavrian Pluton (Goldie 1976), suggest that intrastratal fluids may have penetrated the magma chamber and possibly extracted metals.

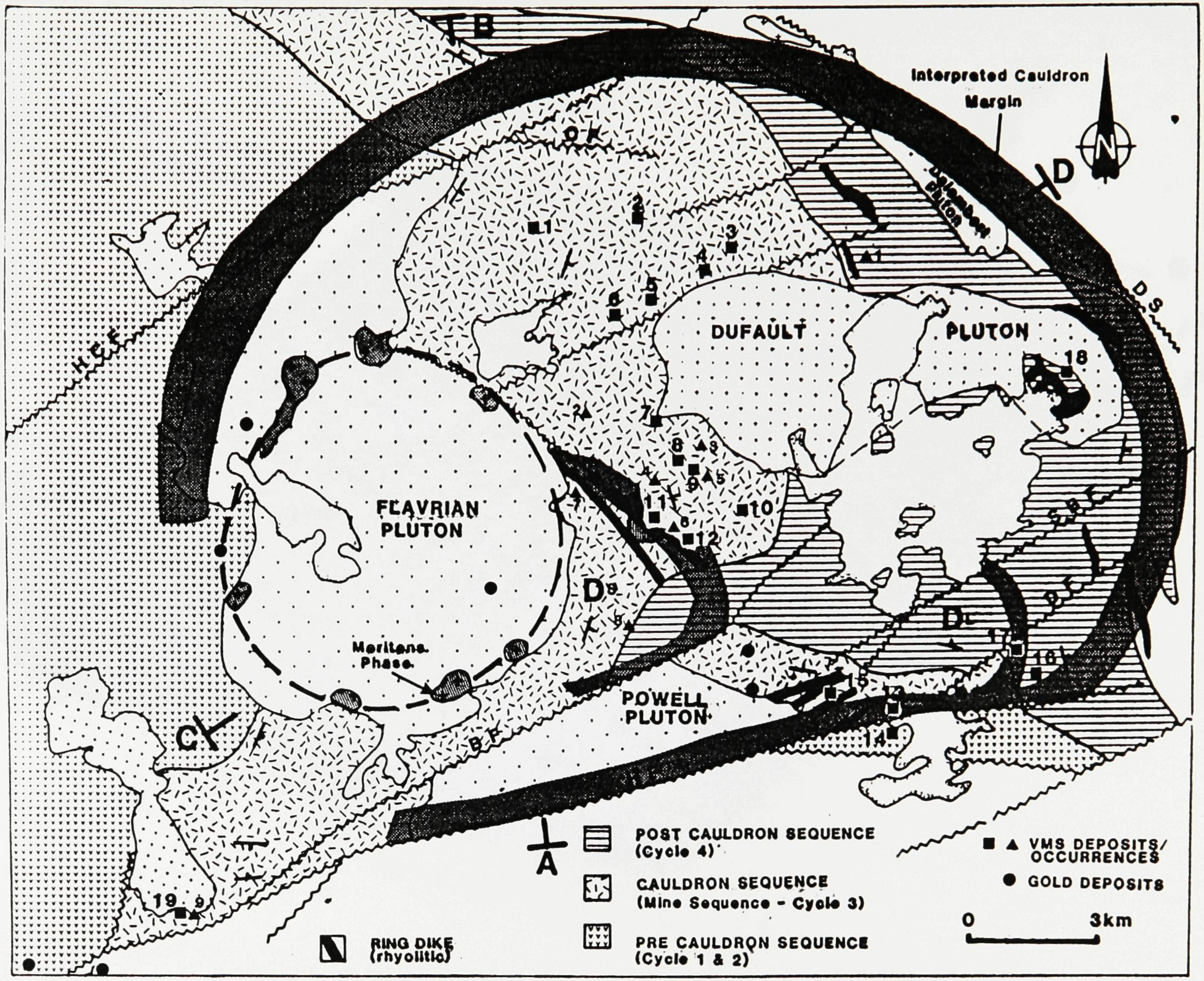

Figure 13.1. Distribution of Volcanogenic Massive Sulphide and gold deposits within the upper part of the Noranda Shield Volcano and Cauldron (see Figure 11.2 for fault abbreviations).

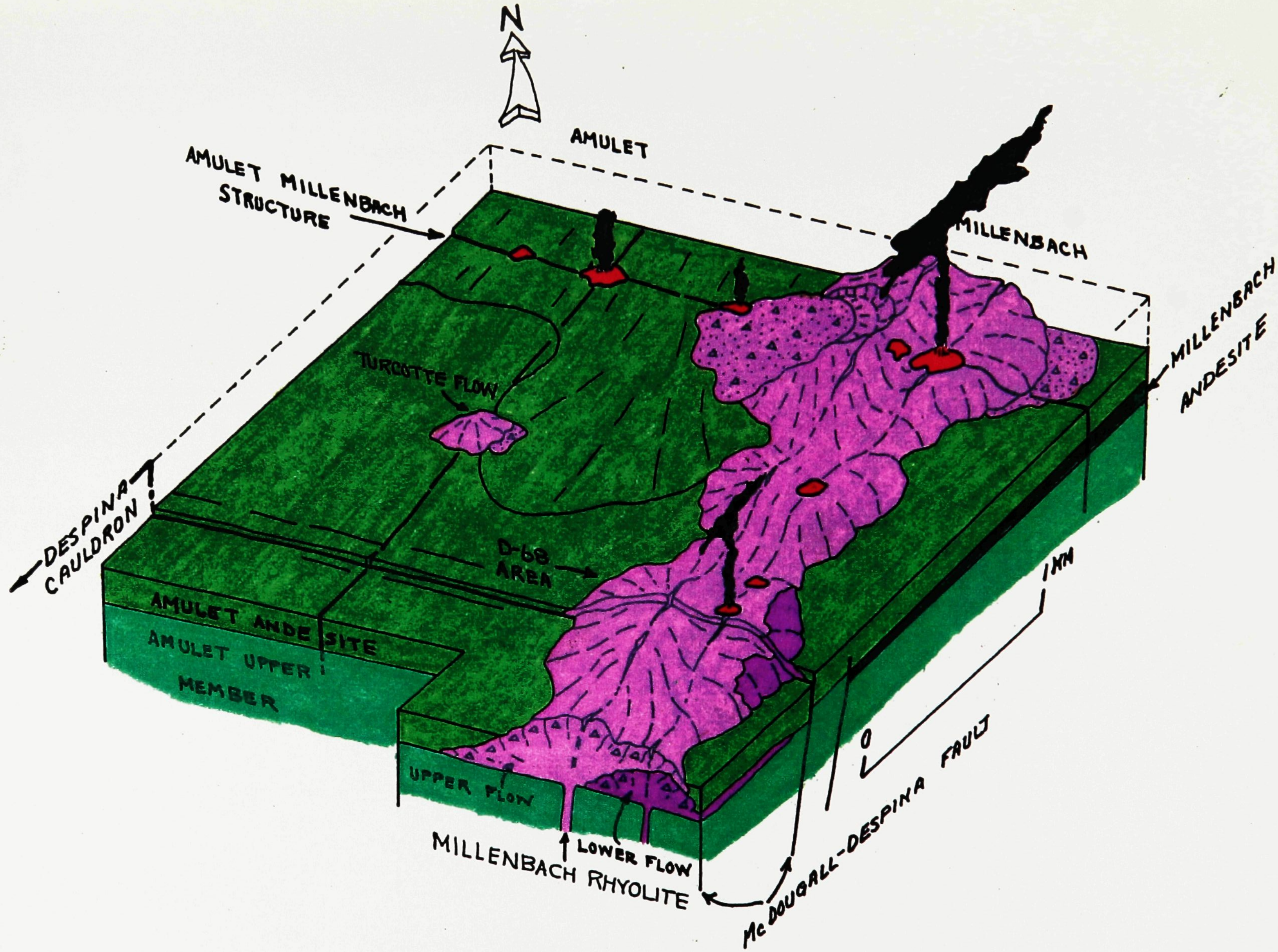

Figure 13.2. Cartoon illustrating an interpreted volcanological reconstruction of the rhyolitic Millenbach - D-68 lava dome/ridge and massive sulphide deposits. The Amulet deposits formed along an inferred andesitic fissure referred to as the Amulet-Millenbach structure.

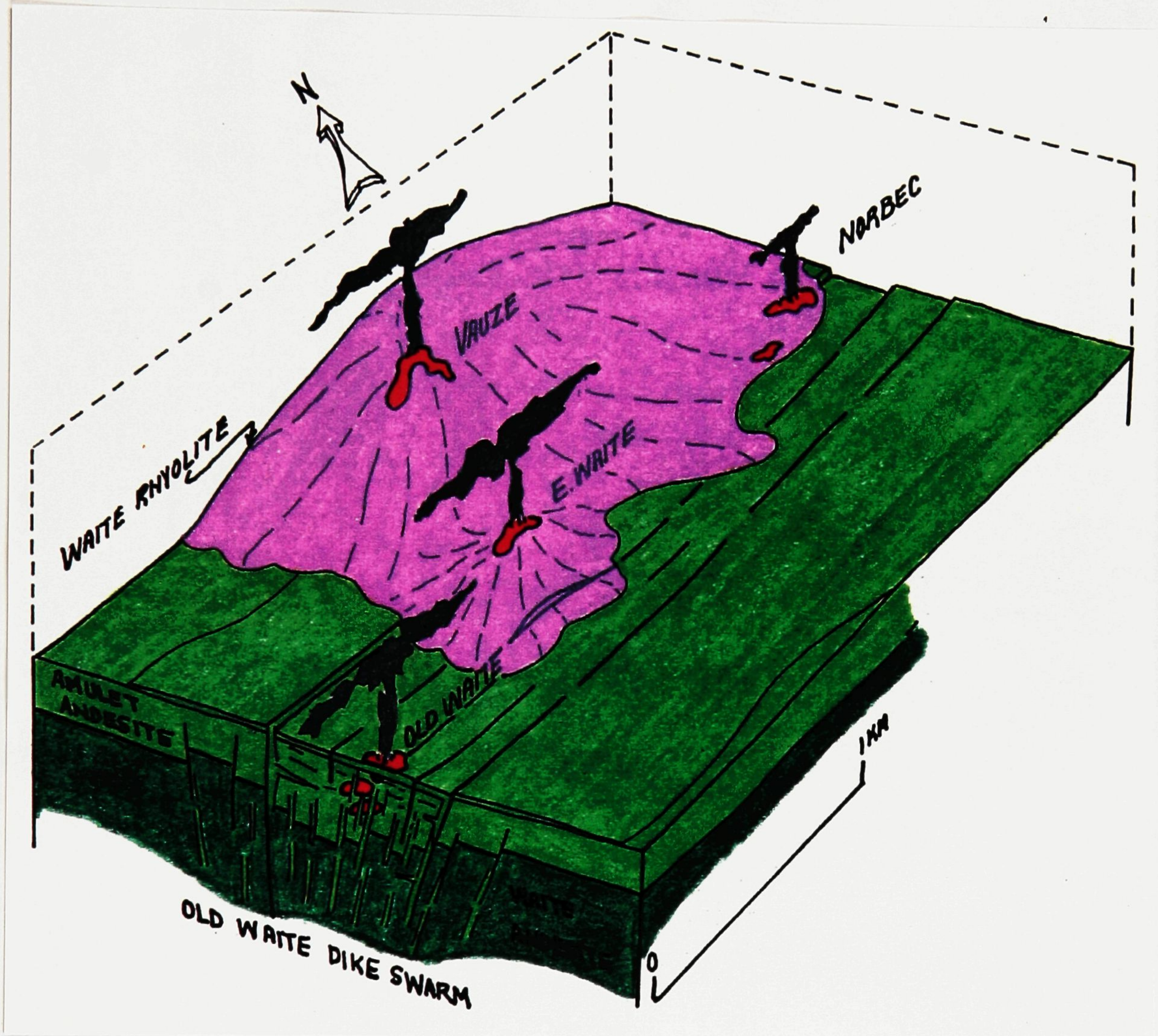

Figure 13.3. Cartoon illustrating an interpreted volcanological reconstruction of contemporaneous rhyolitic (Waite Rhyolite) and andesitic (Amulet Andesite) volcanism and massive sulphide deposits along the Old Waite Dike Swarm (Paleofissure). Note the different "volcanic environments" inferred for the Vauze, Norbec, East Waite and Old Waite massive sulphide deposits.

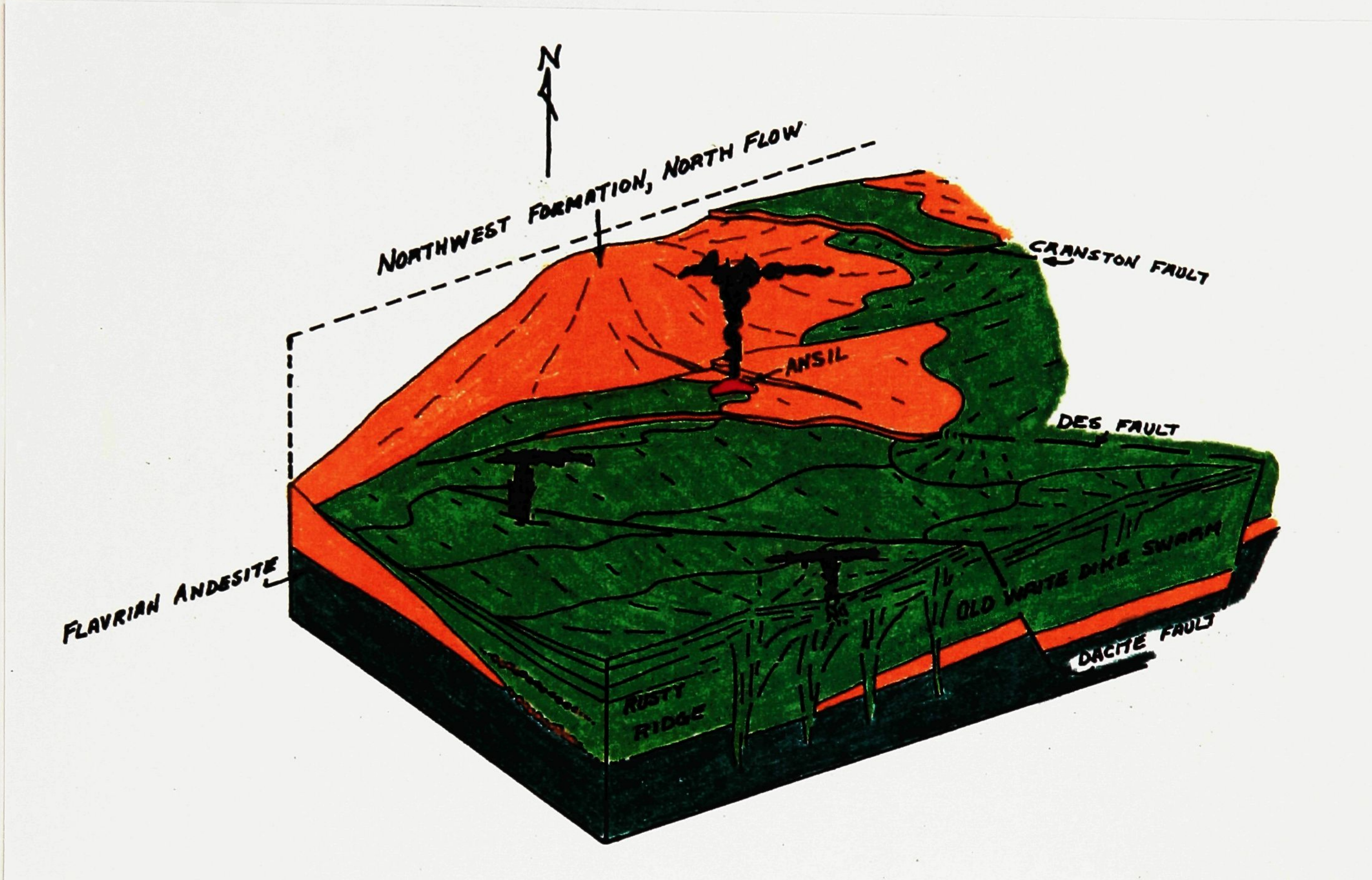

Figure 13.4. Cartoon illustrating an interpreted volcanological reconstruction of the Northwest and Rusty Ridge formations during formation of the Ansil deposit. Andesitic flows of the Rusty Ridge formation issued from fissures localized along the Old Waite Dike Swarm to the south and Cranston Fault to the northeast. The Ansil deposit formed along the flank of the North flow and adjacent to a fault-bounded basin defined by the Des and Dacite Faults.

TABLE 13.1. GRADES AND TONNAGES OF VMS DEPOSITS WITHIN THE NORANDA VOLCANIC COMPLEX

Stratigraphic Position	Deposit	Massive Sulphide	Stringer Sulphide	Multiple Lenses	M/Tons	% Cu	% Zn	oz. Ag	oz. Au	Cu-Zn Ratio
1st Cycle	Four Corners		X							-
	Inmont		X							-
	Yvanex	X								Zn-rich
3rd Cycle	Ansil (1)	X	X		2.1	7.18	0.57	0.80	0.06	92
Mine	Vauze (2)	X	X	X	0.37	2.94	1.00	0.80	0.02	74
Sequence	Norbec (3)	X	X		4.35	2.77	4.50	1.40	0.02	38
	D-Zone (4)	INCLUDED WITH NORBEC (3)								
	East Waite (5)	X	X		1.65	4.10	3.25	0.91	0.05	56
	Old Waite (6)	X	X	X	1.24	4.70	2.98	0.63	0.03	61
	F-Shaft (7)	X	X		0.3	3.40	8.60	1.35	0.01	28
	C Deposits (8)	X	X	X	0.62	2.20	8.50	2.53	0.01	20
	Lower A (9)	X	X		5.17	5.10	5.20	1.29	0.04	49
	Upper A (9)	X	X		0.20	2.30	6.10	1.35	0.06	28
	#11 (9)	X	X		0.49	3.60	2.40	0.63	0.02	60
	Bluff (9)	INCLUDED WITH LOWER A								
	Millenbach (10)	X	X	X	3.92	3.46	4.33	1.64	0.03	44
	Corbet (11)	X	X	X	3.06	3.00	1.96	0.60	0.03	60
	D68 (12)	INCLUDED WITH CORBET								
	Quemont (13)	X	X		16.35	1.20	1.80	0.54	0.12	40
	Aldermac (19)	X	X	X	2.07	1.48	-	0.20	0.01	-
	Newbec (1)		X		0.007	6 to 7				
	Fourcet (2)		X							
	D-62 (3)	X								
	Moosehead (4)	X	X							
	Dufault Zinc (5)	X	X		0.50	-	<3.0	-	-	-
	South Rusty Hill (6)		X							
	Bedford (7)		X		0.09	0.89				
	Ribago (8)	RECENT DISCOVERY - TONNAGE/GRADE UNCERTAIN								
	Aldermac (9)	RECENT DISCOVERY - TONNAGE/GRADE UNCERTAIN								

TABLE 13.1. GRADES AND TONNAGES OF VMS DEPOSITS WITHIN THE NORANDA VOLCANIC COMPLEX (Con't)

Stratigraphic Position	Deposit	Massive Sulphide	Stringer Sulphide	Multiple Lenses	M/Tons	% Cu	% Zn	oz. Ag	oz. Au	Cu-Zn Ratio
4th Cycle	Deldona (17)	X			0.10	0.30	5.00	0.76	0.12	5
	Delbridge (16)	X	X		0.40	0.55	8.60	2.00	0.07	6
	Gallen (18)	X			3.25	0.07	4.77	0.63	0.02	2
5th Cycle	Mobrun[1]	X	?		3.00	0.62	2.30	0.60	0.50	21
	New Lens	TONNAGE/GRADE UNCERTAIN								
Uncertain	Magusi	X			4.11	1.20	3.60	0.90	0.03	25
	New Insco	X	X		1.15	2.11	-	0.50	0.03	-
	Horne (mined)	X	X	X	60.26	2.20	-	0.40	0.17	-
	Horne #5[2]	X	X		144	1.0	0.9			52

(2) and (2) refers to former or operating mines and "uneconomic deposits" respectively.

[1] Some Cu-rich ore removed during earlier mining.
[2] Tonnage and grade of Horne #5 zone from Sangster (1980) and combined with mined tonnage.

Data from Boldy (1979) and unpublished compilations by D. MacNeil (Corp. Falconbridge Copper) and B. Bancroft (Noranda).

Plate 13.1. Massive crudely banded sulphide at the Millenbach Mine. Discontinuous, somewhat lensoidal bands of sphalerite (dark) in a matrix of pyrite-pyrrhotite and chalcopyrite (photo by P.Severin).

Plate 13.2. Brecciated massive sulphide at the Millenbach Mine (photo by P.Severin).

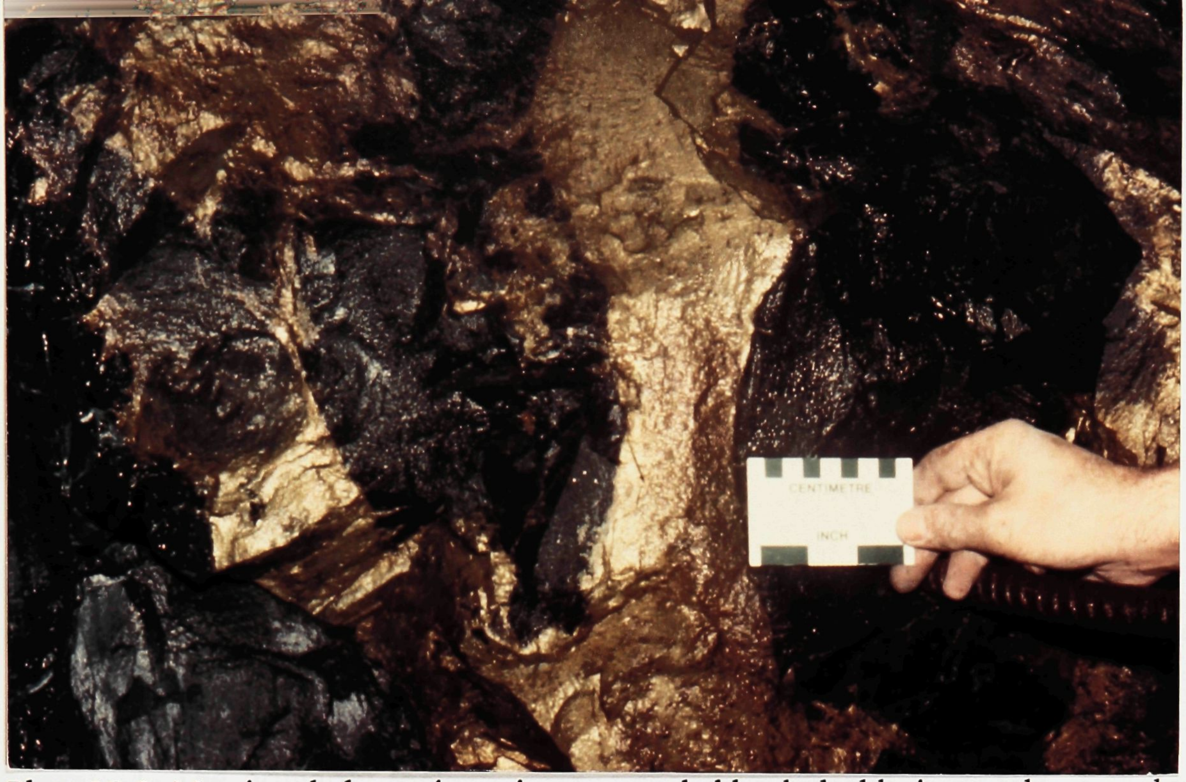

Plate 13.3. Massive chalcopyrite stringers mantled by dark chloritc envelopes at the Corbet Mine.

Plate 13.4. Sericite altered Northwest Rhyolite at the Corbet Mine.

14. CONCLUSIONS

The main conclusions and interpretations are discussed at the end of each chapter and are only summarized below.

1. The primarily tholeiitic formations of the 3000m thick Mine Sequence were erupted during a period of cauldron subsidence within the upper part of the subaqueous Noranda Shield Volcano. The Noranda Shield Volcano is an andesite/basalt - rhyolite bimodal, tholeiitic to calc-alkaline volcanic edifice that may be similar to Tertiary Central Volcanic Complexes in Iceland. The principal area of subsidence, the Noranda Cauldron, has a crudely oval form (approximately 15 x 20 km) with structural margins that lie entirely within the Flavrian and Powell Blocks. The Noranda cauldron is interpreted to have subsided a minimum of approximately 500m and 1200m along its northern and southern margins respectively to produce an asymmetric, trapdoor-like structure that also contains two smaller areas of localized subsidence, the Despina and Delbridge Cauldrons. Subsidence is interpreted to have occurred in response to partial evacuation of an underlying magma chamber now represented by the Flavrian Pluton. Subsidence kept pace with, and accompanied volcanism. The Mine Sequence may be

subdivided into two Cauldron Subsidence Cycles; each cycle began with initial tumescence followed by contemporaneous volcanism and subsidence and ended with a quiet, static period of "sedimentation".

2. Subsidence was essentially passive and piece-meal with effusion of both Mine Sequence rhyolitic and andesitic flows from vents localized along radial and concentric faults. In the Flavrian and Powell Blocks rhyolitic flows were erupted from fissures located primarily along the margins of the Noranda (and Despina) Cauldron whereas andesitic flows were mainly erupted from fissures of the Old Waite Dike Swarm within the core of the cauldron. Mine Sequence flows were confined to the cauldron by faults along the southern margin but commonly overran the northern margin.

3. Mine Sequence rhyolitic flows were subdivided into lobe-hyaloclastite and blocky flows. Lobe-hyaloclastite flows typically consist of aphyric or weakly feldspar porphyritic rhyolite and characteristically formed low relief (<20°), broad plateaus or shields that extended along and 1-2 km away from their feeding fissures. Blocky flows, which typically consist of quartz-feldspar porphyritic rhyolite, formed steep-sided (20-70°) lava domes and ridges restricted to their feeding fissure.

4. Massive and pillowed andesitic flows issued from fissures and produced broad lava plains that inundated and buried topography produced by rhyolitic flows.

5. Pyroclastic eruptions, chiefly phreatomagmatic eruptions that preceded some periods of andesitic and rhyolitic volcanism, were minor. Pyroclastic rocks comprise <5% of the Mine Sequence.

6. The Mine Sequence is interpreted to be a subalkaline, primarily tholeiitic, basalt/andesite - rhyolite bimodal succession. The compositional bimodality of the Mine Sequence flows and feeder dikes, occurrence of contemporaneous rhyolite and andesite-basalt magma in composite dikes, and a general upward trend in the percentage of phenocrysts within the Mine Sequence and an overall greater abundance of phenocrysts in Cycle IV formations is interpreted to be a product of continuous "tapping" of an open, high level, compositionally zoned magma chamber now represented by the Flavrian Pluton. The Amulet upper member may be a product of complete mixing between a more mafic, perhaps differentiated magma and a more felsic magma within the compositionally zoned magma chamber.

7. Deposits of thinly bedded and laminated tuff locally separate flows and formations. The regionally extensive C Contact Tuff, which extends across the Flavrian Block, separates the two Cauldron Cycles.

8. Rhyolitic and andesitic flows have a complex hydrothermal-metamorphic history. Semiconformable alteration, which consists of initial diagenetic alteration followed by spilitization, epidote-quartz alteration and locally by silicification, has affected all flows. Semiconformable alteration is interpreted to be the product of

alteration within a shallow, subseafloor hydrothermal system. Discordant pipe-like areas of chlorite and sericite alteration cross-cut penecontemporaneous semiconformable alteration zones and mark fault controlled conduits that channelled "ore-forming" hydrothermal fluids to the seafloor to form massive sulphide deposits. Mg-chlorite and sericite within the alteration pipes are interpreted to be the products of mixing of a fluid derived from below the Mine Sequence with intrastratal fluids (responsible for semiconformable alteration), downward migrating seawater and boiling of the fluids at or below surface.

9. Pervasive widespread silicification, unlike other types of semiconformable alteration, is essentially confined to the Amulet and Waite upper members. These two units had been previously interpreted as rhyolite. Unlike other Mine Sequence formations the Amulet and Waite upper members are products of uninterrupted flood-type andesitic eruptions. Silicification is interpreted to result from the interaction of these hot, ponded flows with a silica-saturated, intrastratal hydrothermal fluid that, through rapid heating, was driven through the quartz solubility maximum (<700 bars) resulting in the replacement of andesitic and rhyolitic glass by quartz, and quartz precipitation.

10. Epidote-quartz alteration occurs throughout the Mine Sequence but is restricted to andesitic and silicified andesitic flows. Its absence in rhyolitic flows may reflect their low Ca content. The occurrence of epidote-quartz alteration in silicified flows is a reliable criterion for distinguishing silicified andesite from

rhyolite.

11. Volcanogenic massive sulphide (VMS) deposits occur throughout the Noranda Shield Volcano but are concentrated within and along the margins of the Noranda Cauldron where they are localized along synvolcanic radial and concentric faults; they are commonly associated with either rhyolitic or andesitic vents. Although VMS deposits occur throughout the 3000m thick Mine Sequence of the Flavrain Block they preferentially occur in formations immediately above the Amulet formation and C Contact Tuff; i.e., most deposits formed during the onset of the second Cauldron Cycle. The preferential location of VMS deposits to the Noranda Cauldron and Mine Sequence is interpreted to reflect this unique period in the evolution of the Noranda Shield Volcano. Cauldron formation may be regarded as a focusing event that restricted contemporaneous and intense structural, volcanic, and plutonic events to a small volume and area during a "brief" time period. As a result the Noranda Cauldron was a restricted site of anomalously high heat flow and structural permeability that favoured the development of a high temperature hydrothermal system. Metals may have been derived from leaching of aquifer rocks, by an evolved seawater solution, within a simple convection cell or directly from a shallow underlying magma chamber (Flavrian Pluton) that was at its highest position in the crust during cauldron subsidence.

12. Noranda VMS deposits probably formed through a combination of sulphide precipitation and replacement at and below the seafloor much in the same manner as proposed for Mid Ocean Ridge sulphide mounds. Precipitation of these sinter-like deposits in active volcanic vent areas suggests rapid accumulation and mound growth interrupted by contemporaneous volcanic activity; this accounts for their multi-lensed and "stacked" character.

15. REFERENCES

Adamides, N.G., 1980. The form and environment of formation of the Kalavasos ore deposits, Cyprus. In Panayiotou, A.(ed.), Ophiolites, Proceedings of the International Ophiolite Symposium, Cyprus, 1979, Printco, Cyprus, pp.117-128.

Allen, C.C., 1980. Icelandic subglacial volcanism:thermal and physical studies. Journal of Geology, 88: 108-117.

Ambrose, J.W., and Ferguson, S.A., 1945. Geology and mining properties of part of the west half of Beauchastel Township, Temiscamingue County, Quebec. Geological Survey Canada, Paper 45-17.

Anderson, A.T., 1976. Magma mixing: Petrological process and volcanological tool. Journal of Volcanology and Geothermal Research, 1: 3-33.

Anderson, E.M., 1936. The dynamics of the formation of cone sheets, ring-dikes and cauldron-subsidences. Royal Society of Edinburgh Proceedings, 56:128-157.

Andrews, A.J., 1977. Low temperature fluid alteration of oceanic layer 2 basalts, DSDP leg 37. Canadian Journal of Earth Sciences, 14: 911-926.

Arnorsson, S., Gunnlaugsson, E., and Svavarsson, H., 1983a. The chemistry of geothermal waters in Iceland.III. Chemical geothermometry in geothermal investigations. Geochimica et Cosmochimica Acta, 47: 567-577.

Arnorsson, S., Gunnlaugsson, E., and Svavarsson, H., 1983b. The chemistry of geothermal waters in Iceland.II. Mineral equilibria and independent variables controlling water compositions. Geochemica et Cosmochimica Acta, 47: 547-566.

Atkinson, M.L. and Watkinson, D.H., 1980. Copper mineralization and hydrothermal alteration of volcanic rocks at Bedford Hill, Noranda area, Quebec. In Current Research. Part A, Geological Survey of Canada, Paper 80-1A, pp.119-123.

Ayres, L.D., and Thurston, P.C., 1985. Archean supracrustal sequences in the Canadian Shield: An Overview; In Ayres, L.D., Thurston, P.C., Card, K.D. and Weber, W. (eds.), Evolution of Archean Supracrustal Sequences. Geological Association of Canada, Special Paper 28, pp.343-380.

Babcock, R.S., 1973. Computational models of metasomatic processes. Lithos, 6: 279-290.

Ballard, R.D., Holcomb, R.T., and van Andel, T., 1979. The Galapagos Rift at 86° W: 3. Sheet flows, collapse pits, and lava lakes of the Rift Valley. Journal of Geophysical Research, 84: 5407-5422.

Ballard, R.D., and Moore, J.G., 1977. Photographic atlas of the Mid-Atlantic ridge rift valley. Springer Verlag, Berlin.

Baragar, W.R.A., 1984. Pillow formation and layered flows in the Circum-Superior Belt of eastern Hudson Bay. Canadian Journal of Earth Sciences, 21: 781-792.

Baragar, W.R.A., Plant, A.G., Pringle, C.J., and Schau, M., 1977. Petrology and alteration of selected units of Mid-Atlantic Ridge basalts sampled from sites 332 and 335, DSDP. Canadian Journal of Earth Sciences, 14: 837-874.

Baragar, W.R.A., 1968. Major element geochemistry of the Noranda volcanic belt, Quebec-Ontario. Canadian Journal of Earth Sciences, 5: 773-790.

Barnes,, H.L., 1979. Solubilities of ore minerals; In Barnes, H.L.(ed.), Geochemistry of hydrothermal ore deposits, second edition, Wiley, New York, pp. 404-460.

Barton, P.B., 1978. Some ore textures involving sphalerite from the Furutobe Mine, Akita Prefecture, Japanese Mining Geology, 28: 293-300.

Bischoff, J.L., and Rosenbauer, R.J., 1984. The critical point and two phase boundary of seawater, 200-500°C. Earth and Planetary Science Letters, 68: 172-180.

Bischoff, J.L., and Dickson, F.W., 1975. Seawater-basalt interaction at 200 C and 500bars: Implications for the origin of sea-floor heavy-metal deposits and regulation of seawater chemistry. Earth and Planetary Science Letters, 25: 385-397.

Blake, D.H., Elwell, R.W.D. et al., 1965. Some relationships resulting from the intimate association of acid and basic magmas. Quarterly Journal of the Geological Society of London, 121: 31-49.

Bodvarsson, G., and Walker, G.P.L., 1964. Crustal drift in Iceland. Royal Astronomical Society and Geophysics, 8: 285-300.

Bohlke, J.K., Honnorez, J., and Honnorez-Guerstein, B.-M., 1980. Alteration of basalts from site 396B, DSDP:Petrographic and Mineralogic Studies. Contributions to Mineralogy and Petrology, 73: 341-364.

Boldy, J., 1977. Exploration discoveries, Noranda District, Quebec; In Hood,.P.J. (ed.), Geophysics and Geochemistry in the search for metallic ores. Geological Survey of Canada, Report 31, pp.593-604.

Boldy, J., 1968. Geological observations on the Delbridge massive sulphide deposit. Canadian Institute of Mining and Metallurgy, Bull. 61: 1045-1054.

Bonnichsen, B., and Kauffman, D.F., 1987. Physical features of rhyolite lava flows in the Snake river Plain volcanic province, southwestern Idaho. In Fink, J.H.(ed), The Emplacement of Silicic Domes and Lava Flows. Geological Society of America, Special Paper, 212: 119-145.

Buck, M.J., 1981. Hydrothermal alteration and volcanogenic sulphide mineralization near Amulet "F" Shaft, Noranda Area, Quebec. Bsc. thesis, Carleton University, Ottawa, Ontario (unpubl.).

Campbell, I.H., McDougall, T.J., and Turner, J.S., 1984. A note on fluid dynamic processes which can influence the deposition of massive sulphides. Economic Geology, 79: 1905-1913.

Cas, R.A.F., and Wright. J.V., 1987. Volcanic successions: modern and ancient. Allen and Unwin, London.

Carlisle, D., 1963. Pillow breccias and their aquagene tuffs, Quadra Island, B.C. Journal of Geology, 71: 48-71.

Cathles, L.M., 1983. An analysis of the hydrothermal system responsible for massive sulphide deposition in the Hokuroko Basin of Japan. Economic Geology, Monograph 5: 439-487.

Cathles, L.M., 1978. Hydrodynamic constraints on the formation of Kuroko Deposits. Mining Geology, 28: 257-265.

Christiansen, R.L., and Lipman, P.W., 1966. Emplacement and thermal history of a rhyolite lava flow near Fortymile Canyon, southern Nevada. Geological Society of America Bull., 77: 671-684.

Christiansen, R.L., Lipman, P.W., Orkild, P.P., and Byers, F.M., 1965. Structure of the Timber Mountain Caldera, southern Nevada, and its relation to Basin-Range structure. U.S. Geological Survey Prof. Paper 525-B, pp. B43-B48.

Clarke, D.S., 1983. Cu-Zn mineralization and alteration in the Waite Area, Noranda District, Quebec. Msc. thesis, University of Western Ontario, London, Ontario (unpubl.).

Comba, C.D.A., and Gibson, H.L., 1983. Geology of the Millenbach Rhyolite Volcano, Noranda, Quebec. In program with Abstracts, vol. 8, Annual Meeting of the GAC, MAC and CGU, Victoria, B.C.

Comba,C.D.A.,1977. Summary report on the Waite Dufault Mines Ltd. option, Duprat Township, Noranda, Quebec. Falconbridge Copper Ltd., internal report,(Unpubl.).

Comba, C.D.A., 1975. Copper-Zinc zonation in tuffaceous exhalites, Millenbach Mine, Noranda, Quebec. Msc.thesis, Queen's University, Kingston, Ontario (unpubl.).

Cooke,H.C., James, W.F., and Mawdsley, J.B., 1931. Geology and ore deposits of the Rouyn-Harricanaw Region, Quebec. Geological Survey of Canada Mem.166.

Cote, R., and Dimroth, E., 1976. Flow direction of Archean basalts determined from imbricated pillow-breccias. N. Jb. Miner. Mh., H.3: 97-109.

Coussineau, P., and Dimroth, E., 1982. Interpretation of the relations between massive, pillowed and brecciated facies in an Archean submarine andesite volcano - Amulet Andesite, Rouyn-Noranda, Canada. Journal of Volcanology and Geothermal Research, 13: 83-102.

Crera, D.A., and Barnes, H.L., 1976. Ore solution chemistry. V. Solubilities of chalcopyrite and chalcocite assemblages in hydrothermal solution at 200° to 300°C. Economic Geology, 71: 772-794.

de Rosen-Spence, A.P., Provost, G., Dimroth, E., Gochnauer, K., and Owen, V., 1980. Archean subaqueous felsic flows, Rouyn-Noranda, Quebec, Canada and their Quaternary equivalents. Precambrian Research, 12: 43-77.

de Rosen-Spence, A.P., 1976. Stratigraphy, development and petrogenesis of the central Noranda volcanic pile, Noranda, Quebec. Ph.D. thesis, University of Toronto, Toronto, Ont., (unpubl.).

Descarreaux, J., 1973. a petrochemical study of the Abitibi volcanic belt and its bearing on the occurrence of massive sulphide ores. Canadian Institute of Mining and Metallury Bull., 66: 61-79.

Dimroth, E., Imreh, L., Cousineau, P., Leduc, M., and Sanschagrin, Y., 1985. Paleogeographic analysis of mafic submarine flows and its use in the exploration for massive sulphide deposits; In Ayres, L.D., Thurston, P.C., Card, K.D. and Weber, W. (eds.), Geological Association of Canada, Special Paper 28, pp.203-222.

Dimroth, E., Imreh, L., Goulet, N., and Rocheleau, M., 1983A. Evolution of the south- central segment of the Archean Abitibi Belt, Quebec. Part 11: Tectonic evolution and geomechanical model. Canadian Journal of Earth Sciences, 20: 1355-1373.

Dimroth, E., Imreh, L., Goulet, N., and Rocheleau, M., 1983B. Evolution of the south- central segment of the Archean Abitibi Belt, Quebec. Part 111: Plutonic and metamorphic evolution and geotectonic model. Canadian Journal of Earth Sciences, 20: 1374-1388.

Dimroth, E., Imreh, L., Rocheleau, M. and Goulet, N., 1982. Evolution of the South-Central part of the Archean Abitibi Belt, Quebec. Part I: Stratigraphy and paleogeographic model. Canadian Journal of Earth Sciences, 19: 1729-1758.

Dimroth, E., and Lichtblau, A.P., 1979. Metamorphic evolution of Archean hyaloclastites, Noranda Area, Canada. Part I: Comparison of Archean and Cenozoic sea-floor metamorphism. Canadian Journal of Earth Sciences, 16: 1315-1340.

Dimroth,E., Hocq, M., Cousineau, P., Leduc, M., and Sanschagrin, Y., 1978. Structure and organization of Archean subaqueous basaltic flows, Rouyn-Noranda area, Quebec, Canada. Canadian Journal of Earth Sciences, 15: 902-918.

Dimroth, E., 1977. Archean subaqueous volcanic rocks, Rouyn-Noranda area, Quebec: Classification, diagnosis and interpretation. Geological Survey of Canada, Paper 77-1A: 513-522.

Doiron, G., 1983. Geology, reconstruction and targets in the D-68 lava dome. Corp. Falconbridge Copper internal report (unpubl.).

Dostal, J., and Strong, D.F., 1983. Trace-element mobility during low-grade metamorphism and silicification of basaltic rocks from Saint John, New Brunswick. Canadian Journal of Earth Sciences, 20: 431-435.

Dresser, J.A., and Denis, T.C., 1949. Geology of Quebec. Quebec Bur. Mines Geological Report 20, 3: 135-139.

Drummond, S.E., and Ohmoto, H., 1985. Chemical evolution and mineral deposition in boiling hydrothermal systems. Economic Geology, 80: 126-147.

Duffield, W.A., 1969. Concentric structure in elongate pillows, Amador County, California. U.S. Geological Survey Prof. Paper 650-D, pp. D19-D25.

Edwards, R.C.J., 1960. A progress report on the geological interpretation of the Noranda area. Consolidated Zinc Corp. Report (unpubl.).

Eichelberger, J.C., 1978. Andesitic volcanism and crustal evolution. Nature, 175: 21-27.

Eichelberger, J.C., and Gooley, R., 1977. Evolution of silic magma chambers and their relationship to basaltic volcanism; in Heacock,J.G.(ed), The Earths Crust its nature and physical properties, American Geophysical Union Monogram, 20: 57-77.

Eichelberger, J.C., 1975. Origin of andesite and dacite: Evidence of mixing at Glass Mountain in California and at other circum-Pacific volcanoes. Geological Society of America Bull. 86: 1381-1391.

Elders, W.A., Bird, D.K., Williams, A.E., and Schiffman, P., 1984. Hydrothermal flow regime and magmatic heat source of the Cerro Prieto Geothermal system, Baja California, Mexico. Geothermics, 13: 27-47.

Eldridge, C.S., Barton, P.B., and Ohomoto, H., 1983. Mineral textures and their bearing on the formation of the Kuroko orebodies; in Ohomoto, H. and Skinner, B.J. (eds.), The Kuroko and related volcanogenic massive sulphide deposits, Econ. Geology Mono. 5, pp. 241-281.

Faca, G., and Tonai, F., 1967. The self-sealing geothermal field, Bulletin Volcanologique, 30: 271-273.

Fisher, R.V., and Schminke, H.U., 1984. Pyroclastic Rocks. Springer Verlag, Berlin.

Fisher, R.V., and Waters, A.C., 1970. Base surge bed forms in maar volcanoes. American Journal of Science, 268: 157-180.

Fisher, R.V., 1966. Rocks composed of volcanic fragments. Earth-Science Reviews, 1: 287-298.

Fiske, R.S., and Matsuda, T., 1964. Submarine equivalents of ash flows in the Tokiwa Formation, Japan. American Journal of Science, 262: 76-106.

Fiske, R.S., 1963. Subaqueous pyroclastic flows in the Ohanapecosh Formation, Washington. Geological Society of America Bull., 74: 391-406.

Folk, R.L. and Pittman, J.S., 1971. Length-slow chalcedony: A new testament for vanished evaporites. Journal of Sedimentary Petrology 41: 1045-1058.

Fournier, R.O., 1985. The behavior of silica in hydrothermal solutions; in Berger. B.R. and Bethke, P.M. (eds.), Geology and Geochemistry of Epithermal Systems, Reviews in Economic Geology, 2: 45-61.

Fournier, R.O., and Rowe, J.J., 1966. Estimation of underground temperatures from the silica content of water from hot springs and wet-steam wells. American Journal of Science, 264: 685-697.

Franklin, J.M., 1986. Volcanic-associated massive sulphide deposits - an update; in Andrew, C.J., Crowe, W.R.A., Finlay, S., Pennell, W.M. and Pyne, J.F. (eds.), Geology and genesis of mineral deposits in Ireland, Irish Association for Economic Geology.

Franklin, J.M., Sangster, D.F., and Lydon, J.W., 1981. Volcanic-associated massive sulphide deposits. Economic Geology Anniversary Volume, pp. 485-627.

Franklin, J.M., Kasarda, J., and Poulsen, K.H., 1975. Petrology and chemistry of the Alteration Zone of the Mattabi massive sulphide deposit. Economic Geology, 70: 63-79.

Furnes, H., Fridleifsson, I.B., and Atkins, F.B., 1980. Subglacial volcanics. On the formation of acid hyaloclastites. Journal of Volcanology and Geothermal Research, 8: 95-110.

Furnes, H., 1978. Element mobility during palagonitization of a subglacial hyaloclastite in Iceland. Chemical Geology, 22: 249-264.

Gelinas, L., Trudel, P., and Hubert, C., 1984. Chemostratigraphic division of the Blake River Group, Rouyn-Noranda area, Abitibi, Quebec. Canadian Journal of Earth Sciences, 21: 220-231.

Gelinas, L., Lajoie, J., Bouchard, M., Simard, A., Verpaelst, P., and Chalot-Prat, F., 1978. Les complexes rhyoltiques de la region de Rouyn-Noranda. Rapp. Prelim., D.P.V. 583, Quebec Department of Natural Resources.

Gelinas, L., Brooks, C., Perrault, G., Carigan, J., Trudel, P., and Grasso, F., 1977. Chemo-stratigraphic subdivisions within the Abitibi volcanic belt, Rouyn-Noranda District; Iaragar, W.R.A., Coleman, L.C. and Hall, J.M., Volcanic Regimes in Canada, Geological Association of Canada Special Paper 16: 265-296.

Gelinas, L., Brooks, C., and Trzcienski, W.E., 1976. Archean variolites - quenched immiscible liquids. Canadian Journal of Earth Sciences, 13: 210-230.

Gibson, H.L., and Watkinson, D.H., 1986. The Central Mine Sequence, Noranda, Quebec: A caldera-fill sequence. In program with abstracts, Vol.11. GAC, MAC and CGU Annual Meeting, Ottawa, Ontario.

Gibson, H.L., Walker, S.D., and Coad, P.R., 1984. Surface geology and volcanogenic base metal massive sulphide and gold deposits of Noranda and Timmins. Guide Book for Field Trip #14: 124pp., GAC-MAC Annual Meeting, London, Ontario.

Gibson, H.L., Watkinson, D.H. and Comba C.D.A., 1983. Silicification: Hydrothermal alteration in an Archean geothermal system within the Amulet Rhyolite formation, Noranda, Quebec. Economic Geology, 78: 954-971.

Gibson, H.L., 1982. Na-Depletion patterns surrounding the Corbet Cu-Zn Deposit. Corporation Falconbridge Copper Ltd., internal report, (Unpubl.).

Gibson, H.L., and Doiron, G., 1982. Proposed exploration program, Waite Dufault and Jacob options, Duprat Township, Quebec. Corp. Falconbridge Copper internal report (unpubl.)

Gibson, H.L., and O'Dowd, P., 1981. Geological Interpretation and Proposed Exploration program for the West Ansil property. Corp. Falconbridge Copper internal report (unpubl.).

Gibson, H.L., and Watkinson, D.H., 1979. Silicification in the Amulet "Rhyolite" formation. Turcotte Lake section, Noranda area, Quebec. Geological Survey of Canada Paper, 79-B, pp. 111-120.

Gibson, H.L., 1979. Geology of the Amulet Rhyolite formation, Turcotte Lake Section, Noranda area, Quebec. M.Sc. thesis, Carleton University, Ottawa, Ontario, (unpubl.).

Gilmore, P.C., 1965. The origin of massive sulphide mineralization in the Noranda district, northweatern Quebec. Geological Association of Canada Proceedings, 16:63-81.

Goldfarb, M.S., Converse, D.R., Holland, H.D., and Edmond, J.M., 1983. The genesis of hot spring deposits on the East pacific Rise, 21°N. In Ohmoto, H. and Skinner, B.J.(eds.), Kuroko and related Volcanogenic massive sulphide deposits, Economic Geology Mono. 5, pp. 185-197.

Goldie, R., 1979. Consanguineous Archean intrusive and extrusive rocks, Noranda, Quebec: chemical similarities and differences. Precambrian Research, 9: 275-287.

Goldie, R., 1978. Metamorphism of the Flavrian and Powell Plutons, Noranda Area, Quebec. Journal of Petrology, 20: 227-238.

Goldie, R.J., 1976. The Flavrian and Powell Plutons, Noranda Area, Quebec. Phd. thesis, Queen's University, Kingston, Ontario, (unpubl.).

Goodwin, A.M., 1978. Archean volcanic studies in the Timmins-Kirkland Lake-Noranda region of Ontario and Quebec. Geological Survey of Canada Bull 278, 51p.

Gorman, B.E., 1975. Petrography, chemistry and mechanism of deposition of the Don Rhyolites, Rouyn-Noranda, Quebec. Msc. thesis, Queen's University, Kingston, Ontario (unpubl.).

Goulet, N., 1978. Stratigraphy and structural relationships across the Cadillac-Larder Lake Fault, Rouyn-Noranda area, Quebec. Phd. thesis, Queen's University, Kingston, Ontario (unpubl.).

Green, G.R., Ohmoto, H., Date, J., and Takahashi, T., 1983. Whole-rock oxygen isotope distribution in the Fukazawa-Kosaka Area, Hokuroko District, Japan, and its potential application to mineral exploration. In Ohmoto, H. & Skinner, B.J.(eds.), The Kuroko and related volcanogenic massive sulphide deposits, Economic Geology Monograph 5, pp. 395-411.

Greenwood, H., 1957. Geology of the Despina and D68 areas. Lake Dufault Mines Ltd. internal report (unpubl.).

Gresens, R., 1967. Composition-volume relationships of metasomatism. Chemical Geology, 2: 47-65.

Hajash, A., 1975. Hydrothermal processes along mid-ocean ridges. An experimental investigation. Contributions to Mineralogy and Petrology, 53: 205-226.

Hall, B.V., 1982. Geochemistry of the alteration pipe at the Amulet Upper A deposit, Noranda, Quebec. Canadian Journal of Earth Sciences, 19: 2060-2084.

Hargraves, R., and Ayres, L.D., 1979. Morphology of Archean metabasalts flows, Utik Lake, Manitoba. Canadian Journal of Earth Sciences, 16: 1452-1466.

Harley, D.N., 1979. A mineralized Ordovician resurgent caldera complex in the Bathurst-Newcsatle Mining District, New Brunswick, Canada. Economic Geology, 74: 786-796.

Harriagn, D.B., and MacLean, W.H., 1976. Petrography and geochemistry of epidote alteration patches in gabbro dykes at Matagami, Quebec. Canadian Journal of Earth Sciences, 13: 500-511.

Hausback, B.P., 1987. An extensive, hot, vapour-charged rhyodacite flow, Baja California, Mexico. In Fink, J. H. (ed), The Emplacement of Silic Domes and Lava Flows, Geological Society of America, Special Paper 212: 111-118.

Hay, R.L., and Iijima, A., 1967. Petrology of Palagonite tuffs of Koko Craters, Oahu, Hawaii. Contribution to Mineralogy and Petrology, 17: 141-154.

Haymon, R.M., 1982. Growth History of hydrothermal black smoker chimneys. Nature, 301: 695-697.

Haymon, R.M., and Kastner, M., 1981. Hot spring deposits on the east Pacific Rise at 21°N: Preliminary description of mineralogy and genesis. Earth and Planetary Science Letters, 53: 363-381.

Heaton, T.H.E., and Sheppard, S.M.F., 1977. Hydrogen and oxygen isotope evidence for sea-water-hydrothermal alteration and ore deposition, Troodos Complex, Cyprus. In Volcanic Processes and Ore Genesis, Geol. Soc. London, Special Publication 7, pp. 42-57.

Hedenquist, J.W., and Henley, R.W., 1985. Hydrothermal eruptions in the Waiotapu Geothermal System, New Zealand. Their origin, associated breccias, and relation to precious metal mineralization. Economic Geology, 80: 1640-1668.

Hekinian, R., and Fouquet, Y., 1985. Volcanism and metallogenesis of axial and off-axial structures on the East Pacific Rise near 13°N. Economic Geology, 80: 221-249.

Hekinian, R., Francheteau, J., Renard, V. et al., 1983. Intense hydrothermal activity at the axis of the East Pacific Rise near 13°N: Submersible witnesses the growth of a sulphide chimney. Marine Geophysical Research, 6: 1-14.

Hekinian, R., Fevier, M., Bischoff, J.L., Picot, P., and Shanks, C., 1980. Sulphide deposits from the East Pacific Rise near 21°N. Science, 207: 1433-1444.

Hekinian, R., and Hoffert, M., 1975. Rate of palagonitization and manganese coating on basaltic rocks from the rift valley in the Atlantic ocean near 36° 50'N. Marine Geology, 19: 91-109.

Heiken, G., 1974. An Atlas of volcanic ash. Smithsonian contributions to the Earth Sciences, 12.

Heiken, G., 1972. Morphology and petrography of volcanic ashes. Geological Society of America Bull., 83: 1961-1987.

Hildreth, W., 1981. Gradients in silicic magma chambers: Implications for lithospheric magmatism. Journal of Geophysical Research, 86: 10153-10192.

Hodgson, C.J., and Lydon, J.W. 1977. The geologic setting of volcanogenic massive sulphide deposits and active hydrothermal systems. Some implications for exploration. Canadian Institute of Mining and Metallurgy Bull., 70: 95-106.

Holland, H.D., 1972. Granites, solutions and base metal deposits. Economic Geology, 67: 281-301.

Honnerez, J., and Kirst, P., 1975. Submarine basaltic volcanism: morphometric parameters for discriminating hyaloclastites from hyalotuffs. Bulletin Volcanologique, 39: 1-25.

Hubert, C., Trudel, P., and Gelinas, L., 1984. Archean wrench fault tectonics and structural evolution of the Blake River Group, Abitibi Belt, Quebec. Canadian Journal of Earth Sciences, 21: 1024-1032.

Hughes, C.J., 1973. Spilites, keratophyres and the igneous spectrum. Geological Magazine 6: 513:527.

Hunter, A.D., and Gibson, H.L., 1986. A lithostratigraphic correlation of the Aldermac - Amulet/Millenbach areas, Noranda Camp, Quebec. Canadian Institute of Mining and Metallury, 88th Annual Meeting, Montreal, Quebec, Abstract.

Hunter, A.D., and Moore, J.M., 1983. The geologic setting of the Aldermac copper deposit, Noranda, Quebec. Canadian Institute of Mining and Metallurgy Bull., 76: 128-136.

Hunter, A.D., 1979. The geologic setting of the Aldermac Copper deposit, Noranda, Quebec. Msc. thesis, Carleton University, Ottawa, Ontario (unpubl.).

Ikingura, J.R., Bell, K., and Watkinson, D.H., 1989. Hydrothermal alteration and oxygen and hydrogen isotope geochemistry of the D68 Zone Cu-Zn massive sulphide deposit, Noranda District, Quebec, Canada. Mineralogy and Petrology, 40: 155-172.

Ikingura, J.R., 1984. Hydrothermal alteration and Cu-Zn mineralization in the D-68 Zone, Corbet Mine, Noranda District, Quebec, Canada. Msc. thesis, Carleton University, Ottawa, Ontario (unpubl.).

Irvine, T.N., and Baragar, W.R.A., 1971. A guide to the classification of the common volcanic rocks. Canadian Journal of Earth Sciences, 8: 523-549.

Jensen, L.S., 1985. Stratigraphy and petrogenesis of Archean metavolcanic sequences, southwestern Abitibi Subprovince, Ontario; in Ayres, L.D., Thurston, P.C., Card, K.D. and Weber, W. (eds.), Geol. Assoc. Can. Special Paper 28, 65-87.

Jensen, L.S., and Langford, F.F., 1985. Geology and petrogenesis of the Archean Abitibi Belt in the Kirkland Lake Area, Ontario. Ontario Geological Survey Misc. Paper 123, 130p.

Jensen, L.S., 1976. A new cation plot for classifying subalkalic volcanic rocks. Ontario Division of Mines, Miscellaneous Paper 66, 22p.

Jolly, W.T., 1978. Metamorphic history of the Archean Abitibi Belt; In Fraser, J.A. and Haywood, W.W.(eds.), Metamorphism in the Canadian Shield, Geological Survey of Canada, Paper 78-10, pp.63-78.

Jolly, W.T., 1977. Relations between Archean lavas and intrusive bodies of the Abitibi Greenstone Belt, Ontario, Quebec; in Baragar,W.R.A., Coleman, L.C. and Hall, J.M. (eds.), Geological Association of Canada, Special Paper ,6 pp. 311-330.

Jones, J.G., 1970. Intraglacial volcanoes of the Laugarvatn region, south-west Iceland, I. Quarterly Journal of the Geological Society of London, 124: 197-211.

Jones, J.G., 1969. Pillow lavas as depth indicators. American Journal of Science, 267: 181-195.

Jones, J.G., 1968. Pillow lava and pahoehoe. Journal of Geology, 76: 485-488.

Kajiwara, Y., 1970. Chemical composition of ore-forming solutions responsible for the Kuroko type mineralization in Japan. Geochemical Journal, 6: 141-149.

Kalogeropoulos, S.I. and Scott, S.D., 1989. Mineralogy and geochemistry of an Archean tuffaceous exhalite: The Main Contact Tuff, Millenbach Mine area, Noranda, Quebec. Canadian Journal of Earth Sciences, 26: 88-105.

Keith, T.E.C., Muffler, L.J.P, and Cremer, M, 1968. Hydrothermal epidote formed in the Salton Sea geothermal system, California. American Mineralogist, 53: 1653-1644.

Kennedy, G.C., 1950. A portion of the system silica-water. Economic Geology, 45: 629-653.

Knuckey, M.S., Comba, C.D.A., and Riverin, G., 1982. The Millenbach deposit, Noranda district, Quebec - an update on structure, metal zoning and wall rock alteration. Geological Association of Canada, Special Paper 25, pp. 297-318.

Knuckey, M.J. and Watkins, J.J., 1982. The geology of the Corbet massive sulphide deposit, Noranda District, Quebec, Canada. Geological Association of Canada Special Paper 25, pp. 255-296.

Koide, H., and Bhattacharji, S., 1975. Formation of fractures around magmatic intrusions and their role in ore localization. Economic Geology, 70: 781-799.

Kouda, R., and Koide, H., 1978. Ring structures, Resurgent Cauldron and Ore Deposits in the Hokuroko volcanic field, northern Akita, Japan. Mining Geology, 23: 233-244.

Kristmannsdottir, H., 1982. Alteration in IRDP drill hole compared with other drill holes in Iceland. Journal of Geophysical Research, 87: 6525-6531.

Kristmannsdottir, H., 1975. Hydrothermal alteration of basaltic rocks in Icelandic geothermal areas. UN Symposium on the Development and Utilization of Geothermal Resources Proceedings, pp. 441-445.

Krough, T.W., and Davis, G.L., 1971. Zircon U-Pb ages of Archean metavolcanic rocks in the Canadian Shield. Carnegie Institute of Washington, Washington, DC, Geophysical Laboratory Report 1970-1971, pp. 241-242.

Lambert, M.B., 1988. Cameron River and Beaulieu River volcanic belts of the Archean Yellowknife Supergroup, District of Mackenzie, Northwest Territories. Geological Survey of Canada Bull. 382, 145p.

Lambert, M.B., 1974. Bennett Lake cauldron subsidence Complex. B.C. and Y. T. Geological Survey of Canada Bull. 277, 213 p.

Large, R.R., 1977. Chemical evolution and zonation of massive sulphide deposits in volcanic terrains. Economic Geology, 72: 549-572.

Le Maitre, R.W., 1976. The chemical variability of some common igneous rocks. Journal of Petrology, 17: 589-637.

Lesher, C.M., Gibson, H.L., and Campbell, I.H., 1986. Composition-volume changes during hydrothermal alteration of andesite at Buttercup Hill, Noranda District, Quebec. Geochimica et Cosmochimica Acta, 50: 2693-2705.

Lewis, J.V., 1914. Origin of pillow lavas. Geological Society of America Bull. ,2 pp. 591-654.

Lichtblau, A.P., 1983. Preliminary field guide to the Quemont and Powell areas, Noranda, Quebec. Corp. Falconbridge Copper Internal report (unpubl.).

Lichtblau, A.P., and Dimroth, E., 1980. Stratigraphy and facies at the south margin of the Archean Noranda caldera, Noranda, Quebec. In Current Research, Part 1A, Geological Survey of Canada Paper 80-1A, pp. 69-756.

Lickus, R.J., 1965. Geology and geochemistry of the ore deposits at the Vauze Mine, Noranda district, Quebec. Phd. thesis, McGill University, Montreal, Quebec, (unpubl.).

Loney, R.A., 1968. Flow structure and composition of the Southern Coulee, Mono Craters, California - A pumiceous rhyolite flow. Geological Society of America Mem. 116, pp.415-440.

Lorenz, V., 1973. On the formation of Maars. Bulletin Volcanologique, 37: 183-204.

Lorenz, V., 1970. Some aspects of the eruption mechanism of the Big Hole maar, central Oregon. Geological Society of America Bull. 81, pp.823-1830.

Lydon, J.W., 1988. Vocanogenic massive sulphide deposits, Part 2. Genetic models. Geoscience Canada, 15: 43-65.

Lydon, J.W., 1984. Volcanogenic massive sulphide deposits Part 1. A descriptive model. Geoscience Canada, 11: 195-202.

Lydon, J.W., and Jamieson, H.E., 1984. The generation of ore-forming hydrothermal solutions in the Troodos ophiolite complex. Some hydrodynamic and mineralogical considerations. In Current Research, PartA, Geological Survey of Canada, Paper 84-1A, pp. 617-625.

MacDonald, G.A., 1972. Volcanoes. Prentice-Hall, New Jersey.

MacDonald, G.A.,and Katsura. H., 1965. Eruption of Lassen Peak, Cascade Range, California, in 1915: Example of mixed magmas. Geological Society of America Bull. 76, pp.475-482.

MacGeehan, P.J., and McLean, W.H., 1980. An Archean sub-seafloor geothermal system,"calc-alkali" trends, and massive sulphide genesis. Nature 286: 767-771.

MacGeehan, P.J., 1978. The geochemistry of altered volcanic rocks at Matagami, Quebec. A geothermal model for massive sulphide genesis. Canadian Journal of Earth Sciences, 15: 551-570.

Marzouki, F., Kerrich, R., and Fyfe, W.S., 1979. Epidotisation of diorites at Al Hadah, Saudi Arabia: Fluid influx into cooling plutons. Contributions to Mineralolgy and Petrology, 68: 281-284.

Matttnen, P., 1974. Geology of the Hunter Creek Fault area. Falconbridge Copper Ltd., internal report (unpubl.).

McEwen, J.H., and Watkinson, D.H., 1982. Syngenetic deformation in massive sulphides, Gallen Deposit, Noranda, Quebec; In Current Research, Part A, Geological Survey of Canada, Paper 82-1A, pp.275-280.

McKibben, M.A., Williams, A.E., Elders, W.A., and Eldridge, C.S., 1987. Saline brines and metallogenesis in a modern sediment-filled rift: The Salton Sea geothermal system, California, U.S.A.. Applied Geochemistry, 2: 563-578.

Mehegan, J.M., Robinson, P.T., and Delaney, J.R., 1982. Secondary mineralization and hydrothermal alteration in the Reydarfjordur drill core, Eastern Iceland. Journal of Geophysical Research, 87: 6511-6524.

Moore, J.G., 1975. Mechanism of formation of pillow lava. American Scientist, 63: 269-277.

Moore, J.G., and Schilling, J.G., 1973. Vesicles, water and sulphur in Reykjanes Ridge basalts. Contributions to Mineralogy and Petrology, 41: 105-118.

Moore, J.G., Phillips, R.W., Grigg, D., Peterson, W., and Swanson, D.A., 1973. Flow of lava into the sea 1969-1971, Kilauea Volcano, Hawaii. Geological Society of America Bull., 84: 537-546.

Moore, J.G., Cristofolini, R., and Lo Guidice, A., 1971. Development of pillows on the submarine extension of recent lava flows, Mount Etna, Sicily. U.S. Geological Survey Reference Paper 750-C, pp.C89-C97.

Moore, J.G., 1970. Relationship between subsidence and volcanic load, Hawaii. Bulletin Volcanologique, 34: 526-576.

Moore, J.G., and Fiske, R.S., 1969. Volcanic substructure inferred from dredge samples and ocean-bottom photographs, Hawaii. Geological Society of America Bull. 80, pp.1191-1202.

Moore, J.G., 1966. Rates of palagonitization of submarine basalt adjacent to Hawaii. U.S. Geological Survey Prof. Paper 550-D, pp.163-171.

Moore, J.G., 1965. Petrology of deep sea basalt near Hawaii. American Journal of Science, 263: 40-52.

Mortensen, J.K., 1987. Preliminary U-Pb zircon ages for volcanic and plutonic rocks of the Noranda-Lac Abitibi area, Abitibi Subprovince, Quebec. In Current Research, Part A, Geological Survey of Canada, Paper 87-1A, pp581-590.

Mottl, M.J., 1983. Metabasalts, axial hot springs, and the structure of hydrothermal systems at mid-ocean ridges. Geological Society of America Bulletin, 94: 161-180.

Mottl, M.J., and Seyfried, W.E., 1980. Sub-seafloor hydrothermal systems. Rock-vs.seawater-dominated. In Rona, P.A. & Lowell, R.P. (eds.), Seafloor spreading centres - Hydrothermal systems. Dowden, Hutchinson and Ross, Inc., Stroudsburg, Pennsylvania, 424p.

Muffler, L.J., White, D.E., and Truesdell, A.H., 1971. Hydrothermal explosion craters in Yellowstone National Park. Geological Society of America Bull. 82, pp. 723-740.

Nayudu, Y.R., 1964. Palagonite tuffs (hyaloclastites) and the products of post-eruptive processes. Bulletin Volcanologique, 27: 391-410.

Nunes, P.D., and Jensen, L.S., 1980. Geochronology of the Abitibi Metavolcanic belt, Kirkland lake Area - A progress report; in Pye, E.G. (ed.), Summary of Geochronologic Studies, 1971-1979, Ontario Geological Survey, Misc. Paper 92, pp.40-45.

Ohmoto, H., and Takahashi, T., 1983. Part III. Submarine calderas and Kuroko Genesis. In Ohmoto, H., and Skinner, B.J.(eds.), The Kuroko and related volcanogenic massive sulphide deposits, Economic Geology Monograph 5, pp.9-114.

Oudin, E., Picot, P., and Poult, G., 1981. Comparison of sulphide deposits from the East pacific Rise and Cyprus. Nature, 291: 404-407.

Paradis, S., Jonasson, I.R., Le Cheminant, G.M., and Watkinson, D.H., 1988. Two zinc-rich chimneys from the Plume Site, southern Juan De Fuca Ridge. Canadian Mineralogist, 26: 637-654.

Paradis, S., Ludden, J., and Gelinas, L., 1988. Evidence for contrasting compositional spectra in comagmatic intrusive and extrusive rocks of the late Archean Blake river Group, Abitibi, Quebec. Canadian Journal of Earth Sciences, 25: 134-144.

Peacock, M.A., 1926. The volcano-glacial palagonite formation of Iceland. Geology Magazine, 63: 385:399.

Pearce, J.A., and Cann. J.R., 1973. Tectonic setting of basic volcanic rocks determined using trace element analyses. Earth and Planetary Science Letters, 19: 290-300.

Philpotts, A.R., 1982. Compositions of immiscible liguids in volcanic rocks. Contributions to Mineralalogy and Petrology, 80: 210-218.

Phipotts, A.R., 1976. Silicate liguid immiscibility: Its probable extent and petrogenetic significance. American Journal of Science, 276: 1147-1177.

Pichler, H., 1965. Acid Hyaloclastites. Bulletin Volcanologique, 28: 283-310.

Price, P., 1948. Horne Mine; In Structural Geology of Canadian ore deposits. Canadian Institute of Mining and Metallurgy, Geological Division, pp.763-772.

Reynolds, D.L., 1954. Fluidization as a geological process and its bearing on the problem of intrusive granites. American Journal of Science, 252: 577-613.

Richey, J.E., 1961. Scotland: The Tertiary volcanic districts. Department of Science, Industry and Resources, Geological Survey and Museum, Edinburgh, 119pp.

Rickard, D.T., and Zweifel, H., 1975. Genesis of Precambrian sulphide ores, Skellefte District, Sweeden. Economic Geology, 70: 255-274.

Ridge, J.D., 1973. Volcanic exhalations and ore deposition in the vicinity of the seafloor. Mineralium Deposita, 8: 332-348.

Riverin, G., and Hodgson, C.J., 1980. Wall-rock alteration at the Millenbach Cu-Zn mine, Noranda, Quebec. Economic Geology, 75: 424-444.

Riverin, G., 1977. Wall-rock alteration at the Millenbach Mine, Noranda, Quebec. Phd.Thesis, Queen's University, Kingston, Ontario.

Roberts, R.G., and Reardon, E.J., 1978. Alteration and ore-forming processes at Mattagami Lake Mine, Quebec. Canadain Journal of Earth Sciences, 15: 1-21.

Roscoe, S.M., 1965. Geochemical and Isotopic studies, Noranda and Matagami areas: Symposium on stratabound sulphides. Canadian Institute of Mining and Metallurgy, 68: 279-285.

Rosenbauer, R.J. and Bischoff, J.L., 1984. Uptake and transport of heavy metals by heated seawater: A summary of the experimental results. In Rona, P.A., Bostrom, K., Laubier, L. and Smith, K.L.(eds.), Hydrothermal processes at seafloor spreading centres, Plenum, New York.

Rutten, M.G., 1963. Acid lava flow structure (as compared to ignimbrites). Bulletin Volcanologique, 25: 111-121.

Ryerson, F.J. and Hess, P.C., 1975. The partioning of trace elements between immiscible silicate melts (abstract). American Geophyical Union Transactions, pp.456-470.

Sakrison, H.C., 1966. Variations in rock composition around Lake Dufault orebodies, Noranda district. Phd. thesis, McGill University, Montreal, Quebec (unpubl.).

Sangster, D.F., 1980. Quantitative characteristics of volcanogenic massive sulphide deposits. 1. Metal content and size distribution of massive sulphide deposits in volcanic centres. Canadian Institute of Mining and Metallurgy Bull., 73:74-81.

Sangster, D.F., and Scott, S.D., 1976. Precambrian, stratabound, massive sulphide Cu-Zn-Pb sulphide ores of North America; in Wolf, K.H.(ed.), Handbook of Strata-bound and stratiform ore deposits, Elsevier, Amsterdam, 6: 129-222.

Sangster, D.F., 1972. Precambrian volcanogenic massive sulphide deposits in Canada. A review. Geological Survey of Canada Paper 72-22, 44p.

Scarfe, C.M., and Smith, D.G.W., 1977. Secondary minerals in some basaltic rocks from DSDP Leg 37. Canadian Journal of Earth Sciences 14: 903-910.

Scott, R.B., and Hajash, A., 1976. Initial submarine alteration of basaltic pillow lavas: A microprobe study. American Journal of Science 276: 480-501.

Scott, S.D., 1980. Geology and structural control of Kuroko-type massive sulphide deposits. Geological Association of Canada Special Paper 70, pp.301-311.

Scott, S.D., 1978. Structural control of the Kuroko deposits of the Hokuroko district, Japanese Mining Geology, 28:301-311.

Setterfield, T., 1987. Massive and brecciated dikes in the McDougall-Despina faults, Noranda, Quebec, Canada. Journal of Volcanology and Geothermal Research, 31: 87-97.

Setterfield, T., 1984. Nature and significance of the McDougall-Despina fault set, Noranda, Quebec. Msc. thesis, Univ. Western Ontario, London, Ontario (unpubl.).

Seyfried, W.E., Berndt, M.E., and Seewald, J.S., 1988. Hydrothermal alteration processes at mid-ocean ridges: constraints from diabase alteration experiments, hot-spring fluids and composition of the oceanic crust. Canadian Mineralogist, 26, Part 3: 787-804.

Seyfried, W.E., and Janecky, D.R., 1985. Heavy metal and sulphur transport during subcritical and supercritical hydrothermal alteration of basalt. Influence of fluid pressure and basalt composition and crystallinity. Geochimica et Cosmochimica Acta, 49: 2545-2560.

Seyfried, W.E., and Bischoff, J.L., 1981. Experimental seawater-basalt interaction at 300°C, 500 bars. Chemical exchange, secondary mineral formation, and implications for the transport of heavy metals. Geochimica et Cosmochimica Acta, 45: 135-147.

Seyfried, W.E, and Bischoff, J.L., 1979. Low temperature basalt alteration by seawater: An experimental study at 70° C and 150°C. Geochimica et Cosmochimica Acta, 43: 1937-1947.

Seyfried, W.E., and Bischoff, J.L., 1977. Hydrothermal transport of heavy metals by seawater. The role of seawater/basalt ratio. Earth and Planetary Science Letters, 34: 71-77.

Sibson, R.H., Moore, J. and Rankin, A.H., 1975. Seismic pumping - a hydrothermal fluid transport mechanism. Geological Society of London Journal, 131: 653-659.

Sigurdsson, H., and Sparks, R.S.J., 1981. Petrology of Rhyolitic and mixed Magma ejecta from the 1875 eruption of Askja, Iceland. Journal of Petrology, 22: 41-84.

Simmons, B.D., and Geological Staff, 1973. geology of the Millenbach massive sulphide deposit, Noranda, Quebec. Canadian Institute of Mining and Metallurgy Bull., 66: 67-78.

Sinclair, W.D., 1971. A volcanic origin for the No.5 Zone of the Horne Mine. Economic Geology, 66: 1225-1231.

Simmons, B.D., 1972. Geology of the Hunter Creek Fault area. Falconbridge Copper Ltd., internal report (unpubl.).

Skirrow,R.G., 1987. Silicification in a Semiconformable Alteration Zone below the Chisel Lake massive sulphide deposit, Manitoba. MSc. thesis, Carleton University, Ottawa, Ont., (unpubl.).

Smith, R.E., 1968. Redistribution of major elements in the alteration of some basic lavas during burial metamorphism. Journal of Petrology, 9: 191-219.

Smith, R.L., and Bailey, R.A., 1968. Resurgent Cauldrons. Geological Society of America Mem. 116, pp. 613-662.

Smith, T.L., 1984. Textures, field relationships and flow morphology of the Waite Rhyolite Formation, Noranda, Quebec. Bsc.thesis, Carleton University, Ottawa, Ontario (unpubl.).

Smith, W.K., 1983. A petrographic description of the Newbec Breccia, Noranda, Quebec. Bsc. thesis, Univ. of Waterloo, Ontario (unpubl.).

Sparks, R.J.S., Sigurdsson, H., and Wilson, L., 1977. Magma mixing: A mechanism for triggering acid explosive eruptions. Nature, 267: 315-318.

Spence, C.D., 1975. Volcanogenic features of the Vauze sulphide deposit, Noranda, Quebec. Economic Geology, 70: 102-114.

Spence, C.D., and de Rosen-Spence, A.F., 1975. The place of sulphide mineralization in the volcanic sequence at Noranda, Quebec. Economic Geology, 70: 90-101.

Spence, C.D., 1967. The Noranda Area. Canadian Insitute of Mining and Metallurgy, Centennial Field Excursion Guidebook, pp. 36-39.

Spiess, F.N., MacDonald, K.C., Atwater, T., Ballard, R. et al., 1980. East pacific Rise: Hot springs and geophysical experiments. Science, 207: 1421-1433.

Spooner, E.T.C., 1977. Hydrodynamic model for the origin of the ophiolitic cupriferous pyrite ore deposits of Cyprus. In Volcanic processes in ore genesis, Geological Society of London, Special Publication 7, pp. 58-71.

Spooner, E.T.C., and Fyfe, W.S., 1973. Sub-seafloor metamorphism, heat and mass transfer. Contributions to Mineralogy and Petrology, 42: 287-304..

Spring, R.M., 1976. Study of alteration textures on Buttercup Hill, Noranda area, Quebec. B.Sc. thesis, Queen's Univesity, Kingston, Ont., (unpubl.).

Staudigel, H., and Hart, S.R., 1983. Alteration of basaltic glass: Mechanisms and significance for the oceanic crust-seawater budget. Geochimica et Cosmochimica Acta, 47: 337-350.

Stephens, M.B., 1982. Spilitization, volcanic composition and magmatic evolution-their bearing on massive sulphide composition and siting in some volcanic terrains. Transactions of the Institute of Mining and Metallurgy (Section B), 91: B200-B212.

Stevens, T.A., and Lipman, P.W., 1976. Calderas of the San Juan volcanic field, south-western Colorado. U.S. Geological Survey Prof. Paper 958.

Strong, D.F., Dickson, W.L., and Pickerill, R.K., 1979. Chemistry and prehnite-pumpellyite facies metamorphism of calc-alkaline, Carboniferous volcanic rocks of southeastern New Brunswick. Canadain Journal of Earth Sciences, 16: 1071-1085.

Styrt, M.M., Brackmann, A.J., Holland, H.D., Clark, B.C., Pistha-Arnond, V., Eldridge, C.S., and Ohomoto, H., 1981. The mineralogy and the isotopic composition of sulphur in hydrothermal sulphide/sulphate deposits on the East Pacific Rise, 21°N lattitude. Earth and Planetary Science Letters, 53: 382-390.

Swanson, D.A., Dzurisin, D., Holcomb, R.T. et al., 1987. Growth of the lava dome at Mount St. Helens, Washington, (USA), 1981-1983; In Fink, J.H.(ed.), The emplacement of silicic domes and lava flows, Geological Society of America Special Paper 212, pp.1-16.

Swanson, D.A., 1973. Pahoehoe flows from the 1969-1971 Mauna Ula eruption, Kilauea Volcano, Hawaii. Geological Society of America Bull., 84: 615-626.

Taylor, T.R., Vogel, T.A., and Wilband, J.T., 1980. The composite dikes at Mount Desert Island, Maine: An example of coexisting acidic and basic magmas. Journal of Geology, 88: 433-444.

Thurston, P.C., Ayers, L.D., Edwards, G.R., Gelinas, L., Ludden, J.N., and Verpaelst, P., 1985. Archean bimodal volcanism. In Ayers, L.D., Thurston, P.C., Card, K.D., & Weber, W. (eds.), Evolution of Archean supracrustal sequences, Geological Association of Canada Special Paper 28, pp. 7-21.

Thompson, G., 1984. Basalt-seawater interaction; in Rona, P.A., Bostrom, K., Laubier, L., and Smith, K.L. (eds.), Hydrothermal processes at seafloor spreading centres, Plenum, New York, pp.225-277.

Tomasson, J., and Kristmannsdottir, H., 1972. High temperature alteration minerals and thermal brines, Reykjanes, Iceland. Contributions to Mineralogy and Petrology, 36: 123-134.

Urabe, T., Scott, S.D., and Hattori, K., 1983. A comparison of footwall-rock alteration and geothermal systems beneath some Japanese and Canadian Volcanogenic Massive sulphide deposits. In Ohmoto, H. & Skinner,B.J.(eds.), The Kuroko and related volcanogenic massive sulphide deposits, Economic Geology Monograph 5, pp.345-364.

Vallence, T.G., 1974. Spilitic degradation of a tholeiitic Basalt. Journal of Petrology 15: 79-96.

Viereck, L.G., Griffin, B.J., Schmincke H.-U., and Pritchard, R.G., 1982. Volcaniclastic rocks of the Reydarfjordur drill hole, Eastern Iceland 2. Alteration. Journal of Geophysical Research, 87: 6459-6476.

Vivallo, W., and Willden, M., 1988. Geology and geochemistry of an early Proterozoic volcanic sequence at Kristineberg, Skellefte district, Sweden. Geologiska Foreningens i Stockholm Forhandlingar, 110: 1-12.

Vogel, T.A. and Wilband, J.T., 1978. Coexisting acidic and basic melts: Geochemistry of a composite dike. Journal of Geology, 86: 353-371.

Vogel, T.A. and Walker, B.M., 1975. The Tichka Massif, Morocco-an example of contemporaneous acidic and basic plutonism. Lithos, 8: 29-38.

Wachendorf, H., 1973. The rhyolite flows of the Lebombos (SE Africa). Bulletin Volcanologique. 35: 515-529.

Walker, G.P.L., 1973. Lengths of lava flows. Phil. Transactions of the Royal Society of London A274, pp.107-118.

Walker, G.P.L., 1972. Compound and simple lava flows and flood basalts. Bulletin Volcanologique, 35: 579-590.

Walker, G.P.L., and Skelhorn, R.R., 1966. Some associations of acid and basic igneous rocks. Earth Science Reviews, 2: 93-109.

Walker, G.P.L., 1963. The Breiddalur cental volcano, eastern Iceland. Geological Society of London, Quaterly Journal, 119: 29-63.

Walker, G.P.L., 1960a. Zeolite zones and dike distribution in relation to the structure of basalts of eastern Iceland. Mineralogical Magazine 32: 465-477.

Walker, G.P.L., 1960b. The amygdal minerals of the Tertiary lavas of Iceland: III. Regional distribution. Mineralogical Magazine 32: 503-515.

Waters, A.C., 1960. Determining direction of flow in basalts. American Journal of Science, 258: 350-366.

Watkins,J.J., 1980. The geology of the Corbet Cu-Zn deposit and the environment of ore deposition in the Central Noranda area. Msc. thesis, Queen's University, Kingston, Ontario (Unpubl.).

Watkinson, D.H., Gibson, H.L. and Watkins, D.H., 1983. Comparison of Cyprus- and Noranda-Type VMS deposits. In program with abstracts, vol.8, GAC, MAC and CGU Annual Meeting, Victoria, B.C.

Watson, E.B., 1976. Two-liquid partition coefficients: Experimental data and geochemical implications. Contributions to Mineralogy and Petrology, 56: 119-134.

Webber, G.R., 1962. Variation in the composition of the Lake Dufault Granodiorite. Canadian Institute of Mining and Metallurgy, 65: 55-62.

Weibe, R.A., 1973. Relations between coexisting basaltic and granitic magmas in a composite dike. American Journal of Science, 273: 130-151.

Williams, H., and McBirney, A.R., 1979. Volcanology. Freeman, Cooper and Co., San Francisco.

Wilson, M.E., 1941. Noranda district Quebec. Geological Survey of Canada Memoir 229, 162p.

Winchester, J.A., and Floyd, P.A., 1977. Geochemical discrimination of different magma series and their differentiation products using immobile elements. Chemical Geology, 20: 325-343.

Winkler, H.G., 1979. Petrogenesis of metamorphic Rocks. Springer-Verlag, New York.

Wohletz, K.H., and McQueen, R.G., 1984. Volcanic and stratospheric dustlike particles produced by experimental water-melt interaction. Geology, 12: 591-594.

Wohletz, K.H., 1983. Mechanisms of hydrovolcanic pyroclast formation: grain size, scanning electron microscopy and experimental studies. Journal of Volcanology and Geotherm Research, 17: 31-63.

Wohletz, K.H., and Sheridan, M.F., 1983. Hydrovolcanic explosions II. Evolution of basaltic tuff rings and tuff cones. American Journal of Science, 283: 385-413.

Yamada, E., 1973. Subaqueous pumice flow deposits in the Onikobe Caldera, Miyagi Prefecture, Japan. Journal of the Geological Society of Japan, 79: 585-597.

Yamagishi, H., and Dimroth, E., 1985. A comparison of Miocene and Archean rhyolite hyaloclastites: Evidence for a hot and fluid rhyolite lava. Journal of Volcanology and Geothermal Research, 23: 337-355.

Yoder, H.S., 1973. Contemporaneous basaltic and rhyolitic magmas. American Mineralogist, 58: 153-171.

Zachrisson, E., 1982. Spilitization, mineralization and vertical metal zonation at the Stekenjokk strata-bound sulphide deposit, central Scandinavian Caledonides. Transactions of the Institute of Mining and Metallurgy (Section B), 91: B192-B213.